ACS SYMPOSIUM SERIES 1105

Biobased Monomers, Polymers, and Materials

Edited by

Patrick B. Smith and Richard A. Gross

Downloaded by 217.66.152.26 on August 23, 2012 | http://pubs.acs.org
Publication Date (Web): August 16, 2012 | doi: 10.1021/bk-2012-1105.fw001

Biobased Monomers, Polymers, and Materials

In Biobased Monomers, Polymers, and Materials; Smith, P., et al.;
ACS Symposium Series; American Chemical Society: Washington, DC, 2012.

Downloaded by 217.66.152.26 on August 23, 2012 | http://pubs.acs.org
Publication Date (Web): August 16, 2012 | doi: 10.1021/bk-2012-1105.fw001

ACS SYMPOSIUM SERIES **1105**

Biobased Monomers, Polymers, and Materials

Patrick B. Smith, Editor
Michigan Molecular Institute
Midland, Michigan

Richard A. Gross, Editor
Polytechnic University
Brooklyn, New York

Downloaded by 217.66.152.26 on August 23, 2012 | http://pubs.acs.org
Publication Date (Web): August 16, 2012 | doi: 10.1021/bk-2012-1105.fw001

Sponsored by the
ACS Division of Polymer Chemistry, Inc.

American Chemical Society, Washington, DC

Distributed in print by Oxford University Press, Inc.

Downloaded by 217.66.152.26 on August 23, 2012 | http://pubs.acs.org
Publication Date (Web): August 16, 2012 | doi: 10.1021/bk-2012-1105.fw001

Library of Congress Cataloging-in-Publication Data

Biobased monomers, polymers, and materials / Patrick B. Smith, editor, Michigan Molecular Institute, Midland, MI, Richard A. Gross, editor, Polytechnic University, Brooklyn, NY ; sponsored by the ACS Division of Polymer Chemistry, Inc.
pages cm. -- (ACS symposium series ; 1105)
Includes bibliographical references and index.
ISBN 978-0-8412-2767-5
1. Biopolymers--Congresses. I. Smith, Patrick B., Dr., editor of compilation. II. Gross, Richard A., 1957- editor of compilation. III. American Chemical Society. Division of Polymer Chemistry, sponsoring body.
TP248.65.P62B525 2012
572--dc23
2012025700

The paper used in this publication meets the minimum requirements of American National Standard for Information Sciences—Permanence of Paper for Printed Library Materials, ANSI Z39.48n1984.

Copyright © 2012 American Chemical Society

Distributed in print by Oxford University Press, Inc.

All Rights Reserved. Reprographic copying beyond that permitted by Sections 107 or 108 of the U.S. Copyright Act is allowed for internal use only, provided that a per-chapter fee of $40.25 plus $0.75 per page is paid to the Copyright Clearance Center, Inc., 222 Rosewood Drive, Danvers, MA 01923, USA. Republication or reproduction for sale of pages in this book is permitted only under license from ACS. Direct these and other permission requests to ACS Copyright Office, Publications Division, 1155 16th Street, N.W., Washington, DC 20036.

The citation of trade names and/or names of manufacturers in this publication is not to be construed as an endorsement or as approval by ACS of the commercial products or services referenced herein; nor should the mere reference herein to any drawing, specification, chemical process, or other data be regarded as a license or as a conveyance of any right or permission to the holder, reader, or any other person or corporation, to manufacture, reproduce, use, or sell any patented invention or copyrighted work that may in any way be related thereto. Registered names, trademarks, etc., used in this publication, even without specific indication thereof, are not to be considered unprotected by law.

PRINTED IN THE UNITED STATES OF AMERICA

Downloaded by 217.66.152.26 on August 23, 2012 | http://pubs.acs.org
Publication Date (Web): August 16, 2012 | doi: 10.1021/bk-2012-1105.fw001

Foreword

The ACS Symposium Series was first published in 1974 to provide a mechanism for publishing symposia quickly in book form. The purpose of the series is to publish timely, comprehensive books developed from the ACS sponsored symposia based on current scientific research. Occasionally, books are developed from symposia sponsored by other organizations when the topic is of keen interest to the chemistry audience.

Before agreeing to publish a book, the proposed table of contents is reviewed for appropriate and comprehensive coverage and for interest to the audience. Some papers may be excluded to better focus the book; others may be added to provide comprehensiveness. When appropriate, overview or introductory chapters are added. Drafts of chapters are peer-reviewed prior to final acceptance or rejection, and manuscripts are prepared in camera-ready format.

As a rule, only original research papers and original review papers are included in the volumes. Verbatim reproductions of previous published papers are not accepted.

ACS Books Department

Downloaded by 217.66.152.26 on August 23, 2012 | http://pubs.acs.org
Publication Date (Web): August 16, 2012 | doi: 10.1021/bk-2012-1105.pr001

Preface

These continue to be exciting times for the introduction of biobased chemicals. A number of commercial announcements involving biobased chemicals were made within the last year or so including the production of biobased propylene glycol by Archer Daniels Midland, the introduction of bio-isoprene by Danisco and their partnership with Goodyear followed closely by the announcement of the Amyris/Michelin partnership to incorporate bioisoprene into tires, the efforts of soft drink and food packaging companies, Coke, Pepsi and Heinz, to obtain a completely biobased polyethylene terephthalate. Other initiatives which were announced include several biobased plasticizers, biobased acrylic acid, succinic acid, adipic acid and new biobased polymers such as those from Avantium's YXY furanic building blocks, Novomer's CO_2-based polycarbonates and SyntheZyme's ω-hydroxyfatty acid building blocks. The list could go on and on. However, to be fair, last year also saw a large setback for this industry; the termination of the ADM/Metabolix JV to produce poly(hydroxyalkanoates).

Much of the creative invention in this area continues to occur in academia with considerable research in the area of biocatalysis, new biobased building blocks and methods of polymerization. In fact, a number of the new companies mentioned above were spin-offs of this research.

This ACS Symposium Series is the product of a symposium held at the 241st National Meeting of the American Chemical Society in Anaheim, CA on March 27-31, 2011. It includes chapters on new biobased building blocks such as the furandicarboxylic acid, polyesters and polyamides from adipic, succinic and sebacic acids with aliphatic diols such as 1,3-propylene glycol, 1,4-butanediol, 1,12-dodecylenediol and isosorbide. The conversion of hydroxymethylfurfural, the dehydration product of hexose sugars, to succinic acid and 1,4-butanediol to produce poly(butylene succinate) is described in one chapter. Also the synthesis of new polymers from plant-derived olefinic monomers such as tulipalin A and studies of composites from cotton by-products are featured in other chapters.

There is a strong emphasis on biocatalytic synthesis and polymerization within the book. Chapter topics include the synthesis of ω-hydroxyfatty acids and polymers therefrom, an interesting discussion on the structural differences of the products of the biocatalytic and chemical catalytic synthesis of polyesters from oleic diacid and glycerol and the ability to produce polylactic acid (PLA) and PLA-PHA copolyesters within a "microbial cell factory".

Other areas of interest explored in other chapters include recent developments of biobased polymer fibers and oleate-based pressure sensitive adhesives and composites. One chapter describes a large increase in cold-drawn fiber tensile strength by the blending of a small amount of ultrahigh molecular weight (MW)

In Biobased Monomers, Polymers, and Materials; Smith, P., et al.;
ACS Symposium Series; American Chemical Society: Washington, DC, 2012.

poly(3-hydroxybutyrate) with a much lower MW 3-hydroxybutyrate polymer. The addition of a rubber and inorganic fillers to normally brittle PLA was found to dramatically improve its ductility. Finally, there are several chapters on seed oil-based polyurethanes, one on fibers from soy proteins and composites from starch.

The contributions within this ACS Symposium Series are from leading researchers in the field and are drawn from a diverse subject matter. The diversity arises from the feedstocks and chemistries presented within the book and the fact that they originate from leading international researchers in industry, private research institutions, academics and National Labs. We hope you benefit as much from reading this text as we did from editing it.

Patrick B. Smith

Richard A. Gross

Downloaded by 217.66.152.26 on August 23, 2012 | http://pubs.acs.org
Publication Date (Web): August 16, 2012 | doi: 10.1021/bk-2012-1105.pr001

Downloaded by PENNSYLVANIA STATE UNIV on August 28, 2012 | http://pubs.acs.org
Publication Date (Web): August 16, 2012 | doi: 10.1021/bk-2012-1105.ot001

Editors' Biographies

Dr. Patrick B. Smith

Dr. Patrick B. Smith is a Research Scientist at MMI. He spent 32 years with The Dow Chemical Company, rising to the rank of Scientist prior to his retirement in 2007. His areas of research included the synthesis, structure/property relationships and applications of biobased materials, polymer characterization and NMR spectroscopy. He served with Cargill Dow Polymers which launched the Ingeo™ PLA line of products where he defined the processing conditions for PLA films, developed structure/property relationships for oriented films and a PLA service life model. After his retirement from Dow, he consulted with Archer Daniels Midland acting as ADM's R&D leader for their Telles joint venture with Metabolix that commercialized PHA. He also supported ADM's biobased propylene glycol product launch. He is an Adjunct Professor of Chemistry at Central Michigan University and a member of the American Chemical Society (2005 Midland Section Chair). He received the Midland Chapter Sigma Xi Award for the Outstanding Research Publication in 1987 and the Midland Chapter ACS Award for Outstanding Achievement and Promotion of the Chemical Sciences in 1998. He is also the recipient of Dow Analytical Science's V. A. Stenger Award in 1984 and the Dow Michigan R&D Scientists' Award in 1994. He has co-authored nearly 500 Dow technical reports, over 75 publications and 2 patents.

Richard A. Gross

Professor Richard A. Gross has a Ph.D. (1986) in organic/polymer chemistry from Polytechnic University (Brooklyn, New York) under the guidance of Mark Green. He was a Postdoctoral Fellow at the University of Massachusetts (Amherst) working with Robert Lenz, followed by appointment as Assistant Professor, Associate Professor, and full Professor at University of Massachusetts (Lowell) from 1988−1998. Since 1998 he has occupied the Herman F. Mark Chair Professorship at Polytechnic University (New York). His research is focused on developing biocatalytic routes to biobased materials including monomers, macromers, prepolymers, polymers, surfactants, and other biochemicals. He combines chemical methods with cell free and whole-cell biocatalytic systems to investigate biotransformations such as whole-cell routes to biosurfactants, ω-hydroxylation of fatty acids, protease-catalyzed transformations to polypeptides, and lipase-catalyzed routes to biomaterials. Recently he has been exploring using enzymes for surface modification and as "ink" for writing/patterning. He has over 400 publications in peer reviewed journals, been cited about 7000 times, edited 6 books and has granted and filed patents totaling

26. He currently runs a group of 30 consisting of 12 Ph.D. students, 4 postdoctoral fellows, 2 visiting students, 8 masters and 6 undergraduate students. Professor Gross was the recipient of the 2003 Presidential Green Chemistry Award in the academic category. In 2007, he was inducted into the American Institute for Medical and Biological Engineering. In 2010, he was selected as the Turner Alfrey Visiting Professor. He founded SyntheZyme LLC in 2009 and serves as Chief Technology officer. SyntheZyme was established to commercialize technologies developed in Gross's laboratory.

His other Professional activities and honors include: Director of Polymer Research Institute (at POLY), 2003−2006; Director – NSF Center for Biocatalysis and Bioprocessing of Macromolecules (at POLY), 2000−present; NSF Presidential Young Investigator Award, 1990−1995; Presidential Award in Green Chemistry, 2003; Founder and Co-Editor of the Journal of Environmental Polymer Degradation, 1993−1998; Co-founder (with D. Kaplan at Tufts Univ.) of the ACS journal Biomacromolecules, Co-Director of the NSF Biodegradable Polymer Research Center (at UMASS-Lowell), 1993−1998; Past President – U.S. Society on Biodegradable Polymers, 1999; Johnson and Johnson Focused Giving Award, 2000−2002; Editorial Board, Biomacromolecules (2000 to present); Editorial Board, J. Bioactive and Biocompatible Polymers (2001 to 2009); Editorial Board, Industrial Biotechnology (2005 to present); Editorial Board, Journal of Molecular Catalysis B: Enzymatic (2005 to present); Editorial Board Enzyme and Microbial Technology (EMT) (2005 to present); Editorial Board ACS Catalysis (Summer 2011 to present) Engineering Conferences Foundation, Board of Directors (2002−2005); Director: Biomedical Engineering Masters Program (2001−2008, POLY & SUNY Downstate).

Downloaded by PENNSYLVANIA STATE UNIV on August 28, 2012 | http://pubs.acs.org
Publication Date (Web): August 16, 2012 | doi: 10.1021/bk-2012-1105.ot001

Downloaded by 217.66.152.26 on August 23, 2012 | http://pubs.acs.org
Publication Date (Web): August 16, 2012 | doi: 10.1021/bk-2012-1105.ch001

Chapter 1

Furandicarboxylic Acid (FDCA), A Versatile Building Block for a Very Interesting Class of Polyesters

E. de Jong, M. A. Dam, L. Sipos, and G.-J. M. Gruter[*]

Avantium Chemicals BV, Zekeringstraat 29, 1014 BV Amsterdam,
The Netherlands
[*]E-mail: gert-jan.gruter@avantium.com

Avantium (www.avantium.com) is developing a next generation bioplastics based on 2,5-furandicarboxylic acid (FDCA), called "YXY building blocks", which can be produced on the basis of sugars and other, non-food, carbohydrates. Avantium aims to replace oil-based polyesters (such as PET) with Furanics polyesters (such as PEF) in a wide range of applications, including bottles and carpets. The excellent barrier properties, significant reductions in non renewable energy usage and green house gas emissions as well as the calculated cost price indicates that PEF can compete with traditional PET regarding price, performance as well as sustainability issues.

Introduction

Avantium has developed a novel catalytic process which is highly economic to convert carbohydrates into a new class of molecules, YXY building blocks, also known as Furanics. These molecules have been referred to as "Sleeping Giants" because of their enormous market potential, as evidenced by the research of DuPont and DSM in this area and its position in the US Department of Energy top 12 of high-potential biobased products (*1*, *2*). Furanics were never commercialized because they could not be produced in an economic way. Avantium has discovered the chemistry of a revolutionary catalytic process that enables the economic production of Furanics on the basis of a wide range of carbohydrates. The feedstocks that Avantium requires for the production

In Biobased Monomers, Polymers, and Materials; Smith, P., et al.;
ACS Symposium Series; American Chemical Society: Washington, DC, 2012.

of Furanics are carbohydrates that can originate from a variety of crops. The company's feedstock strategy is to have maximal flexibility in feedstock sourcing. Requirements for the feedstock are according to the SARA principle:

- **S**ustainable production
- **A**vailable at the production site
- **R**eliable logistics
- **A**ffordable

Initially Avantium will use carbohydrates that are commercially available today (first generation sugar & starch crops). However the process will be able to use future second and third generation, non-food feedstocks. YXY building blocks can be used to create green materials and fuels (*3*, *4*). The most versatile YXY building block for chemicals and polymer applications seems to be 2,5-furandicarboxylic acid (FDCA). This molecule (also known as dehydromucic- or pyromucic acid), a natural di-acid that is produced in the healthy human body at 3-5 mg quantities per day (*5*, *6*), was first prepared from mucic (galactaric) acid by Fittig and Heinzelmann in 1876 by reacting mucic acid with fuming hydrobromic acid under pressure (*7*). The first review by Henry Hill was already published in 1901 (*8*). Later routes often used 2,5-disubstituted furans such as hydroxymethyl furfural (HMF) as a starting material for FDCA. The literature was reviewed by Lewkowski (*9*) and Rosatella (*10*). Biological transformations (*11–13*) and routes using air oxidation with Co/Mn catalysts in acetic acid were reported recently (*14–16*). FDCA can be used for a range of applications, including green materials, chemicals and biopolymers. The materials market represents a multi-billion-euro market and includes plastics, plasticizers, thermosets and coatings. Relying on competitive price and performance, products based on YXY building blocks will target growth markets where new production capacity will be added and serve existing markets by retrofitting existing production assets from oil-based products to green YXY Building Blocks. Gandini and co-workers extensively reviewed the possibilities of furan-bearing moieties as polymer building blocks (*17*, *18*). In this paper we will discuss the use of FDCA as building block for polyesters.

Downloaded by 217.66.152.26 on August 23, 2012 | http://pubs.acs.org
Publication Date (Web): August 16, 2012 | doi: 10.1021/bk-2012-1105.ch001

Polyesters

Polyesters are a fast-growing group of plastic materials. The most important polyester is PET (polyethylene terephthalate) which is produced using purified terephthalic acid (PTA) and ethylene glycol (EG). Exchanging the EG building block in PET for another diol makes it possible to produce other types of polyesters, such as PBT (polybutylene terephthalate, a polyester based on PTA and 1,4-butanediol) and PPT (polypropylene terephthalate, a polyester based on PTA and 1,3-propanediol), each with its own specific properties, applications and volumes. The main raw material for PTA is *para*-xylene (PX) which is produced by oil refining. EG, the other building block for PET production, is produced on the basis of ethylene, made by oil cracking; EG is now also produced from bioethanol. Avantium aims to replace PTA in oil-based polyester (such as PET) with the YXY building block FDCA to obtain bio-based polyesters such as polyethylene 2,5-furandicarboxylate (PEF) in large applications such as bottles and carpets. When also using renewable EG a 100% renewable PEF can be produced. The market for virgin PET is currently around 50 million tons per year (source: CMAI). PET is well known for its application in packaging, in particular for soft drinks bottles and in fibers for textiles and carpets. PET's transparency, strength and recyclability make it a widely applied material.

FDCA-Based Polyesters

Only 5 years after the first patent application on PET by Calico Printers Association (*19*) Celanese Corporation of America filed a patent application in 1946 on the FDCA analog PEF (*20*). Under melt polymerization conditions FDCA dimethyl ester and 1.6 equivalents of EG were reacted in a transesterification step at ambient pressure between 160 and 220°C, after which the polycondensation was carried out between 190 and 220°C under 3 mm Hg pressure. The product had a reported melting point of 205-210°C and readily yielded filaments from the melt. No additional properties were reported for PEF or other FDCA based polyesters in this 1946 document. An Osaka University publication of 1958 (*21*) describes PEF with a melting point between 220 and 225°C, obtained using a lead catalyst. Also reported were the tri-, tetra-, penta- and hexamethylene diol polyester analogs with reported melting ranges of 115-120°C, 163-165°C, 70°C and 143-145°C, respectively. For the ethylene glycol and 1,4-butanediol polyesters, fiber forming properties were reported. The polymers made were reported to be brown to grayish white. In 1978, Moore (*22*) reported a polyester obtained in the melt from 1,6-hexane diol and dimethyl-2,5-furan dicarboxylate, using calcium acetate and antimony oxide as catalyst. The number average molecular weight was low (M_n less than 10,000), whereas the molecular weight distribution of the greenish product was relatively high (PDI = 2.5). In a patent application by Canon Kabushiki Kaisha (*23*) PEF, PPF (PolyPropylene Furandicarboxylate) and PBF (PolyButylene Furan-dicarboxylate) polymers were obtained by reacting FDCA in an initial step with a 3-fold excess of diol in the presence of a Sn/Ti catalyst. A second step which involved the polycondensation under vacuum was followed by a solid-state polymerization step (step 3) to increase the molecular weight. An (undesired) purification step between steps 2 and 3 (dissolution in hexafluoroisopropanol, precipitation and drying) is reported, probably because these recipes yield strongly colored polymer products. In 2007 Mitsubishi filed a patent application (*24*) describing a method for producing PEF and PBF by performing an ester exchange reaction of the dimethyl ester of FDCA with ethylene glycol or butanediol using a titanium tetrabutoxide / magnesium acetate mixed catalyst system. The PEF produced, showed excellent heat resistance and mechanical physical properties but the reaction time required to achieve a reasonably high molecular weight (reported as solution viscosities) was relatively long (7.5 hours). Gandini and co-workers also have recently published work on FDCA-based polyesters. They applied different polymerization techniques (solution, interfacial polycondensations and polytransesterification). The homopolymerization reactions for PEF and PPF were carried out in bulk using 1 g of bis(hydroxyalkyl)-2,5-furandicarboxylate

Downloaded by 217.66.152.26 on August 23, 2012 | http://pubs.acs.org
Publication Date (Web): August 16, 2012 | doi: 10.1021/bk-2012-1105.ch001

mixed with 1% (w/w) of the catalyst Sb_2O_3. The mixture was heated up to 240–250 °C. They achieved Mn's of 22400 and 21600 and PDI's of 1.99 and 1.28 respectively for PEF and PPF (*25*).

From the above references, it is clear that PEF has been known for more than 70 years and that many different recipes have been used in which temperatures, pressures, diacid/diol stoichiometries, catalysts and precursors (di-acid or di-ester) have been varied. However, a detailed analysis of the polymers formed has never been reported mainly because of the difficulties to produce sufficient amounts of high purity FDCA(dimethylester). The development and up-scaling of Avantium's YXY building blocks technology now makes this possible.

Materials and Methods

Materials

2,5-Furandicarboxylic acid (FDCA) was prepared according to reference (*15*) or purchased from Exclusive Chemistry Ltd. FDCA dimethyl ester was prepared according to reference (*16*). Diols, solvents and catalysts were supplied by Aldrich and used as received.

Analytical Techniques

GPC measurements were performed on a Merck-Hitachi LaChrom HPLC system equipped with two PL gel 5 µm MIXED-C (300x7.5 mm) columns. Chloroform : 2-chlorophenol 6:4 solvent mixture was used as eluent. Calculation of the molecular weight was based on polystyrene standards and carried out by CirrusTM PL DataStream software. UV-visible spectra and absorbances were recorded on a Helios α (ThermoSpectronic) spectrophotometer.

Polycondensation Setup

Small scale polycondensation reactions were carried out in a high-throughput film reactor (*3*). 184 mg (1 mmol) dimethyl 2,5-furan dicarboxylate (dmFDCA), 186 mg (3.0 mmol) ethylene glycol, 1.6 µmol titanium(IV) isopropoxide in 20 µL 0.08 M toluene solution and a magnetic stir bar were placed in each of 9 vials. Other diols were applied at the same molar ratio. The air in the vials was replaced by nitrogen and then they were placed in the reactor block at 190°C. Transesterification was carried out for 1 hour at 160°C, for 1 hour at 170°C, and 2 hours at 180°C. At this stage, dmFDCA conversion was higher than 99% measured by ^{1}H-NMR spectroscopy. Then vacuum was gradually applied and temperature raised to 230°C. The pressure went down below 1 mbar within 2 minutes and then it slowly stabilized at ~0.4 mbar. After 2 hours polycondensation the vacuum was released by nitrogen and the vials were taken out and cooled down.

Downloaded by 217.66.152.26 on August 23, 2012 | http://pubs.acs.org
Publication Date (Web): August 16, 2012 | doi: 10.1021/bk-2012-1105.ch001

Downloaded by 217.66.152.26 on August 23, 2012 | http://pubs.acs.org
Publication Date (Web): August 16, 2012 | doi: 10.1021/bk-2012-1105.ch001

Polymer Analyses and Subsequent Workup

Polymers were weighed and the polymer dissolved in 5 mL dichloromethane:hexafluoro-2-propanol 8:2 solvent mixture. After complete dissolution, part of the material was diluted to 5 mg/mL concentration for absorbance measurements. For GPC, 200 µL stock solution was taken, the solvent evaporated and the polymer dissolved again in 1.0 mL chloroform:2-chlorophenol 6:4 solvent mixture.

Scale Up of Polyester Production

Avantium has recently has started up a sequence of pilot plants at the Chemelot site (Geleen, the Netherlands) to proof the process and the products. Part of this pilot plant set-up is a Tamar polyester pilot plant which was a purpose built rig for producing PET and will be used to produce a wide range of furan-based polyesters. The unit has been designed to mimic large-scale batch PET production, making it an ideal piece of equipment to test our new products, optimize catalysts compositions as well as additives formulations on a small scale. The pilot rig is capable of running under either pressure or vacuum for direct esterification and polycondensation respectively.

Bottle Application Testing

Standard 20 oz straight wall carbonated soft drink (CSD) pre-forms of PEF were made using an Arburg 320M injection molding machine equipped with a unit cavity pre-form tool. These PEF pre-forms were then blow molded using an Sidel SBO1/2 blow molding machine equipped with standard straight wall CSD bottle molds. In the same campaign standard PET control bottles were prepared as reference. Whole bottles were subjected to water loss testing at 23°C and 50% relative humidity (RH). Sidewalls of the bottles obtained were subjected to permeation testing for O_2, and CO_2 at 23°C/50% RH using MOCON Permatran (CO_2) and MOCON Oxtran O_2 methods.

Results and Discussion

The furan precursors which are produced in the Avantium process are a source of a variety of monomers (YXY building blocks) with very different chemical properties. Avantium has focused on FDCA as a building block for materials and application development. This translates into an array of polymers (e.g. polyesters, polyamides, polyurethanes, thermoset resins) covering a broad spectrum of macromolecular materials, potentially capable of replacing a wide range polymer commodities applications, currently predominantly derived from fossil resources. Avantium has put a lot of effort in polymerization research and application development of polyesters. When we compare PEF and PET production there are some distinctions. Whereas PET is typically made with catalysts such as manganese, cobalt and germanium, it was found that these catalysts result in a strongly colored PEF product. Likewise, whereas bright-white

PET can be made directly from PTA and EG, the use of FDCA as monomer inevitably results in a colored product. According to Drewitt and Lincoln (*20*) this is due to decarboxylation of FDCA under the reaction conditions. To prove this concept we added known amounts of FDCA to an FDCA dimethylester – 1,4-butanediol polymerisation set-up.

As can be seen from Figure 1 there is a clear relation between the amount of FDCA and the amount of color formed. Therefore, we concluded that the preferred starting material for furan based polycondensation reactions is the 2,5-furandicarboxylate dimethyl ester.

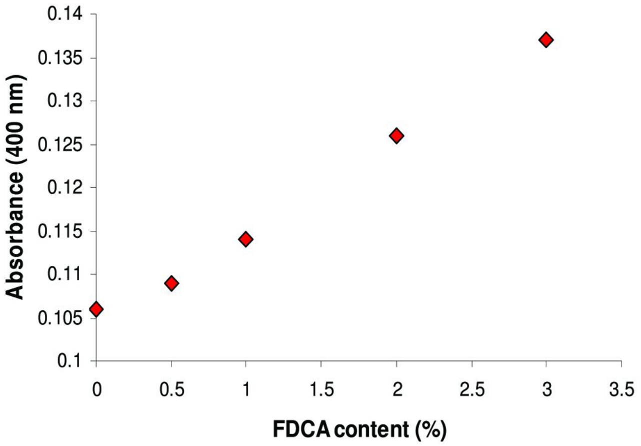

Figure 1. Production of polybutyleneterephthalate (PBF) starting from dmFDCA and 1,4-butanediol with varying concentrations of FDCA. The conditions were: Transesterification and polycondensation temperature was 220 °C, time of transesterification was 20 min, time of polycondensation was 5 hours.

Table 1. Transesterification and polycondensation of PEF starting with dmFDCA and FDCA. Transesterification was done at 190 °C (dmFDCA) and 210 °C (FDCA), polycondensation was at 240 °C. Transesterifaction durations also differed with dmFDCA (2.5 hrs) and FDCA (5 hrs)

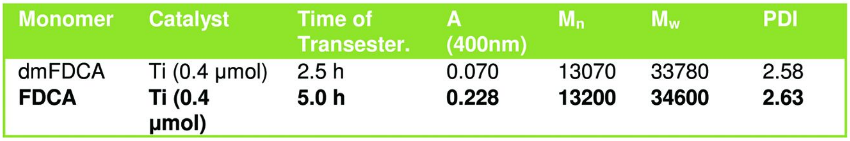

Monomer	Catalyst	Time of Transester.	A (400nm)	M_n	M_w	PDI
dmFDCA	Ti (0.4 µmol)	2.5 h	0.070	13070	33780	2.58
FDCA	**Ti (0.4 µmol)**	**5.0 h**	**0.228**	**13200**	**34600**	**2.63**

In Table 1 the relation between color formation between starting material (FDCA versus FDCA dimethylester) are shown at furthermore similar PEF compositions.

Downloaded by 217.66.152.26 on August 23, 2012 | http://pubs.acs.org
Publication Date (Web): August 16, 2012 | doi: 10.1021/bk-2012-1105.ch001

Downloaded by 217.66.152.26 on August 23, 2012 | http://pubs.acs.org
Publication Date (Web): August 16, 2012 | doi: 10.1021/bk-2012-1105.ch001

The Avantium process (see scheme below) for preparing a polyester comprises a first step *(ii)* wherein dmFDCA is transesterified with ethylene glycol in the presence of a tin(IV) based transesterification catalyst. Transesterfication of the dmFDCA with a diol results in the formation of methanol that is quickly removed by evaporization. This is followed in a second step *(iii)* by a polycondensation reaction, at pressures below 1 mbar, and under melt conditions until a polymer is obtained having a number average molecular weight of at least 10,000. To achieve the desired molecular weights for the selected applications (e.g. fibers, films, bottles) the polymer is subjected to a subsequent Solid-State Polymerization step (SSP, *iv*).

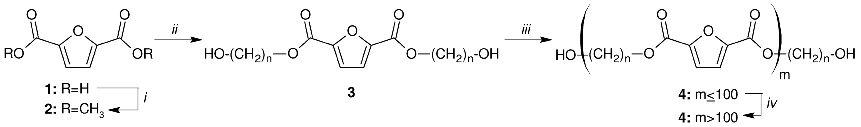

In addition to ethylene glycol a wide range of other diols can be used to prepare polyesters including 1,3-propanediol, 2,2-dimethyl-1,3-propanediol, 1,4-butanediol, 1,6-hexanediol and 1,4-bis(hydroxymethyl) cyclohexane. Some typical properties which can be achieved with these diols are given in Table 2.

Table 2. Some typical characteristics of polyesters made from FDCA and several diols. Numbers are given for molecular weight (M_w); polydispersity index (PDI); glass transition temperature (T_g); starting point of decomposition (T_{start}); inflection point of the TG curve (T_{inf}); and crystallization temperature (T_{cryst})

Diol	M_n	T_g (°C)	T_m (°C)	T_{cryst} (°C)		TG
					T_{st}(°C)	T_{inf}(°C)
Ethylene glycol	18500	86.2	211.4	160.3	312	394
After SSP	50900	88.0	230.6			
1,3-Propanediol	23000	51.4	171.9	140.0	312	392
After SSP	40000	56.2	183.3			
2,2-Dimethyl-1,3-propanediol	15800	67.5	199.6	143.3	294	408
1,4-Butanediol	23500	44.5	171.5	115.3	286	388
Cis-2-Butene-1,4-diol	4000	47.8	164.3	113.0	264	330, 341
1,6-Hexanediol	23500	9.0	144.5	116.3	292	390
After SSP	14000	23.3	126.7	78.4	278	354
1,4-Bis(hydroxyl-methyl) cyclohexane(cis-trans 3-7)	14400		271	229	319	396

Moreover, whereas PET is typically made by polycondensation at polymerization temperatures of 250-280°C and higher, again it was found that the polymers based on FDCA made at such high polymerization temperatures had a high degree of colorization. If the absorbance of a 5 mg/mL solution of the polymer in dichlomethane : hexafluoroisopropanol 8:2 is 0.05 or greater, then the product is deemed inferior.

Solid State Polymerisation

Solid state polymerisation (SSP) is a common process used in the preparation of PET with high molecular weights. In SSP processes pellets, granules, chips or flakes of polymer are subjected for a certain amount of time to elevated temperatures (below the melting point) in a hopper, a tumbling drier or a vertical tube reactor. It was found that with tin(IV)/tin(ll) catalyst system higher molecular weight can be reached than with titanium catalysts. It is also found that dmFDCA is more reactive than dimethylterephthalate, which makes it possible to perform the polymerization reactions at a lower reaction temperature and at a shorter reaction time. The principle of analyzing the effectiveness of SSP is shown in Figure 2. This example shows the evolution of the free carboxylic acid groups (COOH), the methyl groups and the hydroxyl groups in a sample with a high methyl ester content (low starting M_n) during SSP (see scheme below).

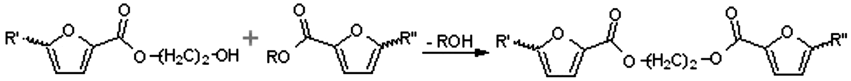

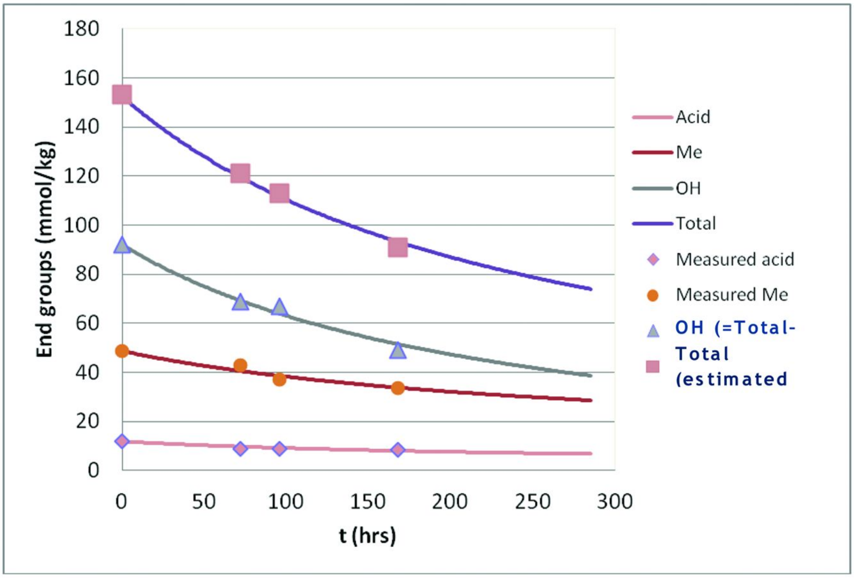

Figure 2. Reduction of the free end groups in a PEF sample with high initial Me ester content and low M_n during SSP according to known procedures for PET (26, 27).

Downloaded by 217.66.152.26 on August 23, 2012 | http://pubs.acs.org
Publication Date (Web): August 16, 2012 | doi: 10.1021/bk-2012-1105.ch001

Downloaded by 217.66.152.26 on August 23, 2012 | http://pubs.acs.org
Publication Date (Web): August 16, 2012 | doi: 10.1021/bk-2012-1105.ch001

Characteristics of Furan-Based Polyesters

PET is the most widely used polyester and is made of purified Terephthalic acid (PTA) and ethylene glycol (EG). Because of sustainability reasons there is currently a lot of interest to make PET more Biobased. In 2010 the Coca Cola company launched the plantbottle, a PET bottle with biobased EG and oil-based PTA (ref). There are also initiatives to replace the PTA part by Biobased PTA but economics and sustainability aspects are still unclear. Avantium pursues a different approach by replacing PTA with FDCA. Together with biobased EG the resulting PEF will be 100% green. For PEF bottles to become a success three key questions compared to oil-based products have to be answered:

- Can PEF compete on performance?
- Can PEF compete on price?
- Can PEF deliver a significantly better environmental footprint?

Recently the first successful bottles were blown. The bottles were not yet made at optimal conditions because the material wanted to stretch further than the mold allowed. Comparing the properties of the newly synthesized PEF relative to PET the following characteristics are observed: The glass transition temperature (Tg) of PEF is higher while the melting temperature (Tm) is lower and PEF has a higher Heat deflection temperature (HDT) than PET.

Table 3. The density (Kg/m^3) of PEF and PET related to the crystallinity of the polyester. PET data are from McGonigle et al (*28*), 100% crystalline PEF data is from Karazyan et al. (*29*)

Material	Crystallinity	
	0%	**100%**
PEF	1428	1565
PET	1335	1453

PEF has higher tensile strength but hardly any elongation to break. This elongation is much lower than with PET. The rate of Quiescent Crystallization is lower than with PET, interestingly preform crystallization is not observed in the required heating window. Drawing & strain hardening/SIC of PEF is similar with PET. PEF does have a higher density than PET both at low and high crystallinity (Table 3), while haze and hydrolysis rates are similar. One of the most important characteristics of polyester bottles are their barrier properties. The oriented PEF bottles have barrier properties for both H_2O (Figure 3) and CO_2 more than 2 times better while the barrier properties for O_2 is even more than 6 times better (Table 4).

In Biobased Monomers, Polymers, and Materials; Smith, P., et al.;
ACS Symposium Series; American Chemical Society: Washington, DC, 2012.

Table 4. CO_2 and O_2 permeation of PET and PEF polyesters (cc*ml/(100 inch^2*day) measured at 23°C and 50% relative humidity

Gas	Method	PEF	PET
CO_2	MOCON Permatran	4.449	10.154
O_2	MOCON Oxtran	0.095	0.891

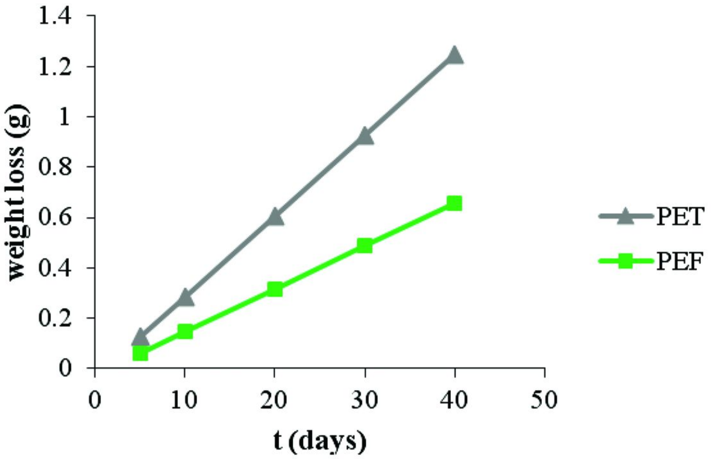

Figure 3. Water loss (grams/day) from PEF bottle at 23°C and 50% Relative Humidity.

Downloaded by 217.66.152.26 on August 23, 2012 | http://pubs.acs.org
Publication Date (Web): August 16, 2012 | doi: 10.1021/bk-2012-1105.ch001

Recycling

Recycling of PET becomes more and more important so to become competitive also the recyclability of PEF should be excellent. Three aspects regarding recycling of PEF needs to be taken into consideration; e.g. reprocessing, depolymerization into starting monomers and potential issues if PEF enters the PET recycling stream. It was successfully shown that mechanical recycling (re-extrusion of polymer after drying) was possible as well as chemical recycling to monomers via hydrolysis, methanolysis and glycolysis. Another important aspect is impact of PET and PEF recycle streams getting mixed. To simulate this mixtures of PET and PEF were injection molded into standard tensile bars using a labscale twin screw extruder and the bars obtained were subjected to analyses (DSC, haze, IZOD notched impact, and tensile). Test results reveal that up to 5% (*w/w*) PEF has no significant effect on the mechanical and physical properties of PET such as haze and impact. Tensile test show that there is no negative influence of small additions of PEF to a PET stream (Figure 4).

Economical Performance

An evaluation of economical performance requires comparison of the cost price of FDCA and PTA. PTA is an oil-based chemical, produced at 50 million tons per year with a current price of 1100 Euro per ton. The main price drivers for PTA are the oil-price and supply/demand. In comparison, FDCA is a bio-based material and we believe that due to superior performance, as shown in this paper, the potential market size of FDCA can exceed 50 million tons per year. The main price drivers for bio-based FDCA are the feedstock-price and economy of scale. However, at >300kT/y scale we believe that the price of FDCA will be < € 1000 per ton, and therefore competitive with PTA produced at the same scale.

Downloaded by 217.66.152.26 on August 23, 2012 | http://pubs.acs.org
Publication Date (Web): August 16, 2012 | doi: 10.1021/bk-2012-1105.ch001

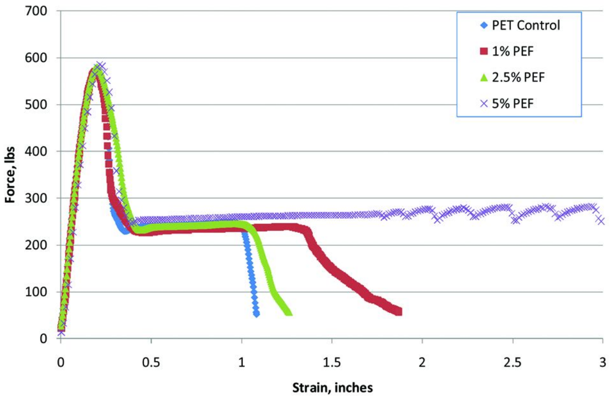

Figure 4. Tensile tests of PET bars containing different amounts of PEF (2 inch/minute strain rate).

Energy and GHG Balance of PEF Production

The production of PEF can reduce the non-renewable energy usage (NREU) approximately 40% to 50% while green house gas (GHG) emissions can be reduced approximately 45% to 55%, compared to PET (using PlasticsEurope's revised dataset of 2010) for the system cradle to grave. These reductions are higher than for other biobased plastics, such as poly lactic acid (PLA) or polyethylene (*30*). More reductions are expected. For instance the use of biobased ethylene glycol substantially improves reductions of NREU and GHG emissions. Furthermore, Avantium continues to improve feedstock and process performance.

Conclusions

Avantium Chemicals BV has developed an attractive route for the conversion of biomass to FDCA. This material can be used to produce PEF, a bio-based alternative to PET. Results so far indicate that PEF can compete with PET on both price and performance, and with a significantly better environmental footprint.

Acknowledgments

The authors would like to thank NatureWorks LLC for the efforts and valuable input during our collaboration on bottle application testing. Also Plastic Technologies, Inc. (PTI) is kindly acknowledged for the execution of the bottle trials.

Downloaded by 217.66.152.26 on August 23, 2012 | http://pubs.acs.org
Publication Date (Web): August 16, 2012 | doi: 10.1021/bk-2012-1105.ch001

References

1. Werpy, T.; Peterson, G. *Top Added chemicals from biomass*. U.S. Department of Energy, 2004, URL www.eere.energy.gov/biomass/pdfs/35523.pdf
2. Bozell, J. J.; Petersen, G. R. *Green Chem.* **2010**, *12*, 539–554.
3. Gruter, G-J. M.; Sipos, L.; Dam, M. A. *Comb. Chem. High Throughput Screening* **2012**, *15*, 180–188.
4. De Jong, E.; Vijlbrief, T.; Hijkoop, R.; Gruter, G-J. M.; van der Waal, J. C. *Biomass Bioenergy* **2012**, *36*, 151–159.
5. Witten, T. A.; Levine, S. P.; King, J. O.; Markey, S. P. *Clin. Chem.* **1973**, *19*, 586–589.
6. Witten, T. A.; Levine, S. P.; Killan, M. T.; Boyle, P. J. R.; Markey, S. P. *Clin. Chem.* **1973**, *19*, 963–966.
7. Fittig, R.; Heinzelmann, H. *Chem. Ber.* **1876**, *9*, 1198.
8. Hill, H. B. *Am. Chem. J.* **1901**, *25*, 439.
9. Lewkowski, J. *ARKIVOC* **2001** (i), 17–54.
10. Rosatella, A. A.; Simeonov, S. P.; Frade, R. F. M.; Afonso, C. A. M. *Green Chem.* **2011**, *13*, 754–793.
11. Hanke, P. D. Patent WO2009/023174, published February 19, 2009.
12. Koopman, F.; Wierckx, N.; de Winde, J. H.; Ruijssenaars, H. J. *Bioresour. Technol.* **2010**, *101*, 6291–6296.
13. Koopman, F.; Wierckx, N.; de Winde, J. H.; Ruijssenaars, H. J. PCT patent WO2011/026913A1, published March 10, 2011.
14. Sanborn, A. PCT patent application WO2010/132740, published November 18, 2010.
15. Muñoz de Diego, C.; Schammel, W. P.; Dam, M. A.; Gruter, G-J. M. PCT patent application WO2011/043660, published April 14, 2011.
16. Muñoz de Diego, C.; Schammel, W. P.; Dam, M. A.; Gruter, G-J. M. PCT patent application WO2011/043661, published April 14, 2011.
17. Gandini, A.; Belgacem, M. N. *Prog. Polym. Sci.* **1997**, *22*, 1203–1379.
18. Gandini, A. *Green Chem.* **2011**, *13*, 1061–1083.
19. Whinfield, J. R.; Dickson, J. T. Br. patent, 578079, filed July 29, 1941.
20. Drewitt, J. G. N.; Lincoln, J. Br. patent, 621971, filed November 12, 1946.

21. Hachihama, Y.; Shono, T.; Hyono, K. *Technol. Rep. Osaka Univ.* **1958**, *8*, 475–480.
22. Moore, J. A.; Kelly, J. E. *Macromolecules* **1978**, *11*, 568–573.
23. Matsuda, K.; Matsuhisa, H.; Horie, H.; Komuro, T. PCT patent application WO2007/052847, filed November 7, 2005.
24. Kato, S.; Kasai, A. Japanese patent application JP2008/291244, filed April 24, 2007.
25. Gomes, M.; Gandini, A.; Silvestre, A. J. D.; Reis, B. *J. Polym. Sci., Part A: Polym. Chem.* **2011**, *49*, 3759–3768.
26. Duh, B. *J. Appl. Polym. Sci.* **2001**, *81*, 1748–1761.
27. Duh, B. *J. Appl. Polym. Sci.* **2002**, *83*, 1288–1304.
28. Kazaryan, L. G.; Medvedeva, F. M. *Vysokomol. Soedin., Ser. B* **1968**, *10*, 305–306.
29. McGonigle, E-A.; Liggat, J. J.; Pethrick, R. A.; Jenkins, S. D.; Daly, J. H.; Hayward, D. *Polymer* **2001**, *42*, 2413–2426.
30. Eerhart, A. J. J. E., Faaij, A. P. C.; Patel, M. K. *Energy Environ. Sci.* 2012, DOI: 10.1039/c2ee02480b.

Downloaded by 217.66.152.26 on August 23, 2012 | http://pubs.acs.org
Publication Date (Web): August 16, 2012 | doi: 10.1021/bk-2012-1105.ch001

Downloaded by COLUMBIA UNIV on August 28, 2012 | http://pubs.acs.org
Publication Date (Web): August 16, 2012 | doi: 10.1021/bk-2012-1105.ch002

Chapter 2

Biobased Pressure-Sensitive Adhesive Derived from Epoxidized and Dihydroxylated Oleate with Phosphoric Acid and Its Chemical Pathways

B. Kollbe Ahn,[1] Stefan Kraft,[2,3] and X. Susan Sun*,[1]

[1]Bio-Materials & Technology Lab, Department of Grain Science & Industry, Kansas State University, Manhattan, KS 66506
[2]Department of Chemistry, Kansas State University, Manhattan, KS 66506
[3]Current adress: 7840 Sunset Ln, Indianapolis, IN 46260
***E-mail: xss@ksu.edu**

Biobased pressure-sesitive adhesives (PSA) were derived from epoxidzed and dihyroxylated soybean oils in the presence of phosphoric acid at ambient temperature. The PSA showed similar peel strength as selected commercial PSAs. The polymerization pathways of the plant oil-based PSA were investigated through model reactions involving epoxides and diols derived from methyl oleate whose conversions could be conveniently monitored by one- and two-dimensional nuclear magnetic resonance (NMR) techniques as well as mass spectroscopy. In this model system, we elucidated two key functions phosphoric acid played: a) acting as a general acid catalyst activating the epoxide toward nucleophilic attack by the diol, thus generating an ether (C-O-C) cross linkage; b) as a reaction partner establishing phosphate ester linkages [(RO)2(O)P-O-C, R = C or H]. The formation of phosphate esters occurred exclusively from H_3PO_4 and epoxide without any incorporation of diol. In contrast, using an excess of isopropanol as the alcoholic component the product distribution could be biased toward ether formation at the expense of

In Biobased Monomers, Polymers, and Materials; Smith, P., et al.;
ACS Symposium Series; American Chemical Society: Washington, DC, 2012.

phosphate ester formation. The role of alcohols as initiators in polyether formations was confirmed by cleanly incorporating one mono-^{18}O labeled diol moiety into polyethers as confirmed by electrospray ionization mass spectrometry (ESI-MS).

Introduction

Obtaining affordable and durable green materials from renewable natural resources is a grand challenge of our time (*1–3*). Plant oil is one of the most inexpensive and readily available feedstocks for biodegradable polymeric materials (*4*, *5*). Soybean is currently the main source of vegetable oil suitable for industrial applications, which include the production of soap, lubricants, coating, paints, and more recently, bioplastics and composite materials (*6*, *7*). The large variety of available tapes (i.e., Scotch tapes, Duck tapes, Post-it) underlines the huge market need for pressure sensitive adhesive (PSA) resins, which are currently derived from petroleum feedstocks.

Triglycerides from plant oils, such as soybean oil, have become attractive feedstocks for chemical functionalizations at the site of their internal alkene-moieties. To create a rigid scaffold with adhesive properties that has potential for PSA applications, the introduced functional groups have to serve a twofold role: establishing polymeric networks and providing polar functional groups (Figure 1). Double bonds of the fatty acid can be functionalized in relatively straightforward way by means of halogenations and oxygenations (*8*), and the resultant functional groups may then provide entries into cross-linking reactions. Typical examples of functionalizations that are geared toward cross-link applications are hydroxylations, epoxidations, acrylation, and maleimide moieties (*7*, *9*). Epoxidation chemistry stands out as it is inexpensive and can be accomplished in up to 98% yield from internal double bonds (*10–12*). Epoxidized triglycerides or fatty esters have been used as plasticizers and stabilizers for polyvinyl chloride (PVC) or as co-reactants for epoxy resins (*13*, *14*). Recently, epoxidized plant oils were cross-linked with inorganic materials to obtain organic-inorganic hybrid materials (*2*, *11*, *12*, *15*, *16*). Furthermore, various cationic polymerizations and radical reactions of epoxidized triglycerides or epoxidized methyl oleate have occurred by photo-initiation (*1*), latent catalysts (*3*), or strong acid catalysts ($HSbF_6$) (*6*, *9*, *15*, *16*). These reactions often require the application of heat. Recently, hydrogels derived from epoxidized soybean oil in the presence of a Lewis acid (BF_3) (*17*) and coatings generated via addition of phosphoric acid (*18*) were delivered using epoxidized soybean oils (ESO); however, chemical scaffolds and reaction pathways of this biobased material were still veiled, and chemical mechanism and structural studies have been required to meet industry needs. Here we investigated polymerization pathways of ESO in the presence of acidic catalysts and identified phosphoric acid as an effective promoter that has relatively low acidity, is inexpensive, and provides reproducible results under moderate conditions.

Downloaded by COLUMBIA UNIV on August 28, 2012 | http://pubs.acs.org
Publication Date (Web): August 16, 2012 | doi: 10.1021/bk-2012-1105.ch002

Downloaded by COLUMBIA UNIV on August 28, 2012 | http://pubs.acs.org
Publication Date (Web): August 16, 2012 | doi: 10.1021/bk-2012-1105.ch002

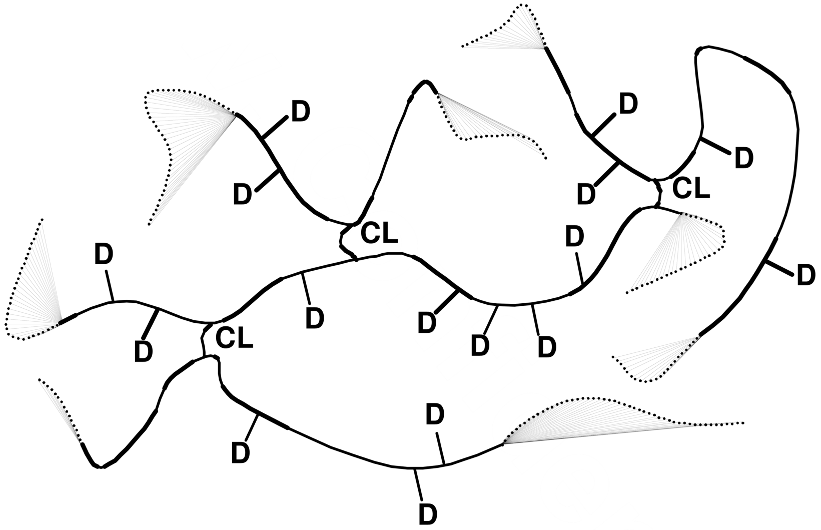

Figure 1. Schematic representation of an pressure sensitive adhesive polymer derived from soybean oil (CL = cross-link; D = Hydrogen Bond Donor.

Several trials have been conducted to develop PSAs from fuctionalized plant oils, but the resultant products had limited potential to reduce the amount of petrochemicals used to produce PSAs (*19*). In this chapter, we summarized the design, synthesis, and characterization of novel soybean oil-based PSAs. The polymerization pathways of the PSA were also eluciated by using a model compound of methyl oleate.

Results and Discussion

The first step toward designing adhesives is to understand the chemistry underlying the formation of cross-links between ESO (**1**) and HSO (**2**), particularly if and to what extent the formation of ethers and/or organic phosphates plays a role in the polymerization process (Figure 1).

In principle, two chemical motifs could result from the interaction of ESO with phosphoric acid. In pathway a (Scheme 1), phosphate esters could form as recently suggested by Guo on the basis of IR-data (*21*). The formation of 2-hydroxyphosphates from epoxides and phosphoric acid that would have to occur as the initial step is well documented (*22*) and has been extensively exploited in material science (*23*, *24*). An alternative pathway b would establish ether networks from the acid-catalyzed reaction of epoxides with nucleophilic alcohols (*25*, *26*) that may have formed from epoxide hydrolysis (Scheme 1). Acid-catalyzed epoxide polymerizations with alcohols (to form polyethers) have been found to go through an activated monomer mechanism (AM) with alcohols

Downloaded by COLUMBIA UNIV on August 28, 2012 | http://pubs.acs.org
Publication Date (Web): August 16, 2012 | doi: 10.1021/bk-2012-1105.ch002

acting as polymerization initiators (*27*, *28*). If pathway b contributes to the overall polymeric network at least in part, deliberate addition of polyols to the reaction mixture would amplify initiation efficiency during polymerization. This would allow for the control of molecular weight at a level suitable for generation of PSAs.

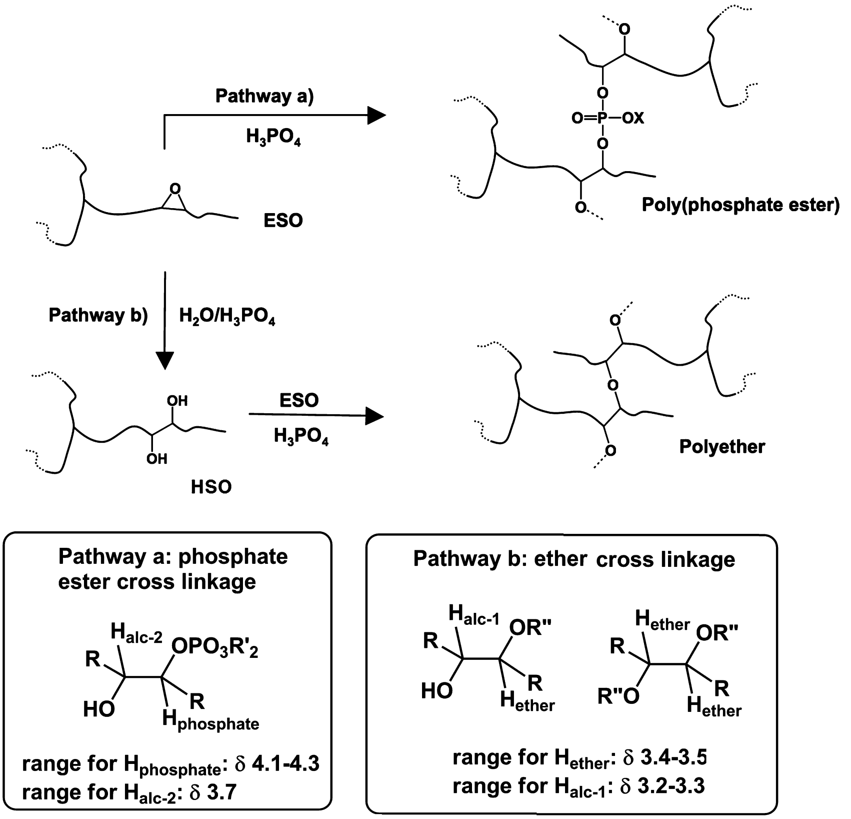
Pathway a)
H_3PO_4
ESO
O=P—OX
Poly(phosphate ester)
Pathway b)
H_2O/H_3PO_4
OH
OH
HSO
ESO
H_3PO_4
Polyether
Pathway a: phosphate ester cross linkage
H_{alc-2}
$OPO_3R'_2$
R
HO
R
$H_{phosphate}$
range for $H_{phosphate}$: δ 4.1-4.3
range for H_{alc-2}: δ 3.7
Pathway b: ether cross linkage
H_{alc-1}
OR"
R
HO
R
H_{ether}
H_{ether}
OR"
R
R"O
R
H_{ether}
range for H_{ether}: δ 3.4-3.5
range for H_{alc-1}: δ 3.2-3.3

Scheme 1. Proposed chemical pathway a and b in ***Polymer-1-2-P*** *formed from epoxidized soybean oil (**1**) and hydroxylated soybean oil (**2**) in the presence of* H_3PO_4*. (Reproduced with permission from ref. (20). Copyright 2011 Royal Society of Chemistry)*

We embarked on mechanistic investigations that would shed light on the establishment of chemical connections in the cross-links. To reduce analytical complexities, we substituted soybean oil for the single-chain platform methyl oleate (**3**) (Scheme 2) and epoxydation with meta-chlorobenzoic acid (mCPBA) (**4**), and subsequent epoxide hydrolysis generated **5** and **6** that would serve as surrogates for **1** and **2**.

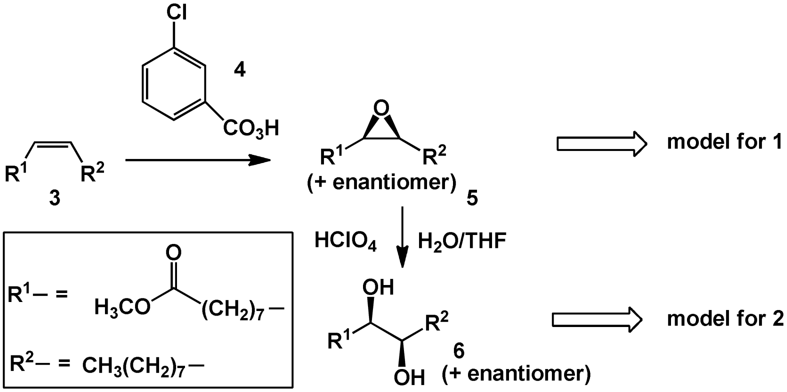

*Scheme 2. Model systems **5** and **6** forming **Polymer-5-6-P***

The chemistry was confirmed by using one- and two-dimensional NMR studies (Figure 2) with a model system using epoxidized methyl oleate (EMO) to avoid the influence of the complexity of multiple functional moieties in triglycerides. NMR spectra indicated the EMO polymer from EMO/H_3PO_4 is consisted of hydroxyl polar sites (doublet signal at δ 3.38) which provide tackiness and cross-linkages of ether (signal at δ 3.55 and δ 3.5 coupled with respectively vicinity alcohol signal at δ 3.3 and δ 3.2) and phosphate ester (signal at δ 4.1-4.3 coupled with vicinity alcohol signal at δ 3.6) (Figure 2).

Downloaded by COLUMBIA UNIV on August 28, 2012 | http://pubs.acs.org
Publication Date (Web): August 16, 2012 | doi: 10.1021/bk-2012-1105.ch002

Downloaded by COLUMBIA UNIV on August 28, 2012 | http://pubs.acs.org
Publication Date (Web): August 16, 2012 | doi: 10.1021/bk-2012-1105.ch002

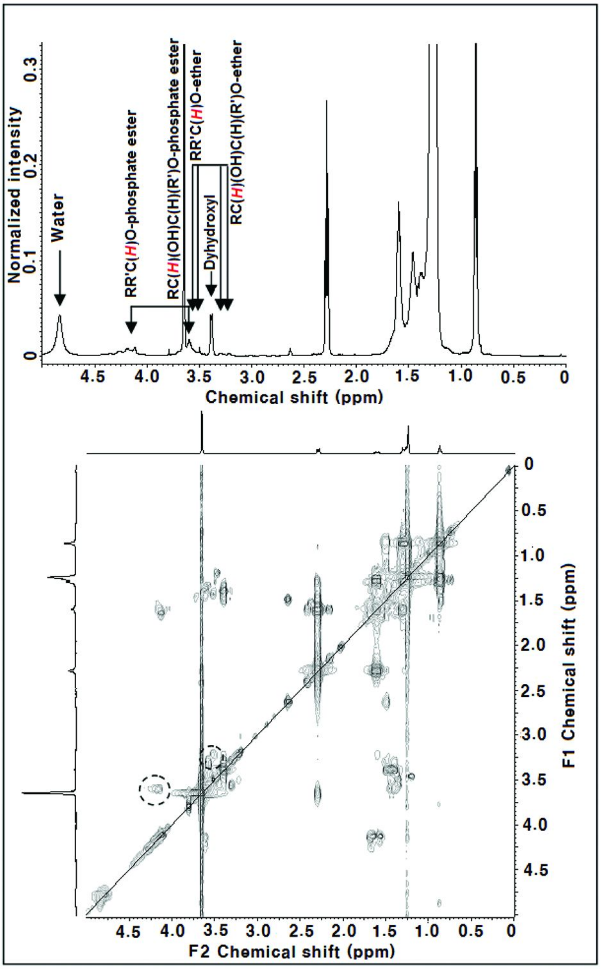

Figure 2. ^1H NMR (top) and $^1H\_^1H$ COSY NMR (bottom) of EMO polymer (EMO/H_3PO_4). (Reproduced with permission from ref. (29). Copyright 2011 American Chemical Society).

Tracking the progression of product development (Figure 3) revealed a near-constant ratio of total ether integral to total phosphate ester integral. We also found that diol **6** increased in concentration over time. Two possible routes (Pathways a and b, Scheme 1) could explain the formation of (poly) ethers under the reaction conditions. Mixtures **5**, **6**, and H_3PO_4 produced **Polymer-5-6-P**, which contained phosphate esters, polyethers, and diols. Based on the chemical pathways, we proposed a chemical scaffold using ESO as the starting material. ESO was polymerized in the presence of phosphate acid to form a copolymeric matrix consisting of phosphoric ester and ether cross-linkages; DSO synthesized from the ESO was added to ESO at a designed ratio to improve tackiness, thus, providing more hydroxyl moieties (Figure 4).

Downloaded by COLUMBIA UNIV on August 28, 2012 | http://pubs.acs.org
Publication Date (Web): August 16, 2012 | doi: 10.1021/bk-2012-1105.ch002

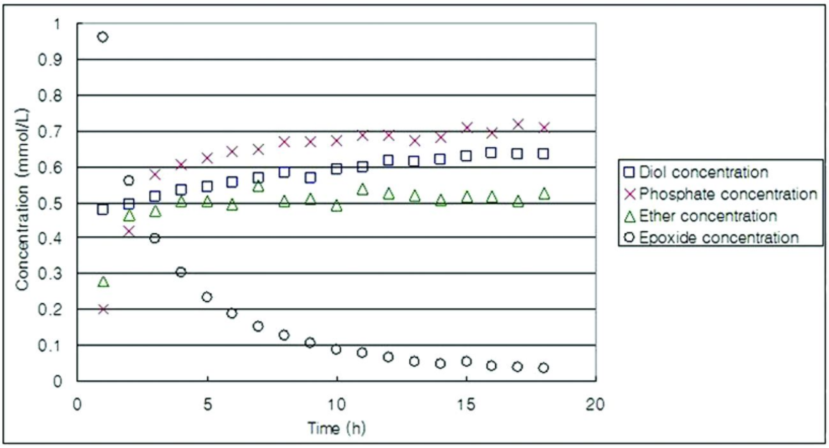

*Figure 3. Concentrations of epoxides, phosphate esters, ethers, and dihydroxide 6 in **Polymer-5-6-P** from NMR integration using a methyl group (δ 0.88) as a quantitative internal standard. ((Reproduced with permission from ref. (20). Copyright 2011 Royal Society of Chemistry).*

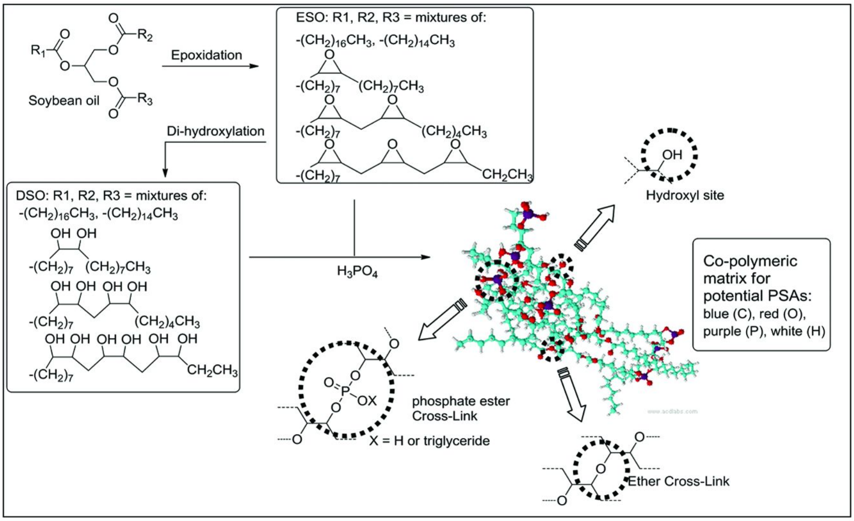
Soybean oil
Epoxidation
ESO: R1, R2, R3 = mixtures of:
Di-hydroxylation
DSO: R1, R2, R3 = mixtures of:
H3PO4
Hydroxyl site
Co-polymeric matrix for potential PSAs:
blue (C), red (O), purple (P), white (H)
phosphate ester Cross-Link
X = H or triglyceride
Ether Cross-Link

Figure 4. Chemical structure of ESO, DSO, and co-polymeric matrix of ESO PSA. (Reproduced with permission from ref. (29). Copyright 2011 American Chemical Society).

Downloaded by COLUMBIA UNIV on August 28, 2012 | http://pubs.acs.org
Publication Date (Web): August 16, 2012 | doi: 10.1021/bk-2012-1105.ch002

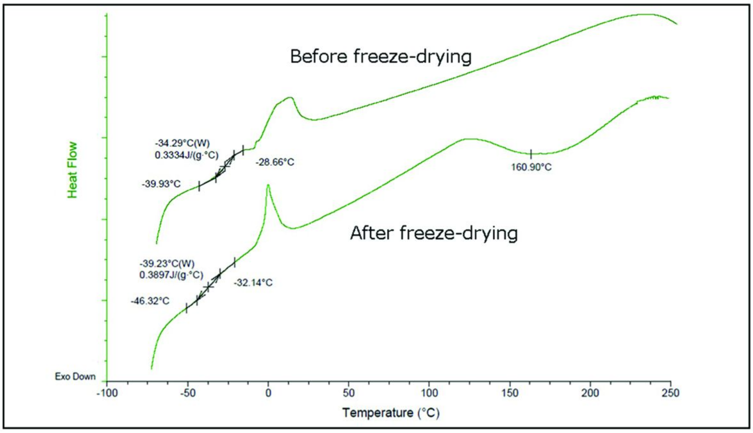

Figure 5. DSC curves of the ESO PSA. (Reproduced with permission from ref. (29). Copyright 2011 American Chemical Society).

The newly developed ESO PSA had small linear coefficient of thermal expansion (CTE) of (14.08 ppm K^{-1}) comparable to the CTE of glass (8.5 ppm K^{-1}), and much lower than that of most flexible plastics (approx. 50 ppm K^{-1}). This can be great advantage of ESO PSA for heat relative application compared to current acryl- and rubber PSAs. Though, we should limit its application in PSA uses with a carrier instead of plastic or thin film since it is unable to stand itself as a thin film due to its low young's modulus (2.05 MPa) and tensile strength (0.16 MPa). The mechanical strength of the ESO PSA film may be able to be improved by several recent reinforcement techniques in advance, but in this study we focused on the PSA application. The differential scanning calorimetry (DSC) (Figure 5) indicated the ESO PSA has great thermal stability (e.g., T_g was -34.29 °C and T_m of ESO PSA were above 250 °C) compared to other PSAs and flexible plastics including polyisoprene, polyethylene (PE) (T_m is about 120-150 °C), and polypropylene (PP) (T_m is about 160 °C). After freeze drying ESO PSA, water moieties trapped in its matrix was slightly removed, the T_g was reduced to -39.23 °C and crystallization was observed at 160 °C (Figure 5). This demonstrates that the ESO PSA film contained moisture and can be a candidate for flexible electronic applications with multiple -OH groups in its matrix. Thermogravimetric Analysis (TGA, Fig 6) indicated that the thermal degradation of the ESO PSA was at 388 °C.

Downloaded by COLUMBIA UNIV on August 28, 2012 | http://pubs.acs.org
Publication Date (Web): August 16, 2012 | doi: 10.1021/bk-2012-1105.ch002

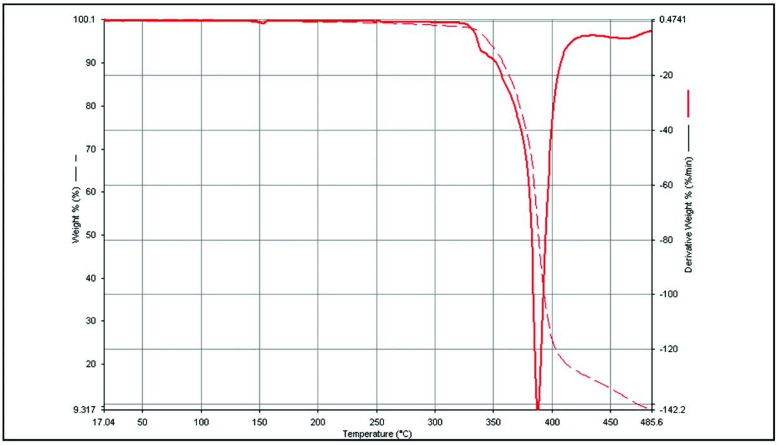

Figure 6. TGA curve of the ESO PSA. (Reproduced with permission from ref. (29). Copyright 2011 American Chemical Society).

It is important to balance the resin ratio of tacky groups and the degree of cross-linking in order to design the ESO PSA with desirable properties. A strong cross-link would make the film too stiff, or cohesion failure would occur if the cross-link is not stronger enough than the adhesion force (*30*). DSO was added as a tackifier to provide more tacky sites to ESO PSAs. Since obtaining a fast reaction and short curing time was essential for commercialization in terms of manufacturing process, we targeted the curing time should be no longer than 60 second. In this novel technology, curing was achieved by air drying to remove the solvent. The ESO PSAs were dried on the one side adhesive treated polyethylene terephthalate (PET) film. Various conditions (ratio, time, temperature) were adjusted for optimum peel strength of PSAs. Based on preliminary peel strength test, we selected several samples with varied ratio of ESO/DSO/H_3PO_4 mixture using PET plastic film as carrier. The ESO PSA of 1.5:1 [ESO/DSO (w/w)] with 5 % (w/w) H_3PO_4 (ESO PSA I) showed fastest drying time (30 s) at 110 °C and had comparable peel strength without cohesion failure (clear removal) (Fig. 7). The ESO PSA I dried at 110 °C for 45 s had an optimum peel strength of 0.77 N/cm (Fig. 7) with glass as a substrate.

Downloaded by COLUMBIA UNIV on August 28, 2012 | http://pubs.acs.org
Publication Date (Web): August 16, 2012 | doi: 10.1021/bk-2012-1105.ch002

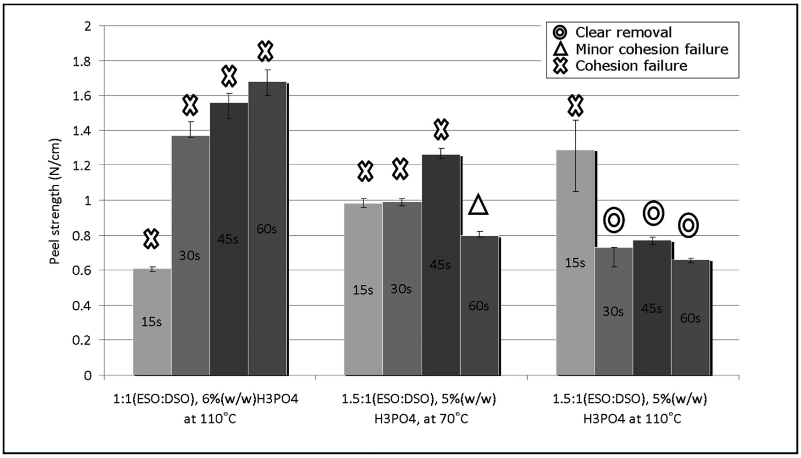

Figure 7. Peel strength of ESO PSAs in terms of drying temperature and time regarding clear removal. (Reproduced with permission from ref. (29). Copyright 2011 American Chemical Society).

The ESO PSA I was selected and evaluated using aluminum foil as carrier, and the peel strength on glass substrate was 2.18 N/cm at 30 s drying, which was comparable to scotch magic tape® and much stronger than to Post-it® (Fig. 8). We believe predominant tack properties on a metal substrate are related to phosphorous polymer adhesion to metal and metal-ion binding characteristics with increased polarity (*29*, *31*) through the phosphate metal attraction (*31*).

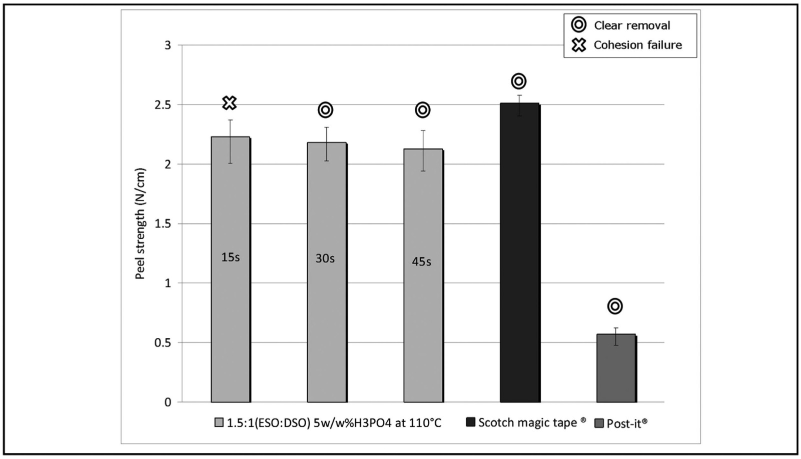

Figure 8. ESO PSA on aluminum foil carrier in terms of drying time vs. Scotch magic tape® and Post-it®. (Reproduced with permission from ref. (29). Copyright 2011 American Chemical Society).

Downloaded by COLUMBIA UNIV on August 28, 2012 | http://pubs.acs.org
Publication Date (Web): August 16, 2012 | doi: 10.1021/bk-2012-1105.ch002

Conclusion

Novel ESO PSA consisted of ethers, phosphate-esters, hydroxyls was successfully synthesized from mixtures of epoxidized and hydroxylated soybean oils (**1** and **2**) in the presence of phosphoric acid. The chemical pathways of this reaction were studied with analogous single-chain model systems **5** and **6**. In the reaction of **5**, **6**, and H_3PO_4 produced a polymer that contained both ether-moieties as well as phosphate ester units in the polymer backbone. A high degree of hydroxy-group loading (with hydrogen-bonding capabilities) in **Polymer-1-2** gives rise to surface tackiness desirable to PSAs, but cohesion failure occurred with excess of DSO. In phosphoric acid, we identified a nontoxic and inexpensive catalyst with relatively low acidity that promotes the polymerization on the timescale of minutes. The peel strength of this novel PSA polymer was comparable to that of commercial PSAs. Importantly, we discovered an environmentally friendly processing method for this biobased PSA by understanding the chemistry of the material.

Acknowledgments

The authors gratefully acknowledge the USB (United soybean board) and KSC (Kansas soybean commission) for financial support for this work. Contribution number 12-212-B from Kansas Agricultural Experimental Station.

References

1. Crivello, J. V.; Narayan, R. *Chem. Mater.* **1992**, *4*, 692.
2. Lligadas, G.; Ronda, J. C.; Galia, M.; Cadiz, V. *Biomacromolecules* **2006**, *7*, 3521.
3. Park, S. J.; Jin, F. L.; Lee, J. R. *Macromol. Rapid Commun.* **2004**, *25*, 724.
4. Cakmakli, B.; Hazer, B.; Tekin, I. O.; Comert, F. B. *Biomacromolecules* **2005**, *6*, 1750.
5. Tsujimoto, T.; Uyama, H.; Kobayashi, S. *Macromolecules* **2004**, *37*, 1777.
6. Andjelkovic, D. D.; Larock, R. C. *Biomacromolecules* **2006**, *7*, 927.
7. Liu, Z. S.; Sharma, B. K.; Erhan, S. Z. *Biomacromolecules* **2007**, *8*, 233.
8. Gandini, A. *Macromolecules* **2008**, *41*, 9491.
9. Lligadas, G.; Ronda, J. C.; Galia, M.; Biermann, U.; Metzger, J. O. *J. Polym. Sci., Part A: Polym. Chem.* **2006**, *44*, 634.
10. Holland, J. M.; Lewis, M.; Nelson, A. *J. Org. Chem.* **2003**, *68*, 747.
11. Lligadas, G.; Ronda, J. C.; Galia, M.; Cadiz, V. *Biomacromolecules* **2007**, *8*, 686.
12. Sharma, B. K.; Adhvaryu, A.; Erhan, S. Z. *J. Agric. Food Chem.* **2006**, *54*, 9866.
13. Chakraborti, A. K.; Rudrawar, S.; Kondaskar, A. *Eur. J. Org. Chem.* **2004**, 3597.
14. Schilling, P. U.S. Patent 4,597,799, 1986.
15. Ballard, R. L.; Tuman, S. J.; Fouquette, D. J.; Stegmiller, W.; Soucek, M. D. *Chem. Mater.* **1999**, *11*, 726.

16. Uyama, H.; Kuwabara, M.; Tsujimoto, T.; Nakano, M.; Usuki, A.; Kobayashi, S. *Chem. Mater.s* **2003**, *15*, 2492.
17. Xu, J. Y.; Liu, Z. S.; Erhan, S. Z. *J. Am. Oil Chem. Soc.* **2008**, *85*, 285.
18. Zhong, B.; Shaw, C.; Rahim, M.; Massingill, J. *J. Coat. Technol.* **2001**, *73*, 53.
19. Bunker, S.; Staller, C.; Willenbacher, N.; Wool, R. *Int. J. Adhes. Adhes.* **2003**, *23*, 29.
20. Ahn, B. K.; Kraft, S.; Sun, X. S. *J. Mater. Chem.* **2011**, *21*, 9498.
21. Guo, Y. Z.; Hardesty, J. H.; Mannari, V. M.; Massingill, J. L. *J. Am. Oil Chem. Soc.* **2007**, *84*, 929.
22. Aberathy, S. M.; Laurent, J. W. *J. Synth. Lubr.* **1993**, *10*, 107.
23. Long, F. A.; Pritchard, J. G. *J. Am. Chem. Soc.* **1956**, *78*, 2663.
24. Moghadam, M.; Tangestaninejad, S.; Mirkhani, V.; Shaibani, R. *Tetrahedron* **2004**, *60*, 6105.
25. Kwart, H.; Goodman, A. L. *J. Am. Chem. Soc.* **1960**, *82*, 1947.
26. Parker, R. E.; Isaacs, N. S. *Chem. Rev.* **1959**, *59*, 737.
27. Penczek, S.; Kubisa, P.; Szymanski, R. *Makromol. Chem., Macromol. Symp.* **1986**, *3*, 203.
28. Nyk, A.; Klosinski, P.; Penczek, S. *Makromol. Chem., Macromol. Chem. Phys.* **1991**, *192*, 833.
29. Ahn, B. K.; Kraft, S.; Wang, D.; Sun, X. S. *Biomacromolecules* **2011**, *12*, 1839.
30. Pocius, A. V. *Adhes. Adhes. Technol.* **1997**, 216.
31. Iliescu, S.; Manoviciu, L.; Ilia, G.; Dehelean, G. *Roum. Chem. Q. Rev.* **1996**, *5*, 267.

Downloaded by COLUMBIA UNIV on August 28, 2012 | http://pubs.acs.org
Publication Date (Web): August 16, 2012 | doi: 10.1021/bk-2012-1105.ch002

Downloaded by UNIV OF GUELPH LIBRARY on August 28, 2012 | http://pubs.acs.org
Publication Date (Web): August 16, 2012 | doi: 10.1021/bk-2012-1105.ch003

Chapter 3

Toughening Modification of Poly(lactic acid) via Melt Blending

Hongzhi Liu and Jinwen Zhang*

**Composite Materials and Engineering Center, Washington State University,
Pullman, WA 99164, U.S.A.
*E-mail: jwzhang@wsu.edu**

For the past decade, cornstarch-based poly(lactic acid) (PLA) has gained increasing interest. PLA is biodegradable and possesses high strength and stiffness. However, the inherent brittleness of PLA has posed a large limitation for its wide applications. To address this major drawback, various strategies, mainly including addition of plasticizers, copolymerization, and melt blending with flexible polymers or rubbers, have been extensively investigated in the literature. Compared to the former, melt blending appears more industrially practical due to the cost-effectiveness. This chapter introduces our efforts to improve the toughness of PLA in terms of non-reactive and reactive melt blending, respectively. Non-reactive blending employed a flexible biodegradable polymer (polybutylene adipate-co-terephthalate), rigid inorganic nanofillers (organically modified montmorillonite and nanosized calcium carbonate), or their combination to modify the performance of PLA materials. In the case of reactive melt blending, an epoxy-containing elastomer and a zinc ionomer were utilized to toughen the PLA materials. Although non-reactive blending gave rise to remarkable enhancement in ductility, reactive blending was shown to be more effective in achieving high impact toughness of PLA.

Downloaded by UNIV OF GUELPH LIBRARY on August 28, 2012 | http://pubs.acs.org
Publication Date (Web): August 16, 2012 | doi: 10.1021/bk-2012-1105.ch003

Introduction

PLA is synthesized from lactic acid (2-hydroxy propionic acid), which is a chiral molecule and exists as two stero isomers (i.e. L- and D- lactic acid). Lactic acid is mainly produced from bacterial fermentation using sugar or enzyme thinned starch (corn, wheat, or rice) as the carbon source. Synthesis of PLA can be conducted by either ring-opening polymerization (ROP) of the lactide (cyclic dimmers of lactic acid) or polycondensation of lactic acid. Direct polycondensation of lactic acid usually yields a low-molecular-weight, brittle, glassy polymer, which, in most cases, is unusable for any applications unless chain-extension agents are added to increase the molecular weight of the polymer. Although Mitsui Chemicals recently commercialized an azeotropic dehydration process to obtain high-molecular-weight PLA (*1*) , ROP is still the most common synthesis route utilized by many other PLA producers, e.g., NatureWorks LLC. The two synthesis routes of PLA is illustrated in Figure 1.

Due to its renewability, competitive cost, good transparency, and excellent stiffness/strength, PLA has attracted increasing interests in many fields as a very promising eco-friendly alternative to some traditional petroleum-based commodity polymers. Unfortunately, its inferior toughness largely limits it wide applications. Therefore, toughening modification of PLA becomes the focus of numerous investigations from academia and industries. Various strategies, including plasticization, copolymerization, and melt blending with flexible polymers or fillers, have been proposed (*2*, *3*). In this chapter, we presented the efforts in our group to improve toughness of PLA via melt blending. Depending on whether chemical reaction occurs during melt blending, our efforts are classified into two categories, i.e. non-reactive blending and reactive blending. In the case of non-reactive blending, poly(butylene adipate-*co*-terephthalate) (PBAT), inorganic rigid nanofillers (organically modified montmorillonite designated as ‘OMMT’ and nanosized calcium carbonate designated as ‘NPCC’), or their combination were employed to improve toughness of PLA, respectively. Finally, a novel ternary blend system involving simultaneous interfacial compatibilization and dynamic vulcanization was presented in the reactive-blending section.

Nonreactive Blending

Toughening with Biodegradable PBAT

PBAT is an aliphatic–aromatic copolyester and is fully biodegradable. PBAT is commercially available under the tradename of Ecoflex® (BASF Co.). It degrades within a few weeks with the aid of naturally occurring enzymes. The PBAT is a flexible thermoplastic designed to process like low-density polyethylene into films, bags or coatings. In view of its high flexibility and biodegradability, PBAT is considered as an ideal toughener candidate for PLA.

Downloaded by UNIV OF GUELPH LIBRARY on August 28, 2012 | http://pubs.acs.org
Publication Date (Web): August 16, 2012 | doi: 10.1021/bk-2012-1105.ch003

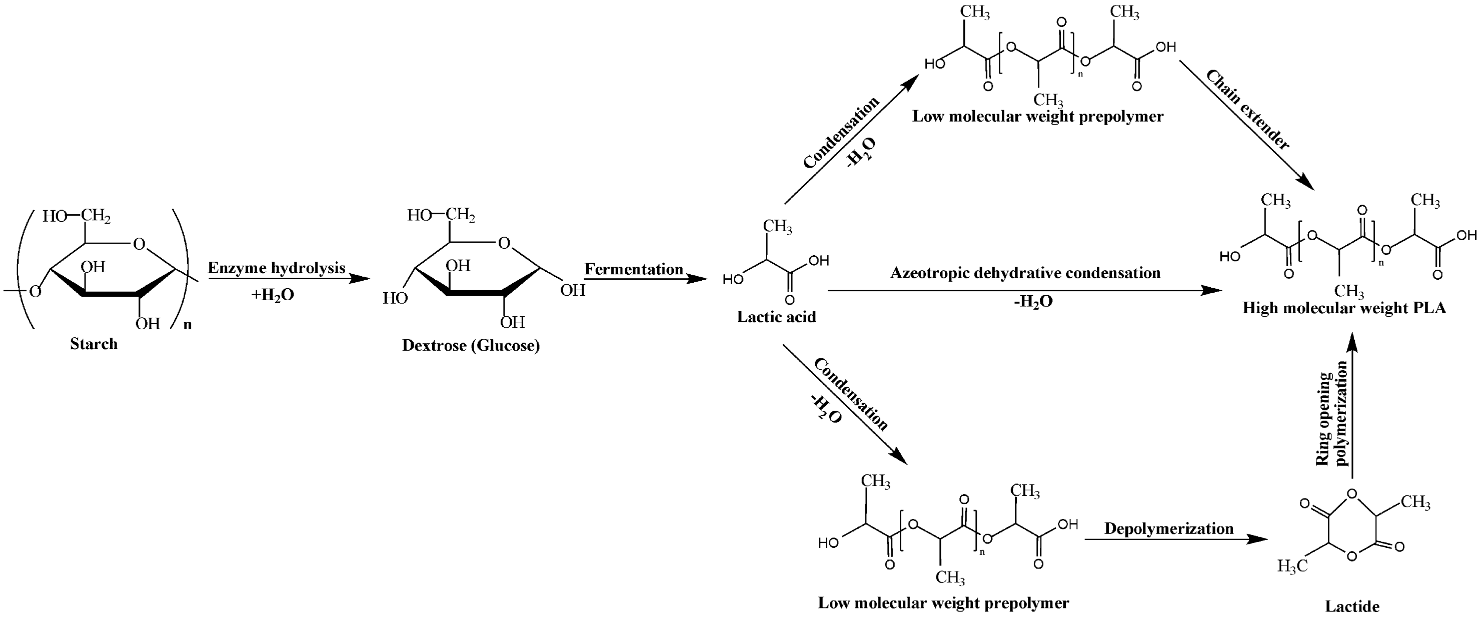
Starch
Enzyme hydrolysis
+H₂O
Dextrose (Glucose)
Fermentation
Lactic acid
Condensation
-H₂O
Low molecular weight prepolymer
Chain extender
Azeotropic dehydrative condensation
-H₂O
High molecular weight PLA
Condensation
-H₂O
Low molecular weight prepolymer
Depolymerization
Lactide
Ring opening polymerization

Figure 1. Detailed synthesis route of poly(lactic acid). Reproduced with permission from reference (3). Copyright 2011 John Wiley & Sons.

Downloaded by UNIV OF GUELPH LIBRARY on August 28, 2012 | http://pubs.acs.org
Publication Date (Web): August 16, 2012 | doi: 10.1021/bk-2012-1105.ch003

Jiang et al. (*4*) first reported the PLA/PBAT blends in the literature and investigated their morphology, tensile properties, and tensile fracture mechanism. Melt blending of PLA/PBAT blends was conducted using a corotating twin-screw extruder (Leistritz ZSE-18) at a barrel temperature profile ranging from 150 to 180°C at a screw speed of 60 rpm. It was found that even without addition of compatibilizers, PBAT was evenly dispersed in PLA. Figure 2 shows stress-extension curves of PLA/PBAT blends as a function of PBAT weight content. It was found that the brittle tensile fracture behavior of PLA was remarkably alerted upon the addition of PBAT and turned ductile. Neat PLA failed at an elongation of 3.7% soon after passing yield point without noticeable necking phenomenon. On the other hand, after yielding all the blends showed stable neck growth through cold drawing, which significantly increased the elongation at break. The elongation of neat PLA was merely 3.7%; however, with only 5 wt % PBAT, the blend exhibited an elongation of 115%. When PBAT content was increased to 20 wt %, elongation of the blend increased to more than 200%.

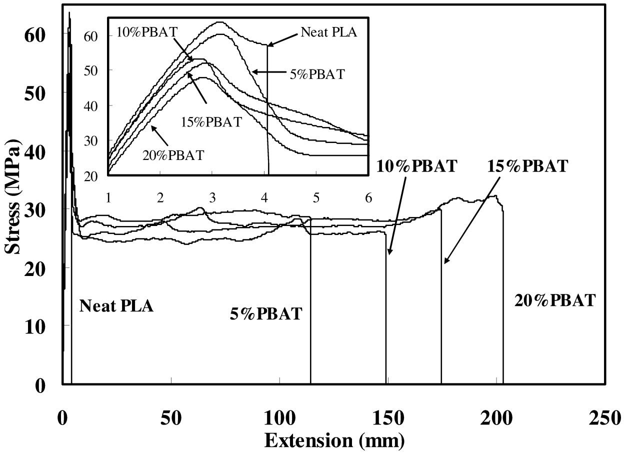

Figure 2. Tensile stress-extension curves of the blends with different weight contents of PBAT. Inset: the stress-extension details of the blends in the neighborhood of yield points. Reproduced with permission from Reference (4). Copyright 2006 American Chemical Society.

Mechanical properties of binary PLA/PBAT blends are listed in Table I. Tensile strength and modulus were found to decrease monotonously with an increase in PBAT content. With addition of 20 wt% PBAT, tensile strength decreased by 25% from 63 MPa (neat PLA) to 47 MPa, whereas elastic modulus decreased by 24% from 3.4 GPa (neat PLA) to 2.6 GPa. Because of weak interfacial adhesion in the blends, impact toughness was only slightly improved. For example, the impact strength of the blend with 20 wt % PBAT was only 4.4 KJ/m^2, as compared to 2.6 KJ/m^2 for neat PLA.

Table I. Tensile and impact properties of PLA/PBAT blends

PBAT content (wt%)	*Tensile strength (MPa)*	*Tensile modulus (GPa)*	*Impact strength (KJ/m²)*
0	63.1	3.43	2.65
5	58.9	3.01	2.72
10	54.1	2.91	2.94
15	51.1	2.76	3.63
20	47.1	2.59	4.44

Downloaded by UNIV OF GUELPH LIBRARY on August 28, 2012 | http://pubs.acs.org
Publication Date (Web): August 16, 2012 | doi: 10.1021/bk-2012-1105.ch003

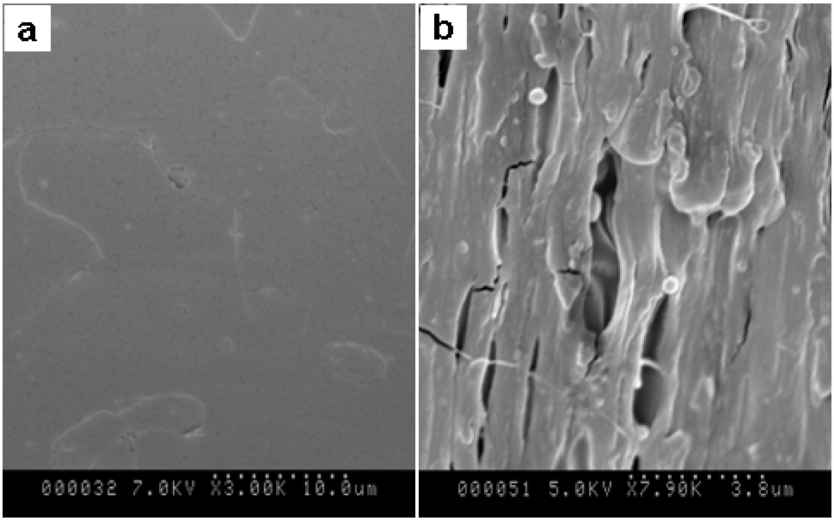

Figure 3. SEM micrograph of the cryo-fractured surface of neat PLA (a) and PLA/PBAT (80/20, w/w) blend (b). Tensile direction is vertical. Reproduced with permission from Reference (4). Copyright 2006 American Chemical Society.

The neck down region of the tensile specimens was cryo-fractured longitudinally (tensile direction) and studied by SEM for tensile fracture mechanism, as shown in Figure 3. Neat PLA, which showed no necking during the tensile test, demonstrated a smooth fracture surface without visible plastic deformation (Figure 3a). Figure 3b shows the micrograph of the cryo-fractured surface of the PLA/PBAT (95/5, w/w) tensile sample, which allowed a clearer view of the PLA matrix deformation and therefore suggested toughening mechanism of PBAT. As shown in Figure 3b, interfacial debonding of spherical

PBAT particles with an average size of ~300 nm under tensile stress can be clearly visible. This behavior occurred during tension when the stress was higher than the bonding strength between the PLA matrix and PBAT inclusions. The cavities formed after the debonding were elongated in the stress direction along with the deformation of the matrix. Since no tensile stress was applied on the PBAT inclusions after the debonding, they remained largely undeformed after sample fracture. It was reasonably concluded that the debonding-induced shear yield was responsible for the remarkable high extensibility of the blends.

Toughening PLA with Inorganic Rigid Particles

As seen in the aforesaid section, the significant improvement in tensile toughness of PLA/PBAT blends was inevitably accompanied by a certain extent of loss in strength and stiffness. To overcome the negative effect of PBAT toughening on the stiffness of PLA blends, Jiang et al. (*5*) further compared the reinforcing and toughening effects of OMMT and NPCC. The two type fillers possesses significantly different geometric structures and surface characteristics. Additionally, the micromechanical deformation process and toughening mechanism were also discussed in the work. OMMT (I.34 TCN, Nanocor Inc.) was modified with methyl dihydroxylethyl hydrogenated tallow ammonium and had a specific surface area of ca. 750 m^2/g and a cation exchange capacity of 92 meq/100g. NPCC (201, NanoMaterials Technology, Singapore) particles were in cubic shapes with an average particle size of ca. 40 nm. Its specific surface area was larger than 40 m^2/g. The surface of NPCC was coated with stearic acid for better dispersion. PLA nanocomposites together with neat PLA control were compounded using the Leistritz ZSE-18 twin screw extruder at a screw speed of 150 rpm. Standard tensile bars were prepared by injection molding subsequently.

As shown in Figure 4, PLA/OMMT nanocomposites exhibited a very different fracture behavior from that of neat PLA and PLA/NPCC nanocomposites. Tensile specimens of neat PLA and PLA/NPCC nanocomposites failed in a similar manner (no necking phenomenon) but larger strains were achieved for PLA/NPCC samples (ca. 5% at 2.5 wt% NPCC and 12~13% at 5 and 7.5 wt% NPCC). For PLA/OMMT samples (Figure 4b), however, necking occurred during tension at 2.5% OMMT, resulting in a relatively large strain at break (ca. 13%). Compared to PBAT toughened PLA blends (Figure 2), the nanoparticles had much inferior tensile tougness. With further increasing OMMT content to 5 and 7.5 wt%, the samples fractured in a complete brittle manner with little stress whitening and the samples failed at stains even lower than that of neat PLA (strains at break of 1.8 and 1.1% for 5 and 7.5 wt% OMMT, respectively). This result was attributed to the presence of large OMMT aggregates in these composites, which acted as material flaws and initiated premature failure.

Downloaded by UNIV OF GUELPH LIBRARY on August 28, 2012 | http://pubs.acs.org
Publication Date (Web): August 16, 2012 | doi: 10.1021/bk-2012-1105.ch003

Downloaded by UNIV OF GUELPH LIBRARY on August 28, 2012 | http://pubs.acs.org
Publication Date (Web): August 16, 2012 | doi: 10.1021/bk-2012-1105.ch003

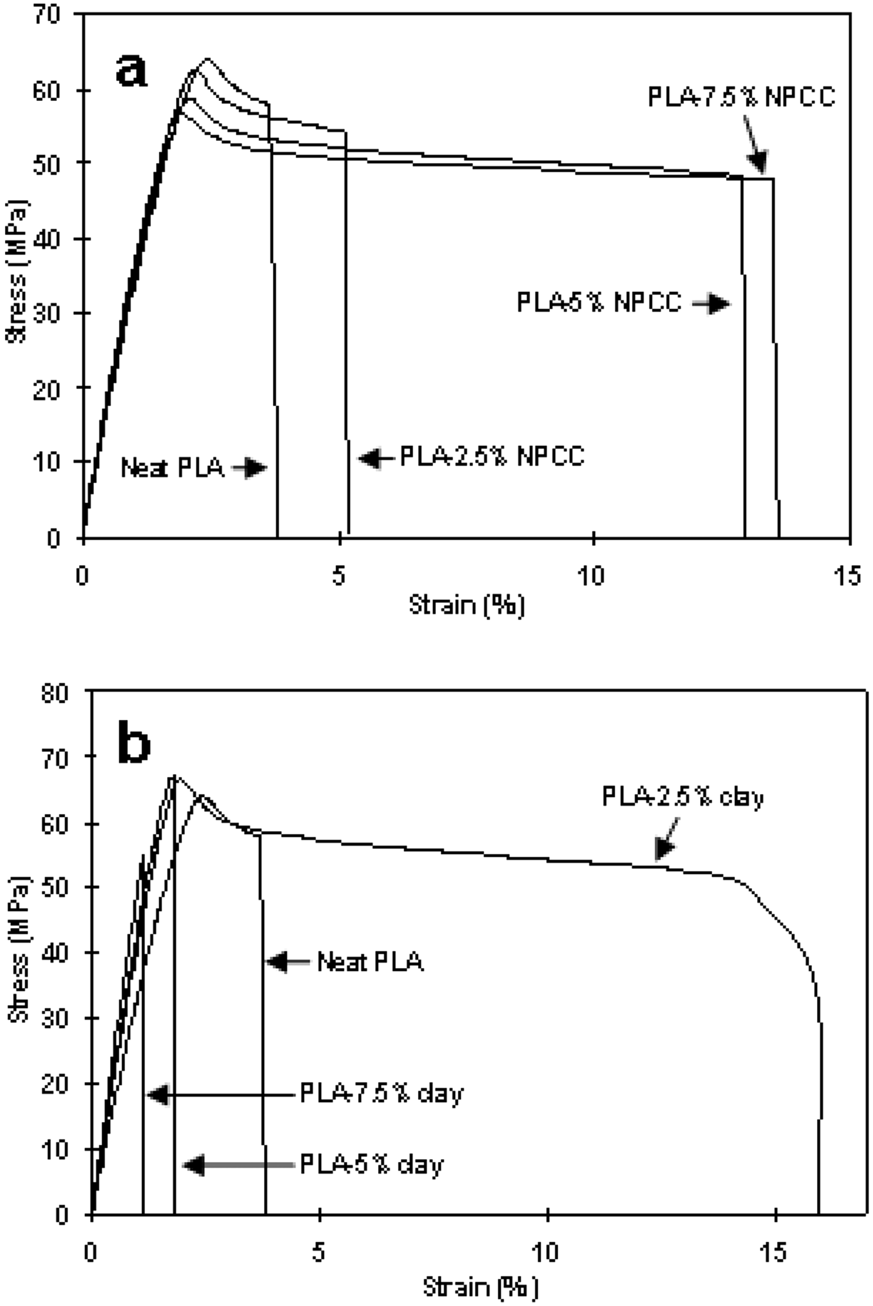

Figure 4. Stress-strain curves of PLA/NPCC (a) and PLA/OMMT (b) composites. Reproduced with permission from Reference (5). Copyright 2007 Elsevier.

Also, the effects of NPCC and OMMT on strength and modulus of the resulting composites were different, as shown in Table II. Tensile strength decreased continuously with increasing NPCC content, while it increased with OMMT content up to 5 wt%. Likewise, compared to NPCC, OMMT also appeared more effective in enhancing the stiffness. The authors attributed the superior reinforcing and toughening effects of OMMT at lower concentrations (i.e. 2.5 and 5 wt%) to the stronger interaction between filler and matrix, larger specific surface area (750 vs. 40 m^2/g) of the OMMT, and higher aspect ratio (~ 40 vs. 1) with respect to NPCC.

Table II. Tensile properties of neat PLA, PLA/NPCC and PLA/OMMT composites

Tensile Properties	*Samples*						
	Neat PLA	*NPCC content (wt%)*			*OMMT content (wt%)*		
		2.5	*5.0*	*7.5*	*2.5*	*5.0*	*7.5*
Strength (MPa)	63.1	62.8	59.5	57.4	65.3	67.2	54.5
Modulus (GPa)	3.4	3.6	3.6	3.7	4.0	4.6	5.1
Strain (%)	3.8	5.1	12.8	12.0	12.4	1.8	1.1

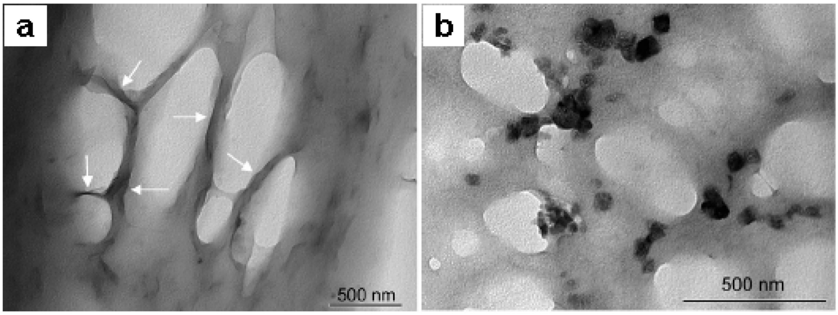

Figure 5. TEM micrographs of PLA/2.5 wt%OMMT (a) and PLA/2.5 wt%NPCC (b) nanocomposites showing cavitation under uniaxial extension. TEM sections were cut from the sub-fracture parts of the samples that had undergone tensile testing. Reproduced with permission from Reference (5). Copyright 2007 Elsevier.

Downloaded by UNIV OF GUELPH LIBRARY on August 28, 2012 | http://pubs.acs.org
Publication Date (Web): August 16, 2012 | doi: 10.1021/bk-2012-1105.ch003

Downloaded by UNIV OF GUELPH LIBRARY on August 28, 2012 | http://pubs.acs.org
Publication Date (Web): August 16, 2012 | doi: 10.1021/bk-2012-1105.ch003

Transmission electron microscopy (TEM) can provide more information on micromechanical deformation behavior of the tensile specimens at a smaller scale, as shown in Figure 5. It is well-accepted that the cavities formed by interfacial debonding are able to release localized strain constraints, thereby triggering shear yielding in the matrix. Besides acting as cavity nucleating sites, OMMT might also prevent the cavities from coalescing and forming catastrophic cracks (Figure 5a). The OMMT platelets (indicated by the arrows in the image) appeared to reside between the elongated cavities and may form the barrier preventing them from coalescence. In PLA/NPCC composites, cavities were formed through NPCC debonding (Figure 5b). However, the cubic-shaped NPCC could not behave in the same way as MMT to prevent the coalescence of the cavities. These cavities inPLA/NPCC nanocomposites could coalesce into cracks at the sites where the cavities most densely located without inducing massive matrix shear deformation. Therefore, necking could not be initiated.

Toughening PLA with Both PBAT and Inorganic Rigid Nanofillers

On the basis of the above results, it was evident that PBAT was more effective in improving tensile toughness (or ductility) of PLA than inorganic rigid nanofillers. Nevertheless, the addition of former also resulted in redcutions in strength and modulus. In contrast, the incorporation of the inorganic nanofillers increased modulus but had little effect on ductility. Therefore, in an attempt to achieve complimentary effect in mechanical properties, PLA ternary composites containing both PBAT and rigid inorganic nanofillers were studied by Jiang et al (*6*). PLA, PBAT and OMMT (or NPCC) were blended using a twin-screw extruder (Leistritz ZSE-18). The content of PBAT was fixed at 10 wt% for all the composites. The content OMMT or NPCC were set at of 2.5 and 5 wt% based on the basis of the total weight of PLA and PBAT. In addition, in order to examine the compatibilizing role of added maleic anhydride grafted PLA (MA-*g*-PLA), 25 wt% pure PLA was replaced by MA-*g*-PLA (0.3 wt% MA) in the ternary composites while maintaining the total polymer contents in the hybrids.

Tensile properties of PLA/PBAT/nanoparticle ternary composites with and without MA-*g*-PLA as a compatibilier are shown in Figure 6. It was found that the addition of 2.5 wt% nanoparticles into the binary PLA/PBAT blends remarkably reduced its strain. For instance, PLA/PBAT/2.5% OMMT and PLA/PBAT/2.5% NPCC showed the strain of 45.4% and 161.4%, respectively, while the strain of the binary PLA/PBAT blend was 243.4%. With addition of the nanoparticles up to 5 wt%, the strain was further reduced to 14.5% for OMMT and 76.4% for NPCC. The reduction in the strain of the ternary composite with respect to the corresponding PLA/PBAT binary one was attributed to the presence of nanoparticle agglomerates. Comparatively, at the same concentration, OMMT resulted in a much larger reduction in strain than NPCC. The authors attributed it to stronger restraints of OMMT on PLA chains since the mobility is essential in large-scale plastic deformation where cooperative chain sliding and rotation occurs. The nanocomposite with OMMT possessed higher stiffness and strength than the ones with NPCC. With 2.5 wt% OMMT, tensile strength of the ternary blend was slightly higher (55.1 vs. 54.1 MPa) but elastic modulus was significantly hiher (3.53 vs. 2.91 GPa) than that of the PLA/PBAT binary blend. The modulus of neat neat PLA was 3.43 GPa. With 5 wt% OMMT, tensile strength and modulus further increased to 55.9 MPa and 3.87 GPa, respectively. In contrast, the addition of NPCC to the binary blend monotonously lowered tensile strength (53.7 MPa at 2.5 wt% and 51.7 MPa at 5.0 wt%). Tensile modulus of the binary blend was only slightly affected by addition of NPCC.

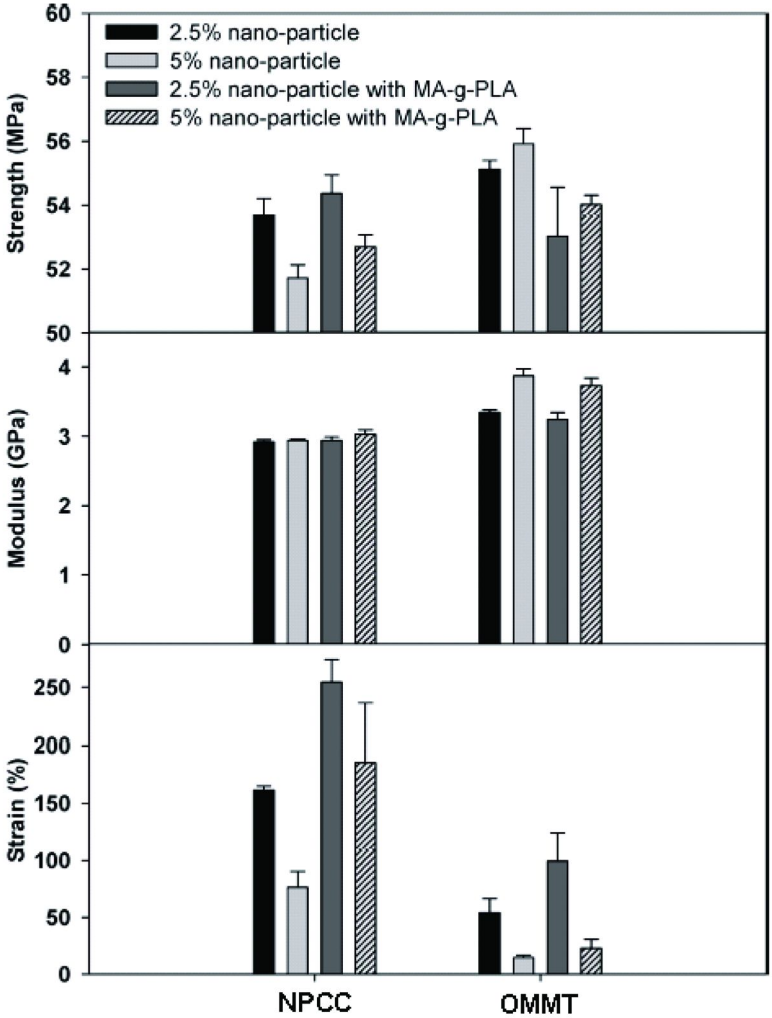

Figure 6. Comparison of tensile properties between the MA -g-PLA compatibilized and noncompatibilized PLA/PBAT/nanoparticle composites. Reproduced with permission from Reference (6). Copyright 2009 American Chemical Society.

Downloaded by UNIV OF GUELPH LIBRARY on August 28, 2012 | http://pubs.acs.org
Publication Date (Web): August 16, 2012 | doi: 10.1021/bk-2012-1105.ch003

The addition of MA-*g*-PLA exhibited negligible effects on the strength and modulus of the ternary composites (Figure 6). However, the strain at break was substantially improved upon addition of MA-*g*-PLA. For the ternary composites filled with NPCC, the strain was increased by 57.6 and 142.5% for addition of 2.5 and 5.0 wt% NPCC, respectively. Likewise, the strain was increased by 83 and 55.6% for the ternary composites with 2.5 and 5.0 wt% OMMT, respectively. Such improvement in tensile toughness was especially crucial for the OMMT ternary composites because they exhibited higher strength and modulus but lower toughness with respect to the NPCC ones. The increase in strain with incorporation of MA-*g*-PLA afforded the OMMT composites better-balanced mechanical performance.

Downloaded by UNIV OF GUELPH LIBRARY on August 28, 2012 | http://pubs.acs.org
Publication Date (Web): August 16, 2012 | doi: 10.1021/bk-2012-1105.ch003

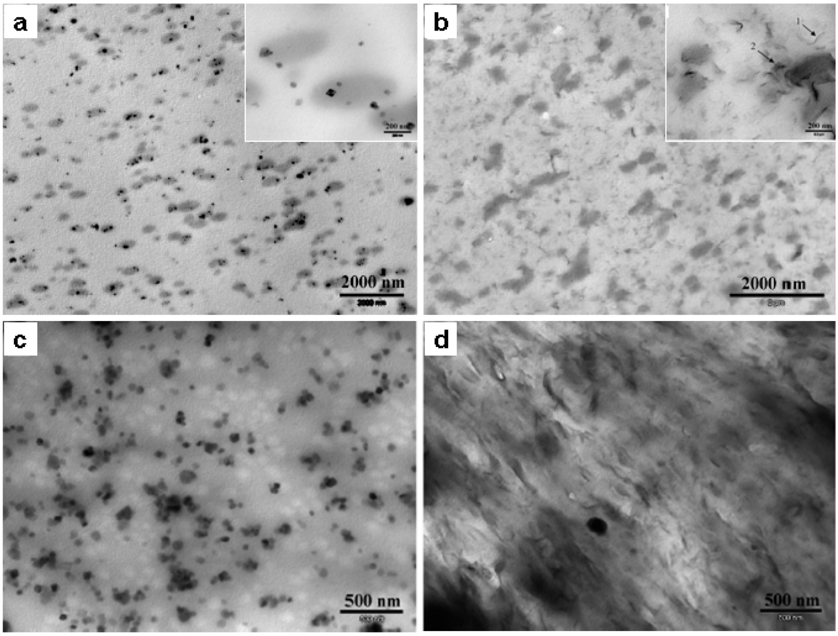

Figure 7. TEM micrographs of PLA/10% PBAT/2.5% NPCC (a,c) and PLA/10% PBAT/2.5% OMMT (b, d) with (a, b; inserts at the right corner: higher magnification) and without MA-g-PLA (c, d) as a compatibilizer, respectively. In the insert of micrograph b, arrow 1 & 2 indicate exfoliated and intercalated OMMT layers. Adapted with permission from Reference (6). Copyright 2009 American Chemical Society.

Figure 7 shows the TEM micrographs of PLA/PBAT/NPCC and PLA/PBAT/OMMT nanocomposites. As shown in Figure 7a & 7b, both PBAT and nanofillers were evenly dispersed in the PLA matrix in the presence of MA-*g*-PLA as a compatibilizer. Moreover, the nanoparticles appeared to distribute inside both PLA and PBAT phases. Without the compatibilization, however, the number and size of the nanoparticle agglomerates evidently became more (Figure 7c & 7d) . The better dispersion level of the nanoparticles upon addition of MA-*g*-PLA could account for the improvement in tensile toughness above.

Downloaded by UNIV OF GUELPH LIBRARY on August 28, 2012 | http://pubs.acs.org
Publication Date (Web): August 16, 2012 | doi: 10.1021/bk-2012-1105.ch003

Reactive Blending − A Novel PLA Ternary Blend System Involving Dual Reactions

As seen from the above results, flexible PBAT proved to be more effective in enhancing tensile toughness or ductility of PLA. However, as for impact strength, especially in the notched state, PBAT only led to a slight improvement. Though a few supertoughened PLA blends (above ~530J/m of notched Izod impact strength) (*7*) have been reported (*8–11*), comprehensive understandings of the relationship between impact toughness and microstructure and toughening mechanism are still missing to date.

Liu et al. (*12*) introduced a novel PLA ternary blend system consisting of an ethylene/n-butyl acrylate/glycidyl methacrylate terpolymer elastomer (EBA-GMA) and a zinc ionomer of ethylene/methacrylic acid copolymer (EMAA-Zn). Unlike the preparations of other toughened PLA blends, the compounding of these ternary blends involved simultaneous vulcanization (crosslinking) of EBA-GMA and interfacial reactive compatibilization between PLA and EBA-GMA. EMAA-Zn was found to catalyze both crosslinking and reactive copatibilization reactions. It needs to mention that in our ternary blend system, PLA matrix behaves as a non-crosslinking thermoplastic phase, wheres the crosslinking only occurred for dispersed EBA-g-MA phase. Therefore, the resultant blends still retain their molten flowability during the compounding, although the crosslinking of the dispersed EBA-GMA phase could lead to a certain level of increase in melt viscosity. In a subsequent study, Liu et al. further found that the balance between interfacial compatibilization and crosslinking was critical to achieve satisfactory toughening effects (*13*). Reactive blending was conducted using a co-rotating twin screw extruder (Leistritz ZSE-18) with a screw diameter of 17.8 mm and an L/D ratio of 40 at a screw speed of 50 rpm. After oven-dried, the pellets were injection-molded (Sumitomo SE50D) into ASTM type-I standard specimens at melt temperature of 190°C and mold temperature of 35°C. Tensile and notched Izod impact impact testing was performed according to ASTM D638 and D256 standards, respectively.

Downloaded by UNIV OF GUELPH LIBRARY on August 28, 2012 | http://pubs.acs.org
Publication Date (Web): August 16, 2012 | doi: 10.1021/bk-2012-1105.ch003

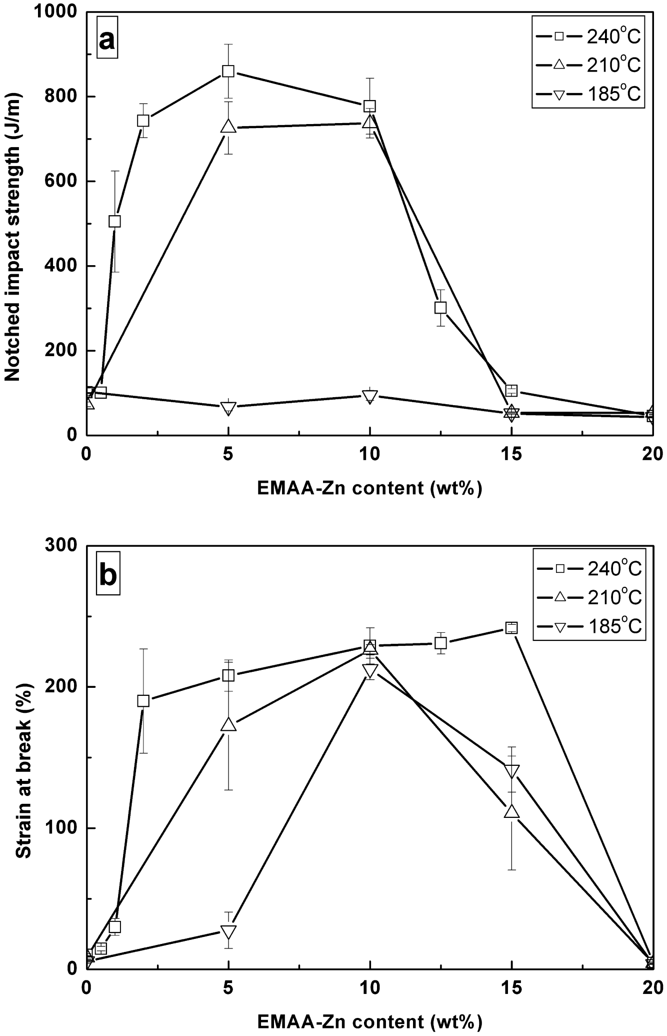

Figure 8. Impact strength (a) and strain at break (b) of PLA/EBA-GMA/EMAA-Zn (80/20-x/x, w/w) blends as a function of weight content of EMAA-Zn under three different extrusion temperatures. Adapted with permission from Reference (12). Copyright 2010 American Chemical Society.

Downloaded by UNIV OF GUELPH LIBRARY on August 28, 2012 | http://pubs.acs.org
Publication Date (Web): August 16, 2012 | doi: 10.1021/bk-2012-1105.ch003

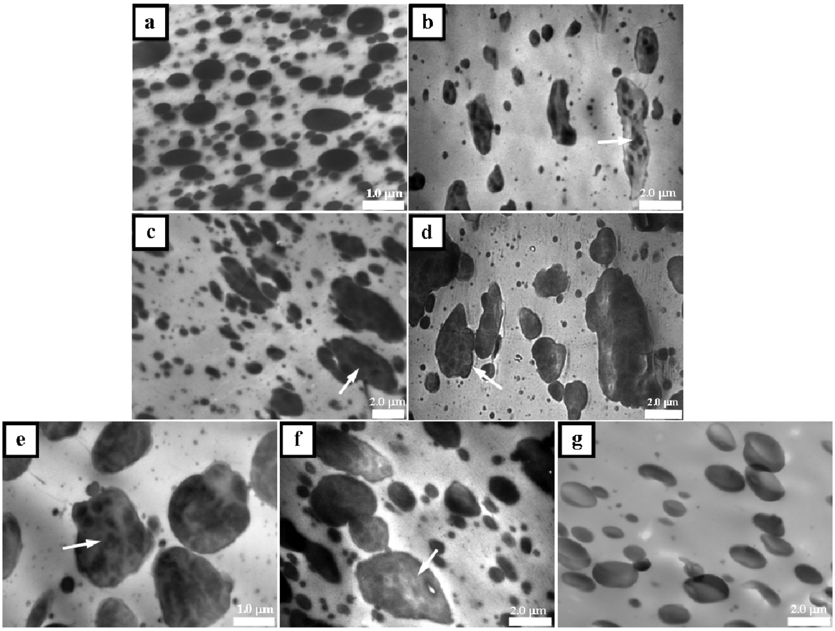

Figure 9. cryo-TEM micrographs of PLA/EBA-GMA/EMAA-Zn blends: (a) 80/20/0 (w/w), 240°C; (b) 80/15/5 (w/w), 240°C; (c) 80/10/10, (w/w), 240°C; (d) 80/10/10, (w/w), 210°C; (e) 80/10/10, (w/w), 185°C; (f) 80/5/15, (w/w), 240°C; (g) 80/0/20 (w/w), 240°C. Adapted with permission from Reference (12, 13). Copyright 2010 & 2011 American Chemical Society.

Figure 8 shows the notched Izod impact strength and strain at break of various PLA/EBA-GMA/EMAA-Zn (80/20-x/x, w/w) blends as functions of weight content of EMAA-Zn under three different extrusion temperatures. A remarkable dependence of impact strength on extrusion temperature and EBA-GMA/EMAA-Zn ratio was found (Figure 8a). The ternary blends prepared at 185°C only exhibited similar impact strength to that of binary blends (i.e. less than three times that of the neat PLA control). In contrast, a considerable toughening effect was observed in the ternary blends prepared at 210°C and 240°C, respectively. Moreover, such improvement in impact toughness was more pronounced when of the EBA-GMA/EMAA-Zn weight ratio was equal to or larger than 1 except for the ternary blend containing 0.5 wt% EMAA-Zn. Especially, the ternary blend with 15 wt% EBA-GMA exhibited the impact strength of 860 J/m, which was approximately 35 times that of neat PLA control (25 J/m). FT-IR results of the dioxane-extracted ternary blends demonstrated that the effective interfacial compatibilization achieved at the elevated blending temperatures was responsible for such significant improvement (*12*). As shown in Figure 8b, the high impact strength was also accompanied by a very high strain (>200%). Evidently, this finding was different from the results by Oyama

Downloaded by UNIV OF GUELPH LIBRARY on August 28, 2012 | http://pubs.acs.org
Publication Date (Web): August 16, 2012 | doi: 10.1021/bk-2012-1105.ch003

in the study of PLA/EGMA (80/20, w/w) binary blend (*8*), which exhibited the similar impact toughness after thermal annealing of the molded specimens but dramatically lower strain at break (≤35%). Unlike impact strength, both tensile strength and modulus of the ternary blends were less affected by reactive blending temperature and elastomer/ionomer ratio and were in the ranges of 35~38 MPa and 2.1~2.4 GPa, respectively (data now shown here).

Since mechanical properties of multicomponent polymer blends depends largely on the resulting phase structure of the blends, TEM was utilized to identify the phase structure of the PLA blends, as shown in Figure 9. Unlike the binary blends (Figure 9a & 9g), the ternary blends displayed a unique 'salami'-like phase structure (indicated by arrows) regardless of variation in extrusion temperature. As shown in Figure 9b & 9c, When the elastomer/ionomer weight ratio was larger than or equal to 1, the blends displayed the occluded ionomer (dark color) inside the elastomer droplets (gray color), which were dispersed in the PLA matrix (white color). When there was more ionomer than rubber in the blends (Figure 9f), however, the structure turned into the the dispersed ionomer droplets with the elastomer as sub-inclusions. This evolution of dispersed phase structure alterted the wetting of the dispersed droplets by the PLA matrix, as will be discussed later.

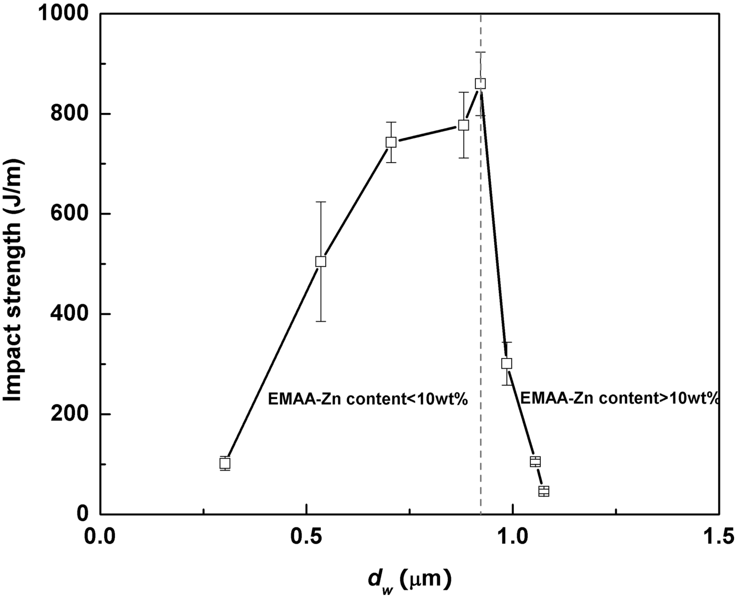

Figure 10. Izod impact strength of PLA/EBA-GMA/EMAA-Zn (80/20-x/x, w/w) blends (240°C) with total content of both modifiers fixed at 20 wt% as a function of weight average particle diameter (d_W). Reproduced with permission from Reference (13). Copyright 2011 American Chemical Society.

Downloaded by UNIV OF GUELPH LIBRARY on August 28, 2012 | http://pubs.acs.org
Publication Date (Web): August 16, 2012 | doi: 10.1021/bk-2012-1105.ch003

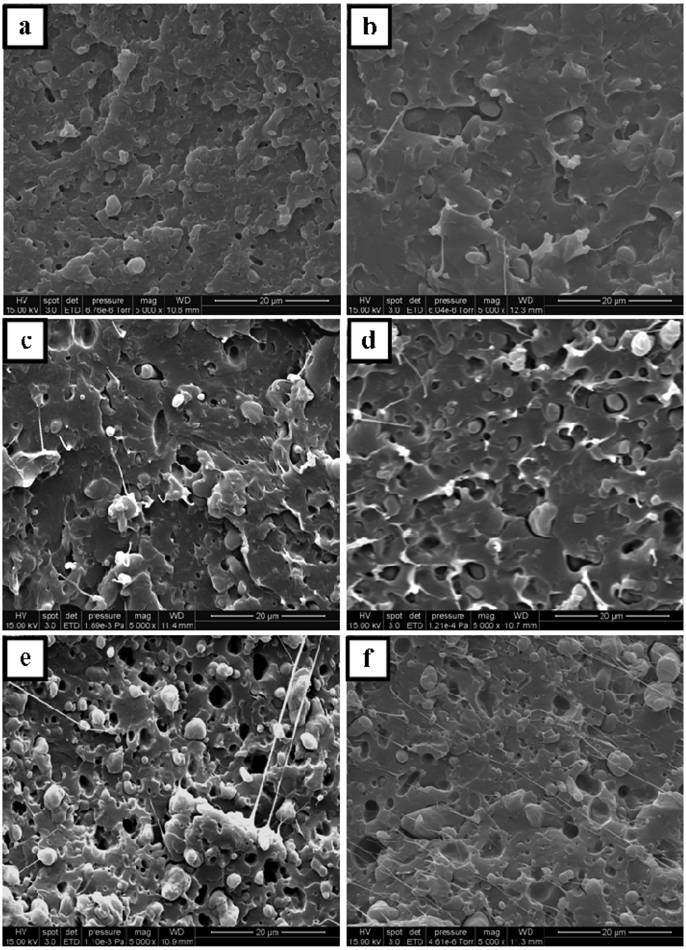

Figure 11. SEM micrographs of impact-fractured surface of PLA/EBA-GMA/EMAA-Zn blends adjacent to the notch: (a) 80/20/0 (w/w), 240°C; (b) 80/15/5 (w/w), 240°C; (c) 80/10/10, (w/w), 240°C; (d) 80/10/10, (w/w), 210°C; (e) 80/10/10, (w/w), 185°C; (f) 80/5/15, (w/w), 240°C. Adapted with permission from Reference (13). Copyright 2011 American Chemical Society.

By correlating dispersed particle size (i.e., weight average particle diameter, d_w) with notched Izod impact toughness, an optimum particle size range (ca. 0.7~0.9 µm) for PLA toughening were identified in the PLA/EBA-GMA/EMA-Zn (80/20-x/x, w/w) blends extruded at 240°C, as shown in Figure 10 (*13*). Likewise, the optimum particle size has also been reported for other thermoplastic matrices containing a variety of rubbers, such as semi-crystalline nylon-6 (PA6: 0.2~0.5 µm) (*14–16*), amorphous nylon (a-PA: 0.2~0.5 µm) (*17*), polycarbonate (PC:

Downloaded by UNIV OF GUELPH LIBRARY on August 28, 2012 | http://pubs.acs.org
Publication Date (Web): August 16, 2012 | doi: 10.1021/bk-2012-1105.ch003

0.10~0.25 μm) (*18*, *19*), poly(methylene methacrylate) (PMMA: 0.2~0.3 μm) (*20–22*), poly(vinyl chloride) (PVC: 0.2 μm) (*23*), poly(styrene-*co*-acrylonitrile) (SAN: 0.75 μm) (*24*), and polystyrene (PS: 0.8~2.5 μm) (*7*, *24*). Wu correlated rubber particle diameter with chain structure parameter of the matrix and claimed that the optimum particle size for toughening decreased as the matrix becomes less brittle (*7*). Because PLA exhibited relatively higher intrinsic brittleness (characteristic chain ratio as a measure of chain flexibility, C_∞=9.5~11.8 (*25–27*) depending on the L/D lactide ratio) than other matrices (e.g., C_∞=6.2 for PA6, C_∞=5.4 for a-PA, C_∞=2.4 for PC, C_∞=8.2 for PMMA, C_∞=7.6 for PVC, C_∞=10.6 for SAN, and C_∞=10.8 for PS) (*7*, *28*), this optimum particle size for the toughened ternary PLAs seemed reasonable. By correlating tensile toughness with dispersed particle diameter in PLLA/conjugated soybean oil binary blends, Gramlich et al. (*29*) also reported a similar range of optimum particle diameter (i.e. 0.5~0.9 μm) for toughening PLA.

In order to study the micromechanical deformation mechanism of the PLA blends, impact-fractured surfaces was analyzed using electron microscopy (*13*). Figure 11 shows SEM fractographs of the impact fractured surface of the blends in the vicinity of the notch. The surface of the PLA/EBA-GMA (80/20, w/w) binary blend compounded at 240°C exhibited some tiny voids but no noticeable matrix yielding (Figure 11a). The well-embedded particles in the matrix were also the evidence of good interfacial wetting. Like the binary blends, good interfacial wetting was also noticible in the ternary PLA/EBA-GMA/EMAA-Zn (80/15/5, w/w) blend compounded at 240°C (Figure 11b) and the PLA/EBA-GMA/EMAA-Zn (80/10/10, w/w) ones (Figure 11c & 11d) compounded at 240°C and 210°C, respectively. In these ternary blends, large cavities around the dispersed particles and matrix plastic deformation were discerned. In contrast, the prevalent debonding of coarse particles from the matrix was seen in the ternary PLA/EBA-GMA/EMAA-Zn (80/5/15, w/w) blend (Figure 11e) compounded at 240°C and ternary PLA/EBA-GMA/EMAA-Zn (80/5/15, w/w) one (Figure 11f) extruded at 185°C. And the matrix plastic deformation did not be seen. Therefore, the fractographic SEM observation of the above blends agreed well with their impact strengths.

Figure 12 further gives TEM micrographs of the sub-fracture surface of the blends (*13*). For the PLA/EBA-GMA (80/20, w/w) binary blend, only tiny debonding around relatively larger particles was observed without internal cavitation (Figure 12a). At higher magnification, the existence of minute fibrillated crazes passing through other neighboring particles was also observed (Figure 12b). Therefore, the interfacial debonding in the PLA/EBA-GMA binary blend was unable to trigger the massive matrix plastic deformation required for high impact toughness. A similar phenomenon was noted in the deformation of the ternary PLA/EBA-GMA/EMAA-Zn (80/5/15, w/w) blend in which debonding at the ionomer/PLA interface prevailed (Figure 12d). On the contrary, the internal cavitation of the EBA-GMA phase was noted in the PLA/EBA-GMA/EMAA-Zn (80/15/5, w/w) blend (Figure 12c). Therefore, the evidence suggested that the high impact toughness observed for some of the ternary blends was attributed to the low cavitation resistance of the dispersed particles in conjunction with suitable interfacial adhesion.

Downloaded by UNIV OF GUELPH LIBRARY on August 28, 2012 | http://pubs.acs.org
Publication Date (Web): August 16, 2012 | doi: 10.1021/bk-2012-1105.ch003

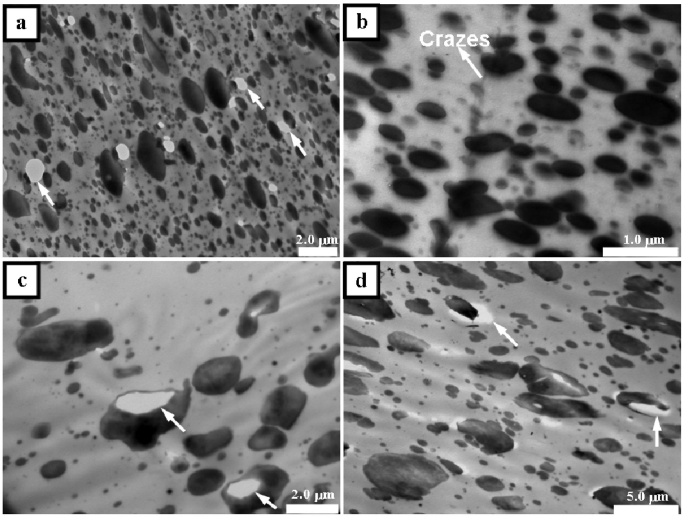

Figure 12. Cryo-TEM micrographs of stress-whitening zone: (a) PLA/EBA-GMA (80/20, w/w) binary blend, low-magnification (x7,500); (b) PLA/EBA-GMA (80/20, w/w) binary blend, high magnification (x30,000) at the localized area; (c) PLA/EBA-GMA/EMAA-Zn (80/15/5, w/w) ternary blend; (d) PLA/EBA-GMA/EMAA-Zn (80/5/15,w/w) ternary blend. Reproduced with permission from Reference (13). Copyright 2011 American Chemical Society.

Conclusions and Outlook

Due to the inherent rigidity of PLA chains, crazing would be favored over shear yielding in the case of neat PLA (*7*). The brittle fracture behavior of PLA in tensile and impact testing is associated with the crazing deformation mechanism through which the polymer fails (*30*, *31*). Based on the above results, reactive blending is shown to be more effective in improving impact toughness of PLA blends than physical melt blending. Super toughness was successfully obtained for the ternary blends in our work. However, the tremenduous improvement in impact toughness was accompanied by a great loss (30~45%) in strength and stiffness. Thus, how to greatly enhance impact toughness while minimizing the reduction in strength and stiffness of the PLA materials still remains challenging. In addition, non-biodegradable petroleum-based polymers (up to 20 wt%) was used in the blends, which compromised the integral biodegradability of the PLA materials. In the long run, the development of high-impact and totally bidegradable PLA materials with moderate strength and modulus and excellent transparency will be ultimate objective in the PLA toughening. Besdies, the in-depth understanding of effects of crystallization (e.g., variation of crystallinity and crystalline structure by the annealing) and tacticty of the PLA matrix on PLA toughening are still insufficient and need to be clarified in the future studies.

Downloaded by UNIV OF GUELPH LIBRARY on August 28, 2012 | http://pubs.acs.org
Publication Date (Web): August 16, 2012 | doi: 10.1021/bk-2012-1105.ch003

References

1. Kawashima, N.; Ogawa, S.; Obuchi, S.; Matsuo, M.; Yagi, T. Polylactic acid LACEA. In *Biopolymers*; Doi, Y., Steinbuchel, A., Eds.; Wiley: New York, 2002; pp 251−274.
2. Anderson, K.; Schreck, K.; Hillmyer, M. Toughening polylactide. *Polym. Rev.* **2008**, *48* (1), 85–108.
3. Liu, H.; Zhang, J. Research progress in toughening modification of poly(latic acid). *J. Polym. Sci., Part B: Polym. Phys.* **2011**, *49* (15), 1051–1083.
4. Jiang, L.; Wolcott, M. P.; Zhang, J. Study of Biodegradable Polylactide/Poly(butylene adipate-co-terephthalate) Blends. *Biomacromolecules* **2006**, *7* (1), 199–207.
5. Jiang, L.; Zhang, J.; Wolcott, M. P. Comparison of polylactide/nano-sized calcium carbonate and polylactide/montmorillonite composites: reinforcing effects and toughening mechanisms. *Polymer* **2007**, *48* (26), 7632–7644.
6. Jiang, L.; Liu, B.; Zhang, J. Properties of poly(lactic acid)/poly(butylene adipate-co-terephthalate)/nanoparticle ternary composites. *Ind. Eng. Chem. Res.* **2009**, *48* (16), 7549–7602.
7. Wu, S. Chain structure, phase morphology, and toughness relationships in polymers and blends. *Polym. Eng. Sci.* **1990**, *30* (13), 753–761.
8. Oyama, H. Super-tough poly(lactic acid) materials: Reactive blending with ethylene copolymer. *Polymer* **2009**, *50* (3), 747–751.
9. Anderson, K. S.; Lim, S. H.; Hillmyer, M. A. Toughening of polylactide by melt blending with linear low-density polyethylene. *J. Appl. Polym. Sci.* **2003**, *89* (14), 3757–3768.
10. Anderson, K.; Hillmyer, M. The influence of block copolymer microstructure on the toughness of compatibilized polylactide/polyethylene blends. *Polymer* **2004**, *45* (26), 8809–8823.
11. Hashima, K.; Nishitsuji, S.; Inoue, T. Structure-properties of super-tough PLA alloy with excellent heat resistance. *Polymer* **2010**, *51* (17), 3934–3939.
12. Liu, H.; Chen, F.; Liu, B.; Estep, G.; Zhang, J. Super Toughened poly(lactic acid) ternary blends by simultaneous dynamic vulcanization and interfacial compatibilization. *Macromolecules* **2010**, *43* (14), 6058–6066.
13. Liu, H.; Song, W.; Chen, F.; Guo, L.; Zhang, J. Interaction of microstructure and interfacial adhesion on impact performance of polylactide (PLA) ternary blends. *Macromolecules* **2011**, *44* (6), 1513–1522.
14. Oshinski, A. J.; Keskkula, H.; Paul, D. R. Rubber toughening of polyamides with functionalized block copolymers: 1. Nylon-6. *Polymer* **1992**, *33* (2), 268–283.
15. Oshinski, A. J.; Keskkula, H.; Paul, D. R. The effect of polyamide end-group configuration on morphology and toughness of blends with maleated elastomers. *J. Appl. Polym. Sci.* **1996**, *61* (4), 623–640.
16. Oshinski, A. J.; Keskkula, H.; Paul, D. R. The role of matrix molecular weight in rubber toughened nylon 6 blends: 2. Room temperature Izod impact toughness. *Polymer* **1996**, *37* (22), 4909–4918.

17. Huang, J. J.; Keskkula, H.; Paul, D. R. Comparison of the toughening behavior of nylon 6 versus an amorphous polyamide using various maleated elastomers. *Polymer* **2006**, *47* (2), 639–651.
18. Cho, K.; Yang, J.; Yoon, S.; Hwang, M.; Nair, S. V. Toughening of polycarbonate: effect of particle size and rubber phase contents of the core-shell impact modifier. *J. Appl. Polym. Sci.* **2005**, *95* (3), 748–755.
19. Xu, H.; Tang, S.; Yang, L.; Hou, W. Toughening of polycarbonate by core-shell latex particles: influence of particle size and spatial distribution on brittle-ductile transition. *J. Polym. Sci., Part B: Polym. Phys.* **2010**, *48* (18), 1970–1977.
20. Dompas, D.; Groeninckx, G. Toughening behaviour of rubber-modified thermoplastic polymers involving very small rubber particles: 1. A criterion for internal rubber cavitation. *Polymer* **1994**, *35* (22), 4743–4749.
21. Cho, K.; Yang, J. H.; Chan Eon, P. The effect of interfacial adhesion on toughening behaviour of rubber modified poly(methyl methacrylate). *Polymer* **1997**, *38* (20), 5161–5167.
22. Cho, K.; Yang, J.; Park, C. E. The effect of rubber particle size on toughening behaviour of rubber-modified poly(methyl methacrylate) with different test methods. *Polymer* **1998**, *39* (14), 3073–3081.
23. Takaki, A.; Yasui, H.; Narisawa, I. Fracture and impact strength of poly(vinyl chloride)/methyl methacrylate/butadiene/styrene polymer blends. *Polym. Eng. Sci.* **1997**, *37* (1), 105–119.
24. Paul, D. R.; Newman, S. *Polymer Blends*; Academic Press: New York, 1978; Vol. 2, pp 100−101.
25. Grijpma, D. W.; Penning, J. P.; Pennings, A. J. Chain entanglement, mechanical properties and drawability of poly(lactide). *Colloid Polym. Sci.* **1994**, *272* (9), 1068–1081.
26. Joziasse, C. A. P.; Veenstra, H.; Grijpma, D. W.; Pennings, A. J. On the chain stiffness of poly(lactide)s. *Macromol. Chem. Phys.* **1996**, *197* (7), 2219–2229.
27. Cooper-White, J. J.; Mackay, M. E. Rheological properties of poly(lactides). Effect of molecular weight and temperature on the viscoelasticity of poly(l-lactic acid). *J. Polym. Sci., Part B: Polym. Phys.* **1999**, *37* (15), 1803–1814.
28. Wu, S. Control of intrinsic brittleness and toughness of polymers and blends by chemical structure: A review. *Polym. Int.* **1992**, *29* (3), 229–247.
29. Gramlich, W. M.; Robertson, M. L.; Hillmyer, M. A. Reactive compatibilization of poly(L-lactide) and conjugated soybean oil. *Macromolecules* **2010**, *43* (5), 2313–2321.
30. Grijpma, D. W.; Pennings, A. J. (Co)polymers of L-lactide, 2. Mechanical properties. *Macromol. Chem. Phys.* **1994**, *195* (5), 1649–1663.
31. Ito, M.; Abe, S.; Ishikawa, M. The fracture mechanism of polylactic acid resin and the improving mechanism of its toughness by addition of acrylic modifier. *J. Appl. Polym. Sci.* **2010**, *115* (3), 1454–1460.

Downloaded by UNIV OF GUELPH LIBRARY on August 28, 2012 | http://pubs.acs.org
Publication Date (Web): August 16, 2012 | doi: 10.1021/bk-2012-1105.ch003

Downloaded by NORTH CAROLINA STATE UNIV on August 28, 2012 | http://pubs.acs.org
Publication Date (Web): August 16, 2012 | doi: 10.1021/bk-2012-1105.ch004

Chapter 4

Biobased Polymeric Materials Prepared from Cotton Byproducts

H. N. Cheng,*,1 Michael K. Dowd,1 and Atanu Biswas2

**1Southern Regional Research Center, USDA Agricultural Research Service,
1100 Robert E. Lee Blvd., New Orleans, LA 70124, U.S.A.
2National Center for Agricultural Resource Utilization, USDA Agricultural
Research Service, 1815 N. University Street, Peoria, IL 61604, U.S.A.
*E-mail: hn.cheng@ars.usda.gov**

Cotton burr and cottonseed hull are relatively inexpensive natural renewable materials from cotton and cottonseed processing. Recently several new polymer applications have been reported involving these byproducts. These new developments are briefly reviewed in this article. In the first application, the cotton byproducts have been used directly as fillers in poly(lactic acid) and low-density polyethylene composites. The composites have been prepared by melt blending and extrusion. The addition of these low-cost fillers has slightly changed the composite's thermal properties but significantly affected the composite's mechanical properties. In the second application, the cotton byproducts have been partly converted into cellulose esters without prior chemical breakdown or physical separation of cellulose, lignin, protein, and other components. The process entails treating these materials with acetic anhydride and iodine, with no solvent involved except during sample workup. In the third application, these materials have been partly converted into carboxymethyl cellulose and carboxymethyl xylan. Potential uses of these materials are discussed.

Not subject to U.S. Copyright. Published 2012 by American Chemical Society
In Biobased Monomers, Polymers, and Materials; Smith, P., et al.;
ACS Symposium Series; American Chemical Society: Washington, DC, 2012.

Downloaded by NORTH CAROLINA STATE UNIV on August 28, 2012 | http://pubs.acs.org
Publication Date (Web): August 16, 2012 | doi: 10.1021/bk-2012-1105.ch004

Introduction

In the past several years there have been a lot of research activities to use natural renewable materials to develop new polymeric products and processes (*1–11*). One of the promising approaches is to utilize agricultural byproducts and wastes as raw materials. In this regard, the byproducts from cotton and cotton processing, such as gin trash, cotton burr, and cottonseed hull, seem attractive. Cotton burr is a byproduct of cotton harvesting and ginning and is often used as fuel for boilers or occasionally as mulch (*12–15*). Cottonseed hull is a byproduct of cottonseed oil extraction and is currently used as roughage in animal feed, as a garden or field mulch, or as a component of the growth media for mushroom production (*12*, *13*). Both materials are readily available and inexpensive.

Recently there have been several reports describing the use of cotton burr and cottonseed hull in polymer applications. In the first application, these materials have been ground into powder and used as fillers in polymer composites (*16*). In the second application, these materials have been chemically converted into cellulose acetates (*17*) and mixed esters (*18*). In the third application, these materials have been converted into cellulose and hemicellulose ethers (*19*). These developments are briefly reviewed in this article.

Polymer Composites

For composite formation (*16*), powdered burr and hull were separately mixed with PLA and LDPE and extruded into ribbons. The scanning electron microscopy (SEM) photomicrographs of the fracture surfaces of PLA, LDPE, and their composites are shown in Figure 1. PLA itself had a smooth fracture surface, but the surfaces of the PLA-burr and PLA-hull composites were more irregular, reflecting the topography of the fillers. In contrast, the LDPE surface appeared somewhat wrinkled; with the fillers, the surface became rougher, with some evidence of polymer-filler separation.

In general, the mechanical properties of PLA (tensile strength, elongation at breakage, and Young's modulus) were reduced by addition of the fillers (Table 1). Maleic anhydride (MA) and peroxide are sometimes used to compatibilize polymer and filler; however, in this case, MA and Lupersol 101 peroxide (L101) caused further reduction in mechanical properties. As for thermal properties, PLA exhibited the expected glass transition (T_g) of ~57 °C, melting temperature (T_m) of ~156 °C, a broad exothermic cold crystallization peak (T_{cc}) starting at ~107 °C, and a low degree of crystallinity (χ_c), consistent with similar values reported in the literature (*20–22*). With filler addition, T_g was reduced, T_m was broadened and shifted to lower temperature, T_{cc} became larger and occurred at lower temperature, and χ_c increased (Table 1). Increasing the amount of filler material in the formulation, either burr or hull, tended to increase the differences, and the use of MA and L101 increased the differences even further. In view of similar effects observed for several other fillers in PLA (*23–25*), the broadening of the peak associated with melting may be due to the presence of different crystallite sizes or levels of crystal perfection as a result of burr addition. The decrease in T_{cc} and the increase in χ_c suggest that filler particles are acting as nucleating sites that enhance cold crystallization (*23–25*). These observations imply some interactions between filler particles and PLA.

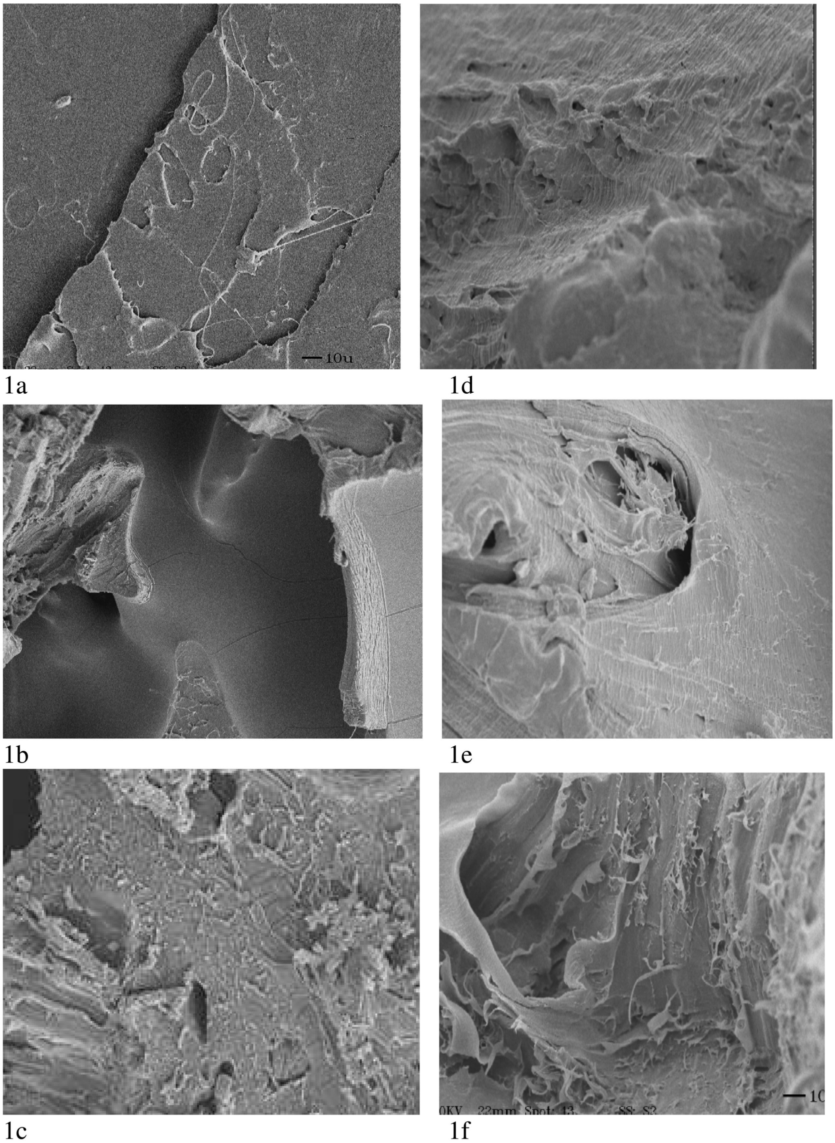

1a 1d

1b 1e

1c 1f

Figure 1. SEM photomicrographs at 500X of PLA by itself (1a), PLA with 20% burr (1b), PLA with 20% hull (1c); LDPE by itself (1d), LDPE with 20% burr (1e), and LDPE with 20% hull (1f). Reproduced with permission from ref. (16). Copyright 2011 Elsevier.

Downloaded by NORTH CAROLINA STATE UNIV on August 28, 2012 | http://pubs.acs.org
Publication Date (Web): August 16, 2012 | doi: 10.1021/bk-2012-1105.ch004

The addition of cotton fillers to LDPE modestly reduced the tensile strength but more severely reduced the elongation of the composite materials (Table 2). The addition of fillers to LDPE, however, increased Young's modulus, the effect being stronger for the addition of burr than for the addition of hull. The effects of MA and L101 were relatively minor. Addition of the fillers to LDPE had relatively small effects on the thermal properties of the composites compared with the thermal effects observed with the addition of fillers to PLA. When fillers were added to LDPE without MA and L101, T_m was almost constant. In the presence of MA and L101, T_m was reduced by at best 1 to 2 °C. Moreover, ΔH_m decreased and χ_c decreased modestly with added filler, and these changes were more pronounced as more filler was added. The use of MA and L101 perhaps slightly increased ΔH_m and χ_c in some composites compared with the same formulation without the added agents. The relatively small impact of fillers on the thermal properties of polyethylene has also been observed with other filler materials (*26*, *27*).

An advantage of using cotton byproducts as fillers in polymers is to decrease the cost. For PLA, the fillers perhaps can be used in applications where cost reduction is important and reduced mechanical properties are acceptable. Possible examples are biodegradable and compostable plastics, such as agricultural mulch films, compost bags, and perhaps disposable dinnerware. As for LDPE, the addition of burr or hull filler materials to LDPE increases the composite material's Young's modulus. Thus for applications needing a stiffer polyethylene at reduced cost, the use of these fillers might be beneficial.

Cellulose Esters

Another method to increase the value of cotton byproducts is to derive chemically modified products from them. Iodine-catalyzed acetylation reaction has been reported earlier (*28*, *29*) and used for cotton byproducts (*17*), e.g.,

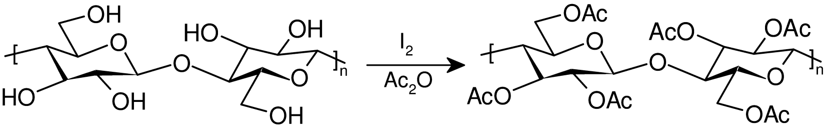

The reaction was conducted with acetic anhydride in the presence of iodine and heat. At 80°C, product yield depended on iodine and acetic anhydride levels (Table 3, samples H1 through H5). As the yield increased, the degree of substitution (DS) tended to decrease. This was probably a result of the crystalline structure of cellulose, which would tend to resist chemical reaction. Thus, acetylation started at amorphous region, and once acetylation took place on an anhydroglucose unit, that same unit became more susceptible to further acetylation reaction, thereby leading to a larger DS. At 100°C, a notable increase in the product yield and a relatively high DS were observed (sample H6). The higher temperature apparently allowed the hull cellulose molecules to be more accessible to acetylation reaction. At 120°C, however, cellulose hydrolysis began

In Biobased Monomers, Polymers, and Materials; Smith, P., et al.;
ACS Symposium Series; American Chemical Society: Washington, DC, 2012.

Downloaded by NORTH CAROLINA STATE UNIV on August 28, 2012 | http://pubs.acs.org
Publication Date (Web): August 16, 2012 | doi: 10.1021/bk-2012-1105.ch004

to become apparent, leading to products with a lower yield and a DS greater than 3.0 (sample H7). Thus, there was an optimal temperature window (at around 100°C) for the acetylation of cottonseed hulls.

The observed product yields from cotton burr also depended strongly on iodine and acetic anhydride levels at 80°C (Table 4, samples B1 through B4). Compared with hull samples, burr seemed to be more susceptible to acetylation (cf. the yields of samples B3 and B4 versus samples H-3 and H-5). At 100°C, burr also showed an increase in yield and DS, similar to what was observed in hull. At 120°C, cellulose hydrolysis became significant with DS exceeding 3.0 and decreasing yield. The optimal temperature for cottonseed burr acetylation was also ~100°C. Because hull or burr contains about 30% cellulose, the maximum weight yield observed (34-37%) corresponds to a conversion and recovery of a significant fraction of the cellulose in each cotton byproduct.

The cellulose in cottonseed hull and burr can also be converted to higher alkyl and mixed cellulose esters using the same reaction; in particular, cellulose acetate propionate and cellulose acetate butyrate have been prepared and characterized in this way (*18*). There are several advantages of using cotton byproducts, such as lower cost and relative ease of reaction. Thus, in this process no prior chemical breakdown or physical separation of cellulose, lignin, protein, and other components is needed. Furthermore, the process entails no solvent during the reaction step, thereby potentially decreasing manufacturing hazards.

Downloaded by NORTH CAROLINA STATE UNIV on August 28, 2012 | http://pubs.acs.org
Publication Date (Web): August 16, 2012 | doi: 10.1021/bk-2012-1105.ch004

Polysaccharide Carboxymethyl Ethers

Another way to derivatize polysaccharides is to form ether derivatives. Indeed, carboxymethyl derivatives have been made earlier from cotton byproducts (*19*), e.g.,

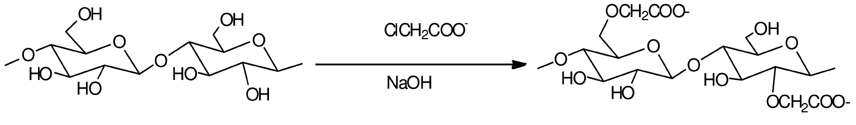

The reaction procedure employed sodium monochloroacetate as the alkylation reagent following standard protocols (*30–33*), and the chemistry was conducted on hull (**H1** and **H2**) and burr (**B1**-**B3**) samples ground to different particle sizes. For comparative purposes, a purified cellulose sample (C) was also treated as a control case (Table 5). As expected, the product derived from the cellulose control was fully water soluble. Reaction of hull (**H1** and **H2**) and burr (**B1**, **B2**, and **B3**) samples yielded water soluble and insoluble fractions, indicating that some components of the samples were recalcitrant to reaction. The weight % of insoluble material from the cotton products was about the same in most of the burr and hull fractions (35-45% of the initial mass).

Downloaded by NORTH CAROLINA STATE UNIV on August 28, 2012 | http://pubs.acs.org
Publication Date (Web): August 16, 2012 | doi: 10.1021/bk-2012-1105.ch004

Table 1. Mechanical and thermal properties of poly(lactic acid) (PLA) and PLA composites formed with cotton burrs and cottonseed hulls[a][b]

PLA:filler:MA:L101	*Thickness (mm)*	*TS (N/mm^2)*	*E (%)*	*YM (MPa)*	T_g (°C)	T_{cc} (°C)	T_m (°C)	ΔH_{cc} (J/g)	ΔH_m (J/g)	χ_c (%)
100 : 0	1.83 (0.10)	62 (2)	16 (1)	550 (19)	58.9	109	156.0	-9	10	2
Burr Filler										
90 : 10	1.64 (0.05)	39 (1)	9 (1)	529 (18)	56.3	107	154.0	-8	14	7
80 : 20	1.90 (0.10)	15 (1)	7 (1)	318 (9)	55.3	104	153.2	-12	19	9
90 : 10 : 2 : 0.5	1.85 (0.08)	24 (3)	9 (1)	362 (36)	54.0	102	153.4	-11	17	8
90 : 10 : 4 : 0.5	2.02 (0.08)	15 (0)	8 (1)	292 (23)	48.0	95	147.4, 153.5	-22	28	8
80 : 20 : 2 : 0.5	1.89 (0.05)	16 (1)	7 (1)	346 (19)	53.8	100	151.4, 154.7	-14	22	11
80 : 20 : 4 : 0.5	1.91 (0.06)	16 (1)	7 (1)	328 (12)	50.8	95	149.2, 154.2	-18	27	13
Hull Filler										
90 : 10	1.88 (0.12)	36 (3)	9 (1)	504 (46)	56.6	105	154.7	-10	13	3
80 : 20	1.76 (0.10)	29 (3)	8 (1)	506 (32)	54.6	103	152.0	-15	22	9
90 : 10 : 2 : 0.5	1.95 (0.05)	19 (1)	8 (1)	338 (14)	51.0	98	149.2, 154.5	-14	23	11
90 : 10 : 4 : 0.5	2.03 (0.05)	15 (2)	8 (2)	284 (16)	46.5	91	144.0, 152.0	-20	31	14
80 : 20 : 2 : 0.5	1.93 (0.05)	18 (3)	8 (2)	350 (6)	51.6	100	150.5, 154.9	-10	20	13
80 : 20 : 4 : 0.5	2.14 (0.05)	11 (1)	7 (1)	254 (9)	47.2	91	145.9, 152.7	-16	28	17

[a] Standard deviations are in parentheses. [b] Data adapted from ref. (*16*); TS = tensile strength, E = elongation during breakage, YM = Young's modulus; the explanation of other acronyms is given in the text.

Downloaded by NORTH CAROLINA STATE UNIV on August 28, 2012 | http://pubs.acs.org
Publication Date (Web): August 16, 2012 | doi: 10.1021/bk-2012-1105.ch004

Table 2. Mechanical and thermal properties of low density polyethylene (LDPE) and LDPE composites formed with cotton burrs and cottonseed hulls[a,b]

LDPE:filler:MA:L101	*Thickness (mm)*	*TS (N/mm^2)*	*E (%)*	*YM (MPa)*	*T^m (°C)*	*ΔH_m (J/g)*	*χ_c (%)*
100 : 0	3.78 (0.11)	9 (1)	549 (128)	44 (3)	110.5	120	40
Burr Filler							
90 : 10	2.97 (0.25)	7 (0)	83 (16)	54 (5)	110.5	102	38
80 : 20	2.40 (0.09)	7 (0)	38 (8)	68 (5)	111.9	89	37
60 : 40	1.97 (0.12)	7 (0)	21 (6)	109 (22)	111.9	71	39
90 : 10 : 2 : 0.5	3.47 (0.23)	8 (0)	76 (22)	55 (5)	109.2	102	39
90 : 10 : 4 : 0.5	4.08 (0.38)	8 (0)	111 (38)	51 (3)	109.9	103	40
80 : 20 : 2 : 0.5	3.08 (0.14)	7 (0)	52 (13)	58 (5)	111.2	82	35
80 : 20 : 4 : 0.5	3.13 (0.16)	7 (1)	52 (8)	56 (3)	109.7	103	45
Hull Filler							
90 : 10	4.01 (0.08)	7 (0)	110 (23)	51 (2)	111.2	106	39
80 : 20	3.42 (0.13)	6 (0)	68 (9)	54 (7)	110.4	88	37
60 : 40	2.34 (0.14)	4 (0)	40 (5)	61 (6)	112.0	49	27
90 : 10 : 2 : 0.5	4.70 (0.18)	7 (1)	108 (32)	48 (3)	110.0	102	39
90 : 10 : 4 : 0.5	4.59 (0.13)	8 (0)	109 (9)	51 (3)	111.0	100	39

Continued on next page.

Downloaded by NORTH CAROLINA STATE UNIV on August 28, 2012 | http://pubs.acs.org
Publication Date (Web): August 16, 2012 | doi: 10.1021/bk-2012-1105.ch004

Table 2. (Continued). Mechanical and thermal properties of low density polyethylene (LDPE) and LDPE composites formed with cotton burrs and cottonseed hulls[a,b]

LDPE:filler:MA:L101	*Thickness (mm)*	*TS (N/mm²)*	*E (%)*	*YM (MPa)*	T_m *(°C)*	ΔH_m *(J/g)*	χ_c *(%)*
80 : 20 : 2 : 0.5	3.98 (0.31)	7 (0)	64 (8)	55 (3)	110.2	85	37
80 : 20 : 4 : 0.5	4.24 (0.48)	6 (0)	54 (9)	53 (5)	109.9	78	34

[a] Standard deviations are in parentheses. [b] Data adapted from ref. (*16*); TS = tensile strength, E = elongation during breakage, YM = Young's modulus; the explanation of other acronyms is given in the text.

Downloaded by NORTH CAROLINA STATE UNIV on August 28, 2012 | http://pubs.acs.org
Publication Date (Web): August 16, 2012 | doi: 10.1021/bk-2012-1105.ch004

Table 3. Iodine-catalyzed acetylation reaction of cottonseed hull, reacted for 20-24 hours[a]

No.	*wt (g)*			*temp (°C)*	*yield*[b] *wt %*	DS_{tot}	DS_6	DS_2	DS_3
	hull	I_2	Ac_2O						
H1	0.57	0.04	3.8	80	1	2.03	0.67	0.69	0.68
H2[c]	0.57	0.08	1.9	80	1	1.98	0.65	0.68	0.65
H3	0.57	0.16	3.8	80	7	1.46	0.45	0.46	0.48
H4	0.57	0.16	0.95	80	2	1.91	0.62	0.69	0.60
H5	0.57	0.32	0.95	80	6	1.69	0.56	0.58	0.55
H6[c]	0.57	0.32	1.9	100	34 [d]	2.03	0.69	0.68	0.66
H7	0.57	0.32	1.9	120	9	3.56	nd [e]	nd	nd

[a] Data taken with permission from ref. (*17*). [b] observed weight of product versus weight of starting hull. [c] Average for duplicate runs. [d] 22% of theoretical yield of cellulose acetate with DS 2.03. [e] nd = not determined.

Table 4. Iodine-catalyzed acetylation reaction of cotton burr, reacted for 20-24 hours[a]

No.	*wt (g)*			*temp (°C)*	*yield[b] wt %*	*DS$_{tot}$*	*DS$_6$*	*DS$_2$*	*DS$_3$*
	hull	*I$_2$*	*Ac$_2$O*						
B1	0.57	0.04	3.8	80	0.4	1.87	0.34	0.30	0.23
B2	0.57	0.08	3.8	80	1	1.66	0.50	0.63	0.53
B3	0.57	0.16	3.8	80	16	1.01	0.38	0.36	0.27
B4	0.57	0.32	0.95	80	18	1.98	0.67	0.66	0.65
B5[c]	0.57	0.32	1.9	100	37 [d]	2.09	0.70	0.70	0.69
B6	0.57	0.32	1.9	120	7	3.84	nd [e]	nd	nd

[a] Data taken with permission from ref. (*17*). [b] observed weight of product versus weight of starting burr. [c] Average for duplicate runs. [d] 24% of theoretical yield of cellulose acetate with DS 2.09. [e] nd = not determined.

Downloaded by NORTH CAROLINA STATE UNIV on August 28, 2012 | http://pubs.acs.org
Publication Date (Web): August 16, 2012 | doi: 10.1021/bk-2012-1105.ch004

Downloaded by NORTH CAROLINA STATE UNIV on August 28, 2012 | http://pubs.acs.org
Publication Date (Web): August 16, 2012 | doi: 10.1021/bk-2012-1105.ch004

Table 5. Yields of water-soluble and water-insoluble fractions from the carboxymethylation of cotton hull and burr fractions[a]

No.	*starting wt (g)*	*water soluble*		*water insoluble*		*total obs'd yield*[b] *%*	*% theoretical yield*[c]
		wt (g)	*obs'd wt %*	*wt (g)*	*obs'd wt %*		
C	5.00	4.5	90	0	0	90	62
H1	5.00	1.8	36	2.2	44	80	68
H2	5.00	2.8	55	2.0	40	95	79
B1	4.64	1.3	28	1.7	36	64	56
B2	5.41	1.6	29	1.9	35	64	55
B3	5.00	1.7	35	2.2	45	80	69

[a] Data taken with permission from ref. (*19*). [b] observed product weight versus weight of starting material. [c] calculated on the assumption of total conversion of cellulose to CMC, sodium salt (DS 0.7), and xylan to CMX, sodium salt (DS 0.4). All hemicellulose is assumed to be xylan. All other components (lignin, lipid, protein, water, inorganics) are considered unchanged and not removed.

The soluble fractions of the reacted hull and burr samples, yielded solution ^{13}C NMR spectra similar to the spectra of reference carboxymethyl cellulose (CMC) and carboxymethyl xylan (CMX) samples (Figure 2). The spectra indicate that these cotton products consist mainly of CMC and CMX.

Thus, with relatively standard procedures, roughly 30% of cotton burr and 45% of cottonseed hull can be converted into soluble carboxymethylated products. These products are readily soluble in water and form films when dried. These materials might be useful as low-cost replacements for CMC or for applications where the properties of CMX are preferred. The insoluble burr and hull products were only slightly carboxymethylated, and they can perhaps be used in conventional applications, such as a soil conditioner or fertilizer or as a source of roughage for animal feeds.

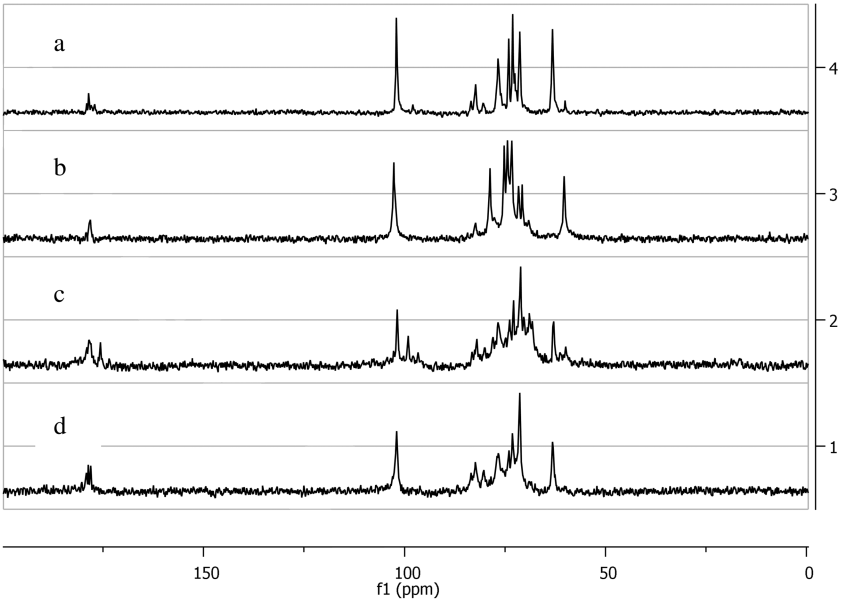

*Figure 2. ^{13}C NMR spectra at 75 MHz in D_2O: a) CMX; b CMC; c) water-soluble fraction of reacted burr sample (**B1**); d) water-soluble fraction of reacted hull sample (**H1**). Reproduced with permission from ref. (19). Copyright 2010 Elsevier.*

Experimental Section

Upland (fuzzy) cottonseed was initially acid delinted in order to remove cellulosic linters and to produce a clean hull material. The seed was then cracked in a Bauer mill, and the hulls were separated by air classification. Cotton burr was obtained as a substantial part of a cotton gin trash sample. Non-burr materials,

Downloaded by NORTH CAROLINA STATE UNIV on August 28, 2012 | http://pubs.acs.org
Publication Date (Web): August 16, 2012 | doi: 10.1021/bk-2012-1105.ch004

such as stem pieces and dried leaves were removed by hand. From proximate analysis (*19*), hull was found to consist of 31% cellulose, 20% hemicellulose, 18% lignin, 2% crude fat, 5% proteins, and 11% moisture. The composition of the burr sample was 31% cellulose, 6% hemicellulose, 17% lignin, 2% crude fat, 8% proteins, and 12% water.

Filler Studies

Both hull and burr samples were ground with a laboratory-scale Wiley mill to pass through the mill's 1-mm opening bottom sieve (*16*). Polymer blends were formulated with 10, 20, or 40% of the milled byproduct filler. Each mixture of materials was manually blended and kept in closed double zip-locked bags for 1 day prior to extrusion.

The data shown in Tables 1-2 were produced from polymer and filler particles that were conditioned in a convection oven at 50°C for 3 days to reduce moisture levels. Several samples were also formulated with maleic anhydride and Lupersol 101 peroxide to promote cross-linking and compatibility of the materials.

Composite ribbons were prepared with a single-screw extruder (C. W. Brabender, South Hackensack, NJ) with four temperature zones that were set from the feed end at 150, 165, 165, and 165°C for the PLA blends, and at 110, 120, 115, 110°C for the LDPE blends. A high-shear screw was employed with a 1-in. ribbon slit die. Screw speed was set at 25 rpm. Sample was fed through a feed throat attached to an air chiller. A conveyor belt was used to take up the ribbon at the same speed as the ribbon exited the die plate.

Ribbons were cut into dog-bone specimens with a MS Instrument Inc., punch press. Tensile properties were measured with an Instron Corp. (Norwood, MA) Universal Testing System Model 4201 tensile tester. Tensile strength, Young's modulus, and elongation at breakage were measured with a cross-head speed of 10 mm/min, a gauge length of 7.62 mm, grip distance of 50 mm, and with a 1 kg load. Each sample was tested five times.

Thermal profiles were determined with a PerkinElmer (Waltham, MA) Model DSC-7 calorimeter and a TAC7/DX controller. Powder samples of 2−3 mg were weighed into stainless steel DSC pans. The calorimeter was programmed to increase the temperature from -20 to 180 °C at a rate of 10 °C/min, then decrease the temperature back to -20 °C at a rate of 10 °C/min, then increase the temperature back to 180 °C, again at a rate of 10 °C/min. Data from the second heating cycle were used to determine T_g, T_{cc}, T_m, ΔH_{cc}, ΔH_m and χ_c. Further details are given in the original reference (*16*).

Stretch-fractured samples from the tensile testing were examined with a JEOL (Peabody, MA) Model 6400V scanning electron microscope, operated with an accelerating voltage of 10 kV. Samples were coated with gold with a SPI (West Chester, PA) sputter coater.

Downloaded by NORTH CAROLINA STATE UNIV on August 28, 2012 | http://pubs.acs.org
Publication Date (Web): August 16, 2012 | doi: 10.1021/bk-2012-1105.ch004

Ester Formation

Burr and the hull samples were pulverized with a hammer mill until they passed through a 16-mesh screen (*17*). They were then stored in capped bottles at room temperature. In a typical reaction, 0.57 g of powder sample, 1.9 g of acetic anhydride, and 0.32 g of iodine were heated at 80–100°C for 20–24 h. The reaction mixture was then cooled to room temperature and treated with 2 mL of a saturated solution of sodium thiosulfate while stirring. The mixture changed color from dark brown to colorless, indicating the transformation of iodine to iodide. The mixture was poured into 50 mL of ethanol and stirred for 30 min. The solid, which contained cellulose acetate, was filtered and washed with water and dried in a vacuum oven at 60°C. The cellulose acetate was then dissolved in methylene chloride and filtered. The filtrate was evaporated under vacuum at room temperature. As the solvent evaporated, cellulose acetate formed a film on the sides of the flask. Ethanol was added to remove the film. The film was washed with ethanol and hot water at ca. 85°C and dried. The % yield (at 5% precision) was calculated as the weight of cellulose acetate versus the weight of starting material.

For mixed esters (*18*), the same procedure was used except that after the reaction mixture was poured into 50 mL of ethanol and stirred for 30 min, the solid was filtered and washed successively with water at 100°C and then washed successively with water and ethanol at room temperature. The remaining solid was then dissolved in chloroform, filtered, and the chloroform removed by evaporation.

The DS was determined by ^{1}H NMR (at 5% precision). Samples were dissolved in $CDCl_3$. Spectra were collected on a Bruker DRX400 spectrometer.

Ether Formation

Burr and hull samples were milled with a kitchen blender (*19*). Hull was separated into a fine powder that passed through the 20-mesh sieve (**H1**) and a medium-sized powder that passed through the 7-mesh sieve but was retained on the 20-mesh sieve (**H2**). Burr was fractioned into a fine powder that passed through the 20-mesh sieve (**B1**), a medium-sized powder that passed the 7-mesh sieve but was retained on the 20-mesh sieve (**B2**) and a coarse fraction that was retained on the top of the 7-mesh sieve (**B3**).

The reaction procedure consisted of three steps (*19*). First, 5 g of ground cotton byproducts was suspended in 125mL of 80% (v/v) isopropanol/water into which 5–6 g of sodium hydroxide was dissolved. The mixture was stirred overnight at room temperature. An alkylation solution was prepared by dissolving 8–12 g of sodium monochloroacetate in 10 mL isopropanol with a minimal amount of water added to facilitate dissolution. The alkylation solution was added slowly to the cellulose/isopropanol sample over a 30-min period, after which the mixture was purged with nitrogen and maintained at 50°C for 2–3 h. The reaction was then stopped by cooling and filtered to separate the solids. The solids was suspended in 70% ethanol/water, neutralized with glacial acetic acid, washed, and refiltered three times with 70% ethanol/water to remove unreacted reagent and salt. The remaining material was then dispersed in 200mL water. For the ground cotton byproducts, this resulted in soluble and insoluble fractions.

Downloaded by NORTH CAROLINA STATE UNIV on August 28, 2012 | http://pubs.acs.org
Publication Date (Web): August 16, 2012 | doi: 10.1021/bk-2012-1105.ch004

The insoluble fraction was separated by filtration, washed with additional water, and dried in a vacuum oven. The soluble material was stripped of water on a rotary evaporator. The % yield (at 5% precision) was calculated as the weight of cellulose acetate divided by the weight of starting material. In addition to the various cotton products, cellulose, xylan, lignin were also carboxymethylated, and the products were used as control materials.

The DS of the CMC was determined by ^{13}C NMR (at 5% precision). Samples were dissolved in D_2O, and spectra were recorded on a Varian Gemini 2000 spectrometer, operating at 75 MHz for ^{13}C.

Downloaded by NORTH CAROLINA STATE UNIV on August 28, 2012 | http://pubs.acs.org
Publication Date (Web): August 16, 2012 | doi: 10.1021/bk-2012-1105.ch004

Acknowledgments

Thanks are due to Janet Berfield (NCAUR) and Catrina Ford (SRRC) for technical work, and Gordon Selling (NCAUR) and Thomas Klasson (SRRC) for encouragement. Mention of trade names or commercial products in this publication is solely for the purpose of providing specific information and does not imply recommendation or endorsement by the U.S. Department of Agriculture. USDA is an equal opportunity provider and employer.

References

1. Mathers, R. T., Meier, M. A. R., Eds.; *Green polymerization methods: Renewable starting materials, catalysis and waste reduction*; Wiley-VCH: Weinheim, Germany, 2011.
2. Cheng, H. N., Gross, R. A., Eds. *Green polymer chemistry: Biocatalysis and Biomaterials*; ACS Symposium Series No. 1043; American Chemical Society: Washington, DC, 2010.
3. Yu, L., Ed.; *Biodegradable polymer blends and composites from renewable resources*; Wiley: Hoboken, NJ, 2009.
4. Belgacem, M. N., Gandini, A., Eds.; *Monomers, polymers and composites from renewable resources*; Elsevier: Oxford, U.K., 2008.
5. Cheng, H. N., Gross, R. A., Eds.; *Polymer Biocatalysis and Biomaterials II*; ACS Symposium Series No. 999; American Chemical Society: Washington, DC, 2008.
6. Luckachan, G. E; Pillai, C. K. S. *J. Polym. Environ.* **2011**, *19*, 637–676.
7. Vroman, I.; Tighzert, L. *Materials* **2009**, *2*, 307–344.
8. Williams, C. K.; Hillmyer, M. A. *Polym. Rev.* **2008**, *48*, 1–10.
9. Gandini, A. *Macromolecules* **2008**, *41*, 9491–9504.
10. Siracusa, V.; Rocculi, P.; Romani, S.; Rosa, M. D. *Trends Food Sci. Technol.* **2008**, *19*, 634–643.
11. Yu, L.; Dean, K.; Li, L. *Prog. Polym. Sci.* **2006**, *31*, 576–602.
12. Bailey, A. E., Ed.; *Cottonseed and Cottonseed Products*; Wiley-Interscience: New York, NY, 1948, pp 873–893.
13. NCPA Publications, National Cottonseed Products Association, Inc., Cordova, TN, 2011. http://www.cottonseed.com/publications/.

14. *Cotton burr compost*; Back to Nature Inc.: Slaton, TX, 2011. www.backtonaturecompost/cbc.html.
15. Thrash, T. K. U.S. Patent 4,670,944, 1987.
16. Sutivisedsak, N.; Cheng, H. N.; Dowd, M. K.; Selling, G. W.; Biswas, A. *Ind. Crops Prod.* **2011**, *36*, 127–134.
17. Cheng, H. N.; Dowd, M. K.; Selling, G. W.; Biswas, A. *Carbohydr. Polym.* **2010**, *80*, 450–453.
18. Cheng, H. N.; Dowd, M. K.; Shogren, R. L.; Biswas, A. *Carbohydr. Polym.* **2011**, *86*, 1130–1136.
19. Cheng, H. N.; Biswas, A. *Carbohydr. Polym.* **2011**, *84*, 1004–1010.
20. Liu, D. Y.; Yuan, X. W.; Bhattacharyya, D.; Easteal, A. J. *Exp. Polym. Lett.* **2010**, *4*, 26–31.
21. Ahmed, J.; Varshney, S. K. *Int. J. Food Prop.* **2009**, *14*, 37–58.
22. Wang, Y.; Mano, J. F. *Eur. Polym. J.* **2005**, *41*, 2335–2342.
23. Shieh, Y.-T.; Liu, G.-L. *J. Polym. Sci., Part B: Polym. Phys.* **2007**, *45*, 1870–1881.
24. Pilla, S.; Gong, S.; O'Neill, E.; Yang, L.; Rowell, R. M. *J. Appl. Polym. Sci.* **2009**, *111*, 37–47.
25. Pilla, S.; Kramschuster, A.; Lee, J.; Clemons, C.; Gong, S.; Turng, L.-S. *J. Mater. Sci.* **2010**, *45*, 2732–2746.
26. Luyt, A. S.; Molefi, J. A.; Krump, H. *Polym. Degrad. Stab.* **2006**, *91*, 1629–1636.
27. Marcovich, N. E.; Villar, M. A. *J. Appl. Polym. Sci.* **2003**, *90*, 2775–2784.
28. Biswas, A.; Selling, G. S.; Shogren, R. L.; Willett, J. L.; Buchanan, C. M.; Cheng, H. N. *Chem. Today* **2009**, *27* (4), 4–6.
29. Biswas, A.; Shogren, R. L.; Willett, J. L. *Biomacromolecules* **2005**, *6*, 1843–1845.
30. Heydarzadeh, H. D.; Najafpour, G. D.; Nazari-Moghaddam, A. A. *World Appl. Sci. J.* **2009**, *6*, 564–569.
31. Choi, Y.; Maken, S.; Lee, S.; Chung, E.; Park, J.; Min, B. *Korean J. Chem. Eng.* **2007**, *24*, 288–293.
32. Adinugraha, M. P.; Marseno, D. W.; Haryadi *Carbohydr. Polym.* **2005**, *62*, 164–169.
33. Dapia, S.; Santos, V.; Parajo, J. C. *Bioresour. Technol.* **2003**, *89*, 289–296.

Downloaded by NORTH CAROLINA STATE UNIV on August 28, 2012 | http://pubs.acs.org
Publication Date (Web): August 16, 2012 | doi: 10.1021/bk-2012-1105.ch004

Downloaded by STANFORD UNIV GREEN LIBR on August 28, 2012 | http://pubs.acs.org
Publication Date (Web): August 16, 2012 | doi: 10.1021/bk-2012-1105.ch005

Chapter 5

Processing, Mechanical Properties, and Structure Analysis of Melt-Spun Fibers of P(3HB)/UHMW-P(3HB) Identical Blend

**Taizo Kabe,[1] Takeharu Tsuge,[2] Takaaki Hikima,[3] Masaki Takata,[4]
Akio Takemura,[1] and Tadahisa Iwata*,[1,4]**

**[1]Graduate School of Agricultural and Life Sciences, The University of
Tokyo, 1-1-1 Yayoi, Bunkyo-ku, Tokyo 113-8657, Japan
[2]Interdisciplinary Graduate School of Science and Engineering,
Tokyo Institute of Technology, 4259 Nagatsuta, Midori-ku,
Yokohama 226-8502, Japan
[3]Research Infrastructure Group, RIKEN Harima Institute/SPring-8 Center,
Kouto, Sayo-cho, Sayo-gun, Hyogo 679-5148, Japan
[4]Structural Materials Science Laboratory, RIKEN Harima Institute,
SPring-8, 1-1-1 Kouto, Sayo-cho, Sayo-gun, Hyogo 679-5148, Japan
*E-mail: atiwata@mail.ecc.u-tokyo.ac.jp**

High tensile strength melt-spun fibers of poly[(*R*)-3-hydroxybutyrate] (P(3HB)) with the addition of a small amount of ultra-high-molecular-weight P(3HB) (UHMW-P(3HB)) were processed by cold-drawing and two-step cold-drawing methods. The mechanical properties and highly ordered structure were investigated by tensile testing, and wide-angle and small-angle X-ray diffraction measurements (WAXD and SAXS) using a synchrotron radiation beam at SPring-8. The molecular weight of P(3HB) decreased drastically within a few minutes during melt-spinning. However, in the case of the blended samples, the degree of molecular weight decrease was slightly reduced by the addition of UHMW-P(3HB). The melt-spun blend fibers stretched at a cold-drawing ratio of 14 showed a tensile strength of 530 MPa. When two-step cold-drawing was applied, the tensile strength increased further to 740 MPa. WAXD and SAXD revealed that the addition of a small amount of UHMW-P(3HB) into P(3HB) induces

In Biobased Monomers, Polymers, and Materials; Smith, P., et al.;
ACS Symposium Series; American Chemical Society: Washington, DC, 2012.

the formation of the β-form (planar zigzag conformation) of molecular chain, increasing the mechanical properties. Based on these results, it seems that the addition of a small amount of UHMW-P(3HB) has a great effect on the thermal stability and processability of melt-spun fibers and increases their final mechanical properties.

Introduction

Poly[(*R*)-3-hydroxybutyrate] (P(3HB)) is produced from renewable carbon resources such as sugar, organic acids or plant oils by a number of microorganisms (*1*, *2*). This polymer is expected to become an alternative to petroleum-based plastics because of its biodegradability and thermoplasticity. However, it is well known that the elongation at break of P(3HB) material is very poor (only 5%), and its mechanical properties degrade with time as a result of secondary crystallization because its glass-transition temperature (T_g) of 4 °C is lower than room temperature (*3*, *4*). For this reason, improvement of the mechanical properties of P(3HB) is of both scientific and practical concern.

Until now, many researchers have tried to prepare high tensile strength fibers of P(3HB) by hot-drawing and cold-drawing methods (*5*–*8*). However, the tensile strengths of the processed fibers were 190-420 MPa, significantly lower than that of petroleum-based plastics such as polypropylene. The major cause of this problem is probably that the melt-spinning temperature of P(3HB) is close to its thermal degradation temperature, and thus thermal degradation occurs during melt-spinning.

Iwata *et al.* reported production of ultra-high-molecular-weight P(3HB) (UHMW-P(3HB)) biosynthesized by using recombinant *Escherichia coli* under specific fermentation conditions and succeeded in obtaining high tensile strength fibers from this UHMW-P(3HB) (*9*). They developed a new drawing method (two-step drawing combined with cold-drawing), and the tensile strength of their UHMW-P(3HB) fiber reached 1,320 MPa, which is higher than that of common plastic fibers. Furthermore, it was revealed by using micro-beam X-ray diffraction that, in this high tensile strength fiber, a new molecular conformation (planar zigzag conformation, *β*-form) was generated at the center part of the fiber, together with the normal molecular conformation (2/1 helix conformation, *α*-form) of P(3HB) (*10*).

However, the biosynthesis of UHMW-P(3HB) using high-density cultivation is very difficult and costly. Accordingly, to use UHMW-P(3HB) efficiently, we report the addition of a small amount of UHMW-P(3HB) into P(3HB), and its effect on thermal properties, melt-spinning processability, and mechanical properties of the P(3HB)/UHMW-P(3HB) identical blend. The highly ordered structure in the P(3HB)/UHMW-P(3HB) blend fibers, which shows two kinds of molecular conformations (*α*-form and *β*-form) was analyzed by wide-angle and small-angle X-ray diffractions using synchrotron radiation at SPring-8. This information will be useful for making P(3HB) fibers with high tensile strength, which is an important step in increasing the industrial use of this polymer.

Downloaded by STANFORD UNIV GREEN LIBR on August 28, 2012 | http://pubs.acs.org
Publication Date (Web): August 16, 2012 | doi: 10.1021/bk-2012-1105.ch005

Downloaded by STANFORD UNIV GREEN LIBR on August 28, 2012 | http://pubs.acs.org
Publication Date (Web): August 16, 2012 | doi: 10.1021/bk-2012-1105.ch005

Experimental Section

Materials

P(3HB) with weight average molecular weight (M_w) = 5.2 × 10^5 and polydispersity (M_w/M_n) = 1.6 was supplied by Monsanto Japan Co. UHMW-P(3HB) with M_w = 3.47 × 10^6 and M_w/M_n = 2.67 was biosynthesized from glucose by recombinant *E. coli* JM109 according to the method of Kahari *et al* (*11*). Both samples were purified by dissolving and precipitating using chloroform and hexane and subsequently dried in vacuum. An identical blend sample consisting of two different molecular weight P(3HB)s was prepared by mixing them in chloroform, followed by precipitating and drying. The composition ratio of UHMW-P(3HB) to P(3HB) was chosen as 5/95.

Melt-Spun Fibers with Cold-Drawing and Two-Step Drawing

The molecular weights of P(3HB)s normally decrease during melt-spinning as a result of the heating process. The change of molecular weight with melt-spinning time and melt-spinning temperature was monitored to determine the optimized melt-spinning conditions. The P(3HB) or blend sample was placed into the spinning apparatus at 180 °C, 190 °C or 200 °C. Die diameter, volume velocity of extruded sample from die, and take-up speed were set at 1 mm, 4 mm^3/s, and 900 mm/s, respectively. The melt-spun fiber was taken up for 1 minute, and the molecular weight was measured using gel permission chromatography (GPC).

The melt-spun fibers were quenched into an ice water bath at around 0 °C to obtain amorphous fibers. These amorphous fibers were then cold-drawn in a water bath at various drawing temperatures (0–8 °C) to various drawing ratios (up to 14 times). Furthermore, two-step cold-drawing (to 2.8 times) was applied to a six times cold-drawn fiber. All drawn fibers were annealed at 80 °C for 30 min in an oven.

Molecular Weight Measurement

Molecular-weight measurements were obtained by GPC at 40 °C, using a Shimadzu 10A GPC system and a 10A refractive index detector with two joint columns of Shodex K-806M and K-802. Chloroform was used as the eluent at a flow rate of 0.8 ml/min, and sample concentrations of 1 mg/ml were used. Polystyrene standards were used to make a molecular-weight calibration curve.

Stress−Strain Test

Mechanical properties of fibers were measured with a tensile tester (EZ-test, Shimadzu Co., Japan) at a cross-head speed of 20 mm/min. The gauge length was 10 mm. These results obtained were averaged over five samples for each condition.

Downloaded by STANFORD UNIV GREEN LIBR on August 28, 2012 | http://pubs.acs.org
Publication Date (Web): August 16, 2012 | doi: 10.1021/bk-2012-1105.ch005

Wide-Angle and Small-Angle X-ray Measurements

The highly ordered structures of the cold-drawn and two-step-drawn fibers were investigated by wide-angle X-ray diffraction (WAXD) and small-angle X-ray scattering (SAXS) using a synchrotron radiation beam. WAXD and SAXS measurements with a wavelength of 0.09 nm at 13.8 keV of synchrotron radiation were carried out at BL45XU beam line at SPring-8, Harima, Japan. The diffraction patterns were recorded with a CCD camera (C7330-12-NR, Hamamatsu Photonics, Japan) with exposure times of 76–1058 ms. The camera lengths for WAXD and SAXS were 126 mm and 2500 mm, respectively.

Results and Discussion

Molecular Weight Changes during Melt-Spinning

Figure 1 shows the changes of weight-average and number-average molecular weights (M_w and M_n) during melt-spinning. Both M_w and M_n decreased drastically within a few minutes, because of thermal degradation of P(3HB). However, the thermal degradation of the blend sample was less than that of the P(3HB).

If the thermal degradation of the P(3HB) molecular chains follows a random cutting model, the number-average degree of polymerization ($P_{n,t}$) at time *t* is given by a reversible reaction with second-order kinetics (Eq. 1) (*12*).

$$\frac{1}{P_{n,t}} = K_d t + \frac{1}{P_{n,0}} \quad \cdot\cdot\cdot (1)$$

In Eq. 1, $P_{n,t}$ and $P_{n,0}$ indicates the number average degree of polymerization at melt-spinning time, 0 and t, respectively. And K_d is a constant of thermal degradation calculated from the slope of 1/ P_n vs melt-spinning time as shown in Figure 1C and F. The K_d values for each sample at various temperatures are summarized in Table I. The K_d value of the blend sample was lower than that of P(3HB) at every melt-spinning temperature. This result indicates that thermal degradation of blend sample was slowed by the addition of a small amount of UHMW-P(3HB).

Optimum Conditions for Melt-Spinning at Various Melt-Spinning Temperatures

It is well known that the melt viscosity of polymers depends on the melt-spinning temperature and melt-spinning time. Table II summarizes the melt-spinning processability of the blend sample at various melt-spinning temperatures. When the melt-spinning temperature was 180 °C, it was impossible to spin the fibers because the “molten” sample remained hard and brittle, indicating that the polymers did not completely melt. When the blend sample was melted at 190 °C, 8 min was required to obtain the melt-spun fibers. At a melt-spinning temperature of 200 °C, 2 min of melting was enough to produce the melt-spun fibers. This melt-spun fiber was easily stretched until a cold-drawing ratio of over 10 times. When the longer melt-spinning time (8 min) was used at 200 °C, continuous spinning was difficult because of the low melt viscosity of the sample. Based on these results, the optimum melt-spinning conditions were selected as 200 °C for 2 min.

Downloaded by STANFORD UNIV GREEN LIBR on August 28, 2012 | http://pubs.acs.org
Publication Date (Web): August 16, 2012 | doi: 10.1021/bk-2012-1105.ch005

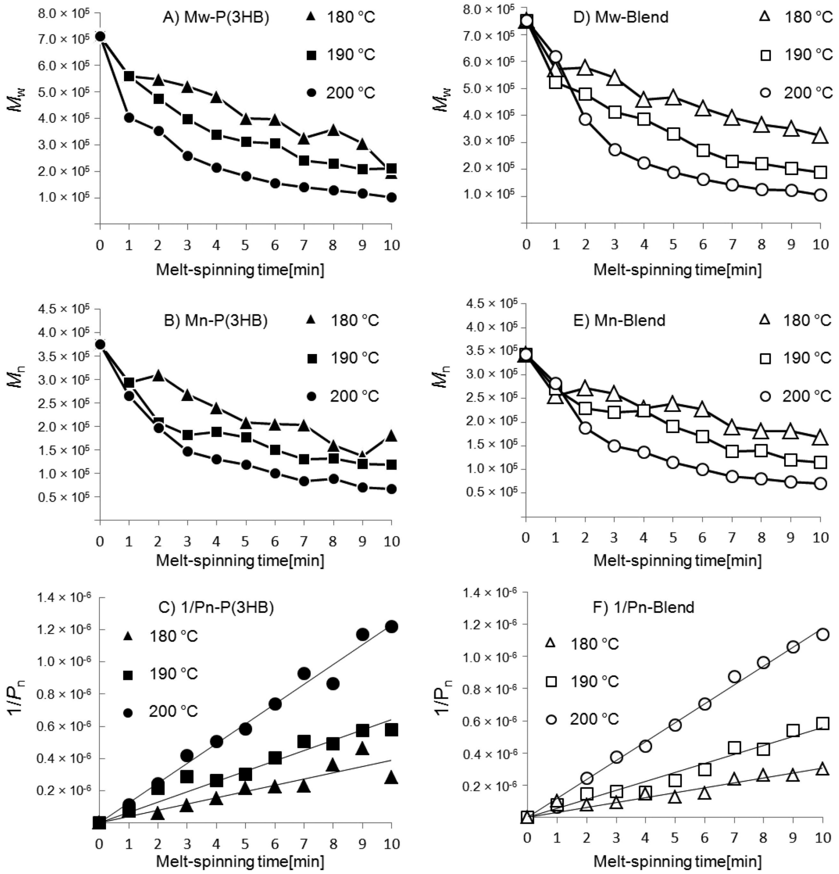

Figure 1. Relationships between molecular weight and melt-spinning time. Left and right columns show results for P(3HB) and the blend, respectively. Weight-average (A, D), and number average (B, E) molecular weights and inverse of number-average degree of polymerization (C, F) are displayed.

Downloaded by STANFORD UNIV GREEN LIBR on August 28, 2012 | http://pubs.acs.org
Publication Date (Web): August 16, 2012 | doi: 10.1021/bk-2012-1105.ch005

Table I. Heat decomposition rate constant of each sample at three temperatures (180, 190, 200 °C), as calculated from the slope of melt-spinning time vs. 1/Mn in Figure 1 (C and F)

Melt-spinning temperature (°C)	*Sample*			
	P(3HB)		*blend*	
180	$(0.323 \pm 0.016) \times 10^{-4}$	min^{-1}	$(0.253 \pm 0.009) \times 10^{-4}$	min^{-1}
190	$(0.533 \pm 0.010) \times 10^{-4}$	min^{-1}	$(0.463 \pm 0.016) \times 10^{-4}$	min^{-1}
200	$(1.021 \pm 0.025) \times 10^{-4}$	min^{-1}	$(0.976 \pm 0.013) \times 10^{-4}$	min^{-1}

Table II. The effects of melt-spinning time and melt-spinning temperature on spinning processability of the blend

Melt-spinning temperature [°C]	*Melt-spinning time [min]*		
	2	*4*	*8*
180	$\times^{a}$	$\times^{a}$	▲
190	$\times^{a}$	▲	○
200	○	○	$\times^{b}$

x^{a}: The melted blend was unable to be spun because that was solid. ▲ : The melted blend was able to be spun but unable to draw. ○ : The melted blend was able to be applied the spinning and drawing. x^{b}: The melted belnd was unable to be spun because the viscosity of that was low.

Effect of Cold-Drawing Temperature on Tensile Strength

Figure 2 shows the tensile strengths of 6 or 12 times cold-drawn blend fibers as a function of the cold-drawing temperature from 0 to 8 °C. Maximum tensile strength appeared when cold-drawing was applied at 4 °C. The T_g of P(3HB) is around 4 °C. Accordingly, cold-drawing at temperatures below T_g did not induce molecular chain orientation because the chain mobility was too low. On the other hand, increasing the cold-drawing temperature seems to accelerate the orientation of molecular chains as a result of increasing molecular chain mobility. However, a high cold-drawing temperature of around 8 °C progresses the growth of crystal nuclei prior to molecular chain orientation. For subsequent experiments, a cold-drawing temperature of 4 °C was selected.

Downloaded by STANFORD UNIV GREEN LIBR on August 28, 2012 | http://pubs.acs.org
Publication Date (Web): August 16, 2012 | doi: 10.1021/bk-2012-1105.ch005

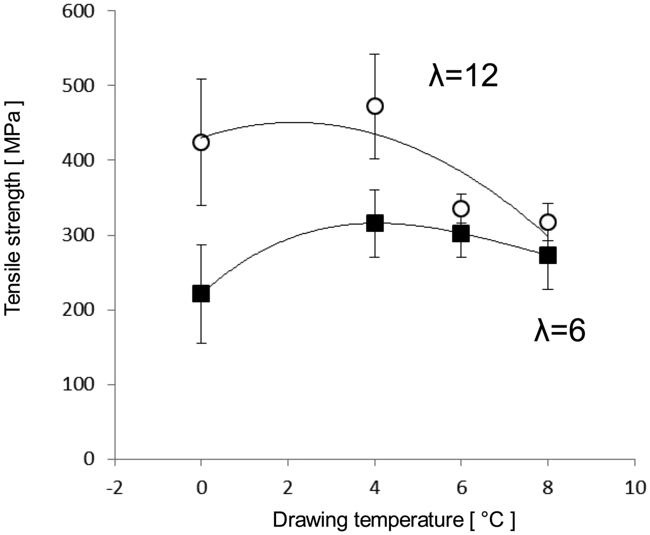

Figure 2. Tensile strength of cold-drawn blend fibers as a function of drawing temperature. Drawing ratios of 6 times and 12 times were used for each sample.

Mechanical Properties of Cold-Drawn and Two-Step-Drawn Fibers

Cold-drawn fibers of both P(3HB) and UHMW-P(3HB)/P(3HB) blend were processed under optimized conditions: melt-spinning temperature (200 °C), melt-spinning time (2 min) and cold-drawing temperature (4 °C). Figure 3 shows the tensile strength of cold-drawn fibers as a function of cold-drawing ratio. Tensile strength increased at cold-drawing ratios of over 4 and 6 for the blend and P(3HB), respectively, suggesting that the addition of a small amount of UHMW-P(3HB) increased the molecular orientation. At a cold-drawing ratio of 14, the tensile strength of the blend and P(3HB) reached 530 MPa and 370 MPa, respectively. Elongation at break and Young's modulus are summarized in Table III.

Figure 4 shows the tensile strength of two-step drawn P(3HB) and blend fibers, as a function of total drawing ratio. Melt-spun fibers were stretched until 6 times at 4 °C in an ice water bath and then two-step cold-drawing was applied until 2.8 times at 8 °C. The two-step drawn fibers were annealed in an oven to fix the two-step drawn molecular chains. Mechanical properties are summarized in Table III. P(3HB) fiber was able to be stretched up to total drawing ratio of 17 and its tensile strength increased to 630 MPa. This value is higher than previously reported (*5–8*). For the two-step drawn blend fibers, the tensile strength further increased to 740 MPa. This value is almost the same as that of common plastic fibers such as polypropylene. This result also indicates that the addition of a small amount of UHMW-P(3HB) contributes to much improved mechanical properties.

Downloaded by STANFORD UNIV GREEN LIBR on August 28, 2012 | http://pubs.acs.org
Publication Date (Web): August 16, 2012 | doi: 10.1021/bk-2012-1105.ch005

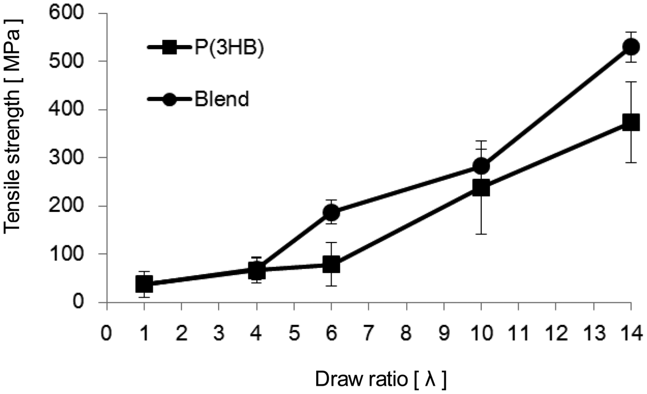

Figure 3. Tensile strength of cold-drawn fibers as a function of drawing ratio.

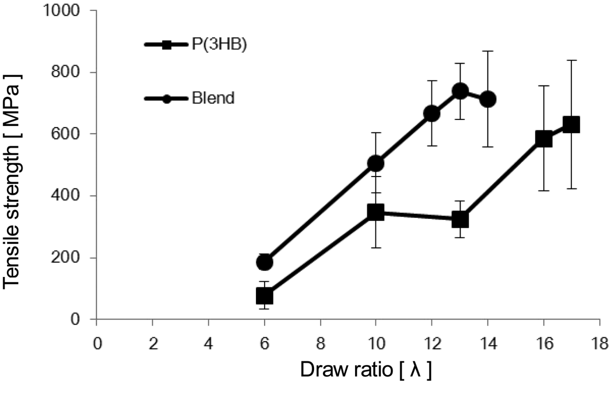

Figure 4. Mechanical properties of P(3HB) and blend fibers prepared by two-step cold-drawing.

Downloaded by STANFORD UNIV GREEN LIBR on August 28, 2012 | http://pubs.acs.org
Publication Date (Web): August 16, 2012 | doi: 10.1021/bk-2012-1105.ch005

X-ray Diffraction and Scattering Measurements

Figure 5 shows WAXD and SAXS of cold-drawn and two-step-drawn P(3HB) and blend fibers. The WAXD and SAXS patterns of undrawn P(3HB) and blend fibers in Figure 5A and B indicate that the molecular chains are slightly oriented in the as-spun fibers. In the case of P(3HB), despite a cold-drawing ratio of 6 times, WAXD and SAXS images were almost the same as those of the as-spun fibers (Figure 5A′ and a′). However, in the case of the blend fiber, one can see a well-oriented diffraction diagram in WAXD (Figure 5B′) and two clear strong reflections along the meridian in SAXS (Figure 5b′), suggesting that molecular chains and lamellar crystals with a 2/1 helix conformation (α-form) (*13*, *14*)are both strongly oriented. Furthermore, a new reflection on the equatorial line indicates that the addition of a small amount of UHMW-P(3HB) induces the planar zigzag conformation (β-form) (*15–17*)in the cold-drawn blend fiber. When 14 times cold-drawing was applied, the WAXD patterns became sharp, indicating highly orientated molecular chains along the cold-drawing direction; the degrees of orientation of P(3HB) and blend fibers are calculated as 0.88 and 0.92, respectively. The intensity of the peaks attributed to the β-form is greater for the blend fiber than for the P(3HB) fiber, suggesting that the addition of a small amount of UHMW-P(3HB) contributes to increased orientation of molecular chains and generation of the planar zigzag conformation. As a result, the mechanical properties are improved.

Until now, it was considered the β-form was generated from the amorphous region between lamellar crystals by two-step cold-drawing (*16*, *17*). However, in this particular cold-drawing process, two-step cold-drawing was not applied. Despite this, in the blend, at a relatively low drawing ratio of 6 times, β-form was generated as shown in Figure 5B′. It is well-known that highly oriented fibers have a shish-kebab structure inside. UHMW-P(3HB) chains seems to be the “shish” region of the shish-kebab structure, which typically consists of extended molecular chains (“shish”) and lamellar crystals (“kebab”) in a three-dimensional structure. The β-form might be generated from the “shish” region of UHMW-P(3HB).

For the two-step drawn blend fibers at a total drawing ratio of 13, the WAXD pattern (Figure 6 B) shows a strong reflection of the β-form compared with that in the cold-drawn fiber (Fig. 5 B″). It turns out that the two-step cold-drawing method promotes the formation β-form and thus improves the mechanical properties. The SAXS pattern of the two-step-drawn blend fiber (Fig. 6 B′) showed a drop-shaped pattern towards the center, which indicates the lengthening of the long period of stacked lamellar crystals by two-step cold-drawing. From these results, it is found that the molecular chains of the P(3HB) in the blend were also oriented highly as a result of the addition of a small amount of UHMW-P(3HB).

Downloaded by STANFORD UNIV GREEN LIBR on August 28, 2012 | http://pubs.acs.org
Publication Date (Web): August 16, 2012 | doi: 10.1021/bk-2012-1105.ch005

Table III. Tensile strengths, Young's modulus, and elongation at break for one- and two-step cold-drawn fibers

Drawing method	*Sample*	*First drawing ratio (λ)*	*Second drawing ratio (λ)*	*Total drawing ratio (λ)*	*Tensile strength (MPa)*	*Elongation at break (%)*	*Young's modulus (GPa)*
one-step cold-drawing	P(3HB)	1	-	1	37 ± 27	9 ± 32	2.49 ± 2.85
		6	-	6	78 ± 45	75 ± 37	3.34 ± 1.64
		14	-	14	370 ± 84	52 ± 45	4.80 ± 4.56
	Blend	1	-	1	37 ± 2	16 ±11	1.44 ± 0.78
		6	-	6	187 ± 25	168 ± 18	2.58 ± 1.73
		14	-	14	530 ± 31	40 ± 12	6.41 ± 0.69
two-step cold-drawing	P(3HB)	6	1	6	78 ± 45	75 ± 37	3.34 ± 1.64
		6	1.7	10	347 ± 114	58 ± 31	4.37 ± 0.86
		6	2.2	13	324 ± 59	50 ± 29	5.04 ± 0.71
		6	2.8	17	630 ± 209	46 ± 18	9.46 ± 4.53
	Blend	6	1	6	187 ± 25	168 ± 18	2.58 ± 1.73
		6	1.6	10	506 ± 97	60 ± 11	5.67 ± 1.32
		6	2.2	13	740 ± 90	50 ± 14	10.6 ± 0.35

Downloaded by STANFORD UNIV GREEN LIBR on August 28, 2012 | http://pubs.acs.org
Publication Date (Web): August 16, 2012 | doi: 10.1021/bk-2012-1105.ch005

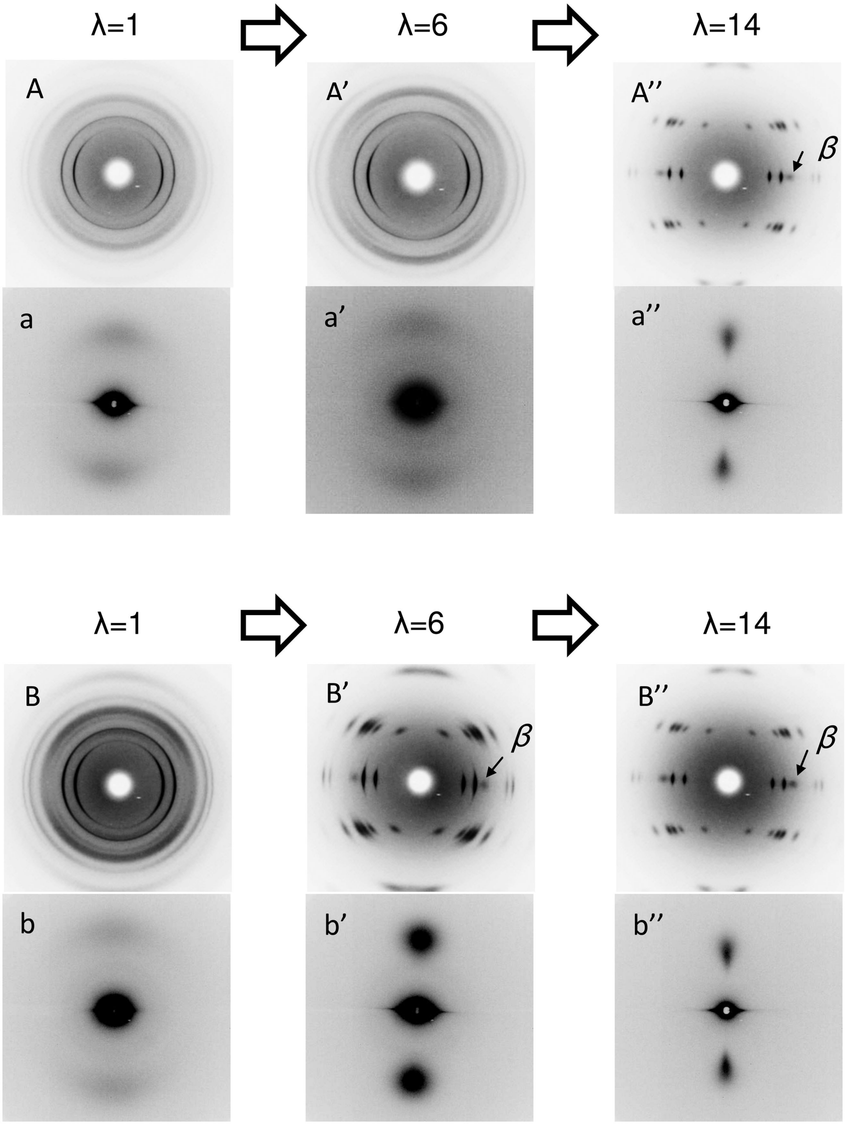

Figure 5. WAXD (capital letters) and SAXS (lower case letters) patterns of cold-drawn fibers. (A,a and (B,b) are P(3HB) and the blend, respectively. Drawing ratios are 6 (') and 14 ('').

Downloaded by STANFORD UNIV GREEN LIBR on August 28, 2012 | http://pubs.acs.org
Publication Date (Web): August 16, 2012 | doi: 10.1021/bk-2012-1105.ch005

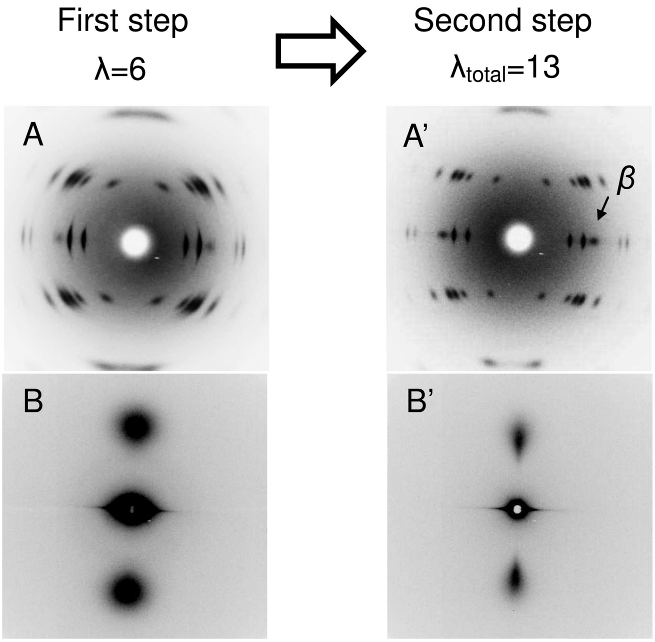

Figure 6. WAXD and SAXS patterns of two-step cold-drawn fibers. (A) and (A'): drawing ratio of 6 (i.e. first step); (B) and (B') two-step cold-drawn fibers with total drawing ratio of 13.

Conclusions

In this paper, the effect of addition of a small amount of UHMW-P(3HB) on the melt-spinning processability, mechanical properties, and highly ordered structure of P(3HB)/UHMW-P(3HB) blend fibers was investigated. The addition of a small amount of UHMW-P(3HB) inhibited the thermal degradation and improved the melt-spinning processability. The tensile strength of the cold-drawn blend fibers is 530 MPa. On the other hand, the two-step-drawn blend fiber had a tensile strength of 740 MPa and Young's modulus of 10.6 GPa together with elongation at break of 50 %. This result indicates that P(3HB) becomes a high tensile strength and high modulus fiber, as well as having adequate elongation at break. WAXD and SAXS measurements showed that the addition of UHMW-P(3HB) to P(3HB) leads to formation of *β*-form crystals at relatively low drawing ratio. This phenomenon seems to be caused by the extended UHMW-P(3HB) molecular chains becoming the "shish" region of the "shish-kebab" structure in the fiber.

Downloaded by STANFORD UNIV GREEN LIBR on August 28, 2012 | http://pubs.acs.org
Publication Date (Web): August 16, 2012 | doi: 10.1021/bk-2012-1105.ch005

Acknowledgments

This work was supported by a Grant-in-Aid for Scientific Research of Japan (A) No.22245026 (2010) and the by New Energy and Industrial Technology Development Organization (NEDO) of Japan.

References

1. Doi, Y. *Microbial polyesters*; VCH Publishers: New York, 1990.
2. Lenz, R. W.; Marchessault, R. H. *Biomacromolecules* **2005**, *6*, 1–8.
3. De Koning, G. J. M.; Lemstra, P. J. *Polymer* **1993**, *19*, 4089–4094.
4. Scandola, M.; Ceccorulli, G.; Pizzoli, M. *Makromol. Chem., Rapid Commun.* **1989**, *10*, 47–50.
5. Gordeyev, S A.; Nekrasov, Yu P. *J. Mater. Sci. Lett.* **1999**, *18*, 1691–1692.
6. Schmack, G.; Jehnichen, D.; Vogel, R.; Tandler, B. *J. Polym. Sci. Part B: Polym. Phys.* **2000**, *38*, 2841–2850.
7. Yamane, H.; Terao, K.; Hiki, S.; Kimura, Y. *Polymer* **2001**, *42*, 3241–3248.
8. Furuhashi, Y.; Imamura, Y.; Jikihara, Y.; Yamane, Y. *Polymer* **2004**, *45*, 5703–5712.
9. Iwata, T.; Aoyagi, Y.; Fujita, M.; Yamane, H.; Doi, Y.; Suzuki, Y. *Macromol. Rapid Commun.* **2004**, *25*, 1100–1104.
10. Iwata, T.; Fujita, M.; Aoyagi, Y.; Doi, Y.; Fujisawa, T. *Biomacromolecules* **2005**, *6*, 1803–1809.
11. Kahar, P.; Agus, J.; Kikkawa; Taguchi, K.; Doi, Y.; Tsuge, T. *Polym. Degrad. Stab.* **2005**, *87*, 161–169.
12. Kunioka, M.; Doi, Y. *Macromolecules* **1990**, *23*, 1933–1936.
13. Okamura, K.; Marchessault, R. H. In *Conformation of Biopolymers*; Romachandra, G. N., Ed.; Academic Press: New York, 1967; Vol. 2, pp 709−720.
14. Yokouchi, M.; Chatani, Y.; Tadokoro, H.; Teranishi, K.; Tani, K. *Polymer* **1973**, *14*, 267–272.
15. Orts, W. J.; Marchessault, R. H.; Bluhm, T. L.; Hamer, G. K. *Macromolecules* **1990**, *23*, 5368–5370.
16. Aoyagi, Y.; Doi, Y.; Iwata, T. *Polym. Degrad. Stab.* **2003**, *79*, 209–216.
17. Iwata, T.; Aoyagi, Y.; Fujita, M.; Yamane, H.; Doi, Y.; Suzuki, Y.; Takeuchi, A.; Uesugi, K. *Macromol. Rapid Commun.* **2004**, *25*, 1100–1104.

Downloaded by OHIO STATE UNIV LIBRARIES on August 28, 2012 | http://pubs.acs.org
Publication Date (Web): August 16, 2012 | doi: 10.1021/bk-2012-1105.ch006

Chapter 6

Biosynthesis of Monomers for Plastics from Renewable Oils

Wenhua Lu,[1] Jon E. Ness,[2] Wenchun Xie,[1] Xiaoyan Zhang,[1] Fei Liu,[1] Jiali Cai,[1] Jeremy Minshull,[2] and Richard A. Gross*,[1]

**[1]Polytechnic Institute of New York University, 6 Metrotech Center,
Brooklyn, NY 11201
[2]DNA2.0 Inc, 1430 O'Brien Drive, Menlo Park, CA 94025
*E-mail: rgross@poly.edu**

Omega-hydroxyfatty acids are excellent monomers for synthesizing a unique family of polyethylene-like biobased plastics. However, ω-hydroxyfatty acids are difficult and expensive to prepare by traditional organic synthesis, precluding their use in commodity materials. Here we report the engineering of a strain of the diploid yeast *Candida tropicalis* to produce commercially viable yields of ω-hydroxyfatty acids. To develop the strain we identified and eliminated 16 genes encoding 6 cytochrome P450s, 4 fatty alcohol oxidases and 6 alcohol dehydrogenases from the *C. tropicalis* genome. We also show that fatty acids with different chain lengths and degrees of unsaturation can be more efficiently oxidized by expressing different P450s within this strain background. Biocatalysis using engineered *Candida tropicalis* is thus a potentially attractive biocatalytic platform for producing commodity chemicals from renewable resources.

Introduction

Poly(ω-hydroxyfatty acids) have the potential to perform as functionally equivalent to versatile plastics like polyethylene while providing other attributes (*1*, *2*). The monomers required to make these polymers are also valuable in chemical products such as lubricants, adhesives, cosmetic ingredients (*3*, *4*) and anti-cancer therapeutics (*5*, *6*). Most work on bioplastics from renewable sources

Downloaded by OHIO STATE UNIV LIBRARIES on August 28, 2012 | http://pubs.acs.org
Publication Date (Web): August 16, 2012 | doi: 10.1021/bk-2012-1105.ch006

has focused on polyhydroxyalkanoates and polylactic acid (*7*, *8*). However, these materials suffer from significant performance deficits that has created difficult challenges to their adoption as general replacements for petroleum-based plastics. Poly(ω-hydroxyfatty acids) appear to overcome the functional limitations of other bioplastics, but the monomers have not been available with economics required for their conversion to commodity plastics (*9*).

In seeking a biological route to production we turned our attention to cytochrome P450s, a powerful and versatile family of enzymes capable of specifically introducing chemical functionality into parts of molecules with low reactivity. Several P450 enzymes are known to hydroxylate aliphatic fatty acids at the omega position (*10–13*). Of particular interest to us were the P450s of *Candida tropicalis* (*14*): a strain of this yeast (H5343) has been engineered to transform fatty acids into α,ω-diacids commercially (*15*), by eliminating the β-oxidation pathway (Figure 1). The key requirement to convert this strain into one capable of producing ω-hydroxyfatty acids is the elimination of enzymes that oxidize the alcohol group (Figure 1); the identity of these enzymes was not known when we began this work.

Fatty alcohol oxidase and inducible wild-type P450 enzymes are generally thought to catalyze the further oxidation of ω-hydroxyfatty acids to α,ω-dicarboxylic acids in *C. tropicalis* (*14*, *16*). However, during the course of this work it was discovered that alcohol dehydrogenases can contribute to the oxidation of ω-hydroxyfatty acids to α,ω-dicarboxylic acids.

Although *C. tropicalis* is an attractive organism for bioprocessing, the relative dearth of established molecular tools to engineer this diploid organism presents serious obstacles to its genetic manipulation. Here we describe the strain and fermentation engineering used to eliminate 16 genes, including cytochrome P450s, fatty alcohol oxidases and alcohol dehydrogenases, to produce strains of *C. tropicalis* capable of converting a range of fatty acids to their corresponding ω-hydroxy fatty acids. A strain that re-reintegrates a select P450 results in the biotransformation of methyl tetradecanoate to 14-hydroxytetradecanoic acid with high yield and purity. Furthermore, when different P450s are integrated into the genome of this strain, different oxidation profiles are obtained from fatty acids with various chain lengths and degrees of unsaturation.

Deletion of Genes from the *C. tropicalis* Genome

DNA constructs for modification of the *C. tropicalis* genome were based on the SAT1-flipper (*17*) and had the general form. The targeting sequences in the deletion constructs were regions ranging in size from 198 bp to 300 bp, identical to the genomic sequences flanking the DNA to be deleted from *C. tropicalis*. For some of the sequences these were based on sequences that had been reported previously (*16*, *18*) : CYP52A17 (GenBank accession AY230504), CYP52A13 (AY230499), CYP52A18 (AY230505), CYP52A14 (AY230500), FAO1 (AY538780), FAO2A (AY538781), FAO2B (AY538782), and CYP52A12 (AY230498).

Downloaded by OHIO STATE UNIV LIBRARIES on August 28, 2012 | http://pubs.acs.org
Publication Date (Web): August 16, 2012 | doi: 10.1021/bk-2012-1105.ch006

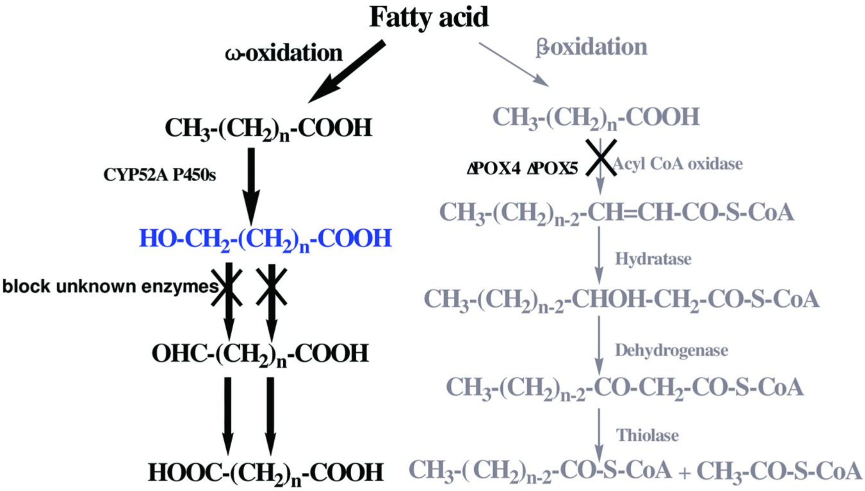
Fatty acid
ω-oxidation
β-oxidation
CH_3-$(CH_2)_n$-COOH
CYP52A P450s
HO-CH_2-$(CH_2)_n$-COOH
block unknown enzymes
OHC-$(CH_2)_n$-COOH
HOOC-$(CH_2)_n$-COOH
CH_3-$(CH_2)_n$-COOH
ΔPOX4 ΔPOX5
Acyl CoA oxidase
CH_3-$(CH_2)_{n-2}$-CH=CH-CO-S-CoA
Hydratase
CH_3-$(CH_2)_{n-2}$-CHOH-CH_2-CO-S-CoA
Dehydrogenase
CH_3-$(CH_2)_{n-2}$-CO-CH_2-CO-S-CoA
Thiolase
CH_3-$(CH_2)_{n-2}$-CO-S-CoA + CH_3-CO-S-CoA

Figure 1. Two pathways for oxidation of fatty acids; the beta oxidation pathway can be blocked by deletion of both copies of the gene encoding the acyl CoA oxidase that catalyzes the first step in the pathway (POX4 and POX5) (15) .

Identification and Deletion of *C. tropicalis* ADH Genes

Two degenerate PCR primers based on the DNA sequences of the structural genes for ADH1A, ADH1B, ADH2A and ADH2B of *C. albicans* (from http://www.candidagenome.org/) were designed to PCR amplify a ~1000 bp fragment corresponding to homologous ADH genes from *C. tropicalis*. These were primers 5′ADH (ACTCAAAAAGCYGTTRTYTTYGAWACCAAYGGTGG) and 3′ADH (GTCCAAKACRTATCTACYCAAGATTTTACCTTCTTC). The primers were used to amplify from genomic DNA isolated from strain H5343 (using the YeaStar™ Genomic DNA Kit from Zymo Research). The resulting amplicon was purified using the QIEXII Gel Purification Kit from Qiagen and cloned. Plasmids were prepared from 96 transformants using Macherey–Nagel‘s Nucleospin Robot 96 plasmid kit and sequenced on an ABI 3730 automated sequencer. For deletion of the first allele of each ADH gene, a targeting construct was created as described above. For the second allele of each, the nested strategy was attempted.

Expression of Synthetic P450s from pXICL

Expression vector pXICL comprised the *C. tropicalis* ICL promoter (*19*), an NcoI site, a stuffer, a NotI site, the *C. tropicalis* ICL transcriptional terminator region, the TEF1 promoter from *S. cerevisiase*, the EM7 prokaryotic promoter, the *Sh ble* gene (which codes for Zeocin™ resistance) recoded for *C. tropicalis*, and the CYC1 transcriptional terminator from *S. cerevisiae*. The sequence of pXICL has been submitted to Genbank (GU046314). Vector pXICL can be propagated in *E. coli* in LB Lennox medium using Zeocin™ at 25 µg/mL. Genes for integration

Downloaded by OHIO STATE UNIV LIBRARIES on August 28, 2012 | http://pubs.acs.org
Publication Date (Web): August 16, 2012 | doi: 10.1021/bk-2012-1105.ch006

into the *C. tropicalis* genome under control of the ICL promoter were optimized for expression in *C. tropicalis* (which uses CUG to encode serine not leucine) and had internal NcoI, NotI and BsiWI sites removed in GeneDesigner (*20*).Prior to transformation into *C. tropicalis*, the vector or its derivatives were linearized at a unique BsiWI site in the ICL promoter region. *C. tropicalis* transformants were selected on YPD agar with Zeocin™ at 200µg/mL. Transformants were screened for integration at ICL by PCR amplification from genomic DNA. Positives were expressed by culturing as described below.

Reactions with Purified Alcohol Dehydrogenase Proteins

Activities of alcohol dehydrogenase from *Saccharomyces cerevisiae* (Cat #: A3263) (from Sigma [St. Louis, MO]) on 12-hydroxydodecanoic acid (Cat #: 198781) and 16-hydroxyhexadecanoic acid (Cat #: H2640) (from Sigma [St. Louis, MO]) were measured by a modification of a previously described procedure (*21*). To a total reaction volume of 6 mL 0.1 M Tris-HCl buffer (pH 9.0) were added 8 mg enzyme, 1 µmol of NAD and 500 µg 12-hydroxydodecanoic acid or 16-hydroxyhexadecanoic acid dissolved in 50 µL of acetone. The reaction was incubated for 1 h at 37 °C. Control reactions without addition of enzyme were performed in parallel. The reaction was terminated by addition of 5 mL 0.1 N HCl. Products were extracted into diethyl ether and formation of fatty aldehydes was determined by ^{1}H NMR and liquid chromatography-mass spectrometry (LC-MS).

Shake-Flask Oxidations of Fatty Acids and ω-Hydroxyfatty Acids by *C. tropicalis*

C. tropicalis strains were precultured in 30 mL YPD medium containing (per liter): yeast extract, 10 g; peptone, 20 g; glucose, 20 g and shaken at 250 rpm, 30 °C for 20 h in 500 mL flask. The cells were inoculated at 10 % (v/v) to 30 mL culture medium consisting of (per liter): peptone, 3 g; yeast extract, 6 g; yeast nitrogen base, 6.7 g; acetic acid, 3 g; K2HPO4, 7.2 g; KH2PO4 9.3 g; glucose, 20 g in 500 ml flask. After 12 h of cultivation at 250 rpm and 30 °C, the biotransformation phase was begun by addition of 30 g/L methyl tetradecanoate. pH was adjusted to 7.5 by addition of 2 mol/L NaOH solution. During the biotransformation, glycerol (50%) was fed (2.5 % per day) as co-substrates and the pH was maintained at ~7.5 by addition of 2 mol/L NaOH solution. For oxidation of ω-hydroxyfatty acids, the preculture of selected *C. tropicalis* strains was diluted in fresh culture medium to A_{600nm} = 1.0, and then continued to cultivate until the A_{600nm} reached to ~5.0. Bioconversion was initiated by adding 5 mL culture to a 125 mL flask together with 50 mg of ω-hydroxyfatty acid and the pH was adjusted to ~7.5 by addition of 2 mol/L NaOH solution. Samples were taken and acidified to pH ~ 1.0 by addition of 6 N HCl. Products were extracted into diethyl ether and the concentrations of products were measured by LC-MS.

Downloaded by OHIO STATE UNIV LIBRARIES on August 28, 2012 | http://pubs.acs.org
Publication Date (Web): August 16, 2012 | doi: 10.1021/bk-2012-1105.ch006

Fermentation Procedure

Selected *C. tropicalis* strains were precultured in 50 mL YPD medium and shaken at 250 rpm, 30 °C for 20 h in 500 mL flask. The cells were inoculated at 10 % (v/v) into 150 mL of conversion medium containing (per liter): glucose, 30 g; $(NH_4)_2SO_4$, 7 g; KH_2PO_4, 5.1 g; $MgSO_4$, 0.5 g; $CaCl_2$, 0.1 g; citric acid, 0.06 g; biotin, 0.0002 g and 1 mL/L of a trace elements solution (H_3BO_3, 0.9; $CuSO_4$, 0.07; KI, 0.18 g; $FeCl_3$, 0.36; $MnSO_4$, 0.72; Na_2MoO_4, 0.36 g; $ZnSO_4$, 0.72 g) in 400 mL DASGIP parallel magnetic-stirrer fermentors (Figure 4B), or in 700 mL of conversion medium in 1.5 L DASGIP parallel over-head driver fermentors (Fig 4C). The cultures were grown at 30 °C at an aeration rate of 1.0 vvm up to 16 hrs as growth phase. The pH was maintained at 6.0 by automatic addition of 6 mol/L NaOH or 2 mol/L H_2SO_4 solutions. Dissolved oxygen was maintained at 70% saturation by agitation and O_2-cascade control mode. After 6 h growth, ethanol was fed into the cell culture to 5 g/L. During the conversion phase, 80% glycerol was fed as co-substrate by dissolved oxygen-stat control mode (the high limit of dissolved oxygen was 75% and low limit of dissolved oxygen was 70%). Temperature was maintained at 35°C for conversion of methyl octadecanoate (C18:0) and 30 °C for the rest of fatty acid substrates (methyl tetradecanoate, methyl hexadecanoate, *cis*-9-octadecenoic acid and *cis*,*cis*-9,12-octadecadienoic acid). Every 12 h, ethanol was added into cell culture to 2 g/L, and substrate was added to 20 g/L or 40 g/L until its total concentration added reached to the predetermined value. To measure the substrate and product concentrations, 2 mL samples were acidified to pH ~ 1.0 by addition of 6 N HCl, extracted into diethyl ether and analyzed by LC-MS. The product concentration (g/L), conversion efficiency (mol-% conversion of substrate to ω-hydroxyfatty acid or α,ω-dicarboxylic acid) and productivity (g/L/h) data were normalized to the initial culture volume by correcting volume change associated with addition of acid, base, glycerol and substrate to the fermentor, to allow an accurate comparison between fermentations.

Liquid Chromatography-Mass Spectrometry

The concentrations of fatty acids, ω-hydroxyfatty acids and α,ω-dicarboxylic acids were measured by LC-MS with authentic reference compounds (obtained from Sigma [St. Louis, MO]) or purified products as standards. Suberic acid was used as internal standard. The solvent delivery system was a Waters Alliance 2795 Separation Module (Milford, MA, USA) coupled with a Waters 2996 photodiode array detector and Waters ZQ detector with an electron spray ionization mode. The separation was carried on a reversed-phase column with dimensions of 150 x 4.6 mm and particle size 5 µm. The mobile phase used for separation contained 10% H_2O, 5% acetonitrile, 5% formic acid solution (1% in water) and 80% methanol.

Downloaded by OHIO STATE UNIV LIBRARIES on August 28, 2012 | http://pubs.acs.org
Publication Date (Web): August 16, 2012 | doi: 10.1021/bk-2012-1105.ch006

Results and Discussion

C. tropicalis converts fatty acids in fermentation media to the corresponding α,ω-dicarboxylic acids, but these are further oxidized to acetyl CoA by the β-oxidation pathway (Figure 1) . Commercially useful levels of α,ω-dicarboxylic acids can be produced from n-alkanes and fatty acids by strains where the first step in β-oxidation is blocked by disruption of the POX4 and POX5 allelic gene pairs encoding acyl coenzyme A oxidases (*15*, *22*) *C. tropicalis* strain H5343 in which β-oxidation is blocked, and which can therefore produce high levels of α,ω-dicarboxylic acids from fatty acids, is thus an attractive starting point for engineering a strain to produce ω-hydroxy fatty acids from renewable sources. Creation of such a strain requires the additional disruption of the enzymes that catalyze the transformation of ω-hydroxy fatty acids to α,ω-dicarboxylic acids.

We initially believed that the enzymes responsible for fatty alcohol oxidation in *C. tropicalis* were inducible cytochrome P450s and fatty alcohol oxidases (FAOs) (*14*, *16*). Therefore, we began our strain construction by deleting from strain H5343 2 allelic pairs of P450s, CYP52A13/CYP52A14 and CYP52A17/CYP52A18: these genes are transcribed during growth on fatty acids (*18*) and their encoded enzymes are known to oxidize fatty acids to dicarboxylic acids (*14*). Genes were deleted by synthesizing 5' and 3' sequences from the target gene, and placing between them two frt sites flanking genes encoding flp recombinase and nourseothricin resistance (*17*). The construct was transformed into *Candida tropicalis*, chromosomal integrants were selected on nourseothricin, the site of integration was confirmed by PCR, and the resistance gene was removed by induction of the recombinase, allowing the use of the same strategy for an unlimited number of genes. Genotypes of strains produced in this study are shown graphically in Figure 2. Strain DP174, in which the four P450 genes had been deleted, was no longer capable of significant fatty acid oxidation (Figure 3A). However, when we grew DP174 in the presence of an ω-hydroxyfatty acid, it oxidized that substrate to the diacid almost as rapidly as the starting strain (Figure 3B), indicating that these P450 genes are responsible for oxidation of the fatty acids to ω-hydroxyfatty acids, but they are not required for subsequent oxidation to the diacids.

To eliminate ω-hydroxyfatty acid oxidation we deleted a further P450 (CYP52A12) that is also induced in *C. tropicalis* upon growth on fatty acids (*18*), as well as the three known fatty alcohol oxidase genes: an allelic pair and a single gene. We also reasoned that because *C. tropicalis* is diploid, there was probably an allelic copy of both CYP52A12 and the unpaired fatty alcohol oxidase (FAO1). We therefore also created constructs to eliminate these two unknown genes. However, we were disappointed to find that strain DP283, lacking 6 CYP450s and 4 FAOs, was almost as active as the starting strain at oxidizing ω-hydroxy fatty acids (Figure 3C).

We next turned our attention to alcohol dehydrogenase (ADH) genes. Although no alcohol dehydrogenases had been sequenced from *C. tropicalis*, it has been reported that alcohol dehydrogenases expressed in the mammalian liver catalyze the metabolism of long chain ω-hydroxyfatty acids to their corresponding fatty acid aldehydes (*21*) and that *Saccharomyces cerevisiae* ADH I and II can

Downloaded by OHIO STATE UNIV LIBRARIES on August 28, 2012 | http://pubs.acs.org
Publication Date (Web): August 16, 2012 | doi: 10.1021/bk-2012-1105.ch006

oxidize long chain alcohols to their corresponding aldehydes (*23*). Based on these reports, we performed an *in vitro* analysis to determine whether a yeast alcohol dehydrogenase from *S. cerevisiae* could oxidize ω-hydroxyfatty acids. LC-MS analysis of reaction products showed that this enzyme catalyzed the conversion of ~25 mol% 12-hydroxydodecanoic acid and ~50 mol% 16-hydroxyhexadecanoic acid to their corresponding fatty aldehydes during one hour incubations (Figure 3D). Because alcohol dehydrogenases are highly expressed enzymes in yeast (*24*), we reasoned that alcohol dehydrogenases could be responsible for some of the ω-hydroxyfatty acid oxidation in *C. tropicalis*.

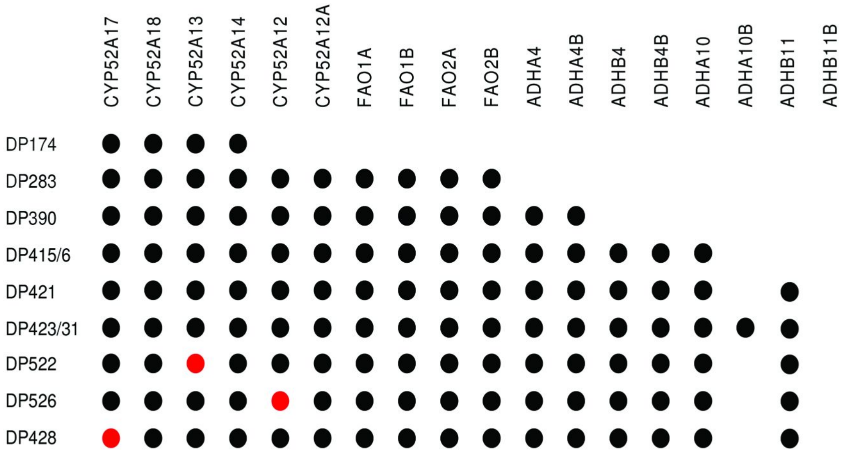

	CYP52A17	CYP52A18	CYP52A13	CYP52A14	CYP52A12	CYP52A12A	FAO1A	FAO1B	FAO2A	FAO2B	ADHA4	ADHA4B	ADHB4	ADHB4B	ADHA10	ADHA10B	ADHB11	ADHB11B
DP174	●	●	●	●														
DP283	●	●	●	●	●	●	●	●	●	●								
DP390	●	●	●	●	●	●	●	●	●	●	●	●						
DP415/6	●	●	●	●	●	●	●	●	●	●	●	●	●	●	●			
DP421	●	●	●	●	●	●	●	●	●	●	●	●	●	●	●		●	
DP423/31	●	●	●	●	●	●	●	●	●	●	●	●	●	●	●	●	●	
DP522	●	●	🔴	●	●	●	●	●	●	●	●	●	●	●	●		●	
DP526	●	●	●	●	🔴	●	●	●	●	●	●	●	●	●	●		●	
DP428	🔴	●	●	●	●	●	●	●	●	●	●	●	●	●	●		●	

Figure 2. Genotypes of strains where black dots indicate deleted genes, red dots indicate deleted wild-type versions of the genes, with a synthetic copy integrated under control of the ICL promoter.

To identify *C. tropicalis* ADH genes we synthesized degenerate oligonucleotide primers based on known sequences of ADHs from *Candida albicans* (*25*, *26*), used these primers to PCR amplify gene fragments out of *C. tropicalis* genomic DNA and cloned the amplicons into *E. coli*. We sequenced 96 clones and about a third of the clones (32 clones) were highly homologous to *C. albicans* ADHs. From these, 5 unique sequences were identified: ADH-A10 (GU056283), ADH-B11 (GU056287), ADH-B2 (GU056285), ADH-A4 (GU056282), and ADH-B4 (GU056286). Translation of the ADH-B2 sequence showed it to contain two in frame stop codons; it is therefore almost certainly a pseudogene. The remaining 4 sequences ADH-A4 and ADH-B4 had the most similar amino acid sequences (87%). In contrast, ADH-A4 was 94% identical to *C. albicans* ADH1A, ADH-B4 was 89% identical to *C. albicans* ADH2A. We therefore concluded that each of the four sequences ADH-A10, ADH-B11, ADH-A4, and ADH-B4 probably represented different *C. tropicalis* ADH genes rather than allelic pairs, and thus each probably had an allelic partner whose sequence was too similar to have been distinguished in the initial set of 32 sequences.

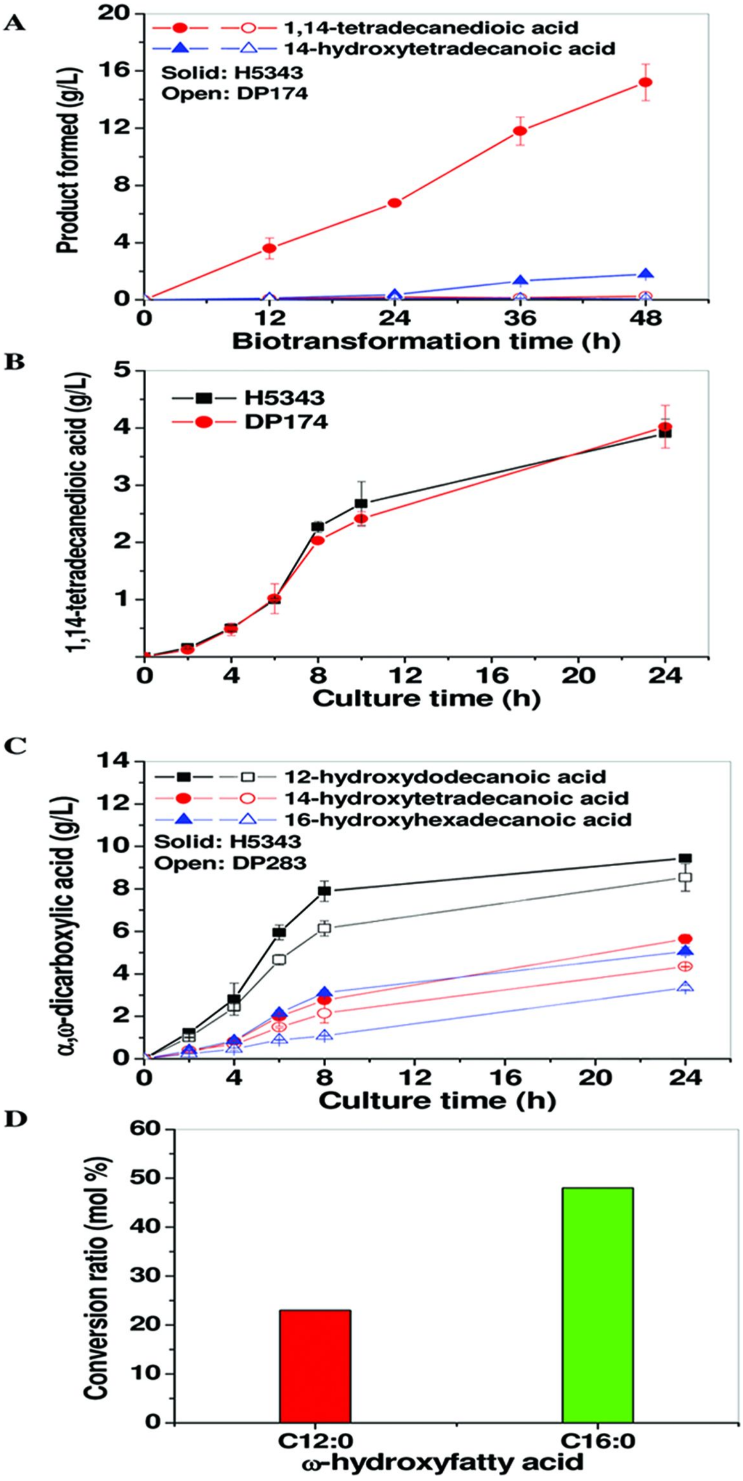

Downloaded by OHIO STATE UNIV LIBRARIES on August 28, 2012 | http://pubs.acs.org
Publication Date (Web): August 16, 2012 | doi: 10.1021/bk-2012-1105.ch006

Downloaded by OHIO STATE UNIV LIBRARIES on August 28, 2012 | http://pubs.acs.org
Publication Date (Web): August 16, 2012 | doi: 10.1021/bk-2012-1105.ch006

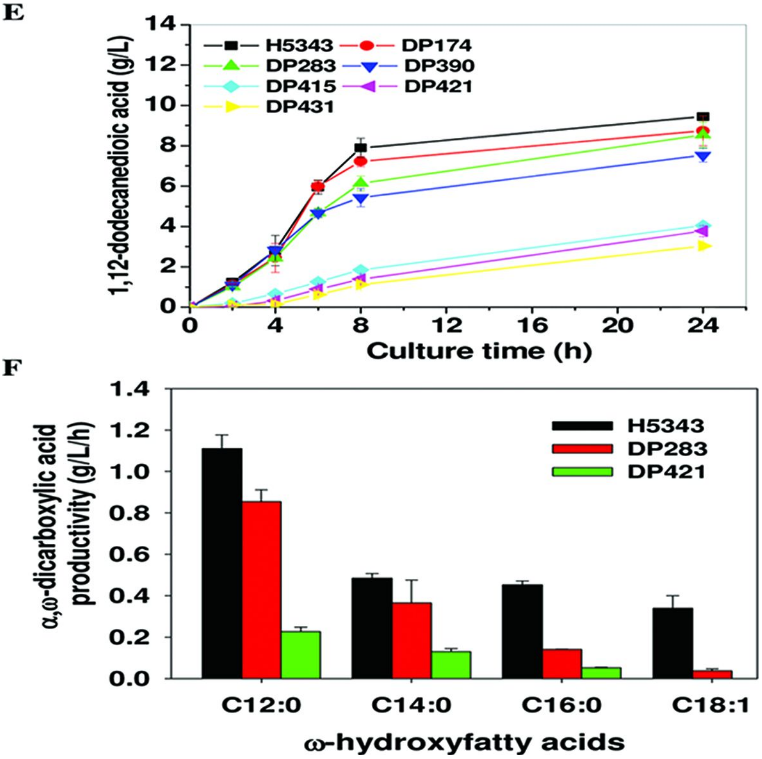

Figure 3. Oxidation of fatty acids and ω-hydroxyfatty acids by engineered strains of Candida tropicalis. (A) Oxidation of tetradecanoic acid to 14-hydroxytetradecanoic acid and 1,14-tetradecanedioic acid by C. tropicalis strains H5343 and DP174. (B) Oxidation of 14-hydroxytetradecanoic acid to 1,14-tetradecanedioic acid by C. tropicalis strains H5343 and DP174. (C) Oxidation of 12-hydroxydodecanoic acid, 14-hydroxytetradecanoic acid and 16-hydroxyhexadecanoic acid to the corresponding α,ω-dicarboxylic acids by C. tropicalis strains H5343 and DP283. (D) Oxidation of 12-hydroxydodecanoic acid and 16-hydroxyhexadecanoic acid to their corresponding fatty aldehydes by purified S. cerevisiae ADH protein. (E) Oxidation of 12-hydroxydodecanoic acid to 1,12-dodecanedioic acid by C. tropicalis strains lacking P450, FAO and ADH genes. (F) Oxidation of 12-hydroxydodecanoic acid, 14-hydroxytetradecanoic acid and 16-hydroxyhexadecanoic acid and 18-hydroxy-9-cis-octadecenoic acid by strains H5343, DP283 and DP421. Oxidation of fatty acids or hydroxyfatty acids by C. tropicalis strains (parts A, B, C, E and F): strains were pre-cultured to A600nm ~5.0 in shake flasks, bioconversion was initiated by addition of substrate and products measured (8 hours of incubation time for part F). Oxidation of hydroxyfatty acids by purified S. cerevisiae ADH protein was performed in an aqueous solution media containing 0.1M Tris-HCl buffer (pH 9.0) with 166 μM NAD. In all cases products were acidified, extracted into diethyl ether and analyzed by LC-MS. The error bars represent the range from two independent experiments.

Downloaded by OHIO STATE UNIV LIBRARIES on August 28, 2012 | http://pubs.acs.org
Publication Date (Web): August 16, 2012 | doi: 10.1021/bk-2012-1105.ch006

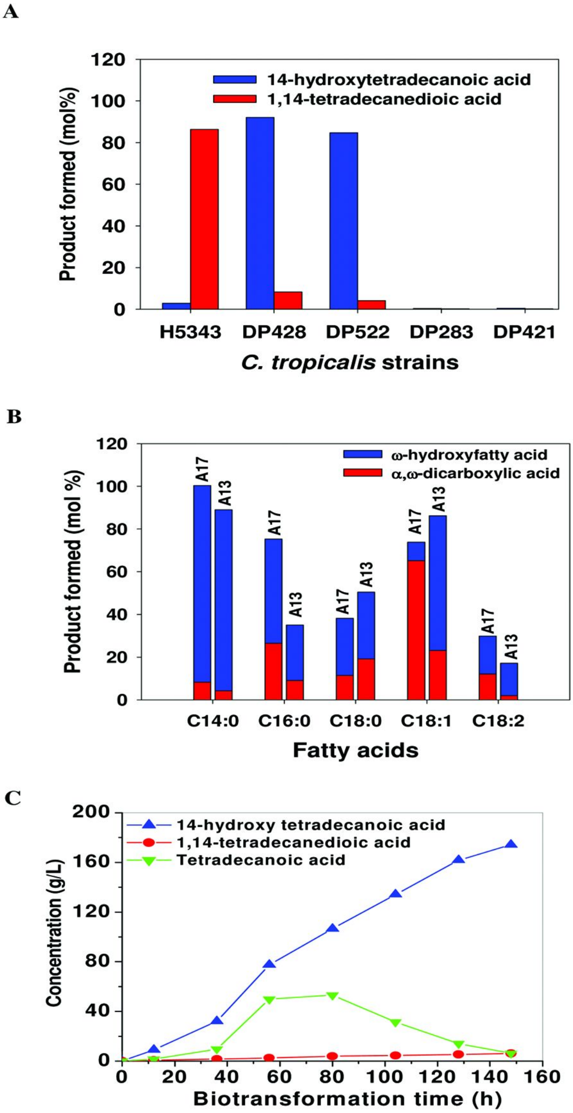

Figure 4. Production of ω-hydroxyfatty acids by engineered Candida tropicalis. Genotypes are as shown in Figure 2. (A) Conversion of tetradecanoic acid (30 g/L) to 14-hydroxytetradecanoic acid and 1,14-tetradecanedioic acid by engineered strains of C. tropicalis. (B) Oxidation of fatty acids (40 g/L) with different chain lengths and degrees of unsaturation by DP428 (CYP52A17) and DP522 (CYP52A13). (C) Conversion of tetradecanoic acid (200 g/L) to 14-hydroxytetradecanoic acid by strain DP428 in a fermentor.

Downloaded by OHIO STATE UNIV LIBRARIES on August 28, 2012 | http://pubs.acs.org
Publication Date (Web): August 16, 2012 | doi: 10.1021/bk-2012-1105.ch006

To eliminate both alleles of each of these 4 alcohol dehydrogenase genes we synthesized a pair of nested knockout constructs for each gene. Following each deletion we tested the ability of the resulting strain to oxidize ω-hydroxy fatty acids to α,ω-dicarboxylic acids. As we deleted each of the *C. tropicalis* ADH genes, we tested the strains for their ability to oxidize 12-hydroxydodecanoic acid. Figure 3E shows that strain DP390, in which the first pair of ADH alleles had been eliminated, oxidized 12-hydroxydodecanoic acid more slowly than DP174 and the starting strain. Progressive deletion of additional ADHs further decreased the rate of oxidation of 12-hydroxydodecanoic acid (Figure 3E, strain genotypes are shown in Figure 2). Strains DP431, in which the second allele of ADH-A10 was deleted appeared much less healthy than the other deletions with smaller colonies and much slower growth times.

We therefore selected strain DP421, lacking both alleles of two of the ADHs (A4 and B4) and one allele of each of the other 2 (A10 and B11), for further development, as it appeared as healthy as the starting strain. In shake flasks, strain DP421 oxidized 12-hydroxydodecanoic acid, 14-hydroxytetradecanoic acid and 16-hydroxyhexadecanoic acid to 12%, 27% and 11%, respectively, of the levels observed after 8 h of incubation time by strain H5343, and almost no oxidation of 18-hydroxy-9-*cis*-octadecenoic acid (ω-OH-C18:1) was detected (Figure 3F).

The deletion of genes to create strain DP421 greatly reduced the oxidation of ω-hydroxyfatty acids, but the elimination of P450 genes also blocked the ω-hydroxylation of fatty acids by this strain. To restore fatty acid ω-hydroxylation activity, we integrated different P450s back into the genome under control of the isocitrate lyase (ICL) promoter; in *C. tropicalis* this promoter is induced by growth with fatty acids, acetate, or ethanol (*19*). We used Gene Designer software (*20*) to design codon-optimized versions of CYP52A17 and CYP52A13 that were synthesized and independently integrated into strain DP421 under control of the ICL promoter to generate strains DP428 and DP522, respectively (Figure 2). Both DP428 and DP522 oxidized tetradecanoic acid in shake flasks to primarily 14-hydroxytetradecanoic acid. In contrast, the starting strain (H5343) yielded primarily 1,14-tetradecanedioic acid, while strains lacking P450s did not oxidize the substrate at all (Figure 4A).

The aim of this work was to develop a general biological route to production of ω-hydroxyfatty acids. Thus, information was needed on the degree to which the oxidation pathway of engineered strains was substrate specific. To accomplish this, the *in vivo* activities and selectivity's of strains DP428 or DP522, carrying the P450's CYP52A17 and CYP52A13, respectively, was assessed by feeding to cultures substrate fatty acids with different carbon chain lengths and unsaturation levels (Figure 4B). Both CYP52A17 and CYP52A13 were capable of efficient ω-hydroxylation of tetradecanoic acid with little dicarboxylic acid formation. However, with longer chain saturated and unsaturated fatty acids, the two strains harboring CYP52A17 and CYP52A13 differed significantly in the efficiency of substrate conversion, indicating that at least some substrate specificity of the pathway resides in the P450 catalyzing the initial oxidation. We also observed that strain DP522 generally yielded a higher ratio of hydroxyfatty acid to dicarboxylic acid. This difference was particularly marked with *cis*-9-octadecenoic acid (C18:1), where DP522 (CYP52A13) produced ω-hydroxyfatty acid and the dicarboxylic acid at a ratio of ~ 5:2, while DP428 (CYP52A17) produced these same products at a ratio of ~ 1:7.5. These results clearly demonstrate that some ω-hydroxyfatty acid oxidation is catalyzed by the P450 itself. It therefore appears that manipulation of substrates transformed and products made by *Candida tropicalis* can be accomplished by introduction into a DP421 background of the appropriate P450, either from a wild type gene from another organism, or by introducing genes encoding artificially engineered enzymes (*27*, *28*).

Finally, we wished to determine whether the *C. tropicalis* platform that we developed could produce commercially useful yields of ω-hydroxyfatty acids. By moving from shake flasks to a fermentor and optimizing growth and transformation conditions, DP428 (carrying CYP52A17) produced yields of over 160 g/L of 14-hydroxytetradecanoic acid, with less than 5% formation of the corresponding dicarboxylic acid (Figure 4C).

Downloaded by OHIO STATE UNIV LIBRARIES on August 28, 2012 | http://pubs.acs.org
Publication Date (Web): August 16, 2012 | doi: 10.1021/bk-2012-1105.ch006

Conclusion

C. tropicalis is an attractive organism for biotransformations: it grows robustly and tolerates high concentrations of substrates which it takes up readily. We created a strain of *C. tropicalis* capable of producing high levels of ω-hydroxyfatty acids by engineering a 90% reduction in the activity of the endogenous pathways that normally metabolize these compounds to diacids. The strain engineering was achieved by identifying target sequences using PCR with degenerate primers based on known *C. tropicalis* and *C. albicans* genes, then eliminating these genes with a 2-step genome modification method that allows indefinite reuse of the same selective marker (*17*).

In preparation for weaning ourselves from a petrochemical society in which the infrastructure for extraction of energy from fossil fuels effectively subsidizes the production of plastics, it is important to develop alternatives that can be synthesized from renewable materials without compromising performance.

The strains described in this report provide the foundation for development of low-cost industrial processes that substitute for chemical approaches to synthesize ω-hydroxy fatty acids.Posssible future modifications include genomic integration of genes for secreted lipases into *C. tropicalis* to allow the direct conversion of natural triglyceride oils to fatty acid substrates and, ultimately, the introduction of pathways for the overproduction of fatty acids by *C tropicalis* itself. Through further P450 engineering and fermentation optimization we expect to achieve high levels of product formation thereby providing a low-cost source of ω-hydroxyfatty acids for a variety of uses. Of particular interest to us is the conversion of ω-hydroxy fatty acids into a family of biobased plastics. Previous work on poly(ω-hydroxypentadecanoate) from a monomer that is just one methylene longer than 14-hydroxytetradecanoic acid has shown that plastics from these monomers are hard, tough materials with an elastic modulus and yield parameters intermediate between low and high density polyethylene (*2*). Polymers from ω-hydroxyfatty acids also present appealing recycling options: conversion of poly(ω-hydroxyfatty acids) to their corresponding alkyl ester monomer units by either a chemical or biological process would result in a biofuel similar in structure to biodiesels such as Soy Gold.

Acknowledgments

We gratefully acknowledge the financial support from the DARPA/DSO under grant BAA 04-12.

References

1. Ceccorulli, G.; Scandola, M.; Kumar, A.; Kalra, B.; Gross, R. A. *Biomacromolecules* **2005**, *6*, 902–907.
2. Focarete, M. L.; Scandola, M.; Kumar, A.; Gross, R. A. *J. Polym. Sci., Part B: Polm. Phys.* **2001**, *39*, 1721–1729.
3. Rawlings, A. V. *Int. J. Cosmet. Sci.* **2003**, *25*, 63.
4. Vandamme, E. J.; Soetaert, W. *J. Chem. Technol. Biotechnol.* **2002**, *77*.
5. Abe, A.; Sugiyama, K. *Anti-Cancer drugs* **2005**, *16*, 543–549.
6. Pohl, E. E.; Voltchenko, A. M.; Rupprecht, A. *BBA-Biomembranes* **2008**, *1778*, 1292–1297.
7. Mehta, R.; Kumar, V.; Bhunia, H.; Upadhyay, S. N. *Polym. Rev.* **2005**, *45*, 325–349.
8. Sudesh, K.; Abe, H.; Doi, Y. *Prog. Polym. Sci.* **2000**, *25*, 1503–1555.
9. Stephan, M. M. S.; Mohar, B. *Org. Process Res. Dev.* **2006**, *10*, 481–483.
10. Bambal, R. B.; Hanzlik, R. P. *Arch. Biochem. Biophys.* **1996**, *334*, 59–66.
11. Hofer, R.; Briesen, I.; Beck, M.; Pinot, F.; Schreiber, L.; Franke, R. *J. Exp. Bot.* **2008**, *59*, 2347.
12. Kitazume, T.; Yamazaki, Y.; Matsuyama, S.; Shoun, H.; Takaya, N. *Appl. Microbiol. Biotechnol.* **2008**, *79*, 981–988.
13. Powell, P. K.; Wolf, I.; Lasker, J. M. *Arch. Biochem. Biophys.* **1996**, *335*, 219–226.
14. Eschenfeldt, W. H.; Zhang, Y.; Samaha, H.; Stols, L.; Eirich, L. D.; Wilson, C. R.; Donnelly, M. I. *Appl. Environ. Microbiol.* **2003**, *69*, 5992–5999.
15. Picataggio, S.; Rohrer, T.; Deanda, K.; Lanning, D.; Reynolds, R.; Mielenz, J.; Eirich, L. D. *Nat. Biotechnol.* **1992**, *10*, 894–898.
16. Eirich, L. D.; Craft, D. L.; Steinberg, L.; Asif, A.; Eschenfeldt, W. H.; Stols, L.; Donnelly, M. I.; Wilson, C. R. *Appl. Environ. Microbiol.* **2004**, *70*, 4872–4879.
17. Reuß, O.; Vik; Kolter, R.; Morschhäuser, J. *Gene* **2004**, *341*, 119–127.
18. Craft, D. L.; Madduri, K. M.; Eshoo, M.; Wilson, C. R. *Appl. Environ. Microbiol.* **2003**, *69*, 5983–5991.
19. Umemura, K.; Atomi, H.; Kanai, T.; Teranishi, Y.; Ueda, M.; Tanaka, A. *Appl. Microbiol. Biotechnol.* **1995**, *43*, 489–492.
20. Villalobos, A.; Ness, J. E.; Gustafsson, C.; Minshull, J.; Govindarajan, S. *BMC Bioinf.* **2006**, *7*, 285.
21. Bjorkhem, I. *Eur. J. Biochem.* **1972**, *30*, 441–451.

Downloaded by OHIO STATE UNIV LIBRARIES on August 28, 2012 | http://pubs.acs.org
Publication Date (Web): August 16, 2012 | doi: 10.1021/bk-2012-1105.ch006

22. Picataggio, S.; Deanda, K.; Mielenz, J. *Mol. Cell. Biol.* **1991**, *11*, 4333–4339.
23. Dickinson, F. M.; Dack, S. *Chem.-Biol. Interact.* **2001**, *130*, 417–423.
24. de Smidt, O.; du Preez, J. C.; Albertyn, J. *FEMS Yeast Res.* **2008**, *8*, 967–978.
25. Bertram, G.; Swoboda, R. K.; Gooday, G. W.; Gow, N. A. R.; Brown, A. J. P. *Yeast* **1996**, *12*, 115–127.
26. Jones, T.; Federspiel, N. A.; Chibana, H.; Dungan, J.; Kalman, S.; Magee, B. B.; Newport, G.; Thorstenson, Y. R.; Agabian, N.; Magee, P. T. *Proc. Natl. Acad. Sci. U.S.A.* **2004**, *101*, 7329.
27. Ehren, J.; Govindarajan, S.; Moron, B.; Minshull, J.; Khosla, C. *Protein Eng. Des. Sel.* **2008**, *21*, 699–707.
28. Liao, J.; Warmuth, M. K.; Govindarajan, S.; Ness, J. E.; Wang, R. P.; Gustafsson, C.; Minshull, J. *BMC Biotechnol.* **2007**, *7*, 16.

Downloaded by OHIO STATE UNIV LIBRARIES on August 28, 2012 | http://pubs.acs.org
Publication Date (Web): August 16, 2012 | doi: 10.1021/bk-2012-1105.ch006

Downloaded by COLUMBIA UNIV on August 28, 2012 | http://pubs.acs.org
Publication Date (Web): August 16, 2012 | doi: 10.1021/bk-2012-1105.ch007

Chapter 7

Synthesis of Biomass-Based Monomers from Biomass-Based Furfural for Polyesters and Evaluation of Their Biomass Carbon Ratios

**Yuya Tachibana,[1] Takashi Masuda,[2] Masahiro Funabashi,[2]
Ken-ichi Kasuya,[1] and Masao Kunioka*,[2]**

**[1]Department of Chemistry and Chemical Biology,
Graduate School of Engineering, Gunma University,
1-5-1 Tenjin, Kiryu, Gunma 376-8515, Japan
[2]National Institute of Advanced Industrial Science and Technology (AIST),
1-1-1 Higashi, Tsukuba, Ibaraki 305-8565, Japan
*E-mail: m.kunioka@aist.go.jp**

Commercially available furfural has been produced from hemicellulose derived from inedible-biomass-based resources, and furfural has been converted into commercially available furan by decarboxylation. These heterocyclic compounds are important chemicals for the production of biomass-based monomers. Oxidation of furfural gave a mixture of maleic acid and FA. These were hydrogenated to give succinic acid. Dimethyl succinate was synthesized from FA by esterification and hydrogenation. These chemicals are useful as biomass-based monomers for biomass-based plastics. Fully biomass-based poly(butylene succinate) (PBS) was obtained by polycondensation of biomass-based 1,4-butanediol and biomass-based succinic acid or dimethyl succinate. Succinic anhydride (SAn) and tetrahydrofuran (THF) were also synthesized from furfural. Fully biomass-based poly(butylene oxide-*co*-butylene succinate) was obtained by ring-opening polymerization of biomass-based SAn and THF. Partially biomass-based poly(butylene terephthalate) was obtained by polycondensation of biomass-based 1,4-butanediol and petroleum-based terephthalic acid. The biomass carbon ratio calculated from ^{14}C concentrations measured by accelerator mass spectroscopy verified that the PBS obtained in this study contained only biomass carbon. The polycondensation of biomass-based 1,4-butanediol and petroleum-based terephthalic acid or dimethyl terephthalate gave partially biomass-based poly(butylene terephthalate), which is an engineering plastic.

Introduction

Biomass-based materials such as wood, silk, and cotton have been used for thousands of years in applications such as buildings, clothing, and furniture. With the development of the petroleum chemical industry, feedstock materials changed from biomass to petroleum, and the level of production has continued to increase. Materials derived from petroleum are used to manufacture plastics. The use of petroleum for plastics production contributes to problems such as global warming caused by CO_2 emissions resulting from the production and incineration of these plastics. Depletion of petroleum supplies is also a problem. Therefore, plastics produced from renewable biomass feedstocks are needed to prevent global warming and to conserve petroleum resources. To reduce the amount of petroleum used for plastics production, plastics-producing companies and research organizations have been developing various biomass-based plastics, and some of these plastics such as poly(lactic acid) (PLA) (*1*, *2*), poly(hydroxylalkanoate) (PHA) (*3–5*), nylon-11 (*6*, *7*), and polyurethane (*8*, *9*) have been used in manufacturing (Table I).

Much attention has been given to PLA produced from corn as a new biomass-based material because of its large-scale production (*1*) and environmentally friendly properties (*2*). The properties of PLA are, however, different from those of commodity plastics like polyethylene, polypropylene, poly(vinyl chloride), and poly(ethylene terephthalate); for example, its physical properties and moldability are inferior to those of commodity plastics. Production companies and researchers have put a great deal of effort into the development of PLA modification technology (*10–13*). A further problem is that PLA is produced from edible biomass. For biomass-based plastics to become widely used, their properties need to be equivalent to those of the commodity plastics currently in use. The best solution would be to produce the commodity plastics currently in use from biomass feedstock. Proposed solutions include large-scale production of polyethylene from bioethanol (*14*, *15*), the supply of acrolein from glycerin waste produced in bio-diesel production (*16*), and synthesis of fully biomass-based poly(ethylene terephthalate) from terpenoids (*17*).

We have focused on another environmental problem caused by plastics, namely plastics waste (*18–20*). To solve the environmental problems caused by plastics wastes, new biorecycling waste-treatment systems such as composting or methane fermentation, and biodegradable materials such as poly(butylene succinate) (PBS) (*21–25*), PLA (*26–28*), poly(hydroxyl alkanoate) (*3–5*), and polycaprolactone (*29–31*) have been developed. PBS is a commercially available biodegradable plastic and was already being used for several purposes when it was being produced from petroleum chemicals. Recently, many researchers

Downloaded by COLUMBIA UNIV on August 28, 2012 | http://pubs.acs.org
Publication Date (Web): August 16, 2012 | doi: 10.1021/bk-2012-1105.ch007

have reported that the PBS monomers, i.e., 1,4-butanediol (BD) and succinic acid (SA), could be produced from biomass feedstocks (*32–34*). SA is a natural biomaterial in the tricarboxylic acid cycle, and SA is found in some animals and plants, e.g., in shellfish. SA is produced by a chemical procedure from benzene via maleic anhydride for use as a raw material for plastics, and as a food additive for seasoning (*35*). We have confirmed that the commercially available SA was derived from petroleum-based materials (*36*). SA can be produced by a fermentation process (*37*, *38*) and can be converted to BD by hydrogenation (*39*). Some companies have announced that in future, SA will be produced from biomass feedstocks by a fermentation process to produce biomass-based PBS (*40–43*). However, no one has yet reported the actual synthesis.

Downloaded by COLUMBIA UNIV on August 28, 2012 | http://pubs.acs.org
Publication Date (Web): August 16, 2012 | doi: 10.1021/bk-2012-1105.ch007

Table I. Commercially available biomass-based plastics

	Partially biomass-based plastic	*Fully biomass-based plastic*
Under developing for manufacturing	poly(butylene succinate) polycarbonate	polypropylene poly(vinyl chloride) poly(acrylic acid)
Commercially available	polyurethane cellulose derivatives	polyethylene poly(lactic acid) poly(hydroxy alkanoate) nylon-11

We have also focused on furan derivatives as the starting materials for monomer synthesis. Hydroxymethylfurfural, furfural, and furan are used industrially as organic solvents or resins, and are valuable biomass compounds as they can be produced from inedible biomass such hemicellulose and cellulose (*44–48*). Hydroxymethylfurfural has six carbon atoms and consists of an aromatic furan moiety, a hydroxymethyl group, and an aldehyde group. Hydroxymethylfurfural is a biomass-based fuel derived from cellulose. Furfural has five carbon atoms and consists of an aromatic furan moiety and an aldehyde group. Around 100 years ago, the chemistry of furfural was studied for its potential as an energy or materials resource, and some chemical reforming methods such as oxidation and reduction were developed to produce chemicals such as furan, which are more useful than furfural (*49–51*).

Several nations currently provide tax and purchase incentives to encourage the use of biomass-based products. When biomass-based PBS is synthesized, a method of verifying that the plastic has been produced from biomass feedstock will be necessary to distinguish it from petroleum-based plastics. Determining the biomass carbon ratio is the most practical and effective method of verifying that a plastic is biomass based. Recently, accelerator mass spectroscopy (AMS) (Figure 1) methods for determining the biomass carbon ratio based on the American Society for Testing and Materials (ASTM) D6866 method, *Standard test methods*

In Biobased Monomers, Polymers, and Materials; Smith, P., et al.;
ACS Symposium Series; American Chemical Society: Washington, DC, 2012.

Downloaded by COLUMBIA UNIV on August 28, 2012 | http://pubs.acs.org
Publication Date (Web): August 16, 2012 | doi: 10.1021/bk-2012-1105.ch007

for determining the biobased content of solid, liquid, and gaseous samples using radiocarbon analysis, have become important in the field of biomass plastics (*52*, *53*). The AMS method has been used for the carbon dating of archaeological and geological samples. The method can also be applied to mass balance studies using low amounts of ^{14}C-labeled metabolic compounds for biological systems. AMS can measure very small ^{14}C concentrations, and can determine $^{14}C/^{12}C$ and $^{14}C/^{13}C$ ratios. The $^{14}C/^{12}C$ ratio in biomass carbon is around 1×10^{-12}. Fossil resources and materials contain no ^{14}C because ^{14}C atoms have a half-life of 5730 years, so all of the ^{14}C will have changed to ^{14}N. We have investigated the suitability of this method for evaluating the biomass carbon ratios of plastics (*54–58*). Plastic that was produced from fully biomass feedstock had a 100% biomass carbon ratio, plastic blended from a fully biomass-based plastic and a fully petroleum-based plastic had a biomass carbon ratio corresponding to the ratio of the plastics, and a composite plastic consisting of a fully biomass-based plastic and an inorganic filler also had a theoretical biomass carbon ratio corresponding to the ratio of biomass-based plastic.

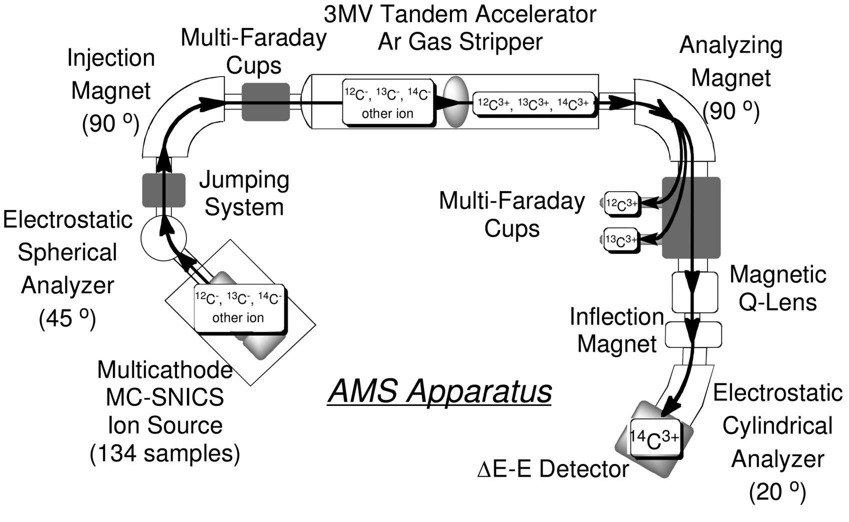
3MV Tandem Accelerator
Ar Gas Stripper
Multi-Faraday Cups
Injection Magnet (90 °)
Analyzing Magnet (90 °)
$^{12}C^-$, $^{13}C^-$, $^{14}C^-$ other ion
$^{12}C^{3+}$, $^{13}C^{3+}$, $^{14}C^{3+}$
Jumping System
Electrostatic Spherical Analyzer (45 °)
Multi-Faraday Cups
$^{12}C^{3+}$
$^{13}C^{3+}$
Magnetic Q-Lens
Inflection Magnet
$^{12}C^-$, $^{13}C^-$, $^{14}C^-$ other ion
Multicathode MC-SNICS Ion Source (134 samples)
AMS Apparatus
$^{14}C^{3+}$
ΔE-E Detector
Electrostatic Cylindrical Analyzer (20 °)

Figure 1. Outline of the accelerator mass spectroscopy (AMS) apparatus (size ca. 15 × 10 m, height 2 m) used to determine the percentage of modern carbon (pMC) from $^{14}C/^{12}C$ (^{14}As) ratios.

In this chapter, we report the first practical synthesis of fully biomass-based PBS from inedible-biomass-based furfural. BD and SA were obtained from furfural by chemical reactions, and polymerized to PBS (Figure 2). We also report that tetrahydrofuran (THF) and succinic anhydride (SAn) could also be synthesized from furfural, and could be polymerized to fully biomass-based poly(butylene oxide-*co*-butylene succinate) (PBBS). The biomass carbon ratios of the synthesized materials were measured by the AMS method. To confirm the validity of the AMS method for the evaluation of biomass-based plastics, PBSs with various ratios of biomass-based monomers and petroleum-based monomers were polymerized and measured by the AMS method; the repeatability was also evaluated. Partially biomass-based poly(butylene terephthalate) (PBT), which is an engineering plastic, was synthesized from the biomass-based BD synthesized in this study and petroleum-based terephthalic acid.

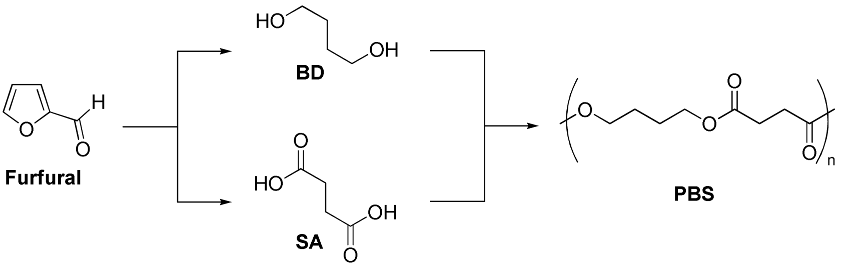

Figure 2. Synthesis of fully biomass-based poly(butylene succinate) (PBS) from 1,4-butane diol (BD) and succinic acid (SA) synthesized from furfural.

Materials and Methods

Furfural was purchased from Wako Pure Chemical Industries (Osaka, Japan) and used after distillation under reduced pressure. Other chemicals were reagent grade and were used without further purification. Nafion® NR50 was purchased from Aldrich Chemical Co. A palladium–rhenium/carbon catalyst was prepared by a previously reported method (*52–57*). ^{1}H NMR spectra were recorded on a 400-MHz NMR spectrometer (JEOL, Tokyo, Japan, JNM-ECX400) using tetramethylsilane as an internal standard. The molecular weight of PBS was determined by gel-permeation chromatography (GPC) with a refractive index detector and a combination of two columns (Tosoh Co., Tokyo, Japan, TSK GMHXL). The columns were eluted with chloroform (flow rate of 0.5 mL/min at 40 °C) and the molecular weights were calibrated with polystyrene standards. The molecular weight of PBT was determined by GPC with a refractive index detector and a column (Showa Denko K.K., Tokyo, Japan, LF-404). The columns were eluted with hexafluoroisopropanol with 5 mM sodium trifluoroacetate (flow rate of 0.14 mL/min at 40 °C), and the molecular weights were calibrated with poly(methyl methacrylate) standards. The melting temperature was determined using a differential scanning calorimetry system (Seiko Instruments Inc., Chiba, Japan, SSC/5520) at a rate of 10 °C/min up to 150 °C.

Downloaded by COLUMBIA UNIV on August 28, 2012 | http://pubs.acs.org
Publication Date (Web): August 16, 2012 | doi: 10.1021/bk-2012-1105.ch007

Downloaded by COLUMBIA UNIV on August 28, 2012 | http://pubs.acs.org
Publication Date (Web): August 16, 2012 | doi: 10.1021/bk-2012-1105.ch007

Sample Preparation for Measurement of Biomass Carbon Ratio

Pretreatment of the samples for AMS and other measurements were performed at the Institute of Accelerator Analysis, Ltd. (IAA) (Fukushima, Japan). All carbon atoms in the samples were transformed into graphite carbons by serial oxidation and reduction reactions, using a quartz-glass tube and a vacuum manifold system. The sample (6.5 mg) was mixed with CuO (1 g) and transferred to a quartz-glass tube. The tube was closed after storage under a vacuum for 10 h. The sample in the tube was oxidized to CO_2 at 500 °C for 30 min and at 850 °C for 2 h. Subsequently, CO_2, CO, and H_2O were cold-trapped, using dry ice/ethanol (−76 °C), in another tube connected to a closed vacuum-line system. The cold-trap step was repeated twice. Pure CO_2 was cold-trapped in a quartz-glass tube with pure ferrous powder in liquid N_2 (−196 °C); the other reactants, i.e., CO_2, CO, and H_2O, were cold-trapped in another tube under dry ice/ethanol. The CO_2 with ferrous powder was reduced to graphite at 650 °C for 10 h. After these processes, the pure graphite and oxidized iron (1 mg) were transferred to a sample holder (small rod-shape; 1 mm hole).

Measurement of Biomass Carbon Ratios

Measurements of the ratios of the three carbon isotopes (^{14}C, ^{13}C, and ^{12}C) using AMS were performed at the IAA. Our measurements were obtained using the 3-MV tandem accelerator system at the IAA. The carbon in graphite from the sample was ionized using a cesium cation beam. The reduced carbon atoms were accelerated using a 3-MV tandem accelerator (National Electrostatics Co., Middleton, WI, USA, Pelletron 9SDH-2). The amounts of ^{12}C and ^{13}C were detected as a current, using multi-Faraday cups. The ^{14}C atoms were detected using a ΔE–E detector. The percentage of modern carbon (pMC) was calculated from the ^{14}C:^{12}C concentration ratios for the sample. The biomass carbon ratio was determined from the ^{14}C concentration measured using AMS based on the ASTM D6866 standard method. Reference materials were measured for the obtained graphite using AMS. The biomass carbon ratios were calculated as follows:

$$^{14}As = {}^{14}C/{}^{12}C \text{ in sample} \quad (1)$$

$$^{14}Ar = {}^{14}C/{}^{12}C \text{ in reference material (NIST SRM 4990c)} \quad (2)$$

$$\Delta^{14}C = [({}^{14}As - {}^{14}Ar)/{}^{14}Ar] \times 1000\ (‰) \quad (3)$$

$$pMC = \Delta^{14}C/10 + 100\ (\%) \quad (4)$$

$$\text{Biomass carbon ratio} = 0.93 \times pMC\ (\%) \quad (5)$$

$\Delta^{14}C$ is the isotope differential ratio of ^{14}C between the sample and reference material. Modern-carbon-based oxalic acid radiocarbon [Standard reference material (SRM) 4990c, National Institute of Standards, USA] was used as the reference material. The pMC for petroleum-based carbon is 0%. The pMC for biomass produced by fixation of CO_2 in the atmosphere by photosynthesis was 108–110% in 2002. The pMC can be slightly higher than 100% because of the continuing but diminishing effects of the 1950s nuclear-testing programs in the atmosphere. During this period, large amounts of ^{14}C were emitted into the atmosphere. Because the ^{14}C in all the samples is referenced to a “prebomb” standard, all pMC values must be multiplied by 0.93 to correct for the bomb carbon and to obtain the true biomass carbon ratio of the sample, as indicated in Eq. (5), based on ASTM D6866.

Downloaded by COLUMBIA UNIV on August 28, 2012 | http://pubs.acs.org
Publication Date (Web): August 16, 2012 | doi: 10.1021/bk-2012-1105.ch007

Direct Polycondensation of BD and SA to PBS (*59*)

A 10-mL flask was charged with SA (3.54 g, 30 mmol), BD (2.97 g, 33 mmol), and titanium tetraisopropoxide (4.2 mg, 14 μmol). The flask was provided with a gas inlet and outlet, and heated at 243 °C for 1 h under a dry N_2 flow to remove the H_2O produced by the esterification reaction. Subsequently, polycondensation was carried out under 10 Pa at 243 °C for 2 h. The resulting solid was dissolved in chloroform (20 mL) and the solution was poured into methanol (100 mL). The precipitate was filtered and dried under a vacuum at 80 °C to give a white solid. The number-average molecular weight was determined by GPC (M_n = 85 000, M_w/M_n = 2.6).

Ring-Opening Polymerization of THF and SAn to PBBS

A 10-mL flask was charged with SAn (10.0 g, 100 mmol), THF (88.7 g, 1.23 mol), glycerin (24 mg, 0.28 mmol), and Nafion® NR50 (2.0 g). The flask was heated at 28 °C for 19 h. The resulting solid was dissolved in chloroform and the solution was poured into methanol. After the solution was filtered, the resulting precipitate was dried under a vacuum at 80 °C to give a white solid (3.1 g). The number-average molecular weight was determined by GPC (M_n = 105 000, M_w/M_n = 1.3). The unit ratio of BD and SA was determined by ^1H NMR (BD:SA = 100:0.8).

Transesterification Polycondensation of THF and Dimethyl Succinate (DS) to PBS (*60*, *61*)

A 10-mL flask was charged with DS, (292 mg, 2.00 mmol), BD (187 mg, 2.08 mmol), and titanium tetraisopropoxide (0.3 mg, 1.0 μmol). The flask was provided with a gas inlet and outlet, and heated at 215 °C for 1 h under a dry N_2 flow to remove the methanol produced as a byproduct of the esterification. Subsequently, polycondensation was carried out under 10 Pa at 215 °C for 4 h. The resulting solid was dissolved in chloroform (2.0 mL) and the solution was poured into methanol

(100 mL). The precipitate was filtered and dried under a vacuum at 80 °C to give a white solid.

Direct Polycondensation of BD and Terephthalic Acid to PBT (*62*)

A 10-mL flask was charged with petroleum-based terephthalic acid (227 mg, 1.37 mmol) and biomass-based BD (209 mg, 2.32 mmol). Butylhydroxytin oxide (0.9 mg, 4.3 μmol) and titanium tetrabutoxide (0.3 mg, 3.0 μmol) were added as a catalyst. The flask was provided with a gas inlet and outlet, and heated at 220 °C for 1 h under a dry N_2 flow to remove the methanol produced as a byproduct of the esterification reaction. Subsequently, polycondensation was carried out under 10 Pa at 250 °C for 3 h. The resulting solid was dissolved in hexafluoroisopropanol (3.0 mL) and the solution was poured into methanol (100 mL). The precipitate was filtered and dried under a vacuum at 80 °C to give a white solid. The number-average molecular weight was determined by GPC (M_n = 7400, M_w/M_n = 2.6).

Transesterification Polycondensation of BD and Dimethyl Terephthalate (*63*)

A 10-mL flask was charged with petroleum-based dimethyl terephthalate (266 mg, 1.37 mmol), biomass-based BD (222 mg, 2.46 mmol), and titanium tetraisopropoxide (0.2 mg, 0.7 μmol). The flask was provided with a gas inlet and outlet, and heated at 220 °C for 1 h under a dry N_2 flow to remove the methanol produced as a byproduct of the esterification reaction. Subsequently, polycondensation was carried out under 10 Pa at 250 °C for 3 h. The resulting solid was dissolved in hexafluoroisopropanol (3.0 mL) and the solution was poured into methanol (100 mL). The precipitate was filtered and dried under a vacuum at 80 °C to give a white solid. The number-average molecular weight was determined by GPC (M_n = 9800, M_w/M_n = 2.4).

Results and Discussion

Conversion of Furfural to Biomass-Based Monomer

The furfural used in this study was a commercially available chemical produced from biomass feedstock such as corn cobs, which is a cellulosic agricultural waste. The AMS method was used to verify that the furfural was biomass based. Furfural is an aromatic aldehyde and is therefore easily oxidized in air to a pale yellow and then red solution (*64*). When an oxidizing reagent and a catalyst are added to furfural, it can be further oxidized to give four-carbon compounds: maleic acid, fumaric acid (FA), furan, and furan derivatives. In the case of addition of a sodium chlorate and vanadium pentoxide catalyst, furfural was converted to a mixture of maleic acid and FA, which are *cis–trans* geometrical isomers (Scheme 1) (*65*). The yield of the mixture of maleic acid and FA was 58% and the ^{1}H NMR spectrum shows that the ratio of maleic acid to FA

Downloaded by COLUMBIA UNIV on August 28, 2012 | http://pubs.acs.org
Publication Date (Web): August 16, 2012 | doi: 10.1021/bk-2012-1105.ch007

was 1:10. Although the mixture of maleic acid and FA can be converted to SA or BD, we purified the mixture to simplify the following reactions. The mixture was purified by recrystallization from 1 M aqueous hydrochloric acid to give FA as white crystals in 47% yield.

FA can be catalytically hydrogenated to BD and SA, which are the monomers of PBS. In general, hydrogenation of the double bonds in carboxylic acids under mild conditions is difficult. The hydrogenation is therefore carried out under high pressure and at high temperature with a heterogeneous catalyst (*66*). The alkene double bond of FA was hydrogenated with a 5% palladium/carbon catalyst under high-pressure hydrogen (13 MPa) at high temperature (160 °C) for 10 h to give SA as white crystals in 98% yield. Hydrogenation of the double bond of a carboxylic acid to an alcohol is more difficult with commercially available catalysts such as palladium/carbon. The hydrogenation of FA to BD has been reported by Pedersen et al. (*67*) FA was hydrogenated with a 5% palladium–rhenium/carbon catalyst under 13 MPa of hydrogen at 160 °C for 10 h to give BD selectively in 63% yield.

Downloaded by COLUMBIA UNIV on August 28, 2012 | http://pubs.acs.org
Publication Date (Web): August 16, 2012 | doi: 10.1021/bk-2012-1105.ch007

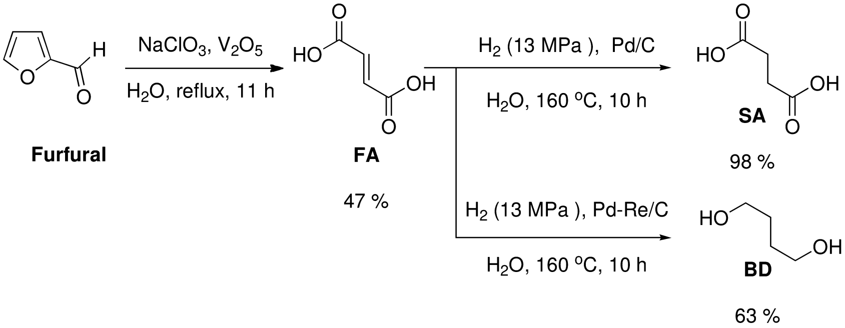

Scheme 1. Synthesis of 1,4-butanediol (BD) and succinic acid (SA) from furfural via fumaric acid (FA)

Hydrogenation of carboxylic compounds hardly occurs under normal pressure, even if the hydrogenation of FA is limited to the alkene double bond. In contrast, the alkene double bond of an alkyl ester can be easily hydrogenated to give an aliphatic ester under normal pressure at room temperature. Because the condensation of a diol and a diester can easily give the corresponding polyester, the synthesis of diester succinate, a monomer of PBS, is useful in establishing the various synthetic routes to biomass-based PBS; the monomer synthesis uses little energy because the reaction takes place at normal pressure. The synthetic route to DS from FA is shown in Scheme 2. DS was synthesized from FA by esterification with concentrated sulfuric acid in a methanol solution to give dimethyl fumarate in 98% yield after purification by recrystallization from methanol. Dimethyl fumarate was hydrogenated under normal pressure at room temperature for 1 h to give DS in 88% yield after distillation.

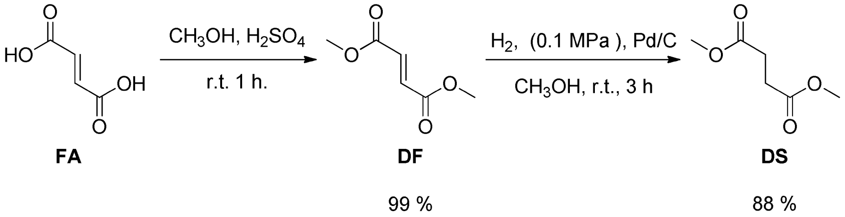

Scheme 2. Synthesis of dimethyl succinate (DS) from FA via dimethyl fumarate (DF)

The synthetic route to THF from furfural is shown in Scheme 3. Disproportionation of an aldehyde to an alcohol and a carboxylic acid using a strong base is known as the Cannizzaro reaction. The disproportionation reaction of furfural with NaOH gave furancarboxylic acid (FCA) as white crystals in 78% yield and hydroxymethylfuran as a byproduct (*68*). FCA can be decarboxylated below 200 °C to give furan as a colorless liquid in 30% yield (*69*). The aromatic ring of furan was then hydrogenated with a palladium oxide catalyst under high-pressure hydrogen (0.7 MPa) at room temperature for 91 h to give THF as a colorless liquid in 83% yield (*70*). Here, we demonstrate the chemical synthesis of furan from furfural. Commercially available furan is also produced from biomass-based furfural. The biomass carbon ratios of the furan synthesized as described in this chapter and of commercially available chemicals are shown in Table II. The synthesis of SAn is carried out using acetyl chloride (Scheme 4) (*71*).

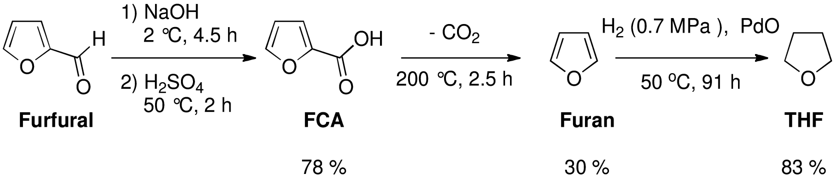

Scheme 3. Synthesis of tetrahydrofuran (THF) from furfural via furancarboxylic acid (FCA) and furan

Biomass Carbon Ratios of Monomers

To verify that the PBS monomers we synthesized were obtained from biomass-based furfural rather than being petroleum-based, the biomass carbon ratios were measured by the AMS method. The biomass carbon ratios of the biomass monomers are shown in Table II. The biomass carbon ratios of furfural, FA, BD, SA, THF, and SAn were 100.8%, 100.4%, 99.4%, 99.9%, 100.7%, and 99.1%, respectively, showing that the chemicals contained only biomass carbon.

Downloaded by COLUMBIA UNIV on August 28, 2012 | http://pubs.acs.org
Publication Date (Web): August 16, 2012 | doi: 10.1021/bk-2012-1105.ch007

In the case of DS, there were four biomass carbon atoms, from the biomass-based SA unit, and two petroleum-based carbon atoms, from the petroleum-based methanol. The biomass carbon ratio of DS was 66.6%, verifying that the DS had 4/6 biomass carbons. It is not well known that commercially available furan is produced from furfural. The biomass carbon ratio of commercially available furan is actually 105.0%. This result certifies that commercially available furan is produced from biomass resources.

Downloaded by COLUMBIA UNIV on August 28, 2012 | http://pubs.acs.org
Publication Date (Web): August 16, 2012 | doi: 10.1021/bk-2012-1105.ch007

Table II. Biomass carbon ratios of biomass-based monomers calculated from $\Delta^{14}C$ measured by accelerated mass spectrometry (AMS), based on ASTM D6866

Entry	*Monomer*	*$\Delta^{14}C$[a] /‰*	*pMC[a] /%*	*Theoretical biomass carbon ratio /%*	*Measured biomass carbon ratio[b] /%*
1	Furfural	84.28	108.43	100	100.8
2	Fumaric acid (FA)	79.28	107.93	100	100.4
3	1,4-Butane diol (BD)	69.09	106.91	100	99.4
4	Succinic acid (SA)	64.68	106.47	100	99.0
5	Dimethyl succinate (DS)	-280.21	71.98	66.7	66.9
6	Tetrahydrofuran (THF)	83.23	108.32	100	100.7
7	Succinic anhydride (SAn)	65.81	106.58	100	99.1
8	Furan[c]	129.93	112.99	-	105.0

[a] Measured by the AMS. [b] Calculation based on Equation 5. [c] Purchased from Wako Pure Chemical Industries.

Fully Biomass-Based PBS by Polycondensation of BD and SA

Production of PBS by polycondensation is already used in industrial manufacturing worldwide. We demonstrated the polycondensation of biomass-based PBS by direct polycondensation of a diol and a dicarboxylic acid. The transesterification polycondensation of a diol and a diester was also carried out. The direct polycondensation of BD and SA, with removal of H_2O, was carried out using a titanium tetraisopropoxide catalyst at 243 °C under 10 Pa for 2 h. The transesterification polycondensation of BD and DS, with removal of methanol, was carried out using a titanium tetraisopropoxide catalyst at 215 °C under 10 Pa for 4 h to give high-molecular-weight PBSs in yields of over 90% (Scheme 5, Table III). The properties of the biomass-based monomers should be the same as those of the petroleum-based monomers, and the properties of the PBS should be the same as those of petroleum-based PBS, except for the biomass carbon ratio.

Downloaded by COLUMBIA UNIV on August 28, 2012 | http://pubs.acs.org
Publication Date (Web): August 16, 2012 | doi: 10.1021/bk-2012-1105.ch007

Table III. Yields, molecular weights, and biomass-based carbon ratios of PBS with various biobased compound monomer ratios

	BD		*Dicarboxylic acid*									
Entry	*Biomass-based*	*Oil-based/%*	*Biomass-based*	*Oil-based/%*	*Theorical biomass carbon ratio /%*	*$\Delta^{14}C$[a]/%*	*pMC[a]/%*	*Measured biomass carbon ratio[b]*	*Tm/°C*	*M_n x 10^{-4}*	*Mw/Mn*	*Yield /%*
9[c]	100	0	100	0	100	75.61	107.56	100.03	114.5	8.5	2.6	97
10[d]	100	0	100	0	100	71.50	107.15	99.65	114.0	4.3	2.0	93
11[d]	100	0	0	100	50	-471.91	52.91	49.11	113.0	7.5	2.2	91
12[d]	0	100	100	0	50	-462.46	53.75	49.99	111.8	3.5	2.6	87
13[d]	50	50	50	50	50	-470.91	52.91	49.21	112.7	3.1	2.6	93
14[d]	10	90	0	100	5	-947.55	5.25	4.88	113.8	3.0	3.0	90
15[d]	0	100	10	90	5	-945.38	5.46	5.08	113.3	2.8	3.1	94

[a] Measured by the AMS. [b] Calculation based on Equation 5. [c] Synthesis from SA as dicarboxylic acid. [d] Synthesis from DS as dicarboxylic acid.

Downloaded by COLUMBIA UNIV on August 28, 2012 | http://pubs.acs.org
Publication Date (Web): August 16, 2012 | doi: 10.1021/bk-2012-1105.ch007

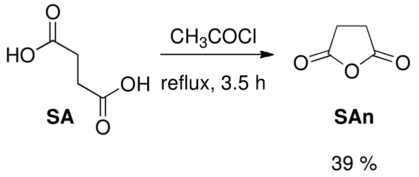

Scheme 4. Synthesis of succinic anhydride (SAn) from SA

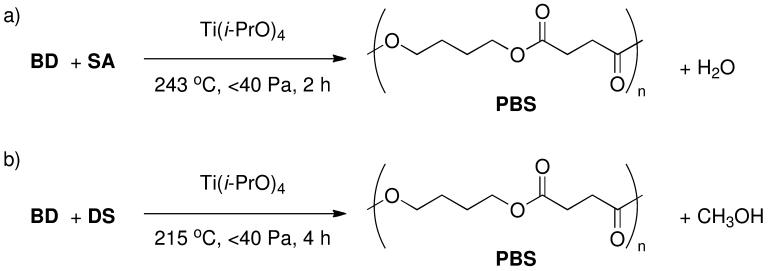

Scheme 5. Polycondensation of PBS: a) direct polycondensation and b) transesterification polycondensation

Biomass Carbon Ratios of Fully and Partially Biomass-Based PBSs

To confirm that the resulting PBSs had biomass carbon, the biomass carbon ratios of the PBSs were measured by the AMS method. The biomass carbon ratio of the PBS polymerized from all-biomass BD and SA was 100% (entry 6 in Table III). This was therefore the first synthesis of fully biomass-based PBS, and it was verified that all the carbon atoms were derived from biomass feedstock. The biomass carbon ratio of the PBS from all-biomass BD and DS was also 100% (entry 7 in Table III). Although the DS included petroleum-based methanol, the resulting PBS was fully biomass-based because the methanol was eliminated in the transesterification polycondensation. To confirm that the biomass carbon ratio depended on the mixture ratio of the biomass-based and petroleum-based monomers, partially biomass-based PBSs with mixtures ofbiomass-based and petroleum-based monomers in various ratios were prepared under the same reaction conditions (entries 8–12 in Table III). PBSs produced from all-biomass-based BD and all-petroleum-based DS, from all-petroleum-based BD and all-biomass-based DS, and from 50% biomass-based BD and 50% biomass-based DS had 50% biomass carbons. The actual biomass carbon ratios were 49.11, 49.99, and 49.21 %, respectively. PBSs including 10% biomass-based BD or DS had 5% biomass carbons. The biomass carbon ratios were 5.08 and 4.88 %, respectively. The biomass carbon ratios of biomass-based PBSs agreed with the theoretical values of the mixture ratios of biomass-based and petroleum-based monomers, showing that the number of biomass carbons in the PBS corresponded to the ratio of the biomass-based monomer in the mixture. We have already reported that the repeatability of the biomass carbon ratio of a partially biomass-based sample, a blend of biomass-based PLA and petroleum-based PBS, was slightly inferior to that of bioethanol, which has only biomass carbons (*55*). It is possible that because the amount of sample used in the AMS method was very small (ca. 10 mg), the heterogeneities of the biomass-based sample and the petroleum-based sample affected the biomass carbon ratio of each measured sample. To evaluate the repeatability of the biomass carbon ratio of the polymer with biomass carbon and petroleum carbon, the biomass carbon ratio of a partially biomass-based PBS, which was a mixture of biomass-based BD and petroleum-based DS (entry 9 in Table III), was measured six times by the AMS method; the results are shown in Table IV. The average value of the biomass carbon ratio was 49.79%. The standard deviation ($1\sigma = 0.25$) of the repeated measurements of the biomass carbon ratio was smaller than the value ($\sigma = 0.84$) for the partially biomass-based sample, which was a blend of biomass-based PLA and petroleum-based PBS (*57*). A mixture of biomass-based and petroleum-based monomers could therefore provide a PBS that had a homogeneous distribution of biomass carbons. These biomass carbon ratio measurements indicated that the AMS method was suitable for the exact evaluation of material produced from biomass feedstock, even if part of the monomer was petroleum based.

Downloaded by COLUMBIA UNIV on August 28, 2012 | http://pubs.acs.org
Publication Date (Web): August 16, 2012 | doi: 10.1021/bk-2012-1105.ch007

Table IV. Repeatability of AMS measurements of biomass-based carbon ratios for partially biomass-based PBS polymer samples (Table III, entry 9)

Entry	*$\Delta^{14}C^{a}$ /‰*	*pMC[a] /%*	*Measured Biomass carbon ratio [b] /%*
16	-462.46	53.75	49.99
17	-461.37	53.86	50.09
18	-462.86	53.31	49.95
19	-462.88	53.31	49.58
20	-466.23	53.28	49.55
21	-466.86	53.31	49.58
average	-463.11	53.47	49.79
standard deviation	1.92	0.26	0.25

[a] Measured by the AMS. [b] Calculation based on Equation 5.

Table V. Yields, molecular weights, and biomass carbon ratios of PBT from biomass-based BD and petroleum-based terephthalic acid derivatives

Entry	*Monomer*		*$\Delta^{14}C$[a] /‰*	*pMC[a] /%*	*Theorical biomass carbon ratio /%*	*Measured biomass carbon ratio[b] /%*	*Yield /%*	*Tm / °C*	*Mn x 10^{-3}*	*Mw/Mn*
22	Biomass-based BD	Petroleum-based terephthalic acid	-637.64	36.24	33.3	33.7	95	224	7.4	2.6
23	Biomass-based BD	Petroleum-based dimethyl terephthalate	-637.64	36.24	33.3	33.7	93	222	9.8	2.4

[a] Measured by the AMS. [b] Calculation based on Equation 5.

Downloaded by COLUMBIA UNIV on August 28, 2012 | http://pubs.acs.org
Publication Date (Web): August 16, 2012 | doi: 10.1021/bk-2012-1105.ch007

Downloaded by COLUMBIA UNIV on August 28, 2012 | http://pubs.acs.org
Publication Date (Web): August 16, 2012 | doi: 10.1021/bk-2012-1105.ch007

Fully Biomass-Based PBBS by Ring-Opening Polymerization of THF and SAn

Previously, we reported ring-opening polymerization of cyclic monomers using a metal triflate as a Lewis-acid catalyst (*72*). The residual catalyst often causes problems such as polymer decomposition, decay of properties, and health risks. Catalyst removal after use is therefore an important step in the production of commercially available polymers. However, it is difficult to recover the catalyst after the polymerization reaction in the case of metal triflate catalysts because the catalyst is homogeneous. Solid acid catalysts, which are easy to separate from the product, have therefore been developed. Nafion® is one such solid acid catalyst, and it is easy to separate from the product. We demonstrated the ring-opening polycondensation of THF and SAn with Nafion® as a solid acid catalyst (Scheme 6). The polymerization was carried out, with glycerin as an initiator, at room temperature for 19 h. The PBS produced using a metal triflate catalyst is a homopolymer, in which the ratio of SA to SAn is 1:1, the polymer produced with Nafion® as the catalyst is a copolymer of poly(butylene oxide) and PBS, and the ratio of butylene units derived from SA and succinate units derived from SAn is 100:0.8. It is postulated that the acid-catalyzed ring-opening polymerization of THF to poly(butylene oxide) is superior to the alternating copolymerization of THF and SAn because Nafion® is a super-acid catalyst.

The biomass carbon ratio of PBBS is 100.1%. The resulting PBBS is therefore also a fully biomass-based polymer, and it was verified that all the carbon atoms were derived from biomass feedstock

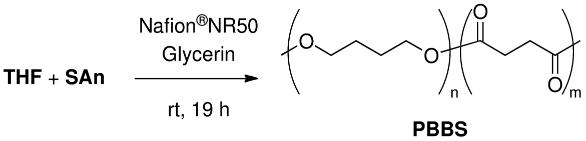

Scheme 6. Ring-opening polymerization of poly(butylene oxide-co-butylene succinate)

Polycondensation of Partially Biomass-Based PBT from BD and Terephthalic Acid

PBT is useful as an engineering plastic because of its high heat-resistance, chemical resistance, electrical properties, and good moldability. PBT is mainly used in automobile parts and in electrical products. The PBT monomer units are BD and terephthalate. PBT polymerized from biomass-based BD, with four carbons, and petroleum-based terephthalic acid, with eight carbons, is a partially biomass-based plastic with 12 carbons in the polymer unit, and the biomass carbon ratio reaches 33.3% [4/(4 + 8)]. Partially biomass-based engineering plastics are important in reducing CO_2 emissions and in conserving petroleum resources, even if the biomass carbon ratio is 33%. We succeeded in synthesizing partially biomass-based PBT from biomass-based BD and petroleum-based terephthalic acid or dimethyl terephthalate (Scheme 7). The ^1H NMR spectrum, molecular weight, and melting point showed that the resulting material was the same as fully petroleum-based PBT. The biomass carbon ratio of both the partially biomass-based PBTs, measured by the AMS method, was 33.7%, which agreed with the theoretical value (see Table V). It was confirmed that the resulting PBTs were partially biomass-based PBT. The synthesis of biomass-based PBT from terpenoids, and fully biomass-based PBT and partially biomass-based PET was reported later (*17*).

Downloaded by COLUMBIA UNIV on August 28, 2012 | http://pubs.acs.org
Publication Date (Web): August 16, 2012 | doi: 10.1021/bk-2012-1105.ch007

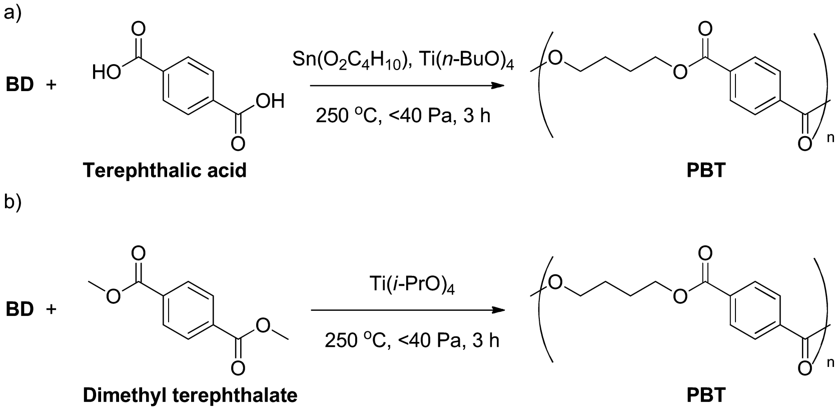

Scheme 7. Polycondensation of partially biomass-based poly(butylene terephthalate) (PBT) with BD synthesized from furfural and petroleum-based terephthalic acid

Conclusions

The effective use of biomass feedstock is a pressing problem. Biomass-based materials are needed for sustainable development, as they can help to decrease CO_2 emissions and help to conserve petroleum resources. Biomass-based PBS is one solution. Furfural has long been known as a biomass chemical, but furfural is only used as a solvent and in special materials. We synthesized biomass-based PBS monomers, i.e., BD, SA and DS, from furfural in polymer grade purity and polymerized these monomers to PBS with arbitrary biomass carbon ratios. This PBS was the first fully biomass-based material; this was verified by the AMS method. A verification method for the biomass carbon ratio of plastics that have both biomass-based monomers and petroleum-based monomers had not been previously reported. Measurements on PBS with a low biomass carbon ratio showed that the AMS method could be useful to verify the biomass carbon ratio from high ratios (100%) to low ratios (5%); the repeatability was stable. We also synthesized biomass-based THF and SAn as monomers of PBBS. This PBBS was also a fully biomass-based material, as verified by the AMS method. Furthermore, partially biomass-based PBT, which is an important engineering material for automobiles and electrical applications, was synthesized from biomass-based BD and petroleum-based terephthalic acid, and identified as a 33.3% (four carbons from biomass-based BD/12 carbons) biomass-based material.

When materials are supplied from biomass feedstocks in the future, this verification method will be indispensable and widely used. We demonstrated the first chemical synthesis of fully biomass-based PBS and evaluated the AMS method as a verification method. This fully inedible-biomass-based PBS will join the biomass plastics family, which includes PLA and PHA. The use of the AMS method as the standard verification method for biomass-based plastics could promote the change from petroleum-based plastics to biomass-based plastics. These fully and partially biomass-based PBSs can be used as standard materials for the measurement of biomass carbon ratios using the AMS method because the PBSs have arbitrary biomass carbon ratios and homogeneous biomass carbon compositions.

Downloaded by COLUMBIA UNIV on August 28, 2012 | http://pubs.acs.org
Publication Date (Web): August 16, 2012 | doi: 10.1021/bk-2012-1105.ch007

Acknowledgments

The authors are grateful for financial support from the New Energy and Industrial Technology Development Organization (NEDO) for the Research Project entitled *Development of preparatory basic bioenergy technologies: Accelerated technology development for biofuel: R&D of method to measure biomass carbon ratio of biopolyolefins*

References

1. Lunt, J. *Polym. Degrad. Stab.* **1998**, *59*, 145–152.
2. Vink, E. T. H.; Rábago, K. R.; Glassner, D. A.; Gruber, P. R. *Polym. Degrad. Stab.* **2003**, *80*, 403–419.
3. Sudesh, K.; Abe, H.; Doi, Y. *Prog. Polym. Sci.* **2000**, *25*, 1503–1555.
4. Sudesh, K.; Doi, Y. *Polym. Adv. Technol.* **2000**, *11*, 865–872.
5. Kim, S.; Dale, B. E. *Environ. Sci. Technol.* **2008**, *42*, 7690–7695.
6. Jones, R. F. *The Future of the Chemical Industry*; Jones, R. F., Ed.; ACS Symposium Series 1026; American Chemical Society: Washington, DC, 2009; pp 1−17.
7. Rincones, J.; Zeidler, A. F.; Grassi, M. C. B.; Carazzolle, M. F.; Pereira, G. A. G. *Polym. Rev.* **2009**, *49*, 85–106.
8. Petrović, Z. S. *Polym. Rev.* **2008**, *48*, 109–155.
9. Dwan'isa, J. P. L.; Mohanty, A. K.; Misra, M.; Drza, L. T.; Kazemizadeh, M. *J. Mater. Sci.* **2004**, *39*, 2081–2087.
10. Ray, S. S.; Okamoto, M. *Macromol. Rapid Commun.* **2003**, *24*, 815–840.
11. Urayama, H.; Kanamori, T.; Fukushima, K.; Kimura, Y. *Polymer* **2003**, *44*, 5635–5641.
12. Kakuta, M.; Hirata, M.; Kimura, Y. *Polym. Rev.* **2009**, *49*, 107–140.

13. Tachibana, Y.; Maeda, T.; Ito, O.; Maeda, Y.; Kunioka, M. *Polym. Degrad. Stab.* **2010**, *95*, 1321–1329.
14. Morschbacker, A. *Polym. Rev.* **2009**, *49*, 79–84.
15. Queiroz, A. U. B.; Collares-Queiroz, F. P. *Polym. Rev.* **2009**, *49*, 65–78.
16. Arita, Y; Takahashi, T.; Okada, M,; Moriguchi, T. U.S. patent 7,847,131.
17. Colonna, M.; Berti, C.; Fiorini, M.; Binassi, E.; Mazzacurati, M.; Vannini, M.; Karanam, S. *Green Chem.* **2011**, *13*, 2543–2548.
18. Moore, C. J. *Environ. Res.* **2008**, *108*, 131–139.
19. Amass, W.; Amass, A.; Tighe, B. *Polym. Int.* **1998**, *47*, 89–144.
20. Siddique, R.; Khatib, J.; Kaur, I. *Waste Manage.* **2008**, *28*, 1835–1852.
21. Polyesters. In *Biopolymers*; Doi, Y., Steinbuchel, A., Eds.; Wiley-VCH: Weinhelm 2002; Vol. 4.
22. Fujimaki, T. *Polym. Degrad. Stab.* **1998**, *59*, 209–214.
23. Gan, Z.; Abe, H.; Doi, Y. *Biomacromolecules* **2001**, *2*, 313–321.
24. Tokiwa, Y.; Calabia, B. P. *Biotechnol. Lett.* **2004**, *26*, 1181–1189.
25. Tachibana, Y.; Giang, N. T. T.; Ninomiya, F.; Funabashi, M.; Kunioka, M. *Polym. Degrad. Stab.* **2010**, *95*, 1406–1413.
26. Kawashima, N.; Ogawa, S.; Obuchi, S., Matsuno, M.; Yagi, T. Poly(lactic acid) "LACEA". In *Biopolymers*; Doi, Y., Steinbuchel, A., Eds.; Wiley-VCH: Weinhelm, 2002; Vol. 4, pp 251−274.
27. Tsuji, H.; Miyaushi, S. *Biomacromolecules* **2001**, *2*, 597–604.
28. Kunioka, M.; Ninomiya, F.; Funabashi, M. *Polym. Degrad. Stab.* **2006**, *91*, 1919–1928.
29. Ohtaki, A.; Sato, N.; Nakasaki, K. *Polym. Degrad. Stab.* **1998**, *61*, 499–505.
30. Funabashi, M; Ninomiya, F; Kunioka, M. *J. Polym. Environ.* **2007**, *15*, 7–17.
31. Kunioka, M; Ninomiya, F; Funabashi, M. *Polym. Degrad. Stab.* **2007**, *92*, 1279–1288.
32. Landucci, R.; Goodman, B.; Wyman, C. *Appl. Biochem. Biotechnol.* **1994**, *45-46*, 677–696.
33. Zeikus, J. G.; Jain, M. K.; Elankovan, P. *Appl. Microbiol. Biotechnol.* **1999**, *51*, 545–552.
34. Shibata, M.; Inoue, Y.; Miyoshi, M. *Polymer* **2006**, *47*, 3557–3564.
35. Furia, T. E. In *Handbook of food additives*; CRC-Press: Boca Raton, Florida, 1973; Vol. 1.
36. Kunioka, M. *Appl. Microbiol. Biotechnol.* **2010**, *87*, 491–497.
37. McKinlay, J. B.; Vielle, C.; Zeikus, J. G. *Appl. Microbibol. Biotechnol.* **2007**, *76*, 727–740.
38. Song, H.; Lee, S. Y. *Enzyme Microb. Technol.* **2006**, *39*, 352–361.
39. Carnahan, J. E.; Ford, T. A.; Gresham, W. F.; Grigsby, W. E.; Hager, G. F. *J. Am. Chem. Soc.* **1955**, *77*, 3766–3768.
40. Xu, J.; Guo, B.-H. In *Plastics from Bacteria: Natural Functions and Applications*; Chen, G. G. Q., Eds.; Springer: Heiderberg, 2010; pp 347−388.
41. Mizukoshi, T. In *ICTABP2*; Hangzhou, China, 2006; p 123.
42. Kato, S.; Tsukahara, T.; Kishimoto, M.; Nagaya, I. In *ICTABP2*; Hangzhou, China, 2006; p 96.
43. Shitani, N.; Kato, S. In *GSC-AON*; Tokyo, Japan, 2007; p 235.

Downloaded by COLUMBIA UNIV on August 28, 2012 | http://pubs.acs.org
Publication Date (Web): August 16, 2012 | doi: 10.1021/bk-2012-1105.ch007

44. Trimble, F. *Ind. Eng. Chem.* **1941**, *33*, 660–662.
45. Brownlee, H. J.; Miner, C. S. *Ind. Eng. Chem.* **1948**, *40*, 201–204.
46. Trickey, J. P.; Miner, C. S.; Brownlee, H. J. *Ind. Eng. Chem.* **1923**, *15*, 65–66.
47. Othmer, D. F.; Tobias, P. E. *Ind. Eng. Chem.* **1942**, *34*, 690–692.
48. Flores, F. D.; Funabashi, M.; Kunioka, M. *J. Appl. Polym. Sci.* **2009**, *112*, 3410–3417.
49. Milas, N. A. *J. Am. Chem. Soc.* **1927**, *49*, 2005–2011.
50. Cass, O. E. *Ind. Eng. Chem.* **1948**, *40*, 216–219.
51. Gandini, A.; Coelho, D.; Gomes, M.; Reis, B.; Silvestre *J. Mater. Chem.* **2009**, *19*, 8656–8664.
52. Narayan, R. *Degradable Polymer and Materials*; Khemani, K. C., Scholz, C., Eds.; ACS Symposium Series 939; American Chemical Society: Washington, DC, 2006, pp 282−306.
53. Narayan, R. *Biobased and Biodegradable Polymer Materials*; ACS Polymer Preprints: San Diego, CA, 2005; pp 319–320.
54. Kunioka, M.; Inuzuka, Y.; Ninomiya, F.; Funabashi, M. *Macromol. Biosci.* **2006**, *6*, 517–523.
55. Kunioka, M.; Ninomiya, F.; Funabashi, M. *J. Polym. Environ.* **2007**, *15*, 281–287.
56. Kunioka, M.; Ninomiya, F.; Funabashi, M. *Int. J. Mol. Sci.* **2009**, *10*, 4267–4283.
57. Funabashi, M.; Ninomiya, F.; Ohara, K.; Kunioka, M. *Bull. Chem. Soc. Jpn.* **2009**, *82*, 1538–1547.
58. Onishi, T.; Ninomiya, F.; Kunioka, M.; Funabashi, M.; Ohara, K. *Polym. Degrad. Stab.* **2010**, *95*, 1276–1283.
59. Mochizuki, M.; Mukai, K.; Yamada, k.; Ichise, N.; Murase, S.; Iwaya, Y. *Macromolecules* **1997**, *30*, 7403–7407.
60. Hirotsu, T.; Tsujisaka, T.; Masuda, T.; Nakayama, K. *J. Appl. Polym. Sci.* **2000**, *78*, 1121–1129.
61. Oishi, A.; Nakano, H.; Fujita, K.; Yuasa, M.; Taguthi, Y. *Polym. J.* **2002**, *34*, 742–747.
62. Hayashi, M.; Ikeuchi, H.; Tanaka, M. U.S. patent 3,936,421.
63. Kibler, C. J.; Bell, A.; Smith, J. G. U.S. patent 2,901,466.
64. Dunlop, A. P.; Stout, P. R.; Swadesh, S. *Ind. Eng. Chem.* **1946**, *38*, 705–708.
65. Tachibana, Y.; Masuda, T.; Funabashi, M.; Kunioka, M. *Biomacromolecules* **2010**, *11*, 2760–2765.
66. Nishimura, S. In *Handbook of Heterogeneous Catalytic Hydrogenation for Organic Synthesis*; Wiley-VCH: New York, 2001.
67. Pedersen, S. E.; Frye, Jr. J. G.; Attig, T. G.; Budge, J. R. U.S. patent 5,698,749.
68. Wilson, W. C. *Org. Synth.* **1941**, Coll. Vol. 1, 276.
69. Wilson, W. C. *Org. Synth.* **1941**, Coll. Vol. 1, 274.
70. Donald, S.; Hixon, R. M. *Org. Synth.* **1943**, Coll. Vol. 2, 566.
71. Fieser, L. F.; Martin, E. L.; Shriner, R. L.; Struck, H. C. *Org. Synth.* **1943**, Coll. Vol. 2, 560.
72. Wang, Y.; Kunioka, M. *Macromol. Symp.* **2005**, *224*, 193–205.

Downloaded by COLUMBIA UNIV on August 28, 2012 | http://pubs.acs.org
Publication Date (Web): August 16, 2012 | doi: 10.1021/bk-2012-1105.ch007

Downloaded by STANFORD UNIV GREEN LIBR on August 28, 2012 | http://pubs.acs.org
Publication Date (Web): August 16, 2012 | doi: 10.1021/bk-2012-1105.ch008

Chapter 8

Poly(oleic diacid-co-glycerol): Comparison of Polymer Structure Resulting from Chemical and Lipase Catalysis

**Yu-Rong Zhang,[1,2] Yi-Xin Yang,[1] Jia-Li Cai,[1] Wen-Hua Lv,[1]
Wen-Chun Xie,[1] Yu-Zhong Wang,[2] and Richard A. Gross*,[1]**

**[1]Center for Biocatalysis and Bioprocessing of Macromolecules,
The Polytechnic Institute of New York University, Six Metrotech Center,
Brooklyn, New York 11201, United States
[2]Center for Degradable and Flame-Retardant Polymeric Materials, College of Chemistry, National Engineering Laboratory of Eco-Friendly Polymeric Materials, Sichuan University, Chengdu 610064, China
*E-mail: rgross@poly.edu**

This study compares the synthesis and structure of poly(oleic diacid-co-glycerol) that results by using Novozym 435 (N435) and dibutyl tin oxide (DBTO) as catalysts. By using N435 catalysis and an oleic diacid to glycerol molar ratio of 1.0:1.0, the resulting polyester Mn were 6000 g/mol at 6h and 9100 g/mol at 24h with low branching degree (Den% of glycerol 13%-16%). Further diversification in polymer structure was achieved by using N435 catalysis and by changing the feed ratio of oleic diacid to glycerol from 1.0:1.0 to 1.5:1.0 in 0.1 increments. Resulting polyesters were not crosslinked, had similar Mn values (generally between 4800 and 6000 g/mol). In contrast, by using DBTO as catalyst and an oleic diacid to glycerol molar ratio of 1.0:1.0, polyester Mn of 1700 g/mol was obtained at 6h and, thereafter, a gel was formed due to cross-linking. As a consequence of N435's ability to deter cross-link reactions owing to steric hindrance at active site, a family of unique, soluble, hyperbranched copolyesters was formed.

Downloaded by STANFORD UNIV GREEN LIBR on August 28, 2012 | http://pubs.acs.org
Publication Date (Web): August 16, 2012 | doi: 10.1021/bk-2012-1105.ch008

Introduction

Fatty acids typically have chain lengths between 12 and 22 carbons, contain variable degrees and sites of unsaturation, and may be hydroxylated. Further diversification of fatty acid structure is achieved by a variety of chemical modification reactions. Examples illustrating routes from fatty acids to diacid building blocks with chain lengths ≥ C10 are described below. The motivation to use long-chain-length fatty acid-derived diacid monomers is due to the properties they impart in resulting polymers such as ductility, high impact strength, hydrolytic stability, hydrophobicity, and lower glass transition temperatures (*1*). Also, many polymers derived from fatty diacids have been found useful in biomedical applications.

Ricinoleic acid was converted to a diacid monomer by esterification with maleic or succinic anhydride. This gave ricinoleic acid maleate (RAM) and ricinoleic acid succinate (RAS), respectively (*2*). Sebacic acid (decanedioic acid) is produced from ricinoleic acid by splitting the molecule with caustic soda at 250-275°C (*3*). Examples of polyesters formed from sebacic acid will be discussed below. Metathesis chemistry has been an important tool in providing versatile routes to fatty diacids. Warwel et al. (*4*) used a Grubbs catalyst to perform metathetical condensation converting 9-decenoic, 10-undecenoic, and 13-tetradecenoic acid methyl esters to their corresponding long-chain, symmetrically unsaturated R,ω-dicarboxylic acid methyl esters (C-18, C-20, C-26). Quinzler and Mecking (*5*) converted methyl oleate, by exposure to carbon monoxide and methanol catalyzed by $Pd(OAc)_2$ /1,2-bis[(di-tert-butylphosphino)methyl]benzenemethanesulfonic acid, to dimethyl-1, 19-nonadecanedioate. Dimer fatty acids are produced on a commercial scale by heating unsaturated fatty acids from tall oil at around 230°C with a montmorillonite followed by distillation (*6*). Resulting C36 dibasic acids are used to prepare polyamides.

In this study, Candida tropicalis ATCC20962 (*7*) was used to prepare 1,18-cis-9-octadecenedioic (oleic diacid) for subsequent polymerization studies. Cognis scientists engineered C. tropicalis ATCC20962 for direct transformation of fed fatty acids into their corresponding R,ω-diacids by eliminating its β-oxidation pathway (*8*, *9*). Recently, our group reported that a diverse family of ω-carboxy fatty acid monomers can be synthesized by using this and related C. tropicalis strains (*10*). For example, bioconversions of oleic, erucic, and epoxy stearic acids by C. tropicalis ATCC20962 in shake flasks produced oleic diacid, 1,22-cis-9-docosenedioic (erucic diacid) and 1,18-cis-9,10-epoxyoctadeca-nedioic. Since these diacids bear sensitive chemical functionalities, our group chose to use N435 for their copolymerization with diols.

Since ω-carboxy fatty acids of medium-to-long chain length are natural metabolic intermediates, and the US Food and Drug Administration has approved glycerol for medical applications, polymers of glycerol and diacids have garnered considerable interest for development of bioresorbable materials (*11–16*). Likely due to the high availability of sebacic acid, much of this work has focused on poly(glycerol sebacate) (PGS). The resulting copolymer of glycerol and sebacic acid was a transparent, almost colorless elastomer (*11*). Low-molecular-weight prepolymers of PGS have also been synthesized for cross-linking in a second step. Research on alternative synthetic approaches in which lipase catalysis was used to avoid cross-linking during propagation of related copolymerizations are described below.

Polyesters from diacids and polyols, such as glycerol and sorbitol, have historically been prepared by chemical methods (*17–21*). However, to prepare linear or controlled branch structures, elaborate protection-deprotection steps are required. Furthermore, at high functional group conversion without protecting group chemistry, reactions that are not terminated prior to gelation give cross-linked materials with limited utility. Special precautions are required to monitor rapid increases in reaction viscosity to indicate the onset of gelation. Other problems encountered are high reaction temperatures (≥150°C) that are energy intensive and lead to product discoloration.

While chemical catalysts used for condensation polymerizations to prepare polyol-polyesters generally lack selectivity, lipases can provide better control over branching while avoiding cross-linking reactions due to steric constraints at enzyme active sites. Reviews describing literature examples of lipase-catalyzed synthesis of polyol-polyesters has been published by us and others (*22–27*). The following are two selected examples from the literature to illustrate how lipases have been used to prepare non-cross-linked polyol-polyesters. N435-catalyzed copolymerization of glycerol, divinyl sebacate, and fatty acids (e.g., oleic, linoleic, and linolenic acids) has been studied as a route to bio-based polymers with unsaturated pendant groups (*28*). Resulting copolymers were non-cross-linked with a high proportion of trisubstituted glycerol units and Mn values that ranged from 3000 to 7000. After epoxidation of fatty acid side chains, resulting polyesters were thermally cured to give transparent high gloss films. Kulshrestha et al. (*29*) formed monophasic solutions of glycerol with adipic acid and 1,8-octanediol and then studied their polymerization in-bulk, catalyzed by N435, at 70°C. Variation of reaction time and glycerol in the monomer feed yielded copolymers with degrees of branching varying from 0% to 58%. Particularly relevant to this study was that N435 catalysis gave linear copolyesters at short reaction times. However, by extending the reaction time to 42h, a branched copolyester (Mn 26 800g/mol) with 27% dendritic units was produced whose structure was presumably thermodynamically controlled.

As studies in developing enzyme-catalyzed routes to polymers progress, it is critical that the performance of enzyme catalysts is compared to their chemical counterparts. This paper describes a comparison between a lipase and an organotin catalyst for synthesis of polyol-polyesters. N435 and dibutyltin oxide (DBTO) were selected as model lipase and chemical catalysts, respectively. The chosen model reaction system is the bulk copolymerization of oleic diacid and glycerol with different molar ratios of monomers. The progression of oligomer and polymer structures that develop as a function of time was studied. Size exclusion chromatography (SEC) with online multiangle laser light scattering (MALLS) was used to determine absolute molecular weight and polydispersity. Inverse gated ^{13}C NMR was used to calculate substitution degree of glycerol unit and relative molar ratio of monosubstituted, linear and dendritic glycerol repeat units. Polyesters were then analyzed by DSC and TGA to characterize their thermal

Downloaded by STANFORD UNIV GREEN LIBR on August 28, 2012 | http://pubs.acs.org
Publication Date (Web): August 16, 2012 | doi: 10.1021/bk-2012-1105.ch008

properties. One of the resulting copolyester compositions was hydrogenated, and the effect of unsaturation level on thermal properties was investigated.

Materials and Methods

Materials

1,18-cis-9-Octadecenedioic acid (oleic diacid, ~99% pure) was produced in our lab as previously reported (*10*). Glycerol (98% pure), toluene (amphorous, 99%), and dibutyltin oxide (DBTO) were purchased from Sigma-Aldrich (St. Louis, MO) and used as supplied. Novozym 435 (specified activity 10 000 PLU g^{-1}) was a gift from Novozymes (Bagsvaerd, Denmark) and consists of Candida Antarctica Lipase B (CALB) physically adsorbed within the macroporous resin Lewatit VPOC 1600 (poly[methyl methacrylate-co-butyl methacrylate], supplied by Bayer). All solvents were of HPLC grade and were used as received without any further purification.

Downloaded by STANFORD UNIV GREEN LIBR on August 28, 2012 | http://pubs.acs.org
Publication Date (Web): August 16, 2012 | doi: 10.1021/bk-2012-1105.ch008

N435-Catalyzed Condensation Polymerization in Bulk

The bulk reaction catalyzed by N435 was performed in a parallel synthesizer (Advantage TM 2050, Argonaut). Oleic diacid (10-15 mmol) and glycerol (10 mmol) were transferred into reactor tubes of the parallel synthesizer at 90°C, and then, 10wt % Novozym 435 relative to monomer was added. Vacuum (10 mmHg) was applied after 2h. To follow the progress of polymerizations, aliquots were withdrawn at 2, 4, 6, 8, 10, and 24h. Reactions were terminated by addition of cooled chloroform, and Novozym 435 was removed by filtration. The filtrates without precipitation were directly analyzed by size exclusion chromatography-multiangle laser light scattering (SEC-MALLS) to determine molecular weight averages and polydispersity and further analyzed by ^{13} C NMR to determine the polyester branching degree. The thermal properties of resulting polyesters were tested by thermogravimetric analysis (TGA) and differential scanning calorimetry (DSC).

DBTO-Catalyzed Condensation Polymerization in Bulk

The bulk reaction catalyzed by DBTO was performed in a parallel synthesizer (Advantage TM 2050, Argonaut). Oleic acid (10, 13, or 15 mmol) and diol (10 mmol) were transferred into reactor tubes of the parallel synthesizer, in the first step; mixture was heated at 150°C under nitrogen for 2h with 1wt % DBTO. Vacuum (10 mmHg) was applied after 2h oligomerization. To follow the progress of polymerizations aliquots were withdrawn at 2, 4, 6, and 8h. Reactions were terminated by addition of cooled chloroform. The filtrates without precipitation were directly analyzed by SEC-MALLS to determine molecular weight averages and polydispersity and further analyzed by ^{13}C NMR to determine the polyester branching degree.

Instrumental Methods

Nuclear Magnetic Resonance (NMR)

Carbon (^{13}C) NMR spectra were recorded on a Bruker DPX300 NMR spectrometer at 300 MHz in deuterated chloroform ($CDCl_3$) as solvent.

Thermogravimetric Analysis (TGA)

Thermal degradation measurements were performed with a TA Instruments TGA-2950 analyzer in a nitrogen atmosphere with about 10 mg of polymer samples at a heating rate of 10°C/min from 25 to 700 °C.

Differential Scanning Calorimetry (DSC)

Differential scannings were recorded using a TA Instruments DSC-2920 analyzer. Polymer samples were heated and cooled under a nitrogen flow rate of 50 mL/min. Samples were first heated to 120°C and cooled to -60°C at the rate of 20°C/min to get homogeneous thermal history, and then samples were heated to 120°C at the rate of 10 °C /min.

Size Exclusion Chromatography-Multiangle Laser Light Scattering (SEC-MALLS)

Absolute molecular weights of copolyesters were determined by SEC with online multiangle laser light scattering (MALLS). The SEC-MALLS system consists of a Shimadzu LC-20AD, Water 717 plus autosampler, Wyatt Optilab-rEX refractive index detector, and a Wyatt HELEOS multiangle laser light scattering detector (MALLS, Wyatt Technology, Santa Barbara, CA) equipped with a GaAs laser emitting at 658nm with a power of 50 mW delivered to the flow cell. Separations based on molecular size were performed using Polymer Laboratories PLgel 500 Å, 10 000 Å columns, in series, with THF as eluent at a flow rate of 0.75 mL/min. Data were collected in 0.25s intervals. MALLS was calibrated by toluene and normalized by polystyrene standards (Sigma-Aldrich) of 29510 g/mol in THF. The measurements were performed at scattering angles from 15° to 155°. After the N435 enzyme particles were removed, the products of polymerization were directly diluted in THF (40 mg polymer/1 mL THF) without any further purification/fraction. A 100 µL solution of each sample was injected into the mobile phase after filtered through a 0.45 µm filter. All measurements were performed at 35°C and then analyzed by ASTRA software (Version 5.3.4.14).

Downloaded by STANFORD UNIV GREEN LIBR on August 28, 2012 | http://pubs.acs.org
Publication Date (Web): August 16, 2012 | doi: 10.1021/bk-2012-1105.ch008

Downloaded by STANFORD UNIV GREEN LIBR on August 28, 2012 | http://pubs.acs.org
Publication Date (Web): August 16, 2012 | doi: 10.1021/bk-2012-1105.ch008

Results and Discussion

This study focused on the synthesis and characterization of poly(oleic diacid-co-glycerol) (Scheme 1) with varied structure (composition and branching) synthesized by either enzymatic (Novozym 435, N435) or chemical (dibutyltin oxide, DBTO) catalyzed polycondensations. Of particular interest was to compare differences in polymer structure resulting from polymerizations conducted using N435 at 90°C and DBTO that requires a higher operating temperature (150°C) for use. Further diversification in polymer structure was achieved by altering the oleic diacid-glycerol feed ratio. All polymerizations were conducted without solvent by combining monomers to create monophasic binary mixtures.

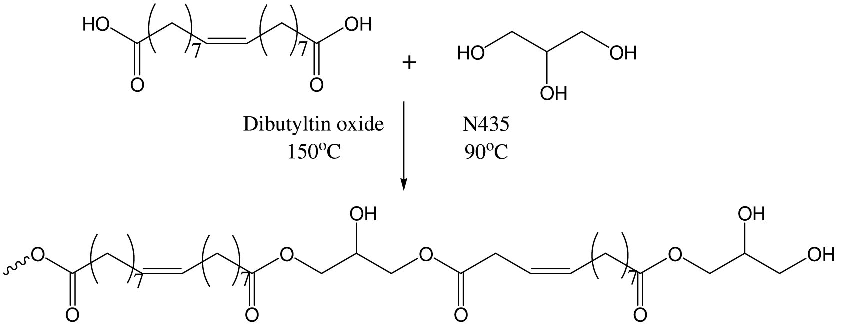

Scheme 1. Condensation polymerization of 1,18-cis-9-octandecenedioic acid (oleic diacid) with glycerol catalyzed by using either N435 or DBTO as catalyst in bulk

Structure Characterization of Poly(oleic diacid-co-glycerol)

Inverse gated ^{13}C NMR was used for structural analysis of poly(oleic diacid-co-glycerol) synthesized by N435 and DBTO catalyzed polymerization. Scheme 2 shows the different substitution patterns of glycerol units along chains and their corresponding methine (-CH-) ^{13}C NMR signals that occur between 68 and 73ppm. Peak assignments agree with those previously reported by Kulshrestha et al. (*29*) for terpolymers of adipic acid, octanediol, and glycerol. Monosubstituted glycerol units were formed by esterification with oleic diacid at either primary or secondary glycerol hydroxyl positions leading to terminal glycerol units (T_g) 1 and/or 2, respectively. The observation of a single peak at 70.3 ppm and the absence of a signal at 75.5ppm (*29*) indicated that, in this polymerization, only T_g units with structure 1 was formed. Trisubstituted or dendritic (Den) glycerol units with structure 3 resulted in an NMR resonance with a peak at 68.9ppm. Disubstituted glycerol units were formed by esterification with oleic diacid at either primary-secondary or primary-primary glycerol hydroxyl positions leading to linear glycerol units designated as $L_{1,2}$ and $L_{1,3}$ with signals at 68.2 and 72.1ppm, respectively.

Downloaded by STANFORD UNIV GREEN LIBR on August 28, 2012 | http://pubs.acs.org
Publication Date (Web): August 16, 2012 | doi: 10.1021/bk-2012-1105.ch008

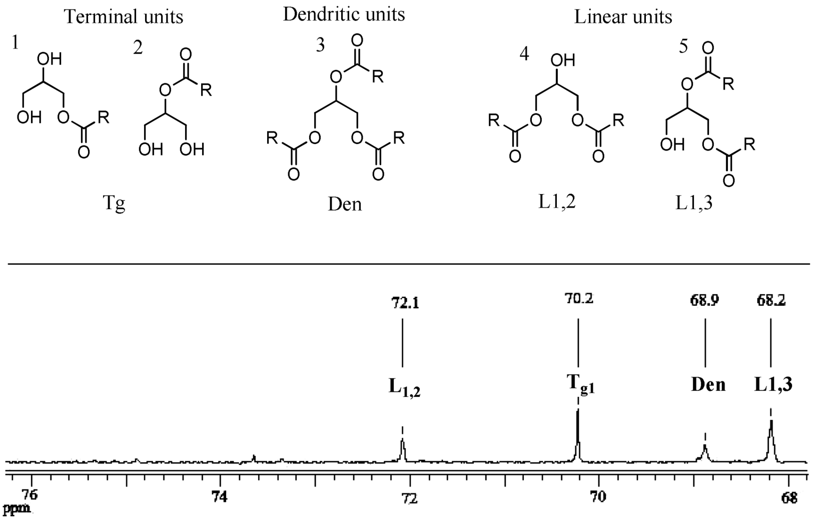
Terminal units
Dendritic units
Linear units
1
2
3
4
5
Tg
Den
L1,2
L1,3
72.1
70.2
68.9
68.2
L1,2
Tg1
Den
L1,3
76
74
72
70
68
ppm

Scheme 2. Expanded Inverse Gated ^{13}C NMR Spectrum of Poly(oleic diacid-co-glycerol), along with Structures and Abbreviations Corresponding to Substitution Patterns of Glycerol Units Leading to the Observed Signals

Equations 1-4 were used to calculate the relative percentages of T_g, $L_{1,2}$, $L_{1,3}$, and Den glycerol units, respectively.

$$T_g\% = \frac{[T_g]_I}{[L_{1,2}]_I + [L_{1,3}]_I + [T_g]_I + [Den]_I} \times 100 \quad (1)$$

$$L_{1,2}\% = \frac{[L_{1,2}]_I}{[L_{1,2}]_I + [L_{1,3}]_I + [T_g]_I + [Den]_I} \times 100 \quad (2)$$

$$L_{1,3}\% = \frac{[L_{1,3}]_I}{[L_{1,2}]_I + [L_{1,3}]_I + [T_g]_I + [Den]_I} \times 100 \quad (3)$$

$$Den\% = \frac{[Den]_I}{[L_{1,2}]_I + [L_{1,3}]_I + [T_g]_I + [Den]_I} \times 100 \quad (4)$$

The average degree of substitution (DS_{avg}) of glycerol units was calculated by eq 5:

$$Substitution = L_{1,2}\% \cdot 2 + L_{1,3}\% \cdot 2 + T_g\% \cdot 1 + Den\% \cdot 3 \quad (5)$$

DBTO-Catalyzed Condensation Polymerization of Oleic Diaicd with Glycerol

DBTO-catalyzed polycondensation of oleic diacid with glycerol (1:1 monomer feed ratio), to prepare poly(oleic diacid-co-glycerol), was performed at 150°C under reduced pressure in bulk. Figure 1 displays number-average molecular weight (Mn) and polydispersity (PDI, Mw /Mn) values as a function of reaction time, determined by SEC-MALLS. By 2h, an oligomer formed with Mn and PDI of 800 g/mol and 1.5, respectively. An increase in the reaction time to 6h showed a modest increase in Mn and PDI to 1750 g/mol and 3.0, respectively. However, as the reaction time increased from 6 to 8h, the gel content in reactions increased based on visual observation. Gel formation is attributed to cross-linking reactions. The gelled product at 8h contained 35 wt % of THF soluble material with Mn and PDI values of 3200 and 9.8, respectively.

Figure 1B displays plots of glycerol repeat unit substitution pattern as a function of reaction time determined by inverse gated ^{13}C NMR spectroscopy. From 2 to 8h, the fraction of T_g units decreased from 60 to 27%, while the fraction of $L_{1,2}$ decreased slightly (21 to 18%). Decreased fractions of T_g and $L_{1,2}$ fractions during the course of reactions was accompanied by increases in both $L_{1,3}$ and Den units. A large increase in the fraction of $L_{1,3}$ units, from 20 to 34%, was observed with increase in reaction time from 2 to 4h. Thereafter, $L_{1,3}$ units increased slowly so that, by 8h, the THF soluble fraction consisted of 39% $L_{1,3}$ units. Den units increased from 0 to 8 and 16% at 2, 4, and 6h, respectively, and, thereafter, remained unchanged.

Another variable of interest was to change the molar feed ratio of oleic diacid to glycerol (Table 1 and Figure 2). If cross-linking can be avoided, changes in monomer stoichiometry can be of value to regulate the extent of branching and carboxylic acid function group formation. Up to 4h, the product Mn and PDI values for these three polyesters with different monomer feed ratios were similar (990 to 1217 g/mol and 1.4 to 1.7, respectively). However, by increasing the molar feed ratio of oleic diacid to glycerol from 1.0:1.0 to 1.3:1.0 and 1.5:1.0, gel formation occurred earlier in the reaction. That is, for oleic diacid-to-glycerol feed ratios 1.3:1.0 and 1.5:1.0, as the reaction time increased from 4 to 6h, the gel content in reactions increased based on visual observation. As anticipated, the time to gel formation was longer (6-8h) for polymerization of the 1.0:1.0 monomer ratio. Gelled products at 6h for 1.3:1.0 and 1.5:1.0 feed ratios contained 45-50 wt % THF soluble material with Mn values of 3020 and 3240 and PDI values of 10.5 and 11.1, respectively. Furthermore, the fraction of Den glycerol units for these products was 32 and 36%, respectively. In contrast, the 6h product for 1.0:1.0 did not have a gel fraction and had values of Mn, PDI, and Den of 1700, 8.9, and 17%, respectively. Another important characterization is the average degree of substitution (DS_{avg}) of glycerol units. For 6h products formed from 1.0:1.0, 1.3:1.0 and 1.5:1.0 feed ratios of oleic diacid to glycerol, DS_{avg} increased from 1.90 to 2.18 and 2.16, respectively.

Downloaded by STANFORD UNIV GREEN LIBR on August 28, 2012 | http://pubs.acs.org
Publication Date (Web): August 16, 2012 | doi: 10.1021/bk-2012-1105.ch008

Downloaded by STANFORD UNIV GREEN LIBR on August 28, 2012 | http://pubs.acs.org
Publication Date (Web): August 16, 2012 | doi: 10.1021/bk-2012-1105.ch008

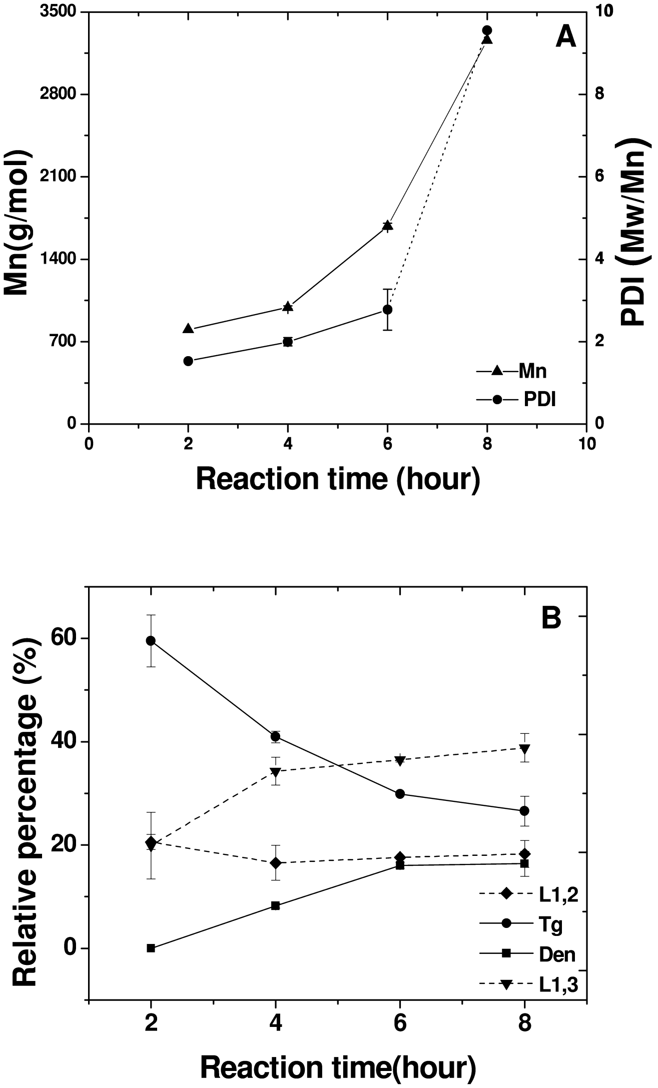

*Figure 1. Poly(oleic diaicid-co-glycerol), synthesized using DBTO as catalyst using a 1:1 molar feed ratio of monomers: (**A**) plots of Mn and PDI (Mw/Mn) as a function of reaction time; (**B**) plots of glycerol repeat unit substitution for products in (A) as a function of reaction time. The error bars represent the experimental precision at 2σ.*

Table 1. Characterization of poly(oleic diaicid-co-glycerol) molecular weight and glycerol substitution after 6 h reactions catalyzed by either N435 or DBTO[a]

Molar ratio (O:G)	*Catalyst*	*Mn*[b]	*PDI*[b] *(Mw/Mn)*	*Substitution Degree*[c] *(DS_{avg})*	*Dendritic Rate*[d]
1.0 :1.0	N435	6 000	3.3	1.84±0.01	12.7±0.4%
1.0 :1.0	DBTO	1 700	8.9	1.90±0.01	16.6±1.7%
1.1 :1.0	N435	4 980	3.1	1.89±0.01	14.0±0.8%
1.2 :1.0	N435	5 100	3.1	2.03±0.02	20.6±1.0%
1.3 :1.0	N435	4 760	2.9	2.06±0.01	21.4±0.8%
1.3 :1.0	DBTO	3 020[e]	10.5	2.18±0.04	31.7±1.4%
1.4 :1.0	N435	5 500	3.1	2.16±0.01	24.6±1.2%
1.5 :1.0	N435	5 200	3.0	2.20±0.06	31.1±2.7%
1.5 :1.0	DBTO	3 240[e]	11.1	2.26±0.02	35.8±0.3%

"O" represented oleic diacid and "G" represented glycerol. [a] polycondensations of oleic diacid with glycerol were performed in bulk at 150 or 90 °C by DBTO or N435, respectively. Samples were taken after 6 hour reaction times. [b] Data from SEC-MALS-VS without fractionation of products. [c] Data were analyzed by ^{13}C-NMR, and calculated based on the equation 4. [d] Data were analyzed by ^{13}C-NMR, and calculated based on the equation 5. [e] Samples were partially cross-linking. The data were based on dissolvable fractions in THF.

Downloaded by STANFORD UNIV GREEN LIBR on August 28, 2012 | http://pubs.acs.org
Publication Date (Web): August 16, 2012 | doi: 10.1021/bk-2012-1105.ch008

N435-Catalyzed Polycondensation of Oleic Diacid and Glycerol

N435-catalyzed polycondensation of oleic diacid with glycerol (1.0:1.0 monomer feed ratio), to prepare poly(oleic diacid-co-glycerol), was performed at 90°C, under reduced pressure, in bulk. Figure 3A displays Mn and PDI values as a function of reaction time. By 2h, an oligomer formed with Mn and PDI of 2300 g/mol and 1.9, respectively. An increase in the reaction time from 4 to 6, 10, and 24h gave products with Mn values of 4400, 6000, 7000, and 9000 g/mol, respectively. PDI values for products formed at 4 to 24h remained near 3.4. A major distinction between DBTO and N435 catalysis is that cross-linking leading to gel formation occurs with the former and not the latter. Therefore, in DBTO-catalyzed reaction, gelation precedes further chain growth and the forming of soluble higher molecular weight polyester. For example, poly(oleic diacid-co-glycerol) gelled by 8h using DBTO catalysis whereas a completely soluble copolyester was formed by N435 catalysis at 10h with Mn and PDI values of 7000 g/mol and 3.4, respectively. Furthermore, N435 catalysis leads to more rapid chain growth relative to DBTO catalysis, even though the latter is conducted at a temperature 60°C above the former. For example, Mn values for 6h polymerizations using a 1.0:1.0 monomer feed ratio, catalyzed by DBTO and N435, are 1700 and 6000 g/mol, respectively. The formation of gels by DBTO catalysis is limiting since they cannot be processed by thermal or solution methods into useful forms such as fibers, films, and other shaped objects.

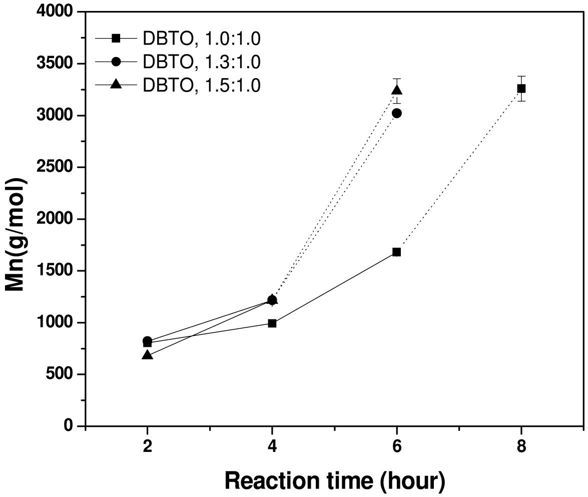

Figure 2. Plots of Mn as a function of reaction time for poly(oleic diaicid-co-glycerol) products, synthesized using DBTO as catalyst, using 1.0:1.0, 1.3:1.0 and 1.5:1 molar feed ratios of oleic diacid-to-glycerol. The error bars represent the experimental precision at 2σ.

It is enzyme regioselectivity that enables the conversion of multifunctional monomers, such as glycerol, to be converted to linear or branched polyesters. The use of lipase catalysis to control the extent of branching along chains and circumvent cross-linking reactions for copolymerizations with monomers having functionality ≥3 was recently discussed as part of a review on enzyme-catalyzed condensation polymerizations (*29*). There, it was concluded that steric constraints imposed by CALB resulted in the formation of soluble branched polyesters instead of crosslinked gels. Previous lipase-catalyzed condensation copolymerizations of glycerol and related alditol monomers focused on reactions with shorter chain diacids, often adipic acid, and involved terpolymerizations so that the concentration of glycerol along chains was diluted using a diol such as octanediol. This study provides a direct comparison of products formed by lipase and chemically-catalyzed polymerization which is critically important for defining what advantages enzyme-catalyzed polymerization methods offer to polymer chemists. Furthermore, in selecting oleic diacid, we explore a difunctional monomer that is similar in chain length to fatty acid substrates normally encountered by lipases. This could potentially lead to unique characteristics

In Biobased Monomers, Polymers, and Materials; Smith, P., et al.;
ACS Symposium Series; American Chemical Society: Washington, DC, 2012.

Downloaded by STANFORD UNIV GREEN LIBR on August 28, 2012 | http://pubs.acs.org
Publication Date (Web): August 16, 2012 | doi: 10.1021/bk-2012-1105.ch008

for lipase-catalyzed polycondensation polymerizations with multifunctional monomers such as glycerol. For example, Kumar et al. (*30*) reported that N435-catalyzed copolymerization of a 1.0:1.0 molar ratio of adipic acid and glycerol, under similar conditions as herein but over a 48h reaction time, resulted in a 50% isolated yield of poly(adipic acid-co-glycerol) with Mn 2600 g/mol. In contrast, 10 and 24h reactions between oleic diacid and glycerol gave nonfractionated poly(oleic diacid-co-glycerol) with Mn values of 7000 and 9100 g/mol, respectively. Fractionation of poly(adipic acid-co-glycerol) prior to analysis makes direct comparison of DP_{avg} values irrelevant.

Figure 3B displays plots of glycerol repeat unit substitution pattern as a function of reaction time determined by inverse gated ^{13}C NMR spectroscopy. From 2 to 24h, the percent of T_g units decreased from 46 to 27% while the percent of L 1,2 showed little variation (15-20%). These trends are similar to those observed for DBTO-catalyzed polymerizations (Figure 1B). The content of $L_{1,3}$ units reached 48% at 4h and, thereafter, remained at about 39%. In contrast, using DBTO catalysis, $L_{1,3}$ units were initially low and increased over reaction time (see Figure 1B). However, comparison of trends observed in Figures 1B and 3B must also consider that the range of poly(oleic diacid-co-glycerol) molecular weights studied for DBTO catalysis is only between Mn 800 and 1700 g/mol at 2 and 6h, respectively, after which the reaction solution began to gel. In contrast, for N435 catalysis, Mn ranged from 2300 to 9100 g/mol. The ratio of $L_{1,3}$ /$L_{1,2}$ units for Mn 1700 and 2300 g/mol samples from DBTO and N435 catalysis is 2.1 and 2.6, respectively. Hence, by using CALB as catalyst instead of DBTO, there is only a small increase in selectivity for primary versus secondary substitution at linear glycerol units. This is reasonable since it is well-known that CALB is not strictly 1,3-selective for esterification of glycerol (*29*, *30*). For example, Kulshrestha et al., (*29*) using N435 to catalyze the reaction between adipic acid, octanediol, and glycerol, found that during the first 18h of a copolymerization with monomer feed ratio 1.0:0.8:0.2 (adipic acid: octanediol: glycerol) the regioselectivity of N435 resulted in linear copolyesters, but as the reaction time extended (42h), hyperbranched copolymers with dendritic glycerol units were obtained. Herein, no Den units were observed during the first 4h of polyester synthesis by N435. Thus, up to Mn 4400 g/mol, poly(oleic diacid-co-glycerol) is linear consisting of a mixture of $L_{1,3}$, $L_{1,2}$, and T_g glycerol units. In contrast, poly(oleic diacid-co-glycerol) prepared during a 6h DBTO catalyzed polymerization has Mn 1700 g/mol (~40% of that from N435 catalysis) and 16% Den units. This result is a direct consequence of steric hindrance at CALB's active site that impedes branching along chains. However, as the N435-catalyzed polymerization is extended to 6h, the reaction moves from kinetic to thermodynamic control and poly(oleic diacid-co-glycerol) with Mn 6000 g/mol and 13% Den glycerol units is formed. The basic trends observed here were also found for an N435 terpolymerization with a shorter diacid (adipic acid) where glycerol units were diluted along the chain with 1,8-octanediol repeat units (four 1,8-octanediol units per glycerol unit) (*29*).

Downloaded by STANFORD UNIV GREEN LIBR on August 28, 2012 | http://pubs.acs.org
Publication Date (Web): August 16, 2012 | doi: 10.1021/bk-2012-1105.ch008

Downloaded by STANFORD UNIV GREEN LIBR on August 28, 2012 | http://pubs.acs.org
Publication Date (Web): August 16, 2012 | doi: 10.1021/bk-2012-1105.ch008

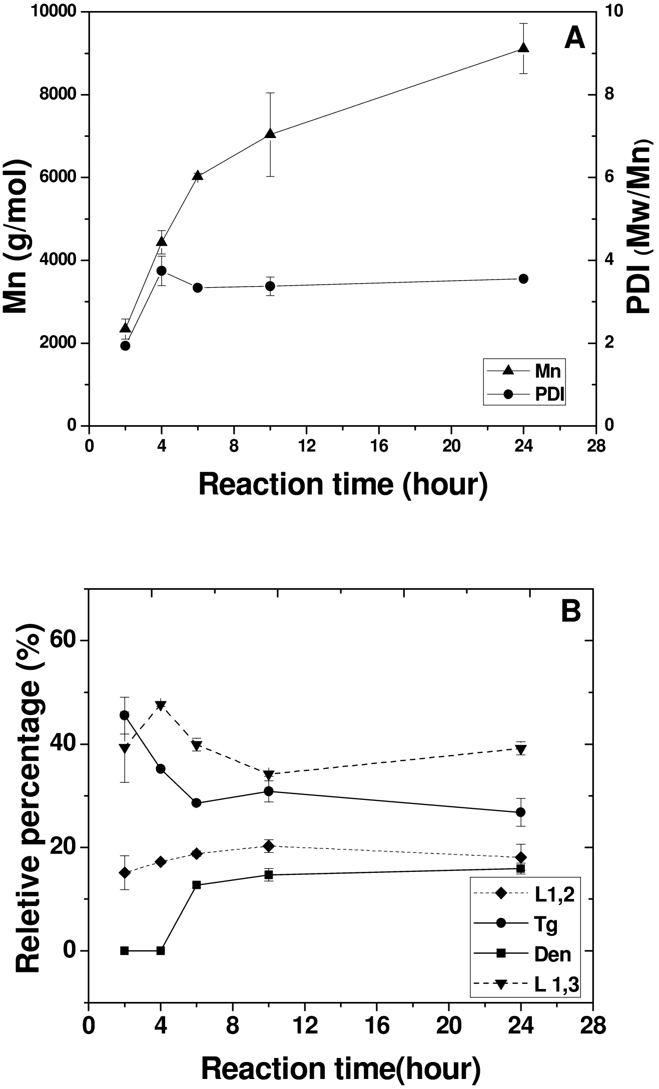

Figure 3. Poly(oleic diacid-co-glycerol), synthesized by N435 catalysis, using a 1:1 molar feed ratio of monomers: ***(A)*** *plots of* M_n *and PDI (*M_w/M_n*) as a function of reaction time,* ***(B)*** *plots of glycerol repeat unit substitution for products in* ***3A*** *as a function of reaction time. The error bars represent the experimental precision at 2σ.*

Further study of results in Figure 3 leads us to a hypothetical model of poly(oleic diacid-co-glycerol) structure (Scheme 3) formed by N435 catalysis. On the basis of the molecular weight and different glycerol unit contents, the average number of glycerol units along poly(oleic diacid-co-glycerol) chains (G_{avg}) were calculated. For polyesters formed at 6, 10, and 24 h, G_{avg} values are 15, 18, and 24, respectively. Poly(oleic diacid-co-glycerol) synthesized after reaction for (i) 6h has G_{avg} 15 with 2 Den, 4 T_g , 3 $L_{1,2}$, and 6 $L_{1,3}$ units (Scheme 3A); (ii) 10 h has G_{avg} 18 with 3 Den, 5 T_g , 4 $L_{1,2}$, and 6 $L_{1,3}$ units (Scheme 3B); and (iii) 24 h has G_{avg} 24 with 4 Den, 6 T_g units, 4 $L_{1,2}$, and 9 $L_{1,3}$ units (Scheme 3C). The depiction of polyester structures suggests there are no free carboxylic acid polyester chain-end groups. Instead, the polyester chain ends consist exclusively of T_g units. These results were also confirmed by ^{13}C NMR spectra of poly (oleic diacid-co-glycerol), synthesized from a 1.0:1.0 ratio of oleic diacid to glycerol, catalyzed by N435 at 90°C for 24h in bulk. Observation of the expended spectral region from 170 to 180 ppm in Figure 4A shows multiple signals at between 173.0 and 174.5 ppm that correspond to oleic diacid carbonyl carbons esterified to glycerol units ($-CH_2-CH_2-CO-O-Gly-$). The origin of multiple signals in this region is due to the numerous ways glycerol units of ester moieties can be substituted (Den, T_g , $L_{1,2}$, and $L_{1,3}$) as well as whether the ester link is between the carbonyl of a secondary or primary hydroxyl group. That no signal corresponding to a free oleic diacid carboxylic acid (-COOH) carbonyl is observed at 178.3ppm confirms that the product structure agrees with the generalized structures displayed in Scheme 3. When DBTO catalysis was used to prepare poly(oleic diacid-co-glycerol) from a 1.0:1.0 ratio of oleic diacid to glycerol, the product after 6h shows signals in the ranges of both 177.5-178.5 and 173.0-174.5ppm, proving the coexistence of both T_g and free acid terminal units.

A question of interest is whether N435 catalysis would provide a means to obtain non-cross-linked poly(oleic diacid-co-glycerol) from polymerizations where the stoichiometry of oleic diacid to glycerol was increased above 1.0:1.0 up to 1.5:1.0. Furthermore, such experiments probe the extent to which cross-link reactions can be avoided by using N435, a selective immobilized lipase catalyst. Results above using DBTO catalysis with oleic diacid-to-glycerol ratios of 1.3:1.0 and 1.5:1.0 (Figure 2) formed gels after only reaching Mn about 1200 g/mol.

Study of results for N435-catalyzed polymerizations in Figure 5 and Table 1 shows that, up to 6h, product Mn and PDI are about 5000 g/mol and 3.0, respectively, and vary little for the five different monomer feed ratios studied. Further increase in reaction time up to 24h for copolymers synthesized from 1.1:1.0 to 1.5:1.0 ratios shows a slow increase in Mn up to about 6500 g/ mol. In comparison, the copolyester synthesized from 1.0:1.0 ratio of monomers reaches Mn 9100 g/mol by 24 h.

From the above we conclude that, even when the ratio of oleic diacid to glycerol in the feed is greater than 1.0:1.0, cross-linking is avoided when reactions are catalyzed by N435 instead of DBTO. Because of N435's ability to deter cross-link reactions, a family of unique, soluble, hyperbranched copolyesters is formed with substantial Mn values. Analysis of copolymer microstructure by inverse gated NMR was carried out for products after 6h reaction times, and the results are listed in Table 1. As the ratio of oleic diacid in the feed was increased, the general trend observed is the Den% glycerol units increased from 12.7 to 31.1%. Accordingly, the DS_{avg} increases from 1.84 to 2.20. Furthermore, the percent T_g units decreased as the feed ratio of oleic diacid to glycerol increased. That is, as the feed ratio of oleic diacid to glycerol increased from 1.0:1.0 to 1.5:1.0, T_g units decreased from 29 to 11%. Thus, by increasing the ratio of oleic diacid to glycerol

Downloaded by STANFORD UNIV GREEN LIBR on August 28, 2012 | http://pubs.acs.org
Publication Date (Web): August 16, 2012 | doi: 10.1021/bk-2012-1105.ch008

in the monomer feed, products are produced with far less T_g but more Den glycerol units so that the functionality of chain ends and branch points is predominantly carboxylic acid groups.

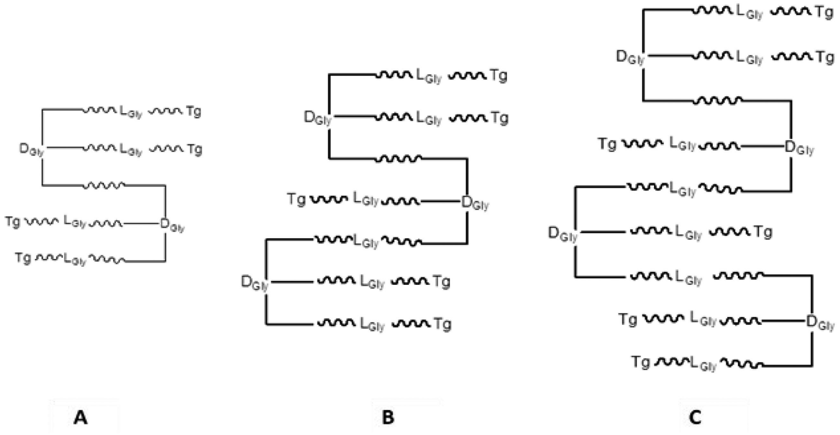

Scheme 3. Predicted structures of poly(oleic diacid-co-glycerol) based on molecular weight and glycerol units content. Polyesters were synthesized by molar ratio 1.0 :1.0 oleic diacid : glycerol, catalyzed by N435 at 90°C in bulk. ***(A)*** *6 hours reaction gave the polyester G_{avg} about 15, with 2 Den and 4 T_g units,* ***(B)*** *10 hours reaction gave the polyester G_{avg} 18, with 3 Den and 5 T_g units,* ***(C)*** *10 hours reaction gave the polyester G_{avg} 24, with 4 Den and 6 T_g units*

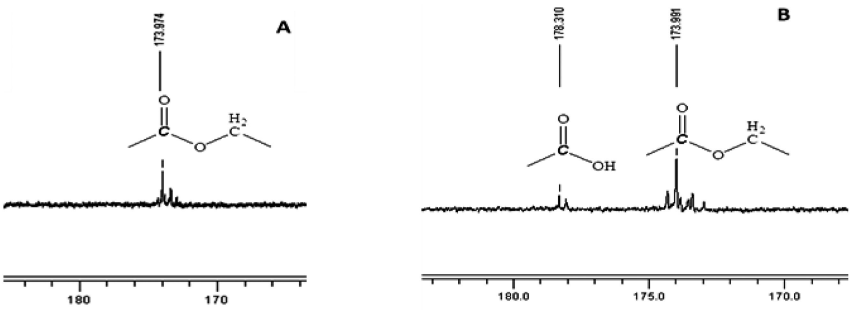

*Figure 4. Expended spectrum of poly(oleic diacid-co-glycerol) at the range about 166-184 ppm. (**A**) Polyester synthesized by N435 at 24 hour; (**B**) Polyester synthesized by DBTO at 6 hour. The oleic diacid carbonyl can be linked to a glycerol in a variety of ways as is depicted in Scheme 2.*

Downloaded by STANFORD UNIV GREEN LIBR on August 28, 2012 | http://pubs.acs.org
Publication Date (Web): August 16, 2012 | doi: 10.1021/bk-2012-1105.ch008

Downloaded by STANFORD UNIV GREEN LIBR on August 28, 2012 | http://pubs.acs.org
Publication Date (Web): August 16, 2012 | doi: 10.1021/bk-2012-1105.ch008

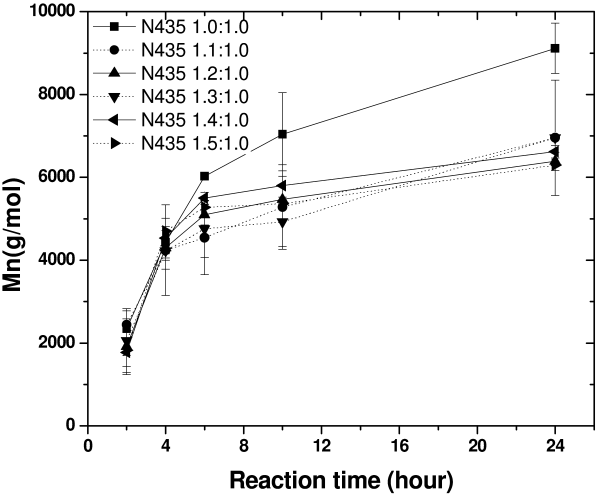

Figure 5. Plots of Mn as a function of reaction time for poly(oleic diaicid-co-glycerol) products, synthesized using N435 as catalyst, using 1.0:1.0, 1.1:1.0, 1.2:1.0, 1.3:1.0, 1.4:1.0 and 1.5:1.0 molar feed ratios of oleic diacid-to-glycerol. The error bars represent the experimental precision at 2σ.

Thermal Properties

As discussed above, a series of poly(oleic diacid-co-glycerol) samples that differ in structural parameters (i.e., end-group/terminal branch composition, degree of branching, and copolymer composition) were prepared by N435 catalysis by varying the ratio of oleic diacid to glycerol in the monomer feed from 1.0:1.0 up to 1.5:1.0 (see Table 1 and Figure 5). Since this series of samples also has similar Mn values at 24h reaction times, they were selected to assess whether structural variations would substantially change their thermal properties. Thermal properties obtained by TGA and DSC experiments are listed in Table 2.

All poly(oleic diacid-co-glycerol) samples in Table 2 exhibited good thermal stabilities both in nitrogen and air. In nitrogen, 10% weight loss of polyesters (T_d) occurred between 380 and 440°C. For each sample, 10% T_d in air was between 20 and 66°C lower than that under nitrogen. This is likely explained by oxidation of polyesters in air, which led to random cleavage events that accelerate material decomposition. Polyesters had similar decomposition peak temperatures (peak T_d) around 470°C in nitrogen and 460°C in air. DSC analyses showed multiple melting peaks during heating scans from which total enthalpies (ΔH m) were calculated. Regardless of structural variations for this series of samples, the lowest melting point transition (peak 1) was observed between -23 and -33°C, which was also the major melting transition step. Differences were found for the secondary melting point (peaks 2 and 3). Higher oleic diacids (e.g., 1.5:1.0) contents in the monomer feed gave lower secondary melting transitions (-15.6°C) than was observed for poly(oleic diacid-co-glycerol) prepared from a lower feed ratio (e.g., 1.0:1.0, 13.7°C). On the basis of the summation of melting transition steps, the total ΔH m values were between 14 and 19 J/g. Further investigations to characterize other properties of poly(oleic diacid-co-glycerol) materials (e.g., biocompatibility, bioerosion rate, mechanical properties) are currently underway in our laboratory.

Table 2. Thermal properties of Poly(oleic diacid-co-glycerol) Samples Prepared by N435[a] Catalysis and Variation in the Monomer Feed Ratio (See Figure 5)

Molar ratio (O:G)	*Mn* [b]	*PDI*[b]	T_d (°C) [c]				T_m(°C) [d]			ΔH_m (J/g)[d]
			N_2		*air*					
			5%	*peak*	*5%*	*peak*	*1*	*2*	*3*	
1.0 :1.0	9120	3.3	384	467	342	460	-26.8	-3.7	13.7	15.4
1.1 :1.0	6960	3.1	381	469	356	461	-24.2	-3.8	13.2	17.4
1.2 :1.0	6390	3.1	434	477	414	459	-22.5	-	-6.9	18.7
1.3 :1.0	6960	2.9	400	470	380	458	-24.4	-	-9.5	19.0
1.4 :1.0	6620	3.1	430	475	406	460	-26.8	-	-11.5	18.4
1.5 :1.0	6300	3.0	397	471	331	453	-32.6	-	-15.6	13.5

"O" represented oleic diacid and "G" represented the glycerol. [a] Polycondensations of oleic diacids with glycerol were performed in bulk at 90 °C by Novozym 435 for 24h. [b] Data from SEC-MALLS were measured using THF as eluent. Samples without precipitation were used for measurements. [c] Decomposition temperatures for 10% or peak weight loss, analyzed by TGA under nitrogen or air atmosphere at a heating rate of 10°C/min from 25 to 700 °C. [d] Data from DSC from the second heating scan run at 10°C/min. [e] ΔHm values were determined by summation of all melting transition steps.

Downloaded by STANFORD UNIV GREEN LIBR on August 28, 2012 | http://pubs.acs.org
Publication Date (Web): August 16, 2012 | doi: 10.1021/bk-2012-1105.ch008

Conclusion

Candida tropicalis ATCC20962 was used to prepare 1,18-cis-9-octadecenedioic (oleic diacid) by selective ω-carboxylation of oleic acid. This work focused on comparing and contrasting the synthesis and structure of poly(oleic diacid-co-glycerol) prepared by polymerizations catalyzed by N435 at 90°C and DBTO at 150°C.

DBTO-catalyzed polycondensation of oleic diacid with glycerol (1:1 monomer feed ratio) proved limiting with respect to the ability to prepare soluble products of substantial molecular weight. By 6h, products formed have Mn and PDI of 1750 g/mol and 3.0, respectively. However, with an increase in reaction time from 6 to 8h, the gel content in reactions increased so that the product contained only 35 wt % THF-soluble material.

In contrast to the above, N435 catalysis of oleic diacid/glycerol (1.0:1.0 monomer feed ratio) gave polyesters with Mn values of 4400, 6000, 7000, and

Downloaded by STANFORD UNIV GREEN LIBR on August 28, 2012 | http://pubs.acs.org
Publication Date (Web): August 16, 2012 | doi: 10.1021/bk-2012-1105.ch008

9000 g/mol at reaction times of 4, 6, 10, and 24h, respectively. Up to 4h, poly(oleic diacid-co-glycerol) is linear with a mixture of $L_{1,3}$, $L_{1,2}$, and T_g glycerol units. PDI values for products remained near 3.4. Cross-linking and gel formation observed with DBTO catalysis were not observed by N435 catalysis. This is a result of steric hindrance at CALB's active site that slows branching and obstructs crosslinking reactions. Gel formation at low molecular weight is limiting while formation of higher molecular weight poly(oleic diacid-co-glycerol) may enable options to process final products by thermal or solution methods into useful forms such as fibers, films, and other shaped objects. Furthermore, poly(oleic diacid-co-glycerol) formed using a 1:1 ratio of oleic diacid to glycerol was found to have exclusively monosubstituted glycerol (T_g) branch and chain-end units. These are intriguing structures for subsequent functionalization and use as prepolymers.

Further diversification of poly(oleic diacid-co-glycerol) structure was achieved using N435 catalysis and by altering the stoichiometry of oleic diacid to glycerol above 1.0:1.0 up to 1.5:1.0. By 6h, product Mn (about 5000 g/mol) and PDI (about 3.0) vary little for the five different monomer feed ratios studied. No cross-linking based in microgel formation is observed, even up to 24h reaction times. With an increase in the oleic diacid to glycerol feed ratio, T_g units decreased from 29% to 11% while Den% glycerol units increased from 12.7 to 31.1%. Thus, variation of the feed ratio enabled the synthesis of a family of unique, soluble, hyperbranched copolyesters.

Studies of poly(oleic diacid-co-glycerol) by thermogravimetric analysis (TGA) showed that the above products from different feed ratios have similar decomposition peak temperatures, around 470°C in nitrogen and 460°C in air. DSC analyses showed multiple melting peaks at temperatures below 14°C. The inability of poly(oleic diacid-co-glycerol) to form a high melting crystal phase is a consequence of carbon-carbon double bonds in oleic diacid units that cause kinks in chains.

References

1. Hill, K. *Pure Appl. Chem.* **2000**, *72*, 1255–1264.
2. Teomim, D.; Nyska, A.; Domb, A. J. *J. Biomed. Mater. Res.* **1999**, *45*, 258–264.
3. Metzger, J. O. *Eur. J. Lipid Sci. Technol.* **2009**, *111*, 865–876.
4. Warwel, S.; Demes, C.; Steinke, G. *J. Polym. Sci., Part A: Polym. Chem.* **2001**, *39*, 1601–1609.
5. Quinzler, D.; Angew, M. S. *Chem. Int. Ed.* **2010**, *49*, 4306–4308.
6. Brütting, A.; Spiteller, G. *Fat Sci. Technol.* **1994**, *96*, 445–451.
7. Eschenfeldt, W. H.; Zhang, Y.; Samaha, H.; Stols, L.; Eirich, L. D.; Wilson, C. R.; Donnelly, M. I. *Appl. Environ. Microbiol.* **2003**, *69*, 5992–5999.
8. Picataggio, S.; Rohrer, T.; Deanda, K.; Lanning, D.; Reynolds, R.; Mielenz, J.; Eirich, L. D. *Nat. Biotechnol.* **1992**, *10*, 894–898.

Downloaded by STANFORD UNIV GREEN LIBR on August 28, 2012 | http://pubs.acs.org
Publication Date (Web): August 16, 2012 | doi: 10.1021/bk-2012-1105.ch008

9. Craft, D. L.; Madduri, K. M.; Eshoo, M. *Appl. Environ. Microbiol.* **2003**, *69*, 5983–5991.
10. Yang, Y.; Lu, W.; Zhang, X.; Xie, W.; Cai, M.; Gross, R. A. *Biomacromolecules* **2010**, *11*, 259–268.
11. Wang, Y. D.; Ameer, G. A.; Sheppard, B. J.; Langer, R. *Nat. Biotechnol.* **2002**, *20*, 602–606.
12. Gao, J.; Crapo, P. M.; Wang, Y. D. *Tissue Eng.* **2006**, *12*, 917–925.
13. Wang, Y. D.; Kim, Y. M.; Langer, R. *J. Biomed. Mater. Res., Part A* **2003**, *66*, 192–197.
14. Sundback, C. A.; Shyu, J. Y.; Wang, Y. D.; Faquin, W. C.; Langer, R. S.; Vacanti, J. P. *Biomaterials* **2005**, *26*, 5454–5464.
15. Motlagh, D.; Yang, J.; Lui, K. Y.; Webb, A. R.; Ameer, G. A. *Biomaterials* **2006**, *27*, 4315–4324.
16. Bettinger, C. J.; Orrick, B.; Misra, A.; Langer, R.; Borenstein, J. T. *Biomaterials* **2006**, *27*, 2558–2565.
17. Stumbe, J.; Bruchmann, B. *Macromol. Rapid Commun.* **2004**, *25*, 921–924.
18. Brioudea, M. M.; Guimar~aesa, D. H.; Boaventura, J. S.; Jose, N. M. *Mater. Res.* **2007**, *10*, 335–339.
19. Wyatt, V. T.; Nunez, A.; Foglia, T. A.; Marmer, W. N. *J. Am. Oil Chem. Soc.* **2006**, *86*, 1033–1039.
20. Guimar~aesa, D. H.; Brioudea, M. M.; Boaventura, J. S.; Jose, N. M. *Mater. Res.* **2007**, *10*, 257–260.
21. Wang, Y.; Ameer, G. A.; Sheppard, B. J.; Langer, R. *Nat. Biotechnol.* **2002**, *20*, 602–606.
22. Gross, R. A.; Ganesh, M.; Lu, W. *Trends Biotechnol.* **2010**, *28*, 435–443.
23. Gross, R. A.; Kumar, A.; Kalra, B. *Chem. Rev.* **2001**, *101*, 2097–2124.
24. Kobayashi, S. *Macromol. Rapid Commun.* **2009**, *30*, 237–266.
25. Kobayashi, S.; Makino, A. *Chem. Rev.* **2009**, *109*, 5288–5353.
26. Kobayashi, S.; Uyama, H.; Kimura, S. *Chem. Rev.* **2001**, *101*, 3793–3818.
27. Varma, I. K.; Albertsson, A. C. *Prog. Polym. Sci.* **2005**, *30*, 949–981.
28. Kelly, A. R.; Hayes, D. G. *J. Appl. Polym. Sci.* **2006**, *101*, 1646–1656.
29. Kulshrestha, A. S.; Gao, W.; Gross, R. A. *Macromolecules* **2005**, *38*, 3193–3204.
30. Kumar, A.; Kulshrestha, A. S.; Gao, W.; Gross, R. A. *Macromolecules* **2003**, *36*, 8219–8221.

Downloaded by PENNSYLVANIA STATE UNIV on August 28, 2012 | http://pubs.acs.org
Publication Date (Web): August 16, 2012 | doi: 10.1021/bk-2012-1105.ch009

Chapter 9

Polymers from Fatty Acids: Poly(ω-hydroxyl tetradecanoic acid) Synthesis and Physico-Mechanical Studies

Chen Liu,[a,¶] Fei Liu,[a] Jiali Cai,[a,¶] Wenchun Xie,[a] Timothy E. Long,[b] S. Richard Turner,[b] Alan Lyons,[c] and Richard A. Gross*,[a]

[a]NSF I/UCRC for Biocatalysis and Bioprocessing of Macromolecules, Department of Chemical and Biological Sciences, Polytechnic Institute of NYU, Six Metrotech Center, Brooklyn, NY 11201
[b]Department of Chemistry, Virginia Tech, 107 Davidson Hall, Blacksburg, VA 24061-0001
[c]Center for Engineered Polymer Materials, Department of Chemistry, College of Staten Island (CUNY), Building 6S - Room 225, 2800 Victory Boulevard, Staten Island, NY 10314
¶Contributed equally to the importance.
***E-mail: rgross@poly.edu.**

This chapter describes the synthesis and physicomechanical properties of bioplastics prepared from methyl-hydroxytetradecanoic acid (Me-ω-OHC14), a new monomer available by a fermentation process using an engineered *Candida tropicalis* strain. Melt-condensation experiments were conducted using titanium tetraisopropoxide ($Ti[OiPr]_4$) as a catalyst in a two stage polymerization (2h at 200 °C under N_2, 4h at 220 °C under 0.1 mmHg). Poly(ω-hydroxytetradecanoate), P(ω-OHC14), M_w, determined by SEC-MALLS, increased from 53K to 110K as the $Ti(OiPr)_4$ concentration increased from 50 to 300 ppm. By varying the polymerization conditions (catalyst concentration, reaction time, second-stage reaction temperature) a series of P(ω-OHC14) samples were prepared with M_w values from 53K to 140K. The synthesized polyesters with M_w ranging from 53K to 140K were subjected to characterization by DSC, TGA, DMTA and tensile testing. Influences of P(ω-OHC14) molecular weight, melting point,

In Biobased Monomers, Polymers, and Materials; Smith, P., et al.;
ACS Symposium Series; American Chemical Society: Washington, DC, 2012.

and enthalpies of melting/crystallization on material tensile properties were explored. Cold-drawing tensile tests at room temperature for P(ω-OHC14) with M_w 53K to 78K showed a brittle-to-ductile transition. In contrast, P(ω-OHC14) with M_w 53K undergoes brittle fracture. Increasing P(ω-OHC14) M_w above 78K resulted in strain-hardening phenomenon and tough properties with elongation at break about 700% and true tensile strength about 50 MPa. Comparisons between HDPE and P(ω-OHC14) mechanical and thermal properties as a function of their respective molecular weights are discussed.

Downloaded by PENNSYLVANIA STATE UNIV on August 28, 2012 | http://pubs.acs.org
Publication Date (Web): August 16, 2012 | doi: 10.1021/bk-2012-1105.ch009

Introduction

The development of bio-based plastics is an important area of research in both academic and industrial laboratories. Biobased plastics, produced from renewable feedstock such as biomass, can decrease our dependency on petroleum and positively impact efforts to curb global warming. The maximum potential of biobased polymers to substitute for their petrochemical counterparts is estimated at 270 Mt, or 90% of the total polymers (*1*). Furthermore, a recent study predicts the worldwide capacity of biobased plastics will increase from 0.36 Mt in 2007 to 2.33 Mt and 3.45 MT in 2013 and 2020, respectively (*1*). Therefore, there is a considerable pull from the consumer market for new biobased materials that meet cost-performance requirements.

Poly(ω-hydroxyfatty acids), P(ω-OHFAs), have structures reminiscent of polyethylene (PE) but, unlike PE, have ester groups separated by moderate stretches of methylene units (generally 13 to 17). The length of methylene units separating ester groups is determined by the fatty acid chain length from which the ω-OHFAs are derived. P(ω-OHFAs) are expected to retain their biodegradability in bioactive environments while solving common problems with existing biobased materials. For example, deficiencies of polylactic acid and microbial polyesters include hydrolytic stability, shelf life and brittleness (*2–4*). Furthermore, P(ω-OHFAs) will solve known shortcomings of PE such as PE's low surface chemical reactivity that causes poor adhesion in composite materials, laminates and blends (e.g. with polyamides and polyesters) (*5–7*).

A roadblock to commercial development of P(ω-OHFAs) is the lack of low cost, practical and environmentally friendly routes to monomer synthesis. Chemical routes to ω-hydroxyfatty acids include: *i*) subjecting ω-hydroxyalkyl-γ-butyrolactones or ω-acyloxyalkyl-γ-butyrolactones to a hydrocracking catalyst in the presence of hydrogen gas (*8*); *ii*) reducing and ring-opening of 2-tetrahydrofuran-undecanoic acid in the presence of a hydrogenation catalyst and a solid acid catalyst (*9*); and *iii*) subjecting an alkali or alkaline earth metal salt of long-chain dicarboxylic acid monoester to a reduction with a borohydride compound or by catalytic hydrogenating reduction (*10*). However, these chemical routes suffer from one or more of the following drawbacks: *i*) require multiple steps, *ii*) use harsh chemical reagents, *iii*) depend on nonrenewable feedstocks, *iv*) exhibit a lack selectivity and *v*) are limited in the range of products formed. All these difficulties create hurdles that limit their commercialization potential.

In a recent report by our laboratory and collaborators, a biotechnological route to ω-OHFAs was disclosed (*11*). An engineered strain of the diploid yeast *Candida tropicalis* was developed that produces commercially viable yields of *ω*-hydroxyfatty acids (*11*). In one experiment, volumetric yields exceeding 160 g/L of 14-hydroxytetradecanoic acid (ω-OHC14) were obtained during a 140 h fermentation. There are plant-derived ω-hydroxyl fatty acids. For example, Veld et al. (*12*) reported that aleuritic acid, with two secondary and one primary (ω-position) hydroxyl group, can be polymerized with a lipase catalyst. Aleuritic acid is derived from ambrettolide that occurs naturally in musk abrette seed oil and is a valued perfume base. Birch outer bark contains suberin from which *cis*-9,10-epoxy-18-hydroxyoctadecanoic acid can be isolated (*5*). However, functional fatty acid monomers from specialty seed oils such as abrette are in low abundance. Furthermore, fatty acids from major seed oil sources lack ω-hydroxyl groups. Moreover, it is difficult to purify components of suberin and cutin that consist of severe mixtures of ω-hydroxylated and other fatty acid structures.

Organometallic catalysts play an important role in condensation polymerizations, accelerating polymerization rates to produce high molecular weight products with desired physicomechanical properties (*13–15*). Currently, metal catalysts based on antimony and germanium dominates industrial condensation polymerization processes. The desire to replace these two catalysts originates from antimony's negative environmental impact and germanium's high cost (*16*, *17*). Titanium alkoxides are emerging as important polyesterification catalysts due to their high activity, general view that they do not cause environmental problems and acceptable pricing for low-cost industrial processes (*18*).

A number of studies attest to the relatively high activity of titanium alkoxide catalysts for polyesterification reactions (*19–24*). Investigation of bulk bis(hydroxyethyl) terephthalate polycondensation reactions to synthesize poly(ethylene terephthalate) (PET) showed that the relative catalyst activity was as follows: Ti > Sn > Sb > Mn > Zn >Pb. Polymer intrinsic viscosities up to 0.66 were attained with 200 ppm potassium titanium oxalate per mole of monomer (*23*). Multiple authors reported that titanium tetra(isopropoxide), ($Ti(OiPr)_4$), was the preferred catalyst for the synthesis by condensation polymerizations of poly(ethylene succinate), poly(tetramethylene succinate) and copolymers (*19–22*). Shirahama et al (*24*), during investigations of condensation polymerization catalysts to prepare aliphatic polyesters, reported that $Ti(OiPr)_4$ was most active of several metal alkoxide catalysts investigated that included $Ti(OEt)_4$, $Zr(OBu)_4$, $Nb(OEt)_5$ and $Ta(OEt)_5$.

The present study was motivated by the recent discovery that ω-OHC14 can be produced from methyl tetradecanoic acid (methyl myristate) by a fermentation process in volumetric yields up to 160 g/L, productivity up to 2.0 g/L/h, with <5 mol% diacid (*11*). The goals of this work was to: *i*) develop an efficient polymerization method to prepare P(ω-OHC14) in high molecular weight and *ii*) investigate the thermal and tensile properties of a press-molded P(ω-OHC14) film. On the basis of our literature review, $Ti(OiPr)_4$ was selected as catalyst for

Downloaded by PENNSYLVANIA STATE UNIV on August 28, 2012 | http://pubs.acs.org
Publication Date (Web): August 16, 2012 | doi: 10.1021/bk-2012-1105.ch009

Downloaded by PENNSYLVANIA STATE UNIV on August 28, 2012 | http://pubs.acs.org
Publication Date (Web): August 16, 2012 | doi: 10.1021/bk-2012-1105.ch009

condensation polymerizations to convert methyl ω-hydroxytetradecanoate (Me-ω-OHC14) to P(ω-OHC14). Effects of $Ti(OiPr)_4$ concentration, reaction time and temperature were investigated. Studies of P(ω-OHC14) thermal and tensile properties were determined as a function of polymer molecular weight. P(ω-OHC14) properties were compared to chemical analogs P(ω-OHC15), prepared by lipase-catalyzed ring-opening polymerization of ω-pentadecalactone (*25*), and high density PE.

Experimental Section

Materials

Methyl ω-hydroxytetradecanoate, Me-ω-OHC14 (>99.95% purity), was a gift from SynthZyme LLC. TYZOR® TPT (titanium tetraisopropoxide, $Ti(OiPr)_4$, 100 % active content) was purchased from DuPont. Chloroform (HPLC grade) was purchased from Pharmaco. 1-Butanol (anhydrous, 99.8%) was purchased from Sigma-Aldrich. All chemicals were used as received.

Preparation of P(ω-OHC14)

In a typical experiment, polymerizations were conducted in a 100 mL single-neck round-bottomed flask equipped with a mechanical overhead stirrer, nitrogen inlet and air condenser. Monomer (10 g) and a predetermined amount of catalyst solution (10 mg/mL $Ti(OiPr)_4$ in 1-butanol) were transferred into the reaction flask. The system was placed under vacuum (0.1 mmHg) and purged with N_2 gas, and this cycle was repeated three times. Subsequently, under N_2 gas, the reaction flask was placed into a preheated 200 °C silicone oil bath and this first stage of the reaction was conducted for 2 h. Thereafter, the second stage of the polymerization was performed by: *i*) raising the temperature of the external silicone oil bath temperature to 220 °C, *ii*) placing the contents of the reaction flask under reduced pressure (0.1 mmHg), *iii*) maintaining these reaction conditions for 4 h. In both stages of the reaction, stirring was carried out using an overhead stirrer at 1500 rpm. The stirrer shaft is made from stainless steel and a swivel blade attached to the shaft mixed reactions. Viscous reaction products were cooled to room temperature under N_2 gas in the reactor flask. Then, to transfer the product from the reaction flask without breaking the flask, we added cold chloroform (~ 50 mL). Products were not fractionated and solvent was removed by rotary evaporation. Remaining volatile compounds were removed from the product in a vacuum oven (2 mmHg, 16 h, 50 °C). Nuclear magnetic resonance (NMR) spectrum (300 MHz, chloroform-*d*) of $–[^{a}C(=O)\text{-}^{b}CH_2\text{-}^{c}CH_2\text{-}^{d}(CH_2)_9\text{-}^{e}CH_2\text{-}^{f}CH_2\text{-}O]\text{-}$: ^{1}H NMR: 4.05 (t, J 6.5Hz, protons *f*); 2.28 (t, J 7.5Hz, protons *b*); 1.59/1.26ppm (brs, protons *c*, *e* and *d*) and ^{13}C NMR: 173.97 (carbon *a*); 64.39 (carbon *f*); 34.40 (carbon *b*); 29.02-29.80 (carbons *d*); 25.95 (carbon *e*); 25.03ppm (carbon *c*). According to published IR spectra from polycaprolactone (*26*) and PE (*27*, *28*), diagnostic peaks in the P(ω-OHC14) IR spectrum were assigned as follows: 2920 cm^{-1} (asymmetric CH_2 stretching); 2850 cm^{-1} (symmetric CH_2 stretching); 1730 cm^{-1} (carbonyl(C=O) stretching); 1460 cm^{-1} (CH_2 bending); 1420 cm^{-1}; 1370 cm^{-1} (CH_2 wagging); 1350 cm^{-1}; 1320 cm^{-1}; 1300 cm^{-1} (C-O and C-C stretching in the crystalline phase); 1270 cm^{-1}; 1250 cm^{-1} (asymmetric C-O-C stretching); 1220 cm^{-1}; 1200 cm^{-1} (OC-O stretching); 1180 cm^{-1} (symmetric C-O-C stretching); 1115 cm^{-1}; 1090 cm^{-1} (C-O and C-C stretching in the amorphous phase); 1030 cm^{-1}; 960 cm^{-1}; 731 cm^{-1} ($[CH_2]_n$ rocking).

Instrumentation

Nuclear Magnetic Resonance (NMR)

^1H and ^{13}C NMR spectra were recorded at room temperature on a DPX300 spectrometer (Bruker Instruments, Inc.) at 300 MHz in chloroform-*d*. Chemical shifts (in parts per million) for ^1H and ^{13}C NMR were referenced relative to tetramethylsilane (internal reference) at 0.00. All synthesized P(ω-OHC14) materials described herein had identical NMR spectra with signals and assignments given above.

Fourier Transform Infrared Spectroscopy

A fourier transform infrared spectroscopy (FTIR) spectrum of P(ω-OHC14) was prepared on a thin film using a Nicolet 6700 FTIR from Thermo Scientific using the following instrumental parameters: 36 scans, resolution 4.0 cm^{-1}, data spacing: 1.928 cm^{-1}, corrected for water and carbon dioxide.

Molecular Weight Measurements

Relative Molecular Weight Measurements

Molecular weight of P(ω-OHC14) samples was determined by gel permeation chromatography (GPC) using the identical Waters HPLC system and experimental method as was described elsewhere (*29*). The number-average molecular weight (M_n) and weight-average molecular weight (M_w) were determined based on a calibration curve generated by narrow molecular weight polystyrene standards (Aldrich Chemical).

Molecular Seight Measurements by Size Exclusion Chromatography with Multiangle Laser Light-Scattering Detection (SEC-MALLS)

The SEC-MALLS system consisted of a Shimadzu LC-20AD pump, a Waters 717 plus autosampler, a Wyatt HELEOS multiangle laser light scattering detector and a Wyatt Optilab-rEX refractive index detector. The polymer was separated on a PLgel 5μm MIXD-D column with a dimension of 300 x 7.5mm from Polymer

Downloaded by PENNSYLVANIA STATE UNIV on August 28, 2012 | http://pubs.acs.org
Publication Date (Web): August 16, 2012 | doi: 10.1021/bk-2012-1105.ch009

Laboratories and the column was kept at a 35°C column chamber. The polymer was eluted from the column by $CHCl_3$ at 1ml/min. The Wyatt HELEOS was calibrated by toluene and normalized by a narrow dispersed 30K polystyrene standard in $CHCl_3$. The software for data collection and processing was ASTRA 5.3.4.14 supplied by Wyatt Technology. The specific refractive index increments dn/dc in $CHCl_3$ were determined at 658 nm using a Wyatt Optilab-rEX refractive index detector by the on-line method using the following assumptions: (1) the sample is compositionally homogeneous at all molecular weights, and (2) the sample is 100% eluted from the column.

Downloaded by PENNSYLVANIA STATE UNIV on August 28, 2012 | http://pubs.acs.org
Publication Date (Web): August 16, 2012 | doi: 10.1021/bk-2012-1105.ch009

Differential Scanning Calorimetry (DSC)

DSC measurements were performed using a differential scanning calorimeter (Model 2920, TA Instruments). Temperature calibration was carried out using an indium standard. Measurements were performed under a nitrogen atmosphere at a flow rate of 50 mL/min. Typical parameters for experimental measurements are as follows: i) samples for dynamic mechanical thermal analysis cooled to 10 °C, ii) heated to 150 °C at 10 °C/min, iii) held at 150 °C for 3 min and iv) cooled at 10 °C/ min to 10 °C. When the temperature reached 10 °C, a second heating scan was performed at 10 °C/min to 200 °C. Values of the melting enthalpy (ΔH_m), peak melting temperature (T_m), crystallization enthalpy (ΔH_c) and crystallization peak temperature (T_{cP}) were analyzed using TA Universal Analysis software.

Thermogravimetric Analysis (TGA)

Thermal stability measurements were conducted using a Perkin-Elmer Pyris 1 TGA instrument. To obtain TGA traces, each polyester sample (about 3.0 mg) was scanned from 50 to 700 °C at heating rate 10 °C/min under dry nitrogen with a flow rate of 45.0 ml/min. To further clarify analysis of thermal stability, peak temperatures at the derivative of TGA traces were denoted as $T_{d(max)}$ and were used as an index to assess the thermal degradation behavior and stabilities of the prepared polyesters.

Dynamic Mechanical Thermal Analysis (DMTA)

P(ω-OHC14) samples were molded into rectangular bars with dimensions 20 mm (length) x 5 mm (width) x 1.5 mm (thickness). DMTA measurements were performed in single-cantilever bending mode using a TA instruments RSA3 Rheometer with an LN2 control system. Measurements were performed from -130 °C to 40 °C at a heating rate of 3 °C/min and frequency of 3 Hz. TA Orchestrator software was used for acquiring and processing experimental data.

Tensile Testing

Dumbbell shaped sample bars with dimensions of 9.0 mm (length) x 3.0 mm (neck width) x 1.0 mm (thickness) were prepared by press-molding at 130 °C and subsequent quenching at ambient temperature. An Instron 5542 tensile testing machine with a 500 N load cell was used. The crosshead speed was 5 mm/min and the test temperature was 25 °C. Merlin software was used to collect and analyze tensile results (stress was calculated according to the initial cross-section area). Values of Young's modulus, elongation at yield and break and stress at yield were obtained by averaging the data obtained from ≥ 5 samples. Young's modulus was measured as the slope of stress-strain curves at strain below 1%, using the linear least square method. Elongation and stress at break measurements were determined at the (x,y) coordinates after which the slope of the stress-strain curve became negative.

Downloaded by PENNSYLVANIA STATE UNIV on August 28, 2012 | http://pubs.acs.org
Publication Date (Web): August 16, 2012 | doi: 10.1021/bk-2012-1105.ch009

Results and Discussion

P(ω-OHC14) Synthesis

Effect of $Ti(OiPr)_4$ Concentration

Polycondensation reactions were performed in two stages. During the first stage, oligomerization of methyl ω-hydroxytetradecanoate, Me-ω-OHC14, was performed with predetermined quantities of $Ti(OiPr)_4$, under N_2, for 2 h, at 200 °C. Subsequently, in stage 2, the pressure was reduced to < 0.1 mmHg, the temperature was increased to 220 °C, and the reaction was conducted for 4 h. The above starting conditions to assess catalyst concentration were selected based on studies of related aliphatic polyester synthesis reactions (*20–24*). Absolute molecular weight values were determined on non-fractionated products by SEC-MALLS. Control experiments, performed under identical conditions as above but without the addition of a catalyst, gave a product with relative (to polystyrene standards) M_w 4000, and polydispersity (PDI, M_w/M_n) 1.7. Figure 1 shows the influence of $Ti(OiPr)_4$ concentration on P(ω-OHC14) M_w. SEC-MALLS determined M_w increased from 53K to 110K as the catalyst concentration was increased from 50 to 300 ppm. Increase in $Ti(OiPr)_4$ concentration from 500 to 800 ppm resulted in a decrease in M_w from 120K to 77K. Further increases in $Ti(OiPr)_4$ concentration up to 1800 ppm resulted in small decreases in M_w to ~67K. Given the uncertainty in M_w values based on the standard deviation determined from three independent experiments at $Ti(OiPr)_4$ concentration 200 ppm ($M_w = 93 \pm 10$ K, see Figure 1) and the desire to use minimum quantities of catalyst in reactions, the preferred catalyst concentration is between 300 and 500 ppm. Since the uncertainty in PDI measurements is ± 0.2, and PDI values ranged from 1.2 to 1.5 over the full range of $Ti(OiPr)_4$ concentrations investigated, we conclude that no substantial change in PDI values was observed in Figure 1. The observation of a maximum in plots of catalyst concentration versus M_w and thus a decrease in M_w above a peak catalyst concentration is consistent with previous literature on related catalyst-monomer polycondensation reactions (*23*, *30*). Shah et al. (*23*) explained that M_w decreases above a peak catalyst concentration during chain propagation due to competitive binding by the catalyst at both intrachain ester units and chain-end groups (e.g. hydroxyl or carboxyl moieties). As the molecular weight increases, it follows that the terminal group concentration decreases. As a consequence, increased metal ion binding to intrachain ester oxygen atoms occurs which can lead to chain scission reactions (*23*). The fact that the decrease in M_w values is not severe at high catalyst concentrations is a consequence of the low frequency of ester groups along chains. This is discussed in greater detail below with respect to P(ω-OHC14) thermal stability.

Downloaded by PENNSYLVANIA STATE UNIV on August 28, 2012 | http://pubs.acs.org
Publication Date (Web): August 16, 2012 | doi: 10.1021/bk-2012-1105.ch009

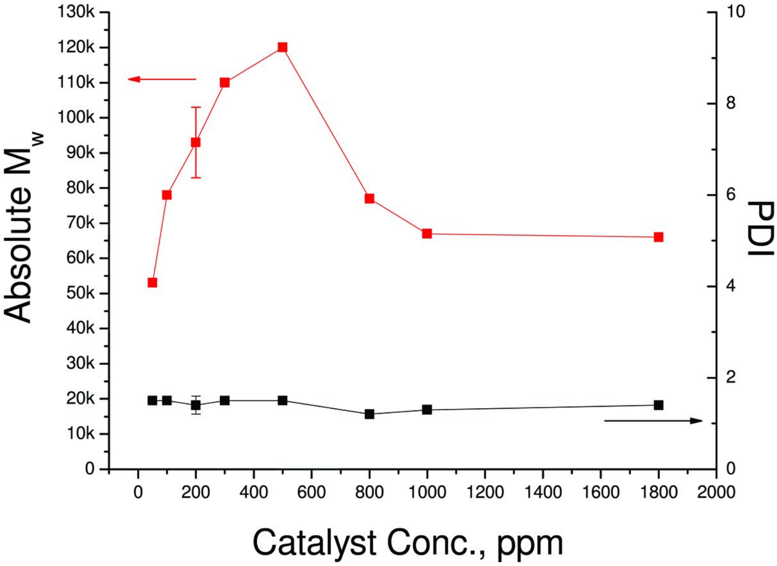

Figure 1. Relationship between Ti(OiPr)$_4$ concentration and P(ω-OHC14) molecular weight. Error bars for the reaction at 200 ppm Ti(OiPr)$_4$ are the standard deviation from the mean for three independent experiments.

Effect of Temperature

The first-stage reaction temperature was kept constant at 200 °C while the second stage reaction temperature was varied. The logic to this approach is, as the molecular weight and corresponding viscosity of P(ω-OHC14) rise, there might be a benefit to increasing the second-stage reaction temperature (*23*). Based on results above, the 200 ppm Ti(OiPr)$_4$ concentration was selected. P(ω-OHC14) molecular weights were measured relative to polystyrene standards. Increase in the second-stage reaction temperature from 220 to 240 and 260 °C resulted in decreased M_w values (160K, 99K and 59K, respectively), whereas PDI values increased from 2.3 to 3.2 and 3.6, respectively. These results suggest that by increasing the second-stage reaction temperature from 220 to 260 °C, there is a corresponding increase in the rate of reactions, leading to intrachain ester cleavage relative to chain propagation.

Progression of P(ω-OHC14) Molecular Weight as a Function of Reaction Time

On the basis of the above results, experiments to determine the preferred second-stage reaction time were performed using 200 ppm $Ti(OiPr)_4$, a first stage reaction at 200 °C under N_2 for 2 h, and a second stage reaction in vacuo (< 0.1 mmHg) at 220 °C. Aliquots were withdrawn at predetermined times during the second-stage polymerization and analyzed by SEC relative to polystyrene standards. Figure 2 illustrates that as the reaction time increased from 2 to 6 h, there was a regular increase in M_w. At 2, 3, 4, 5 and 6 h reaction times, the products had M_w (M_w/M_n in parentheses) values of 20K (2.1), 49K (2.2), 110K (2.0), 130K (2.5) and 140K (2.0). By 6 h, the product viscosity had increased such that the product adhered to the mechanical stirring and mixing was no longer effective.

Downloaded by PENNSYLVANIA STATE UNIV on August 28, 2012 | http://pubs.acs.org
Publication Date (Web): August 16, 2012 | doi: 10.1021/bk-2012-1105.ch009

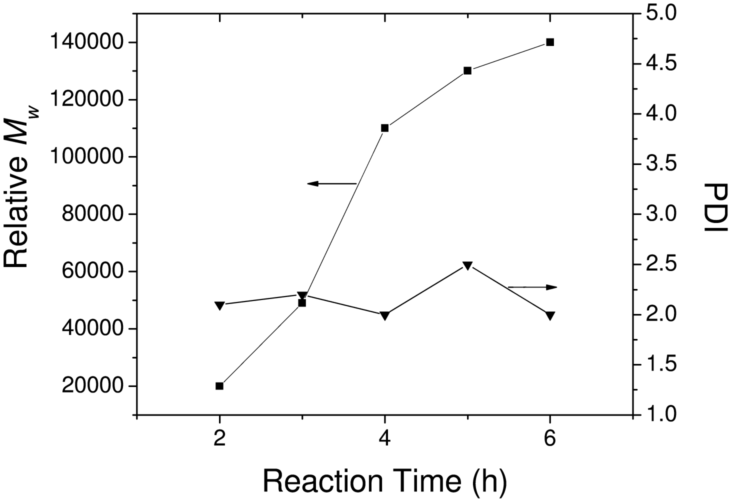

Figure 2. Effect of reaction time on the melt polycondensation to prepare P(ω-OHC14). Reaction conditions were as follows: 200 ppm $Ti(OiPr)_4$, first stage reaction at 200 °C under N_2 for 2 h, second stage reaction in vacuo at 220 °C.

Downloaded by PENNSYLVANIA STATE UNIV on August 28, 2012 | http://pubs.acs.org
Publication Date (Web): August 16, 2012 | doi: 10.1021/bk-2012-1105.ch009

Thermal Properties

Results above illustrate that by changing the catalyst concentration (Figure 1) or the second-stage reaction time (Figure 2), a series of P(ω-OHC14) samples differing in molecular weight can be prepared. These strategies were adopted in order to prepare the series of P(ω-OHC14) samples listed in Table 1. Thus, P(ω-OHC14) samples with M_{w} values of 53K, 78K, 84K and 110K (Samples 1-4) were prepared by varying the catalyst concentration (50, 100, 1800 and 300 ppm, respectively) and by adopting first and second stage reaction conditions of 2 h/200°C and 4 h/220°C, respectively. P(ω-OHC14) with M_{w} 140K was prepared by selecting first and second stage reaction conditions of 2 h/200°C and 3 h/220°C, respectively, and by using 200 ppm $\mathrm{Ti(OiPr)_4}$. The cumulative results of five P(ω-OHC14) samples synthesized with systematic variation in M_{w} values are listed in Table 1. Generally, M_{w} values listed in Table 1, and those shown in Figures 1 and 2 for identical reaction conditions, are in excellent agreement. Thermal analysis by DSC and TGA experiments were conducted on P(ω-OHC14) samples listed in Table 1 to determine whether thermal transitions were significantly altered by changes in P(ω-OHC14) molecular weight.

Table 1. Thermal Transitions from DSC and TGA Experiments for P(ω-OHC14) Samples Differing in Molecular Weight

SampleNo.[a]	*SEC-MALLS*		*DSC scans*						*TGA*
	M_w ×10^{-3} (g/mol)	*PDI*	*First heating*		*Second heating*		*Cooling*		*$T_{d(max)}$*[b] *(°C)*
			ΔH_m[b] *(J/g)*	*ΔT_m*[b] *(°C)*	*ΔH_m*[b] *(J/g)*	*ΔT_m*[b] *(°C)*	*ΔH_c*[b] *(J/g)*	*ΔT_{cp}*[b] *(°C)*	
1	53	1.5	113	100	128	94	116	72	458
2	78	1.5	126	94	118	92	105	71	458
3	84	1.4	116	96	116	96	106	68	455
4	110	1.5	113	93	120	96	105	69	463
5	140	1.8	115	93	119	94	105	70	458

[a] Preparation of samples differing in molecular weight was accomplished by either systematic changes in catalyst concentration or second stage reaction time. Details of these changes are described in the text, above. [b] Following abbreviations were used: melting enthalpy, ΔH_{m}; peak melting temperature, T_{m}; crystallization enthalpy, ΔH_{c}, crystallization peak temperature, T_{cp}; peak temperatures at the derivative of TGA traces, $T_{\mathrm{d(max)}}$.

No observable trends were found when comparing values of melting peak temperatures, T_{m}, and crystallization peak temperatures, T_{cp}, for samples 1-5. In other words, variation in P(ω-OHC14) Mw from 53 to 140K resulted in no significant differences in values of T_{m} and T_{cp}. A decrease in the second heating melting enthalpy, ΔH_m, was observed with an increase in P(ω-OHC14) M_w from 53 to 78K. A corresponding decrease in the crystallization enthalpy, ΔH_c, was observed as P(ω-OHC14) M_w increased from 53 to 78K. For P(ω-OHC14) M_w values ≥ 78K, values of second heating scan ΔH_m and ΔH_c were invariable. In general, for the same sample, values of ΔH_c were smaller than ΔH_m, possibly because of crystal melting, recrystallization, and re-melting of P(ω-OHC14) during heating scans. This result is consistent with that for P(ω-OHC15) samples reported previously (*29*). Unlike P(ω-OHC14) where ΔH_m and ΔH_c values decreased over a small range of the molecular weights investigated, decreases in ΔH_m and ΔH_c values for P(ω-OHC15) were observed over the entire range of M_w values studied (45K to 481K) (*29*). At present, we do not have an explanation for this difference in behavior between P(ω-OHC14) and P(ω-OHC15).

TGA analysis was used to assess the thermal degradation behavior and stabilities of P(ω-OHC14) over the range of M_w values studied herein. Table 1 lists thermal degradation peak temperatures ($T_{d(max)}$) which correspond to the temperature at which the maximum thermal degradation rate occurs and can be observed in the first-derivative curves of TGA traces. Values of $T_{d(max)}$ are about 460 °C and no discernable trends in $T_{d(max)}$ was observed as a function of P(ω-OHC14) M_w. Therefore, for P(ω-OHC14) samples with M_w values from 53K to 140K, $T_{d(max)}$ appears invariable and P(ω-OHC14) exhibits good thermal stability. Even Sample 3, prepared using 1800 ppm of $Ti(OiPr)_4$, a catalyst concentration well above that used to prepare the other Samples studied, showed a similarly high $T_{d(max)}$. It is well known that for polyesters such as poly(tetramethylene succinate) (*30*) and poly(L-lactide) (*31*), their degradation is accelerated at high temperatures by the presence of residual metals which catalyze chain transfer, intra-and intertransesterification and depolymerization reactions (*31*). We believe that the invariable thermal stability as a function of residual metal of P(ω-OHC14) samples studied herein is a consequence of the relatively lower frequency of ester moieties along chains for P(ω-OHC14) relative to the other polyesters discussed above.

Dynamic Mechanical Thermal Analysis (DMTA)

P(ω-OHC14), similar to P(ω-OHC15) (*29*), crystallizes rapidly from the melt so that upon cooling at 10 °C/min in DSC experiments, the resulting fraction of amorphous material is small. As a consequence, the glass transition (T_g) cannot be detected in the DSC curve of the subsequent heating scan from -70°C. In this study, DMTA, a method useful for studying the viscoelasticity of polymers, was employed as a more sensitive method to measure T_g as well as the storage and loss modulus as a function of temperature for the series of P(ω-OHC14) samples 1-5 described in Table 1. Discussions below that relate differences in modulus to DSC results refer to measurements of T_m and ΔH_m during first heating scans. Figure 3a shows that, below -37 °C, the storage modulus does not significantly vary for P(ω-OHC14) samples 1-5. However, above -37 °C, variations in the storage modulus for samples 1-5 are observed. The inserted graph in Figure 3a, in which an expansion of the -25 to 42 °C region of the curve is displayed, indicates that

Downloaded by PENNSYLVANIA STATE UNIV on August 28, 2012 | http://pubs.acs.org
Publication Date (Web): August 16, 2012 | doi: 10.1021/bk-2012-1105.ch009

Downloaded by PENNSYLVANIA STATE UNIV on August 28, 2012 | http://pubs.acs.org
Publication Date (Web): August 16, 2012 | doi: 10.1021/bk-2012-1105.ch009

the higher the P(ω-OHC14) melting point in the first heating scan, the higher the sample's storage modulus. Since crystallinity values of all samples except Sample 2 are very close (see ΔH_m values, Table 1), and a higher melting point indicates better crystal perfection and higher modulus, it follows that samples 1 and 3 have higher storage modulus values than samples 4 and 5. Although the melting point of Sample 2 is intermediate between those of samples 1 and 3, its melting enthalpy is highest of all the samples. At lower temperatures, between -37 °C and 0 °C, Sample 2's storage modulus is relatively low, close to that of samples 4 and 5 with similar T_m values. However, above 10 °C, its storage modulus approaches that of Samples 1 and 3. Thus, Sample 2, because of its relatively low T_m (lower crystal perfection) but high ΔH_m value (higher crystallinity), differs in its storage modulus behavior depending on the temperature region observed.

Variation of loss modulus with temperature for P(ω-OHC14) samples 1-5 is displayed in Figure 3b. The loss modulus vesus temperature curves show that T_g transitions are between -29 and -31 °C, which is slightly lower than the DMTA determined T_g of P(ω-OHC15) at -27 °C (*29*). This can be attributed to that P(ω-OHC15) has higher crystallinity values relative to P(ω-OHC14) samples investigated herein. Hence, the amorphous phase of P(ω-OHC15) is subject to more restriction in motion than that of P(ω-OHC14).

Tensile Testing

Figure 4 shows typical semi-logarithmic stress–strain curves for P(ω-OHC14) samples 1-5. The Young's modulus, elongation to break and stress at break determined from stress-strain curves are listed in Table 2 as the mean plus or minus one standard deviation.

Figure 5 displays four regions according to slope change in stress-strain curves. Manson et al (*32*) assigned these four regions as: I, linear and nonlinear viscoelasticity, II, neck region/strain softening, III, plastic flow, and IV, strain hardening. Inspection of poly(ω-OHC14) samples before stretching and after fracture showed the volume of the bar subjected to high strain was about two times that of the original volume (i.e. 50% polymer and 50% void formations), consistent with observations by Ward on other systems (*32*). Because the stress value in Figure 4 was estimated by the load divided by the initial cross-sectional area, true stress values at break for Samples 2-5 were recalculated using the value of stress at break (in Figure 4, Table 2) multiplied by (1+strain)/2. For Sample 1 at lower strain, the true stress values at break were recalculated by the value of stress at break multiplied by (1+strain), that is, neglecting the effect of volume increase at lower strains. The recalculated values of true stress at break are listed in Table 2.

Downloaded by PENNSYLVANIA STATE UNIV on August 28, 2012 | http://pubs.acs.org
Publication Date (Web): August 16, 2012 | doi: 10.1021/bk-2012-1105.ch009

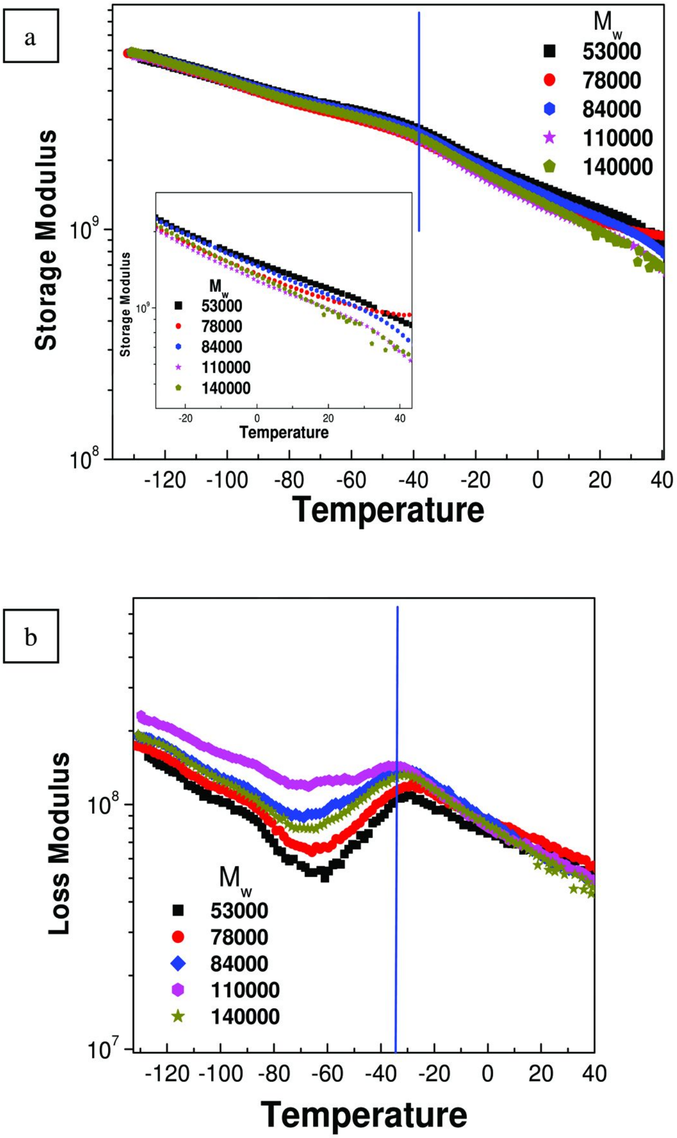

Figure 3. Variation of storage modulus (a) and loss modulus (b) with temperature for the series of P(ω-OHC14) samples differing in Mw as described in Table 1. Inserted graph in 3a is an expansion of the -25 to 42 °C region.

Downloaded by PENNSYLVANIA STATE UNIV on August 28, 2012 | http://pubs.acs.org
Publication Date (Web): August 16, 2012 | doi: 10.1021/bk-2012-1105.ch009

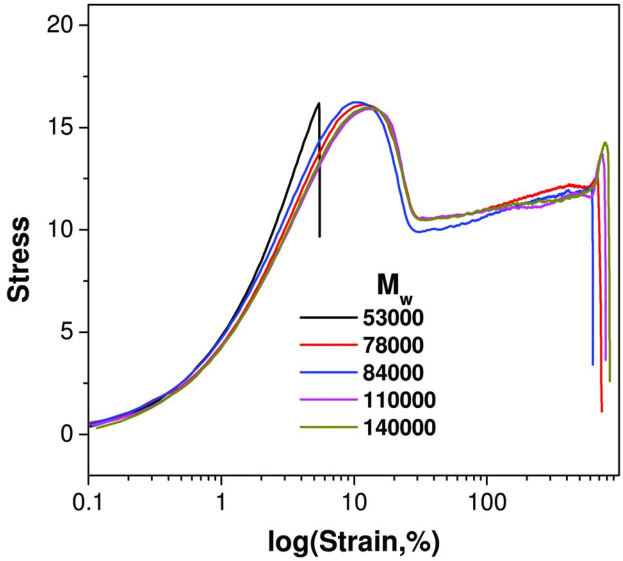

Figure 4. Semi-logarithmic stress–strain plots for tensile tests of P(ω-OHC14) Samples1-5 (see Table 1).

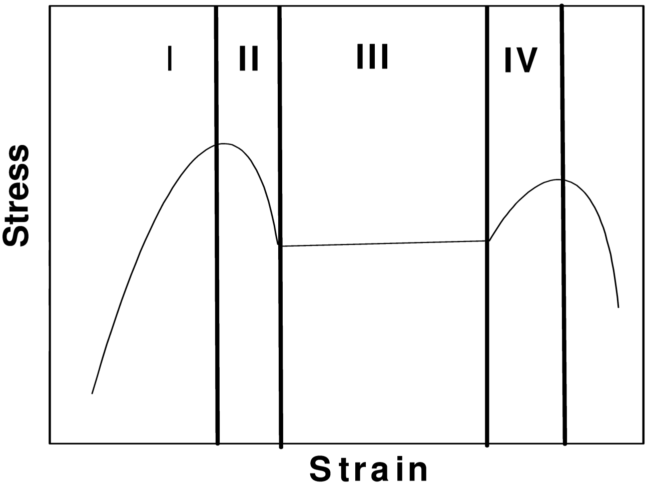

Figure 5. Regions within the stress-strain curves of P(ω-OHC14) samples undergoing stretching. I, linear and nonlinear viscoelasticity, II, neck region/strain softening, III, plastic flow, and IV, strain hardening.

Downloaded by PENNSYLVANIA STATE UNIV on August 28, 2012 | http://pubs.acs.org
Publication Date (Web): August 16, 2012 | doi: 10.1021/bk-2012-1105.ch009

The tensile properties shown in Figure 4 and Table 2 reveal unambigu-ously a dependence on molecular weight. For Sample 1 (M_w =53K), stress first increased rapidly with strain; then, the stress-strain curve slope began to decrease. When the strain reached 5.8 ± 1.2%, the sample fractured. The fracture was homogeneous as is typical for brittle fracture, whereas no neck was observed before fracture. As M_w increased to 78K, the shape of the stress-strain curve (Figure 4) deviated substantially from that of Sample 1. For Sample 2, neck and plastic flow were observed during stretching; stress first reached the maximum value and then decreased, followed by stable propagation before fracture. When the sample bar length reached 638 ± 128% of the initial length, the bar fractured. Thus, with an increase in M_w from 53 to 78K, the elongation at break increases about 100 times and the fracture fashion of P(ω-OHC14) changes from brittle-to-ductile. In addition, a stress-whitening phenomenon was observed during stretching of Sample 2, which is different from Sample 1. Interestingly, for P(ω-OHC14) of M_w = 84K (Sample 3), the elongation at break increases to 677±31% while the strain-hardening phenomenon is also observed. With further increases in M_w, samples exhibited a similar stress-strain curve shape as that of Sample 3, and values of elongation at break remained unchanged (728±80 and 729±21% for M_w 110 and 140K, respectively). These results demonstrate that it's unnecessary to synthesize P(ω-OHC14) with M_w > 78K in order to attain high draw ratios.

Table 2. Young's modulus, elongation to break and stress at break for P(ω-OHC14) samples differing in molecular weight

M_w ×10^{-3}	*PDI*	*Young's Modulus (MPa)*	*Elongation at Break (%)*	*Stress at Break (MPa)*
53	1.5	486±25	**5.8±1.2**	16.1±6.0 (17.0±6.3)[a]
78	1.5	414±50	**638±130**	13.5±2.4 (49.8±8.8)[a]
84	1.4	414±26	677±30	14.0±1.7 (54.4±6.6)[a]
110	1.5	426±50	728±80	15.1±2.8 (62.5±11.6)[a]
140	1.8	419±20	729±20	15.1±1.9 (62.6±7.9)[a]

[a] The true stress at break calculated after correction for the cross-sectional area.

Observation of true stress at break values in Table 2 show a similar trend as elongation at break. That is, the true stress at break increased by about three times (17.0±6.3 to 49.8±8.8) as P(ω-OHC14) M_w increased from 53 to 78K. Whereas further increases in P(ω-OHC14) M_w (78K to 140K) appear to result

Downloaded by PENNSYLVANIA STATE UNIV on August 28, 2012 | http://pubs.acs.org
Publication Date (Web): August 16, 2012 | doi: 10.1021/bk-2012-1105.ch009

in increased stress at break (49.8±8.8 to 62.6±7.9, respectively), these changes are within uncertainty levels. P(ω-OHC14) M_w=53K has the highest Young's Modulus (486±25 Mpa). Increasing P(ω-OHC14) M_w from 53 to 78K resulted in a decrease in Young' s Modulus to 414±50 MPa. With further increases in M_w to 84, 110 and 140K, P(ω-OHC14) exhibited similar Young's Modulus values.

Several studies contend that material's degree of crystallinity is a primary factor affecting its Young's modulus (*33–37*). That is, increases in material crystallinity will generally lead to a higher Young's modulus values. Furthermore, the crystallinity of semi-crystalline materials generally decreases with polymer chain length (*37*). A relevant example is work by Kennedy et al (*37*) who describe decreased Young's modulus values with increasing HDPE M_w. Because P(ω-OHC14) has a similar chemical structure as linear PE, its M_w dependence of Young's modulus may show a similar trend. The crystallinity of Poly(ω-OHC14) was calculated by dividing the cooling crystallization enthalpy by the equilibrium enthalpy of 227 J/g for P(ω-OHC15) (*38*). Percent crystallinity values for P(ω-OHC14) with M_w 53, 78, 84, 110 and 140K are 51, 46, 47, 46 and 46%, respectively. Hence, 53K P(ω-OHC14) has higher crystallinity while crystallinity values of P(ω-OHC14) with M_w 78 to 140K are similar. Table 2 shows that P(ω-OHC14) M_w=53K has the highest Young's Modulus, increasing P(ω-OHC14) M_w from 53 to 78K resulted in a decrease in Young's Modulus and Young's Modulus remained unchanged with further increases in M_w. Thus, effects of P(ω-OHC14) molecular weight and crystallinity are similar to that observed for linear PE (*35–37*). Flory and Yoon (*39*) pointed out that the chain topology initially present in the pure molten polymer, such as entanglements, knots, loops, and related structures, will be conserved during crystallization. Materials of semicrystalline polymers such as P(ω-OHC14) normally consist of the following regions: three-dimensionally ordered crystalline regions, isotropic conformational disordered liquid-like regions, and interfacial regions that connect the two (*37*). Longer chain lengths increase the possibility of polymer chain entanglement in amorphous regions, and, hence, retard crystallization. In a related study by our laboratory and collaborators, the Young's modulus of P(ω-OHC15) (repeating units have one additional methylene than P(ω-OHC14)) decreases with increasing molecular weight (*29*).

Ultimate Properties of Poly(ω-Hydroxyfatty Acids) Relative to HDPE

We are able to examine a brittle-to-ductile transition by increasing P(ω-OHC14) molecular weight. The type of deformation can be characterized by the elongation value for a given molecular weight. A brittle sample is defined as having an elongation value less than 20%. High values of elongation indicate ductile type deformation. As shown in Figure 4 and Table 2, Sample 1 with M_w 53K is brittle with elongation at break 5.8±1.2%. Samples 2-5 show a brittle-to-ductile transition.

Mandelkern et al. (*37*) found that HDPE materials with M_w < 40K are brittle over the accessible range of crystallinities. When HDPE M_w is 71K, the ductile-to-brittle transition can be observed as the crytallinity was increased from 64 to 81%. For higher M_w HDPE (about 316K), the brittle-to-ductile transition was not observed for accessible crystallinity values. Lower elongation (fracture at low strain) for low molecular weight brittle materials is explained as follows: for the set of stacked lamellar crystals, interlamellar regions must possess elements or chain regions which can undergo a ductile deformation. Furthermore, the effective number of deformable sequences within interlamellar structure will be tempered by chain entanglement and interlinking, which is sensitive to molecular weight, crystallinity and interlamellar thickness (*37*). Hence, for low molecular weight polymers such as HDPE with M_w below 40 K (*38*), P(ω-OHC14) with $M_w \leq$ 53K, and P(ω-OHC15) (*30*) (i.e. PPDL) with M_w below 45K, there is an insufficient number of disordered sequences connecting crystallites to transmit tensile force. For HDPE, elongation at break is independent of crystallinity in the ductile region for a given molecular weight, but elongation at break decreases with increasing chain length (*37*). For example, by increasing HDPE molecular weight from 71 to 351K while keeping crystallinity constant, the draw ratio decreases from 12.6 to 5.0. This is explained by an increased density of entanglements that accompanies higher HDPE molecular weight. Because the entanglements are constrained to reside between crystalline lamellae, they act as effective cross-links. Correspondingly, the modulus in this region increases with molecular weight, and the deformability concomitantly decreases (*37*).

The results reported herein for P(ω-OHC14) as a function of molecular weight differs from those published by others for HDPE. The elongation at break of P(ω-OHC14) increased with increasing molecular weight from78K to 140K. The highest value of draw ratio is 7.3 for M_w 140K. For P(ω-OHC15), increasing M_w from 81 K to 280 K increased the draw ratio from 1.4 to 7.0. However, when M_w of P(ω-OHC15) is 481K, the draw ratio decreased to 5.8 (*29*). On the basis of similarities in structure between P(ω-OHC14) and P(ω-OHC15), one would expect a similar decrease in the draw ratio as the molecular weight of P(ω-OHC14) increased. However, P(ω-OHC14) with M_w values above 140K are not currently available because of limitations in condensation polymerization synthetic methods. Perhaps, lactonization of ω-OHC14 to produce ω-tetradecalactone and subsequent ring-opening polymerization would provide a route to higher molecular weight P(ω-OHC14) enabling comparisons of P(ω-OHC14) and P(ω-OHC15) samples with M_w values greater than 200K.

True stress at break of P(ω-OHC14) increased from 17.0 to 62.6MPa for M_w values from 53K to 140K. For P(ω-OHC15) (*29*), true stress showed a similar increase from 21.3MPa to 58.8MPa for M_w values from 75K to 481K. The stress at break for both P(ω-OHC14) and P(ω-OHC15) ranges from 14 to 20MPa. For HDPE (*37*), the stress at break increased from 15 MPa to a maximum value of 50 MPa by increasing HDPE M_w from 71K to 100K and then decreased to 20 MPa when the molecular weight was increased to 1000K. At a similar molecular weight, HDPE has a higher stress at break than both P(ω-OHC14) and P(ω-OHC15).

At present, we are unable to formulate a compelling explanation to explain the differences of mechanical properties as a function of molecular weight between the two P(ω-OHFA)s described herein and HDPE. Further thought would be worthwhile into the potential effects on mechanical property-molecular weight relationships that result by introducing esters within a linear polyethylene backbone. This fundamental difference in structure between HDPE and

Downloaded by PENNSYLVANIA STATE UNIV on August 28, 2012 | http://pubs.acs.org
Publication Date (Web): August 16, 2012 | doi: 10.1021/bk-2012-1105.ch009

P(ω-OHC14)/P(ω-OHC15) means that for the later heterogeneous stress distribution along chains exist during stretching. This is due to the different bond energies between C(=O)–O (110 KJ/mol), O-C (85.5 KJ/mol) and isolated C-C (83 KJ/mol) along chains.

Conclusion

High-molecular-weight P(ω-OHC14) was successfully synthesized by melt-condensation polymerization catalyzed by $Ti(OiPr)_4$. Variation of P(ω-OHC14) M_w from 53K to 140K was achieved by manipulating reaction variables including catalyst concentration and reaction time. Tensile testing, DSC, TGA and SEC-MALLS were used to investigate the effect of molecular weight on mechanical, thermal and crystalline material properties. Cold-drawing tensile tests at room temperature revealed a brittle-to-ductile transition for P(ω-OHC14) with M_w values between 78 and 140K. For P(ω-OHC14) with M_w 53K, the entanglement network strength in noncrystalline regions is insufficient to transmit stress during stretching such that inter-fibrillar slippage dominates until fracture. As P(ω-OHC14) M_w is increased to 78K and above, the entanglement network strength is greatly enhanced and strain-hardening occurs at high strains prior to failure. Furthermore, elongation at break and tensile strength (i.e., true stress at break) reach asymptotic values of 729% and 62.6 MPa, respectively. Moreover, as P(ω-OHC14) M_w is increased from 78K to 140K, values of Young's modulus and second heating melting enthalpy are invariable. Overall comparisons between P(ω-OHC14) and linear high density polyethylene (HDPE) mechanical properties showed similar trends in Young's modulus with molecular weight but differing trends with respect to elongation at break and true stress at break as a function of molecular weight. The latter differences may be related to the persistent density of C–O bonds in ester links of P(ω-OHC14) that is not present in PE. We therefore conclude that P(ω-OHC14) and related P(ω-OHFAs) with similar repeat unit structures (e.g. built from ω-OHC16 and ω-OHC18 units) have excellent potential to function in similar ways to PE whereas the ester bonds of P(ω-OHFAs) introduce sites that allow transesterification (e.g. reactive transesterification between different polyesters), chain hydrolysis (enzymatic and chemically catalyzed) and other reactions that are well known at ester moieties.

Acknowledgments

We acknowledge financial support from SyntheZyme LLC.

References

1. Shen, L.; Haufe, J.; Patel, M. K. *Biofuels, Bioprod. Biorefin.* **2009**, *4*, 25–40.
2. Bhardwaj, R; Mohanty, A. K. *J. Biobased Mater. Bioenergy* **2007**, *1*, 191–209.
3. Garlotta, D. *J. Polym. Environ.* **2001**, *9*, 63–84.
4. Sudesh, K.; Abe, H.; Doi, Y. *Prog. Polym. Sci.* **2000**, *25*, 1503–1555.

Downloaded by PENNSYLVANIA STATE UNIV on August 28, 2012 | http://pubs.acs.org
Publication Date (Web): August 16, 2012 | doi: 10.1021/bk-2012-1105.ch009

5. Olsson, A.; Lindström, M.; Iversen, T. *Biomacromolecules* **2007**, *8*, 757–760.
6. Cole-Hamilton, D. J. *Angew. Chem., Ind. Ed.* **2010**, *49*, 8564–8566.
7. Quinzler, D.; Mecking, S. *Angew. Chem., Ind. Ed.* **2010**, *49*, 4306–4308.
8. Suzuki, K.; Eto, T.; Otsuka, T.; Abe, S.; Yoshikawa, S. U.S. Patent 4,246,182, 1981.
9. Yamanaka, T.; Imai, T. U.S. Patent 4,419,292, 1982
10. Yokota, T.; Akio, W. U.S. Patent 5,191,096, 1992.
11. Lu, W. H.; Ness, J. A.; Xie, W. C.; Zhang, X. Y.; Minshull, J.; Gross, R. A. *J. Am. Chem. Soc.* **2010**, *132*, 15451–15455.
12. Veld, M. A. J.; Palmans, A. R. A.; Meijer, E. W. *J. Polym. Sci., Part A: Polym. Chem.* **2007**, *40*, 5968–5978.
13. Garalehm, M.; LAHCINI, M.; Kricheldorf, H. R.; Weidner, S. M. *J. Polym. Sci Part A: Polym. Chem.* **2009**, *47*, 170–177.
14. Ishii, M.; Okazaki, M.; Shibasaki, Y.; Ueda, M. *Biomacromolecules* **2001**, *2*, 1267–1270.
15. Ajioka, M.; Enomoto, K.; Suzuki, K.; Yamaguchi, A. *Bull. Chem. Soc. Jpn.* **1995**, *68*, 2125–2131.
16. MacDonald, W A *Polym. Int.* **2002**, *51*, 923–930.
17. Thiele, U. K. *Intern. J. Polym. Mater.* **2001**, *50*, 387–394.
18. (a) Waylon, L. J.; Gerry, R.; Mark, R. U.S. Patent 5,143,984, 1992. (b) Hideshi, H.; Fujito, E.; Akiyoshi, S.; Nobumasa, M.; Shoji, H. WO/2002/016467, 2002
19. Montaudo, G.; Rizzarelli, P. *Polym. Degrad. Stab.* **2000**, *70*, 305–314.
20. Cao, A.; Okamura, T.; Ishiguro, C.; Nakayama, K.; Inoue, Y.; Masuda, T. *Polymer* **2002**, *43*, 671–679.
21. Cao, A.; Okamura, T.; Nakayama, K.; Inoue, Y.; Masuda, T. *Polym. Degrad. Stab.* **2002**, *78*, 107–117.
22. Shirahama, H.; Aludin, M. S.; Kawaguchi, Y.; Migita, N.; Yasuda, H. *J. Jpn. Oil. Chem. Soc.* **1997**, *46*, 1391–1397.
23. Shah, T. H.; Bhatty, J. I.; Gamlen, G. A.; Dollimore, D. *Polymer* **1984**, *25*, 1333–1336.
24. Shirahama, H. Y.; Kawaguchi, Y.; Aludin, M. S.; Yasuda, H. *J. Appl. Polym. Sci.* **2001**, *80*, 340–347.
25. Kumar, A.; Kalra, B.; Dekhterman, A.; Gross, R. A. *Macromolecules* **2000**, *33*, 6303–6309.
26. Elzein, T.; Nasser-Eddine, M.; Delaite, C.; Bistac, S.; Dumas, P. *J. Colloid Interface Sci.* **2004**, *273*, 381–387.
27. Krimm, S.; Liang, C. Y.; Sutherland, G. B. B. M. *J. Chem. Phys.* **1956**, *25*, 549–562.
28. Gulmine, J. V.; Janissek, P. R.; Heise, H. M.; Akcelrud, L. *Polym. Test.* **2002**, *21*, 557–563.
29. Cai, J. L.; Liu, C.; Cai, M. M.; Zhu, J.; Zuo, F.; Hsiao, B. S.; Gross, R. A. *Polymer* **2010**, *51*, 1088–1099.
30. Yang, J.; Zhang, S. P.; Liu, X. Y.; Cao, A M. *Polym. Degrad. Stab.* **2003**, *81*, 1–7.
31. Cam, D.; Marucci, M. *Polymer* **1997**, *38*, 1879–1884.

Downloaded by PENNSYLVANIA STATE UNIV on August 28, 2012 | http://pubs.acs.org
Publication Date (Web): August 16, 2012 | doi: 10.1021/bk-2012-1105.ch009

32. Ward, I. M. *Mechanical properties of solid polymers*; John Wiley & Sons: New York, 1983; Vol. 399, Chapter 12.
33. Keith, H. D.; Paden, F. J.; Vadimsky, R. G. *J. Appl. Phys.* **1971**, *42*, 4585–4592.
34. Capaccio, G; Crompton, T. A.; Ward, I. M. *J. Polym. Sci., Part B: Polym. Phys.* **1976**, *14*, 1641–1658.
35. Mandelkern, L. *Polym. J.* **1985**, *17*, 337–350.
36. Mandelkern, L. *Acc. Chem. Res.* **1990**, *23*, 380–386.
37. Kennedy, M. A.; Peacock, A. J.; Mandelkern, L. *Macromolecules* **1994**, *27*, 5297–5310.
38. Cai, J. L.; Hsiao, B. S.; Gross, R. A. *Polym. Int.* **2009**, *58*, 944–953.
39. Flory, P. J.; Yoon, D. Y. *Nature* **1978**, *272*, 226–229.

Downloaded by PENNSYLVANIA STATE UNIV on August 28, 2012 | http://pubs.acs.org
Publication Date (Web): August 16, 2012 | doi: 10.1021/bk-2012-1105.ch009

Downloaded by PENNSYLVANIA STATE UNIV on August 28, 2012 | http://pubs.acs.org
Publication Date (Web): August 16, 2012 | doi: 10.1021/bk-2012-1105.ch010

Chapter 10

Long-Chain Polyesters via Chemical Catalytic Conversions of Fatty Acid Esters

Florian Stempfle, Philipp Roesle, and Stefan Mecking[*]

**Chair of Chemical Materials Science, Department of Chemistry,
University of Konstanz, 78464 Konstanz, Germany
[*]E-mail: stefan.mecking@uni-konstanz.de**

Plant oils with their long linear methylene sequences are attractive substrates for polymeric materials, such as long-chain aliphatic polyesters and polyamides. Existing biotechnological routes for their conversion to long-chain linear α,ω-dicarboxylic acid derivatives have recently been complemented by chemical catalytic conversions. This contribution discusses and compares the conversion of unsaturated fatty acids by olefin metathesis and by isomerizing alkoxycarbonylation, and reviews properties of resulting long-chain aliphatic polyesters. The impact of multiple unsaturated fatty acids present in technical grade plant oils is adressed.

Introduction

At present the chemical industry predominantly relies on fossil feedstocks. This in particular applies to polymer production which is one of the major consumers of these raw materials within the chemical industry. While the predominance of fossil feedstocks will prevail for the forseeable future, the demand for utilization of renewable feedstocks (*1–3*) is increasing due to various issues. On the very long term, the range of fossil feedstocks is limited. Shorter term arguments are the problematic volatility of crude oil prices, the security of supply and the mitigation of greenhouse gases.

At the same time, renewable feedstocks can provide access to polymeric materials with microstructures difficult to generate from fossil feedstocks, and corresponding desirable properties. Fatty acids from plant oils are attractive substrates in this respect (*4–6*) as they contain long-chain linear hydrocarbon segments as well as a carboxy group which is suited for polycondensation or conversion to other functional groups. The hydrocarbon segments can provide e.g. crystallinity, a reduced water uptake and dimensional stability, or flexible segments in polycondensates.

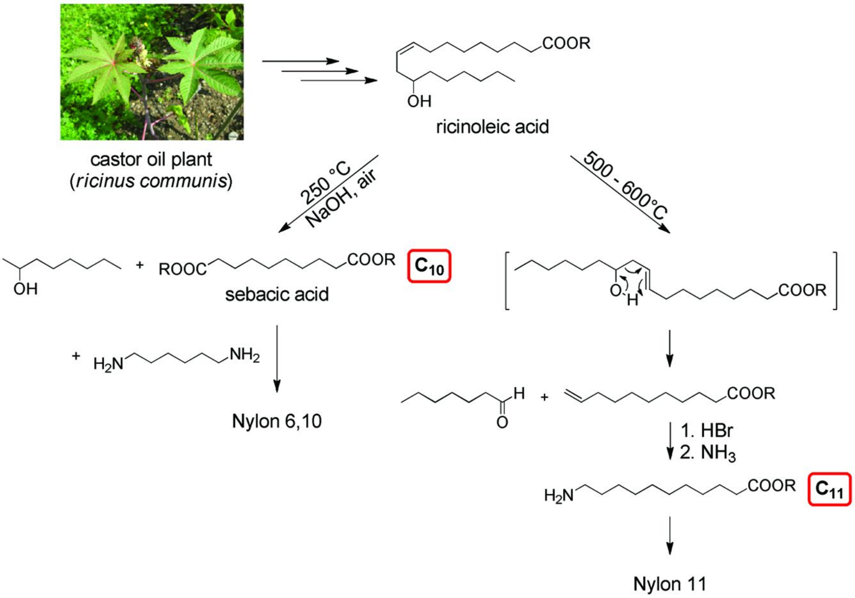

Scheme 1. Medium chain length monomers and polyamides from ricinoleic acid

Medium chain length (number of carbon atoms ranging from 6 to 13) polycondensation monomers have been prepared from ricinoleic acid esters, the major component of castor oil, since many years. Nylon-11 is generated via thermal rearrangement with chain cleavage to yield undecenoic acid (*7*). Likewise, sebacic acid, which is polymerized to Nylon-6,10, is generated by base-catalyzed cleavage of ricinoleic acid (Scheme 1) (*8*). Both of these routes require a hydroxy substituted unsaturated fatty acid, of which ricinoleic acid is the only practically available example. Castor oil is produced on a large scale, but significantly more costly (ca. double the price) than other plant oils like soybean, palm or rapeseed oil.

Moreover, in these transformations only one side of the fatty acid chain with respect to the double bond is incorporated into the monomer and ultimately the polymer. Stoichiometric amounts of less valuable byproducts are formed. These arguments also apply to ozonolysis, which converts monounsaturated fatty acids to α,ω-diacids. The medium chain length diacids azelaic acid (C_9) and brassylic acid (C_{13}) are produced industrially by oxidative cleavage of oleic acid and erucic acid, respectively, affording pelargonic acid as a byproduct (*9*).

Downloaded by PENNSYLVANIA STATE UNIV on August 28, 2012 | http://pubs.acs.org
Publication Date (Web): August 16, 2012 | doi: 10.1021/bk-2012-1105.ch010

In order to employ the potential of the long-chain linear feedstock to provide crystallizable segments and to utilize the feedstock most efficiently, a full linear incorporation of the entire fatty acid chain is desirable. For polyesters in particular, aliphatic materials based on the aforementioned medium chain-length diacids possess low melting points problematic for thermoplastic processing (*10–14*).

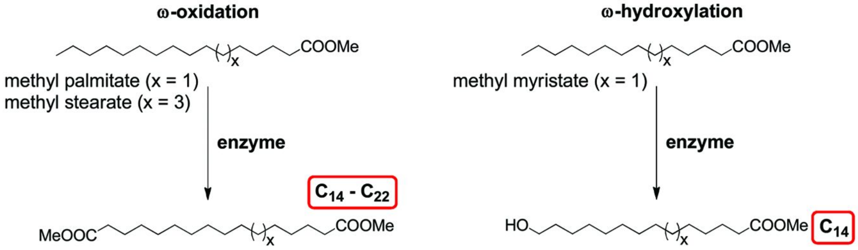

Scheme 2. Biotechnological routes to α,ω-difunctional linear monomers based on different fatty acids

One possible approach to such long-chain α,ω-difunctional compounds is enzymatic ω-oxidation of fatty acids (Scheme 2.) (*15–17*). Linear aliphatic diacids with the same carbon atom number as the fatty acid starting material, that is an even number usually in the range from 14 to 22 can be obtained. Issues of interest are increased space-time yields, and catalytically active microorganisms which can be nurtured by feedstocks less costly than glucose. In a related transformation of fatty acid substrates an ω-hydroxy group is introduced at the unsubstituted hydrocarbon chain end. With modified yeast strains the C_{14} ω-hydroxy fatty acid can be obtained selectively, as reported by Gross et al recently (Scheme 2) (*18*). These unsymmetric compounds can serve as AB-type monomers for polyesters (*19*).

Alternatives to these biotechnological routes based on chemical catalysis have emerged more recently. Self-metathesis of unsaturated fatty acids by ruthenium alkylidenes yields even carbon number monounsaturated diacids, which can be converted to the saturated analogues by hydrogenation of the double bond. Hereby, for example 1,18-octadecanedioates are obtained from oleates. A linear internal olefin is formed as a stoichiometric byproduct (Scheme 3).

Most recently, isomerizing alkoxycarbonylation (Scheme 3) has evolved as a route to long chain α,ω-diacid esters and corresponding polycondensates (*20*). This reaction (*21*), first observed by Cole-Hamilton for fatty acid esters (*22*) converts an internal double bond deep in the hydrocarbon chain very selectively to a terminal ester group by reaction with carbon monoxide and an alcohol. Odd carbon number products are formed, e.g. 1,19-nonadecandioate from oleate.

Downloaded by PENNSYLVANIA STATE UNIV on August 28, 2012 | http://pubs.acs.org
Publication Date (Web): August 16, 2012 | doi: 10.1021/bk-2012-1105.ch010

Downloaded by PENNSYLVANIA STATE UNIV on August 28, 2012 | http://pubs.acs.org
Publication Date (Web): August 16, 2012 | doi: 10.1021/bk-2012-1105.ch010

Results and Discussion

Aliphatic C_{20} Polyester from Olefin Metathesis

As an example of the generation of aliphatic long-chain polyesters via olefin metathesis routes, we have investigated C_{20} polyesters (*23*) from the self-metathesis (*24–26*) of undecenoic acid or its derivatives. Sequences of olefin metathesis, hydrogenation and reduction yield the corresponding long-chain α,ω-functionalized monomers (Scheme 4).

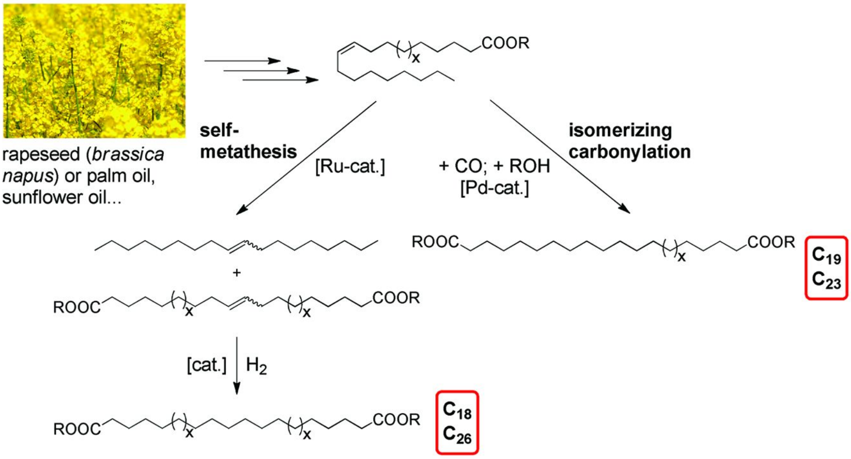
rapeseed (*brassica napus*) or palm oil, sunflower oil...
COOR
x
self-metathesis
[Ru-cat.]
+ CO; + ROH
[Pd-cat.]
isomerizing carbonylation
ROOC
COOR
C_{19}
C_{23}
+
ROOC
COOR
x
[cat.]
H_2
ROOC
COOR
C_{18}
C_{26}

Scheme 3. Chemical routes to α,ω-difunctional linear monomers based on different fatty acids (x = 1: oleic acid; x = 5: erucic acid)

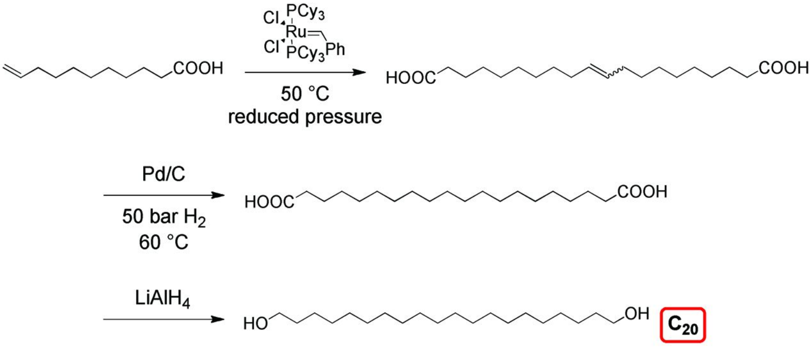
COOH
Cl
PCy3
Ru
Cl
PCy3
Ph
50 °C
reduced pressure
HOOC
COOH
Pd/C
50 bar H2
60 °C
HOOC
COOH
LiAlH4
HO
OH
C_{20}

Scheme 4. Synthesis of C_{20} monomers for polyesterification

Pure 1,20-eicosanedioic acid (>99 %) is obtained by self-metathesis of undecenoic acid with $[(PCy_3)_2Cl_2Ru{=}CHPh]$ (Grubbs 1st generation catalyst), followed by exhaustive hydrogenation. To avoid the formation of shorter chain α,ω-difunctional products, due to metathesis of internal olefins generated from the ω-functionalized 1-olefin substrate by isomerization as a side reaction this catalyst precursor was chosen. Albeit it is known to be less reactive and less tolerant towards polar and protic functionalities by comparison to its N-heterocyclic carbene analogue $[(PCy_3)(\eta\text{-}C\text{-}C_3H_4N_2Mes_2)Cl_2Ru{=}CHPh]$ (Grubbs 2nd generation catalyst), it disfavors olefin isomerization (*27–30*). Moreover isomerization is also assumed to be reduced in the presence of carboxylic acid groups, present in the starting material (*31*, *32*).

The corresponding α,ω-functionalized diol, 1,20-eicosanediole, can be generated by reduction in high purity (also cf. Scheme 6 for catalytic hydrogenation).

Polycondensation of stoichiometric amounts of 1,20-eicosanedioc acid and eicosane-1,20-diol catalyzed by titanium alkoxides in the melt yielded poly[1,20-eicosadiyl-1,20-eicosanedioate]. The material melts with a peak temperature of T_m = 108 °C and crystallizes at T_c = 83 ° (Figure 1).

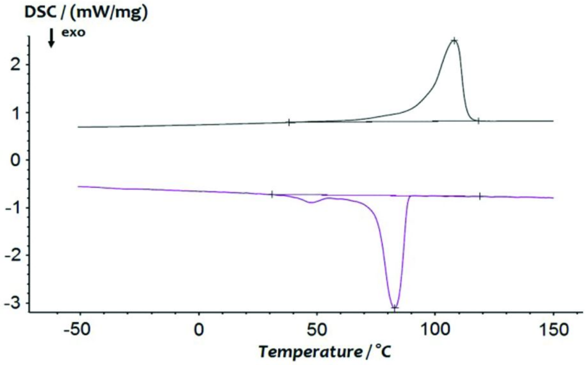

Figure 1. DSC trace of polyester-20,20 (10 K min^{-1}, 2nd heating cycle) (23).

Aliphatic C_{19} and C_{23} Polyesters from Isomerizing Alkoxycarbonylation

The isomerizing alkoxycarbonylation is catalyzed by palladium(II) complexes with very bulky substituted diphosphine ligands, such as 1,2-bis[(di-*tert*-butylphosphino)methyl]benzene (dtpbx). Starting from a fatty acid monoester (*20*) or, as reported recently, directly from different vegetable oils (*33*) including high oleic sunflower oil (*34*) in a one-pot procedure, α,ω-functionalized diesters can be obtained in polymerization grade purity (Scheme 5). Yields correlate with the oleate content of the starting material, but otherwise the catalyst performance appears not to vary dramatically between pure (99 %) oleate starting material and technical grade methyl oleate or triglyceride feed.

Downloaded by PENNSYLVANIA STATE UNIV on August 28, 2012 | http://pubs.acs.org
Publication Date (Web): August 16, 2012 | doi: 10.1021/bk-2012-1105.ch010

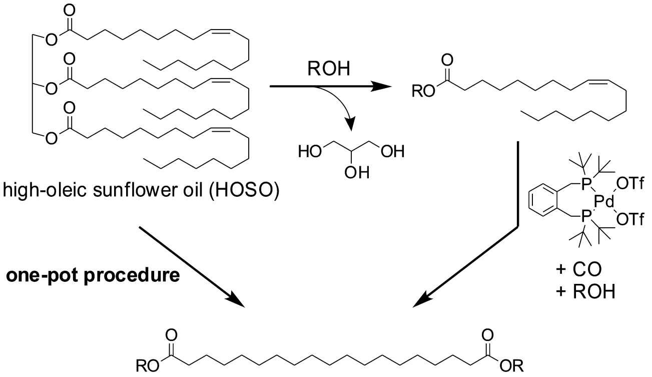

Scheme 5. Synthesis of dimethyl-1,19-nonadecanedioate starting from high-oleic sunflower oil or methyl oleate

Most plant oil sources of monounsaturated fatty acids, like oleate, contain significant amounts of the double unsaturated analogues. For example, palm oil typically contains 40 % of oleate and 10 % of linoleate in the fatty acid portion, soybean oil 25 % vs. 50 % oleate/linoleate and high oleate sun flower oil 93 % vs. 3 % (*35*). Thus, the fate of the double unsaturated fatty acids in isomerizing alkoxycarbonylation is of interest. To this end, the methoxycarbonylation of pure (≥99 %) methyl linoleate was investigated. Under typical reaction conditions, 90 °C and 20 bar CO with [κ^2-P,P-(dtbpx)Pd(OTf)] [OTf] as a well defined catalyst precursor (linoleate to Pd 125:1), the largest part of the starting material is converted as revealed by gas chromatography (GC, cf. experimental section). Of the various products formed, the main product was found to be dimethyl 1,19-nonadecenedioate. Its identity was confirmed by GC-MS, and by further reactions. Upon reacting the crude reaction mixture with bromine, the compound is not observed any more by GC. Also, catalytic hydrogenation with Pd/charcoal results in complete conversion to dimethyl 1,19-nonadecanedioate, as confirmed by enrichment with a genuine sample in GC analyses. The latter experiment also illustrates that the multiple unsaturated fatty acid can be converted to the saturated α,ω-diester by a sequence of isomerizing carbonylation and catalytic hydrogenation.

From the product of isomerizing alkoxycarbonylation of methyl oleate and ethyl erucate, respectively, dimethyl 1,19-nonadecanedioate and diethyl-1,23-tricosanedioate crystallize in >99 % purity. These novel linear long-chain substances can be utilized as platform chemicals for the synthesis of a range of α,ω-functionalized compounds, which can serve amongst others as novel polycondensation monomers (Scheme 6) (*36*). Amongst others, long-chain α,ω-diols are accessible by catalytic hydrogenation in high purity.

Downloaded by PENNSYLVANIA STATE UNIV on August 28, 2012 | http://pubs.acs.org
Publication Date (Web): August 16, 2012 | doi: 10.1021/bk-2012-1105.ch010

Downloaded by PENNSYLVANIA STATE UNIV on August 28, 2012 | http://pubs.acs.org
Publication Date (Web): August 16, 2012 | doi: 10.1021/bk-2012-1105.ch010

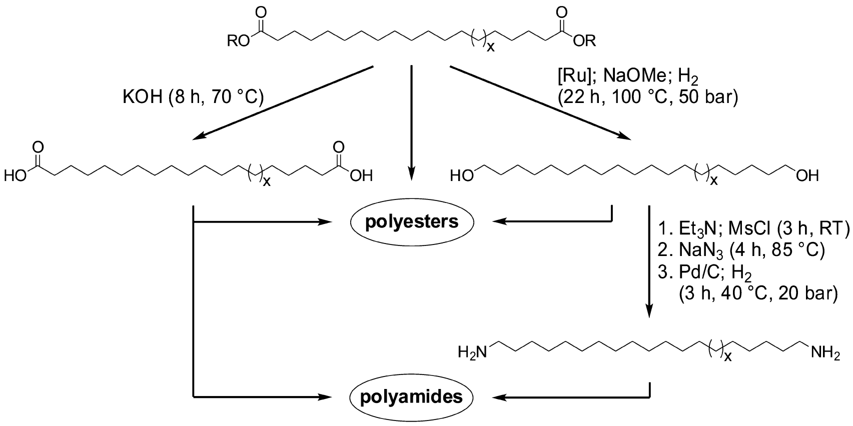

Scheme 6. Long-chain α,ω-difunctional compounds from unsaturated fatty acids (x = 1, oleic acid as starting material; x = 5, erucic acid) (36)

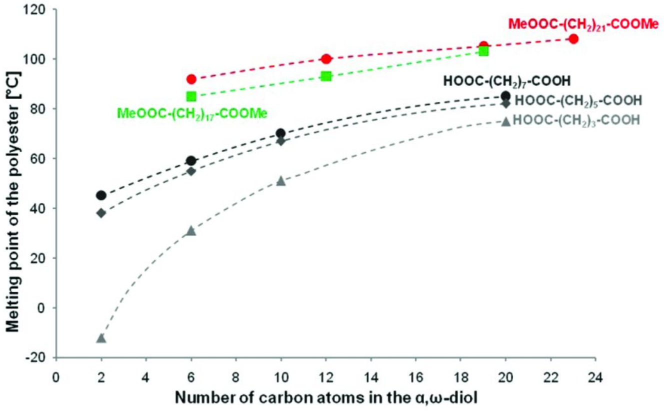

Figure 2. Melting points of polyesters obtained by polycondensation of dimethyl-1,19-nonadecanedioate and diethyl-1,23-tricosanedioate, and of azelaic, pimelic, andglutaric acid with α,ω-diols of different chain lengths (10, 20, 36).

Polyesters prepared from these long-chain dicarboxylic acid esters by polycondensation with the corresponding diols, namely poly[1,19-nonadecadiyl-1,19-nonadecanedioate] and poly[1,23-tricosadiyl-1,23-tricosanedioate], possess melting points above 100 °C and crystallization temperatures around 90 °C (*20*). These thermal properties compare with typical thermoplastics, and in this respect are significantly higher than for medium chain length aliphatic polyesters. For example, poly(decamethylene sebacate) melts at T_m = 80 °C (*12*). The enthalpies of fusion of the crystalline portion of these long-chain aliphatic polyesters and their crystalline structures as revealed by WAXS approach those of polyethylene, reflecting their largely hydrocarbon character. High crystallinities of χ = 70 to 75 % are observed (*20*).

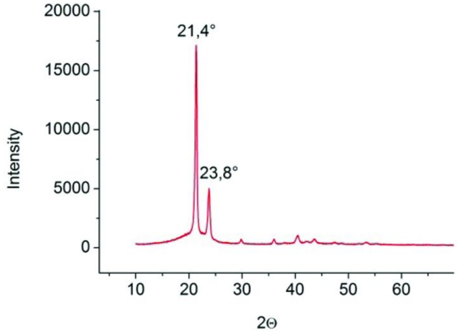

Figure 3. WAXS diffraction pattern of poly[1,6-hexadiyl-1,19-nonadecanedioate] (36).

Substantial melting and crystallization points, and crystallinities can also be achieved by combination of the long-chain diacids with shorter chain petrochemistry- or renewable-resource based monomers (Figures 2 and 3). E.g., polyesters with 1,6-hexanediole or 1,12-dodecanediole melt in the range of 86 to 100 °C, and crystallize above 70 °C.

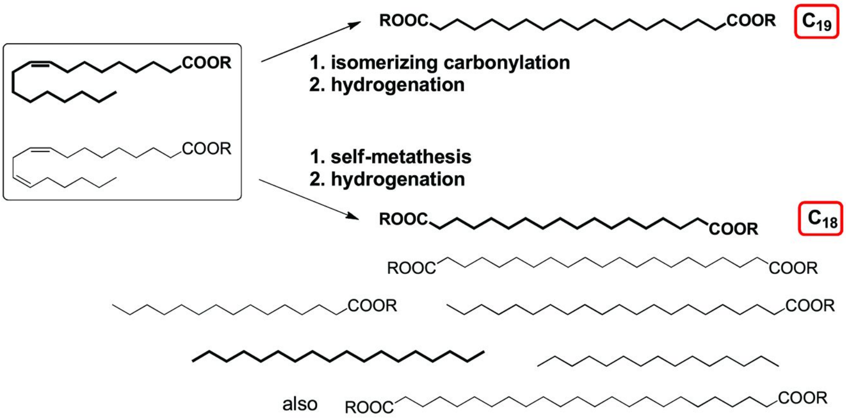
ROOC
COOR
C_{19}
COOR
1. isomerizing carbonylation
2. hydrogenation
COOR
1. self-metathesis
2. hydrogenation
ROOC
COOR
C_{18}
ROOC
COOR
COOR
COOR
also
ROOC
COOR

Scheme 7. Major products obtained by isomerizing alkoxycarbonylation (top) and self-metathesis (bottom) of an oleate and its double unsaturated analogue linoleate, followed by double bond hydrogenation

Downloaded by PENNSYLVANIA STATE UNIV on August 28, 2012 | http://pubs.acs.org
Publication Date (Web): August 16, 2012 | doi: 10.1021/bk-2012-1105.ch010

Downloaded by PENNSYLVANIA STATE UNIV on August 28, 2012 | http://pubs.acs.org
Publication Date (Web): August 16, 2012 | doi: 10.1021/bk-2012-1105.ch010

Summary and Conclusion

Olefin metathesis and isomerizing alkoxycarbonylation are promising catalytic routes for the generation of long-chain α,ω-difunctional monomers, and corresponding polymers and materials. A significant difference between these two routes is the spectrum of products formed, particularly from technical plant oil feedstocks which contain substantial portions of multiple unsaturated fatty acids in addition to the monounsaturated major component. Metathesis will convert the multiple unsaturated fatty acids to additional α,ω-diacid esters of different chain length. A range of hydrocarbons is formed as stoichiometric byproducts, as illustrated in Scheme 7 for a sequence of self-metathesis and double bond hydrogenation. By contrast, in isomerizing alkoxycarbonylation the multiple unsaturated fatty acids can in principle be converted to the same α,ω-diacid esters as formed as the main product from the monounsaturated fatty acid starting material. This difference between olefin metathesis and isomerizing carbonylation can be related to a fundamental characteristic of these reactions: in olefin metathesis, often equilibria are obtained and there is no extreme kinetic preference for a particular product. The isomerizing carbonylation, on the other hand, is strictly kinetically controlled and yields a product not representing the thermodynamically favored outcome.

These considerations illustrate that metathesis of technical plant oils generates a range of interesting products for polycondensation chemistry. On the other hand, effective seperation procedures are required. Note that in a technical process, recycling of selected metathesis products prior to hydrogenation could narrow the product spectrum.

Concerning future developments, olefin metathesis of plant oils appears to be feasible on a larger scale. Concrete plans have been announced for the construction of a biorefinery for the large scale conversion of palm oil by metathesis with 1-butene. This process would yield also substantial amounts of self-metathesis byproducts, that is in particular 1,18-octadecenedioate (*37*). Isomerizing alkoxycarbonylation of plant oil has been disclosed on a kilogramm scale to date (*34*). Carbonylation reactions in general are well established processes in industry. A large scale process for the methoxycarbonylation of ethylene to methylpropionate (as a part of a novel route to MMA) which likely uses a very similar catalyst as employed here for the isomerizing alkoxycarbonylation of fatty acids went into operation in 2008 (*38*, *39*). While in the isomerizing reaction improving catalyst productivity is an issue, this illustrates the principal feasibility of such reactions.

These developments provide broad perspectives for novel polycondensates and materials. One example are thermoplastic semicrystalline aliphatic polyesters.

Downloaded by PENNSYLVANIA STATE UNIV on August 28, 2012 | http://pubs.acs.org
Publication Date (Web): August 16, 2012 | doi: 10.1021/bk-2012-1105.ch010

Experimental Section

Materials and General Considerations

Unless stated otherwise, all manipulations were carried out under inert gas atmosphere using standard Schlenk or glovebox techniques. Methanol was distilled from magnesium turnings and iodine. THF was distilled from sodium/benzophenone under inert conditions. All other solvents were used in technical grade as received. Carbon monoxide (3.7) and hydrogen (5.0) were supplied by Air Liquide. Methyl linoleate (≥ 99 %) was supplied by Sigma Aldrich. All solvents were degassed by three freeze-pump-thaw cycles prior to use. Methyl palmitate (≥99 %) was supplied by Sigma Aldrich and palladium/charcoal (activated; 10 % Pd) was purchased from Merck. The complex [κ^2-(P^P)Pd(OTf)][OTf] was prepared according to a previously reported method (*36*).

Gas chromatographic analysis were performed using a Perkin-Elmer (PE) Clarus 500 instrument equipped with a flame ionization detector and an Elite-5 column (crosslinked 5 % diphenyl- 95 % dimethyl polysiloxane). The temperature of the oven was kept at 90°C for 1 min, then heated from 90°C to 280°C with a heating rate of 30°C per minute and was finally held at this temperature for 8 min. Helium of 99.995 % purity was used as the carrier gas. Injector and detector temperature were both set to 280°C. A sample volume of 1 µL was injected via autosampler. Analysis of the retention times and peak areas were performed using the TotalChrom software (Perkin Elmer).

Mass spectra (GC-MS) were received from an Agilent Technologies 7890A Series GC system with an Agilent Technologies 5975C Mass Selective Detector (electron impact ionization with 70 eV). The GC apparatus was equipped with a Phenomenex ZB-5 column (5 % diphenyl- 95 % dimethylpolysiloxane) of 30 m length, 0.25 mm inner diameter and 0.25 µm film thickness. The initial temperature of 50 °C was kept for 1 min, after which the column was heated at a rate of 30 °C per minute up to 280 °C. The final temperature was kept for 8 min. Helium of 99.995 % purity was used as the carrier gas. The injection temperature was set to 250°C.

Alkoxycarbonylation of Methyl Linoleate

Carbonylations were carried out in a 20 mL stainless steel magnetically stirred pressure reactor equipped with a heating jacket and a glass inlay. Prior to a carbonylation experiment the reactor was purged several times with nitrogen. [κ^2-(P^P)Pd(OTf)] [OTf] (P^P = 1,2-bis[(di-tert-butylphosphino)methyl]benzene) (38 mg, 0.048 mmol) was weighed into a Schlenk tube under an inert atmosphere and dissolved in 10 mL of methanol. Methyl linoleate (2.0 mL; 6.0 mmol) and as an internal standard methyl palmitate (5 mol-%) were added. After stirring for a few minutes, the homogenous reaction mixture was cannula transferred into the pressure reactor. The reactor was closed, pressurized with 20 bar carbon monoxide and then heated to 90 °C. After 5 d the reactor was cooled to room temperature and vented. The crude product was dissolved in methylene chloride and filtrated over a Buchner funnel to remove solid residues. Removing the

In Biobased Monomers, Polymers, and Materials; Smith, P., et al.;
ACS Symposium Series; American Chemical Society: Washington, DC, 2012.

Downloaded by PENNSYLVANIA STATE UNIV on August 28, 2012 | http://pubs.acs.org
Publication Date (Web): August 16, 2012 | doi: 10.1021/bk-2012-1105.ch010

solvent in vacuo yielded a yellow oil, which was analyzed by GC (Figure 4). GC-MS analysis of the main peak (retention time 8.95 min) yielded: m/z (relative intensity) = 354 (3) [M^+]; 323 (17); 322 (24); 305 (3); 304 (6); 291 (32); 290 (54); 262 (12); 151 (11); 149 (11); 137 (16); 135 (16); 133 (12); 123 (22); 121 (22); 121 (19); 109 (28); 98 (42); 95 (53) 81 (68); 74 (62); 69 (52); 67 (64); 59 (42); 55 (100).

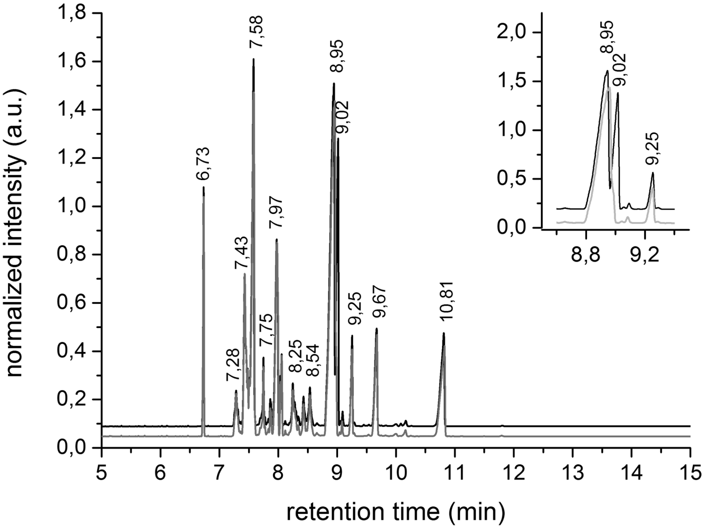

Figure 4. Gas chromatogram of the crude reaction mixture from isomerizing carbonylation of methyl linoleate. Insert: close-up of main peak (gray scale) and enrichment with a genuine sample of dimethyl 1,19-nonadecanedioate (black). Assignments of selected peaks: 6.73 min methyl palmitate added as internal standard (5.3 area %)., 7.58 methyl linoleate residual starting material (16.4 %), 8.95 dimethyl 1,19-nonadecenedioates (37.7 %), tentatively: 9.25 dimethyl 1,19-nonadec-2-endioate (3.1 %).

Catalytic Hydrogenation

The crude product of the alkoxycarbonylation of methyl linoleate was dissolved in 50 mL of dry and degassed THF. After addition of Pd/C (10 % Pd) (200 mg, 0.19 mmol Pd), the resulting mixture was cannula-transferred into a 280 mL stainless steel mechanically stirred (1500 rpm) pressure reactor equipped with a glas inlay and a heating/cooling jacket controlled by a thermocouple dipping into the reaction mixture, which was purged several times with argon prior to the reaction. The reactor was closed and pressurized with 50 bar of hydrogen and heated to 70 °C. After 12 h the reactor was cooled to room temperature and vented. The reaction mixture was then filtrated over a Buchner funnel to remove catalyst residues. After removing the solvent in vacuo an off-white solid was obtained, which was subsequently dissolved in methylene chloride and analyzed by GC (Figure 5). ^{1}H NMR shows that all double bonds are hydrogenated completely.

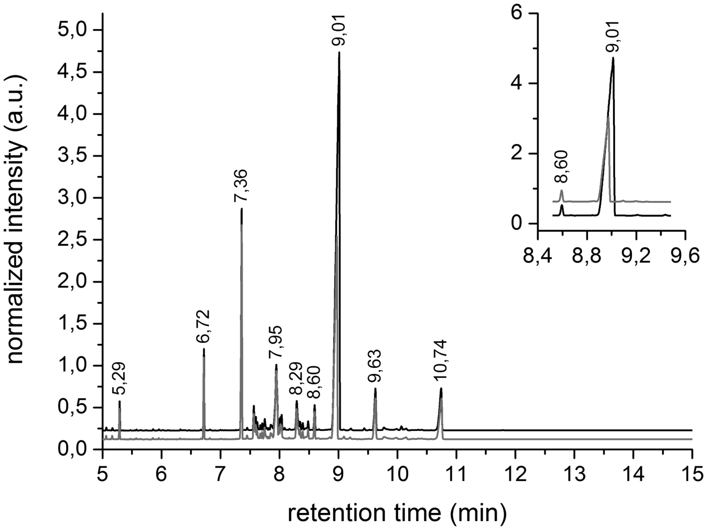

Figure 5. Gas chromatogram of hydrogenated reaction mixture from isomerizing carbonylation of methyl linoleate. Insert: close-up of main peak (gray scale) and enrichment with a genuine sample of dimethyl 1,19-nonadecanedioate (black). Assignments of selected peaks: 6.72 min methyl palmitate added as internal standard (5.2 area %), 7.36 methyl stearate (17.9 %), 9.01 dimethyl 1,19-nonadecanedioate (41.6 %).

Downloaded by PENNSYLVANIA STATE UNIV on August 28, 2012 | http://pubs.acs.org
Publication Date (Web): August 16, 2012 | doi: 10.1021/bk-2012-1105.ch010

References

1. Dodds, D. R.; Gross, R. A. *Science* **2007**, *318*, 1250–1251.
2. Mecking, S. *Angew. Chem., Int. Ed.* **2004**, *43*, 1078–1085.
3. Ulber, R.; Sell, D.; Hirth, T. Renewable Raw Materials: New Feedstocks for the Chemical Industry; Wiley-VCH: Weinheim, 2011.
4. Meier, M. A. R.; Metzger, J. O.; Schubert, U. S. *Chem. Soc. Rev.* **2007**, *36*, 1788–1803.
5. Xia, Y.; Larock, R. C. *Green Chem.* **2010**, *12*, 1893–1909.
6. Biermann, U.; Bornscheuer, U.; Meier, M. A. R.; Metzger, J. O.; Schäfer, H. J. *Angew. Chem., Int. Ed.* **2011**, *50*, 3854–3871.
7. Genas, M. *Angew. Chem.* **1962**, *74*, 535–540.
8. Naughton, F. C. *J. Am. Oil Chem. Soc.* **1974**, *51*, 65–71.

9. Stevens, C. V.; Verhé, R. Renewable bioresources: scope and modification for non-food applications; Wiley: Chichester, 2004; pp 208−250.
10. Evans, R. D.; Mighton, H. R.; Flory, P. J. *J. Am. Chem. Soc.* **1950**, *72*, 2018–2028.
11. Korshak, V. V.; Vinogradova, S. V. *Polyesters*; Pergamon Press: Oxford, U.K., 1965.
12. Mandelkern, L.; Alamo, R. G. In *Physical Properties of Polymers Handbook*; Mark, J. E., Ed.; Springer: New York, 2007; pp 165– 186.
13. Quinzler, D.; Mecking, S. *Chem. Commun.* **2009**, 5400–5402.
14. Yamamoto, M.; Witt, U.; Skupin, G.; Beimborn, D.; Müller, R.-J. In *Biopolymers*; Steinbüchel, A.; Doi, Y., Eds.; Wiley-VCH: Weinheim, 2002; Vol. 4, pp 299−311.
15. Picataggio, S.; Rohrer, T.; Deanda, K.; Lanning, D.; Reynolds, R.; Mielenz, J.; Eirich, L. D. *Nat. Biotech.* **1992**, *10*, 894–898.
16. Zibek, S.; Wagner, W.; Hirth, T.; Rupp, S.; Huf, S. *Chem. Ing. Tech.* **2009**, *81*, 1797–1808.
17. Schörken, U.; Kempers, P. *Eur. J. Lipid Sci. Tech.* **2009**, *111*, 627–645.
18. Lu, W.; Ness, J. E.; Xie, W.; Zhang, X.; Minshull, J.; Gross, R. A. *J. Am. Chem. Soc.* **2010**, *132*, 15451–15455.
19. Liu, C.; Liu, F.; Xie, W.; Long, T. E.; Turner, S. R.; Lyons, A.; Gross, R. A. *Biomacromolecules* **2011**, *12*, 3291–3298.
20. Quinzler, D.; Mecking, S. *Angew. Chem. Int. Ed.* **2010**, *49*, 4306–4308.
21. Pugh, R. I.; Drent, E.; Pringle, P. G. *Chem. Commun.* **2001**, 1476–1477.
22. Jiménez-Rodriguez, C.; Eastham, G. R.; Cole-Hamilton, D. J. *Inorg. Chem. Commun.* **2005**, *8*, 878–881.
23. Trzaskowski, J.; Quinzler, D.; Bährle, C.; Mecking, S. *Macrom. Rapid Commun.* **2011**, *32*, 1352–1356.
24. Dinger, M. B.; Mol, J. C. *Adv. Synth. Catal.* **2002**, *344*, 671–677.
25. Ngo, H.; Jones, K.; Foglia, T. *J. Am. Oil Chem. Soc.* **2006**, *83*, 629–634.
26. Warwel, S.; Demes, C.; Steinke, G. *J. Polym. Sci., Part A: Polym. Chem.* **2001**, *39*, 1601–1609.
27. Bielawski, C. W.; Grubbs, R. H. *Angew. Chem., Int. Ed.* **2000**, *39*, 2903–2906.
28. Lehman, S. E.; Wagener, K. B. *Macromolecules* **2001**, *35*, 48–53.
29. Lehman, S. E., Jr; Schwendeman, J. E.; O'Donnell, P. M.; Wagener, K. B. *Inorg. Chim. Acta* **2003**, *345*, 190–198.
30. Djigoué, G. B.; Meier, M. A. R. *Appl. Catal. A* **2009**, *368*, 158–162.
31. Hong, S. H.; Sanders, D. P.; Lee, C. W.; Grubbs, R. H. *J. Am. Chem. Soc.* **2005**, *127*, 17160–17161.
32. Gimeno, N.; Formentín, P.; Steinke, J. H. G.; Vilar, R. *Eur. J. Org. Chem.* **2007**, *2007*, 918–924.
33. Furst, M. R. L.; Le Goff, R.; Quinzler, D.; Mecking, S.; Botting, C. H.; Cole-Hamilton, D. J. *Green Chem.* DOI:10.1039/C1GC16094J.
34. Walther, G.; Deutsch, J.; Martin, A.; Baumann, F.-E.; Fridag, D.; Franke, R.; Köckritz, A. *ChemSusChem* **2011**, *4*, 1052–1054.

Downloaded by PENNSYLVANIA STATE UNIV on August 28, 2012 | http://pubs.acs.org
Publication Date (Web): August 16, 2012 | doi: 10.1021/bk-2012-1105.ch010

35. Thomas, A. Fats and Fatty Oils. In *Ullmann's Encyclopedia of Industrial Chemistry*, 6th ed.; Gerhartz, W., Elvers, B., Eds.; Wiley-VCH: Weinheim, 2005.
36. Stempfle, F.; Quinzler, D.; Heckler, I.; Mecking, S. *Macromolecules* **2011**, *44*, 4159–4166.
37. Form S1 SEC filing by Elevance Renewable Sciences of September 20, 2011 (IPO registration).
38. Clegg, W.; Eastham, G. R.; Elsegood, M. R. J.; Tooze, R. P.; Wang, X. L.; Whiston, K. *Chem. Commun.* **1999**, 1877–1878.
39. Tullo, A. H. *Chem. Eng. News* **2009**, *87*, 22–23.

Downloaded by PENNSYLVANIA STATE UNIV on August 28, 2012 | http://pubs.acs.org
Publication Date (Web): August 16, 2012 | doi: 10.1021/bk-2012-1105.ch010

Downloaded by OHIO STATE UNIV LIBRARIES on August 28, 2012 | http://pubs.acs.org
Publication Date (Web): August 16, 2012 | doi: 10.1021/bk-2012-1105.ch011

Chapter 11

Advances in the Use of BiOH® Polyols in Polyurethanes

Timothy W. Abraham[*]

Cargill Inc. Minnesota, MN 55343, U.S.A.
[*]E-mail: Tim_Abraham@cargill.com

An exponential increase in the utilization of petroleum for transportation fuels, energy and industrial chemicals that has taken place over the past several decades is widely accepted as being unsustainable. Additionally, increased concerns about the environment and global warming have given rise to worldwide efforts devoted to utilizing biobased resources for fuels and industrial chemicals. Natural oils are seen as one such inexpensive, abundant renewable resource. The versatility of natural oils in industrial applications is demonstrated by the ability to introduce various functional groups, such as epoxy, hydroxyl and carboxylic acid groups, onto the fatty acid chains, which enables their use in numerous applications. The utilization of natural oils in polyurethanes is accomplished by introducing hydroxyl groups. Cargill has introduced a family of natural oil-based polyols for polyurethane foams under the BiOH® tradename. The basic technology involves epoxidation and reaction of the epoxides with nucleophiles yielding polyols that have the desired molecular weight and functionality range. BiOH® polyols have been used to partially replace petrochemical-based polyols in flexible molded foams and flexible slabstock foams, including viscoelastic foams, and to partially substitute copolymer polyols in high resilience foams.

In Biobased Monomers, Polymers, and Materials; Smith, P., et al.;
ACS Symposium Series; American Chemical Society: Washington, DC, 2012.

Downloaded by OHIO STATE UNIV LIBRARIES on August 28, 2012 | http://pubs.acs.org
Publication Date (Web): August 16, 2012 | doi: 10.1021/bk-2012-1105.ch011

Introduction

The beginnings of the modern petroleum industry can be traced back to the 1850s when fractionation of petroleum by distillation was first demonstrated. Subsequently, a rapid expansion in the utilization of petroleum took place in the 1900s resulting from the introduction of the internal combustion engine, followed by a steady growth in the exploration and discovery of petroleum resources. A rapid increase in the utilization of petroleum for transportation fuels, energy and industrial chemicals has taken place over the past several years, mainly driven by increasing energy demands due to population growth and improved living standards across the globe. However, it has also become quite clear in recent years, even to the most ardent supporters of the petroleum industry, that petroleum as a portable, dense energy source powering the vast majority of vehicles, and as the base for many industrial chemicals, is not sustainable.

A consequence of this acute dependence on a finite resource is an increase in carbon dioxide emissions, which is known to be a major contributor to global warming and climate change. Increasing concerns about the environment and sustainability has fueled growing worldwide efforts devoted to utilizing renewable resources for energy and industrial chemicals, with the aim of reducing the world's dependence on fossil fuels. Bio-based resources are renewable and CO_2 neutral, in contrast to fossil fuels. In some instances, bio-based products may even possess unique properties, such as biodegradability and biocompatibility, thus providing additional benefits. There has been a positive change in the attitude of the general public over the past several years towards environmentally friendly products. However, the demand from many customers and consumers is for products that are equivalent in price and performance to the petroleum-based products that are being replaced.

Although a few bio-based products are able to garner a higher price than their petrochemical-based counterparts, processes for the conversion of renewable raw materials into industrial chemicals need to be cost competitive for a vast majority of biobased products, if they are to compete against the incumbent petrochemical-based products. This competitiveness is inevitable, with the continuous increase in the price of petroleum as the world approaches peak oil production, as well as advances being made in new technologies for biobased products. Ironically, it's the same natural materials that had originally been displaced as raw materials, when fossil fuels became cheaper to extract and convert to useful products at the turn of the last century, that are once again attracting attention as renewable, environmentally friendly materials for fuels and industrial chemicals. The development of technologies that utilize agricultural, animal, forestry and municipal waste as renewable feedstocks presents a significant opportunity for the manufacture of biobased fuels and industrial chemicals. Significant progress is being made in developing such value-added chemicals (*1–3*).

Cargill Inc. has been at the forefront of investing in new technologies to manufacture industrial chemicals from renewable resources. It has been supplying starch-based products to the papermaking industry for over 75 years, for use in coatings and sizing, and has also supplied starch-based products to other industries, such as corrugated boards for packaging, construction materials, and feedstocks for various biochemicals. Recent additions to this portfolio of starches are xanthan gum, scleroglucan, carageenan, alginates and pectin. In 2002, Natureworks LLC, a subsidiary of Cargill, opened the world's first global-scale manufacturing facility for polylactic acid, a biobased plastic resin from carbohydrates, demonstrating its vision and commitment to such efforts. Cargill has also, for many decades, used natural oils and their derivatives in a variety of applications, such as paints & coatings, inks, dielectric fluids, lubricants, adhesives, biodiesel, water treatment, dust control and oilfields. Its access to various oilseeds across the global, from soy in the US and South America, to canola and sunflower in Europe, palm in Asia, and cottonseed in Australia, coupled with a strong global supply chain, places Cargill in a unique position to supply these various industries. In 2005, Cargill introduced natural oil-based BiOH® polyols for the replacement of petroleum-based polyols in polyurethane foams.

Downloaded by OHIO STATE UNIV LIBRARIES on August 28, 2012 | http://pubs.acs.org
Publication Date (Web): August 16, 2012 | doi: 10.1021/bk-2012-1105.ch011

Natural Oils in Industrial Applications

Worldwide economic and scientific interest in natural oils (lipids) as inexpensive, abundant renewable resource has grown, and has already been the subject of significant research efforts globally. It represents a major potential alternative source of chemicals suitable for developing environmentally safe and consumer friendly products. Natural oils have been used since the beginning of civilization in non-food applications, and its use in coatings for wood and metal, decorative arts, printing inks, lacquers, and as lubricants goes back many thousands of years. These applications take advantage of the natural oil's lubricating and solvent like nature, and its ability to cross-link in the presence of air, resulting in polymeric films that are tough, elastic, waterproof, and adhere tightly to the substrate (*4*).

Natural oils are primarily fatty acid triesters of glycerol (also known as triacylglycerols or triglycerides). The fatty acids usually have an even number of carbons and can be 6-carbons to 22-carbons in length, but the most common fatty acids are 12-carbons to 18-carbons long. Many of the fatty acids possess one or more double bonds, and a few of them have other functional groups, such as hydroxyl groups or epoxide groups. The general structure of soybean oil (Figure 1*)* shows the glycerol backbone onto which are attached fatty acid chains, primarily oleic, linoleic, linolenic, stearic and palmitic acids.

Modern industrial methods of extracting and refining yield vegetable oils with well defined specifications and in high purity. In some cases, natural fats and oils can be used directly as building blocks for polymers, but often they are modified or functionalized to intermediates which are more suitable for polymer formation. Although currently not economical for industrial applications, genetic engineering offers a way to further optimize the properties of natural oil-based polymers by controlling the fatty acid distribution, and changing the composition of plant oils to control the structures and produce polymers with improved properties. Natural oils can be used directly for energy, or easily processed into biofuels, such as their conversion to biodiesel or jet fuel. However, the value of lipids as an abundant

Downloaded by OHIO STATE UNIV LIBRARIES on August 28, 2012 | http://pubs.acs.org
Publication Date (Web): August 16, 2012 | doi: 10.1021/bk-2012-1105.ch011

source for industrially useful chemicals is demonstrated by the versatile methods that have been developed to introduce functional groups, such as hydroxyl, epoxy, carbonyl and carboxylic acid groups, on the fatty acid chains (*5*).

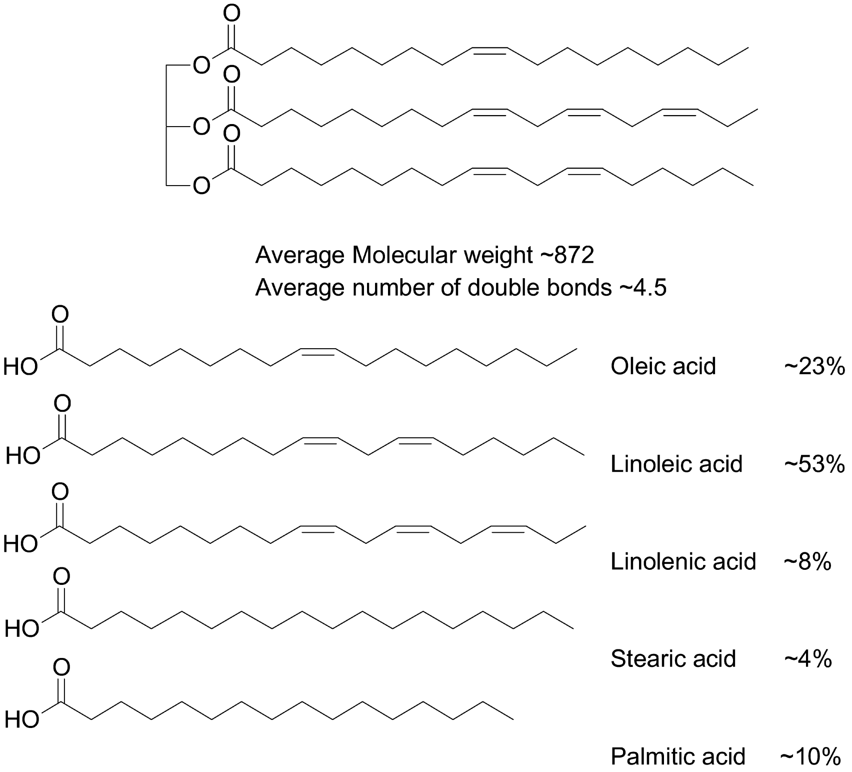

Figure 1. General structure of soybean oil.

Synthetic methods involving radical, electrophilic, nucleophilic, and pericyclic reactions have been applied extensively to the carbon-carbon double bonds of natural oils and fatty acids for selective functionalization (*6–12*). Natural oils that already possess hydroxyl or epoxide groups can be used directly in some applications (*13*, *14*). Polymeric materials from natural oils have also been investigated extensively (*15*, *16*)*,* with the above-mentioned reactions being utilized to synthesize useful monomers for polymers which are used as coatings, and toughening agents for epoxy resins (*17*). Certain vegetable oils and their derivatives, such as polyol products, are utilized as alternative feedstocks to produce additives or components for composites or polymers (*18*). More recently, natural oils have been used in creating engineering composites (*19*, *20*) and pressure-sensitive adhesives (*21*).

Downloaded by OHIO STATE UNIV LIBRARIES on August 28, 2012 | http://pubs.acs.org
Publication Date (Web): August 16, 2012 | doi: 10.1021/bk-2012-1105.ch011

Natural Oils in Polyurethanes

Polyurethanes can be broadly classified into Flexible foams (~50%), Rigid foams (~30%) and CASE (Coatings, Adhesives, Sealants and Elastomers, ~20%) applications. Flexible polyurethane foams are used in such items as home and office furniture, mattresses, carpet backing and automotive seats. Rigid polyurethane foams are used in insulation materials (eg. coolers, vending machines, refrigerators, and panels for walls and roofs), automotive parts, and various structural materials. CASE applications span a variety of industries from coatings for cars, floors, and basketball courts, to various adhesives, sealants (eg. caulking materials), and elastomeric materials (eg. tracks, shoe soles, and artificial leather). The polyurethane industry is about a 20 billion dollar global industry which used about 11 billion pounds of polyols in 2006 (*22*). About a third of polyurethanes are sold in North America, another third in Europe, and the rest in Asia Pacific and South America.

The seminal work of Frankel and others, beginning in the 1960s, at the USDA's Northern Regional Research Laboratory, demonstrated the potential for utilizing hydroformylation reactions to convert natural oils into polyols for use in polyurethanes (*23–32*). There has been a renewed interest (*33–35*) in recent years to utilize such hydroxylated natural oils in polyurethanes due to the volatility of the petroleum-based polyols market. Various natural oils, such as soybean oil (*36–39*), sunflower oil (*38*, *40*), rapeseed oil (*40*, *41*), and palm kernel oil (*42*), have been tested in the synthesis of polyols. Polyurethanes produced from natural oil polyols present some excellent properties, such as enhanced hydrolytic and thermal stability (*43*, *44*). In recent years, the availability of inexpensive blown soybean oil, which has hydroxyl groups that are introduced by blowing air or oxygen through the heated oil (*45*, *46*), provided an impetus for the development of various natural oil-based polyols. Subsequent generations of blown oil-based polyols include products with higher functionality, obtained by transesterifying blown oils with polyols like glycerol and sorbitol (*45*, *46*).

The initial success demonstrated with blown oils led to the accelerated development of other proven technologies for the introduction of hydroxyl groups onto fatty acids and natural oils. Although the use of polyols obtained by the hydroformylation of oils in making rigid polyurethanes had been demonstrated by Frankel and others (*23–32*), the versatility of these polyols in a number of different polyurethane applications was demonstrated by Rogier (*47*), who synthesized liquid polyols for elastomers and microcellular foams. The hydoroformylation reaction provides a valuable method to introduce primary hydroxyl groups onto fatty acid chains, while maintaining the molecular weight of the oil. More recently, Guo and others (*48–51*) studied the physical and mechanical properties of polyurethane foams made with polyols derived from the hydroformylation of natural oils. In order to build high-MW polyols from hydroformylated fatty acids, Peerman and Rogier (*52*) had developed a novel method of polymerizing hydroxymethyl-containing alkyl esters of fatty acids onto polyol, polyamine, and aminoalcohol initiators, which enabled the synthesis of previously unseen high molecular weight, non-gelling polyols. These polyols were used in the preparation of elastomeric polyurethanes that exhibited low water absorption, good retention of strength after exposure to hot water, and good flexibility. Building on this work, the Dow Chemical Company has synthesized polyols from natural oils in a similar manner, and have tested them in various polyurethane applications (*53–58*). In order to understand structure-property relationships, Petrovic et. al. (*59*) synthesized a series of triols from methyl oleate, which have a more uniform structure than polyols synthesized from a heterogeneous mixture of fatty acids, and studied the effect of the molecular weight of these polyols on the properties of the resulting polyurethanes.

Epoxidation of natural oils, followed by reaction of the epoxides with nucleophiles is another method to introduce hydroxyl groups (*60*). Industrially, the epoxidation of natural oils is performed utilizing a peracid, such as performic acid or peracetic acid (*61–64*). Various nucleophiles have been used in the reaction with epoxidized oils, such as water, alcohols, carboxylic acids, amines, amino alcohols and thiols (*39*, *65–69*). The reaction with carboxylic acids results in polyols with vicinal hydroxyl and ester groups. These reactions usually result in the introduction of secondary hydroxyl groups. Ozonolysis (*70*) is another method of introducing primary hydroxyl groups onto fatty acids. However, unlike in the case of hydroformylation, ozonolysis results in oxidative cleavage of the carbon-carbon double bonds. Azelaic acid (nonanedioic acid) and Pelargonic acid (nonanoic acid) are produced as bulk industrial chemicals by ozonlysis. The reaction of double bonds in natural oils with ozone results in the formation of ozonides, which are converted to polyols using different reducing agents (*71*). Hydroformylation introduces primary hydroxyl groups without decreasing the molecular weight of the oil, while ozonolysis of fatty acid chains results in low molecular weight compounds, which limits their use to mostly rigid polyurethanes. A mixture of low molecular weight polyester polyols and highly functionalized glyceride alcohols can be obtained when vegetable oils are directly subjected to ozonolysis in the presence of polyols like glycerol (*72–74*).

BiOH® Polyols

BiOH® polyols are synthesized utilizing the epoxidation route, where the double bonds in natural oils are first converted to epoxides, and the epoxides are then reacted with nucleophiles, such as monoalcohols, in the presence of an acid catalyst, to introduce hydroxyl groups *((75*, *76*) Figure 2*)*.

A variety of polyols have been synthesized using this basic technology, by choosing different types of natural oils, partially or fully epoxidizing the oils, and varying the type and functionality of the nucleophiles. The reaction of epoxidized oils with nucleophiles can also be performed in a manner as to cause intermolecular reactions resulting in the formation of polyether bonds (*77*), yielding natural oil-based oligomeric polyols that are suitable for use in manufacturing flexible foams (*78*, *79*). Polymerization of epoxidized oils, via ether bonds, can also be accomplished by reacting the epoxidized oils with multifunctional nucleophiles, such as ethylene glycol, trimethylolpropane, or an amino alcohol. A portfolio of BiOH® polyols have been developed utilizing the epoxidation technology, and is shown in Table I.

Downloaded by OHIO STATE UNIV LIBRARIES on August 28, 2012 | http://pubs.acs.org
Publication Date (Web): August 16, 2012 | doi: 10.1021/bk-2012-1105.ch011

Downloaded by OHIO STATE UNIV LIBRARIES on August 28, 2012 | http://pubs.acs.org
Publication Date (Web): August 16, 2012 | doi: 10.1021/bk-2012-1105.ch011

Table I. Typical properties of BiOH® polyols

BiOH® polyol	***5000***	***5300***	***5400***	***2300***	***1000***	***2100***
OH# (mg KOH/g)	56	119	129	160	200	225
Viscosity (cp @ 25C)	4,000	5,500	4,400	4,900	3,900	8,900
Molecular weight (Mn)	1721	1,447	1,300	1,335	1,164	1,215
Functionality (Fn)	1.7	3.1	3.0	3.8	4.2	4.9
Acid value (mg KOH/g)	0.5	0.72	0.6	0.84	0.55	1.7
Water (ppm)	500	1,600	500	1,300	700	3,000
Color (Gardner)	<1	<1	<1	<1	<1	<2

Table II. BiOH® 5000 polyols synthesized from different oils

	OH number (mg KOH/g)	***Viscosity (Pa.s)***	***Mn***	***Fn***	***Mw***	***Mw/Mn***
Soybean	57.0	4.1	1800	1.83	9592	5.3
Canola	56.4	3.1	1703	1.71	6280	3.7
Palm olein	53.4	1.6	1677	1.60	2981	1.8

In general, the hydroxy number (OH#), which is a measure of the concentration of OH groups in a polyol, ranges from about 56 to 225 mg KOH/gm of polyol, the molecular weight ranges from about 1100 to 1700, and the hydroxyl functionality, which is the average number of OH groups per molecule, ranges from 1.7 to 4.9. The high OH#, high functionality, low MW polyols are generally suitable for making rigid foams, while the low OH#, low functionality, high MW polyols are suitable for making flexible foams. Since a monoalcohol was the choice of nucleophile in the reaction with epoxides, the hydroxyl groups are all secondary, and are located internally. The pendant chains can slow down crosslinking due to steric hindrance when these polyols are reacted with isocyanates or other polyfunctional compounds, and also have a plasticizing effect on the resulting polymers.

Downloaded by OHIO STATE UNIV LIBRARIES on August 28, 2012 | http://pubs.acs.org
Publication Date (Web): August 16, 2012 | doi: 10.1021/bk-2012-1105.ch011

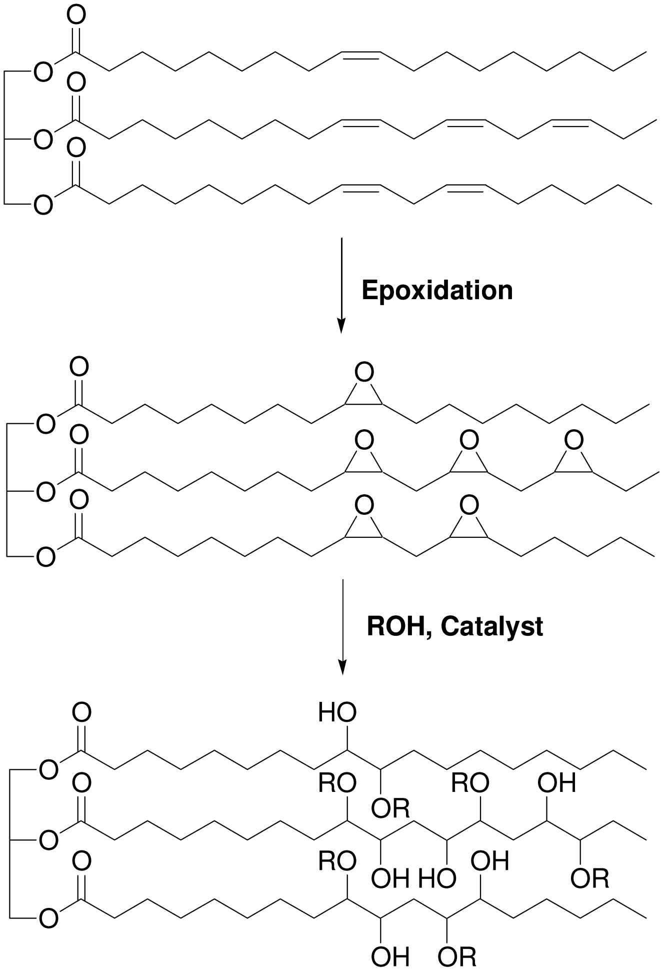

Figure 2. Synthesis of BiOH^(R) polyols.

Castor oil which contains hydroxylated fatty acids, as well as other natural oils that have been hydroxylated by the methods described above, have been used in polyurethanes for several years. However, their broader use has been limited due to challenges with odor, color and consistency, which are essential in many commercial applications. Overcoming these challenges was critical in introducing natural oil-based polyols in flexible polyurethane foams, especially for foams used in the furniture and bedding industries. Cargill's knowledge and experience in the processing of oilseeds played a key role in the successful introduction of BiOH® polyols with a light color and low odor into the flexible foams market. Initial success in developing polyols for the polyurethanes industry began with BiOH® 2100 (Figure 3), which was used to partially substitute copolymer polyols in molded flexible foams. In petroleum-based polyurethane foams, Styrene-Acrylonitrile (SAN) copolymer polyols provide improved load bearing capabilities to flexible foams, and are synthesized by grafting styrene and acrylonitrile onto polyether polyols. Partial substitution of copolymer polyols with BiOH® 2100 was achieved, which provided the desired hardness while retaining other foam physical properties *((80, 81)* Figure 3*).*

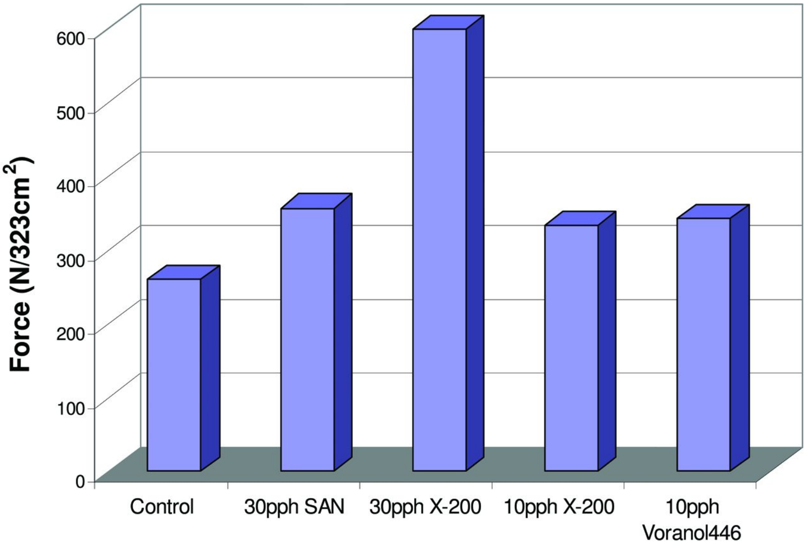

Figure 3. Load bearing properties of flexible molded foams containing BiOH® 2100 (X-200).

BiOH® 5000 has become one of the most successful biobased polyols for replacing the base polyol in flexible slabstock foams (*77–79*). Although there are claims of 50% substitution of petroleum-based polyols by natural oil-based polyols in flexible slabstock foams (*82*)*,* most PU foam manufacturers are comfortable in substituting 20-30% of a petroleum-based polyol in a polyurethane formulation, and being able to retain the desired physical properties of the foam. Attempts to go above these levels usually result in a deterioration of some foam properties, especially tensile, tear, elongation, and compression sets. Achieving higher levels of incorporation will require new biobased polyols with a high molecular weight and low functionality, which are more uniform in structure. They should also enable a significant mass of the polyols to be a part of the polyurethane network (less pendant chains), which will improve extensive properties of the foam.

Downloaded by OHIO STATE UNIV LIBRARIES on August 28, 2012 | http://pubs.acs.org
Publication Date (Web): August 16, 2012 | doi: 10.1021/bk-2012-1105.ch011

BiOH® polyols can be synthesized from different natural oils, and as shown in Table II, BiOH® 5000 polyols were synthesized from soybean oil, canola oil and palm olein. The high level of polyunsaturated fatty acids in soybean oil results in a polyol with a high polydispersity and viscosity, that is lower in the palm olein-based polyol which has a high level of monounsaturated and saturated fatty acids.

BiOH® 5300 and BiOH® 5400

In order to expand the use of BiOH® polyols in flexible polyurethane foams, and to mitigate some of the risks associated with the volatility of the grain commodities market, higher value polyols were developed from natural oils, which provide performance benefits beyond what the petroleum-based polyol being replaced can provide. BiOH® 5300 was developed to replace copolymer polyols (CPP) in flexible slabstock foams. As mentioned previously, copolymer polyols are standard polyether polyols onto which are grafted styrene and acrylonitrile copolymers that form white, solid particles, and impart a certain level of hardness to the foams. However, there are problems associated with using copolymer polyols, in addition to the fact that hazardous compounds (styrene & acrylonitrile) are used in their production. The wear and tear that polyols containing solids cause to manufacturing equipment, the plugging of filters, and densification (where the bottom of the foam is harder than the top) are additional challenges. BiOH® 5300 was introduced to partially replace CPP in flexible slabstock foams, while providing the same level of hardness as a CPP, but containing no solids.

Table III shows the properties of high resilience (HR) foams made on a production line, in which BiOH® 5300 was partially substituted for a CPP.

Replacing 10 pph (parts per hundred) of the CPP with 10 pph BiOH® 5300 showed no deterioration of the properties. The indentation force deflections (IFDs), support factor (SAG factor), resilience (also known as ball rebound), tensile strength and tear are all similar. The % elongation is slightly lower, but is adequate since the specification calls for an elongation of >100%. The last two rows are flammability tests, which were also similar. The last column shows the properties of foams where both the CPP and the base polyol in a HR foam were partially replaced with BiOH® 5300 and BiOH® 5000 respectively. Once again, the foam properties were as good as the control, and met all specifications.

BiOH® 5300 also imparts a more uniform IFD spread across the foam compared to CPP (*83*, *84*). A higher isocyanate index or cross-linkers are often used to achieve the desired hardness in low density CO_2-blown foams, where CPP is not traditionally used, especially during the summer months. BiOH® 5300 can be used as an alternative to increasing the isocyanate index (*83*, *84*), thereby decreasing the cost of producing the foam, and also reducing the maximum temperature from the exotherm.

BiOH® 5400 was developed for the viscoelastic (VE, memory) foams market, where it can partially replace the higher value petrochemical polyols that are specifically synthesized for this application. Petrochemical polyols that have been developed for use in VE foams are often blends of several polyols of

Downloaded by OHIO STATE UNIV LIBRARIES on August 28, 2012 | http://pubs.acs.org
Publication Date (Web): August 16, 2012 | doi: 10.1021/bk-2012-1105.ch011

different molecular weight, hydroxy number and functionality (*85–90*). They are specially formulated to impart specific properties to the foam, such as to have a glass transition temperature (Tg) close to room temperature, and a very low resiliency. Table IV shows a comparison of the properties of VE foams in which 30 pph of the petrochemical polyol was replaced with BiOH® 5400. The 'ball rebound' test shows that both foams have the desired low resilience. IFD's are slightly better for the foam made with BiOH® 5400, and the SAG factor is about the same. While the tensile strength is better, and % elongation about the same, the tear strength is a little lower but met specifications, and the compression sets for both foams were excellent.

Downloaded by OHIO STATE UNIV LIBRARIES on August 28, 2012 | http://pubs.acs.org
Publication Date (Web): August 16, 2012 | doi: 10.1021/bk-2012-1105.ch011

Table III. Foam properties of high resilience Slabstock foams containing BiOH® polyols

		Control 25 pph CPP	*10pph BiOH® 5300 15 pph CPP*	*10 pph BiOH® 5300 20 pph BiOH® 5000 15 pph CPP*
Density	**kg/m3**	28.0	30.0	32.0
25% IFD	**N**	114.3	132.1	132.1
65% IFD	**N**	262.0	319.8	340.3
Support factor		2.3	2.4	2.6
Air flow	**cfm**	1.23	1.20	1.17
Ball Rebound	**%**	46	48	48
Tensile strength	**Kpa**	107.6	108.3	122.0
Tear	**N/m**	245.1	262.7	262.7
Elongation	**%**	143	140	120
Cal 117	**cm**	6.60	6.35	6.60
Smolder	**% loss**	3.97	2.27	2.37

Some additional benefits have been observed when using BiOH® 5400 in visco foams. The foams stay soft even when the temperature drops below room temperature *(unpublished),* which is not always the case with most petroleum-based foams, that tend to get very hard and are unsuitable for certain applications, such as for outdoor use during the winter. Faster heat dissipation has also been observed in foams containing BiOH® 5400 *(unpublished),* which makes the foams feel cooler when compared to petroleum polyol-based foams with the same density. Studies are ongoing to understand the reasons for this "cooling effect". The foam properties are optimum when a lower index is used. i.e. the amount of isocyanate used in preparing the polyurethane foam is lower than what is needed to react with all the hydroxyl groups present in the polyol formulation, resulting in additional savings for the foam manufacturer.

Table IV. BiOH® 5400 in a viscoelastic foams

	Units	*Control*	*BiOH® 5400 30 pph*
Density	Kg/m3	83.45	82.81
Resilience	%	2	3
25% IFD	N	21.8	23.2
65% IFD	N	43.9	45.9
SAG factor		2	2
Tensile strength	Kpa	56	65
Elongation	%	137	139
Tear	N/m	193	180
90% Compression set (dry)	%	0	0

Increasing the Incorporation Level of Natural Oil-Based Polyols

One of the challenges of using natural oil-based polyols in flexible foams is the fact that even after the introduction of hydroxyl groups the polyols are still quite hydrophobic. This can pose a challenge when attempting to utilize these polyols in aqueous polyol formulations that have been optimized around hydrophilic, petroleum-based polyols. In response to these challenges, changes are being made to the components of these formulations, such as the surfactants and catalysts. It has been observed that the use of bismuth compounds as catalysts in foams made using natural oil-based polyols provide a wide processing window and give foams with reduced shrinkage, fine cells, low odor, and low VOCs when compared with traditional catalysts, such as tin octoate (*91*). A natural oil-based polyol can form a homogeneous mixture with a petroleum-based polyol in the absence of water. However, the addition of even a small amount of water to this mixture, which is needed for the manufacture of flexible and many rigid foams, usually results in the formation of two phases. Formulations that do not phase separate have been prepared by synthesizing natural oil-based polyols containing nitrogen, making them more hydrophilic (*92*), or developing new surfactants which enable the formation of much better dispersions (*93*, *94*). The incorporation level of biobased polyols can also be increased by improved mixing, for example by using high shear mixers, and by making prepolymers of the natural oil-based polyols, which are known to improve the properties of the resulting foams (*95–98*). Continuous improvements to polyol structures, formulations,

Downloaded by OHIO STATE UNIV LIBRARIES on August 28, 2012 | http://pubs.acs.org
Publication Date (Web): August 16, 2012 | doi: 10.1021/bk-2012-1105.ch011

Downloaded by OHIO STATE UNIV LIBRARIES on August 28, 2012 | http://pubs.acs.org
Publication Date (Web): August 16, 2012 | doi: 10.1021/bk-2012-1105.ch011

and processing conditions will progressively increase the incorporation level of natural oil-based polyols in polyurethanes.

Conclusions

Natural oils have been used since pre-historic times in non-food applications. Even its use in coatings, paints and lubricants goes back many thousands of years. However, over the past 150 years or so, the ability to inexpensively extract petroleum from underground reservoirs, and refine it in very large amounts to industrially useful chemicals resulted in a decrease in the use of natural oils in industrial applications, purely due to economic reasons, except in cases where the natural oils provided a functional benefit. It is evident from the variety of natural oils available, and the numerous methods of introducing functional groups, that natural oils are an abundant resource for industrially useful chemicals. An obvious advantage of many natural oils is the presence of double bonds, which in some cases make the oils useful as they are, and in other cases make it easier to convert them into industrially useful chemicals, including monomers for polymers.

A variety of synthetic methods have been applied extensively for the selective functionalization of natural oils that afford a vast array of compounds with interesting properties. Further developments in innovative technologies will continue to provide high-value industrial products from natural oils, thus promoting the increased use of this renewable resource. This is also helped by improved agricultural practices and scientific advancements in developing improved breeds, which has increased the yield of crops, as well as due to the scale at which farming is done in many developed countries.

BiOH® polyols were synthesized to replace petrochemical polyols in polyurethanes applications, especially in flexible foams. Currently, partial substitution of petrochemical polyols can be achieved, without compromising the physical properties of the foam, which is a measure of the foams performance and durability during its use lifetime. BiOH® polyols have a high renewable content (≥95%), and are manufactured by processes that do not use propylene oxide or ethylene oxide. Cargill is able to take advantage of its globally integrated supply chain, and proprietary knowledge in processing oilseeds, to manufacture BiOH® polyols that have gained recognition in the polyurethanes industry as having brought a new supply option, supply stability, and an opportunity for performance differentiation.

References

1. Hackett, M. *Chemical building blocks from renewable resources*; SRI Report, Menlo Park, CA. 2011 Sep.
2. Bozell, J. J.; Petersen, G. R. *Green Chem.* **2010**, *12* (4), 539–554.
3. Werpy, T., Petersen, G., Ed.; *Top value added chemicals from biomass*; US Department of Energy report, 2004.
4. Abraham, T. W., Höfer, R. Lipid-based polymer building blocks & polymers. In *Polymers for Sustainable Environment and Energy*, Comprehensive

Polymer Science, 2nd ed.; McGrath, J., Höfer, R., Eds.; Elsevier Ltd.: Oxford, London; Vol. 10, chapter 10.1 (in press).

5. Pryde, E. H., Princen, L. H., Mukherjee, K. D., Eds.; *New sources of fats and oils*; American Oil Chemists Society: Champaign, IL, 1981; Monograph No. 9.
6. Biermann, U.; Friedt, W.; Lang, S.; Luhs, W.; Machmuller, G.; Metzger, J. O.; Rusch gen. Klaas, M.; Schafer, H.; Schneider, M. P. *Angew. Chem. Int. Ed.* **2000**, *39* (13), 2206–2224.
7. Knothe, G., Derksen, P., Eds.; *Recent Developments in the Synthesis of Fatty Acid Derivatives*; AOCS Press: Champaign, IL, 1999.
8. Nachwachsende, R. *Perspektiven fur die Chemie*; Eggersdorfer, M., Warwel, S., Wulff, G., Eds.; VCH: Weinheim, 1993.
9. Eierdanz H., Eds.; *Perspektiven nachwachsender Rohstoffe in der Chemie*; VCH: Weinheim, 1996.
10. Baumann, H.; Buhler, M.; Fochem, H.; Hirsinger, F.; Zoebelein, H.; Falbe, J. *Angew. Chem., Int. Ed. Engl.* **1988**, *27* (1), 41–62.
11. Biermann, U.; Furmeier, S.; Metzger, J. O. In *Oleochemical Manufacture and Applications*; Gunstone, F. D., Hamilton, R. J., Eds.; CRC Press, LLC: Boca Raton, FL, 2001; pp 266–299.
12. Biermann, U.; Metzger, J. *Top. Catal.* **2004**, *27* (1-4), 119–130.
13. Barrett, L. W.; Sperling, L. H.; Murphy, C. J. *J. Am. Oil Chem. Soc.* **1993**, *70*, 523–534.
14. Carlson, K. D.; Chang, S. P. *J. Am. Oil. Chem. Soc.* **1985**, *62*, 934–939.
15. Hill, K. *Pure Appl. Chem.* **2000**, *72* (7), 1255–1264.
16. Gandini, A.; Belgacem, M. N. *J. Polym. Environ.* **2002**, *10* (3), 105–114.
17. Kirschenbauer, H. G. *Fats and Oils: An Outline of Their Chemistry and Technology*; Reinhold Publishing: New York, 1960; pp 146–156.
18. Nayak, P. L. *J. Macromol. Sci., Polym. Rev.* **2000**, *40* (1), 1–21.
19. Wool, R. P.; Kusefoglu, S. H.; Palmese, G. R.; Zhao, R.; Khot, S. N. U.S. Patent 6,121,398, 2001.
20. Khot, S. N.; Lascala, J. J.; Can, E.; Morye, S. S.; Williams, G. I.; Palmese, G. R.; Kusefoglu, S. H.; Wool, R. P. *J. Appl. Polym. Sci.* **2001**, *82* (3), 703–723.
21. Bunker, S. P.; Wool, R. P. *J. Polym. Sci., Part A: Polym. Chem.* **2002**, *40*, 451–458.
22. 2008 End-Use Market Survey on the Polyurethanes Industry, American Chemistry Council, Washington, DC, 2008.
23. Frankel, E. N.; Metlin, S.; Rohwedder, W. K.; Wender, I. *J. Am. Oil Chem. Soc.* **1969**, *46* (3), 133–138.
24. Frankel, E. N. *J. Am. Oil Chem. Soc.* **1971**, *48* (5), 248–253.
25. Frankel, E. N. U.S. Patent 3,787,459, 1974.
26. Frankel, E. N.; Pryde, E. H. *J. Am. Oil Chem. Soc.* **1977**, *54* (11), A873–A881.
27. Frankel, E. N.; Thomas, F. L. *J. Am. Oil Chem. Soc.* **1972**, *49* (1), 10–14.
28. Pryde, E. H.; Frankel, E. N.; Cowan, J. C. *J. Am. Oil Chem. Soc.* **1972**, *49* (8), 451–456.
29. Frankel, E. N.; Thomas, F. L.; Rohwedder, W. K. *Ind. Eng. Chem. Prod. Res. Dev.* **1973**, *1*, 47–53.

Downloaded by OHIO STATE UNIV LIBRARIES on August 28, 2012 | http://pubs.acs.org
Publication Date (Web): August 16, 2012 | doi: 10.1021/bk-2012-1105.ch011

30. Frankel, E. N. *Ann. N. Y. Acad. Sci.* **1973**, *214*, 79–93.
31. Khoe, T. H.; Otey, F. H.; Frankel, E. N. *J. Am. Oil Chem. Soc.* **1972**, *49*, 615–618.
32. Lyon, C. K.; Garrett, V. H.; Frankel, E. N. *J. Am. Oil Chem. Soc.* **1974**, *51* (8), 331–334.
33. (a). Hu, Y. H.; Gao, Y.; Wang, D. N.; Hu, C. P.; Zu, S.; Vanoverloop, L.; Randall, D. *J. Appl. Polym. Sci.* 2002, *84,* 591–597.
34. DwanIsa, L. J. P.; Mohanty, A. K.; Misra, M.; Drzal, L. T.; Kazemizadeh, M. *J. Polym. Environ.* **2003**, *11*, 161–168.
35. Guo, A.; Demydov, D.; Zhang, W.; Petrovic, Z. S. *J. Polym. Environ.* **2002**, *10*, 49–52.
36. Guo, A.; Javni, I.; Petrovic, Z. S. *Polym. Mater.: Sci. Eng.* **1999**, *80*, 503–504.
37. John, J.; Bhattaacharia, M.; Turner, R. *J. Appl. Polym. Sci.* **2002**, *86*, 3097–3107.
38. Javni, I.; Petrovic, Z. S.; Guo, A.; Fuller, R. *J. Appl. Polym. Sci.* **2000**, *77* (8), 1723–1734.
39. Guo, A.; Petrovic, Z. S. *J. Appl. Polym. Sci.* **2000**, *77*, 467–473.
40. Stirna, U.; Yakushin, V.; Sevastyanova, I.; Misane, M. *Latv. J. Chem.* **1999**, *4*, 91–99.
41. Hu, Y. H.; Gao, Y.; Wang, D. N.; Hu, C. P.; Zu, S.; Vanoverloop, L.; Randal, D. *J. Appl. Polym. Sci.* **2002**, *84* (3), 591–597.
42. Badri, K. H.; Ahmad, S. H.; Zakaria, S. *J. Appl. Polym. Sci.* **2001**, *81* (2), 384–389.
43. Javni, I.; Zhang, W.; Petrovic, Z. S. *J. Polym. Environ.* **2004**, *12* (3), 123–129.
44. Zlatanic, A.; Petrovic, Z. S. *Abstr. Pap. Am. Chem. Soc.* **2002**, *223*, D77.
45. Kurth, T. M. U.S. Patents 6,180,686, 2001; 6,465,569, 2002; 6,624,244, 2003; 6,864,296, 2005; 6,867,239, 2005; 6,881,763, 2005.
46. Mahlum, L. U.S. Patents 6,476,244, 2002; 6,759,542, 2004.
47. Rogier, E. R. U.S. Patents 4,216,343, 1979; 4,216,344, 1979; 4,229,562, 1979; 4,304,945, 1979; 4,582,946, 1979.
48. Guo, A.; Demydov, D.; Zhang, W.; Petrovic, Z. S. *J. Polym. Environ.* **2002**, *10* (1/2), 49–52.
49. Kandanarachchi, P.; Guo, A.; Petrovic, Z. *J. Mol. Catal. A* **2002**, *184* (1-2), 65–71.
50. Petrovic, Z. S.; Guo, A.; Javni, I.; Zhang, W. *Polyurethanes Conference 2000, Proceedings of the Polyurethanes Conference*, Boston, MA, Oct. 8–11, 2000; Alliance for the Polyureth. Ind.: Arlington, VA, 2000; pp 323–327.
51. Guo, A.; Zhang, W.; Petrovic, Z. S. *J. Mater. Sci.* **2006**, *41* (15), 4914–4920.
52. Peerman, D. E.; Rogier, E. R. U.S. Patents 4,423,162, 1983; 4,496,487, 1985; 4,534,907, 1985; 4,543,369, 1985.
53. Lysenko, Z.; Morrison, D. L.; Babb, D. A.; Bunning, D. L.; Derstine, C. W.; Gilchrist, J. H.; Jouett, H. R.; Kanel, J. S.; Olson, K. D.; Peng, W.-J.; Phillips, J. D.; Roesch, B. M.; Sanders, A. W.; Schrock, A. K.; Thomas, P. J. U.S. Patent 7,615,658, 2004.

Downloaded by OHIO STATE UNIV LIBRARIES on August 28, 2012 | http://pubs.acs.org
Publication Date (Web): August 16, 2012 | doi: 10.1021/bk-2012-1105.ch011

Downloaded by OHIO STATE UNIV LIBRARIES on August 28, 2012 | http://pubs.acs.org
Publication Date (Web): August 16, 2012 | doi: 10.1021/bk-2012-1105.ch011

54. Lysenko, Z.; Schrock, A. K.; Babb, D. A.; Sanders, A. W. U.S. Patent Appl. 2006/0276609, 2006.
55. Wiltz, E. P.; Lysenko, Z.; Aguirre, F.; Sanders, A.; Tsavalas, J.; Babb, D. A.; Schrock, A. K. EP 1627003, 2006; U.S. Patent Appl. 2006/0293400, 2006.
56. Peng, W.-J.; Babb, D.; Sanders, A.; Derstine, C. W.; Jiminez, J.; Lysenko, Z.; Olson, K.; Phillips, J.; Roesch, B.; Schrock, A. PCT WO 2008/073729, 2007.
57. Frycek, G. J.; Feist, S. D.; Frank, T. C.; Lysenko, Z.; Phillips, J. D.; Pynnonen, B. W. PCT WO 2009/009271, 2009.
58. Gruenbauer, H.; Meerbote, M.; Thoen, J.; Van der Wal, H. PCT WO 2009/129292, 2009.
59. Petrovic, Z. S.; Cvetkovic, I.; Hong, D. P.; Wan, X.; Zhang, W.; Abraham, T. W.; Malsam, J. *Eur. J. Lipid Sci. Technol.* **2010**, *112*, 97–102.
60. Swanson, R. R.; Rogier, E. R. CA 671033, 1963.
61. Gall, R. J.; Greenspan, F. P. GB 755778, 1954.
62. Rowland, S. P.; White, R. G. U.S. Patent 3,051,672, 1958.
63. Dieckelmann, G.; Heinz, H. J. *The Basics of Industrial Oleochemistry*; Oleochem. Consulting Int.: Mülheim, Germany, 1988.
64. Köckritz, A.; Martin, A. *Eur. J. Lipid Sci. Technol.* **2008**, *110* (9), 812–824.
65. Höfer, R.; Gruber, B.; Meffert, A.; Grützmacher, R. EP 259722, 1987.
66. Hellbardt, S.; Schlandt, K.; Zech, W. DE 4125031, 1991.
67. Daute, P.; Grützmacher, R.; Klein, J.; Hofer, R.; Dobrich, P.; Beuer, B. EP 0689556, 1994.
68. Bauer, S.; Meyer, S. EP 1981926, 2007.
69. Casper, D. M., Newbold, T. U.S. Patent 7,893,287, 2011.
70. Pryde, E. H.; Anders, D. E.; Teeter, H. M.; Cowan, J. C. *J. Am Oil Chem. Soc* **1961**, *38*, 375–379.
71. Petrovic, Z. S.; Zhang, W.; Javni, I. *Biomacromolecules* **2005**, *6*, 713–719.
72. Narayan, R.; Graiver, D.; Farminer K. W.; Tran, P. T.; Tran, T., U.S. Patent 7,589,222, 2006.
73. Benecke, H. P.; Garbark, D. B.; Vijayendran, B. R. U.S. Patent Appl. 2009/0216040, 2009.
74. Narine, S.; Sporns, P.; Yue, J. U.S. Patent 7,538,236, 2009.
75. Petrovic, Z.; Guo, A.; Javni, I. U.S. Patent 6,107,433, 2000.
76. Petrovic, Z.; Guo, A.; Javni, I.; Zhang W. U.S. Patent 6,433,121, 2002.
77. Petrovic, Z. S.; Javni, I.; Zlatanic, A.; Guo, A. U.S. Patent 7,786,239, 2010.
78. Abraham, T. W.; Carter, J. A.; Dimitri, D.; Malsam, J. U.S. Patent 7,691,914, 2006.
79. Abraham, T. W.; Dai, D. G.; De Genova, R.; Malsam, J. U.S. Pat. Appl. 2010/0048754, 2010.
80. Herrington, R.; Malsam, J. U.S. Patent Appl. 2005/0070620, 2005.
81. Zhang, L.; Jeon, H. K.; Malsam, J.; Herrington, R.; Macosko, C. W. *Polymer* **2007**, *48*, 6656–6667.
82. *Furniture Today* 2010, April 12th; pp 40.
83. Gower, W. C.; De Genova, R. *New Polyols Based on High Renewable Content for the Production of High Resilience Flexible Slabstock Foams.* UTECH Europe 2009, Maastricht, The Netherlands.

In Biobased Monomers, Polymers, and Materials; Smith, P., et al.;
ACS Symposium Series; American Chemical Society: Washington, DC, 2012.

84. Gower, W. C.; De Genova, R. *New Polyols Based on High Renewable Content for the Production of High Resilience Flexible Slabstock Foams.* Center for the Polyurethanes Industry, Polyurethanes 2008 Technical Conference, San Antonio, Austin, TX.
85. Yu, J. U.S. Patent 6,946,497, 2005.
86. Lockwood, R. J.; Poole, V. D. U. S. Patent 7,022,746, 2006.
87. Obi, B.; Schrock A.; Gamboa, R.; Shafi, A. PCT WO 2010/009205, 2010.
88. Hager, S. L.; Jividen, V.; Triouleyre, S. P.; Joulak, F. U.S. Patent 6,391,935, 2002.
89. Hager, S. L.; Haider, K. W.; Jividen, V.; Moore, M. N.; Dai, D. G. U.S. Patent Appl. 2007/0299153, 2007.
90. Frericks, A.; Lutter, H.-D.; Stadler, E.; Schroeder, H.-J.; Simon, K.; Meyer, A.; Pomeris, F. U.S. Patent Appl. 2011/0218258, 2011.
91. Casati, F.; Sonney, J.-M.; Wuilay, H. PCT WO 2009/029621, 2009.
92. Casati, F. PCT WO 2009/111215, 2009.
93. Terheiden, A.; Hubel, R. *Scientific Approach to the Question "Why Natural Oil Based Polyols Affect the Physical Properties of Conventional Slabstock Foam"*; Proceedings from the Conference of Polyurethane Industries, Oct 2010, Houston, Texas.
94. Bunting, B.; Vidakovic, M.; Glos, M. *Choosing an Optimal Surfactant to Maximize the Usage Level and Processing Performance of NOPs in HR Molded Foams*; Proceedings from the Conference of Polyurethane Industries, Oct 2010, Houston, Texas.
95. Erdem, B.; Bhattacharjee, D.; Argyropoulos, J. N. U.S. Patent Appl. 2008/0096995, 2008.
96. Koonce, W.; Latham, D.; Jenkines, R.; Bhattacharjee, D.; Lysenko, Z.; Chen, H.; Sonnenschein, M.; Schiller, K.; Leibig, C.; Schrock, A. PCT WO 2009/009571, 2009.
97. Casati, F. M.; Munshi, I. U.S. Patent Appl. 2011/0086215, 2011.
98. Rowlands J. P.; Paap, F. PCT WO 2010/100421, 2010.

Downloaded by OHIO STATE UNIV LIBRARIES on August 28, 2012 | http://pubs.acs.org
Publication Date (Web): August 16, 2012 | doi: 10.1021/bk-2012-1105.ch011

Downloaded by STANFORD UNIV GREEN LIBR on August 28, 2012 | http://pubs.acs.org
Publication Date (Web): August 16, 2012 | doi: 10.1021/bk-2012-1105.ch012

Chapter 12

Carbohydrate Hydrogenolysis

Patrick B. Smith*

**Michigan Molecular Institute, 1910 West St. Andrews Road,
Midland, MI 48640**
***E-mail: smith@mmi.org**

Hydrogenolysis is defined as a reaction in which a carbon-carbon or carbon-heteroatom bond is cleaved by the addition of hydrogen. It has been most widely practiced in the refining industry for hydrodesulfurization of petroleum feedstocks. The hydrogenolysis of carbohydrate feedstocks has also been widely explored, its history dating back to the 1930s. Today it is seeing renewed interest for the conversion of glycerol and carbohydrate feedstocks into commercially valuable polyols such as propylene glycol, ethylene glycol and glycerol. This chapter provides a review of the research on carbohydrate (excluding glycerol) hydrogenolysis. Supported heterogeneous transition metal catalysts have been most commonly and successfully used for carbohydrate hydrogenolysis together with base promoters. Most often sugar alcohols were hydrogenolyzed rather than the corresponding saccharides.

Introduction

A transition in the chemicals and fuels industries is taking place from petroleum-derived products to those derived from biological sources (*1*). This transition will, most certainly, be cautious and deliberate because fossil feedstocks will continue to be abundant into the foreseeable future. However, their price will also most certainly continue to rise due to at least two factors; the rising global demand for oil and a shift away from the cheaper oil to more expensive sources such as that from secondary and tertiary oil recovery, tar sands and oil shale. Regulatory pressures relative to CO2 emissions may also contribute to price volatility as may the fact that a greater proportion of the conventional oil is owned by OPEC nations (*2*), many of which are politically unstable.

In Biobased Monomers, Polymers, and Materials; Smith, P., et al.;
ACS Symposium Series; American Chemical Society: Washington, DC, 2012.

Downloaded by STANFORD UNIV GREEN LIBR on August 28, 2012 | http://pubs.acs.org
Publication Date (Web): August 16, 2012 | doi: 10.1021/bk-2012-1105.ch012

The commercialization of biobased commodities will have to be done wisely, evaluating their advantages and disadvantages relative to the competitive fossil feedstock infrastructure. Certainly, the historical cost disadvantage is eroding due to the large increases in the price and price volatility of oil. Other disadvantages of biobased feedstocks relative to fossil feedstocks include the fact that refining and chemical processing infrastructure is in place, highly integrated in terms of feedstocks, byproducts and energy, and depreciated such that new processes are enormously disadvantaged from a capital cost perspective. As an aside, life cycle assessments often compare new biobased processes to mature petrochemical processes with their highly integrated infrastructure, putting the biobased process at another disadvantage.

Biobased feedstocks are most often composed of carbon, hydrogen and oxygen. Therefore, it is usually still not economically competitive to produce hydrocarbons from them (except in certain geographies like Brazil where there is both a competitive cost advantage for ethanol fermentation, combined with a need to increase polyethylene capacity in the region). This feedstock composition disadvantage is turned into an advantage if one is interested in making oxygenated products such as ethanol, ethylene and propylene glycol, lactic acid, acrylic acid, succinic acid, etc., from carbohydrate feedstocks. Many of these compounds have already found commercial success.

One of the most prominent methods for converting carbohydrates to useful chemicals is fermentation. Lactic acid, lysine and 1,3-propanediol are good examples of commercially successful commodity carbohydrate fermentation products (*3*). Thermochemical process such as pyrolysis and gasification are becoming quite successful for converting a wide range of biomass feedstocks into products like pyrolysis oil and syngas (*1*). Companies such as Enerkem, Woodland Biofuels and Range Fuels catalytically upgrade the syngas to fuels. Others such as Ineos Bio and Coskata use the syngas as a fermentation substrate for conversion to ethanol. Companies such as Virent, Ensyn and Anellotech have announced the production of p-xylene from biomass using a thermochemical process. p-Xylene is one of the key feedstocks in the petrochemical process for production of terephthalic acid.

Carbohydrate feedstocks have been successfully converted to value-added chemicals by chemical catalysis, one notable catalytic process being hydrogenolysis. Hydrogenolysis has found considerable application for the chemical conversion of glycerol, sugars and sugar alcohols to chemical products such as ethylene and propylene glycol (*4*). Hydrogenolysis is defined as a reaction by which a carbon-carbon or carbon-heteroatom bond is cleaved by the addition of hydrogen and has been commonplace in the petroleum industry for hydrodesulfurization, or the removal of sulfur, from fossil feedstocks (*5*). Hydrogenolysis has also been extensively explored for the conversion of carbohydrate feedstocks to, for example, 1,2-propylene glycol which was described as early as 1933 (*6*) but never commercialized due to the much cheaper chlorohydrin process from propylene (*7*). However, with advances in catalytic processes and the cost competitiveness of carbohydrate feedstocks relative to petroleum-based feedstocks, hydrogenolysis of carbohydrate feedstocks has become commercially interesting again (*8*). This chapter provides a review

Downloaded by STANFORD UNIV GREEN LIBR on August 28, 2012 | http://pubs.acs.org
Publication Date (Web): August 16, 2012 | doi: 10.1021/bk-2012-1105.ch012

the carbohydrate hydrogenolysis literature excluding glycerol. The glycerol hydrogenolysis literature is extensive with several companies announcing processes to convert glycerol to propylene glycol (PG) (*8*). Selectivities to PG of over 90 mole% have been achieved at conversions of over 90% (*9*). Since the glycerol hydrogenolysis literature has been thoroughly reviewed elsewhere (*10*), no attempt is made here to provide a thorough review of this literature.

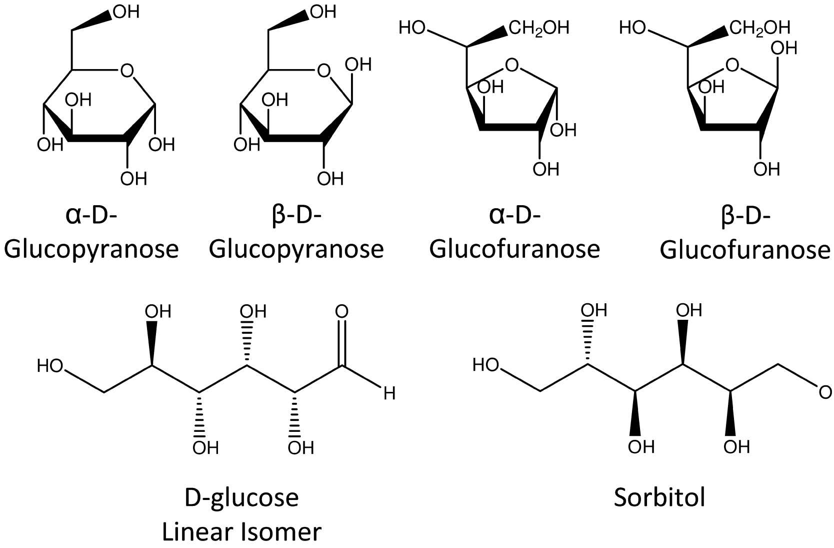

Figure 1. Isomeric structures of sucrose; anomeric pyranoses and furanoses, the linear glucose isomer and sorbitol, the sugar alcohol.

Hydrogenolysis Reaction Mechanism

Recent developments in the commercialization of hydrogenolysis processes for carbohydrate feedstocks have primarily targeted glycerol and sugar alcohols, especially sorbitol. Historically, the yields from direct hydrogenolysis of sugars were not as high as those from sugar alcohols due to the fact that sugars exist as several equilibrium isomeric structures in solution as shown in Figure 1 for glucose. Hydrogenation of sugars to sugar alcohols converts these isomeric forms into one linear sugar alcohol isomer, in this case, sorbitol. However, the first step in the hydrogenolysis mechanism proposed by Sun and Liu is the dehydrogenation of the sugar alcohol back to the carbonyl intermediate followed by a base-catalyzed retro-aldol bond cleavage as shown in Figure 2 for xylitol (*11*). The products of the retro-aldol condensation for xylose, glycolaldehyde and glyceraldehyde, when hydrogenated yield ethylene glycol and glycerol. These steps are reversible, especially with glycerol which can be converted to propylene glycol and lactic acid through a pyruvaldehyde intermediate. These products often become more prominent at higher xylitol conversions. Zhao et al. also noted that the reversibility

Downloaded by STANFORD UNIV GREEN LIBR on August 28, 2012 | http://pubs.acs.org
Publication Date (Web): August 16, 2012 | doi: 10.1021/bk-2012-1105.ch012

of the retro-aldol condensation under basic conditions often leads to scrambling of the products and that increasing the base concentration accelerated the scrambling (*35*). They suggested the use of calcium hydroxide instead of sodium hydroxide as a basic promoter to provide enough base to promote the reaction but at the same time moderating the pH extremes by its limited solubility. The fact that lactic acid is produced as an unwanted byproduct, adds a further complication to the chemistry in that it neutralizes the basic promoter, quenching the hydrogenolysis reaction.

Controlling the selectivities to the products of interest while maintaining good substrate conversion and conversion rates has been the focus of research over the last several decades. Pentose sugar alcohols, such as xylitol, can be cleaved by hydrogenolysis at the bond between carbons 1 and 2, yielding C1 structures such as CO or formic acid and a C4 sugar alcohol, or at carbons 2 and 3 yielding EG, glycerol, PG or lactic acid as shown in Figure 2. Hexose sugar alcohols, such as sorbitol, have still more cleavage points leading to even more potential product scrambling. Therefore, specificity to a given product is even more tenuous. The recovery of the high value products from a complex reaction mixture is expensive as is an inefficient process that generates a significant level of waste. This is the primary reason that glycerol hydrogenolysis, rather than that of higher carbohydrates, was the first process to be commercialized.

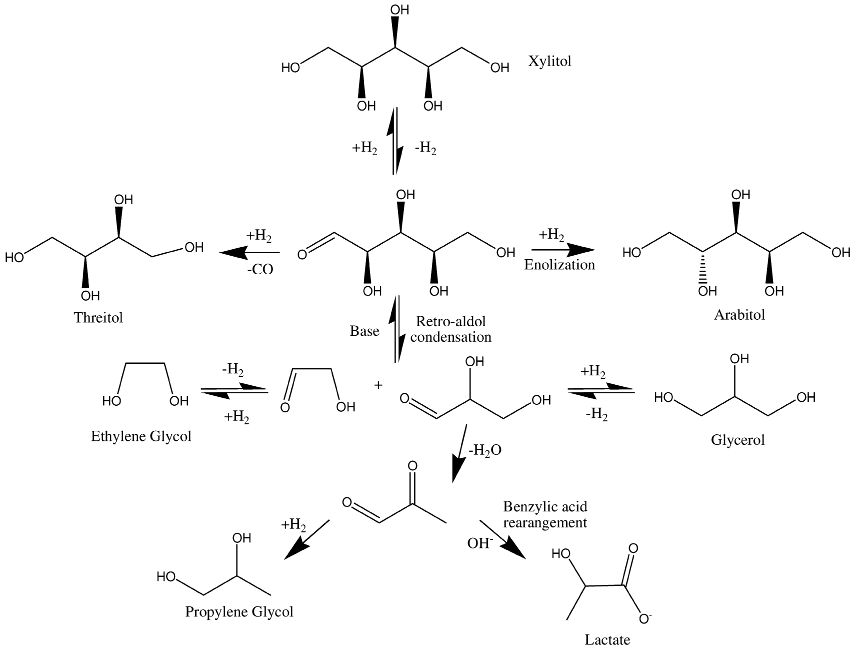

Figure 2. The proposed mechanism for the xylitol hydrogenolysis.

The maximum theoretical selectivity for a hydrogenolysis reaction depends on which substrate and products are considered. For example two moles of glycerol can be produced from one mole of sorbitol for a 200 mole% selectivity which corresponds to a 101 weight% selectivity. Two moles of PG can be produced from one mole of sorbitol, giving a 200 mole% selectivity corresponding to 83.5 weight% selectivity. If EG is one of the products, 1 mole of sorbitol can produce 1 mole of EG and 1 mole PG which corresponds to 34.1 and 41.8 weight% EG and PG, respectively. For EG and glycerol as products, 100 mole% selectivity for each product corresponds to 34.1 and 50.5 weight% selectivity. If the sorbitol is converted completely to EG, the molar selectivity is 300% corresponding to a 102.2 weight% selectivity. These values are summarized in Table 1 for both sorbitol and xylitol.

Downloaded by STANFORD UNIV GREEN LIBR on August 28, 2012 | http://pubs.acs.org
Publication Date (Web): August 16, 2012 | doi: 10.1021/bk-2012-1105.ch012

Table 1. The Maximum Theoretical Selectivities for Sorbitol and Xylitol Given in Mole% and Weight%

Reactant	*Products*	*Maximum Theoretical Mole% Selectivity*	*Maximum Theoretical Weight% Selectivity*
Sorbitol	Glycerol	200	101
Sorbitol	PG	200	83.5
Sorbitol	EG, PG	100, 100	34.1, 41.8
Sorbitol	EG	300	102.2
Xylitol	EG, Glycerol	100, 100	40.8, 60.5
Xylitol	EG, PG	100, 100	40.8, 50.0
Xylitol	EG	200	81.6

The following discussion reviews the carbohydrate hydrogenolysis literature in a chronological fashion with focus on the catalyst and conditions used in the reaction and the resulting conversions and selectivities. One disclaimer for the data presented is that it is not always clear in the patent literature whether the values for the conversions and selectivities are expressed in weight or mole%. An attempt was made within this review to consistently express these values in weight% for comparison purposes.

Downloaded by STANFORD UNIV GREEN LIBR on August 28, 2012 | http://pubs.acs.org
Publication Date (Web): August 16, 2012 | doi: 10.1021/bk-2012-1105.ch012

Table 2. Catalysts, Conditions, and Selectivities for the Conversion of C5 and C6 Sugars to PG, EG, and Glycerol

Catalyst, solvent	*Temp°C/ ATM H_2*	*Sub-strate*	*PG/EG/ Glycerol Selectivity (wt.%)*	*Conver-sion*	*Reference*
copper-chromium oxide, ethanol	250/ 300	Sugars, sugar alcohols	Primarily PG	>90	Zartman (*6*)
copper-aluminum oxide, methanol	240/ 102	sucrose, dextrose	40% PG	>90	Lenth (*12*)
nickel on kieselguhr/ 0.4% calcium hydroxide, water	Varied T and P	sorbitol, xylitol	17/16/40	>90	Clark (*13*)
copper-magnesium chromite	250/ 200	Sucrose	62/ - /0	>90	Boul-houwer (*14*)
copper-beryllium chromite, methanol	235/ 155	Sucrose	6/ - /61		
nickel on kieselguhr, $Ca(OH)_2$, pH = 12, water	230/ 130	Sucrose	21/15/32	99%	Tamins (*15*)
nickel-tungsten oxide on kieselguhr, water	220/ 136	Sugars	33% glycerol	>90	Wright (*16*)
$CuO\text{-}Ce\text{-}O_2\text{-}SiO_2$, 4% $Ca(OH)_2$, CH_3OH/H_2O	225/ 200	Sucrose	18/16/31	84%	Van Ling (*17*)
60% nickel on kieselguhr, 1% $Ca(OH)_2$, water	230/ 120	Sorbitol	Primarily glycerol	30 to 70%	Chao (*18*)
	260/ 120		Primarily EG and PG		
nickel on kieselguhr, 1% $Ca(OH)_2$, water	230/ 13.6-81.6	Sorbitol	70% glycerol	35%	Sirkar (*19*)
Ni on silica/alumina, 5/1 xylitol/$NaOCH_3$ molar, CH_3OH	240/ 272	Xylitol	30/46/14	99%	Tanikella (*21*)
sulfide-modified ruthenium on carbon, 2% CaO, water	250/ 163	Sor-bitol, xylitol	54/27/3	89%	Dubeck (*22*)
ruthenium on titanited alumina, 4% $Ba(OH)_2$, water	180/ 218	Sorbitol	18/3/21	58%	Arena (*23*)
$H_2Ru(PPh_3)_4$, 4.7mM KOH, NMP	100/ 204	Fruc-tose	1/8/36	92	Andrews (*25*)

Continued on next page.

Downloaded by STANFORD UNIV GREEN LIBR on August 28, 2012 | http://pubs.acs.org
Publication Date (Web): August 16, 2012 | doi: 10.1021/bk-2012-1105.ch012

Table 2. (Continued). Catalysts, Conditions, and Selectivities for the Conversion of C5 and C6 Sugars to PG, EG, and Glycerol

Catalyst, solvent	*Temp°C/ ATM H_2*	*Substrate*	*PG/EG/ Glycerol Selectivity (wt.%)*	*Conversion*	*Reference*
phosphated Co/Cu/Mn, 0.4% MgO/K_2O, water	260/ 296	Sucrose	23/11/18	>90	Shuster (*26*)
ruthenium/palladium/ copper mixed metal catalyst on carbon, 6/1 Sorbitol/NaOH (molar)	235/ 148	Sorbitol	44/20/6	100	Gubitosa (*27*)
Ruthenium/activated carbon	200/ 49.3	Hydrolyzed starch	Primarily methanol	>90%	Abreu (*29*)
ruthenium on carbon, 1% KOH, water	231/82	Sorbitol, xylitol	45/39/13	45%	Chopade (*30*)
rhenium-nickel on carbon (and other bimetallic catalysts), 1% KOH, water	200/ 122	Xylitol	30/35/10	85%	Werpy (*31*)
ruthenium/organic phosphine (no promoter), water	200-250/ 54-68	Glucose, NMP/ water	47/23/0.5	>90%	Crabtree (*33*)
Ruthenium on carbon nanofiber, 0.6% CaO, water	220/79	Sorbitol	32/21/16	36%	Zhou (*34*)
Ruthenium on Carbon, 0.8% $Ca(OH)_2$, water	200/ 39.5	Xylitol	21/33/10	25%	Sun (*11*)
Ni (6%), Pt (1%) on Na-Y, no promoter, water	220/59	Sorbitol	72/10/7	59%	Banu (*36*)
tungsten carbide on mesoporous carbon, water	245/59	Microcrystalline cellulose	5/73/ -	100%	Zhang (*41*)
nickel/tungsten carbide on activated carbon, NH_3, water	245/59	Pretreated corn stalks	14/18/ -	96	Pang (*42*)

In Biobased Monomers, Polymers, and Materials; Smith, P., et al.;
ACS Symposium Series; American Chemical Society: Washington, DC, 2012.

Downloaded by STANFORD UNIV GREEN LIBR on August 28, 2012 | http://pubs.acs.org
Publication Date (Web): August 16, 2012 | doi: 10.1021/bk-2012-1105.ch012

Chronological Review

Pre-1970

The carbohydrate hydrogenolysis literature dates back to the 1930s where common hexose sugars (mono and disaccharides) and sugar alcohols were hydrogenolyzed over a copper-chromium oxide catalyst at 250°C and 300 atmospheres of hydrogen by Zartman and Adkins (*6*). Although the activity of this catalyst was not very high, the primary product of the reaction was propylene glycol (PG) with several other compounds also identified. The attributes of the hydrogenolysis catalysts, conditions and selectivities are summarized in Table 2.

Lenth and DuPuis hydrogenolyzed sucrose and dextrose over copper-aluminum oxide at 240°C and 1500 psi H_2 with a selectivity of 40% to PG and remainder being glycerol and other polyols at high conversions (*12*). Clark recognized that sugar alcohols required lower temperatures and gave better selectivity when hydrogenolyzed to polyols than the corresponding saccharides (*13*). Sorbitol and xylitol were hydrogenolyzed using nickel on kieselguhr with a calcium hydroxide promoter to study hydrogenolysis selectivities as a function of temperature, reaction time and H_2 pressure. The main hydrogenolysis products were glycerol, PG and ethylene glycol (EG) but the yields and selectivities were low.

Boelhouwer et al. hydrogenolyzed sucrose in methanol over several different types of supported catalysts; nickel, nickel-thorium oxide, copper-magnesium chromite and copper-beryllium chromite catalysts (*14*). The authors obtained 62% selectivity to PG and no glycerol with the copper-magnesium chromite catalyst, and 61% selectivity to glycerol with 6% PG with the copper-beryllium chromite catalyst. Tamins, Ems and Haldenstein used nickel on kieselguhr at 180 to 200°C and 60 to 180 atm. H_2 pressure with the pH controlled to about 12 with calcium hydroxide to hydrogenolyze cane sugar and sorbitol/mannitol (*15*). Conversions of nearly 99% were obtained but the selectivity to any given product was low. The primary products were glycerol (32%), PG (21%) and EG (15%).

1970s

Sugars were hydrogenolyzed by Wright using nickel-tungsten oxide supported on kieselguhr. The primary hydrogenolysis product was glycerol with highest yields being about 33% (*16*). Sucrose was hydrogenolyzed using a CSTR process over a CuO-CeO_2 catalyst on silica by Van Ling et al. who achieved similar selectivities to glycerol (*17*).

1980s

Sorbitol was hydrogenolyzed by Chao and Huibers using 60% nickel on kieselguhr with a calcium hydroxide promoter as a function of temperature, pressure and liquid hourly space velocity (*18*). The selectivity to glycerol, PG and EG was strongly dependent on temperature, 230°C giving roughly 36% selectivity to glycerol with little PG and EG and 260°C favoring PG and EG conversion.

Sirkar hydrogenolyzed sugar alcohols using a kieselguhr supported nickel catalyst and a calcium hydroxide promoter (*19*). Glycerol yields as high as 70% were obtained with sorbitol at 230°C and 200 to 1200 psi H_2. In another study, the same author used a two stage process to hydrogenolyze sugar feedstocks. The sugar was hydrogenated to the sugar alcohol in the first stage which was subsequently hydrogenolyzed in the second stage using a silica-alumina supported nickel catalyst (*20*). Glycerol yields were given only in approximate terms. Tanikella used a supported nickel catalyst on silica/alumina in the presence of strong base to hydrogenolyze sugar alcohols, the best yield being obtained for xylitol (*21*). The products were 46% EG, 30% PG, 14% glycerol with 10% "others". The xylitol conversion exceeded 95%.

Dubeck and Knapp hydrogenolized sorbitol and xylitol using a sulfide-modified ruthenium on carbon catalyst with a base promoter (*22*). They obtained greater than 89% sorbitol conversion with 84% selectivity to EG (27%), PG (54%) and glycerol (3%). Arena hydrogenolyzed sugar alcohols to EG, PG and glycerol with poor selectivity using a ruthenium on titanited alumina catalyst and barium oxide as promoter (*23*). Sohounloue et al. hydrogenolyzed sorbitol with a Ru on silica catalyst and with a Raney nickel catalyst using a $Ca(OH)_2$ promoter, attempting to find conditions where selectivity to one of the products, EG, PG and glycerol, was strongly favored (*24*). They concluded that "good selectivity is not achievable in a basic medium" for these products.

1990s

A homogeneous ruthenium-based catalyst, $H_2Ru(PPh_3)_4$, was used for the hydrogenolysis of fructose yielding conversions as high as 92% but with very poor selectivities (*25*). Shuster used a phosphated cobalt, copper, manganese, molybdenum catalyst to hydrogenolyze sugars (*26*). The selectivity to PG was 23% and to EG, 11%. Sorbitol hydrogenolysis was carried out using a ruthenium, palladium, copper mixed metal catalyst on carbon in the presence of sodium hydroxide by Gubitosa and Casale (*27*). Their best selectivity was 44% for PG, 20% EG and 6% glycerol. Hawley et al. investigated the mechanism of hydrogenolysis using 1,3-diol model compounds (*28*). They concluded that the mechanism for bond cleavage was by retro-aldol condensation followed by dehydration of the hydroxyl β to the carbonyl (see Figure 2). This is the preferred mechanism today. Acid depolymerized (5 weight% aqueous H_2SO_4) corn starch was used as a substrate for hydrogenolysis by Abreu et al. (*29*). These authors studied the relative rates of C-C and C-O bond splitting using a ruthenium on carbon catalyst, apparently at acidic pH. Methanol was the primary product, leading them to conclude that C-C bonds were preferentially hydrogenolyzed over C-O bonds with this catalyst.

2000 to Present

Chopade et al. hydrogenolyzed sugar alcohols such as sorbitol and xylitol using a ruthenium on carbon catalyst with a potassium hydroxide promoter (*30*). There was a tradeoff between xylitol conversion and selectivity but in one case a

In Biobased Monomers, Polymers, and Materials; Smith, P., et al.;
ACS Symposium Series; American Chemical Society: Washington, DC, 2012.

Downloaded by STANFORD UNIV GREEN LIBR on August 28, 2012 | http://pubs.acs.org
Publication Date (Web): August 16, 2012 | doi: 10.1021/bk-2012-1105.ch012

Downloaded by STANFORD UNIV GREEN LIBR on August 28, 2012 | http://pubs.acs.org
Publication Date (Web): August 16, 2012 | doi: 10.1021/bk-2012-1105.ch012

xylitol conversion of 45% was obtained with molar selectivities to PG of 71%, EG 75% and glycerol of 17%. These correspond to 36% PG, 31% EG and 10% glycerol on a weight basis. At a sorbitol conversion of 63%, the molar selectivity to PG was 76%, EG, 52% and glycerol, 51% (32%, 18%, 26% on a weight basis). Still better selectivities were obtained at lower conversions. This same team investigated supported rhenium multimetallic catalysts to hydrogenolyze glycerol, xylitol and sorbitol (*31*). Rhenium-nickel, rhenium-ruthenium, rhenium-palladium and rhenium-rhodium bimetallic catalysts were evaluated. The rhenium-nickel on carbon provided the conversion/selectivity for glycerol with, for example, a conversion of 53% and selectivities for PG of 79%, EG of 11% and lactate of 10%. These catalysts also effectively hydrogenolyzed sugar alcohols giving at 85% conversion, 30% selectivity for PG, 10% for glycerol and 35% for EG from xylitol. Catalysts were found (Ru-Re/C) that effectively hydrogenated lactic acid to stereo-regular PG with, for example, a selectivity of 96.3% at 95.8% conversion. This same group used a carbon-supported nickel-rhenium catalyst to hydrogenolyze glycerol to PG obtaining 88 mole% selectivity to PG at 61% glycerol conversion (*32*). Lactic acid was also reduced to PG with greater than 95% selectivity and conversion.

Crabtree and Tylers hydrogenolyzed sugar alcohols and sugars using ruthenium/organic phosphine catalysts (*33*). The unusual thing about this catalyst was that base was not required to enhance its selectivity but higher temperatures (200 to 250°C) and H_2 pressures (800 to 1000 psig) were used instead. When sugars were used as substrates, they were first converted to sugar alcohols at lower temperatures (150 to 200°C) in a pre-reduction step and then the temperature and pressure were raised for subsequent hydrogenolysis. Solvents such as NMP or THF were also used. Glucose, NMP/water and catalyst with a pre-reduction temperature of 200°C and a hydrogenolysis temperature of 260°C attained a selectivity of 47% PG, 23% EG and 0.5% glycerol.

Zhou et al. used ruthenium supported on mesoporous carbon nanofibers with a CaO promoter to hydrogenolyze sorbitol (79 atm. H_2 pressure and 220°C) at yields of 32% PG, 21% EG and 16% glycerol at 36% sorbitol conversion (*34*, *35*). Sun and Liu carried out the hydrogenolysis of biomass-derived xylitol evaluating several different catalysts and solid supports as a function of temperature and pressure while keeping the partical size of the catalysts constant (*11*). They evaluated activated carbon and several metal oxide solid supports as well as metals such as Ru, Rh, Pd and Pt and promoters such as calcium and magnesium hydroxide and calcium carbonate. Pt was found to be most active metal but the best combination of selectivity and activity occurred with Ru/C.

Banu et al. hydrogenolyzed sorbitol using a Ni (6%) - Pt (1%) catalyst on Na-Y zeolite with a $Ca(OH)_2$ promoter (*36*). They obtained good selectivity to PG (72%) at low sorbitol conversion.

Sorbitol was hydrogenolyzed to a mixture of C_4 to C_6 polyols for alkyd resins by Blanc et al. (*37*). They used CuO-ZnO catalysts and achieved greater than 73% selectivity to C_4 and greater polyols. Cellulose was hydrolyzed to sugars followed by hydrogenolysis in one process by combining noble metal catalysts (Pt, Pb, Ru) with mineral acids (sulfuric and phosphoric acid) by Palkovits et al. (*38*). Glucose and sorbitol yields from cellulose as high as 64% were achieved but very little hydrogenolysis was observed. The primary products were glucose and sorbitol. Zhang et al. used a nickel phosphide catalyst on activated carbon support to convert microcrystalline cellulose (Merck) to primarily sorbitol, 48%, but small amounts of PG, 2% and EG, 8%, were also produced (*39*). This same group hydrogenolyzed microcrystalline cellulose directly to polyols, primarily EG, using a supported metal carbide catalyst (*40*). Several metal carbides were evaluated but the best selectivity to EG, 61% based on cellulose, was obtained using a Ni promoted tungsten carbide catalyst on an activated carbon. Small amounts of PG, 7.6%, were also obtained with this catalyst. In another study, this group achieved 73% selectivity to EG with a tungsten carbide catalyst on mesoporous carbon (*41*). This catalysts was much less prone to deactivation than the earlier catalysts.

Corn stalks, after one of various pretreatment steps, were directly hydrogenolyzed to primarily EG and PG using a nickel-promoted tungsten carbide catalyst by Pang et al. (*42*). Their best selectivities to EG (55 wt%) and PG (8%) came from microcrystalline cellulose purchased from Merck. They were only able to achieve 18 wt% selectivity for EG and 14% for PG from pretreated corn stalks at 96% conversion.

In conclusion, the catalysts which were found to have the greatest selectivities were supported ruthenium catalysts with a base promoter. The best performance was achieved by Chopade et al. who hydrogenolized sorbitol using a ruthenium on carbon catalyst with potassium hydroxide promoter (*30*). They obtained greater than 45% xylitol conversion with about 97 wt% selectivity to EG (39%), PG (45%) and glycerol (13%). The best performance for xylitol conversion was obtained using a nickel on silica/alumina with strong base promoter by Sirkar, who obtained 35% PG, 40%EG and 4% glycerol (*19*). The distribution of products from either substrate was shown to be a function of catalyst and conditions.

Most of the carbohydrate hydrogenolysis investigations were performed in aqueous media although some used such solvents as methanol, ethanol, THF and NMP (see Table 2 for the reaction conditions, including solvents, which were used in the investigations). Undoubtedly the choice of solvent has an effect the selectivity of the catalyst. A thorough, systematic investigation of the effect of solvent on the hydrogenolysis products seems to be an area worthy of further investigation.

This review would not be complete without mentioning the separation difficulties associated with the purification of EG, PG and glycerol. Each have high boiling points, that for EG being 197°C, PG being 188°C and glycerol, 290°C. Their separation by distillation is difficult due to the high boiling points and the fact that the boiling points of EG and PG are separated by less than 10°C. Polyols are prone to stability problems at these temperatures if the pH varies much from neutral and in the presence of oxygen. One separation process developed by Chopade et al. to circumvent this high temperature distillation utilizes an acetal-derivatization process (*43*, *44*). The glycols are converted to the corresponding lower boiling cyclic acetals using an aldehyde or ketone such as formaldehyde, acetaldehyde or acetone and then purified by distillation. Subsequent to distillation, the acetals are acid hydrolyzed back to the polyols and aldehyde or ketone, which is recycled.

Downloaded by STANFORD UNIV GREEN LIBR on August 28, 2012 | http://pubs.acs.org
Publication Date (Web): August 16, 2012 | doi: 10.1021/bk-2012-1105.ch012

Summary

Considerable research has been performed on the conversion of carbohydrate feedstocks to polyols. One major component of this research, the conversion of glycerol to PG, was not covered in this manuscript. The hydrogenolysis of 5 and 6 carbon sugars is much less selective than that for glycerol due to the multiplicity of isomers present and the statistically higher number of carbon-carbon bond cleavage possibilities. The multiplicity of isomeric forms can be eliminated by hydrogenating sugars to sugar alcohols. Sugar alcohols are most often used for hydrogenolysis for this reason, even though the first step in the hydrogenolysis of sugar alcohols is apparently the dehydrogenation back to the linear carbonyl form. Many combinations of hydrogenolysis conditions, including catalysts and solvents, have been investigated. Optimal catalysts need to possess high selectivities and rates as well as being robust to fouling, i.e., resistant to coking, poisoning, sintering and metal leaching, thereby maintaining their activity for long periods of time and in a number of different upset conditions. The catalysts which have had greatest selectivities were supported ruthenium catalysts with a base promoter. The best performance was achieved by Chopade et al. who hydrogenolized sorbitol using a ruthenium on carbon catalyst with potassium hydroxide promoter (*30*). This group obtained greater than 45% xylitol conversion with about 97wt% selectivity to EG (39%), PG (45%) and glycerol (13%). The best performance for xylitol conversion was obtained using a nickel on silica/alumina with strong base promoter by Sirkar, who obtained 35% PG, 40% EG and 4% glycerol (*19*). The distribution of products from either substrate was shown to be a function of catalyst and conditions.

Downloaded by STANFORD UNIV GREEN LIBR on August 28, 2012 | http://pubs.acs.org
Publication Date (Web): August 16, 2012 | doi: 10.1021/bk-2012-1105.ch012

References

1. *ACS Symposium Series 1063*; Payne, G. F., Smith, P. B., Eds.; American Chemical Society: Washington, DC, 2011; Chapter 1.
2. Nashawi, I. S.; et al. *Energy Fuels* **2010**, *24*, 1788–1800.
3. Bozell, J. J.; Petersen, G. R. *Green Chem.* **2010**, *12*, 539–554.
4. (a) Zhou, C.-H.; Beltramini, J. N.; Fan, Y.-X.; Lu, G. Q. *Chem. Soc. Rev.* **2008**, *37,* 527−549. (b) Zheng, T.; Chen, X.; Shen, Y. *Chem. Rev.* **2008**, *108*, 5253−5277. (c) Choi, W. J. *Recent Patents Biotechnol.* **2008**, *2*, 173−180. (d) Nakagawa, Y.; Tomishige, K. *Catal. Sci. Technol.* **2011**, *1*, 179−190.
5. Topsøe, H.; Clausen, B. S.; Massoth, F. E. *Hydrotreating Catalysis–Science and Technology*; Anderson, J. R, Boudart, M., Eds.; Springer Verlag: Berlin, 1996; Vol. 11.
6. Zartman, W. H.; Adkins, H. *J. Am. Chem. Soc.* **1933**, *55*, 4559–4563.
7. SRI Report 2. *Propylene Oxide*; SRI Consulting, 2003.
8. Smith, P. B. Revitalizing Chemurgy: Chemicals from Agricultural Resources. In *Renewable and Sustainable Polymers*; Payne, G. F., Smith, P. B., Eds.; ACS Symposium Series 1063; American Chemical Society: Washington, DC, 2011; Chapter 6.
9. Bloom, P. U.S. Patent 7,928,148 B2, 2011.

10. (a) Zhou, C.-H.; Beltramini, J. N.; Fan, Y.-X.; Lu, G. Q. *Chem. Soc. Rev.* **2008**, *37*, 527−549. (b) Zheng, Y.; Chen, X.; Shen, Y. *Chem. Rev.* 2008, *108*, 5253−5277. (c) Behr, A.; Eilting, J.; Irawadi, K.; Leschinski, J.; Lindner, F. *Green Chem.* **2008**, *10*, 13−30. (d) Kenar, J. A. *Lipid Technol.* **2007**, *19*, 249−253
11. Sun, J.; Liu, H. *Green Chem.* **2011**, *13*, 135–142.
12. Lenth, C. W.; DuPuis, R. N. *Ind. Eng. Chem.* **1945**, *37*, 152–157.
13. Clark, I. T. *Ind. Eng. Chem.* **1958**, *50*, 1125–1126.
14. Boulhouwer, C.; Korf, D.; Waterman, H. I. *J. Appl. Chem.* **1960**, *10*, 292–296.
15. Tamins, F. C.; Ems, G. B.; Haldenstein, J. G. U.S. Patent 3,030,429, 1962.
16. Wright, L. W. U.S. Patent 3,691,100, 1972.
17. (a) Van Ling, G.; Driessen, A. J.; Piet, A. C.; Vlugter, J. C. *Ind. Eng. Chem. Prod. Res. Develop.* **1970**, *9*, 210−212. (b) Van Ling, G.; Ruijterman, C.; Vlugter, J. C. *Carbohyd. Res.* **1967**, *4*, 380−386. (c) Van Ling, G.; Vlugter, J. C. *J. Appl. Chem.* **1969**, *19*, 43.
18. Chao, J. C.; Huibers, D. T. A. U.S. Patent 4,366,332, 1982.
19. Sirkar, A. K. U.S. Patent 4,338,472, 1982.
20. Sirkar, A. K. US Patent 4,380,678, 1983.
21. Tanikella, M. S. S. R. U.S. Patent 4,404,411, 1983.
22. (a) Dubeck, M.; Knapp, G. G. U.S. Patent 4,476,331, 1984. (b) Dubeck, M.; Knapp, G. G. U.S. Patent 4,430,253, 1984.
23. (a) Arena, B. J. U.S. Patent 4,496,780, 1985. (b) Arena, B. J. U.S. Patent 4,401,823, 1983.
24. Sohounloue, D. K.; Montassier, C.; Barbier, J. *React. Kinet. Catal. Lett.* **1983**, *22*, 391–397.
25. (a) Andrews, M. A.; Klaeren, S. A. U.S. Patent 5,026,927, 1991. (b) Andrews, M. A.; Klaeren, S. A. *J. Am. Chem. Soc.* **1989**, *111*, 4131−4133.
26. Shuster, L. U.S. Patent 5,107,018, 1992.
27. (a) Gubitosa, G.; Casale, B. U.S. Patent 5,326,912, 1994. (b) Gubitosa, G.; Casale, B. U.S. Patent 5,543,379, 1996. (c) Gubitosa, G.; Casale, B. U.S. Patent 5,354,914, 1994. (d) Gubitosa, G.; Casale, B. U.S. Patent 5,600,028, 1997. (e) Gubitosa, G.; Casale, B. U.S. Patent 5,600,028, 1997, (f) Casale, B.; Gomez, A. M. U.S. Patent 5,214,219, 1993.
28. Wang, K.; Hawley, M. C.; Furney, T. D. *Ind. Eng. Chem. Res.* **1996**, *34*, 3766–3770.
29. Abreu, C. A. M.; Lima, N. M.; Zoulalian, A. *Biomass Bioenrgy* **1995**, *9*, 487–492.
30. Chopade, S. P.; Miller, D. J.; Jackson, J. J.; Werpy, T. A.; Frye, J. G.; Zacher, A. H. U.S. Patent 6,291,725, 2001.
31. Werpy, T. A.; Frye, J. G.; Zacher, A. H.; Miller, D. J. U.S. Patent 6,479,713, 2002.
32. (a) Werpy, T. A.; Frye, J. G.; Zacher, A. H.; Miller, D. J. U.S. Patent 6,841,085, 2005. (b) Werpy, T. A.; Frye, J. G.; Zacher, A. H.; Miller, D. J. U.S. Patent 7,038,094, 2006.
33. Crabtree, S. P.; Tylers, V. T. U.S. Patent 2007/0123739 A1.

Downloaded by STANFORD UNIV GREEN LIBR on August 28, 2012 | http://pubs.acs.org
Publication Date (Web): August 16, 2012 | doi: 10.1021/bk-2012-1105.ch012

In Biobased Monomers, Polymers, and Materials; Smith, P., et al.;
ACS Symposium Series; American Chemical Society: Washington, DC, 2012.

34. Zhou, L.; Zhou, J. H.; Sui, Z. J.; Zhou, X. G. *Chem. Eng. Sci.* **2010**, *65*, 30–35.
35. Zhou, J. H.; Zhang, M. G.; Zhou, L.; Li, P.; Zhou, X. G.; Yuan, W. K. *Catal. Today* **2009**, *147S*, S225–S229.
36. Banu, M.; Sivasanker, S.; Sankaranarayanan, T. M.; Venuvanalingam, P. *Catal. Commun.* **2011**, *12*, 673–677.
37. Blanc, B.; Bourrel, A.; Gallezot, P.; Haas, T.; Taylor, P. *Green Chem.* **2000**, *2*, 89–91.
38. Palkovits, R.; Tajvidi, K.; Procelewska, J.; Rinaldi, R.; Ruppert, A. *Green Chem.* **2010**, *12*, 972–978.
39. Ding, L.-N.; Wang, A.-Q.; Zheng, M.-Y.; Zhang, T. *ChemSusChem* **2010**, *3*, 818–821.
40. Ji, N.; Zhang, T.; Zheng, M.; Wang, A.-Q.; Wang, H.; Wang, X.; Chen, J. G. *Angew. Chem. Int. Ed.* **2008**, *47*, 8510–8513.
41. Zhang, Z.-H.; Wang, A.-Q.; Zhang, T. *Chem. Commun.* **2010**, *46*, 862–841.
42. Pang, J.; Zheng, M.-Y.; Wang, A.-Q.; Zhang, T. *Ind. Eng. Chem. Res.* **2011**, *50*, 6601–6608.
43. Chopade, S. P.; Sharma, M. M. *React. Funct. Polym.* **1997**, *34*, 37–45.
44. Miller, D. J.; Jackson, J. E.; Chopade, S. P.; Dhale, A. D.; Clark, A. M.; Kiesling, C. W. U.S. Patent 6,713,640, 2004.

Downloaded by STANFORD UNIV GREEN LIBR on August 28, 2012 | http://pubs.acs.org
Publication Date (Web): August 16, 2012 | doi: 10.1021/bk-2012-1105.ch012

Downloaded by NORTH CAROLINA STATE UNIV on August 28, 2012 | http://pubs.acs.org
Publication Date (Web): August 16, 2012 | doi: 10.1021/bk-2012-1105.ch013

Chapter 13

Biobased Polymers from Plant-Derived Tulipalin A

Seema Agarwal,*[*] Qiao Jin, and Samarendra Maji

Philipps-Universität Marburg, Fachbereich Chemie,
Hans-Meerwein Strasse, D-35032, Marburg, Germany
[*]E-mail: agarwal@staff.uni-marburg.de

A few interesting examples of plant-derived naturally originated vinyl monomers are known. These plant-derived monomers can be easily classified into three categories (olefinic, styrenic and acrylate types) in resemblance to their chemical structures with the corresponding petro-derived monomers. One of these monomers, α-methylene-γ-butyrolactone (MBL) (Tulipalin A) belongs to the class of sesquiterpene lactone family and considered as cyclic analog of most common vinyl monomer methyl methacrylate (MMA). By virtue of its exo-methylene double bond, it can be used as a naturally originated vinyl monomer in order to synthesize biopolymers. Having a natural source origin inculcates biocompatibility, biodegradability, eco-friendly, and renewable characteristics in the resulting polymers. The present chapter highlighted the structure, synthesis, properties, and specialty polymers obtained from this naturally occurring Tulipalin A monomer.

Introduction

Fossil resources like oil and gas as well as bio mass are used for the production of the synthetic polymers which are indispensable in the modern society. In general, fossil or bio-based renewable raw materials undergo chemical modification to make value added products. The choice of raw material (fossil/bio-based) is highly important keeping in-view the rapidly depleting fossil fuels. Although bio-based polymers are not new but in recent times, there is a great awareness for using bio-based or naturally originated monomers for making

In Biobased Monomers, Polymers, and Materials; Smith, P., et al.;
ACS Symposium Series; American Chemical Society: Washington, DC, 2012.

Downloaded by NORTH CAROLINA STATE UNIV on August 28, 2012 | http://pubs.acs.org
Publication Date (Web): August 16, 2012 | doi: 10.1021/bk-2012-1105.ch013

polymers (*1–3*). In fact the use of renewable feed stock is one of the twelve principles of GREEN CHEMISTRY.

There are different types of bio-based polymers in which monomers are either bio-based (derived from renewable resources by modification) or naturally originated from plants etc. These monomers were then polymerized by different techniques like condensation polymerization (*4–9*), ring-opening polymerization (*10*), metathesis polymerization (*11–13*), vinyl polymerization (*14*, *15*) etc. Some of the highly used renewable raw materials in the chemical industry include plant oils, polysaccharides, sugars etc. These renewable resources have been successfully used for the synthesis of a variety of monomers as well as linear and cross-linked polymers of different types e.g. polyolefns, polyesters, polyethers, polyamides, epoxy and polyurethane resins etc (*2*). In contrast, there are some plant-derived vinyl monomers which could be directly polymerized to vinyl polymers. These monomers and their corresponding polymers are also known in the literatures. α-Methylene-γ-butyrolactone (MBL) is one of these plant-derived monomers and is the highlight of this article. The polymerization techniques, different macromolecular architectures and properties of poly α-methylene-γ-butyrolactone (PMBL) are presented in this article. The polymerization capability of MBL with electron donors and without any initiator for the formation of high molecular weight polymers is also emphasized.

Plant-Derived Naturally Originated Vinyl Monomers

Plant-derived naturally originated vinyl monomers can be easily classified into three categories in resemblance to their chemical structures with the corresponding petro-derived monomers (Table 1).

Table 1. Classification of plant-derived vinyl monomers

Type	Chemical Structure	Representative examples of Petro-derived vinyl monomers	Representative examples of Plant-derived vinyl monomers [ref]
Olefinic monomers (including cyclic)	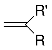	Ethylene, Propylene, 1,3-Butandiene, etc.	α-pinene, β-pinene, Limonene, Myrcene, etc. [16-18]
Styrenic monomers	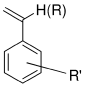	Styrene, α-methyl styrene, etc.	Anethole, Isosafrole, Isoeugenol, Cinnamic acid, etc. [19-21]
(meth)acrylic monomers	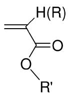	Methyl methacrylate, n-butyl acrylate, etc.	α-methylene-γ-butyrolactone, Itaconic acid, etc. [22-27]

Downloaded by NORTH CAROLINA STATE UNIV on August 28, 2012 | http://pubs.acs.org
Publication Date (Web): August 16, 2012 | doi: 10.1021/bk-2012-1105.ch013

Phenylpropanoids (PPs) (Styrenic type) and terpenoids (Ts) (Olefinic type) are the secondary metabolites in plants and have been used as vinyl monomers for making corresponding polymers for different purposes. Terpenoids are one of the well studied members of this class of monomers. They have isoprene (2-methyl-1,4-butadiene) as carbon skeleton building block (*16*). The terpenes which can be easily isolated in appreciable amounts from turpentine like α-pinene, β- pinene, limonene, and myrcene (Chart 1) have been investigated for polymerization by cationic or radical methods (*17*, *18*).

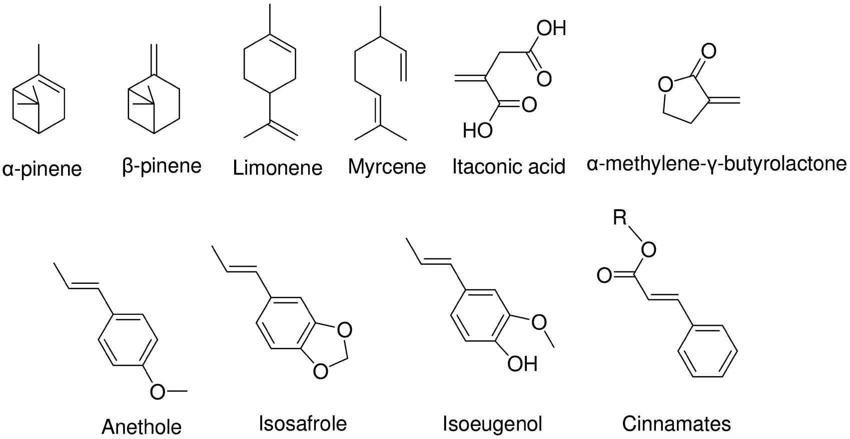

Chart 1. Chemical structures of plant-derived monomers

PPs belong to the largest group of secondary metabolites produced by plants. The plants produce them mainly, in response to biotic or abiotic stresses for example infections, wounding, UV irradiation, exposure to ozone, pollutants etc. Cationic polymerizations of some of these PPs like isosafrole (1,2-methylene-dioxy)-4-propenyl benzene) (*19*), anethole (trans-1-methoxy-4-(prop-1-enyl) benzene) (*20*), isoeugenole (Phenol, 2-methoxy-4-(1-propenyl)-) (*21*), (Chart 1) have been carried out in past. The chemical structure of PPs resemble to that of petrochemical derived styrene. Depending upon the chemical structures they provided low to high molecular weight polymers. Itaconic acid and its derivatives resembling acrylate and methacrylate structures of petro-derived monomers were also studied for vinyl polymerizations. Itaconic acid can be fermented from starch derived glucose and sucrose (*22*, *23*). Other compounds like β-methyl-α-methylene-γ-butyrolactone (γ-MBL or MMBL) and γ-methyl-α-methylene-γ-butyrolactone (MeMBL), and α-methylene-γ-butyrolactone (MBL) belonging to the class of sesquiterpene lactone family have been isolated from various plants. These α-methylene-γ-butyrolactones [dihydro-3-methylene-2(3H)furanones] constitute an important group of natural products and possess wide-ranging biological activities (*24–27*). They have been studied for their antibacterial and antitumor properties. One of these sesquiterpene lactones is MBL also known as Tulipalin A, which is found to be present in white tulips. By virtue of its exo-methylene double bond, it can be used as a naturally originated vinyl monomer in order to synthesize biopolymers. Having a natural source origin inculcates biocompatibility, biodegradability, eco-friendly and renewable characteristics in these compounds. It is generally considered as cyclic analog of most common vinyl monomer methyl methacrylate (MMA) (Scheme 1).

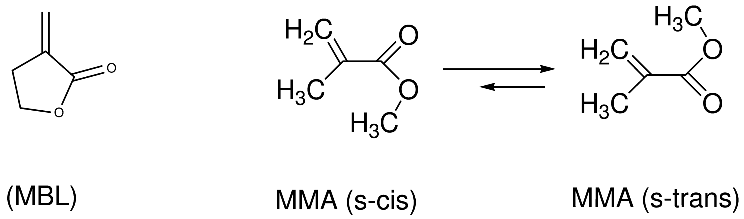

Scheme 1. Chemical structure resemblance of α-methylene-γ-butyrolactone (MBL) to methyl methacrylate (MMA). (reproduced from Stansbury, J. W.; Antonucci, J. M. Dent. Mater. ***1992,*** *8, 270−273)*

Free-Radical Homo- and Copolymerization of MBL

The very first free radical polymerization of such compounds was reported in a patent by Mc Graw in 1953 (*28*). Prior to which more attention was given by medicinal chemists for biomedical applications due to their cytotoxicity and tumor inhibitory properties (*29*). Polymerization of MBL using radical initiator azobisisobutyronitrile (AIBN) has been carried out many times (Scheme 2) providing linear polymer with high molecular weight (*30–32*).

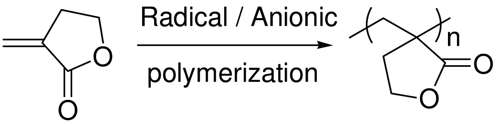

Scheme 2. Free-radical polymerization of α-methylene-γ- butyrolactone (MBL) at vinylic double bond

The overall polymerization rate constant k was found to be 190 % conversion/h at 55 °C which is little higher than bulk polymerization of MMA at 60 °C (128 % conversion/h) (*33*). The major difference between MBL and MMA is the planar structure of MBL. These results in the favorable interaction between the growing radical and the approaching monomer thereby led to higher reactivity as compared to MMA. The PMBL prepared by radical polymerization is amorphous, atactic (p_{rr} = 0.43, p_{mr} = 0.44, p_{mm} = 0.13). The glass transition temperature (T_g) is 195 °C. It is highly thermally stable (major decomposition at more than 320 °C) polymer, thermally depolymerize to monomer. It is soluble in DMF and DMSO with tensile strength of 9100 psi, ultimate elongation of 6.5% and tensile modulus of 2.9 x 10^5

Downloaded by NORTH CAROLINA STATE UNIV on August 28, 2012 | http://pubs.acs.org
Publication Date (Web): August 16, 2012 | doi: 10.1021/bk-2012-1105.ch013

psi. MBL is also copolymerizable with other vinyl monomers like styrene and its derivatives and MMA (*34*). MBL showed high reactivity during copolymerization with reactivity parameters like $r_{st} = 0.14$ and $r_{MBL} = 0.87$ for copolymerization with styrene (*31*) and $r_{MMA} = 0.6$ and $r_{MBL} = 1.67$ for copolymerization with MMA (r = reactivity ratio) (*30*). Apart from this, the group transfer polymerization of MBL using tris-(dimethylamino) sulfonium difluoride as a catalyst is also known (*35*). Although the yield of PMBL was reasonable (> 60%) but molecular weight obtained was low.

Precision Polymerizations and Different Macromolecular Architectures

The term precision polymerization in this chapter is referred to the techniques leading to controlled polymerization of MBL. The result of such polymerization methods was the achievement of pre-determined molecular weight, low polydispersities as determined by the ratio of M_w/M_n (M_w = weight average molecular weight; M_n= number average molecular weight) and the possibility of making different macromolecular architectures like block, and star polymers. Controlled radical polymerization (atom transfer radical polymerization; ATRP) of MBL has been done by Matyjaszewski and Mosnacek (*36*) wherein, CuBr/2,2'-bipyridine (bpy) catalyst complex and bromopropionitrile (BPN) initiator were used to synthesize homopolymers of MBL. The resulting PMBL had very low polydispersities (1.09 – 1.14) and controlled molecular weights as evidenced by a good match between the experimental (determined by ^{1}H NMR) and calculated molecular weights. Also, they obtained well defined diblock and triblock copolymers by chain extension of various macroinitiators, for example, PMMA and P(n-BA) with MBL, using CuBr/N,N,N',N",N"-pentamethyldiethylenetriamine (PMDETA) as a catalyst. Further, block copolymers of PMBL and polybutyl acrylate (PBA) were studied with an aim of getting thermoplastic elastomeric properties (*37*). The idea was to use PMBL block as hard segment and PBA block as soft segment (Scheme 3).

The block copolymers were made by ATRP and showed microphase separated morphology of cylindrical PMBL domains hexagonally arranged in the PBA matrix (Fig 1). All polymers showed a broad rubbery plateau range extending up to temperatures of 300 °C.

The corresponding star block copolymers containing middle soft poly(n-butyl acrylate) (PBA) block and outer hard poly(α-methylene-γ-butyrolactone) (PMBL) block also maintained phase separated morphologies till high temperatures (around 300 °C) and showed elastomeric properties in a broad range of service temperatures (*38*). The star shaped macromolecular architecture provided better mechanical properties as compared to the linear counterpart of the same composition. Although the star polymers showed improved strength and elongation at break as compared to the corresponding linear polymers of the same molecular weight but the range of elongation shown was still less than the conventional thermoplastic elastomers (TPEs). Although the use of MBL for making bio-based thermoplastic elastomers is highly promising and the authors

Downloaded by NORTH CAROLINA STATE UNIV on August 28, 2012 | http://pubs.acs.org
Publication Date (Web): August 16, 2012 | doi: 10.1021/bk-2012-1105.ch013

have presented encouraging results, further research is required in terms of different soft segments, block lengths etc in order to compete with the mechanical properties of conventional styrene-butadiene based TPEs. This is an area still open for further research.

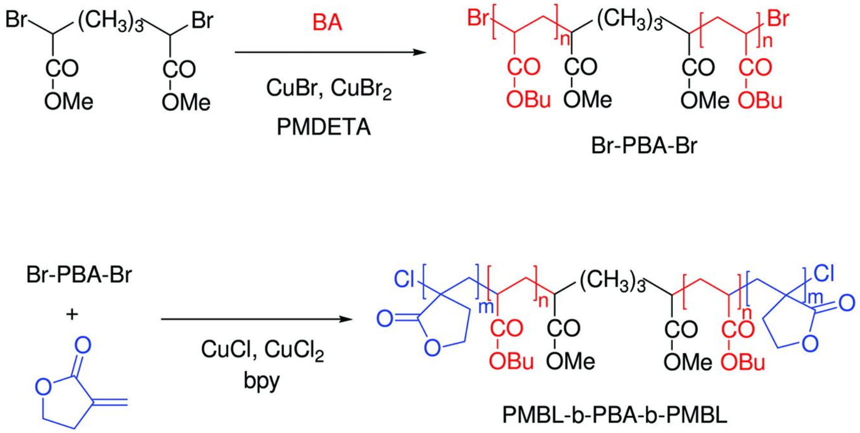
Br
(CH3)3
Br
CO
OMe
CO
OMe
BA
CuBr, CuBr2
PMDETA
Br
n
(CH3)3
Br
n
CO
OBu
CO
OMe
CO
OMe
CO
OBu
Br-PBA-Br
Br-PBA-Br
+
O
O
CuCl, CuCl2
bpy
Cl
m
n
(CH3)3
n
m
Cl
O
O
CO
OBu
CO
OMe
CO
OMe
CO
OBu
O
O
PMBL-b-PBA-b-PMBL

*Scheme 3. Block copolymers of α-methylene-γ-butyrolactone (MBL) with butyl acrylate synthesized by atom transfer radical polymerization (ATRP). (reproduced from Mosnacek, J.; Yoon, J. A.; Juhari, A.; Koynov, K.; Matyjaszewski, K. Polymer **2009,** 50, 2087−2094)*

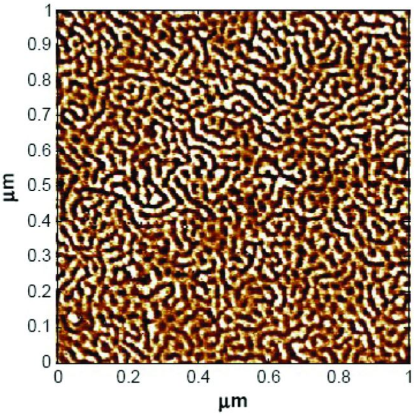
1
0.9
0.8
0.7
0.6
0.5
0.4
0.3
0.2
0.1
0
µm
0
0.2
0.4
0.6
0.8
1
µm

Figure 1. AFM phase image of PMBL-b-PBA-b-PMBL (poly(α-methylene-γ-butyrolactone)-b-poly(butylacrylate)-b-poly(α-methylene-γ-butyrolactone) triblock copolymer (22.7 wt% PMBL). (reprinted with permission from Mosnacek, J.; Yoon, J. A.; Juhari, A.; Koynov, K.; Matyjaszewski, K. Polymer ***2009,*** *50, 2087−2094)*

Downloaded by NORTH CAROLINA STATE UNIV on August 28, 2012 | http://pubs.acs.org
Publication Date (Web): August 16, 2012 | doi: 10.1021/bk-2012-1105.ch013

Downloaded by NORTH CAROLINA STATE UNIV on August 28, 2012 | http://pubs.acs.org
Publication Date (Web): August 16, 2012 | doi: 10.1021/bk-2012-1105.ch013

The chemical structure of MBL has resemblance to MMA and contains a vinylic double bond in conjugation with carbonyl carbon. This makes double bond of MBL susceptible to anionic polymerzation. Anionic polymerization of MBL with PhMgBr (phenylmagnesium bromide) in toluene and 9-fluorenyllithium in THF at -78 °C provided isotactic polymer as compared to atactic PMBL obtained by radical polymerization (*30*). Zhu et al. (*39*) have used resorbable potassium salts of hydride (K[H]), enolate ($Me_2C{=}C(OiPr)OK$) (K[E]) and allyl ($K[1,3\text{-}(SiMe_3)_2\text{-}C_3H_3]$ (K[A]) for controlled anionic polymerization of MBL. These salts themselves at ambient temperatures showed very low to moderate activity. The formation of ate complex ($K^+[HA(C_6F_5)_3]^-$ by mixing $Al(C_6F_5)_3$ ($K[H] / 2Al(C_6F_5)_3$) showed high efficacy for MBL polymerization i.e. shift of TOF (turn over frequency) (mole of monomer consumed per mol catalyst per h) from 0 to 100 from K[H] to ate complex. These polymerizations were possible at ambient temperature.

Metal-Catalyzed Polymerization of MBL

Highly efficient polymerizations at ambient temperatures were possible for MBL with metal catalysts. The major advantage of metal-catalyzed polymerizations is reactions under mild conditions with high conversions, catalyst efficiency, and steroregularity. Metal-catalyzed coordination addition polymerization of polar vinyl monomer like MMA is well-known (*40–42*). MBL resembles structurally to MMA and therefore expected to show chemical reactions similar to it. Chen et al. (*43*) reported the first example of coordination-addition polymerization of MBL using neutral lanthocene(II), non-lanthocene(III), and cationic group 4 metallocene catalysts. The Samarocene (II) catalyst, $Sm(Cp^*)_2(THF)_2$ provided high molecular weight PMBL at ambient temperature with high TOF (turn over frequency) of 30000 h^{-1} and quantitative initiator efficiency. The reaction took place through one electron transfer from Sm(II) ($Sm(Cp^*)_2(THF)_2$) to MBL leading to the formation of Sm(III) cation and MBL radical anion as shown in the Scheme 4. The similar mechanism was shown by us (*44*) and others (*45*) previously for the reaction of MMA with other divalent samarocene compounds. Interestingly the polymerization was controlled and led to the formation of block copolymer with MMA.

Recently, alane-based classical and frustrated Lewis pairs (FLPs) consisting of a bulky N-heterocyclic carbine base and strong acid provided fast polymerization of MBL (*46*). FLPs were formed by a sterically encumbererd Lewis acids and a base, in which these two components cannot form classical donor-acceptor adducts. FLPs consisting of bulky phosphine (e.g. tBu_3P) and the strong acid $Al(C_6F_5)_3$ exhibited a TOF of 7660 h^{-1} with high molecular weight and moderate polydispersity (Scheme 5).

The few examples of metal-catalyzed polymerization of MBL open the field of copolymerization of MBL with other comonomers wide for property tuning and for making functional polymers.

Downloaded by NORTH CAROLINA STATE UNIV on August 28, 2012 | http://pubs.acs.org
Publication Date (Web): August 16, 2012 | doi: 10.1021/bk-2012-1105.ch013

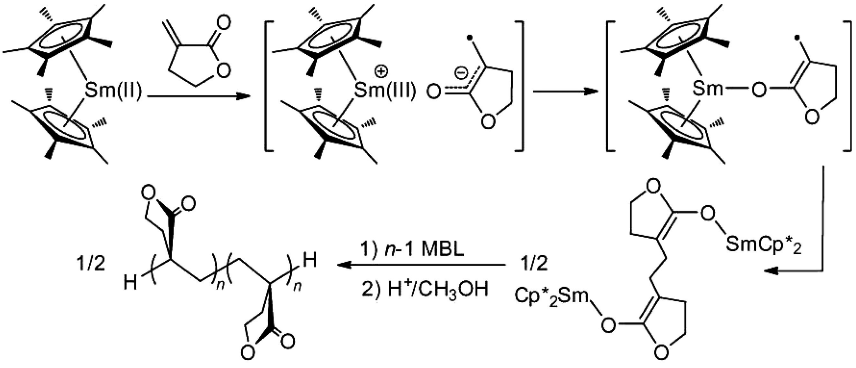
Sm(II)
Sm(III)
Sm
SmCp*₂
Cp*₂Sm
1/2
1) n-1 MBL
2) H⁺/CH₃OH
O
H
n

Scheme 4. Proposed mechanism of polymerization of α-methylene-γ-butyrolactone (MBL) with Sm(Cp)₂(THF)₂. (reproduced from Miyake, G. M.; Newton, S. E.; Mariott, W. R.; Chen, E. Y. X. Dalton Trans.* ***2010,*** *39, 6710−6718)*

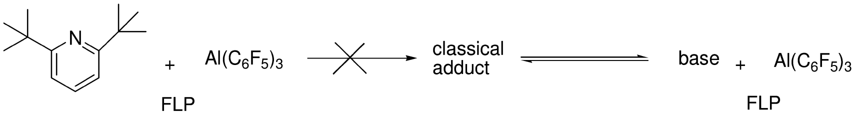
N
+
Al(C6F5)3
classical adduct
base
FLP

Scheme 5. A representative frustrated Lewis pair (FLP) used for the polymerization of α-methylene-γ-butyrolactone (MBL). (reproduced from Zhang, Y.; Miyake, G. M.; Chen, E. Y. X. Angew. Chem., Int. Ed. ***2010,*** *49, 10158−10162)*

Functional and Specialty Polymers from MBL

The chemical structure of MBL has two possible polymerization sites i.e. a vinylic double bond and a γ-butyrolactone (cyclic ester) ring (Scheme 6).

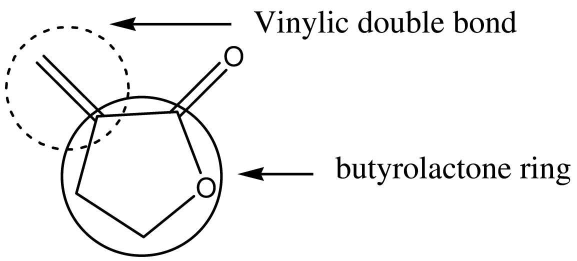
Vinylic double bond
O
butyrolactone ring
O

Scheme 6. The chemical structure of α-methylene-γ-butyrolactone (MBL) with two possible polymerization sites

Vinylic double bonds are already shown to undergo radical, anionic and metal-catalyzed polymerizations as described above. In general, lactones (cyclic esters) like caprolactone are also very well known to undergo anionic, cationic and metal-catalyzed polymerizations (*47*). In contrast, γ-butyrolactone, a five membered cyclic ester is highly stable and does not undergo ring-opening homopolymerization. Previously, using Sm based catalysts we showed participation of γ-butyrolactone during copolymerization with caprolactone (*48*). MBL has similar kind of γ-butyrolactone ring. The tendency of butyrolactone ring of MBL to undergo ring-opening polymerization (Scheme 7) was shown for the first time by Ritter et al. (*49*) during copolymerization with another cyclic ester like ε-caprolactone.

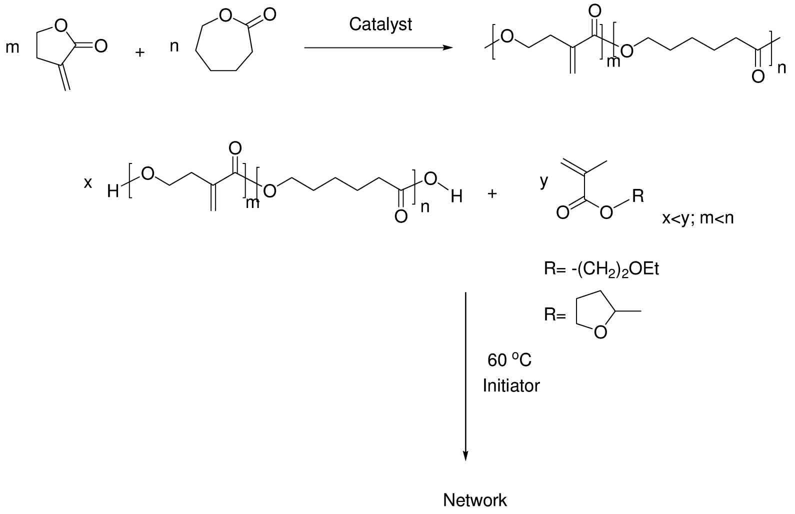

Scheme 7. Ring-opening copolymerization of α-methylene-γ-butyrolactone (MBL) with caprolactone and subsequent cross-linking using vinyl monomer and radical initiator. (reproduced from Zhou, J.; Schmidt, A. M.; Ritter, H. Macromolecules ***2010,*** *43, 939−942)*

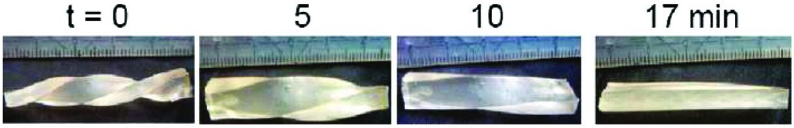

Figure 2. Photo series demonstrating the shape memory effect of the polymer network (from left to right) showing the transition from a temporary shape to a permanent shape at room temperature after twisting and freezing at -20 °C depending on time. (reprinted with permission from Zhou, J.; Schmidt, A. M.; Ritter, H. Macromolecules ***2010,*** *43, 939−942. Copyright American Chemical Society 2010.)*

Downloaded by NORTH CAROLINA STATE UNIV on August 28, 2012 | http://pubs.acs.org
Publication Date (Web): August 16, 2012 | doi: 10.1021/bk-2012-1105.ch013

Bismuth (III) trifluoro methane sulphonate was used as the ring-opening polymerization catalyst. Resulting unsaturated polyesters were cross linked with methacrylates to obtain transparent bicomponent networks which showed shape memory effect (Figure 2). The elasticity and the glass transition temperature of the material could be controlled in a range of -26 °C up to 29 °C. Although the present system showed very long time for recovery but provided the basis for further research in this direction of making bio-based plant-derived shape memory polymers. Such polymers have large applications in biomedical fields.

The butyrolactone ring (BL) of PMBL can also be utilized in polymer analogous reactions for the formation of new materials with modified characteristics. For example, Akkapedi et al. (*30*) showed this property by alkaline hydrolysis at 100 °C and hydrazinolysis of the side butyrolactone ring (Scheme 8). Hydrazinolysis made new water soluble polymers. Unfortunately, there is not much done regarding the polymer analogous reactions of PMBL but there is a great potential in using BL ring of PMBL for further reactions and for generating new properties and new bio-based polymers.

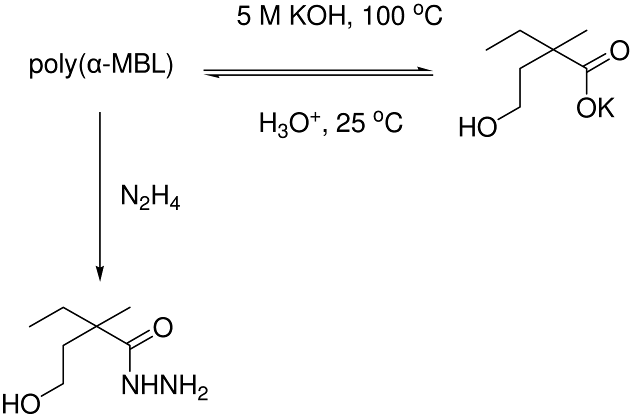

Scheme 8. Polymer ananlogous reactions at butyrolactone ring of α-methylene-γ-butyrolactone (MBL). (reproduced from Akkapeddi, M. K. Macromolecules ***1979,*** *12, 546−551)*

The use of MBL in solid polymer electrolyte is also shown with an aim to obtain a polymer electrolyte with high conductivity but small temperature dependence. Uno et al. (*50*) have made use of high rigidity and polarity of PMBL backbone and expected conductivity due to hopping mechanism. The PMBL showed smaller temperature dependence of ionic conductivity. Further the authors have used this property of PMBL combined with the segmental motion conduction mechanism of poly(ethylene oxide) methyl ether methacrylate (PEOMA) and made different hybrid structures like blends, block copolymers and random copolymers (Figure 3).

Downloaded by NORTH CAROLINA STATE UNIV on August 28, 2012 | http://pubs.acs.org
Publication Date (Web): August 16, 2012 | doi: 10.1021/bk-2012-1105.ch013

Downloaded by NORTH CAROLINA STATE UNIV on August 28, 2012 | http://pubs.acs.org
Publication Date (Web): August 16, 2012 | doi: 10.1021/bk-2012-1105.ch013

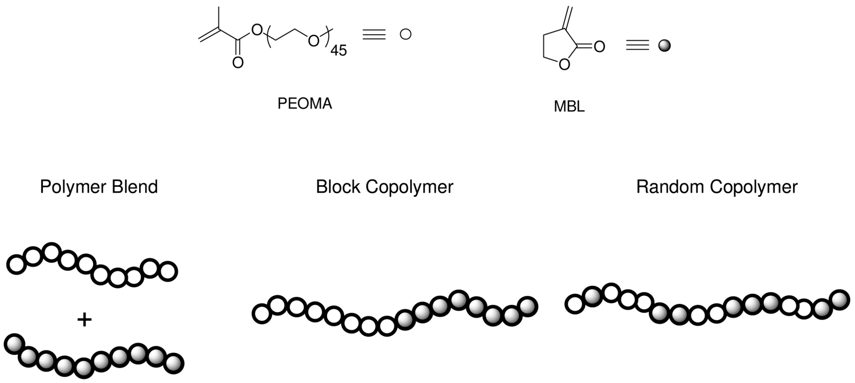

Figure 3. Different macromolecular architectures and blend of poly(ethylene oxide) methyl ether methacrylate (PEOMA) and α-methylene-γ-butyrolactone (MBL) used as solid electrolyte. (reproduced from Uno, T.; Kawaguchi, S.; Kubo, M.; Itoh, T. J. Power Sources ***2008,*** *178, 716−722)*

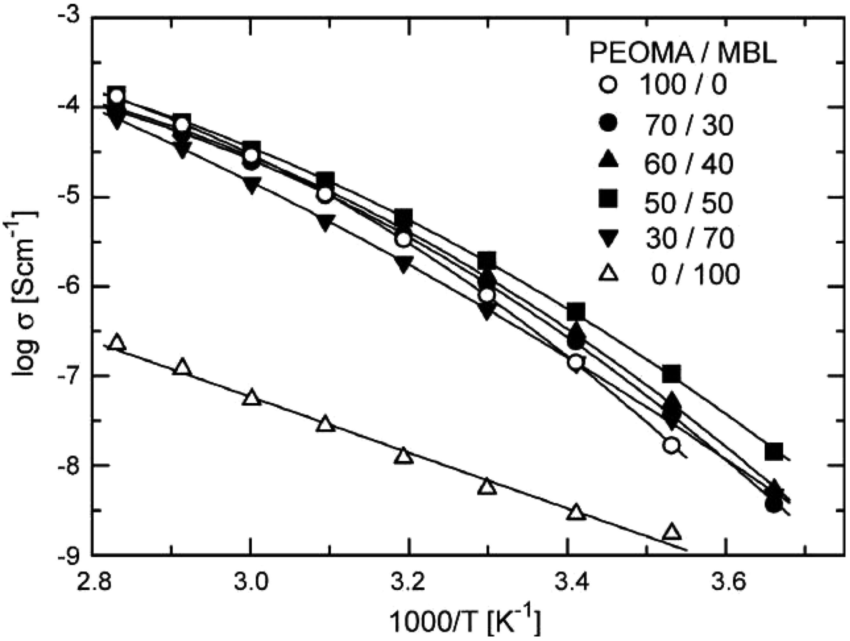

Figure 4. Temperature dependence of the ionic conductivities for the polymer blend electrolytes with fixed [Li]/[O] ratio of 1/12 at the different PEOMA/MBL ratios of 70/30 (●), 60/40 (▴), 50/50 (■), and 30/70 (▾), and for the poly(PEOMA) (○) and poly(MBL) (□) electrolytes with fixed [Li]/[O] ratio of 1/12. (reproduced from Uno, T.; Kawaguchi, S.; Kubo, M.; Itoh, T. J. Power Sources ***2008,*** *178, 716−722)*

Downloaded by NORTH CAROLINA STATE UNIV on August 28, 2012 | http://pubs.acs.org
Publication Date (Web): August 16, 2012 | doi: 10.1021/bk-2012-1105.ch013

Blends of PMBL and poly(PEOMA) were compared with the corresponding statistical and block copolymers for lithium (Li) ion conductivity at different lithium salt concentrations ([Li]/[O] ratios of 1/8, 1/12, and 1/16). The ionic conductivity showed a significant difference depending upon the combination manner of PEOMA and MBL units, the highest conductivities were obtained at the different hybrid polymer compositions for the blend (Figure 4) (*50*).

The use of MBL as a diluent monomer in dental resin composition was also aimed by Stansbury et al (*51*). The advantage of MBL in such applications was the high reactivity as compared to MMA. The incorporation of small amounts of MBL into bis-glycidyl methacrylate (Bis-GMA) significantly reduced the amount of unreacted monomer in the dental composition. Improved diametral tensile and transverse strengths were also observed.

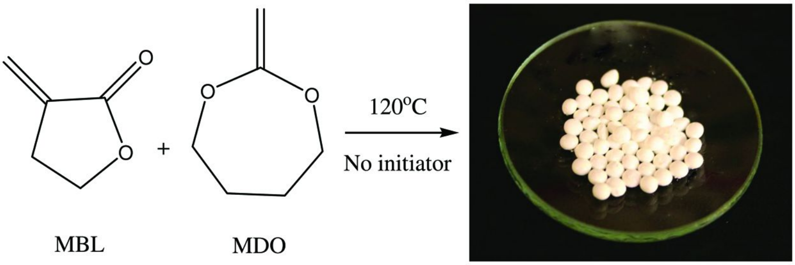

Figure 5. Preparation of polymers in the form of white pellets by radical ring opening polymerization in combination with free radical polymerization of a cyclic ketene acetal, 2-methylene-1,3-dioxepane (MDO) with α-methylene-γ-butyrolactone (MBL) without initiator. (reprinted with permission from Agarwal, S.; Kumar, R. Macromol. Chem. Phys. ***2011,*** *212, 603−612)*

We made use of MBL in providing transparent, degradable, and high glass transition temperature polymers with good processability (*52*). Such material could be used for many different applications including packaging. In order to provide degradability to PMBL backbone, ester linkages were introduced. Cyclic ketene acetals (CKAs) are a group of exocyclic methylene compounds which have a tendency to undergo ring-opening polymerization in the presence of free radical initiator. The outcome is the formation of polyesters by free-radical polymerization. The copolymerization of CKAs with other vinyl monomers incorporates ester linkages in the otherwise "stable" vinyl polymer backbone randomly, thus rendering degradability. Already in our lab, we have synthesized a large number of such degradable and useful polymers (*53–59*). To make targeted degradable, high T_g MBL based polymers, radical ring opening polymerization in combination with free radical polymerization of a cyclic ketene acetal, 2-methylene-1,3-dioxepane (MDO) with MBL was carried out (*60*). During the copolymerization studies, surprisingly, the two monomers reacted even in the absence of any radical initiator at 70 °C and above. For a 50:50 monomer feed ratio (α-MBL:MDO) polymers in the form of white pellets of very high molecular weights ($M_n = 2.6 \times 10^5$ and 7.9×10^4 for spontaneous polymerizations at 70 & 120 °C, respectively) were obtained even without any initiator (Figure 5).

Further, the amount of ester linkages by ring-opening of MDO and hence the properties of polymers could be easily controlled by controlling the temperature of mixing or by feed composition. Two parallel reaction mechanisms i.e. zwitterionic and biradical mechanism were running in the system, which could be easily controlled to get the desired microstructure (Scheme 9).

During copolymerization MBL acted as an acceptor for highly nucleophilic monomer MDO and made an acceptor-donor complex. Therefore, it was also possible to tune the reactions by adding either the radical trapping agent like hydroquinine or radical generators like AIBN in the system. Hydrolytic degradability of the backbone was also proved. This study provided hydrolytically degradable polymers having ester linkages with varied glass transition temperatures, having high thermal stability and suitable mechanical properties using bio-based MBL and cyclic ketene acetal.

Downloaded by NORTH CAROLINA STATE UNIV on August 28, 2012 | http://pubs.acs.org
Publication Date (Web): August 16, 2012 | doi: 10.1021/bk-2012-1105.ch013

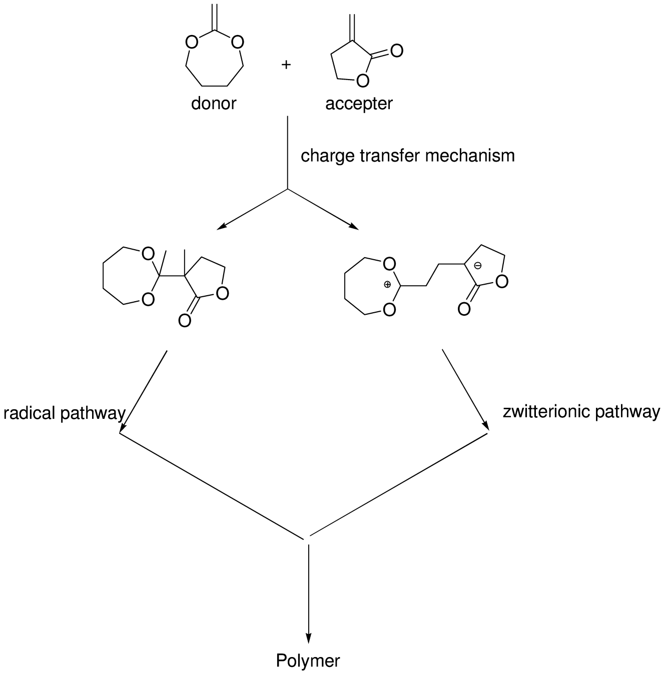

Scheme 9. Expected copolymerization routes of α-methylene-γ-butyrolactone (MBL) and 2-methylene-1,3-dioxepane (MDO) at 70 °C and 120 °C via donor-acceptor mechanism. (reproduced from Agarwal, S.; Kumar, R. Macromol. Chem. Phys. ***2011,*** *212, 603−612)*

Downloaded by NORTH CAROLINA STATE UNIV on August 28, 2012 | http://pubs.acs.org
Publication Date (Web): August 16, 2012 | doi: 10.1021/bk-2012-1105.ch013

Conclusions

MBL is an interesting naturally occurring monomer with two polymerizable sites. It can undergo vinyl polymerizations at the double bond as well as metal-catalyzed ring-opening polymerization at its γ-butyrolactone ring with other cyclic esters. The important characteristics of the resulting linear homo PMBL made by vinyl polymerization are high glass transition temperatures and very high thermal stability. Although the basic polymerization characteristics and properties of PMBL are highly promising for replacing conventional petro-derived vinyl monomers like MMA by MBL for many applications but there is hardly any commercial utilization of this monomer till date. The problems could be its limited solubility (only soluble in high boiling solvents like DMF and DMSO), difficult processing because of very high glass transition temperature and brittle nature. The properties of PMBL can be easily tuned by copolymerization with other vinyl monomers. This gives promising scenario for its applications in future. There are other aspects of this polymer which have not been either tested or utilized in full. For example, it would be interesting to compare the antibacterial and antitumor properties of PMBL with the corresponding monomer. Also, the butyrolactone ring can undergo further chemistry and can be utilized for making different macromolecular architectures generating wide variety of properties which at present is under utilized.

References

1. Meier, M. A. R.; Metzgerb, J. O.; Schubert, U. S. *Chem. Soc. Rev.* **2007**, *36*, 1788–1802.
2. Williams, C. K.; Hillmyer, M. A. *Polym. Rev.* **2008**, *48*, 1–10.
3. Ishimoto, K.; Arimoto, M.; Ohara, H.; Kobayashi, S.; Ishii, M.; Morita, K.; Yamashita, H.; Yabuuchi, N. *Biomacromolecules* **2009**, *10*, 2719–2723.
4. Deng, Y.; Fan, X. -D.; Waterhouse, J. *J. Appl. Polym. Sci.* **1999**, *73*, 1081–1088.
5. Tsujimoto, T.; Uyama, H.; Kobayashi, S. *Macromol. Biosci.* **2002**, *2*, 329–335.
6. Cermak, S. C.; Isbell, T. A. *J. Am. Oil Chem. Soc.* **2001**, *78*, 557–565.
7. Cermak, S. C.; Isbell, T. A. *J. Am. Oil Chem. Soc.* **2004**, *81*, 297–303.
8. Peláeza, M.; Orellanaa, C.; Marquésa, A.; Busquetsb, M.; Guerreroc, A.; Manresa, A. *J. Am. Oil Chem. Soc.* **2003**, *80*, 859–866.
9. Harry-O kuru, R. E.; Isbell, T. A.; Weisleder, D. *J. Am. Oil Chem. Soc.* **2001**, *78*, 219–222.
10. Warwel, S.; Brüse, F.; Demes, C.; Kunz, M. *Ind. Crops Prod.* **2004**, *20*, 301–309.
11. Warwel, S.; Brüse, F.; Demes, C.; Kunz, M.; Rüsch gen. Klaas, M. *Chemosphere* **2001**, *43*, 39–48.
12. Tian, Q.; Larock, R. C. *J. Am. Oil Chem. Soc.* **2002**, *79*, 479–488.
13. Xia, Y.; Lu, Y.; Larock, R. C. *Polymer* **2010**, *51* (1), 53–63.
14. La Scala, J. J.; Sands, J. M.; Orlicki, J. A.; Robinette, E. J.; Palmese, G. R. *Polymer* **2004**, *45*, 7729–7737.

15. Agarwal, S.; Choudhary, V.; Varma, I. K. *J. Appl. Polym. Sci.* **1992**, *46*, 1707–1712.
16. Silvestre, A. J. D.; Gandini, A. *Terpenes: major sources, properties and applications, in Monomers, Polymers and Composites from Renewable Resources*; Belgacem, M. N., Gandini, A., Eds.; Elsevier: Amsterdam, 2008, Chapter 2.
17. Mathers, R. T.; Damodaran, K.; Rendos, M. G.; Lavrich, M. S. *Macromolecules* **2009**, *42*, 1512–1518.
18. Satoh, K.; Matsuda, M.; Nagai, K.; Kamigaito, M. *J. Am. Chem. Soc.* **2010**, *132*, 10003–10005.
19. Trumbo, D. L. *Polym. Bull.* **1994**, *33*, 643–649.
20. Rooney, J. M. *Macromol. Chem.* **1978**, *179*, 2419–2430.
21. Pailer, M. *Monatsh. Chem.* **1947**, *77*, 45–51.
22. Tate, B. E. *Adv. Polym. Sci.* **1967**, *5*, 214–232.
23. Marvel, C. S.; Shepherd, T. H. *J. Org. Chem.* **1959**, *24*, 599–605.
24. Hoffmann, H. M. R.; Rabe, J. *Angew. Chem., Int. Ed. Engl.* **1985**, *24*, 94–110.
25. Wong, H. F.; Brown, G. D. *Phytochemistry* **2002**, *59*, 99–104.
26. Vučković, I.; Vujisić, L.; Vajs, V.; Tešević, V.; Janaćkovic, P.; Milosavljević, S. J. *J. Serb. Chem. Soc.* **2006**, *71*, 127–133.
27. Trendafilova, A.; Todorova, M.; Mikhova, B.; Vitkova, A.; Duddeck, H. *Phytochemistry* **2006**, *67*, 764–770.
28. McGraw, W. J. U.S. Patent 2624723, 1953.
29. Kupchan, S. M. *Bioorg. Chem.* **1971**, *1*, 13–31.
30. Akkapeddi, M. K. *Macromolecules* **1979**, *12*, 546–551.
31. Ueda, M.; Takahashi, M.; Imai, Y.; Pittman, C. U. *J. Polym. Sci., Part A: Polym. Chem.* **1982**, *20*, 2819–2828.
32. Brink, M. D.; Smulders, W.; Herk, A. M.; German, A. L. *J. Polym. Sci., Part A: Polym. Chem.* **1999**, *37*, 3804–3816.
33. Luskin, L. S.; Meyers, R. J. In '*Encyclopedia of Polymer Science and Technology*' Vol 1, Interscience, NY, 1964, p 264.
34. Trumbo, D. L. *Polymer Bulletin* **1995**, *35*, 265–269.
35. Sogah, D. Y.; Herter, W. R.; Webster, O. W.; Cohen, G. M. *Macromolecules* **1987**, *20*, 1473–1488.
36. Mosnacek, J.; Matyjaszewski, K. *Macromolecules* **2008**, *41*, 5509–5511.
37. Mosnacek, J.; Yoon, J. A.; Juhari, A.; Koynov, K.; Matyjaszewski, K. *Polymer* **2009**, *50*, 2087–2094.
38. Juhari, J.; Mosnacek, J.; Yoon, J. A.; Nese, A.; Koynov, K.; Kowalewski, T.; Matyjaszewski, K. *Polymer* **2010**, *51*, 4806–4813.
39. Hu, Y.; Gustafson, L. O.; Zhu, H.; Chen, E. Y. X. *J. Polym. Sci. Part A: Polym. Chem.* **2011**, *49*, 2008–2017.
40. Yasuda, H.; Yamamoto, H.; Yamashita, M.; Yokota, K.; Nakamura, A.; Miyake, S.; Kai, Y.; Kanehisa, N. *Macromolecules* **1993**, *26*, 7134–7143.
41. Yasuda, H.; Yamamoto, H.; Yokota, K.; Miyake, S.; Nakamura, A. *J. Am. Chem. Soc.* **1992**, *114*, 4908–4909.
42. Boffa, L. S.; Novak, B. M. *Macromolecules* **1997**, *30*, 3494–3506.

Downloaded by NORTH CAROLINA STATE UNIV on August 28, 2012 | http://pubs.acs.org
Publication Date (Web): August 16, 2012 | doi: 10.1021/bk-2012-1105.ch013

Downloaded by NORTH CAROLINA STATE UNIV on August 28, 2012 | http://pubs.acs.org
Publication Date (Web): August 16, 2012 | doi: 10.1021/bk-2012-1105.ch013

43. Miyake, G. M.; Newton, S. E.; Mariott, W. R.; Chen, E. Y. X. *Dalton Trans.* **2010**, *39*, 6710–6718.
44. Agarwal, S. *Eur. Polym. J.* **2004**, *40*, 2143–2152.
45. Boffa, L. S.; Novak, B. M. *Macromolecules* **1994**, *27*, 6993–6995.
46. Zhang, Y.; Miyake, G. M.; Chen, E. Y. X. *Angew. Chem. Int. ed.* **2010**, *49*, 10158–10162.
47. Agarwal, S.; Mast, C.; Anfang, S.; Dehnicke, K.; Greiner, A. *Macromol. Rapid Commun.* **2000**, *21*, 195–212.
48. Agarwal, S.; Xie, X. *Macromolecuels* **2003**, *36*, 3545–3549.
49. Zhou, J.; Schmidt, A. M.; Ritter, H. *Macromolecules* **2010**, *43*, 939–942.
50. Uno, T.; Kawaguchi, S.; Kubo, M.; Itoh, T. *J. Power Sources* **2008**, *178*, 716–722.
51. Stansbury, J. W.; Antonucci, J. M. *Dent. Mater.* **1992**, *8*, 270–273.
52. Agarwal, S.; Kumar, R. *Macromol. Chem. Phys.* **2011**, *212*, 603–612.
53. Agarwal, S.; Kumar, R.; Kissel, T.; Reul, R. *Polym. J.* **2009**, *41*, 650–660.
54. Agarwal, S. *Polym. J.* **2007**, *39*, 163–174.
55. Wickel, H.; Agarwal, S.; Greiner, A. *Macromolecules* **2003**, *36*, 2397–2403.
56. Wickel, H.; Agarwal, S. *Macromolecules* **2003**, *36*, 6152–6159.
57. Agarwal, S.; Bognitzki, M. *Polym. Preprints (Am. Chem. Soc., Div. Polym. Chem.)* **2006**, *7*, 528.
58. Lutz, J. –F.; Andrieu, J.; Uzgun, S.; Rudolph, C.; Agarwal, S. *Macromolecules* **2007**, *40*, 8540–8543.
59. Ren, L.; Speyer, C.; Agarwal, S. *Macromolecules* **2007**, *40*, 7834–7841.
60. Ren, L.; Agarwal, S. *Macromol. Chem. Phys.* **2007**, *208*, 245–253.

Downloaded by OHIO STATE UNIV LIBRARIES on August 28, 2012 | http://pubs.acs.org
Publication Date (Web): August 16, 2012 | doi: 10.1021/bk-2012-1105.ch014

Chapter 14

Biological Lactate-Polymers Synthesized by One-Pot Microbial Factory: Enzyme and Metabolic Engineering

John Masani Nduko, Ken'ichiro Matsumoto, and Seiichi Taguchi*

Division of Biotechnology and Macromolecular Chemistry,
Graduate School of Engineering, Hokkaido University,
N13W8, Kita-ku, Sapporo 060-8628, Japan
***E-mail: staguchi@eng.hokudai.ac.jp. Tel/Fax: +81-11-706-6610**

Polylactic acid (PLA) is a representative commodity polyester synthesized from renewable resources. The benefits of PLA over the conventional petrochemical-based plastics are; it is biodegradable, it requires less energy to produce and reduces greenhouse gas production. PLA is mainly produced via a two step bio-chemo process where lactate produced by microorganisms is converted into lactides which are then polymerized by metal catalysts to form high molecular weight PLA. In 2008, microbial LA-based polyester production systems were for the first time established as microbial cell factories (MCFs). This paradigm shift is based on a conversion of a two-step chemical process into a single-step MCF. This breakthrough was triggered by the discovery of an engineered LA-polymerizing enzyme (LPE). LPE was discovered among a collection of polyhydroxyalkanoate (PHA) synthase mutants from *Pseudomonas* sp. 61-3 through a long-term evolutionary engineering study. The MCF has been advanced by combination of further evolution of LPE with metabolic engineering for improved monomer precursor production. This chapter reviews the backgrounds on the establishment of the MCFs for the synthesis of LA-based polyesters to near PLA homopolymer, structures and properties of LPE-catalyzed polymers and challenges of LA-based polymer production system as well as future perspectives on the microbial LA-based polyesters.

In Biobased Monomers, Polymers, and Materials; Smith, P., et al.;
ACS Symposium Series; American Chemical Society: Washington, DC, 2012.

Downloaded by OHIO STATE UNIV LIBRARIES on August 28, 2012 | http://pubs.acs.org
Publication Date (Web): August 16, 2012 | doi: 10.1021/bk-2012-1105.ch014

Introduction

Due to the dwindling nature of petroleum and other fossil resources and increased emission of greenhouse gases into the atmosphere, bio-based polymers have gained enormous attention as alternatives to petroleum-derived plastics (*1*, *2*). Poly(lactic acids) (PLAs) are representative bio-based polymers with good processability, highly transparent and widely used as packaging materials, for making containers and stationery (*1*). Moreover, due to their biodegradability and biocompatibility, PLAs have found applications in agriculture and medicine (*3–6*). The interest of PLA research stems from not only their improved productivity but also developing modifications for the addition of functions and/or properties such as heat resistance/or impact resistance through copolymerization, surface treatment, stereocomplexation or blending to make the materials suitable for a wide range of applications (*7–9*). In typical examples, plasticizers have been applied to help make PLAs flexible, and PLAs have served as component nano-alloys in creating engineering plastics whereas copolymerization has led to formation of materials with new properties and functions (*10–13*) . PLAs are produced from renewable biomass (such as corn starch and sugar beets) through the two-step bio-chemo fusion process combining the fermentative production of lactate (LA) and chemical polymerization via a lactide intermediate that uses either chiral form of LA 2-hydroxy propionic acid) or combinations (*14*, *15*) . The most common way for the industrial production of high-molecular-weight PLAs is ring-opening polymerization (ROP) that is catalyzed by heavy metal catalyst systems but typically tin due to its high catalytic activity, high solubility in molten lactide and low racemization of the polymer while giving polymers of high molecular weight (*8*, *16*). However, despite these positive achievements by metal catalysts, the remnants of heavy metal catalysts are unfavorable for medical and food use applications due to their potential harmfulness (*6*). In addition, the two-step bio-chemo process for PLA synthesis turns out to be costly as the need for lactate purification alone contributes up to 50% of production cost of the monomer and therefore limiting the competitiveness of PLA over the conventional petrochemical-derived plastics (*17*).

To overcome those challenges, efforts towards the replacement of the two-step bio-chemo process which employs heavy metal catalysts have been directed on the potentially safe and environmentally friendly metal-free one-pot process that employs enzymes or/and whole-cell catalysts. This alternative process has become an attractive and hot point of research as enzymes are preferable as natural non-harmful biocatalysts that function under ambient conditions (*18*). Furthermore, enzymes could catalyze highly selective biotransformations and whole-cell systems harboring them are capable of synthesizing polymers with enantiomerically pure structure from inexpensive raw materials (*6*, *19*). On the other hand, the bio-chemo process for PLA synthesis requires monomers with extremely high purity to avoid causing side reactions, and for the anhydrous and high temperature conditions to proceed (*8*). In such a situation, a single-step biosynthesis of PLA by microorganisms is an enormous challenge for both academia and industry. Typically, a lactate-polymerizing enzyme (LPE), which can function in place of the metal catalysts, would be desirable to establish the single-step bio-process as envisaged in Figure 1.

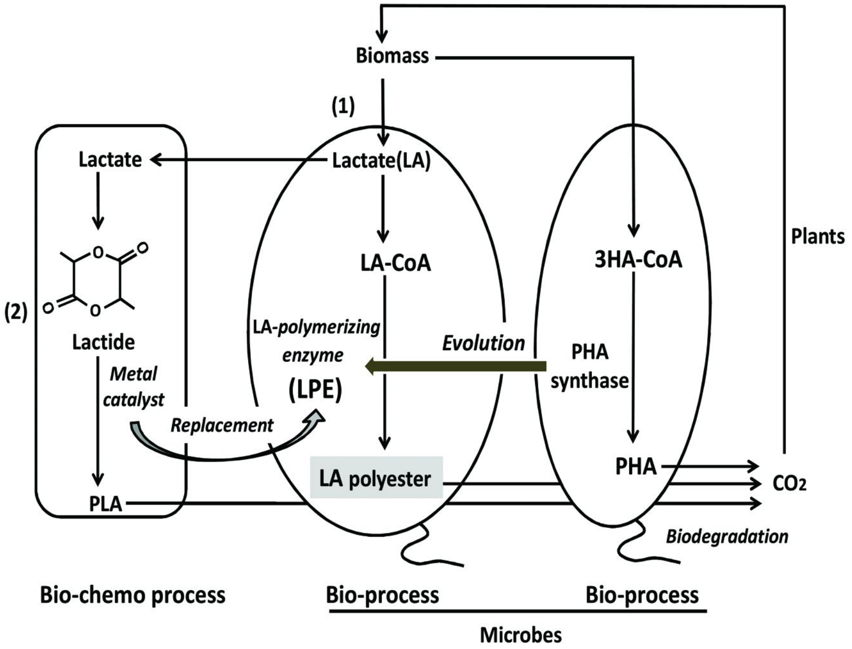
Biomass
(1)
Lactate
Lactate(LA)
LA-CoA
3HA-CoA
Plants
(2)
Lactide
LA-polymerizing enzyme
(LPE)
Evolution
PHA synthase
Metal catalyst
Replacement
PHA
CO2
LA polyester
PLA
Biodegradation
Bio-chemo process
Bio-process
Bio-process
Microbes

Figure 1. Process conversion for the production of lactate (LA)-based polyesters from the two-step; (1) fermentation and (2) chemical polymerization bio-chemo process into a single-step metal free bio-process using microbes. The LA-polymerizing enzyme (LPE) which is an evolved PHA synthase is a key to the process conversion.

The best way for the production of PLA in a single-step process could have been the discovery of a PLA-producing microorganism, but hitherto this route is unknown (*20*). With these obstacles at hand, Taguchi et al. focused on the microbial biosynthetic system for polyhydroxyalkanoates (PHAs) with the aim of engineering bacteria to analogously biosynthesize PLA. These efforts were an attempt to convert the two-step bio-chemo process of PLA synthesis into a one-pot bioprocess based on the well-established metabolic pathways for the synthesis of PHAs (*20*). PHAs are natural polyesters accumulated by bacteria as energy storage materials (*20*, *21*). PHAs are biocompatible bio-based polyesters with properties similar to synthetic thermoplastics and elastomers e.g. polypropylene and rubber, and are completely and effectively degraded by bacteria in soil or water (*22*). The most abundant PHA is polyhydroxybutyrate [P(3HB)] and the natural or recombinant bacteria cultivated on glucose can accumulate up to 95% of their cellular dry weights in P(3HB), making these microorganisms miniature

Downloaded by OHIO STATE UNIV LIBRARIES on August 28, 2012 | http://pubs.acs.org
Publication Date (Web): August 16, 2012 | doi: 10.1021/bk-2012-1105.ch014

bioplastic factories (*23*). The synthesis of P(3HB) is dependent on two steps i.e. monomer supply and polymerization. Polymerization is the crucial step that is catalyzed by PHA synthases which are the key enzymes for polymerizing various monomers depending on their substrate specificity (*24*, *25*). Upon supply of monomers, some PHA synthases have been reported to polymerize a variety of monomers (*24*). Therefore, based on the broad substrate specificity of PHA synthases and the fact that the monomeric constituents of PHA share the common chemical structure, hydroxyl acid, with 2-hydroxypropionate (LA) (*6*), the prospects of conferment of PHA synthases with LA polymerizing capability was envisioned. Additionally, it was thought that if a PHA synthase catalyzing the polymerization of LA were to be obtained, heterologous expression of that synthase in recombinant cells would lead to the synthesis of PLA. Indeed in a landmark experiment in the year 2008, Taguchi et al. formally reported the first enzyme-driven microbial cell factory (MCF) for the biosynthesis of LA-based polyesters [P(6 mol% LA-*co*-3HB)] (*20*). Although PLA homopolymer synthesis was not obtained, this study laid the foundation upon which a series of studies on the LA-enrichment of the copolymers that led to the synthesis of near PLA homopolymer were conducted (*15*, *26*–*30*). In this chapter review, current developments in the newly established one-pot LA-based polyester synthetic bioprocess will be comprehensively mentioned from the viewpoints of enzyme engineering (the most important key strategy), aspects of metabolic engineering, the properties of LA-based polyesters i.e. hybrid polymers of rigid PLA and flexible PHA and future perspectives of LA-based polyester research.

Studies Toward the Discovery of a Lactate-Polymerizing Enzyme (LPE)

Challenges on the Creation of an MCF for LA-Based Polyester Biosynthesis

Direct *in vivo* polymerization of LA to generate PLA is an attractive but a challenging target. The absence of natural LA-polymerizing enzymes presented obstacles that had to be overcome in order to create an MCF for the production of LA-based polyesters. However, considering the facts that PLA is structurally analogous to PHAs and LA is a fermentation product of sugars, the prospects of designing an LA-polymerizing enzyme based on the bacterial PHAs synthetic system became evident (*20*). PHAs are wholly synthesized *in vivo* as intracellular carbon and energy storage compounds (*31*, *32*). If PLA can be intracellularly synthesized in a similar manner to PHAs, PLA could be produced from biomass-derived LA in a single-step bioprocess without the involvement of the multiple chemical processes such as; extraction of LA, synthesis and purification of lactides and ring-opening polymerization of lactides using metal catalysts (*1*). Thus far, there are limited studies on the creation of an *in vivo* system for the synthesis of LA-based polyesters and at the beginning, the question was, how could an LPE be obtained to drive a MCF? Nonetheless, a PHA synthase with broad substrate spectra formed the basis upon which a series of studies that led to the microbial synthesis of LA-based polyesters were conducted.

Downloaded by OHIO STATE UNIV LIBRARIES on August 28, 2012 | http://pubs.acs.org
Publication Date (Web): August 16, 2012 | doi: 10.1021/bk-2012-1105.ch014

Downloaded by OHIO STATE UNIV LIBRARIES on August 28, 2012 | http://pubs.acs.org
Publication Date (Web): August 16, 2012 | doi: 10.1021/bk-2012-1105.ch014

Natural and Artificially Engineered PHA Synthases

In the PHAs biosynthetic system, the PHA synthases are key enzymes that catalyze the incorporation of the hydroxyacyl moieties of the CoA esters, hydroxyacyl-CoAs into the polymer concomitantly releasing CoA (*33*). Generally, the continuous esterification by the PHA synthase yields high-molecular weight polyesters in a living manner polymerization (*6*). Typically, the 3 or 4-hydroxyacyl-CoAs and the most common monomeric constituent, 3-hydroxybutyryl-CoA (3HB-CoA) can be incorporated into PHA depending on the substrate specificity of a PHA synthase (*25*). Much work has been done in the search of PHA synthases with new function and properties for industrial PHA production and the nucleotide sequences of over 80 PHA synthases have been identified, cloned and assigned (*25*, *34*).

The PHA synthases are classified into four major classes depending on their primary sequences, substrate specificities and subunit structures as shown in Table I (*25*). Class I PHA synthases comprise enzymes consisting of one subunit (PhaC) e.g. the PHA synthase from *Cupriavidus necator* that has relatively narrow substrate specificity and preferentially uses CoA thioesters comprising 3-5 (C3-C5) carbon atoms, the short-chain-length (SCL) (*35*). The class II PHA synthases also consist of one subunit (PhaC) and are represented by Pseudomonads and exhibit substrate specificity towards medium-chain-length (MCL), (C6-C12) CoA thioesters (*21*). On the other hand, Class III polyester synthases e.g. PHA synthase from *Allochromatium vinosum* comprise enzymes with two subunits (PhaC and PhaE) and have substrate specificity similar to Class I synthases (*35*). The Class IV PHA synthases such as PHA synthase from *Bacillus megaterium* have two subunits (PhaC and PhaR) that combine for the exhibition of enzyme activity as do the class III PHA synthases (*25*).

Table I. The four classes of PHA synthases

Class	*Subunits*	*Representative species*	*Substrate*
I	PhaC	*Cupriavidus necator*	C3 - C5
II	PhaC	*Pseudomonas aeruginosa*	≥ C5
III	PhaC - PhaE	*Allochromatium vinosum*	C6 - C8
IV	PhaC - PhaR	*Bacillus megaterium*	$3HA_{SCL}$ - CoA

Downloaded by OHIO STATE UNIV LIBRARIES on August 28, 2012 | http://pubs.acs.org
Publication Date (Web): August 16, 2012 | doi: 10.1021/bk-2012-1105.ch014

The production and properties of PHAs are closely related to the performances of PHA synthase involved in their synthesis. Polyester synthases determines polyester composition and molecular weight as well as strongly impact on the efficiency of PHA production (*33*). As such, over the last few years, directed evolution of PHA synthase experiments have demonstrated enhanced PHA synthase activity and broader substrate specificity resulting in creating polyesters with tailor-made properties (*36–38*). There are a number of enzyme resources on the engineered PHA synthases. For example, there are reports on the engineered class I and II PHA synthases (*39–42*). Of these PHA synthases, the class II PHA synthase (PhaC1$_{Ps}$) from *Pseudomonas* sp. 61-3 has been an attractive target for engineering because of its intrinsic broad substrate specificity (*20*, *38*, *43*). PhaC1$_{Ps}$ catalyzes the polymerization of MCL and SCL monomers but with low activity towards SCL monomers (*44*). Although suitable structural models for any PHA synthase have been hard to achieve, earlier studies based on semi-rational approaches were successful in fine-tuning the monomer composition of SCL/MCL PHAs using beneficial mutants of PhaC1$_{Ps}$ with enhanced activity towards SCL (*30*, *32–34*, *45*). The beneficial positions of PhaC1$_{Ps}$ (130, 325, 477 and 481) illustrated in Figure 2A, are closely related to the enzyme properties and are addressed in these references (*34*, *43*, *46*).

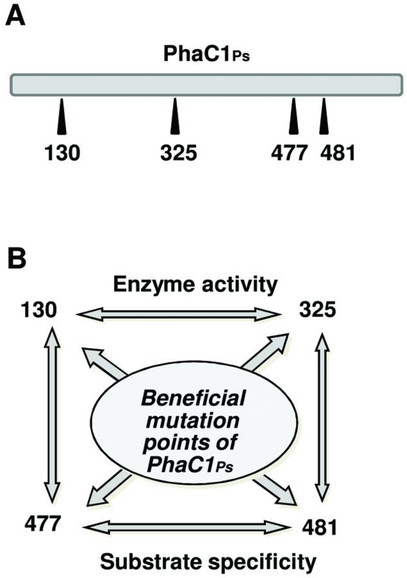

Figure 2. Evolutionary engineering of a PHA synthase (PhaC1$_{Ps}$) to obtain desired mutants. ***A****, beneficial positions of PhaC1$_{Ps}$ for enhanced activity or substrate specificity.* ***B****, the combinations of the beneficial mutations further enhanced enzyme activity or substrate specificity.*

These beneficial mutations have been evolved to various directions such as activity increase (130 and 325) and substrate specificity alteration (477 and 481) (Figure 2B) (*37*). Of particular interest was the double mutant, Ser325Thr/Gln481Lys (PhaC1$_{Ps}$STQK) that had enhanced *in vivo* and *in vitro* activities (*38*). Eventually, this is the mutant PHA synthase that led to the discovery of the LPE.

The Discovery of a Lactate Polymerizing Enzyme (LPE)

The pioneering work on the exploration of LA-polymerizing activity by PHA synthases was reported by Valentin et al. (*47*). In that attempt, the PLA biosynthesis was carried out by monitoring the activity of PHA synthases towards synthetic LA-CoAs (*R* and *S* enantiomers). Several PHA synthases were evaluated for LA-polymerizing activities and a class III PHA synthase from *Allochromatium vinosum* exhibited a weak CoA releasing activity (*47*). In a similar report, Yuan et al. reported in detail the activity of *A. vinosum* PHA synthase towards (*R*)-LA-CoA (*48*). Unfortunately, in either case, polymerization was not observed/was negligible suggesting that PHA synthase could hydrolyze CoA ester to release CoA but not progress from there with polymerization to form a polymer (*47*, *48*).

As these initial efforts by Valentin et al. and Yuan et al. showed little promise with natural PHA synthases towards LA polymerizing activity, Taguchi et al. focused on artificially evolved PHA synthases and formally reported the first prototype LPE in the year 2008 as a PHA synthase with an acquired LA-polymerizing activity through *in vitro* and *in vivo* experiments (*20*). The first clue of LA-polymerizing activity was obtained through a water-organic solvent two-phase *in vitro* system. In that study, the activity of LA polymerization was judged by the formation of a white precipitate (probably a polymer). The activity towards LA-CoA was tested in the absence or presence of 3HB-CoA using representative PHA synthases belonging to the four classes of PHA synthases; PHA synthase from *Ralstonia eutropha* (class I), *Pseudomonas* sp. 61-3 (class II), *Synechosysytis* sp. PCC6803 (Class III) and *Bacillus* sp. INT005 (class IV) and three engineered (PhaC1$_{Ps}$ mutants) from *Pseudomonas* sp. 61-3. The engineered PHA synthases were two single mutants [Ser325Thr (ST) and Gln481Lys (QK)] and one double mutant carrying the two mutations (STQK). The two mutants were selected based on their improved activity and/or broader substrate specificity (*34*, *38*).

In the water-organic solvent two-phase *in vitro* system (illustrated in Figure 3) (*49*), the wild type synthases and mutants did not form a clear-polymer like precipitation with LA-CoA but did with 3HB-CoA. However, when LA-CoA was supplied together together with 3HB-CoA, one mutant, PhaC1$_{Ps}$(STQK) clearly exhibited a polymer-like precipitation. However to confirm polymer synthesis, it was necessary to verify polymer formation by further analysis. As reported in the first paper, the analysis of the precipitant revealed that the precipitant consisted of 36 mol% of the LA unit. Therefore, this was the first report ever of a PHA synthase with ability to incorporate LA unit [lactate-polymerizing enzyme (LPE)] to form P(LA-*co*-3HB) (*20*, *49*).

Downloaded by OHIO STATE UNIV LIBRARIES on August 28, 2012 | http://pubs.acs.org
Publication Date (Web): August 16, 2012 | doi: 10.1021/bk-2012-1105.ch014

Downloaded by OHIO STATE UNIV LIBRARIES on August 28, 2012 | http://pubs.acs.org
Publication Date (Web): August 16, 2012 | doi: 10.1021/bk-2012-1105.ch014

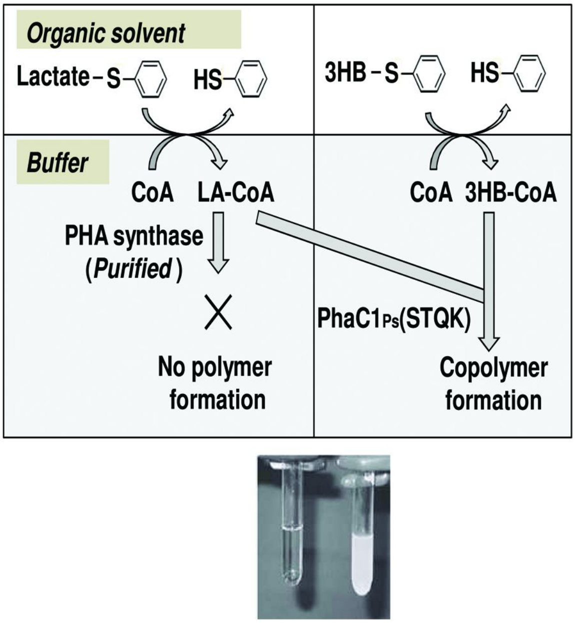

Figure 3. A two-phase in vitro polymerization assay system for the quantitative detection of LA-polymerizing activity of various PHA synthases. Polymer-like precipitation is shown on the right tube (white).

A key finding in this study was the LA polymerization dependence on the presence of 3HB-CoA. This showed that LA-polymerization proceeded in the presence of the preferred substrate of PhaC1$_{Ps}$ (STQK), (3HB-CoA). A similar phenomenon had been reported earlier during the synthesis of SCL/MCL using wild type PhaC1$_{Ps}$ where the addition of the preffered substrate (3HA-CoA) led to enhanced polymerization of the less favoured substrate (3HB-CoA) (*50*). Analogously, the mutant PhaC1$_{Ps}$(STQK) incorporated the less preferred substrate (LA-CoA) in the presence of the preferred substrate (3HB-CoA).

The finding that PhaC1$_{Ps}$(STQK) could polymerize LA was a demonstration of evolutionary engineering as a powerful tool for the generation of biocatalysts with desired properties. By demonstrating the *in vitro* activity of PhaC1$_{Ps}$(STQK) towards LA-CoA, it was presumed that heterologous expression of this LPE could result into an *in vivo* synthesis of LA-based polyesters thus creating a system for LA-based polyesters synthesis.

Downloaded by OHIO STATE UNIV LIBRARIES on August 28, 2012 | http://pubs.acs.org
Publication Date (Web): August 16, 2012 | doi: 10.1021/bk-2012-1105.ch014

Biosynthesis of Lactate (LA)-Based Polyesters

The Establishment of the First MCF for LA-Based Polyester Production

The finding of an LPE in an *in vitro* system aroused interest in the creation of an *in vivo* whole-cell system, for the production of LA-based polyesters such as P(LA-*co*-3HB). The whole-cell system offers several potential advantages over the *in vitro* biocatalysis, including the opportunity to interface heterologous reactions with intrinsic metabolic pathways (e.g. supply of LA from sugars via glycolysis) and the fact that enzyme preparation steps are eliminated. Furthermore, when employing cofactor mediated reactions such as NADPH-dependent redox reactions, cofactor regeneration is achieved during sugar metabolism in the cells (*51*).

In the microbial LA-based polyester production, the LA-CoA monomer supply for LPE was necessary. Intrinsically, the microorganisms employed as hosts, *Escherichia coli* JM109 could produce LA (*52*). However, LA and LA-CoA metabolic link had to be constructed and this was done by heterologously expressing a propionyl-CoA transferase (PCT) gene in *E. coli* (*20*). PCT catalyzes the inter-transfer reactions of CoA between CoA esters of small carbonic acids and their free acids such as acetate, propionate and LA. Prior to the assembly of the pathways for the construction of the MCF for LA-based polyester production, confirmation of LA-CoA supply *in vivo* was essential. By capillary electrophoresis/MS (CE/MS), the Megasphaera elsdenii PCT was shown to supply LA-CoA monomer better than the other assayed PCT enzymes *in vivo* (*20*). The biosynthetic pathway for LA-based polyesters production is illustrated in Figure 4. The PCT, LPE and 3HB-CoA monomer supplying enzymes could be expressed from a vector construct and be functional *in vivo* (*20*). The 3HB supplying enzymes employed, PhaA which is a β-ketothiolase and PhaB, NADPH dependent acetoacetyl-CoA reductase from *Ralstonia eutropha* have already been reported to be functional in *E. coli* (*53–55*) .

Therefore, the recombinant *E. coli* cells harboring the vector carrying all the essential genes and cultivated on a medium supplemented with sugars such as glucose could be expected to synthesize P(LA-*co*-3HB) in a similar fashion as the *in vitro* assay. Then after cultivation of the recombinant cells, several analyses were essential to confirm LA incorporation into the polymers. GC/MS analysis detected ethyl-LA (ethanolysis product of LA) suggesting the *in vivo* incorporation of LA unit into the polymer to form P(6 mol% LA-*co*-3HB) (*20*). However, further analysis was necessary to confirm LA incorporation into the polymer. NMR techniques have been applied successfully to the analysis of polymers including polyesters and ^{1}H NMR spectra permits determination of polymer composition (*56*). When the purified polymer sample was subjected to ^{1}H NMR, it exhibited signals characteristic of a copolymer and the first LA-based polyester synthesized in the prototype MCF was confirmed to be P(LA-*co*-3HB). In agreement with the *in vitro* experiment, in the absence of 3HB-CoA monomer supplying pathway, there was no polymer formation, confirming the requirement of 3HB-CoA for LA polymerization to proceed (*20*).

When polymers are copolymerized, the properties of the materials are altered as a result of decreased crystallinity and melting temperatures (T_m) (*56*). Therefore, the incorporation of 6 mol% LA was expected to affect properties of P(3HB). The characterization of the P(6 mol% LA-*co*-3HB) polymer demonstrated that the copolymer had a different properties e.g. lower melting temperature (T_m) in comparison to P(3HB) (*20*). This analysis indicated that varying the LA fraction in the copolymer could vary polymer properties (*20*). Therefore, towards the complete biological production of PLA, further engineering of LPE with reduced or lost 3HB-polymerizing activity was thought to be crucial. For the enrichment of the LA fraction in the copolymer, the same LPE was targeted to synthesize LA-based polyesters with new properties. Additionally, such strategies such as metabolic engineering were as well expected to enrich the LA fractions in the copolymers.

Downloaded by OHIO STATE UNIV LIBRARIES on August 28, 2012 | http://pubs.acs.org
Publication Date (Web): August 16, 2012 | doi: 10.1021/bk-2012-1105.ch014

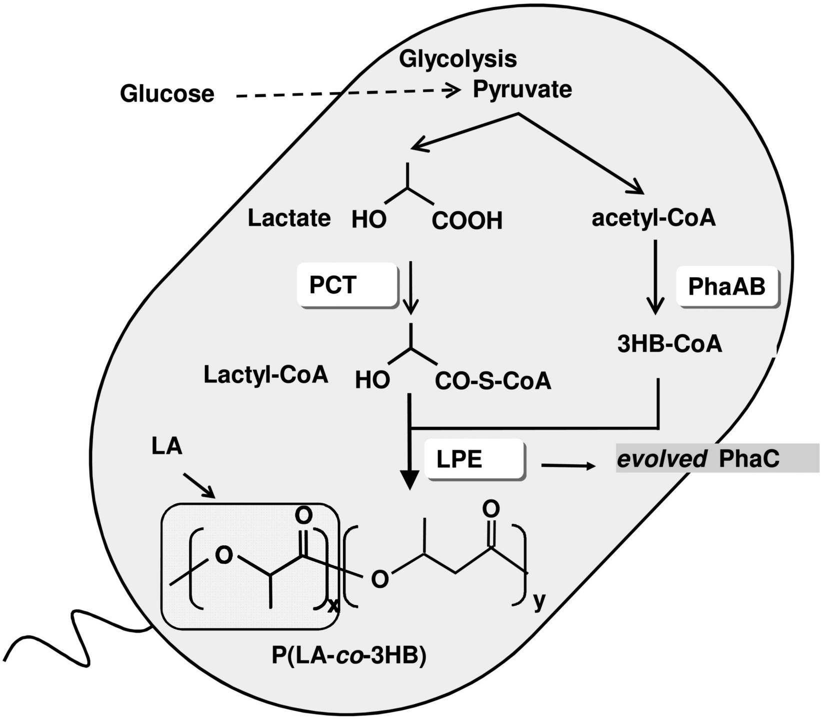

Figure 4. The microbial cell factory (MCF), Escherichia coli harboring PCT, PhaAB and LPE for the production of P(LA-co-3HB). Lactic acid is intrinsically produced by E. coli.

Downloaded by OHIO STATE UNIV LIBRARIES on August 28, 2012 | http://pubs.acs.org
Publication Date (Web): August 16, 2012 | doi: 10.1021/bk-2012-1105.ch014

LA Unit Enrichment in the Copolymers

Copolymers exhibit various mechanical and thermal properties depending on monomer composition therefore they could be useful for many applications (*57*). During the *in vitro* synthesis of P(LA-*co*-3HB), 3HB-CoA and LA-CoA were added in equimolar proportions and P(LA-*co*-3HB) with 36 mol% LA was synthesized (*20*). The low *in vivo* LA fraction in the copolymer was thought to be limited by the supply of LA-CoA. Therefore, in a subsequent study, the enhancement of LA supply and reduction of 3HB supply was attempted (*58*). *E. coli* metabolizes glucose via glycolysis to produce pyruvate which is sequentially converted to acetyl-CoA under aerobic conditions (*59*). Conversely, lactate is well produced from pyruvate under anaerobic conditions since lactate dehydrogenase (*ldhA*) is induced under anaerobic conditions and acidic pH (*58–60*). *E. coli* W3110, which overproduces LA under anaerobic conditions was used as a host strain for P(LA-*co*-3HB) synthesis in place of the earlier used *E. coli* JM109 under anaerobic conditions (*52*, *61*). Under these conditions, the recombinant *E. coli* W3110 cells expressing PCT, LPE and 3HB-CoA supplying enzymes accumulated P(LA-*co*-3HB) with 47 mol% LA however with reduced polymer content (2%). These results indicated that the use of anaerobic conditions was effective in enriching the LA fraction in the copolymers however, it was inefficient due to low polymer yields (*58*).

To increase polymer content of the LA-enriched copolymers, focus was directed towards another metabolically engineered LA-overproducing mutant strain. The *E. coli* JW0885 (Δ*pflA*), that shuts off the formate production node and consequently produces large amounts of LA from glucose was used for P(LA-*co*-3HB) synthesis (*59*, *62*). As predicted this mutation led to improved LA fraction (26 mol %) in the copolymer with relatively high polymer content (44 wt %) under aerobic conditions (*27*). This clearly indicated that this metabolic engineering strategy was effective in improving LA fractions and polymer yields simultaneously.

Further Engineering of LPE

To further create LA-based polyesters with higher LA fractions and polymer content, *E. coli* JW0885 was used as a controllable MCF platform for P(LA-*co*-3HB) polyester production. In a subsequent study, based on the improved activity of a point mutation at position 420 (F420S) of a class I PHA synthase ($PhaC_{Re}$) from *Ralstonia eutropha,* a similar mutation was introduced into the ancestral LPE [$PhaC1_{Ps}$(STQK)] to create a triple mutant of LPE with S325T and Q481K along with a new mutation, F392S which corresponds to F420S of $PhaC_{Re}$ (*27*, *39*). When the new further engineered LPE [$PhaC1_{Ps}$ (STQKFS)] was expressed along with PCT and PhaAB in *E. coli* JW0885, a copolymer with 45 mol% LA and polymer content of 62 wt% was synthesized in comparison with P(26 mol% LA-*co*-3HB) obtained with the ancestral LPE, $PhaC1_{Ps}$(STQK) under aerobic culture conditions (*27*). Additionally, the cells harboring $PhaC1_{Ps}$ (STQKFS) synthesized P(LA-*co*-3HB) with 62 mol% LA with polymer content of 12 wt% under anaerobic culture conditions. During the same study, saturation mutagenesis of LPE on the same site (position 392) yielded mutants that gave varying LA fractions in the copolymers however; F392S was superior to the other mutants in incorporating LA. This study demonstrated the effectiveness of enzyme engineering of the LPE towards two directions; there was improved LA incorporation and polymer yield improvement for both aerobic and anaerobic culture conditions (*27*).

Synthesis of LA-Based Polyesters with Different Monomeric Units

Despite the wide acceptance of PLA for many applications, flexibility limits its range of applicability (*15*). The chemically synthesized PLA has been modified by means of adding plasticizers, copolymerization or cross-linkage of polymer chains (*10*, *12*). For biologically synthesized LA-based polymers, composition control of monomer constituents is effective to alter polymer properties (*6*). Some reports have indicated that copolymerization of 3HB with other PHA constituents e.g. 3HV, 3-hydroxyhexanoate (3HHx) and other MCL 3-hydroxyalkanoates (MCL-3HAs) to form P(3HB-*co*-3HV), P(3HB-*co*-3HHx), and P(3HB-*co*-MCL-3HAs), respectively results into copolymers exhibiting flexibility and altered thermal and physical properties compared to P(3HB) homopolymer (*31*, *43*, *50*, *63*, *64*). Based on these reports, the incorporation of 3HV could be thought to render LA-based polyesters more flexible. In a study investigating 3HV incorporation into LA-based polyesters, Shozui et al. used propionate as a precursor for generating 3HV in *E. coli*. When employing *E. coli* as a host for the production of 3HV-containing polyesters, 3HV precursor supply is essential and propionate or valerate have already been shown to be suitable precursors (*64*, *65*). In *E. coli*, propionate can be converted by the heterologously expressed PhaAB to form the 3HV monomer; 3-hydroxyvaleryl-CoA which could be finally polymerized into the copolymer by the LPE with broad substrate specificity (*29*, *43*, *45*, *64*). In that study various concentrations of propionate were used so as to regulate the 3HV fraction (*29*). The analysis of the copolymers produced under this system revealed the incorporation of 3HV to form a terpolyester, P(LA-*co*-3HB-*co*-3HV) with up to 7.2 mol% of 3HV and varying mole fractions of LA. Further analysis of this terpolyester by NMR revealed an interesting finding; the presence of the dyad sequence, LA-3HV suggesting that LPE could connect LA with other monomeric constituents and thus synthesizing various LA-based polyesters with random sequences (*29*).

Analogously, Shozui et al. investigated the production of LA-based polyesters incorporating long-chain HAs which are known to add flexibility to polyesters (*42*, *66*). The terpolyester, P(LA-*co*-3HB-*co*-3HHx) was synthesized by expressing LPE together with PhaJ4 [(*R*)-specific enoyl-CoA hydratase from *Pseudomonas aeruginosa*] and PCT in *E. coli* (*66*, *67*). By supplying butyrate, 3HHx could be incorporated via the fatty acid biosynthesis pathway by the action of PhaJ4 (*45*, *68*). Analysis of the synthesized polymers indicated that the HHx mole fractions were varied by butyrate concentrations and up to 38 mol% of HHx-containing LA-based terpolyesters were produced (*66*). Furthermore, Matsumoto et al. demonstrated the incorporation of MCL (C4-C12) monomers into LA-based polyesters (*69*). Interestingly, under the same study, LPE was found to polymerize glycolate which is structurally similar to LA but naturally

Downloaded by OHIO STATE UNIV LIBRARIES on August 28, 2012 | http://pubs.acs.org
Publication Date (Web): August 16, 2012 | doi: 10.1021/bk-2012-1105.ch014

Downloaded by OHIO STATE UNIV LIBRARIES on August 28, 2012 | http://pubs.acs.org
Publication Date (Web): August 16, 2012 | doi: 10.1021/bk-2012-1105.ch014

not known to be polymerized by PHA synthases (*69*). All these results further demonstrated that LPE is capable of polymerizing a number of monomers to produce LA-based polymers with new properties and thus expanding potential applications.

High LA-Containing Polyesters

In the initial reports, P(6 mol% LA-*co*-3HB) was synthesized by copolymerization of the two monomeric units, LA and 3HB (*20*). The LA-CoA monomer was supplied by propionyl-CoA transferase (PCT) and 3HB-CoA generated via successive reactions catalyzed by β-ketothiolase (PhaA) and acetoacetyl-CoA reductase (PhaB), respectively (*55*). In the absence of 3HB-CoA supplying pathway, polymer formation was not detected, demonstrating that 3HB was essential for LA polymerization (*20*, *49*). In the follow-up studies, emphasis was on anaerobic culture conditions, use of LA overproducing *E. coli* mutants and further evolution of LPE so as to increase LA fraction in the copolymers (*27*, *58*). These combined strategies elevated LA fraction up to 62 mol%. Characterization of the copolymers by NMR demonstrated the LA-clustering sequence suggesting that LPE was capable of polymerizing LA sequentially (*58*). Therefore, in the next stage of improved LA fraction polymer production, a system lacking the expression of PhaAB that eliminated the supply of the preferred monomer, 3HB-CoA was designed. However, due to the absolute requirement of 3HB-CoA by LPE, the 3HB-CoA monomer was substituted by 3HV-CoA to enhance LA polymerization since the formation of LA-3HV sequence LPE had been demonstrated (*29*). By using this design, LPE could be expected to form P(LA-*co*-3HV) with LA being regulated by varying the concentration of 3HV precursor. The system employed recombinant *E. coli* cells harboring PCT, LPE [PhaC1$_{Ps}$(STQK)] and PhaJ4 that could supply 3HV from valerate through the β-oxidation pathway as illustrated in Figure 5 (*30*, *67*).

By varying the valerate concentrations, polymers with different LA fractions were obtained. Interestingly, terpolyester [P(LA-*co*-3HB-*co*-3HV)] with 96 mol% LA was synthesized at valerate concentrations of 0.5 $g\ l^{-1}$ (*30*). This polymer having 96 mol% of LA, designated as LA96, could be thought to be similar in material properties to PLA homopolymer hence its analysis was of interest. The monomer composition was; 96 mol% LA, 1 mol% 3HB and 3 mol% 3HV. The thermal properties of LA96 were comparable to those of chemically synthesized PLAs however; the slight differences could be accounted for by the presence of 3HB and 3HV monomers in LA96 (*30*). Furthermore, LA96 was shown to be capable of stereocomplexing with chemically synthesized PLLA as well as PDLA.

Although hypothetically it seems possible to synthesize 100% PLA by microorganisms, the synthesis of PLA-like polymer, LA96 was a tremendous achievement and it indicated that LA-based polyesters with high LA fractions could be synthesized microbially. Indeed, other PLA-like polymers were synthesized when the prototype LA-based polymer production system was transferred to *Corynebacterium glutamicum*. When *C. glutamicum* expressing LPE and LA-CoA and 3HB-CoA monomer supplying pathways along with *ldhA* (lactate dehydrogenase) for the supply of LA, P(LA-*co*-3HB) with 96.8 mol%

LA was synthesized (*26*). Unlike *E. coli*, recombinant *C. glutamicum* with the absence of 3HB-CoA supplying pathway could synthesize P(LA-*co*-3HB) with 99.3 mol% LA (*26*). Although the *C. glutamicum* platform is at its infancy, the results demonstrated *C. glutamicum* as an applicable platform for the synthesis of food grade PLA-like polyesters (*26*). All these reports underscore the fact that PLA-like polyesters can be synthesized microbially in a single-step process. The production of these PLA-like polyesters was coupled with low polymer content and the polymers had low molecular weights compared with polymers with low LA fractions (*26*, *30*). However, these challenges could be addressed in future as more information about biosynthesis of LA-based polyesters becomes available.

Downloaded by OHIO STATE UNIV LIBRARIES on August 28, 2012 | http://pubs.acs.org
Publication Date (Web): August 16, 2012 | doi: 10.1021/bk-2012-1105.ch014

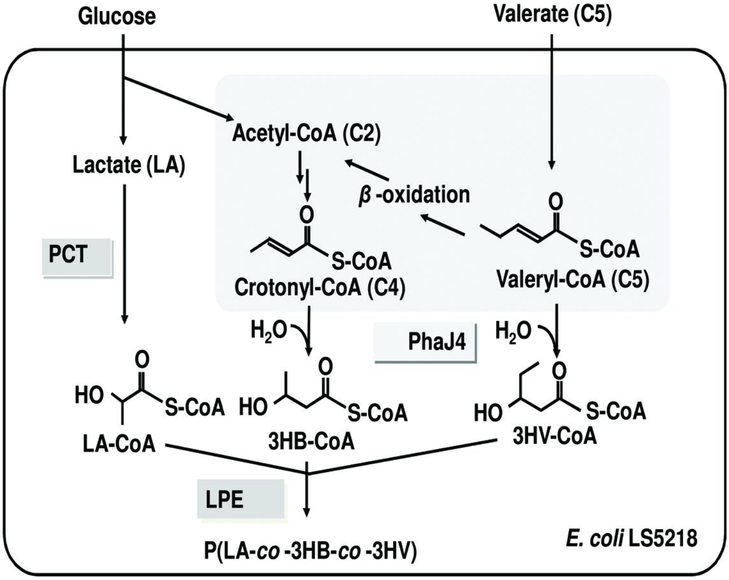
Glucose
Valerate (C5)
Acetyl-CoA (C2)
Lactate (LA)
β-oxidation
PCT
S-CoA
Crotonyl-CoA (C4)
S-CoA
Valeryl-CoA (C5)
H2O
PhaJ4
H2O
HO
S-CoA
LA-CoA
HO
S-CoA
3HB-CoA
HO
S-CoA
3HV-CoA
LPE
P(LA-co-3HB-co-3HV)
E. coli LS5218

Figure 5. Metabolic pathways for the synthesis of high LA-containing polyesters including LA96.

Characteristics of LA-Based Polyesters

Enantiomeric Purity of LA in the Copolymers

The full characterization of these new members of the PHA family is essential for precise estimation of the quality and performance of the biosynthesized polymers. The enantiomeric purity has attracted the attention of a number of professionals as it influences the properties of materials (*1*). In the synthesis of LA-based polyesters, the enantiospecificity can be ascribed to LPE that takes part in the ultimate step of polymerization (*20*, *49*, *58*). The conformation of the LA enantiomer incorporated into the polyester was analyzed chiral HPLC and the sample of P(LA-*co*-3HB) exhibited peaks characteristic of (*R*)-LA and (*R*)-3HB (*58*). Already the wild type PHA synthases have been reported to specifically incorporate the *R*-form in the 3HA units, 3HB inclusive (*33*, *70*). Accordingly, the engineered PHA synthase, PhaC1$_{\mathrm{Ps}}$(STQK) (LPE), was found to retain its enantiospecificity and it synthesized P[(*R*)-LA-*co*-(*R*)-3HB] *in vivo*. Furthermore, in an *in vitro* analysis, when (*S*)-LA-CoA was supplied together with (*R*)-3HB-CoA for the synthesis of a copolymer, only P(3HB) homopolymer was formed (*20*, *49*). This confirmed that LPE cannot polymerize (*S*)-LA (*49*). In another study regarding the enantiospecificity of native PHA synthases, Valentin et al. demonstrated that the rate of hydrolysis of LA-CoA by the *A. vinosum* PHA synthase was faster with (*R*)-LA-CoA than (*S*)-LA-CoA (*47*). This result gives further support on the preference of LPE for (*R*)-LA-CoA.

The enantioselectivity towards LA in the *in vivo* system should as well be considered on the side of monomer supplying enzymes i.e., LDH and PCT. Typically, there are two kinds of LDH, which selectively catalyze the formation of either (*R*)-LA or (*S*)-LA from pyruvate (*52*, *71*). *E. coli* intrinsically produces (*R*)-LA which is catalyzed by D-LDH. The (*R*)-LA is subsequently converted into LA-CoA by PCT. However, PCT has no strict enantiospecificity and could catalyze the CoA transfer towards the formation of both (*R*)-LA-CoA and (*S*)-LA-CoA (*6*). Generally, the enantiomeric configuration of LA in the LA-based polyesters is determined by the enantiospecificity of LDH and LPE.

The chirality of LA affects properties of the polymers and the homopolymers of either enantiomer, P[(*S*)-LA](PLLA) and P[(*R*)-LA] (PDLA) are crystalline with melting temperatures (T_m) of about 180°C and glass transition temperatures (T_g) of 55°C (*57*). The stereocomplexation between PLLA and PDLA has been achieved and this has led to polymers with high thermostability (T_m of 245°C) (*72*). It cannot therefore be overemphasized that the control LA enantiomer is crucial in regulating polymer properties. In the current bio-chemo process system for the synthesis of PLA, the enantiomeric purity (e.e) of LA-based polymers solely relies on the e.e. of the monomers (*1*, *8*). Therefore, the need of optically pure monomers increases production costs. The fermentation process for the production of LA proceeds at ambient temperatures (30°C) which are enough to avoid thermal epimerization of LA. It is therefore practical for the MCF to synthesize polyesters with high enantiomeric purity without any requirement for chiral separation procedures (*6*). This high enantioselectivity of microorganisms is an advantage in relation to the conventional processes for the synthesis of PLA and its copolymers.

Sequential Structures of LA-Based Polyesters

The sequence of monomers in the copolymer i.e. random or block copolymers does affect polymer properties (*73*). NMR is one of the most powerful tools that can be employed for the analysis of monomer distribution in the copolymer (*12*). The NMR signals of the LA unit are affected by both neighboring monomeric units and a triad sequence of LA units can be distinctly recognized by NMR

Downloaded by OHIO STATE UNIV LIBRARIES on August 28, 2012 | http://pubs.acs.org
Publication Date (Web): August 16, 2012 | doi: 10.1021/bk-2012-1105.ch014

Downloaded by OHIO STATE UNIV LIBRARIES on August 28, 2012 | http://pubs.acs.org
Publication Date (Web): August 16, 2012 | doi: 10.1021/bk-2012-1105.ch014

spectral analysis (*6*, *56*). In particular, the methine group of the LA unit is a good 'fingerprint' for characterization. In the case of P(LA-*co*-3HB), four triad sequences for the LA unit could be expected in principle i.e., LA-LA -LA, LA-LA -3HB, 3HB-LA -3HB and 3HB-LA -LA. On analysis of P(LA-*co*-3HB) synthesized by *E. coli*, the ^{1}H-^{13}C COSY-NMR profile showed sufficient amounts of LA clustering sequences, LA-LA and LA-LA-LA in the random copolymer (*58*). This indicated that LPE is capable of incorporating LA unit next another LA unit sequentially. However, it should be noted that the copolymer synthesized was a random copolymer. The clustering of LA units next to each other suggested that LA-enriched copolymers could be biosynthesized. Indeed, polymers with 96 mol% of LA (LA96) were synthesized (*30*). The ^{13}C-NMR spectra of LA96 showed strong signals for LA and weak signals for 3HB and 3HV, indicating LA96 was rich in LA. The ^{1}H-NMR spectra showed signals which were equal to the characteristic resonances for an LA unit neighboring a 3HB unit in P(LA-*co*-3HB) as reported by Yamada et al. (*58*). Additionally, when a terpolymer, P(LA-*co*-3HB-*co*-3HV), with lower LA fractions was analyzed, ^{1}H-NMR confirmed that LA and 3HV units were incorporated in the same polymer chain (*29*). These signals clearly indicated that LA96 was a P(LA-*co*-3HB-*co*-3HV) terpolymer and not a blend of PLA and P(3HB-*co*-3HV). Here, it could be seen that the prototype LPE is a truly LA-polymerizing enzyme with broad substrate specificity. Its derivatives could be expected to expand substrate specificity and reactivity.

Molecular Weights

The molar mass of polymers has been known to affect polymer properties related to processability and mechanical properties such as tensile strength (*8*, *74*). In the synthesis of LA-based copolymers, there was an inverse relationship between molecular weight and the LA fraction in the copolymer (Table II) (*28*). This phenomenon maybe attributed to two factors; the relative supply of LA-CoA or the relatively higher incorporation activity of LA over that of 3HB by LPE. However, this inverse relationship between LA fraction and molecular weight is not clear at the moment hence more work is expected to clarify this phenomenon.

Thermal and Mechanical Properties of LA-Based Polyesters

The quality of polymeric materials is determined by polymer properties such as heat resistance and crystallinity (*57*). The glass transition temperature (T_g) and melting temperature (T_m) affects the quality and determines the suitability of polymers for application. These thermal properties can be well determined by differential scanning calorimetry (DSC) (*8*). Table II summarizes the thermal and mechanical properties of LA-based polyesters with various LA fractions along with their corresponding molecular weights. To gain insight into the properties of microbially synthesized LA-based polyesters, their thermal and mechanical properties are compared with those of chemically synthesized PLA and P(3HB). PLA and P(3HB) have T_gs of 61°C and -7°C, respectively. These differences in T_gs accounts for the transparent and opaque nature of PLA and P(3HB), respectively. On the other hand, the copolymers, P(LA-*co*-3HB) displayed T_g values of -6 to 34°C depending on the LA fraction of the copolymers as shown in Table II (*28*). On the other hand, the melting temperatures (T_ms) and melting enthalpies (ΔH_m) of copolymers with 29 - 47 mol% LA were lower than those of P(3HB) and PLA homopolymers. This suggested that the packing of the crystals in the copolymers is looser hence copolymerization inhibited the tight packing of crystals associated with the individual homopolymers (*15*). This observation of altered thermal properties was in tandem with earlier reported cases whereby copolymerization of 3HB with 3-hydroxyalkanoates decreased crystallinity depending on the HA fractions anderson (*56*, *74*). When the films of the copolymers were prepared, the P(LA-*co*-3HB)s had semitransparent films and transparency was observed to increase with increase in LA fraction in the P(LA-*co*-3HB) copolymer (*28*). In particular, the copolymers with LA fraction more than 15 mol%, transparency was significant suggesting that crystallinity was effectively lowered concomitant with lowered T_m and ΔH_m. Conversely, the P(3HB) homopolymer film was noted to shrink and became opaque whereas the chemically synthesized PLA homopolymer formed a clear film (*28*).

The P(LA-*co*-3HB)s displayed mechanical properties different from their respective PLA and P(3HB) copolymers. The Young's modulus of the copolymers were; 148 - 905 Mpa and were lower than that of PLA (1020 Mpa) and P(3HB)(1079 Mpa). The young modulus showed an inverse relationship with LA fractions in the copolymers. Additionally, the elongation at break of the P(LA-*co*-3HB) copolymers was relatively higher than that of PLA and P(3HB). Particularly, the elongation of P(LA-*co*-3HB) with 29 mol% LA had an elongation to break of 150%. This clearly demonstrated that the copolymers are more stretchy and pliable than the respective homopolymers. PLA and P(3HB) lack impact resistance hence this drawback could be overcome by using the copolymers of P(LA-*co*-3HB). The stretching properties of P(LA-*co*-3HB) copolymers compared favorably with those of P(3HB-*co*-3HA) copolymers reported by Matsusaki et al., although the T_gs of the two sets of the copolymers distinguishes them (*28*, *50*).

Additionally, the PLA-like polymer, LA96 polymer that had similar properties as chemically synthesized PLA as described in Table II. (*30*). Furthermore, LA96 showed that it could form a stereocomplex with chemically synthesized PLLA of the same molecular weight. The stereocomplex formed had a much higher T_m (201.9°C) which was higher than that of each polymer (*30*). Although there were small fractions of 3HB and 3HV, the properties of LA96 suggested that PLA-like polymers could be synthesized microbially and it could be used as PLA homopolymer for certain functions.

Downloaded by OHIO STATE UNIV LIBRARIES on August 28, 2012 | http://pubs.acs.org
Publication Date (Web): August 16, 2012 | doi: 10.1021/bk-2012-1105.ch014

Downloaded by OHIO STATE UNIV LIBRARIES on August 28, 2012 | http://pubs.acs.org
Publication Date (Web): August 16, 2012 | doi: 10.1021/bk-2012-1105.ch014

Table II. Thermal and mechanical properties of P(LA-*co*-3HB)s[a] and LA96[b]

monomer composition (mol%)		*molecular weights*		*mechanical properties*			*thermal properties*		
LA	*3HB*	M_w *(x10⁴)*	M_w/M_n	*tensile strength (Mpa)*	*Young's modulus (Mpa)*	*elongation at break (%)*	T_g *(°C)*	T_m *(°C)*	ΔH_m *(cal g⁻¹)*
100[c]	0	20		52±2	1020	2	60	153	2.2
47	53	7	2.3	7±2	153±15	84±20	-8, 34	140, 157	0.4, 1.9
40	60	7	3.5	6±0	148±10	64±7	-8, 30	140, 156	0.3, 1.4
29	71	9	2.2	7±7	154±5	156±34	-8, 25	141,158	0.2, 0.9
15	85	82	2.4	10±0	194±5	75±2	-9, 19	149, 167	0.6, 3.2
4	96	74	4.6	30±4	905±136	7±1	-6	160, 174	1.8, 5.4
0	100	70	2.3	19±1	1079±215	9±1	-7	159, 176	1.6, 9.9
LA96		1.3	1.7	ND	ND	ND	49.3	153.3	9.5

[a] Data from Yamada et al. (*28*); [b] Shozui et al. (*30*); [c] Zaman et al. (*75*) .

Downloaded by OHIO STATE UNIV LIBRARIES on August 28, 2012 | http://pubs.acs.org
Publication Date (Web): August 16, 2012 | doi: 10.1021/bk-2012-1105.ch014

Conclusions and Future Perspectives

PLA is one of the most promising bio-based biodegradable polymers for a wide range of applications and with potential to replace petrochemical-derived commodity plastics. At the inception of the biosynthesis of LA-based polyesters project, LA was regarded special as it is a monomeric constituent of PLA. Up to the first pioneering report of LA inclusion to form LA-based polyesters in 2008, there was no clear answer as to why LA was not a member of the over 150 members of the PHA family, some of which are shown in Figure 6.

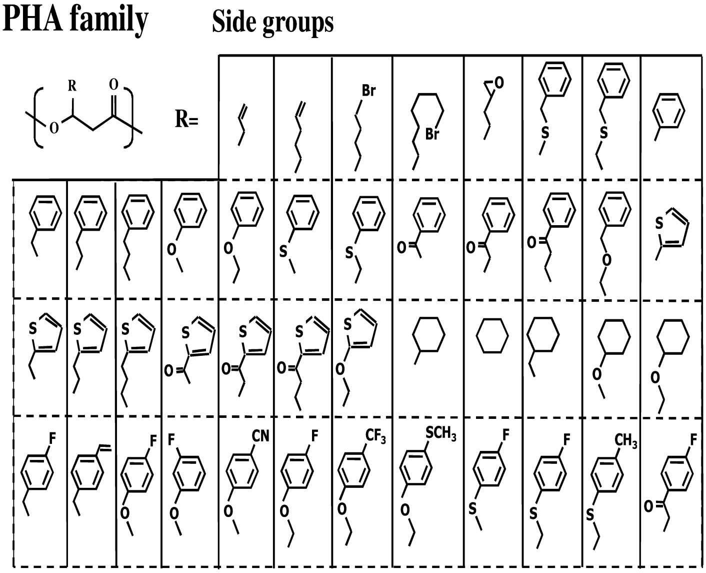

Figure 6. Some of the monomeric constituents of the PHA family. LA-based polyesters could be synthesized to incorporate any monomeric constituent with the above diversity of side groups to create materials with novel properties.

The incorporation of LA unit into the PHA family was due to the discovery of LPE. In this case, this was a rare discovery of engineering an enzyme to polymerize a compound naturally not known to be polymerized. This discovery eventually led to the establishment of microbial systems for the synthesis of LA-based polyesters with high enantiomeric purity and was a leap forward in the field of PLA research and already the same principle has been adopted by some research groups (*76*). In this project, pathway optimization concept for LA metabolism was made evident and indeed the utilization of a pathway-engineered mutant of the host strain was effective for enhanced LA fraction in the copolymers as well as the use of anaerobic conditions for polyester production.

Downloaded by OHIO STATE UNIV LIBRARIES on August 28, 2012 | http://pubs.acs.org
Publication Date (Web): August 16, 2012 | doi: 10.1021/bk-2012-1105.ch014

At present, LA-based polymers with up to 99.3 mol% LA have been biosynthesized. Strategies such as using different microorganisms with intrinsic ability or metabolically engineered to produce high LA may be useful towards the biosynthesis of PLA homopolymer as already demonstrated by employing *C. glutamicum*. Furthermore, the continued directed evolution of LPE might be useful towards the engineering of mutants with superior LA-polymerizing ability. This was evident on the mutation of the LPE at F392S which led to improved LA fractions in the LA in the copolymers as well as improved polymer yields compared to the ancestral LPE [PhaC1$_{Ps}$ (STQK)]. In addition, site specific mutations of other PHA synthases corresponding to positions at beneficial sites of the ancestral LPE might be useful towards high LA incorporation in the copolymers.

Although this review characterizes a milestone in the single-step synthesis of LA-based polyesters, incorporation of the other monomeric units along with LA will be an attractive point of research e.g. the creation of functionalized polymers. Already, the incorporation of 3HV, 3HHx and MCL-3HAs (C4-C12) into LA-based polymers was achieved. Further, it is interesting to note that copolymers incorporating 2-hydroxy acids such as 2-hydroxybutyrate and glycolate may lead to copolymers with novel properties (*77*). Meanwhile, the issue of inverse relationship between LA fractions and molecular weights as well as improved polymer yields remains to be addressed.

This chapter has reviewed the background of LA-based polyester biosynthesis from monomers supplied by a single carbon source, glucose. Regarding this system for LA-based polymer production, it forms a platform transferrable to other microorganisms. As already mentioned, the transfer of LA-based polymer production system into *Corynebacterium glutamicum* led to the synthesis of almost 100% PLA. Therefore, the transfer of LA-based polymer production to other microorganisms such as lactic acid bacteria as well as plants is an attractive target. Further optimization of this system and recruitment of cheaper carbon sources such as molasses, municipal wastes and even cellulosic biomass will definitely lead to the cost-effective industrial production of LA-based polyesters with high optical purity and a full industry independent of the chemical synthesis of PLA.

References

1. Auras, R.; Harte, B.; Selke, S. *Macromol. Biosci.* **2004**, *4*, 835–864.
2. Carrasco, F.; Pages, P.; Gamez-Perez, J.; Santana, O. O.; Maspoch, M. L. *Polym. Degrad. Stab.* **2010**, *95*, 116–125.
3. Lasprilla, A. J.; Martinez, G. A. R.; Lunelli, B. H.; Jardini, A. L.; Filho, R. M. *Biotech. Adv.* **2011**, DOI: 10.1016/j.biotechadv.2011.06.019.
4. Gupta, B.; Revagade, N.; Hilborn, J. *Prog. Polym. Sci.* **2007**, *32*, 455–482.
5. Tokiwa, Y.; Calabia, B. P. *Appl. Microbiol. Biotechnol.* **2006**, *72*, 244–251.
6. Taguchi, S. *Polym. Degrad. Stab.* **2010**, *95*, 1421–1428.
7. Rasal, R. M.; Janorkar, A. V.; Hirt, D. E. *Prog. Polym. Sci.* **2010**, *35*, 338–356.

Downloaded by OHIO STATE UNIV LIBRARIES on August 28, 2012 | http://pubs.acs.org
Publication Date (Web): August 16, 2012 | doi: 10.1021/bk-2012-1105.ch014

8. Inkinen, S.; Hakkarainen, M.; Albertsson, A. C.; Sodergard, A. *Biomacromolecules* **2011**, *12*, 523–532.
9. Zhang, M.; Thomas, N. L. *Adv. Polym. Tech.* **2011**, *30*, 67–79.
10. Saulnier, B.; Ponsart, S.; Coudane, J.; Garreau, H.; Vert, M. *Macromol. Biosci.* **2004**, *4*, 232–237.
11. Lim, L. T.; Auras, R.; Rubino, M. *Prog. Polym. Sci.* **2008**, *33*, 820–852.
12. Kricheldorf, H. R. *Chemosphere* **2001**, *43*, 49–54.
13. Ozkoc, G.; Kemaloglu, S. *J. Appl. Polym. Sci.* **2009**, *114*, 2481–2487.
14. Chisholm, M. H. *Pure Appl. Chem.* **2010**, *82*, 1647–1662.
15. Drumright, R. E.; Gruber, P. R.; Henton, D. E. *Adv. Mater.* **2000**, *12*, 1841–1846.
16. Nampoothiri, K. M.; Nair, N. R.; John, R. P. *Bioresour. Technol.* **2010**, *101*, 8493–8501.
17. Corma, A.; Iborra, S.; Velty, A. *Chem. Rev.* **2007**, *107*, 2411–2502.
18. Matsumoto, K.; Taguchi, S. *Appl. Microbiol. Biotechnol.* **2010**, *85*, 921–32.
19. Pleiss, J. *Curr. Opin. Biotechnol.* **2011**, *22*, 611–617.
20. Taguchi, S.; Yamadaa, M.; Matsumoto, K.; Tajima, K.; Satoh, Y.; Munekata, M.; Ohno, K.; Kohda, K.; Shimamura, T.; Kambe, H.; Obata, S. *Proc. Natl. Acad. Sci. U.S.A.* **2008**, *105*, 17323–17327.
21. Rehm, B. H. A. *Biotechnol. Lett* **.2006**, *28*, 207–213.
22. SteinbŰchel, A.; Hein, S. *Adv. Biochem. Eng. Biotechnol.* **2001**, *71*, 81–123.
23. Gross, R. A.; Kalra, B. *Science* **2002**, *297*, 803–807.
24. SteinbŰchel, A.; Lutke-Eversloh, T. *Biochem. Eng. J.* **2003**, *16*, 81–96.
25. Rehm, B. H. *Curr. Issues Mol. Biol.* **2007**, *9*, 41–62.
26. Song, Y.; Matsumoto, K.; Yamada, M.; Gohda, A.; Brigham, J.; Sinskey, A. J.; Taguchi, S. *Appl. Microbiol. Biotechnol.* **2011**, DOI:10.1007/s00253-011.007.
27. Yamada, M.; Matsumoto, K.; Shimizu, K.; Uramoto, S.; Nakai, T.; Shozui, F.; Taguchi, S. *Biomacromolecules* **2010**, *11*, 815–819.
28. Yamada, M.; Matsumoto, K.; Uramoto, S.; Motohashi, R.; Abe, H.; Taguchi, S. *J. Biotechnol.* **2011**, *154*, 255–260.
29. Shozui, F.; Matsumoto, K.; Nakai, T.; Yamada, M.; Taguchi, S. *Appl. Microbiol. Biotechnol.* **2010**, *85*, 949–954.
30. Shozui, F.; Matsumoto, K.; Motohashi, R.; Sun, J. A.; Satoh, T.; Kakuchi, T.; Taguchi, S. *Polym. Degrad. Stab.* **2011**, *96*, 499–504.
31. Chen, G. Q. *Chem. Soc. Rev* **.2009**, *38*, 2434–2446.
32. Lutke-Eversloh, T.; Steinbuchel, A. *FEMS Microbiol. Lett* **.2003**, *221*, 191–196.
33. Rehm, B. H. A. *Biochem. J.* **2003**, *376*, 15–33.
34. Nomura, C. T.; Taguchi, S. *Appl. Microbiol. Biotechnol.* **2007**, *73*, 969–979.
35. Stubbe, J.; Tian, J. *Nat. Prod. Rep* **.2003**, *20*, 445–457.
36. Matsumoto, K.; Takase, K.; Aoki, E.; Doi, Y.; Taguchi, S. *Biomacromolecules* **2005**, *6*, 99–104.
37. Matsumoto, K.; Aoki, E.; Takase, K.; Doi, Y.; Taguchi, S. *Biomacromolecules* **2006**, *7*, 2436–2442.
38. Takase, K.; Taguchi, S.; Doi, Y. *J. Biochem* **.2003**, *133*, 139–145.

39. Normi, Y. M.; Hiraishi, T.; Taguchi, S.; Sudesh, K.; Najimudin, N.; Doi, Y. *Biotechnol. Lett* .**2005**, *27*, 705–712.
40. Taguchi, S.; Maehara, A.; Takase, K.; Nakahara, M.; Nakamura, H.; Doi, Y. *FEMS Microbiol. Lett.* **2001**, *198*, 65–71.
41. Matsumoto, K.; Takase, K.; Yamamoto, Y.; Doi, Y.; Taguchi, S. *Biomacromolecules* **2009**, *10*, 682–685.
42. Kichise, T.; Taguchi, S.; Doi, Y. *Appl. Environ. Microbiol.* **2002**, *68*, 2411–2419.
43. Taguchi, S.; Doi, Y. *Macromol. Biosci.* **2004**, *4*, 146–156.
44. Matsumoto, K.; Matsusaki, H.; Taguchi, K.; Seki, M.; Doi, Y. *Biomacromolecules* **2002**, *3*, 787–792.
45. Takase, K.; Matsumoto, K.; Taguchi, S.; Doi, Y. *Biomacromolecules* **2004**, *5*, 480–485.
46. Hiraishi, T.; Taguchi, S. *Mini-Rev. Org. Chem.* **2009**, *6*, 44–54.
47. Valentin, H. E.; Steinbuchel, A. *Appl. Microbiol. Biotechnol.* **1994**, *40*, 699–709.
48. Yuan, W.; Jia, Y.; Tian, J. M.; Snell, K. D.; Muh, U.; Sinskey, A. J.; Lambalot, R. H.; Walsh, C. T.; Stubbe, J. *Arch. Biochem. Biophys.* **2001**, *394*, 87–98.
49. Tajima, K.; Satoh, Y.; Satoh, T.; Itoh, R.; Han, X. R.; Taguchi, S.; Kakuchi, T.; Munekata, M. *Macromolecules* **2009**, *42*, 1985–1989.
50. Matsusaki, H.; Abe, H.; Taguchi, K.; Fukui, T.; Doi, Y. *Appl. Microbiol. Biotechnol.* **2000**, *53*, 401–409.
51. Cirino, P. C.; Sun, L. H. *Biotechnol. Progr.* **2008**, *24*, 515–519.
52. Zhou, S. D.; Causey, T. B.; Hasona, A.; Shanmugam, K. T.; Ingram, L. O. *Appl. Environ. Microbiol.* **2003**, *69*, 399–407.
53. Schubert, P.; Steinbuchel, A.; Schlegel, H. G. *J. Bacteriol.* **1988**, *170*, 5837–5847.
54. Peoples, O. P.; Sinskey, A. J. *J. Biol. Chem.* **1989**, *264*, 15293–15297.
55. Matsumoto, K.; Kobayashi, H.; Ikeda, K.; Komanoya, T.; Fukuoka, A.; Taguchi, S. *Bioresour. Technol.* **2011**, *102*, 3564–3567.
56. Anderson, A. J.; Dawes, E. A. *Microbiol. Rev.* **1990**, *54*, 450–472.
57. Sodergard, A.; Stolt, M. *Prog. Polym. Sci.* **2002**, *27*, 1123–1163.
58. Yamada, M.; Matsumoto, K.; Nakai, T.; Taguchi, S. *Biomacromolecules* **2009**, *10*, 677–681.
59. Zhu, J.; Shimizu, K. *Appl. Microbiol. Biotechnol.* **2004**, *64*, 367–375.
60. Alexeeva, S.; de Kort, B.; Sawers, G.; Hellingwerf, K. J.; de Mattos, M. J. T. *J. Bacteriol.* **2000**, *182*, 4934–4940.
61. Shukla, V. B.; Zhou, S.; Yomano, L. P.; Shanmugam, K. T.; Preston, J. F.; Ingram, L. O. *Biotechnol. Lett.* **2004**, *26*, 689–693.
62. Baba, T.; Ara, T.; Hasegawa, M.; Takai, Y.; Okumura, Y.; Baba, M.; Datsenko, K. A.; Tomita, M.; Wanner, B. L.; Mori, H. *Mol. Syst. Biol.* **2006**, *2*, 2006–0008.
63. Doi, Y.; Kitamura, S.; Abe, H. *Macromolecules* **1995**, *28*, 4822–4828.
64. Slater, S.; Gallaher, T.; Dennis, D. *Appl. Environ. Microbiol.* **1992**, *58*, 1089–1094.

Downloaded by OHIO STATE UNIV LIBRARIES on August 28, 2012 | http://pubs.acs.org
Publication Date (Web): August 16, 2012 | doi: 10.1021/bk-2012-1105.ch014

Downloaded by OHIO STATE UNIV LIBRARIES on August 28, 2012 | http://pubs.acs.org
Publication Date (Web): August 16, 2012 | doi: 10.1021/bk-2012-1105.ch014

65. Nduko, J. M.; Suzuki, W.; Matsumoto, K.; Kobayashi, H.; Ooi, T.; Fukuoka, A.; Taguchi, S. *J. Biosci. Bioeng.* **2011**, DOI:10.1016/j.jbiosc.2011.08.021
66. Shozui, F.; Matsumoto, K.; Motohashi, R.; Yamada, M.; Taguchi, S. *Polym. Degrad. Stab.* **2010**, *95*, 1340–1344.
67. Tsuge, T.; Fukui, T.; Matsusaki, H.; Taguchi, S.; Kobayashi, G.; Ishizaki, A.; Doi, Y. *FEMS Microbiol. Lett.* **2000**, *184*, 193–198.
68. Sato, S.; Nomura, C. T.; Abe, H.; Doi, Y.; Tsuge, T. *J. Biosci. Bioeng.* **2007**, *103*, 38–44.
69. Matsumoto, K.; Ishiyama, A.; Sakai, K.; Shiba, T.; Taguchi, S. *J. Biotechnol.* **2011**, *156*, 214–217.
70. Amass, W.; Amass, A.; Tighe, B. *Polym. Int.* **1998**, *47*, 89–144.
71. Matjan, F.; Alam, K. Y.; Clark, D. P. *J. Bacteriol.* **1989**, *171*, 342–348.
72. Tsuji, H. *Macromol. Biosci.* **2007**, *7*, 1299–1299.
73. Wolf, F. F.; Friedemann, N.; Frey, H. *Macromolecules* **2009**, *42*, 5622–5628.
74. Sudesh, K.; Abe, H.; Doi, Y. *Prog. Polym. Sci.* **2000**, *25*, 1503–1555.
75. Zaman, H. U.; Song, J. C.; Park, L. S.; Kang, I. K.; Park, S. Y.; Kwak, G.; Park, B. S.; Yoon, K. B. *Polym. Bull.* **2011**, *67*, 187–198.
76. Yang, T. H.; Jung, Y. K.; Kang, H. O.; Kim, T. W.; Park, S. J.; Lee, S. Y. *Appl. Microbiol. Biotechnol.* **2011**, *90*, 603–614.
77. Park, S. J.; Kim, T. W.; Kim, M. K.; Lee, S. Y.; Lim, S. *Biotech. Adv.* **2011**, DOI:10.1016/j.biotechadv.2011.007.

Downloaded by STANFORD UNIV GREEN LIBR on August 28, 2012 | http://pubs.acs.org
Publication Date (Web): August 16, 2012 | doi: 10.1021/bk-2012-1105.ch015

Chapter 15

Synthesis of Amylose-Grafted Polysaccharide Materials by Phosphorylase-Catalyzed Enzymatic Polymerization

Jun-ichi Kadokawa*

**Graduate School of Science and Engineering, Kagoshima University,
1-21-40 Korimoto, Kagoshima 890-0065, Japan
*E-mail: kadokawa@eng.kagoshima-u.ac.jp**

This chapter reviews the synthesis of polysaccharide materials having amylose graft-chains by means of phosphorylase-catalyzed enzymatic polymerization. The synthesis of amylose-grafted heteropolysaccharides composed of abundant polysaccharide main-chains, such as chitin/chitosan, cellulose, alginate, and xanthan gum, was performed by combining the phosphorylase-catalyzed enzymatic polymerization forming amylose with the appropriate chemical reaction (chemoenzymatic method). In addition, glycogen-based polysaccharide materials having the elongated amylose graft-chains were prepared by the phosphorylase-catalyzed polymerization from glycogen.

Introduction

Polysaccharides are one of three major classes of biopolymers in nature, which are vital materials for important in vivo functions such as providing an energy resource, acting as a structural material, and conferring specific biological properties (*1*, *2*). They are structurally composed of monosaccharide units linked through glycosidic linkages. A glycosidic linkage is a type of covalent bond that joins a monosaccharide residue to another group, which may or may not be another saccharide residue. Natural polysaccharides have very complicated structures owing not only to a structural diversity of monosaccharide residues, but also to the differences in stereo- and regio-types of glycosidic linkages. In contrast, the other two major biopolymers of proteins and nucleic acids have relatively

In Biobased Monomers, Polymers, and Materials; Smith, P., et al.;
ACS Symposium Series; American Chemical Society: Washington, DC, 2012.

simple structures because they are constructed by a type of specific linkage between 20 kinds of amino acids and several kinds of nucleotides, respectively (*3*). The large diversity of polysaccharide structures contributes to serve a whole range of biological functions in the host organism, and a subtle change in the chemical structure has a profound effect on the properties and functions of the polysaccharides (*4–6*). Therefore, synthesis of new artificial polysaccharides has attracted much attention because of their potential applications as materials in the field of medicine, pharmaceutics, cosmetics, and food industries.

In addition to linear polysaccharides such as cellulose and amylose, branched structures have often been observed in natural polysaccharides, where a polysaccharide of the main-chain accompanies different kinds of branched polysaccharide chains by covalent linkages (*2*). Such chemical structures probably contribute to their promising and high-performance functions in nature. For example, arabinoxylan, gum arabic, and guar gum play important roles in moisture maintenance and protection against bacteria. On the basis of the above viewpoint, the development of an efficient method for the preparation of the branched or grafted artificial polysaccharides using common polysaccharides is a promising topic in carbohydrate and material research fields.

Polysaccharides are theoretically produced by the repeated glycosylations of a glycosyl donor with a glycosyl acceptor to form a glycosidic linkage (*7–9*). Figure 1 shows a typical schematic reaction of the glycosylation from two glucose substrates for possible formation of α-(1→4)- and β-(1→4)-linked glucose dimers (maltose and cellobiose, respectively). For stereo- and regioselective construction of the glycosidic linkage, a leaving group, protective groups, a catalyst, and a solvent should appropriately be selected. Among multiple fashions of the glycosidic linkages produced by the glycosylation, in the chemical synthesis of polysaccharides, only one kind of linkage during the repeated glycosylations must be constructed to give the products with well-defined structures. As appeared in two representative natural polysaccharides, i.e., cellulose and starch, the importance of the glycosidic linkages in the polysaccharides is significant for their functions. Cellulose and starch are composed of the same structural unit, i.e., an anhydroglucose unit, but are linked through different α-(1→4)- and β-(1→4)-glycosidic linkages, respectively. Owing to the difference in such stereochemistry of glycosidic linkages in cellulose and starch, their roles in nature are completely different; the former is the structural material and the latter acts as the energy resource. However, the perfection of the selectivities in glycosidic linkages still remains a difficult barrier in the general chemical glycosylations (*10*). Furthermore, the chemical glycosylations require the protection-deprotection processes of the hydroxy groups. During such multiple reaction steps for the synthesis of polysaccharides via the repeated chemical glycosylations, therefore, undesired side-reactions often take place.

To develop a superior method for the synthesis of polysaccharides, the in vitro approach by enzymatic catalysis has been significantly investigated because enzymes have remarkable catalytic advantages compared with other types of catalyst in terms of the stereo- and regioselectivities. Enzymes are generally categorized into six main classes, which are oxidoreductase (EC1), transferase (EC2), hydrolase (EC3), lyase (EC4), isomerase (EC5), and ligase

Downloaded by STANFORD UNIV GREEN LIBR on August 28, 2012 | http://pubs.acs.org
Publication Date (Web): August 16, 2012 | doi: 10.1021/bk-2012-1105.ch015

Downloaded by STANFORD UNIV GREEN LIBR on August 28, 2012 | http://pubs.acs.org
Publication Date (Web): August 16, 2012 | doi: 10.1021/bk-2012-1105.ch015

(EC6) (*11*). In such main classes, two enzymes, i.e., transferases and hydrolases, have been practically applied as catalysts for the in vitro enzymatic synthesis of polysaccharides (*12–17*).

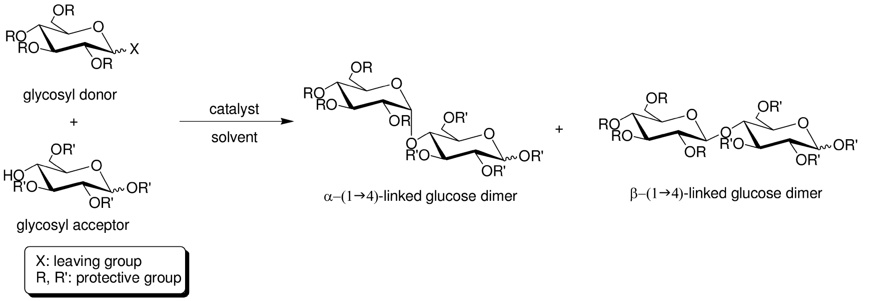
OR
RO
RO
O
X
OR
glycosyl donor
+
OR'
HO
R'O
O
OR'
OR'
glycosyl acceptor
X: leaving group
R, R': protective group
catalyst
solvent
α-(1→4)-linked glucose dimer
+
β-(1→4)-linked glucose dimer

Figure 1. Typical reaction manner of glycosylation between two glucose substrates.

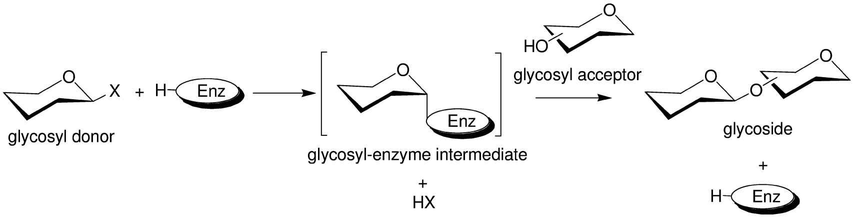
glycosyl donor
X
+
H
Enz
glycosyl-enzyme intermediate
+
HX
HO
glycosyl acceptor
glycoside
+
H
Enz

Figure 2. General reaction scheme for enzymatic glycosylation.

Similar to the general chemical glycosylation, enzymatic formation of a glycosidic linkage between C-1 atom of a monosaccharide and one of hydroxy groups of the other monosaccharide can be realized by the reaction of a activated glycosyl donor and a glycosyl acceptor (Figure 2) (*18*, *19*). First, the glycosyl donor is recognized by an enzyme to form a glycosyl-enzyme intermediate. Then, the intermediate is attacked by the hydroxy group of the glycosyl acceptor, giving a glycoside. The enzymatic glycosylation is a very powerful tool for the stereo- and regioselective construction of the glycosidic linkages under mild conditions, where a glycosyl donor and a glycosyl acceptor can be employed in their unprotected forms, leading to the direct formation of the unprotected glycoside in aqueous media. Thus, repetition of the enzymatic glycosylations, i.e., enzymatic polymerization, forms polysaccharides with well-defined structure. As aforementioned, the enzymes involved in the synthesis of polysaccharides are glycosyl hydrolases and glycosyl transferases (Figure 3). Furthermore, the latter is mainly subclassified into synthetic enzymes (Leloir glycosyltransferases) (*20*) and phosphorolytic enzymes (phosphorylases) (*21*).

Downloaded by STANFORD UNIV GREEN LIBR on August 28, 2012 | http://pubs.acs.org
Publication Date (Web): August 16, 2012 | doi: 10.1021/bk-2012-1105.ch015

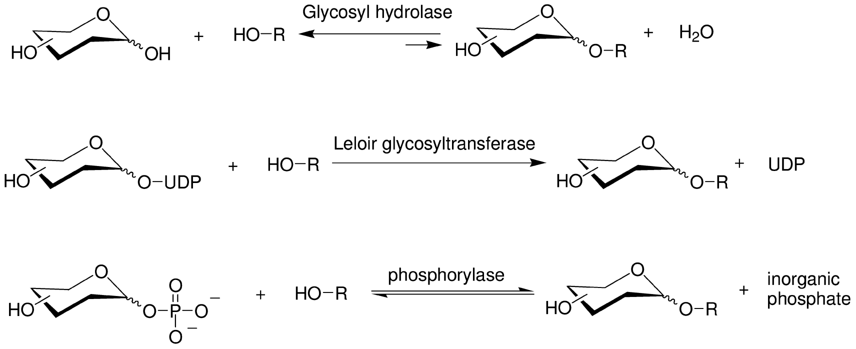

Figure 3. Typical enzymes involved in synthesis of polysaccharides

Leloir glycosyltransferases are biologically important because they perform the role for synthesizing saccharide chains in vivo (*22*). The reactions of the enzymes are irreversible in the synthetic direction because of equipment for cleavage of the high-energy linkage of glycosyl nucleotide substrates. However, Leloir glycosyltransferases are generally transmembrane-type proteins, present in less amount in nature, and unstable for isolation and purification. Therefore, the in-vitro enzymatic reaction using Leloir glycosyltransferases is not common for practical synthesis of the polysaccharides.

Glycosyl hydrolyses, so-called glycosidases and glycanases, have been frequently employed in the hydrolysis of polysaccharides such as starch. The glycosyl hydrolase catalysis using natural polysaccharides readily proceeds in the hydrolysis direction under normal conditions in aqueous media. However, when an enzyme-substrate intermediate is formed, glycosyl hydrolases catalyzing in vivo are able to catalyze a glycosylation in vitro to produce a glycoside. This view is based on a hypothesis that the structures of transition states are very similar in both in vivo and in vitro reactions (*12*, *14*, *15*). For the synthesis of polysaccharides by the glycosyl hydrolase-catalyzed enzymatic polymerization, therefore, the substrates should be designed as the structure of a transition state analogue. On the basis of this concept, two types of substrates, i.e., glycosyl fluorides and sugar oxazolines, have been designed to be efficiently recognized by glycosyl hydrolases (*13*)(*23*). An anomeric carbon of the starting sugars is activated by introducing fluoride or an oxazoline group (1,2-oxazoline derived from 2-acetamido-2-deoxysugar), giving the substrates which have structures close to a transition state of the suitable enzymatic reactions and efficiently form the enzyme-substrate complexes. By the enzymatic polymerization of glycosyl fluorides catalyzed by glycosyl hydrolases, cellulose, amylose, xylan, and related polysaccharides have been synthesized (*12–17*, *24–26*), and the glycosyl hydrolase-catalyzed enzymatic polymerization using sugar oxazolines produced chitin, hyaluronan, chondroitin, and related aminopolysaccharides (*14–17*, *23*, *27–32*). The former proceeds via polycondensation through leaving hydrogen

Downloaded by STANFORD UNIV GREEN LIBR on August 28, 2012 | http://pubs.acs.org
Publication Date (Web): August 16, 2012 | doi: 10.1021/bk-2012-1105.ch015

fluoride, whereas the ring-opening polyaddition is the mechanism of the latter case.

Phosphorylases catalyze phosphorolytic cleavage of a glycosidic linkage in the saccharide chain in the presence of inorganic phosphate to produce glycose 1-phosphate and the saccharide chain with one smaller degree of polymerization (DP) (*21*). Because the bond energy of the glycose 1-phosphate product is comparable with that of the glycosidic linkage, the phosphorylase-catalyzed reactions show reversible nature. Therefore, the phosphorylases can be employed in the practical synthesis of saccharide chains via glycosylation. In such glycosylation, the glycose 1-phosphates are used as a glycosyl donor and the glycose unit is transferred from the substrate to a nonreducing end of an appropriate glycosyl acceptor to form a stereo- and regiocontrolled glycosidic linkage accompanied with the production of inorganic phosphate. Of the phophorylases, which have been known so far, α-glucan phosphorylase (glycogen phosphorylase, starch phosphorylase, hereafter, this enzyme is simply called 'phosphorylase' in this chapter) is the most extensively studied and found in animals, plants, and microorganisms. The role of phosphorylase is though to be in utilization of storage polysaccharides in the glycolytic pathway.

Characteristic Features of Phosphorylase-Catalyzed Enzymatic Polymerization to Produce Amylose

Phosphorylase catalyzes the reversible phosphorolysis of α-(1→4)-glucans at the nonreducing end, such as glycogen and starch, in the presence of inorganic phosphate, giving rise to α-D-glucose 1-phosphate (Glc-1-P) (*21*). By means of the reversibility of the reaction, α-(1→4)-glycosidic linkage can be constructed by the phosphorylase-catalyzed glycosylation using Glc-1-P as a glycosyl donor (*33*). As a glycosyl acceptor, maltooligosaccharides with DPs higher than the smallest one recognized by phosphorylase are used. The glycosyl acceptor is often called a 'primer.' The smallest glycosyl acceptor for the phosphorylase-catalyzed glycosylation is typically maltotetraose (Glc_4), whereas that for the phosphorolysis is typically maltopentaose (Glc_5). In the glycosylation, a glucose unit is transferred from Glc-1-P to a nonreducing end of the primer to form α-(1→4)-glycosidic linkage. When the excess molar ratio of Glc-1-P to the primer is present in the reaction system, the successive glycosylations occur as a propagation of polymerization to produce the α-(1→4)-glucan chain, i.e., amylose (Figure 4). Because the phosphorylase-catalyzed polymerization proceeds analogously to a living polymerization, the molecular weight distribution of the amylose produced is a narrow ($M_w/M_n < 1.2$) and can be controlled by the Glc-1-P/primer feed molar ratios (*34*). Phosphorylase is the only enzyme that can produce amylose with the desired average molecular weight.

The enzymatic polymerization by phosphorylase catalysis is completely different from the aforementioned enzymatic polymerization by glycosyl hydrolase catalysis. The former proceeds by a chain-growth polymerization, where the polymerization is initiated from a chain end of the primer, and the propagation proceeds via successive transfer of glucose residues from monomers to the nonreducing end (propagating end). On the other hand, the latter is a step-growth polymerization, where monomers react each with other stepwise by enzymatic catalysis to produce the saccharide chain. Therefore, the phosphorylase-catalyzed enzymatic polymerization can initiate from the primer modified at a reducing end, located opposite the nonreducing end in an unreacted reaction (Figure 5) (*35*). This is one of the most characteristic and advantageous features of the phosphorylase-catalyzed reactions that are not possible in the glycosyl hydrolase-catalyzed reaction.

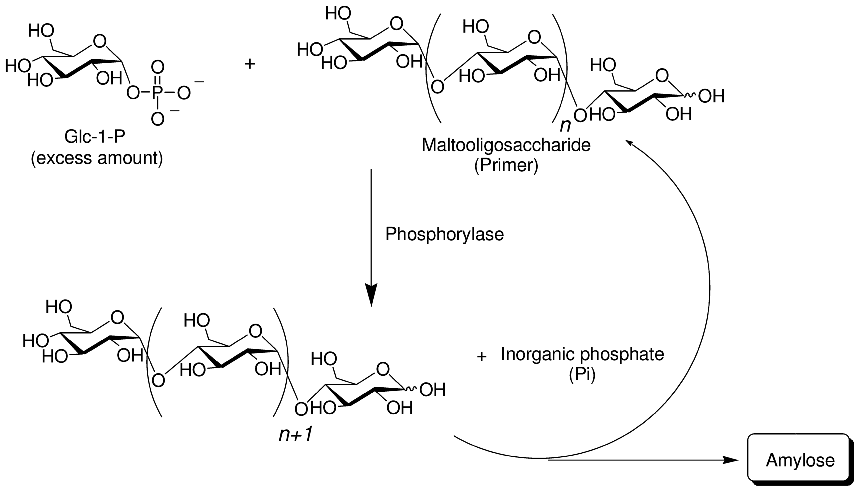

Figure 4. Phosphorylase-catalyzed enzymatic polymerization to amylose.

By means of this characteristic of the phosphorylase catalysis, a styrene-type macromonomer having a amylose chain was prepared by the phosphorylase-catalyzed polymerization using a primer having a polymerizable group at the reducing end (*36*). Then, radical polymerization of the macromonomer gave an amylose-grafted polystyrene. This material was also prepared by the radical polymerization of a styrene-type macromonomer having a maltooligosaccharide, followed by the phosphorylase-catalyzed polymerization from the chain ends of the primers on the product (*36*). By this approach, other amylose-grafted polymers such as dimethylsiloxane, poly(L-glutamic acid), polyacetylene, and poly(vinyl alcohol) have been synthesized (*37–41*).

Downloaded by STANFORD UNIV GREEN LIBR on August 28, 2012 | http://pubs.acs.org
Publication Date (Web): August 16, 2012 | doi: 10.1021/bk-2012-1105.ch015

Downloaded by STANFORD UNIV GREEN LIBR on August 28, 2012 | http://pubs.acs.org
Publication Date (Web): August 16, 2012 | doi: 10.1021/bk-2012-1105.ch015

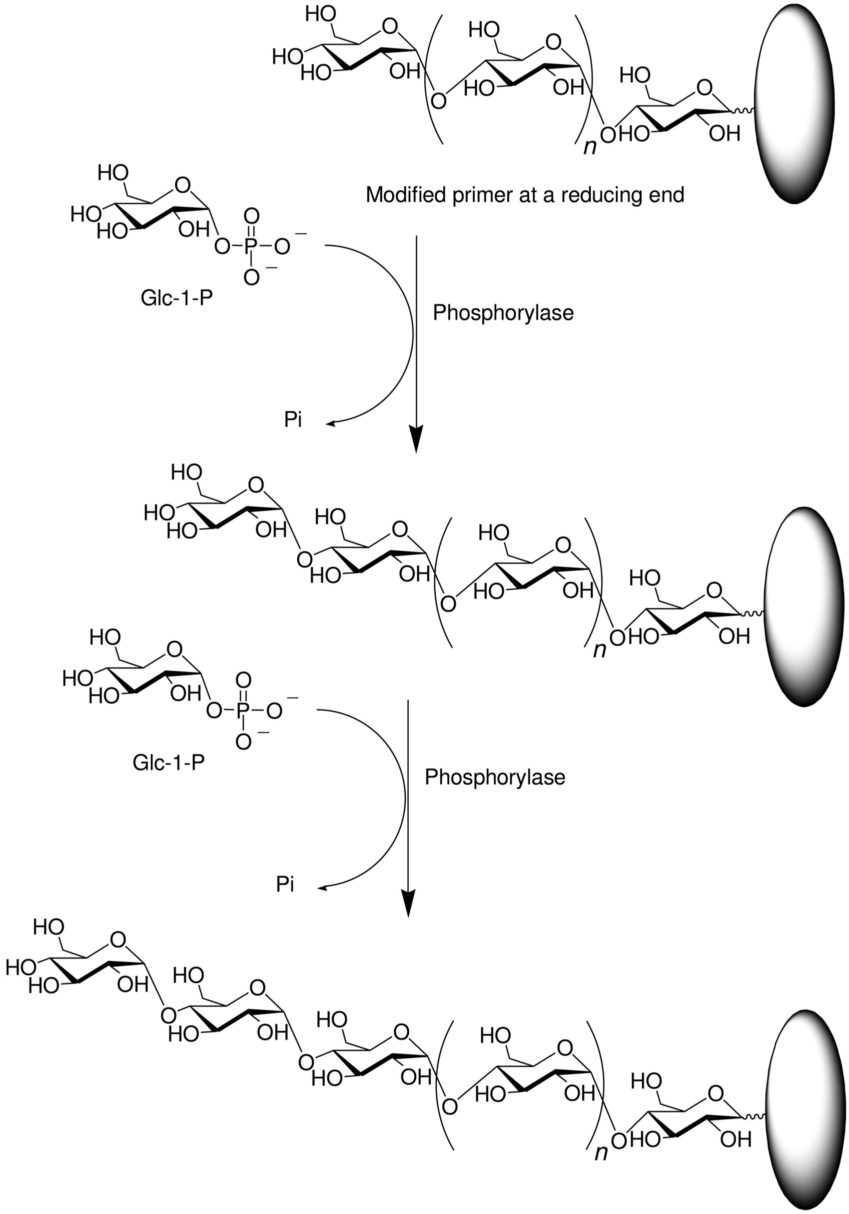
Modified primer at a reducing end
Glc-1-P
Phosphorylase
Pi
Glc-1-P
Phosphorylase
Pi
n

Figure 5. Enzymatic propagation using modified primer by phosphorylase catalysis.

Downloaded by STANFORD UNIV GREEN LIBR on August 28, 2012 | http://pubs.acs.org
Publication Date (Web): August 16, 2012 | doi: 10.1021/bk-2012-1105.ch015

Chemoenzymatic Synthesis of Amylose-Grafted Heteropolysaccharides

Amylose-grafted heteropolysaccharides have been synthesized by the phosphorylase-catalyzed enzymatic polymerization of Glc-1-P. As aforementioned, maltooligosaccharides as a primer have to be present to initiate the polymerization. To obtain the amylose-grafted heteropolysaccharides, therefore, the maltooligosaccharides are first introduced onto the polysaccharides of the main-chain by appropriate chemical reactions, and then the phosphorylase-catalyzed polymerization is performed using the products as a macroprimer (chemoenzymatic method). Two types of chemical reactions have been employed to introduce the primer chains onto the main-chain polysaccharides; one is reductive amination of the maltooligosaccharides with cationic polysaccharides having amino groups using reductants and the other one is condensation of amine-functionalized maltooligosaccharides with anionic polysaccharides having carboxylate groups using condensing agents (Figure 6) (*42*, *43*).

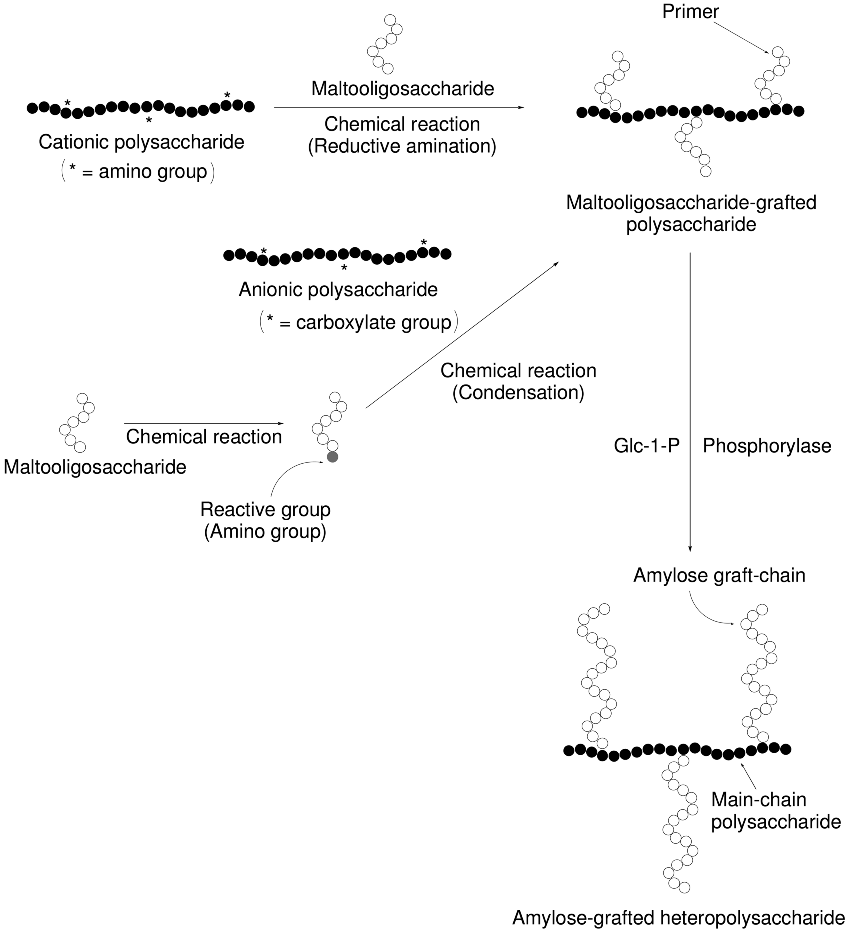
Maltooligosaccharide
Chemical reaction
(Reductive amination)
Cationic polysaccharide
(* = amino group)
Primer
Maltooligosaccharide-grafted polysaccharide
Anionic polysaccharide
(* = carboxylate group)
Chemical reaction
(Condensation)
Maltooligosaccharide
Chemical reaction
Reactive group
(Amino group)
Glc-1-P
Phosphorylase
Amylose graft-chain
Main-chain polysaccharide
Amylose-grafted heteropolysaccharide

Figure 6. Chemoenzymatic synthesis of amylose-grafted heteropolysaccharides.

In Biobased Monomers, Polymers, and Materials; Smith, P., et al.;
ACS Symposium Series; American Chemical Society: Washington, DC, 2012.

Downloaded by STANFORD UNIV GREEN LIBR on August 28, 2012 | http://pubs.acs.org
Publication Date (Web): August 16, 2012 | doi: 10.1021/bk-2012-1105.ch015

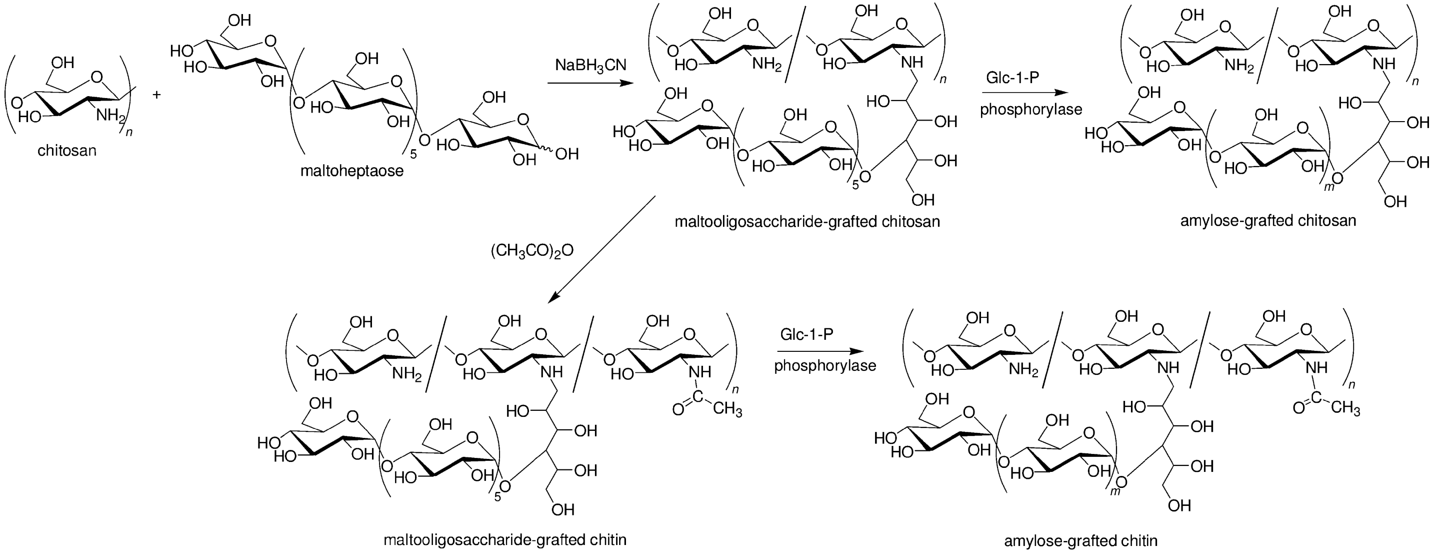
chitosan
+
maltoheptaose
NaBH3CN
maltooligosaccharide-grafted chitosan
Glc-1-P
phosphorylase
amylose-grafted chitosan
(CH3CO)2O
maltooligosaccharide-grafted chitin
Glc-1-P
phosphorylase
amylose-grafted chitin

Figure 7. Chemoenzymatic synthesis of amylose-grafted chitin and chitosan.

Downloaded by STANFORD UNIV GREEN LIBR on August 28, 2012 | http://pubs.acs.org
Publication Date (Web): August 16, 2012 | doi: 10.1021/bk-2012-1105.ch015

By means of the chemoenzymatic approach, amylose-grafted chitin and chitiosan were synthesized (Figure 7) (*44*, *45*). Chitin is a (1→4)-linked 2-acetoamido-2-deoxy-β-D-glucan and chitosan is the *N*-deacetylated derivative of chitin. First, maltoheptaose (Glc_7) was introduced to chitosan by the reductive amination using $NaBH_3CN$ in a mixed solvent of aqueous acetic acid/methanol to give a maltooligosaccharide-grafted chitosan. This material was converted into a maltooligosaccharide-grafted chitin by *N*-acetylation using acetic anhydride. Then, the phosphorylase-catalyzed enzymatic polymerization of Glc-1-P from the maltooligosaccharide chains as the primer on the chitin and chitosan derivatives was performed to obtain the amylose-grafted chitin and chitosan. The products were insoluble in any solvents, e.g., aqueous acetic acid and DMSO, which were good solvents for chitosan and amylose, respectively. The hydrogel of the amylose-grafted chitosan could be formed by drying the reaction mixture slowly in the vessel at 40 – 50 °C.

The chemoenzymatic approach for amylose-grafted heteropolysaccharides was extended to the synthesis of an amylose-grafted cellulose (Figure 8) (*46*). The two representative natural polysaccharides, cellulose and amylose, are composed of the same structural unit, i.e., anhydroglucose unit, but linked through the different β-(1→4)- and α-(1→4)-glucosidic linkages, respectively. Therefore, the amylose-grafted cellulose has a very interesting and unique structure because it is composed of two polysaccharide chains with the same structural unit but with the different linkages. For the preparation of such a material, the amino groups must be introduced to cellulose because the amino groups efficiently react with maltooligosaccharides by the reductive amination as was previously performed using chitosan. Therefore, the synthesis of amine-functionalized cellulose was first performed, which was successfully obtained by three reaction steps; the partial tosylation of the OH groups at C-6 positions, the displacement of the tosylates by the azido groups, and the reduction to amino groups. Then, maltooligosaccharide primers were introduced on cellulose main-chain by reductive amination of the amine-functionalized cellulose with Glc_7. Subsequently, the amylose-grafted cellulose was synthesized by the phosphorylase-catalyzed polymerization of Glc-1-P from the maltooligosaccharide primers on the cellulose derivative. When the reaction mixture obtained by the enzymatic polymerization was left standing in a Petri dish at room temperature for several days, it totally converted to the gel form. The hydrogel product was washed with water several times to remove some contaminants such as the unreacted Glc-1-P. This hydrogel was tougher than that formed from the amylose-grafted chitosan. The hydrogel was converted further into the solid material by drying under the ambient atmosphere. The addition of water to the solid gave the gelled material again. The cycle between the solid and gel was repeated by the drying and wetting process. Furthermore, the above property of the amylose-grafted cellulose allowed the formation of a film. The reaction mixture of the enzymatic polymerization was spread thinly on a glass plate, and subsequently left standing at room temperature, giving rise to a wet and swollen film. This material was converted into the soft film by drying under the ambient atmosphere. The cycle between the swollen and dried films was also repeated by wetting and drying.

Downloaded by STANFORD UNIV GREEN LIBR on August 28, 2012 | http://pubs.acs.org
Publication Date (Web): August 16, 2012 | doi: 10.1021/bk-2012-1105.ch015

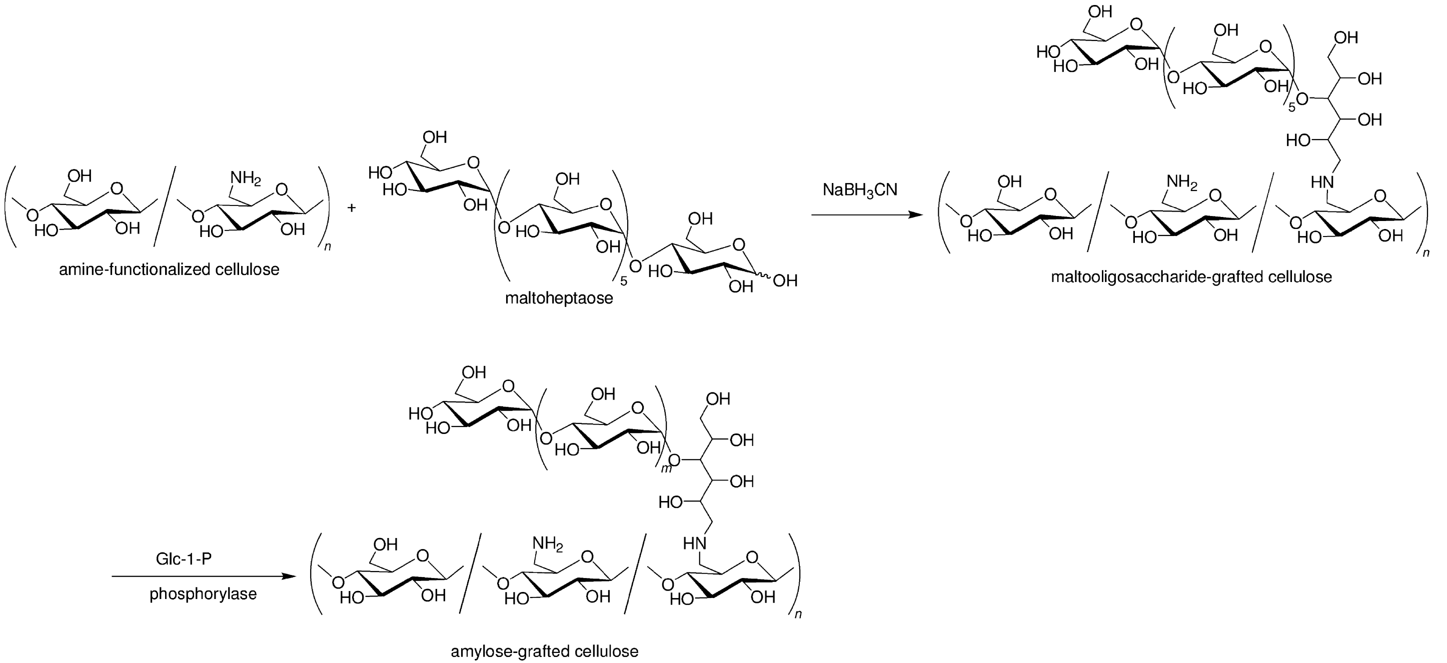
amine-functionalized cellulose
maltoheptaose
NaBH3CN
maltooligosaccharide-grafted cellulose
Glc-1-P
phosphorylase
amylose-grafted cellulose

Figure 8. Chemoenzymatic synthesis of amylose-grafted cellulose.

Downloaded by STANFORD UNIV GREEN LIBR on August 28, 2012 | http://pubs.acs.org
Publication Date (Web): August 16, 2012 | doi: 10.1021/bk-2012-1105.ch015

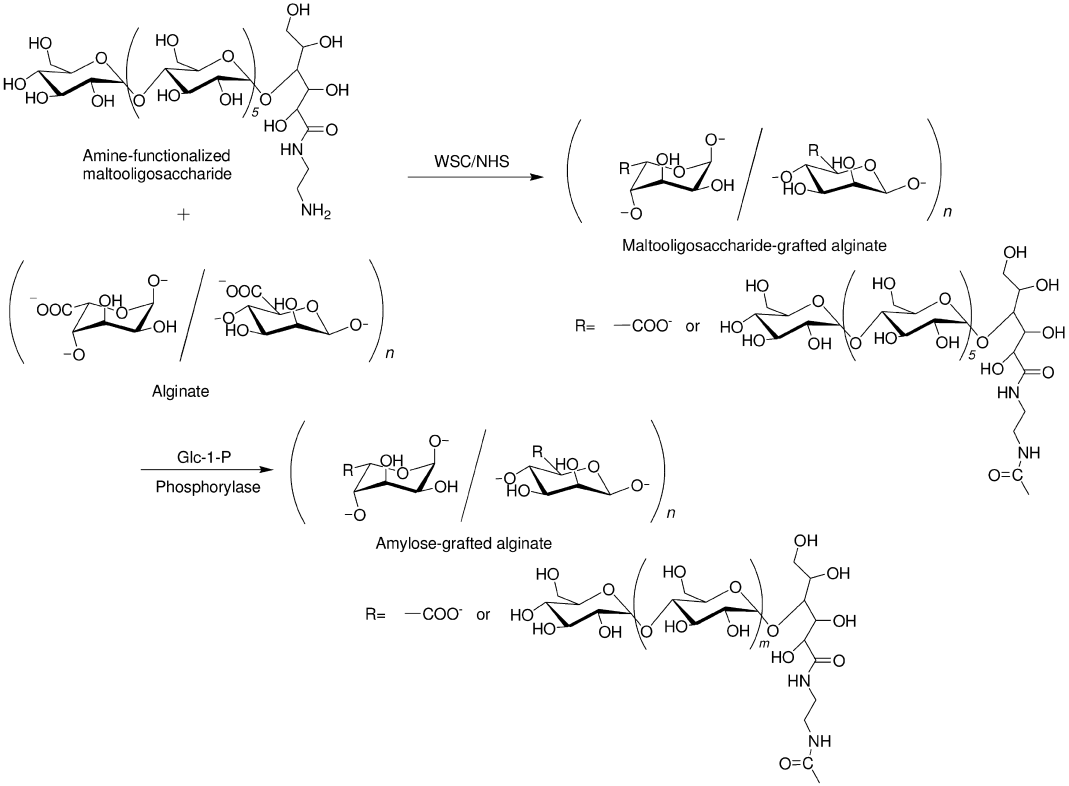
Amine-functionalized maltooligosaccharide
+
Alginate
WSC/NHS
Maltooligosaccharide-grafted alginate
R= —COO⁻ or
Glc-1-P
Phosphorylase
Amylose-grafted alginate
R= —COO⁻ or
n
5
m

Figure 9. Chemoenzymatic synthesis of amylose-grafted alginate.

Downloaded by STANFORD UNIV GREEN LIBR on August 28, 2012 | http://pubs.acs.org
Publication Date (Web): August 16, 2012 | doi: 10.1021/bk-2012-1105.ch015

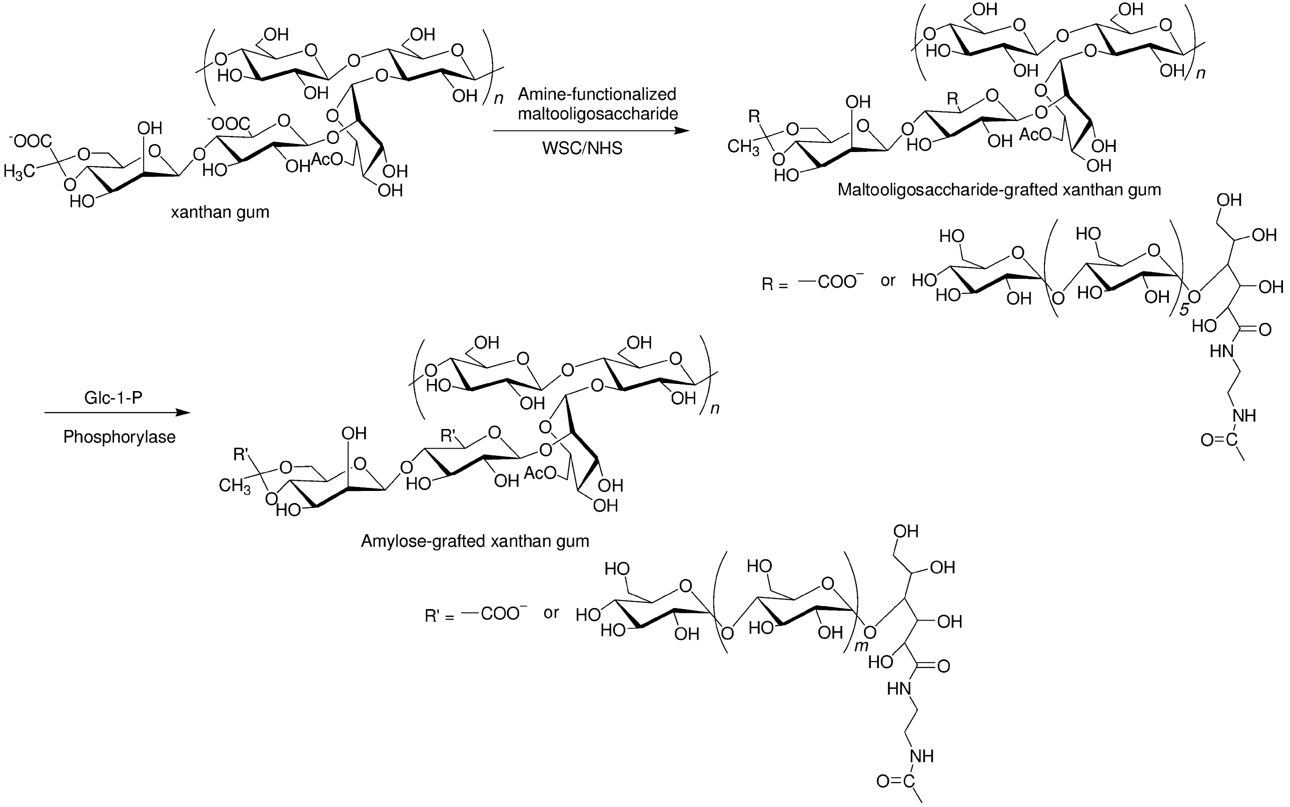
xanthan gum
Amine-functionalized maltooligosaccharide
WSC/NHS
Maltooligosaccharide-grafted xanthan gum
R = —COO⁻ or
Glc-1-P
Phosphorylase
Amylose-grafted xanthan gum
R' = —COO⁻ or

Figure 10. Chemoenzymatic synthesis of amylose-grafted xanthan gum.

Downloaded by STANFORD UNIV GREEN LIBR on August 28, 2012 | http://pubs.acs.org
Publication Date (Web): August 16, 2012 | doi: 10.1021/bk-2012-1105.ch015

Water-soluble anionic polysaccharides, such as alginic acid and xanthan gum, have reactive carboxylate groups in the polysaccharide main-chains, which are condensed with amine-functionalized maltooligosaccharides using condensing agents. Therefore, the chemoenzymatic method has been extended to the use of such anionic polysaccharides as the main-chain polymers for the amylose-graftied heteropolysaccharides (Figure 9) (*47*). Alginic acid is a linear polysaccharide composed of (1→4)-linked β-D-mannuronic acid and (1→4)-linked α-L-guluronic acid units. For the chemoenzymatic approach, an amine-functionalized maltooligosaccharide, which was prepared by the reaction of maltooligosaccharide lactone with 2-azidoethylamine, followed by the reduction using $NaBH_4$, was chemically introduced to sodium alginate by condensation with carboxylates of the alginate using water-soluble carbodiimide (WSC)/*N*-hydroxysuccinimide (NHS) as the condensing agent to produce a maltooligosaccharide-grafted alginate. Then, the phosphorylase-catalyzed enzymatic polymerization of Glc-1-P from the maltooligosaccharide primers on the alginate main-chain was conducted to produce the amylase-grafted alginate. The preparation of beads from the resulting product was attempted by adding its alkaline solution into calcium chloride aqueous solution. Consequently, beads were obtained from the amylose-grafted alginate containing shorter amylose chains (DP < ca. 50), whereas that possessing longer amylose graft chains (DP = ca. 100) did not afford formation of beads. This result indicated that the longer amylose graft chains attached to the alginate main-chain disturb the formation of stable matrices composed of the cross-linked calcium alginates, resulting in difficulty in beads formation. After beads were produced, their enzymatic degradation was investigated by β-amylase-catalyzed reaction. When the beads were kept standing in the presence of β-amylase in a stirred acetate buffer at 40 °C for 6 h, the solution gradually became turbid, indicating disintegration of the beads. Furthermore, the enhancement of the release rate of an entrapped dye compound from inside of the beads by the β-amylase treatment was observed, which was reasonably explained by the hydrolysis of the amylose graft-chains in the beads by β-amylase.

The chemoenzymatic method was also investigated using xanthan gum for other anionic polysaccharides as a main-chain of amylose-grafted heteropolysaccharide (Figure 10) (*48*). Xanthan gum, which is a water soluble polysaccharide produced by *Xanthomonas* campestris, has a cellulose-type main-chain (β-(1→4)-glucan) with trisaccharide side-chains (mannose-β-(1→4)-glucuronic acid-β-(1→2)-mannose-α-(1→3)-) attached to alternating glucose units in the main-chain. The α-mannoside unit is acetylate at position 6 and the β-mannoside unit is partially pyruvated at positions 4 and 6. Because the side chain contains carboxylate groups, xanthan gum is an anionic polysaccharide. The chemoenzymatic synthesis of an amylose-grafted xanthan gum was performed as follows. The amine-functionalized maltooligosaccharide was chemically introduced to xanthan gum by condensation with its carboxylate functionality using WSC/NHS as the condensing agent to produce a maltooligosaccharide-grafted xanthan gum. Then the phosphorylase-catalyzed enzymatic polymerization of Glc-1-P from the maltooligosaccharide primers on the xanthan gum main-chain was performed, giving the amylose-grafted xanthan

In Biobased Monomers, Polymers, and Materials; Smith, P., et al.;
ACS Symposium Series; American Chemical Society: Washington, DC, 2012.

Downloaded by STANFORD UNIV GREEN LIBR on August 28, 2012 | http://pubs.acs.org
Publication Date (Web): August 16, 2012 | doi: 10.1021/bk-2012-1105.ch015

gum. The product formed a gel with an ionic liquid, 1-butyl-3-methylimidazolium chloride, which was converted into a hydrogel with high water content by replacement of the ionic liquid by water. An ionically cross-linked hydrogel with trivalent metal cations was produced by soaking the hydrogel product in $FeCl_3$ aqueous solution. When the mechanical properties of the ionically cross-linked hydrogels with Fe^{3+} were evaluated by compressive testing, the fracture strain values increased with increasing functionalities or DPs of the amylose graft-chains, whereas the fracture stress values were mostly unchanged regardless of the functionalities or DPs. It appears that the Fe^{3+}-treated hydrogels of the amylose-grafted xanthan gums were constructed by not only the ionically cross-linking with Fe^{3+} and the double helix conformation of xanthan gum chains, but also the double helix conformation of amylose graft-chains, because amylose is known to readily form the double helix conformation. The presence of the double helix structure between amylose graft-chains probably contributed to the formation of a looser network structure in the hydrogels, resulting in the enhancement of the fracture strain values.

Preparation of Glycogen-Based Polysaccharide Materials Having Elongated Amylose-Graft Chains by Phosphorylase-Catalyzed Polymerization

Glycogen is known to be a high molecular-weight and water soluble polysaccharide, which is composed of linear chains containing an average of 10 to 14 (1→4)-linked α-glucose residues, interlinked by α-(1→6)-glycosidic linkages to form highly branched structure. Besides glycogen being for the in vivo phosphorolysis by glycogen phosphorylase, it was used as the primer for phosphorylase-catalyzed polymerization (Figure 11) (*49*). When the phosphorylase-catalyzed polymerization of Glc-1-P from glycogen was carried out, followed by standing further at room temperature for 24 h, the reaction mixture turned into a hydrogel form. The hydrogelation was caused by the formation of junction zones based on the double helix structure of the elongated amylose graft-chains among glycogen molecules. The stress-strain curves of the hydrogels obtained by various Glc-1-P/glycogen ratios under compressive mode showed that the gels became stronger and then became brittle with increasing amounts of glycogen. Because the number of elongated amylose chains increased with increasing amounts of glycogen, the gel strength increased as more junction zones were formed. However, further increases in the number of junction zones probably induced the brittle nature.

The hydrogels were facilely converted into xerogels by lyophilization of the hydrogels. The stress-strain curves of the xerogels under compressive mode showed that the harder xerogels were obtained when the amount of glycogen used for the preparation of the hydrogels increased. This is probably due to formation of tighter networks because the larger number of junction zones were formed from the larger amounts of glycogen. The XRD profile of the xerogel showed diffraction peaks due to the crystalline structure of the double helix amylose chains (*50*). This result indicated that the networks in the xerogel were constructed based on the double helical entanglement of the elongated amylose graft-chains which in turn supported the presence of the junction zones by the double helix formation in the hydrogel.

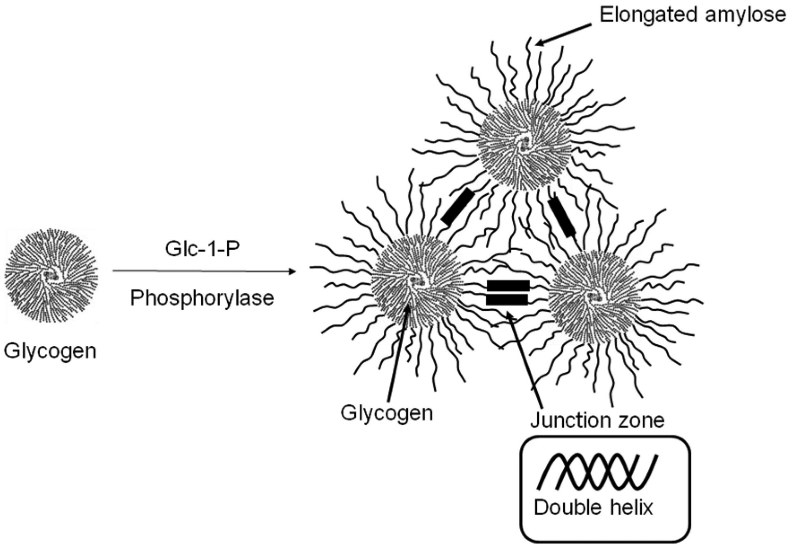
Elongated amylose
Glc-1-P
Phosphorylase
Glycogen
Glycogen
Junction zone
Double helix

Figure 11. Schematic reaction for phosphorylase-catalyzed polymerization using glycogen to form hydrogel.

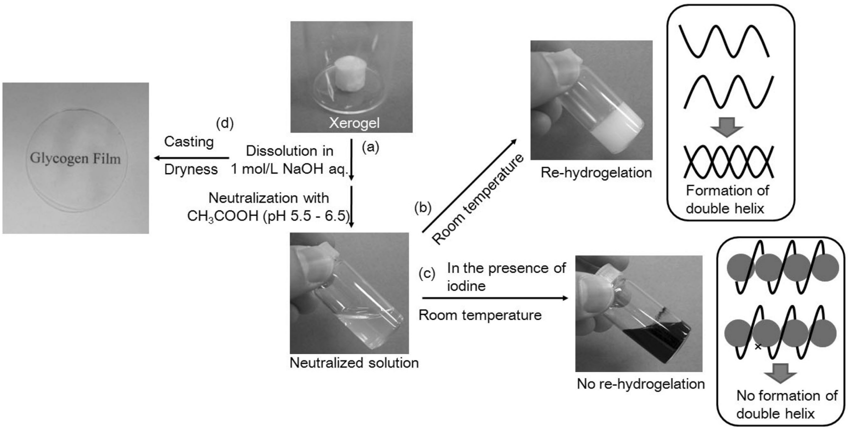
Xerogel
Glycogen Film
(d)
Casting
Dryness
Dissolution in
1 mol/L NaOH aq.
(a)
Neutralization with
CH_3COOH (pH 5.5 - 6.5)
(b)
Room temperature
Re-hydrogelation
Formation of
double helix
Neutralized solution
(c)
In the presence of
iodine
Room temperature
No re-hydrogelation
No formation of
double helix

Figure 12. Dissolution of xerogel (a), re-hydrogelation (b), suppression of re-hydrogelation (c), and formation of film (d).

Downloaded by STANFORD UNIV GREEN LIBR on August 28, 2012 | http://pubs.acs.org
Publication Date (Web): August 16, 2012 | doi: 10.1021/bk-2012-1105.ch015

Downloaded by STANFORD UNIV GREEN LIBR on August 28, 2012 | http://pubs.acs.org
Publication Date (Web): August 16, 2012 | doi: 10.1021/bk-2012-1105.ch015

When an aqueous solution of the xerogel was prepared by dissolution in aqueous NaOH solution, followed by neutralization with acetic acid to pH 5.5 – 6.5, it gradually turned into the hydrogel form (Figure 12(a)-(b)). These cycles could be repeated up to 5 times. When the standard iodine-iodide solution was added to the neutralized solution immediately after it was prepared by the same procedure as above, and the resulting mixture was left standing, the re-hydrogelation did not take place (Figure 12(c)). In this experiment, iodine was included by the elongated amylose chain to form the well-known amylose/iodine inclusion complex, which suppressed the formation of the double helix as the junction zone. Furthermore, a transparent film was obtained by casting the alkaline solution of the xerogel on a glass plate and evaporating to dryness (Figure 12(d)).

Conclusions

In this chapter, the synthesis of amylose-grafted polysaccharide materials by means of the phosphorylase-catalyzed enzymatic polymerization has been overviewed. Because the enzymatic polymerization by the phosphorylase catalysis proceeds with highly controlled stereo- and regioselectivities, the amylose chains with well-defined structure have efficiently been synthesized, which has been applied to the construction of the complicated polysaccharide structures like amylose-grafted heteropolysaccharides. Additionally, the motivation for the studies of phosphorylase-catalyzed enzymatic synthesis of the polysaccharides has strongly been based on the viewpoints that the greener and sustainable processes should be developed in the fields not only of fundamental research, but also of practical applications of polymer and material chemistries. Thus, besides the control of stereo- and regiochemistries, the methods described in this chapter have the additional advantages over the conventional chemical process; (i) the reactions proceed under the mild conditions in aqueous media, (ii) renewable resources from natural and related sources can be employed as the substrates of the reactions, (iii) the products have biodegradability in most cases, and (iv) enzymes are renewable and nontoxic.

The polysaccharides and the related compounds have been attracting much attention because of their potential for new functional materials applications in many research fields such as medicines, pharmaceutics, foods, cosmetics. Therefore, the polysaccharide materials prepared by means of the present chemoenzymatic method will be increasingly important and useful in the future.

References

1. Berg, J. M.; Tymoczko, J. L.; Stryer, L. *Biochemistry*, 6th International ed.; W. H. Freeman & Co.: New York, 2006; Chapter 11.
2. Schuerch, C. *Polysaccharides in Encyclopedia of Polymer Science and Engineering*, 2nd ed.; John Wiley & Sons: New York, 1986; Vol. 13, pp 87−162.

3. McMurry, J.; Castellion, M. E.; Ballantine, D. S.; Hoeger, C. A. *Fundamentals of General, Organic, and Biological Chemistry*, 6th ed.; Prentice Hall Inc.: New Jersey, 2009.
4. *Carbohydrates in Chemistry and Biology*; Ernst, B., Hart, G. W., Sinaÿ, P., Eds.; Wiley-VCH: Weinheim, 2000.
5. *Glycoscience*, 2nd ed.; Fraser-Reid, B. O., Tatsuta, K., Thiem, J., Coté, G. L., Flitsch, S., Ito, Y., Kondo, H., Nishimura, S. -I., Yu, B., Eds.; Springer: Berlin, 2008.
6. *Essentials of Glycobiology*, 2nd ed.; Varki, A., Cummings, R. D., Esko, J. D., Freeze, H. H., Stanley, P., Bertozzi, C. R., Hart, G. W., Etzler, M. E., Eds.; Cold Spring Harbor Laboratory Press: New York, 2009.
7. Paulsen, H. *Angew. Chem., Int. Ed. Eng.* **1982**, *21*, 155–173.
8. Schmidt, R. R. *Angew. Chem., Int. Ed. Eng.* **1986**, *25*, 212–235.
9. Toshima, K.; Tatsuta, K. *Chem. Rev.* **1993**, *93*, 1503–1531.
10. Mydock, L. K.; Demchenko, A. V. *Org. Biomol. Chem.* **2010**, *8*, 497–510.
11. *Enzyme Nomenclature 1992, Recommendations of the NCIUBMB on the Nomenclature and Classification of Enzymes*; Webb, E. C., Ed.; International Union of Biochemistry and Molecular Biology; Academic Press: San Diego, 1992.
12. Kobayashi, S.; Uyama, H.; Kimura, S. *Chem. Rev.* **2001**, *101*, 3793–3818.
13. Kobayashi, S. *J. Polym. Sci., Part A: Polym. Chem.* **2005**, *43*, 693–710.
14. Kobayashi, S. *Proc. Jpn. Acad., Ser. B* **2007**, *83*, 215–247.
15. Kobayashi, S.; Makino, A. *Chem. Rev.* **2009**, *109*, 5288–5353.
16. Kadokawa, J.; Kobayashi, S. *Curr. Opin. Chem. Biol.* **2010**, *14*, 145–153.
17. Kadokawa, J. *Chem. Rev.* **2011**, *111*, 4308–4345.
18. Shoda, S.; Fujita, M.; Kobayashi, S. *Trends Glycosci. Glycotechnol.* **1998**, *10*, 279–289.
19. Shoda, S.; Izumi, R.; Fujita, M. *Bull. Chem. Soc. Jpn.* **2003**, *76*, 1–13.
20. *Handbook of Glycosyltransferases and Related Genes*; Taniguchi, N., Honke, K., Fukuda, M., Eds.; Springer: Tokyo, 2002.
21. Kitaoka, M.; Hayashi, K. *Trends Glycosci. Glycotechnol.* **2002**, *14*, 35–50.
22. Rupprath, C.; Schumacher, T.; Elling, L. *Curr. Med. Chem.* **2005**, *12*, 1637–1675.
23. Makino, A.; Kobayashi, S. *J. Polym. Sci., Part A: Polym. Chem.* **2010**, *48*, 1251–1270.
24. Kobayashi, S.; Kashiwa, K.; Kawasaki, T.; Shoda, S. *J. Am. Chem. Soc.* **1991**, *113*, 3079–3084.
25. Kobayashi, S.; Shimada, J.; Kashiwa, K.; Shoda, S. *Macromolecules* **1992**, *25*, 3237–3241.
26. Kobayashi, S.; Wen, X.; Shoda, S. *Macromolecules* **1996**, *29*, 2698–2700.
27. Kobayashi, S.; Kiyosada, T.; Shoda, S. *J. Am. Chem. Soc.* **1996**, *118*, 13113–13114.
28. Kobayashi, S.; Morii, H.; Itoh, R.; Kimura, S.; Ohmae, M. *J. Am. Chem. Soc.* **2001**, *123*, 11825–11826.
29. Kobayashi, S.; Fujikawa, S.; Ohmae, M. *J. Am. Chem. Soc.* **2003**, *125*, 14357–14369.

Downloaded by STANFORD UNIV GREEN LIBR on August 28, 2012 | http://pubs.acs.org
Publication Date (Web): August 16, 2012 | doi: 10.1021/bk-2012-1105.ch015

Downloaded by STANFORD UNIV GREEN LIBR on August 28, 2012 | http://pubs.acs.org
Publication Date (Web): August 16, 2012 | doi: 10.1021/bk-2012-1105.ch015

30. Ohmae, M.; Fujikawa, S.; Ochiai, H.; Kobayashi, S. *J. Polym. Sci., Part A: Polym. Chem.* **2006**, *44*, 5014–5027.
31. Kobayashi, S.; Ohmae, M.; Ochiai, H.; Fujikawa, S. *Chem. Eur. J.* **2006**, *12*, 5962–5971.
32. Ohmae, M.; Makino, A.; Kobayashi, S. *Macromol. Chem. Phys.* **2007**, *208*, 1447–1457.
33. Ziegast, G.; Pfannemüller, B. *Carbohydr. Res.* **1987**, *160*, 185–204.
34. Takata, H.; Takaha, T.; Okada, S.; Takagi, M.; Imanaka, T. *J. Ferment. Bioeng.* **1998**, *85*, 156–161.
35. Kitamura, S.; Yunokawa, H.; Mitsuie, S.; Kuge, T. *Polym. J.* **1982**, *14*, 93–99.
36. Kobayashi, K.; Kamiya, S.; Enomoto, N. *Macromolecules* **1996**, *29*, 8670–8676.
37. von Braunmühl, V.; Jonas, G.; Stadler, R. *Macromolecules* **1995**, *28*, 17–24.
38. Kamiya, S.; Kobayashi, K. *Macromol. Chem. Phys.* **1998**, *199*, 1589–1596.
39. Kadokawa, J.; Nakamura, Y.; Sasaki, Y.; Kaneko, Y.; Nishikawa, T. *Polym. Bull.* **2008**, *60*, 57–68.
40. Sasaki, Y.; Kaneko, Y.; Kadokawa, J. *Polym. Bull.* **2009**, *62*, 291–303.
41. Kaneko, Y.; Matsuda, S.; Kadokawa, J. *Polym. Chem.* **2010**, *1*, 193–197.
42. Kaneko, Y.; Kadokawa, J. In *Handobook of Carbohydrate Polymers*; Ito, R., Matsuo, Y., Eds.; Nova Science Publishers, Inc.: Hauppauge NY, 2009; Chapter 23; pp 671−691.
43. Omagari, Y.; Kadokawa, J. *Kobunshi Ronbunshu* **2011**, *68*, 242–249.
44. Matsuda, S.; Kaneko, Y.; Kadokawa, J. *Macromol. Rapid Commun.* **2007**, *28*, 863–867.
45. Kaneko, Y.; Matsuda, S.; Kadokawa, J. *Biomacromolecules* **2007**, *8*, 3959–3964.
46. Omagari, Y.; Matsuda, S.; Kaneko, Y.; Kadokawa, J. *Macromol. Biosci.* **2009**, *9*, 450–455.
47. Omagari, Y.; Kaneko, Y.; Kadokawa, J. *Carbohydr. Polym.* **2010**, *82*, 394–400.
48. Arimura, T.; Omagari, Y.; Yamamoto, K.; Kadokawa, J. *Int. J. Biol. Macromol.* **2011**, *49*, 498–503.
49. Izawa, H.; Nawaji, M.; Kaneko, Y.; Kadokawa, J. *Macromol. Biosci.* **2009**, *9*, 1098–1104.
50. Putaux, J. –L.; Potocki-Véronèse, G.; Remaud-Simeon, M.; Buleon, A. *Biomacromolecules* **2006**, *7*, 1720–1728.

Downloaded by NORTH CAROLINA STATE UNIV on August 28, 2012 | http://pubs.acs.org
Publication Date (Web): August 16, 2012 | doi: 10.1021/bk-2012-1105.ch016

Chapter 16

Novel Nanocomposites Reinforced with Polysaccharide (Starch) Nanocrystals: From Interfacial Ring-Opening Polymerization to Melt-Processing Implementation

**J.-M. Raquez,*,[a] A.-L. Goffin,[a] E. Duquesne,[a] Y. Habibi,[a,b]
A. Dufresne,[b] and Ph. Dubois[a]**

[a]Laboratory of Polymeric and Composite Materials, Center of Innovation and Research in Materials and Polymers (CIRMAP), University of Mons, Place du Parc 23, B-7000 Mons, Belgium
**[b]Grenoble Institute of Technology, The International School of Paper, Print Media and Biomaterials (PAGORA), BP65,
38402 Saint Martin d'Hères cedex, France**
***E-mail: jean-marie.raquez@umons.ac.be. Fax: +32.65.37.34.84**

A "grafting from" approach was employed to chemically modify the surface of starch nanocrystals (SNCs) with poly(epsilon-caprolactone) (PCL) chains via $Sn(Oct)_2$-catalyzed ring-opening polymerization (ROP) of epsilon-caprolactone (CL). The grafting efficiency was evaluated by suspension tests of resulting SNCs grafted with PCL chains (SNC-*g*-PCL) carried out in toluene as well as infrared analyses. In a subsequent step, the resulting SNC-*g*-PCL nanohydrids and neat SNCs were melt-blended in a commercial PCL matrix using extrusion techniques in order to investigate the thermo-mechanical properties of resulting bio(nano)composites. The morphological analyses provided by Atomic Force Microscopy showed that the starch nanoplatelets within the SNC-*g*-PCL nanohydrids maintained their initial morphology and dimensions even after melt-processing at high temperature. Thermo-mechanical properties were evaluated by differential scanning calorimetry and dynamic mechanical thermo-analysis. They showed a substantial improvement of

In Biobased Monomers, Polymers, and Materials; Smith, P., et al.;
ACS Symposium Series; American Chemical Society: Washington, DC, 2012.

the crystallinity and storage modulus of the PCL matrix when filled with 4 and 8 wt% SNC-*g*-PCL.

Introduction

Over the past decades, starch - anhydroglucosidic polymer - has attracted considerable attention as an interesting structural platform for the manufacture of sustainable and biodegradable plastic packaging due to its biodegradability, renewability and low cost (*1*). Starch is composed by two isomers: amylose (linear isomer formed by alpha-D-(1,4)-glycoside linkages) and amylopectin (highly branched isomer formed by alpha-D-(1,4)-glycoside linkages and alpha-D-(1,6)-glycoside linkages) (*2*). Native starch can be used as granular microgranules or converted into thermoplastic starch in the presence of plasticizers like water and glycerol (*3–8*).

Recently, an increasing interest has been addressed to starch nanoparticles that are obtained from the crystalline fraction present within starch granules, *that is*, via the acid-hydrolysis of amorphous parts (*9*, *10*). Adding these starch nanoparticles to polymeric materials could reinforce the polymer matrix performances at low filler content in relation with their nano-sized features (*11*). However, some experimental difficulties were encountered during their preparation and recovery by controlled acid-hydrolysis, hampering their study as nanofillers. Initially, the hydrolytic procedure used for starch nanocrystals (SNCs) required very long reaction times (several weeks), ending up with low recovery yields (less than 15 wt%). Interesting enough, in order to optimize the recovery yields of SNCs, new hydrolytic procedures developed by other groups have been reported and discussed in a recent review paper (*12*).

SNCs have been mainly incorporated within polar or apolar polymers (*11*, *13–20*). Although numerous publications and reviews concern cellulose nanowhiskers (the most studied polysaccharide-based nanofillers), SNCs have remained not so much investigated (*21–27*)*, mainly in matrices* such as poly(styrene-co-butyl acrylate), natural rubber, pullulan, polylactide, thermoplastic starch, polyvinyl alcohol, soy protein, waterborne polyurethanes. Some of these studies revealed interesting mechanical and barrier properties in relation with their platelet-like morphology although the reinforcing effect provided by these SNC nanoparticles has not been completely understood yet.

However, there were some obstacles to be addressed when processed with polymeric matrices (*15*, *28–30*). Indeed, SNCs are recovered and stored in an aqueous medium due to strong hydrogen bonding (i), are poorly dispersible in common polymer solvents such as toluene (ii) without any surface modification, and present a low thermal stability when heated at moderated temperatures (iii).

To alleviate these drawbacks the surface modification of SNCs is therefore required as (*15*, *28–30*): surface-functionalization by low molecular weight organic compounds, “grafting onto” methods of pre-synthesized polymer chains and “grafting from” methods via polymerization initiated directly from the reactive surface of SNCs. The “grafting from” methods however represent the

Downloaded by NORTH CAROLINA STATE UNIV on August 28, 2012 | http://pubs.acs.org
Publication Date (Web): August 16, 2012 | doi: 10.1021/bk-2012-1105.ch016

Downloaded by NORTH CAROLINA STATE UNIV on August 28, 2012 | http://pubs.acs.org
Publication Date (Web): August 16, 2012 | doi: 10.1021/bk-2012-1105.ch016

most efficient way to achieve highest grafting density (*31–34*) as well as to significantly improve the mechanical performances of unfilled matrix.

This chapter aims at reporting on the synthesis of poly(ε-caprolactone) (PCL)-grafted SNCs via "*grafting from*" approach, and then their addition into a commercial PCL matrix, for the first time to the best of our knowledge, using melt-extrusion techniques. In this work, PCL was selected as polymeric matrix due to its biodegradability and recently-reported renewability, yielding the formation of fully renewable bio(nano)composites (*35*). Moreover, commonly used to process thermoplastic polymers, the melt-extrusion techniques have never been employed for the preparation of SNC-based (nano)composites. In this respect, ring-opening polymerization (ROP) of epsilon-caprolactone (CL) was initiated from the hydroxyl groups present at the SNC surface. As-synthesized nanohybrids (SNC-g-PCL) were finely dispersed within PCL matrix by melt-blending using a twin-screw extruder at 120°C. Both Dynamical Mechanical Thermal Analysis (DMTA) and Differential Scanning Calorimetry (DSC) were carried out in order to investigate the thermo-mechanical properties of the produced bio(nano)composites. Some revealing results were in relationship with the material morphology as studied by Atomic Force Microscopy (AFM).

Experimental Part

Materials

Waxy maize starch granules were obtained from Waxylis, Roquette S.A. (France). Sulphuric acid (95 %), acetone (99 %) and toluene (anhydrous, 99.8 %) were obtained from Sigma-Aldrich. Toluene was dried under CaH_2, and was distilled prior to use. Poly(ε-caprolactone) (PCL) under the tradename CAPA 6500 with a M_n of 50,000 g/mol was supplied by former Solvay Interox (UK) and used as received. ε-caprolactone (CL) supplied by Sigma-Aldrich was dried over calcium hydride and distilled under reduced pressure just before use. Tin(II) ethylhexanoate ($Sn(Oct)_2$) (95 %, Aldrich) was used as received.

Starch Nanocrystal Preparation

Waxy maize starch granules were submitted to acid-hydrolysis with a 3.16 M H_2SO_4 solution at 40 °C for 5 days under continuous stirring at 100 rpm. The suspension was washed with water until neutrality by using centrifugation for 10 min at 10,000 rpm and dialysis against deionized water. The resulting suspension was filtered through a N°.1 glass sinter in order to remove unhydrolyzed starch fraction, and the suspension was concentrated, providing the stock suspension. A freeze-drying procedure was applied just before polymerization or melt-processing.

Ring-Opening Polymerization of ε-Caprolactone

The freeze-dried starch nanocrytals (1.4 g) was introduced into a two-neck flask equipped with a three-way stopcock and a magnetic stirring bar under

Downloaded by NORTH CAROLINA STATE UNIV on August 28, 2012 | http://pubs.acs.org
Publication Date (Web): August 16, 2012 | doi: 10.1021/bk-2012-1105.ch016

nitrogen flow. Thereafter, 10 mL of CL (10.6 g, 93 mmol) and 2 wt% $Sn(Oct)_2$ (with respect to the monomer) were added to the reaction flask using flame-dried syringes. The polymerization was carried out for 24 h at 90°C and then stopped by adding a few drops of diluted aqueous hydrochloric acid solution (0.1 M). The surface-modified starch nanocrystals were recovered by precipitation with heptane, filtered and dried until constant weight at 40 °C under vacuum.

Melt-Blending Preparation of PLA-Based (Nano)composites

CAPA650-based (nano)composites were prepared by melt-blending in a ThermoHaake MiniLab Rheomex CTW5 mini-extruder at 120°C and at 150 rpm for 10 min. Rectangular samples (35x 12x3 mm^3) were prepared by injection-molding at 120°C for Dynamical Mechanical Thermal Analysis (DMTA). Different materials were prepared: the unfilled matrix and corresponding (nano)composites: direct SNC dispersion and SNC-*g*-PCL dispersion as masterbatch at nanofiller contents of 2, 4 and 8 wt% (Table 1).

Table 1. Composition of PCL/SNCs-based (nano)composites prepared by melt-blending

Polymer matrix	*Starch content*
CAPA 6500	0%
CAPA 6500	2, 4 and 8wt% SNC
CAPA 6500	2, 4 and 8wt% SNC-g-PCL

Characterization

Fourier transform infrared (FTIR) spectra were recorded using a BIO-RAD Excalibur spectrometer equipped with an ATR Harrick Split Pea™. Spectra were recorded using a spectral width ranging from 700 to 4000 cm^{-1}, with 4 cm^{-1} resolution and an accumulation of 16 scans. The morphology of the (nano)composites was analyzed by Atomic Force Microscopy (AFM). The samples were cryo-microtomed at -100 °C by an Ultracut FC4E microtome from Reichert-Jung. AFM images were recorded using a Nanoscope IIIa Multimode microscope operating in tapping mode at room temperature under air. Commercial probes were used with a spring constant of 20-80 N/m and a resonance frequency of about 298-335 kHz. Thermal characterizations using Differential Scanning Calorimetry (DSC) were performed using a TA Instruments Q200 apparatus. A heat/cool/heat procedure was applied using a temperature range from -80 °C to 100 °C at a heating/cooling rate of 10 °C/min. The crystallization temperature (T_c), crystallization enthalpy and melting enthalpy (ΔH_m) was determined from the second heating scan. The enthalpy values were calculated taking into account the final content of SNCs. Dynamic Mechanical Thermal Analyses (DMTA) of the (nano)composites were performed under ambient atmosphere using a 2980 DMTA apparatus from TA Instruments using a dual cantilever module. The measurements were carried out at a constant frequency of 1 Hz, a temperature range from -100 to 30 °C for PCL-based materials at a heating rate of 3 °C/min. Three samples were characterized for each composition.

Results and Discussion

Synthesis of SNC-g-PCL Nanohybrids

The synthesis of SNC-*g*-PCL nanohybrids was carried out by "grafting from" method, *that is*, via ring-opening polymerization of CL initiated onto the surface of starch nanocrystals (Figure 1). However, we first attempted the same experimental conditions used for the synthesis of PCL grafted onto cellulose nanowhiskers (*36*) with unsatisfactory results. For instance, after 24 hours of reaction, the PCL recovery yield was only of 20 wt% and complete and instantaneous sedimentation of the SNCs was observed during suspension tests carried out in toluene (a good solvent of PCL). This indicated that no PCL chains (or only few PCL chains) were grafted onto the SNC surface. In addition, it was observed that the medium became more and more yellowish and gelatinous in the course of reaction. This suggested the occurrence of SNC degradation during this tentative surface treatment. Some attempts to neutralize any residual acidic compounds derived from the preparation of SNCs were also envisioned with NaOH as base, but the results were not satisfactory again. Such results could be explained with the multi-step treatments used for recovering SNCs leading to their thermal degradation. Indeed, in contrast to cellulose and its derivatives, starch and its derivatives proved highly sensitive to both hydrolytic and thermal degradations in relation with their weak alpha-glucoside linkages (*1*).

Downloaded by NORTH CAROLINA STATE UNIV on August 28, 2012 | http://pubs.acs.org
Publication Date (Web): August 16, 2012 | doi: 10.1021/bk-2012-1105.ch016

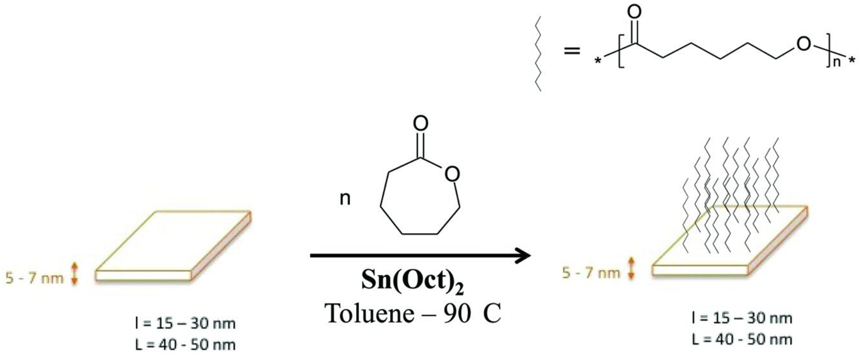

Figure 1. Ring-opening polymerization (ROP) of CL initiated onto the surface of SNCs.

Downloaded by NORTH CAROLINA STATE UNIV on August 28, 2012 | http://pubs.acs.org
Publication Date (Web): August 16, 2012 | doi: 10.1021/bk-2012-1105.ch016

Therefore, in order to avoid any further solvent exchange and distillation steps, SNCs were recovered by freeze-drying method and directly used for ROP of CL. $Sn(Oct)_2$-catalyzed ROP of CL was carried out starting from these as-freeze-dried SNCs at 90°C for 24 hours. Interestingly, no yellowish coloration from the medium was observed. In addition, a high recovery yield was achieved (97 %), for a final content of SNC within the nanohydrids close to 12 wt% (Table 2). FTIR analyses show the presence of two intense peaks centered at 1730 cm^{-1} and 2866 cm^{-1}, ascribed to the stretching of the PCL ester groups and the PCL methylene groups (Figure 2). In addition, the free-hydroxyl band at 3300 cm^{-1} was largely decreased, all confirming PCL-grafting onto SNC nanoparticles.

Table 2. Experimental composition and recovery yield obtained for the synthesis of SNC-g-PCL nanohybrid (bulk, time = 24 h, T = 90 °C)

Name	m_{SNC} *(g)*	m_{CL} *(g)*	$m_{SNC\text{-}g\text{-}PCL}$ [a] *(g)*	*Yield* [a] *(%)*	*% CNWr* [b]
SNC-g-PCL	1.4	10.6	11.6	97	12

[a] Determined by gravimetry ; [b] $\%SNC = (m_{SNC}/m_{SNC\text{-}g\text{-}PCL})*100$

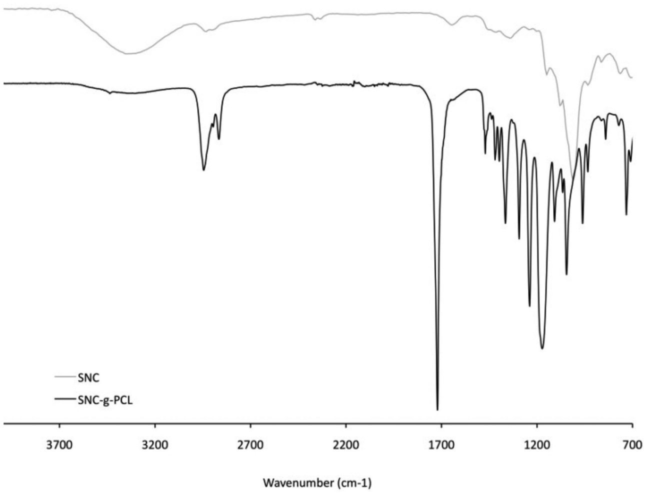

Figure 2. FTIR spectra of SNCs (A) before and (B) after PCL grafting reaction.

Downloaded by NORTH CAROLINA STATE UNIV on August 28, 2012 | http://pubs.acs.org
Publication Date (Web): August 16, 2012 | doi: 10.1021/bk-2012-1105.ch016

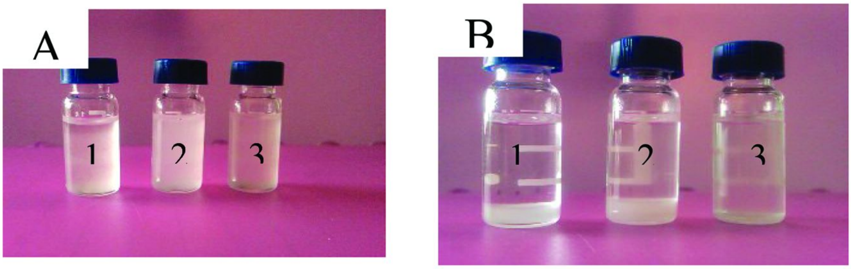

Figure 3. (1) Neat SNCs, (2) homo-PCL + SNCs simple mixture, and (3) SNC-g-PCL nanohybrids in toluene suspension: pictures recorded (A) immediately after stopping the stirring agitation and (B) after 20 minutes.

The grafting efficiency was indirectly evaluated by suspension tests carried out in a good solvent of PCL, *i.e.,* toluene, and compared with neat SNCs and a physical mixture of SNCs and PCL. As shown in Figure 3, the suspension of SNC-g-PCL nanohybrids remains stable in the apolar solvent after 20 minutes. In contrast, the other samples settled down rapidly. In the case of SNC-g-PCL nanohybrids, the fine dispersion of SNCs in toluene could be consequently attributed to the covalent polymer grafting on the starch nanoparticle surface.

PCL-Based Bio(nano)composites

PCL-based (nano)composites were prepared by dispersing SNC-*g*-PCL nanohybrids or SNCs within a commercial PCL matrix using melt-processing techniques. The melt-blending process was carried out at 120°C in a twin-screw co-rotating micro-compounder (10 min, 150 rpm). The content in SNCs (grafted or not) was varied from 2 to 8 wt% (see Table 1). In the case of neat SNCs, the morphological analyses revealed a poor dispersion of neat SNCs within the polymeric matrix, as shown by the presence of micron-sized aggregates (Figure 4). In the case of SNC-*g*-PCL, the morphology is quite different with the presence of individual SNC nanoparticles, together with only a few aggregates. It is worth noting that the origin of these aggregates may be raised from the freeze-drying step. Interestingly, individual starch nanoplatelets have the same nanometric dimensions as those reported by Angellier et al (*16*), attesting that the inherent structure of SNCs is still preserved after melt-processing.

The isochronal evolution of storage modulus (E′) against temperature was determined with the unfilled PCL matrix, SNC-filled (nano)composite and the SNC-*g*-PCL-filled (nano)composites (Figure 5). E′ was normalized at -100°C. From Figure 5, after the relaxation observed at -60°C associated to the glass transition temperature of PCL, a clear increase of the E′ is observed on increasing SNCs contents. This increase is much pronounced when SNC-*g*-PCL nanohydrids is used. This is also confirmed by the E′ determined at 20°C (Table 3). For instance, E′ increases from 423 MPa for the neat PCL matrix to 570 MPa for PCL/8 wt% SNCs-based composition and 710 MPa for PCL/8 wt% SNC-g-PCL-based nanocomposites.

Downloaded by NORTH CAROLINA STATE UNIV on August 28, 2012 | http://pubs.acs.org
Publication Date (Web): August 16, 2012 | doi: 10.1021/bk-2012-1105.ch016

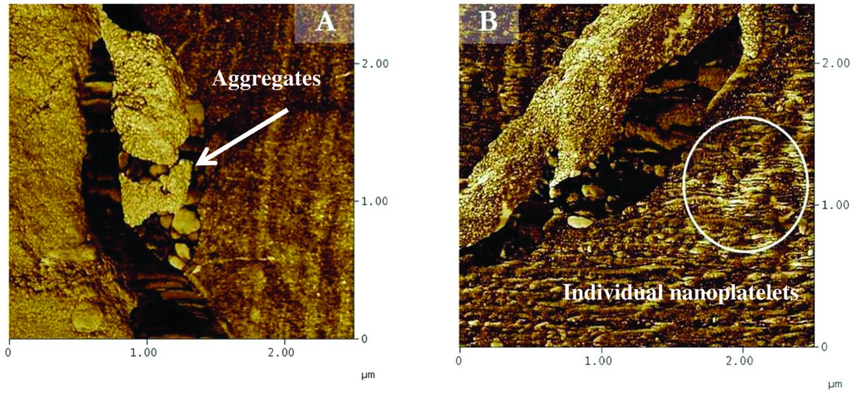

Figure 4. AFM images (phase) of CAPA6500/8wt% SNCs (A) and CAPA6500/8wt% SNC-g-PCLs (B).

Table 3. Evolution of E′ (determined at 20°C) for SNC-based (nano)composites (SNCs grafted or not) and comparison to neat PCL

Entry	*Samples*	*E′ 20°C (MPa)*
1	CAPA6500	423±99
2	+2wt%SNC	505±27
3	+4wt%SNC	515±105
4	+8wt% SNC	570±62
5	+2wt%SNC-g-PCL	539±25
6	+4wt%SNC-g-PCL	615±59
7	+8wt%SNC-g-PCL	710±70

Table 4 summarizes the DSC results obtained with PCL (nano)composites, compared with neat PCL. In the case of neat PCL, a melting temperature at 59 °C is observed with a crystallization peak at 35 °C. Under these DSC conditions, the glass transition temperature was hardly discerned and therefore not reported. From these results, both the melting (T_m) and crystallization temperatures (T_c) are similar, regardless of the SNCs loading and nature. While having melting (ΔH_m) and crystallization enthalpies (ΔH_c) for non-grafted SNCs comparable, these values are modified on addition of SNC-g-PCL based-nanohybrids, reaching an enhancement of ca. 50 % for CAPA6500/8wt%SNC-g-PCL (entry 7, Table 4). The covalent grafting of PCL onto these SNCs nanoparticles allows enhancing the PCL matrix crystallinity, dispersed starch nanoparticles, acting therefore as nucleating agents.

Downloaded by NORTH CAROLINA STATE UNIV on August 28, 2012 | http://pubs.acs.org
Publication Date (Web): August 16, 2012 | doi: 10.1021/bk-2012-1105.ch016

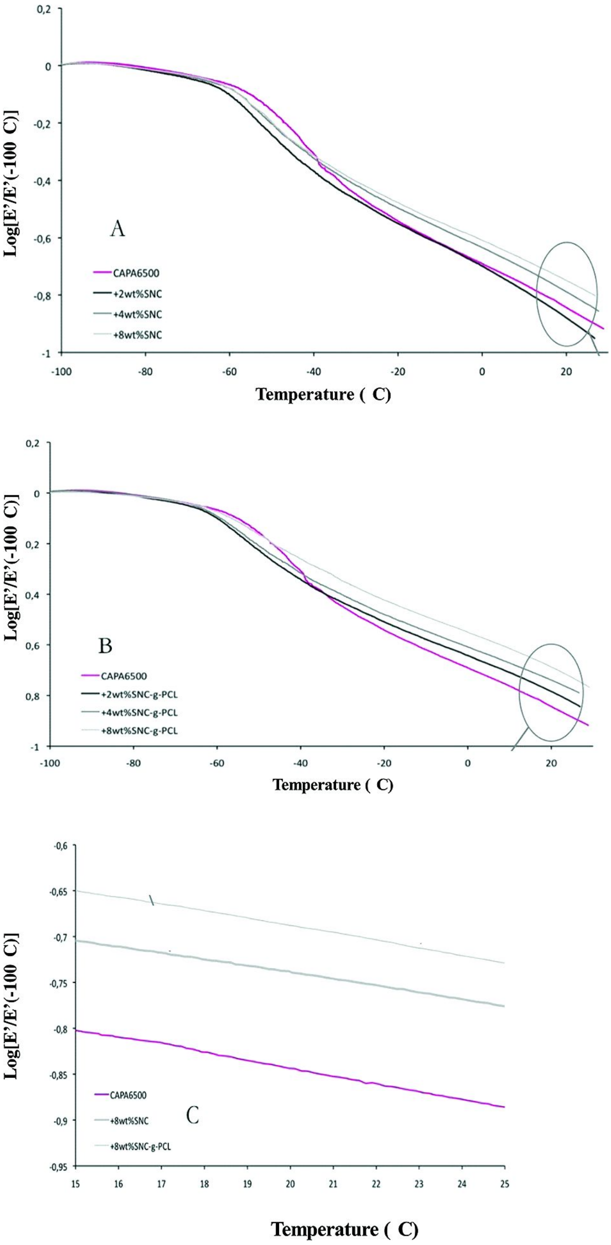

Figure 5. Logarithmic evolution of E' vs. temperature for bio(nano)composites reinforced with SNCs (A) and SNC-g-PCL (B). Zoom of E' values for 8wt% SNCs (C).

Downloaded by NORTH CAROLINA STATE UNIV on August 28, 2012 | http://pubs.acs.org
Publication Date (Web): August 16, 2012 | doi: 10.1021/bk-2012-1105.ch016

Table 4. DSC analyses of unfilled CAPA6500, CAPA6500/SNCs and CAPA6500/SNC-g-PCL (2, 4, and 8wt%) (Heat/Cool/Heat from -80 to 100°C - heating rate of 10°C/min)

Entry	*Samples*	T_c (°C)	ΔH_c (J/g)	T_m (°C)	ΔH_m (J/g)
1	CAPA6500	35	58	59	56
2	+2wt%SNC	34	60	58	58
3	+4wt%SNC	35	59	57	58
4	+8wt%SNC	35	58	58	60
5	+2wt%SNC-g-PCL	33	64	58	63
6	+4wt%SNC-g-PCL	35	81	57	79
7	+8wt%SNC-g-PCL	36	76	58	75

Conclusions

In the chapter, PCL chains were covalently grafted onto the SNC surface via a ‘grafting from’ approach on the basis of *in situ* $Sn(Oct)_2$-catalyzed ring-opening polymerization of CL. When melt-blended using extrusion techniques at high temperature, this PCL grafting allowed enhancing the SNC dispersion via an interfacial compatibilization between starch nanoparticles and PCL. This also led to some improvements in terms of mechanical and crystalline properties for the resulting PCL bio(nano)composites. Although better improvements must be still obtained, this first study shows the potential applications of SNCs as reinforcing agents of polymer matrix in order to prepare new bio(nano)composites with interesting high-performance properties.

Acknowledgments

The authors are grateful to the “Région Wallonne” and European Community (FEDER, FSE) in the frame of “Pôle d’Excellence Materia Nova” and the excellence program “OPTI^{2}MAT” for their financial support. LPCM thanks the “Belgian Federal Governement Office Policy of Science (SSTC)” for general support in the frame of the PAI-6/27. A.-L. Goffin thanks F.R.I.A. for her PhD thesis grant. J.-M. Raquez is “chargé de recherches” from the F.R.S.- FNRS. R. Lazzaroni and his collaborators (CIRMAP) are warmly thanked for their help in AFM characterization.

References

1. Gross, R. *Science* **2002**, *297*, 803.
2. Mohanty, A. K.; Misra, M.; Hinrichsen, G. *Macromol. Mater. Eng.* **2000**, *276/277*, 1.

Downloaded by NORTH CAROLINA STATE UNIV on August 28, 2012 | http://pubs.acs.org
Publication Date (Web): August 16, 2012 | doi: 10.1021/bk-2012-1105.ch016

3. de Graaf, R.; Karman, A.; Janssen, L. *Starch/Stärke* **2003**, *55*, 80.
4. Forssell, P.; Mikkila, J.; Suortti, T.; Seppala, J.; Poutanen, K. *J. Macromol. Sci., Pure Appl. Chem.* **1996**, *A33*, 703.
5. Nabar, Y.; Raquez, J-M.; Dubois, P.; Narayan, R. *Biomacromolecules* **2005**, *6*, 807.
6. Nayak, P. *J. Macromol. Sci., Rev. Macromol. Chem. Phys.* **1999**, *C39* (3), 481.
7. Stepto, R. *Macromol. Symp.* **2003**, *201*, 203.
8. Van Soest, J.; Benes, K.; de Witt, D. *Polymer* **1996**, *37*, 3543.
9. Angellier, H.; Choisnard, L.; Molina-Boisseau, S.; Ozil, P.; Dufresne, A. *Biomacromolecules* **2004**, *5*, 1545.
10. Viguie, J.; Molina-Boisseau, S.; Dufresne, A. *Macromol. Biosci.* **2007**, *7*, 1206.
11. Dufresne, A.; Cavaillé, J.-Y. *J. Polym. Sci., Part B: Polym. Phys.* **1998**, *36*, 2211.
12. Le Corre, D.; Bras, J.; Dufresne, A. *Biomacromolecules* **2010**, *11*, 1139.
13. Angellier, H.; Molina-Boisseau, S.; Dufresne, A. *Macromolecules* **2005**, *38*, 9161.
14. Kristo, E.; Biliaderis, C. G. *Carbohydr. Polym.* **2007**, *68*, 146.
15. Yu, J.; Ai, F.; Dufresne, A.; Gao, S.; Huang, J.; Chang, P. R. *Macromol. Mater. Eng.* **2008**, *293*, 763.
16. Angellier, H.; Molina-Boisseau, S.; Dole, P.; Dufresne, A. *Biomacromolecules* **2006**, *7*, 531.
17. Lin, N.; Yu, JH.; Chang, P. R.; Li, J. L.; Huang, J. *Polym. Comp.* **2011**, *32*, 472.
18. Garcia, N. L.; Ribba, L.; Dufresne, A.; Aranguren, M. I.; Goyanes, S. *Macromol. Mater. Eng.* **2009**, *294*, 169.
19. Chen, Y.; Cao, X.; Chang, P. R.; Huneault, M. A. *Carbohydr. Polym.* **2008**, *73*, 8.
20. Zheng, H.; Ai, F.; Chang, P. R.; Huang, J.; Dufresne, A. *Polym. Compos.* **2009**, *30*, 474.
21. Samir, M.; Alloin, F.; Dufresne, A. *Biomacromolecules* **2005**, *6*, 612.
22. Siqueira, G.; Bras, J.; Dufresne, A. *Biomacromolecules* **2008**, *10*, 425.
23. Dubief, D.; Samain, E.; Dufresne, A. *Macromolecules* **1999**, *32*, 5765.
24. Habibi, Y.; Lucia, L. A.; Rojas, O. J. *Chem. Rev.* **2010**, *110*, 3479.
25. Ljungberg, N.; Cavaillé, J.-Y.; Heux, L. *Polymer* **2006**, *47*, 6285.
26. Chazeau, L.; Cavaillé, J.-Y.; Canova, G.; Dendievel, R.; Boutherin, B. *J. Appl. Polym. Sci.* **1999**, *71*, 1797.
27. Favier, V.; Chanzy, H.; Cavaille, J.-Y. *Macromolecules* **1996**, *28*, 6365.
28. Namazi, H.; Dadkhah, A. *J. Appl. Polym. Sci.* **2008**, *110*, 2405.
29. Thielemans, W.; Belgacem, M. N.; Dufresne, A. *Langmuir* **2006**, *22*, 4804.
30. Chang, P. R.; Ai, F.; Chen, Y.; Dufresne, A.; Huang, J. *J. Appl. Polym. Sci.* **2009**, *111*, 619.
31. Heux, L.; Chauve, G.; Bonini, C. *Langmuir* **2000**, *16*, 8210.
32. Kvien, I.; Bjom, S. T.; Oksman, K. *Biomacromolecules* **2005**, *6*, 3160.
33. Goussé, C.; Chanzy, H.; Exoffier, G.; Soubeyrand, L.; Fleury, E. *Polymer* **2002**, *43*, 2645.

34. Grunert, M.; Winter, W. T. *J. Polym. Environ.* **2002**, *10*, 27.
35. Buntara, T.; Noel, S.; Phua, P. H.; Melián-Cabrera, I.; de Vries, J. G.; Heeres, H. J. *Ang. Chem., Int. Ed.* **2011**, *50*, 7083.
36. Habibi, Y.; Goffin, A.-L.; Schiltz, N.; Duquesne, E.; Dubois, Ph.; Dufresne, A. *J. Mat. Chem.* **2008**, *18*, 5002.

Downloaded by NORTH CAROLINA STATE UNIV on August 28, 2012 | http://pubs.acs.org
Publication Date (Web): August 16, 2012 | doi: 10.1021/bk-2012-1105.ch016

Downloaded by UNIV OF GUELPH LIBRARY on August 28, 2012 | http://pubs.acs.org
Publication Date (Web): August 16, 2012 | doi: 10.1021/bk-2012-1105.ch017

Chapter 17

Oleic Acid and Undecylenic Acid as Platform Chemicals for Thermoplastic Polyurethanes

Gerard Lligadas, Juan C. Ronda, Marina Galià, and Virginia Cádiz[*]

Departament de Química Analítica i Química Orgànica, Universitat Rovira i Virgili, C/ Marcel.lí Domingo s/n, 43007 Tarragona, Spain
[*]E-mail: virginia.cadiz@urv.cat

Nowadays, the utilization of raw materials derived from renewable feedstock is in the spotlight of the chemical industry. Vegetable oils are an important platform chemicals due to their universal availability, inherent biodegradability and low price. Taking into account that polyurethanes are one of the most versatile industrial products suitable for use in many fields, here we present our research on exploiting oleic and undecylenic acids in the preparation of biobased polyols and derived thermoplastic polyurethanes.

Introduction

Renewable resources are recently gaining a lot of attention to substitute petroleum for producing polymers (*1*). It is not only a consideration for the future shortage of petroleum supplies, but also a sense of environmental protection. Vegetable oils are one of the cheapest and most abundant biological sources available in large quantities and are predominantly mixtures of triglyceride molecules, which have the three-armed star structure shown in Figure 1. Triglycerides are made up of three fatty acids joined at a glycerol junction. Most of the common oils contain fatty acids that vary from 12 to 22 carbons in length, with 0 to 3 double bonds per fatty acid. Thus, triglycerides have a non-perfect molecular structure which contains a statistical number of various fatty acid chains. Classical and well-established oleochemical transformations occur preferently at the ester functionality of the native triglycerides, such as hydrolysis to free fatty acids and glycerol and transesterification to fatty acid methyl esters (*2*). The annual global production of the major vegetable oils

In Biobased Monomers, Polymers, and Materials; Smith, P., et al.;
ACS Symposium Series; American Chemical Society: Washington, DC, 2012.

(from palm, soy, rapeseed, cotton, sunflower, palm kernel, olive, and coconut) amounted to 84.6 million tons (Mt) in 1999/2000 and increased to 137.3 Mt in 2009/2010 (an increase of 62%). The production of fatty acids is the highest volume oleochemical process and accounts for about 52% of industrially used oils and fats. The world supply of fatty acids has almost doubled from 2001 to 2008 (*3*).

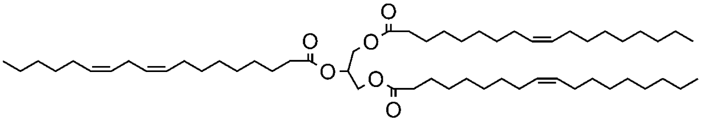

Figure 1. Schematic representation of triglyceride molecule structure.

Their use as starting materials has numerous advantages: for example, low toxicity, inherent biodegradability, and high purity (*3*), thus they are considered to be one of the most important classes of renewable resources for the production of biobased polymers (*4*). Nevertheless, the non-perfect molecular structure of triglycerides can be an issue when well-defined polymers are targeted.

Polyurethanes (PUs) are one of the most important and versatile classes of polymers and can vary from thermoplastic to thermosetting materials. The industrial production of PUs is normally accomplished through the polyaddition reaction between organic isocyanates and compounds containing active hydroxyl groups, such as polyols. Usually, both isocyanate and polyol are petroleum-based. Due to uncertainty about the future cost of petroleum as well as the desire to move toward more environmentally friendly feedstocks, many recent efforts have focused on replacing all or part of the conventional petroleum-based polyols with those made from vegetable oils. Combined with isocyanates, vegetable-oil based polyols produce PUs that can compete in many ways with PUs derived from petrochemical polyols. Moreover, due to the hydrophobic nature of triglycerides, vegetable oil-based polyols produce PUs that have excellent chemical and physical properties such as enhanced hydrolytic and thermal stability (*5*).

With the exception of castor oil, vegetable oils must be functionalized with hydroxyl groups to be used as polyols for PU synthesis. Triglycerides and fatty acids contain several active sites amenable to chemical reaction, being double bonds and ester groups the most important. These active sites open up various strategies to tailor new biosourced target molecules exhibiting the architectural features and chemical functionalities of the currently available PU precursors of petrochemical origin, polyether and polyester polyols.

The preparation of polyols from vegetable oils has been recently reviewed by us (*6*). Traditionally, plant oil-based polyols have been prepared starting from triglyceride molecules. These polyols have been succesfully prepared by different

Downloaded by UNIV OF GUELPH LIBRARY on August 28, 2012 | http://pubs.acs.org
Publication Date (Web): August 16, 2012 | doi: 10.1021/bk-2012-1105.ch017

Downloaded by UNIV OF GUELPH LIBRARY on August 28, 2012 | http://pubs.acs.org
Publication Date (Web): August 16, 2012 | doi: 10.1021/bk-2012-1105.ch017

ways, being the epoxidation of carbon-carbon double bonds and further oxirane ring-opening with alcohols or other nucleophiles the most common approach. Other methodologies involve the transesterification with multifunctional alcohols and the combination of hydroformylation or ozonolysis and subsequent reduction of carbonyl groups. More recently, thiol-ene addition has been applied to rapeseed oil to prepare biobased polyols (*7*). Polyols have also been prepared from fatty acids and fatty acid methyl esters by polycondensation of hydroxyl containing fatty acid with multifunctional alcohols, ring-opening polymerization of epoxidized fatty acids and subsequent partial reduction of ester groups or cyclotrimerization of alkyne-containing fatty acids and subsequent reduction (*6*).

Limited attention has been paid to the preparation of diols from fatty acids with functionality 2, requirement for thermoplastic polyurethane (TPU) formulations. Dimerization of oleic and linoleic acids, producing a complex mixture known as dimer acid, and consecutive reduction of carboxylate groups is a classical procedure for the synthesis of long-chain diol known as dimer diol. This methodology was originally introduced in the 1950s by General Mills Chemicals and Emery (now Cognis Corp.) (*8*, *9*). Dimer diol, dimer diol oligoethers (manufactured by acid-catalyzed dehydration of dimer diol), and dimer diol oligocarbonates (synthesized by transesterification with dimethyl carbonate) are commercially available. Due to their improved stability toward hydrolysis and oxidation, dimer diol polyethers (and dimer diol polycarbonates) are used as soft segments in the preparation of saponification-resistant TPU sealings. Recently, Cramail et al. have reported some procedures for the preparation of diols from oleic and ricinoleic acids (*10*).

The metathesis reaction is also a prominent tool for the preparation of fatty acid-derived diols, including dimer fatty acids and derivatives (*6*, *11*, *12*). By taking advantage of this methodology, 1,18-octadec-9-endiol, a long chain diol from oleic acid, was synthesized using second generation Grubbs catalyst. Alternatively, 1,9-nonanediol was synthesized by cleaving oleic acid via ozonolysis followed by oxidation to azealic acid and reduction of carboxylate groups. Classical polycondensation reactions have also been used for the preparation of oligomeric diols from methyl ricinoleate and diethylene glycol by polycondensation at high temperatures. This product was used as soft segment in the preparation of segmented PUs.

In this context, our research is focused on the preparation of diols from oleic acid (OL) and undecylenic acid (UD) applying thiol-ene click additions. OL is a C18 fatty acid containing a carbon-carbon double bond at 9th position that can be found in several natural oils such as olive oil (71%), canola oil (61%), sunflower oil (42%) and palm oil (39%). Modern genetic engineering techniques are already able to develop natural oils with much higher content of an individual fatty acid. For example, “high oleic” sunflower oil with an oleic acid content of more than 90% is available. UD is a C11 fatty acid-derivative with a terminal carbon-carbon double bond. It can be easily obtained from castor oil. Up to 90% of the fatty acid fraction in castor oil is ricinoleic acid. UD can be obtained by heating ricinoleic acid under vacuum pyrolysis. Several mechanisms, including a McLafferty-type rearrangement (Figure 2) and a free-radical mechanism (*13*), have been proposed for the transformation of ricinoleic acid into UD and heptaldehyde.

Downloaded by UNIV OF GUELPH LIBRARY on August 28, 2012 | http://pubs.acs.org
Publication Date (Web): August 16, 2012 | doi: 10.1021/bk-2012-1105.ch017

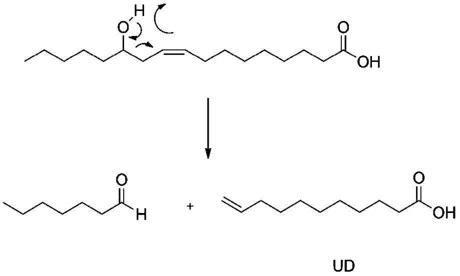

Figure 2. McLafferty-type rearrangement of ricinoleic acid to UD and heptaldehyde.

Classically the reaction between a thiol and a double bond has received significant attention as candidate for many applications including coatings, adhesives, dental materials, and imprinting lithography. Resurgence over the past decades has occurred in response to the many benefits thiol-ene coupling presents for polymer synthesis: tolerance to many different reaction conditions/solvents, clearly defined reaction pathways/products, and facile synthetic strategies from a range of easily obtained starting materials (*14*). Thus, thiol-ene chemistry has recently emerged as a powerful tool for synthetic chemistry and polymer functionalization that has the potential to fall within the realm of click chemistry (*15–17*). The thiol-ene coupling makes use of the high nucleophilicity of the sulfhydryl moiety and proceeds under physiological conditions. The formed thioether linkage is very stable under physiological conditions and resists a strong basic or acidic environment and is also stable toward reducing agents; however, it is susceptible toward oxidizing agents. The robust nature of thiol-ene chemistry allows for the preparation of well-defined materials with few structural limitations and synthetic requirements (*18*). While both heat and light have been used to generate radicals that initiate the thiol-ene radical chain process, the use of light has enormous advantages for small molecule synthesis, surface and polymer modification, and polymerization reactions. A vast array of work has been performed in an effort to understand and implement radical-mediated thiol-ene reactions, primarily focusing on the photo-initiated reactions. This large body of literature is detailed in very recent review articles (*19–22*).

In the last decade, many authors have reported the use of vegetable oils as feedstock for UV-curable systems (*23–25*), and although UV-curable chemistries based upon thiol-ene functionality offer many advantages (*26*, *27*), only recently thiol-ene UV-curable coatings using vegetable oils is reported (*28*).

In particular, thiol-ene click chemistry of fatty acid derivatives obtained from plant oils (*29*), is a promising route that can be used for the synthesis of novel chemical intermediates from renewable resources.

Downloaded by UNIV OF GUELPH LIBRARY on August 28, 2012 | http://pubs.acs.org
Publication Date (Web): August 16, 2012 | doi: 10.1021/bk-2012-1105.ch017

OL and UD-Based Diols and Derived Polyurethanes

Naturally occurring undecylenic and oleic acids were used as raw materials for the synthesis of novel biobased diols (*30*). UDM-diol and OLM-diol (Figure 3A and B) were obtained in high yields applying photoinitiated thiol-ene coupling with 2-mercaptoethanol (ME) to methyl esters of undecylenic and oleic acids (UDM and OLM respectively), and the subsequent reduction.

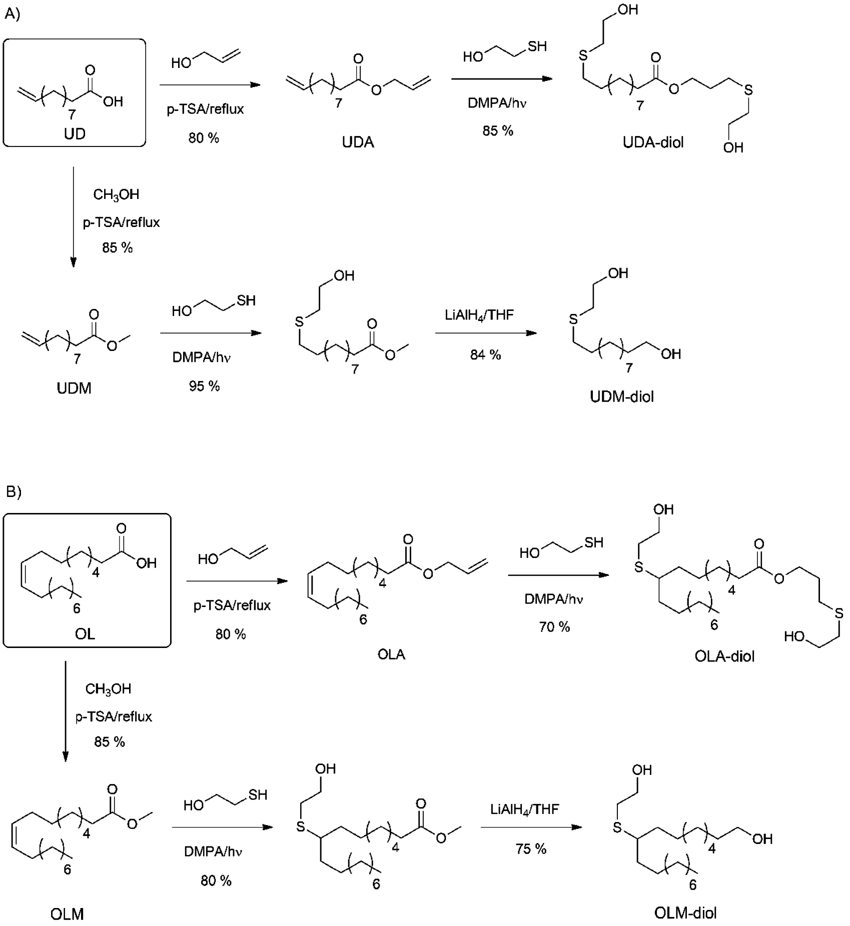
A)
UD
7
OH
p-TSA/reflux
80 %
UDA
DMPA/hν
85 %
UDA-diol
CH₃OH
p-TSA/reflux
85 %
UDM
DMPA/hν
95 %
LiAlH₄/THF
84 %
UDM-diol
B)
OL
4
6
p-TSA/reflux
80 %
OLA
DMPA/hν
70 %
OLA-diol
CH₃OH
p-TSA/reflux
85 %
OLM
DMPA/hν
80 %
LiAlH₄/THF
75 %
OLM-diol

Figure 3. Synthetic procedure for the preparation of UD- and OL-derived diols using thiol-ene click coupling as a key step.

As expected, the addition of ME to UDM reached 100% conversion in few minutes, whereas the addition to OLM required longer reaction times (90 min to reach 99% conversion). This difference in reactivity is due to reversible addition of thyil radical to internal C=C bonds which is accompanied with an *cis/trans* isomerisation process. ^{1}H NMR spectra during the photoinitiated thiol-ene coupling between ME and methyl oleate (MO) shows how as the reaction proceeds, a new signal corresponding to *trans* C=C bonds appears confirming that *cis/trans* isomerization is taking place (Figure 4).

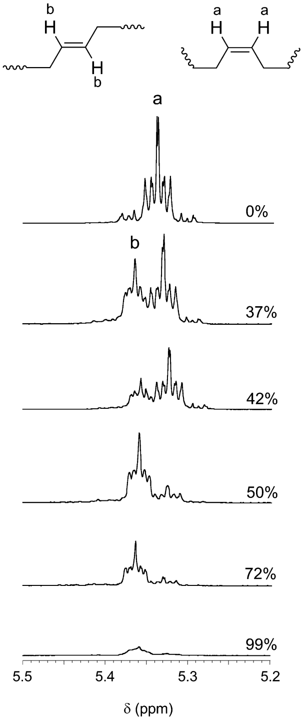

Figure 4. Expansion of the 400 MHz ^{1}H NMR spectra during the photoinitiated thiol-ene coupling between 2-mercaptoethanol and methyl oleate.

ME addition was also applied to undecylenic and oleic acid allyl ester derivatives (UDA and OLA, respectively) leading to two ester containing biobased diols, UDA-diol and OLA-diol. Although allyl alcohol is a large-scale industrial chemical, UDA and OLA are potentially 100% biomass-derived monomers since allyl alcohol can be easily obtained from glycerol (*31*). Polyester and polyanhydride precursors have also been prepared from fatty acids via thiol-ene additions with functional tiols (*32*, *33*)

In Biobased Monomers, Polymers, and Materials; Smith, P., et al.;
ACS Symposium Series; American Chemical Society: Washington, DC, 2012.

Downloaded by UNIV OF GUELPH LIBRARY on August 28, 2012 | http://pubs.acs.org
Publication Date (Web): August 16, 2012 | doi: 10.1021/bk-2012-1105.ch017

Linear PUs with molecular weight of 36-83 KDa range were obtained in DMF solution in high yields by polymerization of the above mentioned diols with 4,4'-methylenebis(phenylisocyanate) (MDI) applying conventional heating (50 °C) for 24 h using tin (II) 2-ethylhexanoate as catalyst. High intensity ultrasound irradiation was also utilized for comparison to the preparation of the PU derived from UDA-diol. In this case, the sonochemical reaction proceeded faster in the early stages and led to higher molecular weight PU (Figure 5).

Downloaded by UNIV OF GUELPH LIBRARY on August 28, 2012 | http://pubs.acs.org
Publication Date (Web): August 16, 2012 | doi: 10.1021/bk-2012-1105.ch017

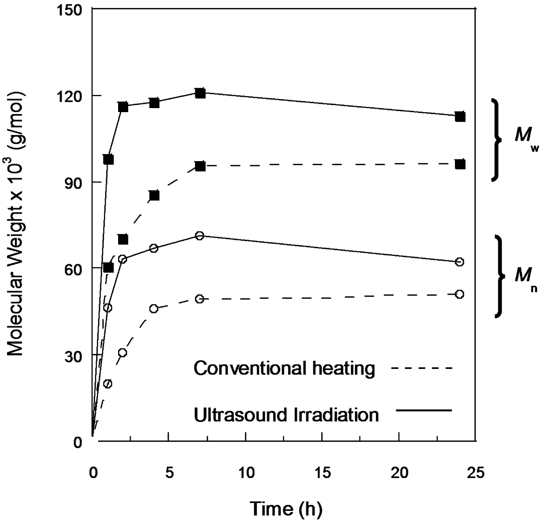

Figure 5. Polyaddition of UDA-diol with MDI. Evolution of M_n and M_w versus time under conventional heating and ultrasound irradiation.

All synthesized PUs showed good thermal stabilities ($T_{5\%}$ weight loss 270-300°C) and excellent hydrolytic resistance at pH 7.4 (no weight loss and decrease in the molecular weight were observed after 6 months in a sodium phosphate buffer solution at 60 °C) due to its high hydrophobicity. This hydrophobic character can be exploited in moisture-sensitive environments and long-term applications. DSC analysis showed that synthesized PUs crystallinity is dependent on the parent diol structure. PUs from undecylenic acid derivatives UDM-diol and UDA-diol showed higher crystallynity than those PUs derived from oleic acid-based diols (OLM and OLA). This can be related to the presence of pendant chains that difficult packing in OL derivatives. This fact determined the different stress-strain behaviour observed for all the synthesized PUs (Figure 6). The stress-strain behaviour of PUs from undecylenic acid derivatives UDM-diol and UDA-diol shows a yield point as a result of the presence of crystalline domains which act increasing the rigidity of the material.

Downloaded by UNIV OF GUELPH LIBRARY on August 28, 2012 | http://pubs.acs.org
Publication Date (Web): August 16, 2012 | doi: 10.1021/bk-2012-1105.ch017

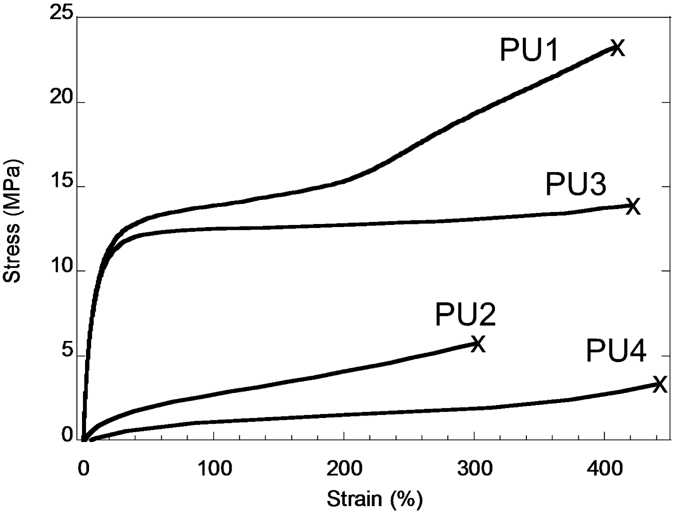

Figure 6. Stress-strain curves of the polyurethanes (PU1: from UDM-diol; PU2: from OLM-diol; PU3: from UDA-diol; PU4: from OLA-diol).

Cytotoxicity of PUs was evaluated using the MTT assay for testing the toxicity of eluates. The MTT assay is a colorimetric assays for measuring the activity of enzymes that reduce MTT to formazan dye, giving a purple color. This test can be used to determine cytotoxicity of potential medicinal agents and toxic materials, since those agents would stimulate or inhibit cell viability and growth. Figure 7 shows that cell viability was not affected by the presence of extracts from any PU systems within seven days, reaching values higher than 85% of the control TMX in all polymers. These initial cytotoxicity tests indicates that these materials are promising for biomedical purposes, however, further testing is required to ascertain whether they are compatible.

To further explore the potential of thiol-ene coupling in the functionalization of plant oil derivatives, we developed an efficient and versatile “one pot” method for the preparation of well-defined telechelic diols from UDA via two sequential thiol-ene click processes: step-growth photopolymerization and post-polymerization end group modification (Figure 8) (*34*). A major problem for the preparation of telechelic polymers and particularly for the transformation of end-groups is the incompleteness of the reactions. Thus, it is essential to develop synthetic methodologies involving high efficient reactions such as thiol-ene coupling.

Downloaded by UNIV OF GUELPH LIBRARY on August 28, 2012 | http://pubs.acs.org
Publication Date (Web): August 16, 2012 | doi: 10.1021/bk-2012-1105.ch017

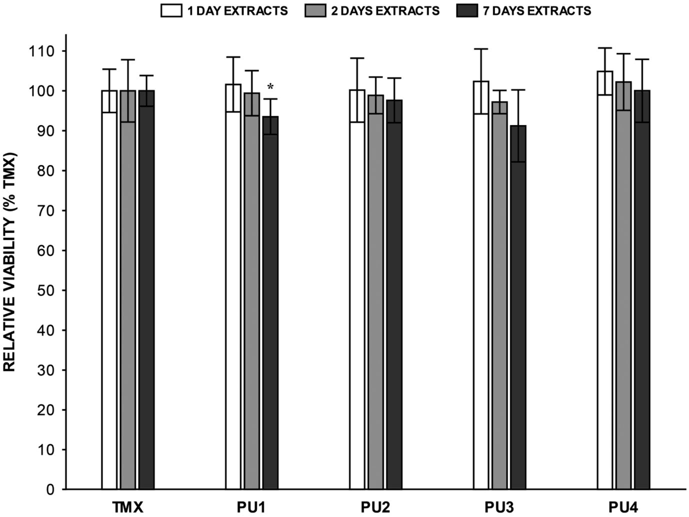

*Figure 7. MTT cytotoxicity results for control TMX and polyurethanes (PU1: from UDM-diol; PU2: from OLM-diol; PU3: from UDA-diol; PU4: from OLA-diol). Results are the mean ± standard deviation. Statistical analysis (n=12) of each polymer was performed with respect to TMX at a significance level of *: $p < 0.05$.*

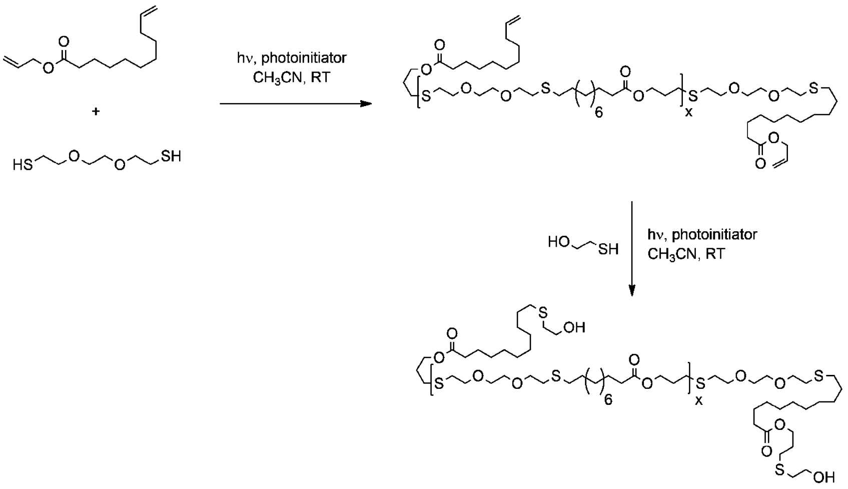

Figure 8. Synthetic procedure for the preparation of telechelics from UDA, 3,6-dioxa-1,8-octanedithiol and 2-mercaptoethanol through two consecutive thiol-ene click reactions.

Downloaded by UNIV OF GUELPH LIBRARY on August 28, 2012 | http://pubs.acs.org
Publication Date (Web): August 16, 2012 | doi: 10.1021/bk-2012-1105.ch017

UDA and a 3,6-dioxa-1,8-octanedithiol were "clicked" to prepare alkene-functionalized linear polymers with variable molecular weight by thiol-ene click step-growth polymerization. Thereafter, the modification at the polymer terminus has been done using ME to prepare new biobased telechelic diols with targeted molecular weight up to 3000 g/mol. An exhaustive ^{1}H NMR and MALDI-TOF MS analyses demonstrated the highly end-group fidelity of this methodology being an interesting procedure for the accelerated preparation of telechelics derived from divinyl monomers. Figure 9 shows the complete chain ends modification with ME by MALDI-TOF MS. It can be seen that series corresponding to alkene-terminated oligomers complete disappears and a new series corresponding to the hydroxyl-containing oligomers appears 157 mass units above the former series. This value corresponds to two times the molar mass of ME and confirms the click joining of two ME at both polymer end groups.

UDA-based telechelic diols prepared using this methodology were reacted with MDI and 1,4-butanediol as chain extender to obtain multiblock poly(ester urethane) with phase separated morphology. A two-step PU synthetic method resulted in a segmented TPU with a low temperature T_g and a melting point at -45 °C and -9 °C, respectively. A second T_g with a midpoint of approximately 55 °C and a broad melting endotherm at 190 °C corresponding to 1,4-butanediol/MDI domains support the phase separated morphology.

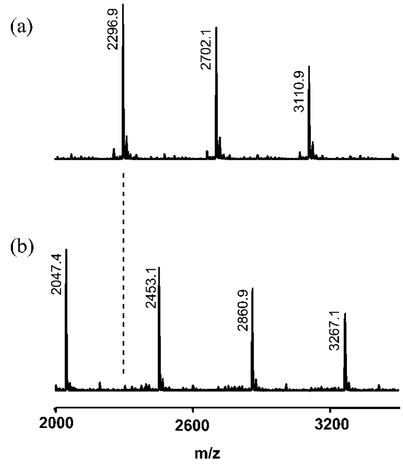

Figure 9. Expanded MALDI-TOF MS spectra of (a) alkenyl-terminated oligomer and (b) the corresponding diol, recorded during the preparation of telechelic diols from UDA.

Downloaded by UNIV OF GUELPH LIBRARY on August 28, 2012 | http://pubs.acs.org
Publication Date (Web): August 16, 2012 | doi: 10.1021/bk-2012-1105.ch017

Conclusions

We developped a general route via thiol-ene addition to obtain diols and oligomeric diols from fatty acid derivatives. The resulting monomers were polymerized with MDI to produce the corresponding linear PUs. Ultrasound irradiation has been proved to improve the PU synthesis. The prepared PUs were characterized and revealed good thermal and mechanical properties, making them possible candidates for the substitution of petroleum based materials. The above presented results envision that thiol-ene click chemistry is a promising route for designing novel bio-inspired monomers and shaping structural and functional polymers.

Acknowledgments

The authors express their thanks to CICYT (Comisión Interministerial de Ciencia y Tecnología) (MAT2008-01412) for financial support, and Dr. J. Parra for cytotoxicity assays.

References

1. Gandini, A. *Macromolecules* **2008**, *41*, 9491–9504.
2. Anneken, D. J.; Both, S.; Christoph, R.; Fieg, G.; Steinberner, U.; Westfechtel, A. Fatty Acids. In *Ullmann's Encyclopedia of Industrial Chemistry*, Online ed.; Wiley-VCH: Weinheim, Germany, 2006.
3. Biermann, U.; Bornscheuer, U.; Meier, M. A. R.; Metzger, J. O.; Schäfer, H. J. *Angew. Chem. Int. Ed.* **2011**, *50*, 3854–3871.
4. Montero de Espinosa, L.; Meier, M. A. R. *Polymer* **2011**, *47*, 837–852.
5. Petrovic, Z. S. *Polym. Rev.* **2008**, *48*, 109–155.
6. Lligadas, G.; Ronda, J. C.; Galià, M.; Cádiz, V. *Biomacromolecules* **2010**, *11*, 2825–2835.
7. Desroches, M.; Caillol, S.; Lapinte, V.; Auvergne, R.; Boutevin, B. *Macromolecules* **2011**, *44*, 2489–2500.
8. Fischer, E. M. U.S. Patent 3,157,681, 1964.
9. Myers, L. D.; Goebel, C.; Barreto, F. O. U.S. Patent 2,955,121, 1960.
10. (a) Cramail, H.; Boyer, A.; Cloutet, E.; Bakhiyi, R.; Alfos, C. WO2011030076, FR2950051. (b) Cramail, H.; Boyer, A.; Cloutet, E.; Alfos, C. WO 2011030075, FR2950052. (c) Cramail, H.; Boyer, A.; Cloutet, E.; Alfos, C. WO 2011045536, FR2951166.
11. Meier, M. A. R. *Macromol. Chem. Phys.* **2009**, *210*, 1073–1079.
12. Ngo, H. L.; Jones, K.; Foglia, T. A. *J. Am. Oil Chem. Soc.* **2006**, *83*, 629–634.
13. Van der Steen, M.; Stevens, C. V. *ChemSusChem* **2009**, *2*, 692–713.
14. Hoyle, C. E.; Lee, T. Y.; Roper, T. *J. Polym. Sci., Part A: Polym. Chem.* **2004**, *42*, 5301–5338.
15. Hoyle, C. E.; Lowe, A. B.; Bowman, C. N. *Chem. Soc. Rev.* **2010**, *39*, 1355–1387.

16. Killops, K. L.; Campos, L. M.; Hawker, C. J. *J. Am. Chem. Soc.* **2008**, *130*, 5062–5064.
17. Campos, L. M.; Killops, K. L.; Sakai, R.; Paulusse, J. M. J.; Damiron, D.; Drockenmuller, E.; Messmore, B. W.; Hawker, C. J. *Macromolecules* **2008**, *41*, 7063–7070.
18. Kade, M. J.; Burke, D. J.; Hawker, C. J. *J. Polym. Sci., Part A: Polym. Chem.* **2010**, *48*, 743–750.
19. Hoyle, C. E.; Bowman, C. N. *Angew. Chem. Int. Ed.* **2010**, *49*, 1540–1573.
20. Lowe, A. B. *Polym. Chem.* **2010**, *1*, 17–36.
21. Van Dijk, M.; Rijkers, D. T. S.; Liskamps, R. M. J.; Van Nostrum, C. F.; Hennick, W. E. *Bioconjugate Chem.* **2009**, *20*, 2001–2016.
22. Dondoni, A. *Angew. Chem. Int. Ed.* **2008**, *47*, 8995–8997.
23. Yu, X. E.; Homan, J. G.; Connor, T. J.; Cooper, S. L. *J. Appl. Polym. Sci.* **1991**, *43*, 2249–2257.
24. Crivello, J. V.; Narayan, R.; Sternstein, S. S. *J. Appl. Polym. Sci.* **1997**, *64*, 2073–2087.
25. Crivello, J. V.; Chakrapani, S. J. *J. Macromol. Sci., Part A: Pure Appl. Chem.* **1998**, *35*, 1–20.
26. Carioscia, J. A.; Stansbury, J. W.; Bowman, C. N. *Polymer* **2007**, *48*, 1526–1532.
27. Phillips, J. P.; Mackey, N. M.; Confait, B. S.; Heaps, D. T.; Deng, X.; Todd, M. L.; Stevenson, S.; Zhou, H.; Hoyle, C. E. *Chem. Mater.* **2008**, *20*, 5240–5245.
28. Black, M.; Rawlins, J. W. *Eur. Polym. J.* **2009**, *45*, 1433–1441.
29. Samuelsson, J.; Jonsson, M.; Brinck, T.; Johansson, M. *J. Polym. Sci., Part A: Polym. Chem.* **2004**, *42*, 6346–6352.
30. González, R. J.; Lluch, C.; Lligadas, G.; Galià, M.; Ronda, J. C.; Cádiz, V. *J. Polym. Sci., Part A: Polym. Chem.* **2011**, *49*, 2407–2416.
31. Arceo, E.; Marsden, P.; Bergman, R. G.; Ellman, J. A *Chem. Comm.* **2009**, *23*, 3357–3359.
32. Turünç, O.; Meier, M. A. R. *Macromol. Rapid Commun.* **2010**, *31*, 1822–1826.
33. Lluch, C.; Lligadas, G.; Ronda, J. C.; Galià, M.; Cádiz, V. *Macromol. Rapid Commun.* **2011**, *32*, 1343–1251.
34. Lluch, C.; Ronda, J. C.; Galià, M.; Lligadas, G.; Cádiz, V. *Biomacromolecules* **2010**, *11*, 1646–1653.

Downloaded by UNIV OF GUELPH LIBRARY on August 28, 2012 | http://pubs.acs.org
Publication Date (Web): August 16, 2012 | doi: 10.1021/bk-2012-1105.ch017

Downloaded by COLUMBIA UNIV on August 28, 2012 | http://pubs.acs.org
Publication Date (Web): August 16, 2012 | doi: 10.1021/bk-2012-1105.ch018

Chapter 18

Novel Biomass-Based Polymers: Synthesis, Characterization, and Application

**Bart A. J. Noordover,*[,1,2] Lidia Jasinska-Walc,[1,2,3]
Inge van der Meulen,[1,2] Robbert Duchateau,[1,2] and Cor E. Koning[1,2]**

**[1]Laboratory of Polymer Chemistry, Eindhoven University of Technology,
Den Dolech 2, P.O. Box 513, 5600 MB Eindhoven, The Netherlands
[2]Dutch Polymer Institute (DPI), P.O. Box 902,
5600 AX Eindhoven, The Netherlands
[3]Department of Polymer Technology, Chemical Faculty, Gdansk University
of Technology, G. Narutowicza Str. 11/12, 80-952 Gdansk, Poland
*E-mail: b.a.j.noordover@tue.nl**

A wide range of polymers were prepared from biomass-derivatives, using different polymerization mechanisms. Well-defined, fully hydroxy-functional polyesters based on aliphatic diols were synthesized, using either conventional metal-based catalysts or the organic superbase 1,5,7-triazabicyclododecene (TBD). Unsaturated polyesters were also made, offering additional functionality to these biobased resins. Metal-catalyzed or enzymatic ring-opening polymerization of macrolactones afford novel, renewable materials with good mechanical properties similar to those of polyethylene. In addition to polyesters, aliphatic polycarbonates based on 1,4:3,6-dianhydrohexitols (DAH) were prepared, which proved very suitable for application in thermosetting coating systems. Polyamides from sebacic acid, 1,4-diaminobutane and diaminoisoidide are very interesting polymers, in which the diaminoisoidide residues cocrystallize in the polyamide 4.10 matrix. Another type of polymers studied were the polyurethanes. Thermoplastic polyurethanes and polyureas from biomass can be effectively synthesized through either isocyanate-based or isocyanate-free strategies. Also, poly(ester/carbonate urethane) networks from renewable polymer resins are very promising systems for coating

In Biobased Monomers, Polymers, and Materials; Smith, P., et al.;
ACS Symposium Series; American Chemical Society: Washington, DC, 2012.

applications. The chemical, thermal and mechanical properties of the mentioned biobased polymers could be tuned by varying the molecular structure, the composition, the end-group functionality and the molecular weight.

Introduction

After a century of petrochemistry-based advances in polymer chemistry, numerous researchers in the field have recently shifted their attention to biomass-derived starting materials to prepare macromolecules. One of the driving forces behind these activities is the desire to move away from fossil feedstock and its price volatility. Also, the ever-looming threat of crude oil depletion and the required reduction of our carbon footprint have motivated scolars and commercial parties to look for alternatives. For polymer chemists and material scientists, another important driver exists: curiosity. What do these novel biobased materials have to offer in terms of differentiated properties? Can we make polymers from renewable feedstock which match or even outperform the currently available library of materials? What clever chemistry and catalysis can we come up with to selectively convert the plethora of functionalities into the desired products, while operating at mild reaction conditions? These and many other questions need to be answered to effectively use the resources offered to us by nature in a way that makes sense economically and environmentally.

For almost a decade, a significant part of the research efforts of the Polymer Chemistry Group at the Eindhoven University of Technology have been aimed at studying alternative routes to performance polymers, including engineering plastics, elastomers, coatings and fibers. This chapter provides an overview of our recent activities in the field of biomass-based polymers prepared via novel (catalytic) routes.

Downloaded by COLUMBIA UNIV on August 28, 2012 | http://pubs.acs.org
Publication Date (Web): August 16, 2012 | doi: 10.1021/bk-2012-1105.ch018

Biomass-Based Saturated Polyesters through Melt Polycondensation

Linear Dihydroxyl-Terminated Polyesters

Natural products such as starch, cellulose and vegetable oils are sources of a wide range of monomers for polyester synthesis (*1*). Diols including 1,3-propanediol (1,3-PD) (*2*, *3*), 1,4-butanediol (1,4-BD) (*4*), 2,3-butanediol (2,3-BD) (*5*, *6*) and polyhydric alcohols such as glycerol (GLY) (*7*, *8*) can be derived from biomass. In addition, several dicarboxylic acids can be produced from similar feedstock, including succinic acid (SA) (*1*), adipic acid (AA) (*9*, *10*) and sebacic acid (SebA) (*11*). For some of these chemicals, further development of the demonstrated synthetic pathways is required before they can compete with the corresponding petrochemicals from an economic point of view.

Different polymerization routes can be applied to prepare polyesters, including direct polycondensation reactions between diols and dicarboxylic acids, transesterifications between diols and dialkyl esters of dicarboxylic acids, enzymatic synthesis and ring-opening polymerization (ROP) of lactones (*vide*

Downloaded by COLUMBIA UNIV on August 28, 2012 | http://pubs.acs.org
Publication Date (Web): August 16, 2012 | doi: 10.1021/bk-2012-1105.ch018

infra). Recently, metal-free organic catalysts have been studied intensively, for example in the field of ROP of cycloesters (*12–14*). Fokou et al. showed that the organic, bicyclic guanidine 1,5,7-triazabicyclododecene (TBD) also catalyzes transesterification reactions at relatively low temperatures (*15*). In addition, polyesters were prepared from fatty acid derivatives through polycondensation (*16*, *17*). In this paragraph, we describe telechelic OH-functional polyesters synthesized through transesterification reactions between selected biobased diols and dimethyl esters, catalyzed by TBD.

For transesterification reactions, often metal-based catalysts are used including titanium alkoxides, tin (II) octoate and bismuth (III) carboxylates. Such catalysts require the reactions to be performed at temperatures above 150 °C, to achieve acceptable reaction rates. Instead, when using TBD it was found that the reaction temperature may be significantly reduced to approx. 120 °C. By choosing the appropriate molar ratio of the dimethyl ester and the diol, the end-group structure can be controlled very effectively. In this way, fully hydroxyl-functional polyesters are prepared, using either primary or secondary diols (Scheme 1). Their glass transition temperatures (T_g) range from -38 °C (for poly(1,2-dimethylethylene adipate), PDMEA) to -70 °C (for poly(1,4-butylene adipate), PBA and poly(1,3-propylene adipate), PPA) and these polyesters are typically thermally stable up to approx. 270 °C.

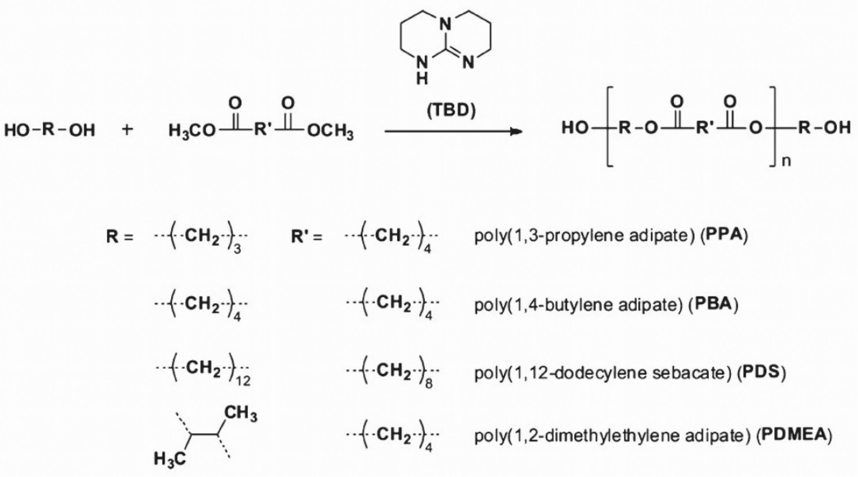
HO–R–OH
+
H₃CO–C(O)–R'–C(O)–OCH₃
(TBD)
HO–[R–O–C(O)–R'–C(O)–O]n–R–OH
R =
R' =
poly(1,3-propylene adipate) (PPA)
poly(1,4-butylene adipate) (PBA)
poly(1,12-dodecylene sebacate) (PDS)
poly(1,2-dimethylethylene adipate) (PDMEA)

Scheme 1. TBD-catalyzed synthesis of biomass-based polydiols. Figure taken from reference (18). Copyright 2011, John Wiley & Sons. Reproduced with permission.

By combining different molecular characterization techniques such as Matrix-Assisted Laser Desorption Ionization Time-of-Flight Mass Spectrometry (MALDI-ToF-MS), Nuclear Magnetic Resonance spectroscopy (NMR) and titration, the telechelic character of these polyesters can be ascertained.

Downloaded by COLUMBIA UNIV on August 28, 2012 | http://pubs.acs.org
Publication Date (Web): August 16, 2012 | doi: 10.1021/bk-2012-1105.ch018

Figure 1 shows the MALDI-ToF-MS spectrum of the novel polyester poly(1,2-dimethylethylene adipate) (PDMEA).

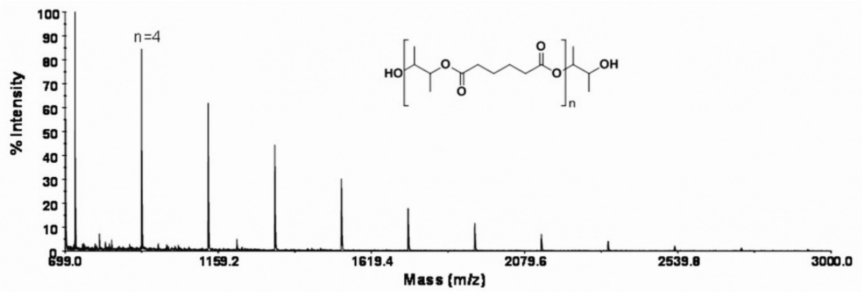

Figure 1. MALDI-ToF-MS spectrum of dihydroxy-functional PDMEA. Figure taken from reference (18). Copyright 2011, John Wiley & Sons. Reproduced with permission

By using an initial diol/dimethylester ratio equal to 3.0 (similar to the procedure applied in the production of poly(butylene terephthalate)) and subsequently stripping off the excess of diol during vacuum processing, an OH-functional telechelic polyester was obtained. This particular polyester is a very interesting prepolymer for the preparation of thermoplastic polyurethanes, as will be discussed in the final section of this chapter.

Linear and Branched Polyester Resins from 1,4:3,6-Dianhydrohexitols

From glucose, a very interesting class of bicyclic monomers are obtained: 1,4:3,6-dianhydrohexitols (DAH). Depending on the orientation (*endo* or *exo*) of their two secondary hydroxyl groups, three DAH isomers can be distinguished (Figure 2): isosorbide (1,4:3,6-dianhydro-D-glucitol), isoidide (1,4:3,6-dianhydro-L-iditol) or isomannide (1,4:3,6-dianhydro-D-mannitol). To prepare isosorbide, first D-glucose is hydrogenated, yielding sorbitol. This polyhydric alcohol is subsequently dehydrated, resulting in the *endo*/*exo* isomer. Isomannide (*endo*/*endo*) is derived from D-mannose via D-mannitol, while isoidide (*exo*/*exo*) is prepared based on L-fructose via L-iditol (*19*).

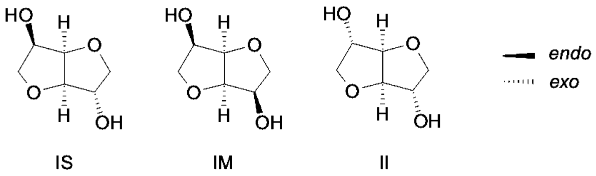

Figure 2. The 1,4:3,6-dianhydrohexitols: isosorbide (IS), isomannide (IM) and isoidide (II).

These diols have been intensively studied in recent years, as their relatively rigid structures afford polymers with rather high T_g values. Isosorbide has been successfully incorporated in several high performance polyesters such as poly(ethylene terephthalate) (PET) and poly(butylenes terephthalate) (PBT), leading to new copolymers with enhanced thermal properties (*20–23*). However, melt polycondensation reactions using these sugar derivatives should be performed with care, preferably at temperatures below 250 °C and under an inert atmosphere (e.g. nitrogen or argon) to avoid thermal and/or oxidative degradation of these compounds.

Linear aliphatic polyesters based on DAHs were described by several authors (*24–28*). As it is available on an appreciable scale at high purity, isosorbide is most commonly studied. Its symmetric counterpart isoidide, although slightly more reactive as a result of the *exo*/*exo* orientation of the OH-groups, is more laborious (and thus, more expensive) to produce. Isomannide has received little attention so far, which is mainly due to its limited thermal stability (*21*, *29*, *30*). When copolymerizing isosorbide with aliphatic dicarboxylic acids of increasing chain length, the T_g of the resulting polyesters decreases from approx. 75 °C for succinic acid (one of the main products of glucose fermentation) to values between -10 and 0 °C for longer diacids. For the shorter diacids, ranging from succinic acid (containing two CH_2 segments) to azeleic acid (containing seven CH_2 segments), the IS-based polyesters are amorphous materials due to the asymmetric, bulky structure of the diol, prohibiting close packing of the polymer chains. Longer diacid residues afford semi-crystalline polyesters. Isoidide-based polyesters, on the other hand, are all semi-crystalline regardless of the dicarboxylic acid length. Polyesters based on isomannide are also semi-crystalline at shorter diacid lengths.

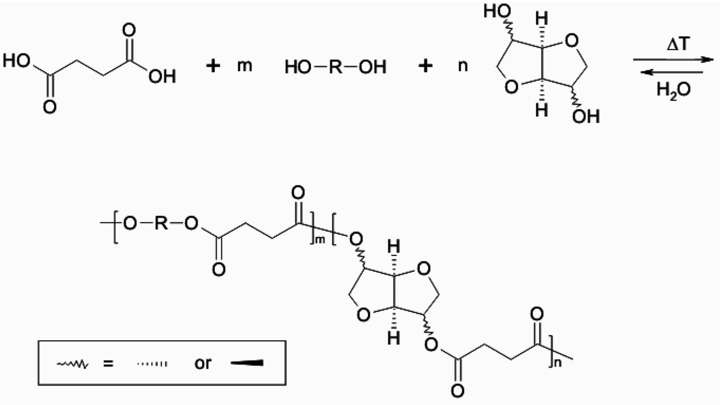

Scheme 2. Polycondensation reaction to form copolyesters from the DAH isomers, diol comonomers and succinic acid. Adapted with permission from reference (31). Copyright 2006, American Chemical Society

Downloaded by COLUMBIA UNIV on August 28, 2012 | http://pubs.acs.org
Publication Date (Web): August 16, 2012 | doi: 10.1021/bk-2012-1105.ch018

Through the incorporation of comonomers (Scheme 2), the T_g, the melting temperature (T_m), the degree of crystallinity and the crystallization temperature (T_c) of DAH-based polyesters can be effectively controlled. Figure 3 demonstrates the influence on the T_g of the incorporation of 1,3-PD, 2,3-BD and neopentyl glycol (NPG) in copolymers of isosorbide and succinic acid (*31*).

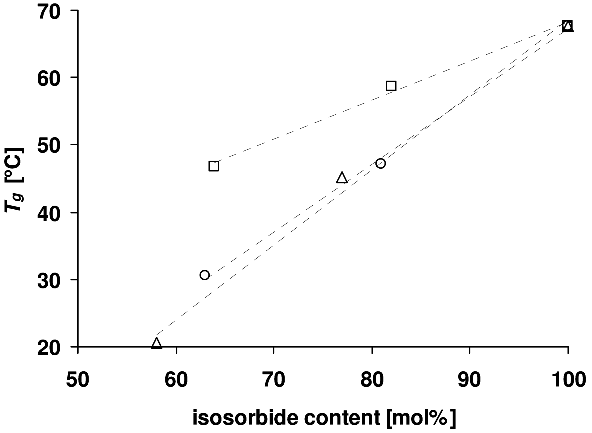

Figure 3. T_g vs. isosorbide content for several SA/IS-based polyesters containing the following comonomers: 1,3-propanediol (▵), neopentyl glycol (○) or 2,3-butanediol (□). Reprinted with permission from reference (31). Copyright 2006, American Chemical Society.

Polyester polyols are often applied in polyurethane systems, requiring strict control of their end-group structures. Typically, the type of end-groups (e.g. hydroxyl or carboxylic acid) can be set by choosing the appropriate stoichiometry during the synthesis. In the case of isosorbide-based polyesters, predominantly OH-terminated chains are indeed obtained when using an excess of diols (ratio succinic acid/diol = 1.15), as confirmed by end-group titration, NMR spectroscopy and MALDI-ToF-MS. These glassy, transparent copolyesters have properties enabling their application in, for example, thermosetting powder coatings (*vide infra*) or in toner resins. In powder coating systems, usually branched semi-aromatic polyesters are applied, which have average functionalities larger than two. Glycerol is a useful trifunctional monomer to facilitate branching in fully biobased polyesters (*32*).

Interestingly, the preparation of carboxylic acid-terminated DAH-based polyesters is less straightforward. Even when a 0.2 molar excess of SA is used relative to the amount of diols, high intensity peaks corresponding to hydroxyl end-groups are observed in the MALDI-ToF-MS spectrum, alongside the expected peaks assigned to carboxylic acid-functionalized chains. The concentration of hydroxyl end-groups is found to be in the same order of magnitude as carboxylic acids, as determined by titration. Apparently, this is due to the reduced reactivity of the secondary hydroxyls, in particular at chain ends when additional steric

Downloaded by COLUMBIA UNIV on August 28, 2012 | http://pubs.acs.org
Publication Date (Web): August 16, 2012 | doi: 10.1021/bk-2012-1105.ch018

constraints are present (i.e. *endo*-orientation of the OH-group). Therefore, the synthesis of fully acid-functional, linear isosorbide polymers cannot be achieved under these reaction conditions, when using non-activated diacid species (*31*).

An attractive method was found to prepare carboxylic acid functional polymers based on DAHs, as was described previously (*33*). A predominantly OH-functional polymer can be reacted with citric acid (CA), yielding a COOH-terminated product with an improved average functionality (Scheme 3). Even though citric acid contains non-activated carboxylic acid groups, the reaction with the moderately reactive secondary OH-groups of isosorbide does proceed as a result of a special feature of the citric acid molecule. Upon heating to around the melting temperature of CA (T_m = 153 °C), citric acid anhydride is formed which is more reactive towards the secondary hydroxyl groups. This modification should be performed under well-controlled conditions to avoid excessive decomposition of CA through dehydration and/or decarboxylation at temperatures in excess of 180 °C.

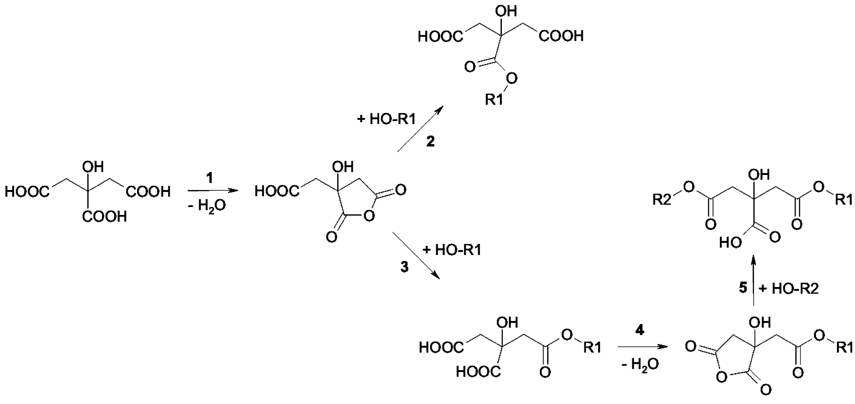

*Scheme 3. Citric acid anhydride formation (**1**), followed by its esterification with an OH-terminated species (**2**, **3**). The citrate end-group resulting from reaction **3** can again form a cyclic anhydride (**4**) and react once more with a hydroxyl-terminated polyester chain (**5**). Adapted with permission from reference (33). Copyright 2007, American Chemical Society*

In theory, the CA-modification transforms a linear, OH-functional chain with a maximum functionality of F_n = 2 into a carboxylic acid-terminated chain with a functionality of F_n = 4. In reality, some branching also occurs, as evidenced from a broadening of the molecular weight distribution upon reaction. The increase of the average number of reactive end-groups per chain is clearly demonstrated by the emergence of a high acid value (*AV*, measure for the number of carboxylic acid groups per gram of sample), while the hydroxyl value (*OHV*) stays virtually constant. After all, the number of OH-groups should in theory stay constant, as CA carries a tertiary OH-functionality. In Table 1, the *AV* and *OHV* are listed together with other key polyester characteristics.

Downloaded by COLUMBIA UNIV on August 28, 2012 | http://pubs.acs.org
Publication Date (Web): August 16, 2012 | doi: 10.1021/bk-2012-1105.ch018

Downloaded by COLUMBIA UNIV on August 28, 2012 | http://pubs.acs.org
Publication Date (Web): August 16, 2012 | doi: 10.1021/bk-2012-1105.ch018

Table 1. Properties of isosorbide-based polyesters with enhanced functionality

composition[a]	T_g *[°C]*	M_n[b] *[g·mol^{-1}]*	*PDI*[b]	*AV*[b] *[mgKOH·g^{-1}]*	*OHV*[c] *[mgKOH·g^{-1}]*
SA:IS [1:1.09]	56.5	3,000	2.0	1.5	65.0
SA:IS:CA[d] [1:1.11:0.2]	68.7	3,500	2.3	108.3	65.2

[a] SA = succinic acid, IS = isosorbide, CA = citric acid. Composition determined by ^{1}H NMR spectroscopy. [b] Determined by SEC in HFIP, relative to PMMA standards. [c] *AV* = acid value, *OHV* = hydroxyl value; determined by titration. [d] The amount of citric acid added to the OH-functional polyesters was based on the *OHV* data of the polymers.

Carboxylic acid-functional polyesters such as the CA-modified compounds can be cross-linked with either epoxy- or *β*-hydroxyalkylamide curing agents to form polyester networks. Potentially, part of the citric acid end-groups, having two carboxylic acid moieties available, will form five-membered anhydrides during curing at elevated temperatures. This is advantageous for the network formation, as acid anhydride/epoxy curing systems are known to afford higher reaction rates, conversions and cross-link densities and are less sensitive to variations in the formulation stoichiometry (*34*). The curing reaction between a CA-modified polyester and a 60:40 (wt/wt) mixture of diglycidyl terephthalate (DGT) and triglycidyl trimellitate (TGT) (Figure 4, structures **I** and **II**) was investigated by dynamic mechanical analysis (Figure 5).

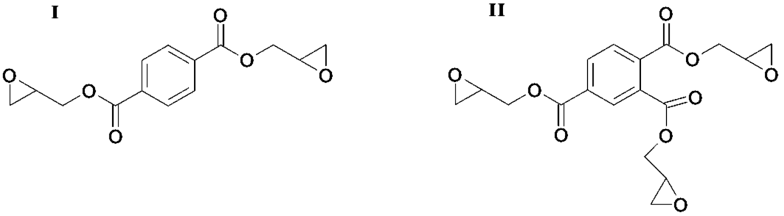

*Figure 4. Chemical structures of (**I**) diglycidyl terephthalate (DGT) and (**II**) triglycidyl trimellitate (TGT).*

After an initial drop in modulus upon heating, *G′* starts to increase when the curing reaction commences. At *T* = 165 °C (and *t* = 46 minutes), the *G′* of the formulation has reached its plateau modulus value of approximately 420 kPa at high *T*. Powder coating of such formulations onto aluminum substrates followed by thermal curing yields glossy coatings, having excellent solvent and impact resistance. In the case of catalyzed formulations, fully cured coatings can be prepared within 15 minutes at 150 °C (*32*, *33*).

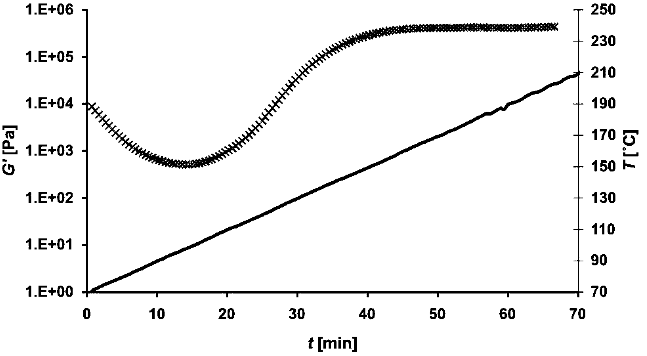

Figure 5. Shear modulus G' (X) for a TiO_2 pigmented, hexadecyltrimethylammonium bromide catalyzed coating formulation and temperature T (−) as functions of time during polyester network formation. The temperature sweep was performed at 2 °C ·min^{-1}. using a rheometer with parallel plate geometry. Figure adapted from reference (32). Copyright (2009), with permission from Elsevier.

Downloaded by COLUMBIA UNIV on August 28, 2012 | http://pubs.acs.org
Publication Date (Web): August 16, 2012 | doi: 10.1021/bk-2012-1105.ch018

Isosorbide-Derived Unsaturated Polyesters for Coating Applications

Introduction

The natural origin of monomers has become a fundamental topic in the synthesis of pharmaceuticals, liquid crystalline materials and polymers. Some of the most frequently reported biobased building blocks are the 1,4:3,6-dianhydrohexitols (DAH) (*27*, *31*, *33*, *35–38*). The limited flexibility of the five-membered rings and the sufficient reactivity of the secondary hydroxyl groups of the isohexitols offer great opportunities for their use in the synthesis of polymers as T_g enhancing agents. Currently, many possibilities are also provided by the synthesis of biobased, unsaturated polyesters (PEs), which can be cross-linked by unsaturated or polyfunctional monomers as well as by an UV curing method (*39–46*). Furthermore, the presence of unsaturated bonds results in a wide scope of modification possibilities via the incorporation of diverse functionalities into the PEs backbone.

Nowadays, the driving force for the development of environmentally friendly coating technologies is the synthesis of water-soluble or dispersible and biobased polymers. Also in this field isosorbide, as a “green” comonomer, has been recently regarded as one of the best alternatives for non-renewable compounds. As reported before (*40*), isosorbide in combination with poly(ethylene glycol) and maleic anhydride can successfully replace some of the organic solvent-borne polymers for coating applications.

Downloaded by COLUMBIA UNIV on August 28, 2012 | http://pubs.acs.org
Publication Date (Web): August 16, 2012 | doi: 10.1021/bk-2012-1105.ch018

Structure-Properties Relations of Unsaturated and Cured Polyesters

The unsaturated PEs (Figure 6) based on isosorbide, maleic anhydride, succinic acid and/or poly(ethylene glycol) were synthesized via step-growth bulk polymerization, as reported before (*39*, *40*). By choosing the molar ratio of [OH/COOH] of the used monomers slightly above 1.0, hydroxyl-functional products were obtained, which was also proven by 2D NMR experiments.

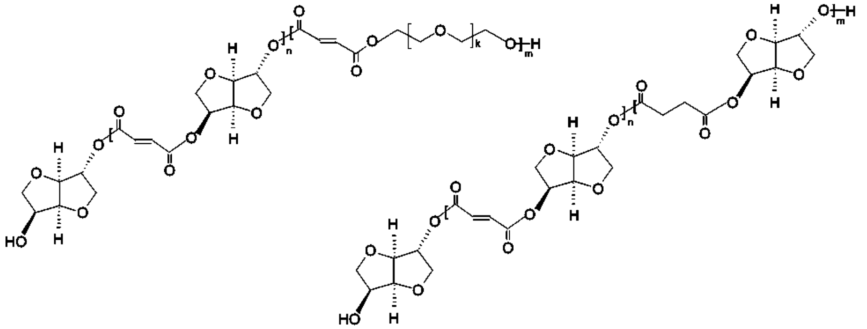

Figure 6. The structure of the unsaturated polyesters. Reproduced with permission from reference (39, 40). Copyright 2011, John Wiley & Sons.

To afford a variety of unsaturated polyesters, including water-soluble materials, different monomers and reaction conditions were investigated (Table 2). The polyesters were subsequently cross-linked with non-toxic and water-soluble, unsaturated monomers *viz.* 2-hydroxyethyl methacrylate (HEMA) or *N*-vinyl-2-pyrrolidinone (NVP).

The performed 2D NMR experiments clearly indicate that during the polycondensation of maleic anhydride with isosorbide or poly(ethylene glycol) (PEG 600) the unsaturated moieties are entirely transformed into fumaric acid units. The analysis of the cross-peaks in the ^{1}H-^{1}H Correlation Spectroscopy (COSY) and ^{1}H-^{13}C Heteronuclear Multiple-Bond Correlation spectra (HMBC) proved that isosorbide and poly(ethylene glycol) are bonded to fumaric and/or succinic acid residues, with one or both OH-groups. The molecular analysis also revealed that the functionality of the polyesters can be influenced by Michael addition of the used diols and/or water on unsaturated bonds. Nevertheless, still a sufficient amount of the unsaturated bonds (above 80% of the theoretical iodine value) can participate in the curing process.

The evaluation of thermal properties of the investigated polyesters confirmed the previously reported results (*31*, *33*) concerning amorphous, isosorbide-based polymers. As reported (*39*, *40*), with an increase of the molecular weight and amount of the unsaturated bonds of PEs their glass transition temperature (T_g) increased. This practical approach towards isosorbide-derived, unsaturated polymers leads to materials with T_g values in the interval 50-70 °C (Table 2). An exception is the composition based on isosorbide, poly(ethylene glycol) (PEG) and maleic anhydride. Due to the presence of flexible PEG units in the polymer chain, the T_g value of this water-soluble product was noted at around -17 °C.

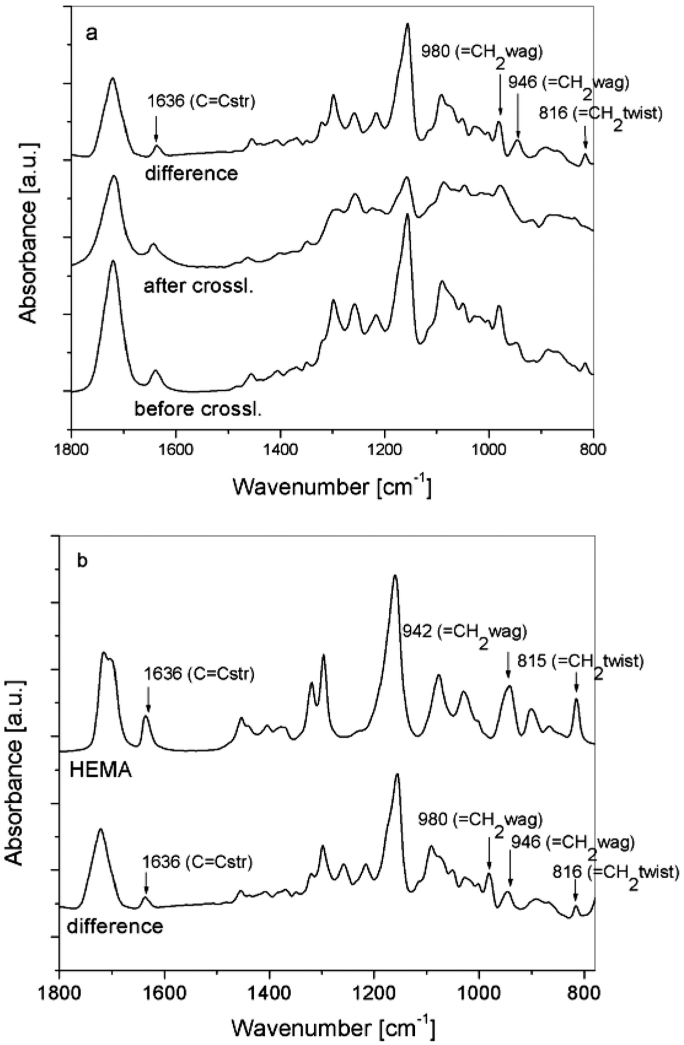

Figure 7. a) FT-IR spectra of PEs 5 before and after cross-linking with 2-hydroxyethyl methacrylate and the difference spectrum obtained by subtracting of these spectra, subtracting factor = 1. b) FT-IR difference spectrum of PEs 5 and FT-IR spectrum of HEMA. Reproduced with permission from reference (39, 40). Copyright 2011, John Wiley & Sons.

Downloaded by COLUMBIA UNIV on August 28, 2012 | http://pubs.acs.org
Publication Date (Web): August 16, 2012 | doi: 10.1021/bk-2012-1105.ch018

Downloaded by COLUMBIA UNIV on August 28, 2012 | http://pubs.acs.org
Publication Date (Web): August 16, 2012 | doi: 10.1021/bk-2012-1105.ch018

Table 2. Properties of the unsaturated polyesters with different content of unsaturated bonds synthesized from isosorbide, maleic anhydride, succinic acid, and poly(ethylene glycol). Reproduced with permission from reference (*39*, *40*). Copyright 2011, John Wiley & Sons

PEs	***molar ratio*** [a] *IS/MA/SA/PEG*	***AV*** [b] *[mgKOH·g^{-1}]*	***OHV*** [b] *[mgKOH·g^{-1}]*	***M_n*** [c] *[g·mol^{-1}]*	***T_g*** [d] *[°C]*
1	1.1/0.25/0.75/0	6.6	79.4	3370	49
2	1.1/0.33/0.66/0	3.8	59.6	3100	61
3	1.1/0.66/0.33/0	19.7	79.9	2900	61
4	1.1/0.75/0.25/0	19.5	88.8	3250	76
5	1.1/1/0/0	14.8	119.6	2400	52
6	0.95/1/0/0.2	16.6	73.7	4450	-17

[a] IS = isosorbide, MA = maleic anhydride, SA = succinic acid, PEG = poly(ethylene glycol). [b] *AV* = acid value, *OHV* = hydroxyl value. [c] M_n = molecular weight determined using SEC method with PMMA standards in HFIP. [d] T_g = glass transition temperature.

To illustrate the potential of the unsaturated, biobased polyesters the polymers were used in the cross-linking process initiated by 2-butanon peroxide with unsaturated curing monomers such as HEMA and NVP. On account of the solubility characteristics exclusively PEs containing PEG units were cured in the aqueous solutions of HEMA or NVP, while for the materials with T_g above 40 °C the radical copolymerization was performed in chloroform. The curing process, caused by radical copolymerization with the cross-linking agents, was successfully monitored using Fourier Transform Infrared (FT-IR) spectroscopy. The FT-IR spectra, analyzed before and after cross-linking, proved that along with the reaction progress the bands at 1636 cm^{-1}, 980 cm^{-1}, 942-946 cm^{-1} originating from νC=C and =CH$_{wag}$ (wagging) had almost disappeared (Figure 7a, 7b). The decrease of these peak area intensities implies the disappearance of double bonds from both the polyester and the curing agents.

An evaluation of the cross-linked materials with regard to thermal properties and their solubility is very important for their use in coating applications. Since the investigated polyesters are amorphous materials they do not show endothermic melting transitions in DSC thermograms. In many cases, the cured coatings exhibit a significant T_g reduction in comparison to the corresponding PEs before curing (Table 3). This effect is caused by the presence of plasticizing oligo(HEMA) or oligo(NVP) units in the cured compositions. The cured products were also investigated for their thermal stability. The initial weight loss of PEs cross-linked with HEMA was noted above 200 °C. Simultaneously, the thermal stability of the compositions containing NVP was lower in comparison to the products cross-linked with HEMA. Nevertheless, the main degradation of all investigated coatings occurred above 380 °C, which suggests their sufficiently high thermal stability.

Table 3. Thermal properties and solubility parameters of the polyesters cross-linked with 2-hydroxyethyl methacrylate (HEMA) and *N*-vinyl-2-pyrrolidinone (NVP). Reproduced with permission from reference (*39*, *40*). Copyright 2011, John Wiley & Sons

PEs	*curing agent*	T_g [a] [°C]	$T_{5\%}$[a] [°C]	T_{max}[a] [°C]	*water solub.*[b] [wt%]	$CHCl_3$ *solub.*[b] [wt%]
1	HEMA	64	249	403	5.8	7.4
2	HEMA	53	242	397	4.4	4.9
3	HEMA	65	226	413	7.9	9.6
4	HEMA	56	196	406	11.4	10.1
4	NVP	62	153	414	9.2	6.9
5	HEMA	60	199	396	12.3	8.7
6	HEMA	n.d.[c]	238	392	7.7	5.0
6	NVP	n.d.[c]	202	384	9.1	1.2

[a] T_g = glass transition temperature, $T_{5\%}$ = temperature at which 5% mass loss is observed in TGA, T_{max} = temperature of maximal rate of decomposition. [b] the soluble fraction of the cross-linked polyesters in water or $CHCl_3$. [c] n.d. = not detected.

The solubility parameters of the cross-linked polyesters, determined by performing swelling experiments, show that for isosorbide-based compositions the content of the uncross-linked part is generally below 10 wt%. This implies a high conversion of the curing process. Because of the different chemical compositions of the unsaturated polyesters influencing the solubility and their different initial molecular weights, a reliable correlation between the content of unsaturated bonds and their solubility was not observed.

Conclusions

The preparation of well-defined, biobased polyesters offers excellent possibilities for coating technologies. An additional advantage is the opportunity to provide functionality *viz.* double bonds, which can be easily cured with non-toxic monomers. Taking these perspectives into account, unsaturated polyesters from isosorbide, succinic acid, maleic anhydride and optionally poly(ethylene glycol) were synthesized and characterized. The step-growth polymerization leads to amorphous and unsaturated products. Despite that after polycondensation and before curing a measurable part of the unsaturated bonds of PEs had disappeared, as a result of oxidation processes or Michael addition of isosorbide or PEG onto double bonds, still a sufficient amount of C=C bonds remained available for a subsequent curing process. The curing resulted in thermally stable coatings having good solvent resistance.

Downloaded by COLUMBIA UNIV on August 28, 2012 | http://pubs.acs.org
Publication Date (Web): August 16, 2012 | doi: 10.1021/bk-2012-1105.ch018

Downloaded by COLUMBIA UNIV on August 28, 2012 | http://pubs.acs.org
Publication Date (Web): August 16, 2012 | doi: 10.1021/bk-2012-1105.ch018

Ring-Opening Polymerization of Macrolactones

Polyolefins are the most widely used type of polymers and cover around 65% of the total polymer market. Replacing polyolefins with biobased polymers is the least to say a challenging task. Poly-β-hydroxybutyrates have properties similar to isotactic polypropylene (*i*-PP) but degrade rapidly (*47*), which limits their use to disposable, short-term applications. Poly-α,ω-hydroxy fatty acids show good mechanical properties reminiscent of those of polyethylenes and their relatively high hydrolytic stability allows long-term applications (*48*, *49*). Poly-α,ω-hydroxy fatty acids can be produced via polycondensation of the ω-hydroxy fatty acids (*17*, *50*, *51*) or via enzymatic (*48*, *49*, *52–54*) or catalytic (*55*, *56*) ring-opening polymerization of the corresponding lactones. ω-Pentadecalactone (PDL), 16-hexadecalactone (HDL) and their unsaturated analogues globalide (Gl) and ambrettolide (Am) are naturally occurring macrocyclic musks that are used in the fragrance industry. Gross and coworkers recently reported a high potential route to transform fatty acids into the corresponding ω-hydroxy fatty acids (*17*), which opens the road to cheap monomers.

Polymer Synthesis

Being reminiscent of polyethylene, poly-α,ω-hydroxy fatty acids rely on crystallinity and entanglements for their mechanical properties, which requires high molecular weights. Ring-opening polymerization is a well-controlled polymerization mechanism that generally affords higher molecular weight products than polycondensation. We therefore studied the enzymatic and metal-catalyzed ring-opening polymerization of macrolactones.

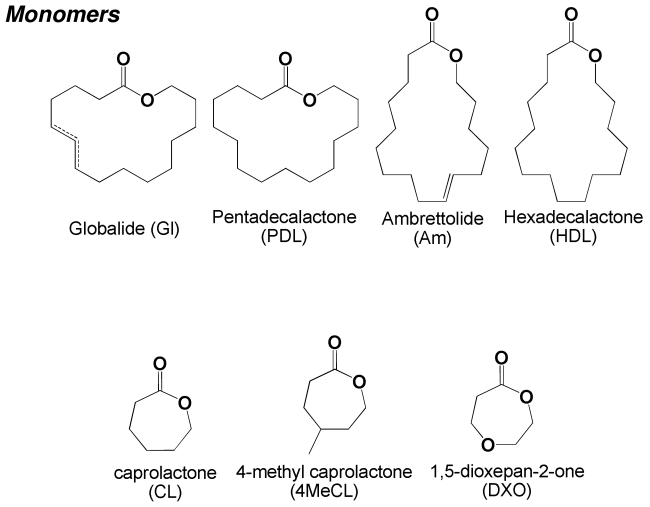

Figure 8. The different lactones that are used for the enzymatic and metal-catalyzed ring-opening polymerization.

Enzymatic Ring-Opening Polymerization of Macrolactones.

The enzymatic ring-opening polymerization of a family of macrolactones containing PDL, HDL, Am and Gl was studied (Figure 8).

It appeared that very high molecular weights of $M_w \approx 300{,}000\ g{\cdot}mol^{-1}$ could be obtained (*48*). These high molecular weight polymers have been used to produce fibres. In order to compare the reactivity of the unsaturated lactones with PDL in enzymatic ring-opening polymerization, a kinetic study was performed (*49*). For all homopolymers the polymerization behavior is similar and follows Michaelis-Menten kinetics.

Furthermore, to systematically investigate the tunability of the properties of copolymers from unsaturated macrolactones, Gl and Am were copolymerized with 4-methyl caprolactone (4MeCL) and 1,5-dioxepan-2-one (DXO) in various ratios (*54*). Thermal investigation showed that incorporating the comonomers lowered the melting points of the polymers compared to the macrolactone homopolymers. The decrease was dependent on the comonomer ratio.

Usually, aliphatic main chain double bonds are difficult to cross-link due to their unreactive character (*57*). However, two pathways were found to effectively cure these main chain double bonds present in Gl and Am residues. Thermal curing using dicumyl peroxide as initiator resulted in rapid cross-linking of polyambrettolide (PAm) and all materials showed a gel content of above 95% (*54*). A set of copolymers with different amounts of cross-linkable comonomer was made and it was found that 10% of cross-linkable monomer is sufficient to obtain complete network formation. The second cross-linking route utilizes UV-light and thiol-ene chemistry (*58*). The thiol-ene chemistry is rapid and within 15 minutes exposure to UV-light the curing is finished. The obtained products were less densily cross-linked than thermally cured products. Interestingly, the cured materials were completely amorphous, which makes the crystallinity a tunable property (Figure 9).

Downloaded by COLUMBIA UNIV on August 28, 2012 | http://pubs.acs.org
Publication Date (Web): August 16, 2012 | doi: 10.1021/bk-2012-1105.ch018

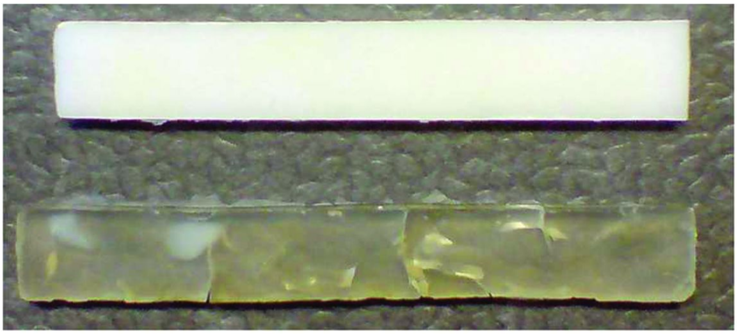

Figure 9. PAm before curing (top) and after curing (bottom). Copyright 2008, American Chemical Society.

Metal-Catalyzed Ring-Opening Polymerization of Macrolactones.

It was found that salen-based aluminum complexes effectively catalyze the ring-opening polymerization of macrolactones to high molecular weight products (Figure 10). The remarkably high efficiency of the catalysts in these polymerizations was immediately evident from the fast increase in viscosity of the reaction medium and within 10 minutes agitation stopped completely. The molecular weights obtained reached $M_w > 300{,}000$ g·mol^{-1}, which matches the highest molecular weights reported for polymacrolactones obtained by enzymatic ring-opening polymerization. The linear correlation between molecular weight and conversion (Figure 10) is characteristic for a living-like catalytic behavior. However, the polypentadecalactones (PPDL) showed rather high (PDI ≥ 2) polydispersity indices, which was attributed to concurrent rapid chain transfer via transesterification.

Downloaded by COLUMBIA UNIV on August 28, 2012 | http://pubs.acs.org
Publication Date (Web): August 16, 2012 | doi: 10.1021/bk-2012-1105.ch018

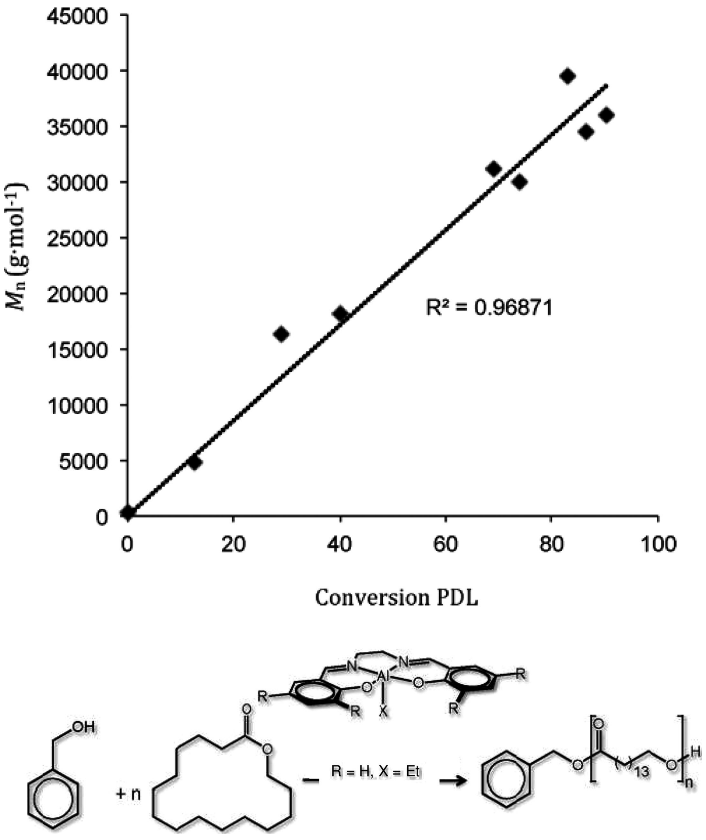

Figure 10. M_n versus conversion plot for PPDL prepared by bulk polymerization at a monomer to initiator ratio of 100. Copyright 2011, American Chemical Society.

In Biobased Monomers, Polymers, and Materials; Smith, P., et al.;
ACS Symposium Series; American Chemical Society: Washington, DC, 2012.

Downloaded by COLUMBIA UNIV on August 28, 2012 | http://pubs.acs.org
Publication Date (Web): August 16, 2012 | doi: 10.1021/bk-2012-1105.ch018

Besides macrolactones, also small ring lactones ε-caprolactone (CL) and δ-valerolactone (VL) as well as the medium-sized decalactone (DL) and undecalactone (UL) could be polymerized using the salen aluminum catalyst. Although the polymerization rate of the medium-sized lactone is the lowest, the rate is still respectable and considerably higher than for the enzymatic ring-opening polymerization or the rate of alkaline hydrolysis of these medium-sized lactones (*59*, *60*).

Why the salen aluminum system is such a suitable catalyst for the ring-opening polymerization of macrolactones to high molecular weight polymers whereas the common catalysts are not, is still a matter of debate. Nevertheless, these results show that it is possible to polymerize macrolactones to unprecedentedly high molecular weights (M_w > 300,000 $g \cdot mol^{-1}$) polyethylene-like polymers using cheap and robust metal-based catalysts. By copolymerizing macrolactones with strained-ring lactones such as ε-CL and lactide, copolymers with varying properties and degradability could be obtained. The observation that even the so-called medium-sized lactones (ring size: 9–12) can be polymerized with a reasonably good activity to high molecular weight products is truly exceptional. These results complement the common theory of ring-tension driven catalytic ring-opening polymerization.

Characterization

A detailed analysis of all polymers was carried out by NMR, DSC, high temperature SEC and tensile testing (*17*, *48*, *49*, *54*).

The tensile modulus (*E*) of compression molded films PPDL is around 420 MPa. The stress at break (σ_{break}) was observed to be as high as 38 MPa. Typically, the strain at break of the high molecular weight PPDL synthesized in this study, being ε_{break} > 1200%, is much higher than the previously reported values (ε_{break} = 100-700%). This difference could be an effect of the higher molecular weight of our samples, as low molecular weight fractions act as plasticizers and have a deleterious effect on the elongation at break.

The monomer ratio found in the copolymers as determined by ^1H NMR spectroscopy corresponded well to the feed ratio. Using ^{13}C NMR, the randomness of all copolymers was studied (Figure 11). Enzymatic ring-opening polymerization afforded fully random copolymers. Using sequential feed and a metal-based catalyst allowed the formation of block copolymers poly(PDL-*b*-CL). Thermal analysis of the homopolymers showed that the unsaturated analogues have a lower melting temperature and lower crystallinity than their saturated congeners. The melting points and melting enthalpies of the copolymers can be tuned by incorporating more or less comonomer, which is in agreement with a study by Andronova *et al.* stating that the incorporation of amorphous DXO will lower the melting and crystallization temperatures of the resulting polyesters (*57*).

Downloaded by COLUMBIA UNIV on August 28, 2012 | http://pubs.acs.org
Publication Date (Web): August 16, 2012 | doi: 10.1021/bk-2012-1105.ch018

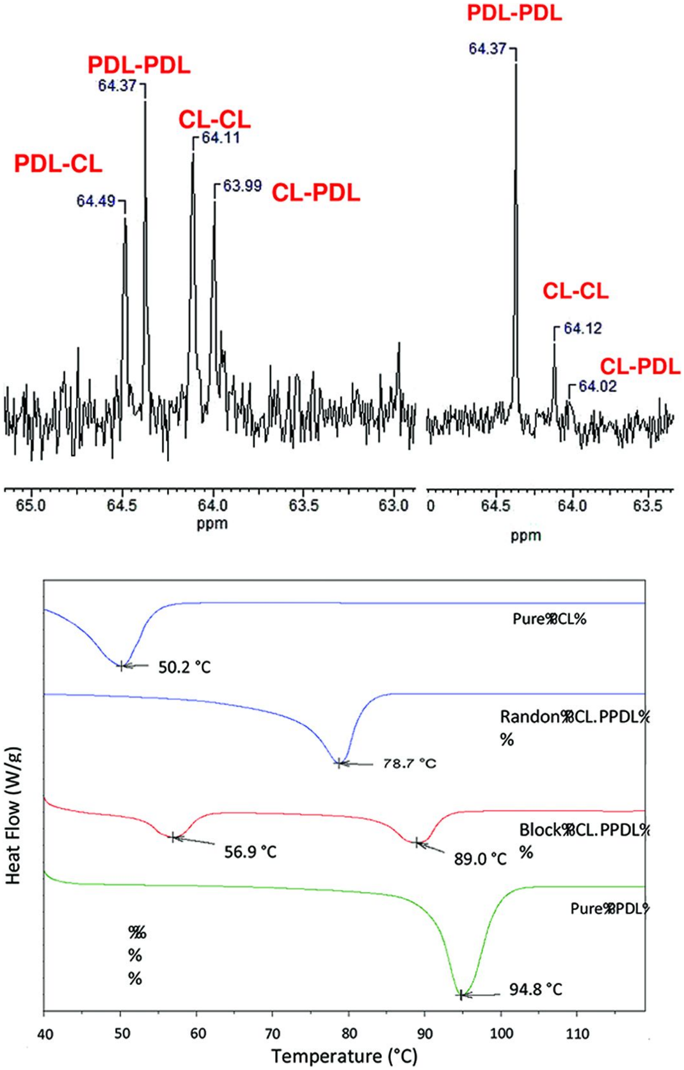

Figure 11. -CH_2O- region in the ^{13}C NMR spectra of a random poly(CL-co-PDL) and block poly(Cl-b-PDL) and the DSC traces of PCL, poly(CL-co-PDL), poly(Cl-b-PDL) and PPDL.

Downloaded by COLUMBIA UNIV on August 28, 2012 | http://pubs.acs.org
Publication Date (Web): August 16, 2012 | doi: 10.1021/bk-2012-1105.ch018

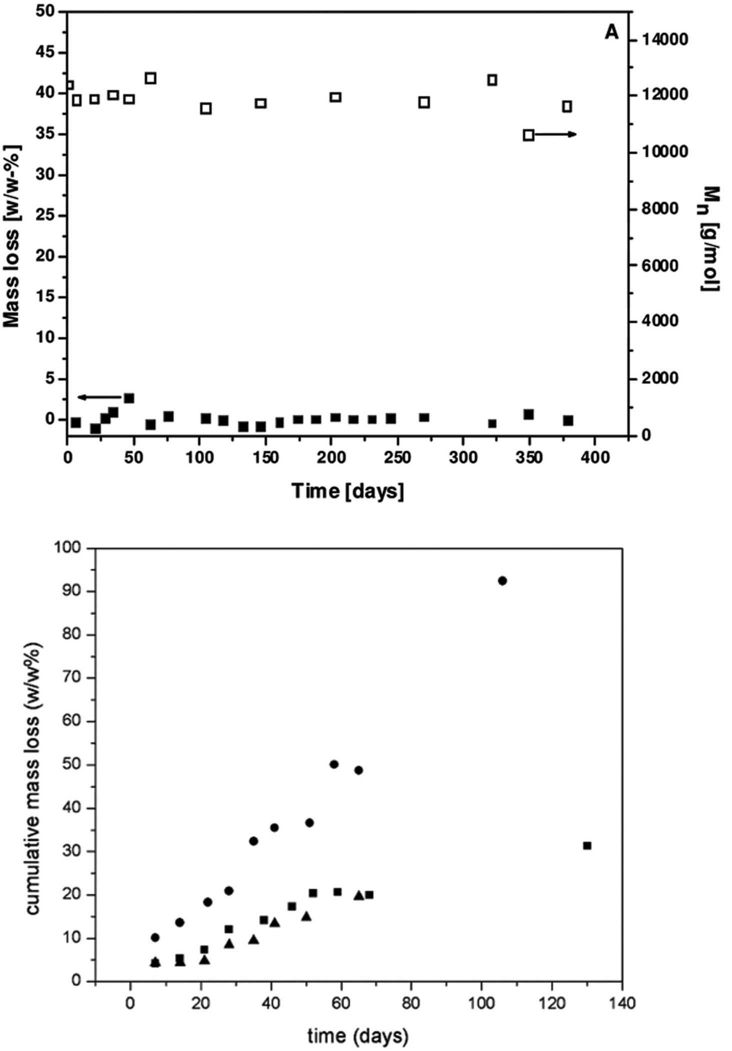

Figure 12. Hydrolytic degradation of polypentadecalactone strand in phosphate buffered saline (PBS buffer) at 37 °C. Cumulative mass loss and molecular weight, M_n as a function of degradation time (top). Enzymatic degradation of selected cross-linked copolymers in PBS buffer at 37 °C. Cumulative mass loss as a function of degradation time ● P(Am-co-DXO) (25/75), ■ P(Gl-co-4MeCL) (53/47), ▲ P(Am-co-DXO) (50/50) (bottom). Copyright 2008, 2011, American Chemical Society.

Downloaded by COLUMBIA UNIV on August 28, 2012 | http://pubs.acs.org
Publication Date (Web): August 16, 2012 | doi: 10.1021/bk-2012-1105.ch018

Hydrolytic and Enzymatic Degradation

A crucial structural difference between polymacrolactones and polyethylene is the presence of ester bonds in the polymer main chain of the former, which gave rise to the suggestion that these materials might be biodegradable (*61–64*). However, their hydrolytic stability is surprisingly high. Over a period of two years neither mass loss nor a reduction of the molecular weight of PPDL was detected (Figure 12 shows the data for a period of 375 days). Moreover, the crystallinity of the samples did not change over this time period. The same experiment was repeated with polyambrettolide (PAm) and polyglobalide (PGl) for 100 days and also here, no degradation took place. Additionally, PPDL, PAm and PGl do not degrade enzymatically. Even amorphous cross-linked PGl and PAm are not degradable under physiological conditions. Only upon incorporation of hydrophilic and non-crystalline comonomers like 4MeCL or DXO the enzymatic degradability could be enhanced (*54*). The molecular weight evolution could not be monitored due to the network formation upon cross-linking. As can be seen in Figure 12, mass loss was detected for both copolymers, however, DXO copolymers degrade faster. The degradation can be tuned by altering the comonomer ratio and nature of the copolymer.

Conclusions

Using either enzymatic or metal-catalyzed ring-opening polymerization of renewable macrolactones offers tremendous opportunities for the development of novel, renewable materials with good mechanical properties reminiscent of those of polyethylene. Using the right processing conditions, strong fibers can be made out of high molecular weight PPDL. Cross-linking polymers containing unsaturated macrolactones leads to strong 3D networks avoiding creep. Due to their biocompatibility these materials can be used for biomedical applications. Furthermore, introduction of comonomers affords the production of polyesters with tunable properties, such as degradability.

Polycarbonates from 1,4:3,6-Dianhydrohexitols

Introduction

Conventional polycarbonates, such poly(bisphenol-A carbonate), are known for their toughness, excellent transparency and good solvent and hydrolysis resistance. Aromatic polycarbonates, however, show poor UV-stability which hampers their use in outdoor applications. In addition, bisphenol-A (BPA) is suspected to have adverse health effects and is under pressure (*65*). Aliphatic alternatives are therefore of interest and several materials have been studied, including oligo- and polycarbonates based on different linear glycols, polymers synthesized by using cyclic carbonate monomers as carbonyl sources and systems based on oxiranes, using CO_2 as the carbonyl donor (*66*, *68–70*). Other aliphatic polycarbonates were based on 1,4-bis(hydroxymethyl) cyclohexane (*71*). Poly(isosorbide carbonate) was described for the first time in 1964 (*72*) and

Downloaded by COLUMBIA UNIV on August 28, 2012 | http://pubs.acs.org
Publication Date (Web): August 16, 2012 | doi: 10.1021/bk-2012-1105.ch018

DAH-based (co)polycarbonates have subsequently received attention from other researchers in recent decades (*28*, *73–82*). Poly(isosorbide carbonate) has a T_g up to 175 °C and molecular weights up to 50,000 g·mol^{-1} have been reported. Interestingly, the T_g and mechanical properties of the DAH-based polymer are comparable to those of poly(bisphenol-A carbonate) (*24*). In this paragraph, we focus on the preparation of DAH-based copolycarbonates having moderate molecular weights and well-defined end-group structures as well as tunable thermal properties. Potential applications of such materials are thermosetting coating systems, potentially affording highly transparent, tough cross-linked networks. The molecular weight between cross-links as well as the end-group structure can be influenced by carefully controlling the reaction stoichiometry and the average functionality of the applied monomers (*83*). In polycarbonate systems, the most logical approach is to target OH-functional polymers, which can subsequently be reacted with polyisocyanate curing agents. Cured poly(carbonate urethane) systems will be discussed later on.

Different polymerization routes can be applied to prepare linear or branched (co)polycarbonates. Phosgenation of diol monomers is a common, although hazardous, approach. In research laboratories, phosgene derivatives such as the liquid diphosgene or the solid triphosgene are often used, as these compounds are more convenient to handle. When polymerizing isosorbide through pyridine-catalyzed phosgenation (using triphosgene), the *endo*-oriented OH-group shows a higher conversion (97%) than its *exo*-oriented counterpart (88%). This observation can be explained by the fact that the *endo*-oriented hydroxyl is involved in intramolecular H-bonding (as illustrated in Figure 13), enhancing its nucleophilic character (*29*, *84*, *85*).

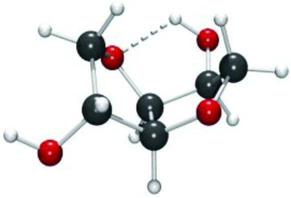

Figure 13. Structure of isosorbide, showing intramolecular H-bonding of its endo-oriented OH-group.

Another effect of the different OH-group orientations of the three DAH isomers is that the predominant chain conformation of the resulting polymers differs. Isoidide-based homopolycarbonates appear to consist almost exclusively of linear chains, whereas the isomannide-based samples seem to contain an abundance of cyclic species, as determined by MALDI-ToF-MS. Possibly, the conformation of poly(isomannide carbonate) chains is such that cycle formation is favored, whereas the *exo*-oriented hydroxyl groups present in isoidide favor the formation of more extended, linear polymer chains. Although MALDI-ToF-MS is not a quantitative technique, the trend observed here is similar to results

Downloaded by COLUMBIA UNIV on August 28, 2012 | http://pubs.acs.org
Publication Date (Web): August 16, 2012 | doi: 10.1021/bk-2012-1105.ch018

published for polycarbonates prepared from IS and IM using diphosgene as a carbonyl source (*75*). An advantage of preparing polycarbonates through phosgenation is that controlling the polymer composition is straightforward, meaning that the feed ratio of different diol monomers is reflected in the final polymer composition. The molecular weights of the prepared polycarbonates can in principle be controlled by adapting the reaction stoichiometry. The T_g of the polymers depends on the ratio between the rigid DAHs and more flexible comonomers such as 1,3-propanediol or glycerol.

However, using highly reactive compounds such as phosgene may lead to side-reactions. Also, several different types of end-groups can be formed depending on the stoichiometry, reaction conditions and the subsequent work-up procedure. Furthermore, balancing the molecular weight and the functionality can be rather difficult and the required procedure may differ depending on the type of comonomers used.

Table 4. Composition and properties of DAH-based (co)polycarbonates prepared in the melt using DPC, $T_{r,max}$ = 250 °C

composition [a]	T_g [b] *[°C]*	M_n [c] *[g·mol⁻¹]*	M_w [c] *[g·mol⁻¹]*	***PDI*** [c] *[-]*	***OHV*** [d] *[mgKOH·g⁻¹]*
IS [-]	138.0	3,200	7,200	2.2	55.0
II [-]	148.2	4,600	10,300	2.2	34.0
IS/1,3-PD [0.57:0.43]	48.1	3,200	5,300	1.7	57.2

[a] IS = isosorbide, II = isoidide, 1,3-PD = 1,3-propanediol. Composition determined by ^{1}H NMR spectroscopy. [b] Determined from the second heating curve of the DSC thermogram. [c] Determined by SEC in HFIP, using PMMA calibration. [d] Hydroxyl-value, determined by potentiometric titration.

Instead of phosgenation, melt polycondensation of diols with carbonyl donors such as diphenyl carbonate (DPC) is an effective way to prepare polycarbonates. The reaction between an OH-functional compound (in this case: a 1,4:3,6-dianhydrohexitol) and DPC is a type of transesterification reaction which is also referred to as transcarbonation (*86*). The condensation product phenol has to be removed from the increasingly viscous reaction mixture at relatively high temperature and reduced pressure. In such reactions, secondary alcohols like the DAHs require longer reaction times and/or higher temperatures to achieve high conversion. It was found that isoidide, the DAH isomer having two *exo*-oriented OH-groups, is the more reactive isomer, as was also observed during esterification reactions in the melt (*vide supra*). Some properties of polycarbonates made via the DPC-route are listed in Table 4.

By adjusting the stoichiometry of the reaction mixture, predominantly OH-functional polycarbonates can be prepared relatively easily. No phenyl carbonate end-groups are observed when applying a sufficient excess of diol or polyols monomers relative to DPC. In addition to linear chains, cyclic polycarbonates species are formed during these melt reactions (Figure 14). Due to the moderate reactivity of the DAHs, temperatures up to 250 °C are needed to drive the reaction forward. At these high reaction temperatures decarboxylation may occur, resulting in ether linkages along the polycarbonate main chain. In addition, volatile comonomers such as 1,3-propanediol may be partially lost from the reaction mixture, making it more difficult to control the reaction stoichiometry, the final polymer composition and end-group structure. Isomannide proved to be insufficiently stable to withstand these temperatures, resulting in cross-linked, strongly coloured products.

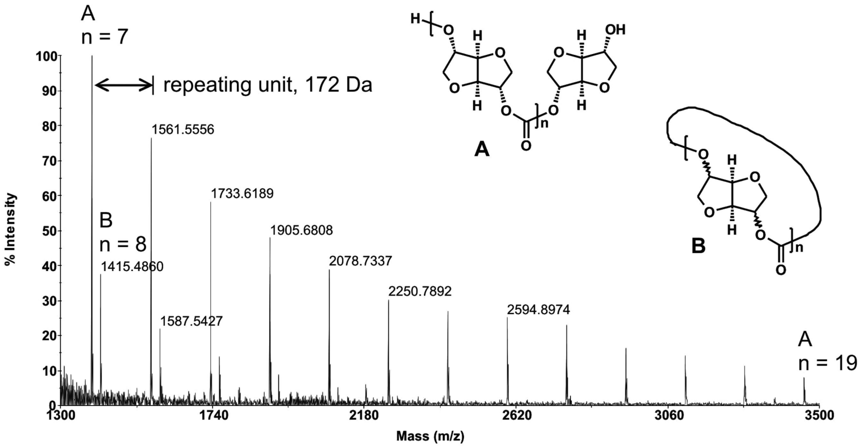

*Figure 14. MALDI-ToF-MS spectrum of poly(isoidide carbonate), where species **A** represent linear chains and species **B** represent cyclic chains. Figure taken from reference (83). Copyright 2011, John Wiley & Sons. Reproduced with permission.*

To enhance the control over the polymer composition, as well as to reduce the required reaction temperature, another route to DAH-based polycarbonates was studied. In this approach, dialkyl or diaryl (*77*, *78*) carbonate DAH-derivatives are prepared, which can subsequently react with primary diols and/or triols such as biomass-based alkylene diols or glycerol in the presence of a transesterification catalyst (Scheme 4).

Downloaded by COLUMBIA UNIV on August 28, 2012 | http://pubs.acs.org
Publication Date (Web): August 16, 2012 | doi: 10.1021/bk-2012-1105.ch018

Downloaded by COLUMBIA UNIV on August 28, 2012 | http://pubs.acs.org
Publication Date (Web): August 16, 2012 | doi: 10.1021/bk-2012-1105.ch018

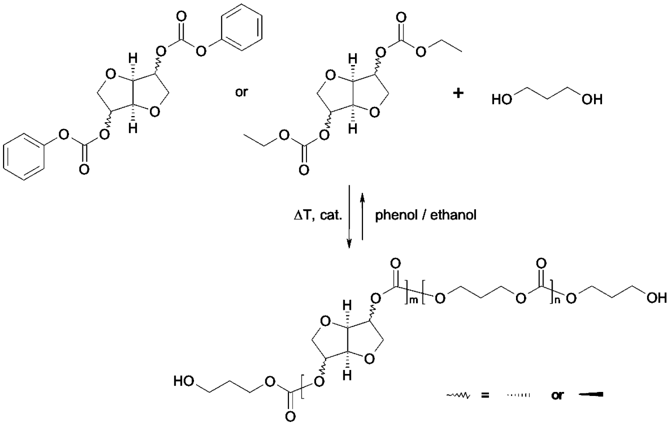

Scheme 4. Synthesis of poly(isohexide-co-propylene carbonate) from a dianhydrohexitol bis(phenyl/ethyl carbonate) and 1,3-propanediol

Table 5. Composition and properties of DAH-based (co)polycarbonates prepared in the melt using DAH bis(alkyl/aryl carbonates), $T_{r,max}$ = 210 °C

composition [a,e]	***T_g*** [b] *[°C]*	***M_n*** [c] *[g·mol^{-1}]*	***M_w*** [c] *[g·mol^{-1}]*	***PDI*** [c]	***OHV*** [d] *[mgKOH·g^{-1}]*
IS/1,3-PD [0.57:0.43]	90	4,200	8,100	1.9	47.3
IS/1,3-PD [f] [0.67:0.33]	64	2,200	3,700	1.7	*n.d.*
II/1,3-PD [0.44:0.56]	36	3,100	6,400	2.1	76.4
II/1,3-PD [f] [0.83:0.17]	67	1,900	3,100	1.6	*n.d.*
IS/1,4-BD [0.45:0.55]	38	5,000	9,800	2.0	32.1
II/1,4-BD [0.44:0.56]	36	6,300	14,400	2.3	39.0
IS/1,3-PD/TMP [1:0.28:0.06]	79	3,600	11,600	3.2	50.4
II/1,3-PD/TMP [1:0.24:0.05]	83	2,900	6,600	2.3	56.8

[a] IS = isosorbide, II = isoidide, 1,3-PD = 1,3-propanediol, 1,4-BD = 1,4-butanediol, TMP = trimethylolpropane. Composition determined by ^{1}H NMR spectroscopy. [b] Determined from the second heating curve of the DSC thermogram. [c] Determined by SEC in HFIP, using PMMA calibration. [d] Hydroxyl-value, determined by potentiometric titration. Measurements were only performed on materials available in sufficient quantities and at full solubility of the resins in NMP. [e] Prepared using the DAH bis(phenyl carbonate)s (unless stated otherwise). [f] Prepared using the corresponding DAH bis(ethyl carbonate)s.

Downloaded by COLUMBIA UNIV on August 28, 2012 | http://pubs.acs.org
Publication Date (Web): August 16, 2012 | doi: 10.1021/bk-2012-1105.ch018

The higher reactivity of primary alcohols facilitates a significant reduction of the polymerization temperature compared to direct reactions between DAHs and DPC. In addition, this procedure gives improved control over especially the polycarbonate end-groups. Although the formation of cyclic polymer chains cannot be avoided, otherwise fully OH-functional materials can be obtained. This approach is similar to a method described by Sablong et al. to incorporate isosorbide into poly(butylene terephthalate) (*23*). Table 5 gives an overview of some of the properties of linear and branched copolycarbonates prepared using the DAH bis(alkyl/aryl carbonate)s. These copolycarbonates are typically colorless or pale yellow transparent polymers. Their T_g values depend on the molecular weight as well as on the composition of the copolycarbonates. The monomers are built into the polymer chains in the same ratio as the initial monomer feed and significant losses of volatile diols were not observed, indicating that the reaction temperatures were sufficiently low to control the reaction stoichiometry and the final polymer composition. MALDI-ToF-MS spectra mainly show signals which can be attributed to linear chains having two hydroxyl end-groups. The DAH-based copolycarbonates are thermally stable up to at least 250 °C, while the homopolycarbonates are stable up to 300 °C.

From Diaminoisoidide to Biobased Polyamides

Introduction

The number and types of applications utilizing polyamides (PA) generate new trends in the selection of monomers used in their synthesis. Nowadays, biomass-derived chemicals offer an enormous potential to replace the depleting fossil feedstock and are considered as environmentally friendly alternatives. Despite the obvious benefits offered by renewable resources, biobased polymers are often believed to be unsuitable for high temperature industrial processes and applications. However, recent results have shown that, based on a thorough understanding of the structure-property relations of different polyamides, it is now possible to prepare fully biobased nylons having equally good thermal and mechanical properties as their counterparts from petrochemical origin (*87*).

Widely reported biobased monomers in this field are sebacic acid, brassylic acid, 1,4-diaminobutane or isohexides (*24*, *87–100*). Since an extensive evaluation of isohexide derivatives revealed their numerous interesting properties, they can be successfully used in the synthesis of polyamides and poly(ester amides) (*87*, *88*, *91*). Towards isohexide-based polyamides, both bulk polycondensation and interfacial polymerization was applied. As reported (*87*), the difficulties associated with low thermal stability of these bicyclic compounds have been overcome by using mild reaction conditions.

The presence of isohexides in the polyamide backbone, causing a disturbance of the polymer chain regularity, can significantly affect its crystal structure. In an attempt to reduce the hydrogen bond density and the melting point of the polyamides, which is relevant in terms of their processing, the incorporation of biobased diaminoisoidide, the *exo-exo* diamine derivative of isomannide, into the polymer backbone is considered as one of the promising alternatives

(*87*, *88*). Furthermore, in view of their expected higher moisture absorption isohexide-based polyamides might be proposed for fiber applications.

Evaluation of Polyamides Based on Diaminoisoidide

The polyamides (PAs) entirely based on renewable monomers *viz.* sebacic acid (SebA), 1,4-diaminobutane (DAB) and diaminoisoidide (2,5-diamino-2,5-dideoxy-1,4;3,6-dianhydroiditol, DAII) (Figure 15) were synthesized either by melt polycondensation of the nylon salts followed by solid state polymerization (SSP) or by interfacial polycondensation (*87*). The unique properties of the synthesized polyamides resulted from the presence of diaminoisoidide units in the polymer backbone. By using a new route towards DAII the monomer, utilized subsequently in the synthesis of the polyamides, was isolated with a high yield and purity (*87*, *101*). The monomer combination used in the synthesis of the polyamides allowed to obtain relatively high molecular weight products, which significantly influenced their thermal and mechanical properties. As is well-known, higher molecular weight of the PAs promote higher thermal stability and melting points.

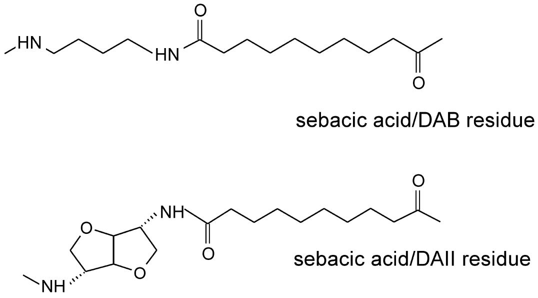

Figure 15. Chemical structure of the repeat units in the synthesized polyamides. Reproduced with permission from reference (87). Copyright 2011, American Chemical Society.

The measurements of the molecular weights of the polyamides, examined before and after SSP, provided the expected results. Due to the limited reactivity of the exo-oriented secondary diamine, the DAII-rich products revealed lower molecular weights in comparison to PA 4.10 (in Table 6 presented as PA1). Nevertheless, for compositions with a DAII content below 40 mol%, the applied conditions resulted in copolymers with molecular weights above 18,000 g·mol^{-1} and polydispersity indices below 3.0.

As demonstrated by DSC measurements, the incorporation of diaminoisoidide into the structure of PA 4.10 reduced the melting temperature (T_m) of the copolymers. This behavior proved that the changes in the polyamide chain regularity affect their crystal structure. The presence of DAII units in the copolymers allowed to reduce the T_m from 246 °C (noted for PA 4.10) to about 180 °C (as recorded for the copolyamide containing 43 mol% of DAII instead

Downloaded by COLUMBIA UNIV on August 28, 2012 | http://pubs.acs.org
Publication Date (Web): August 16, 2012 | doi: 10.1021/bk-2012-1105.ch018

Downloaded by COLUMBIA UNIV on August 28, 2012 | http://pubs.acs.org
Publication Date (Web): August 16, 2012 | doi: 10.1021/bk-2012-1105.ch018

of DAB). The impact of the copolyamide structure associated with the presence of diaminoisoidide was also pronounced in their thermal stability. Given the structure of DAII one might anticipate that the first step of the thermal degradation of the polymers is related to the oxidation at the carbon atom in the α-position of the ether oxygen of the cyclic diamine (*87*). Indeed, the diaminoisoidide-based polyamides reveal lower thermal stability than PA 4.10. However, in combination with their lower melting temperature and reduced enthalpy of the transition (see Table 6) these materials can be successfully processed.

The hydrogen bonding efficiency influencing the crystal structure of the polyamides was analyzed by FT-IR. Infrared spectroscopy revealed a direct correlation between an increased content of DAII in PAs and their NH stretch bands position and intensities. The signals at around 3300-3315 cm^{-1} attributed to hydrogen bonded NH groups (*102–105*) become broader and weaker, which implies the decrease of the crystalline order of the DAII-based copolyamides (Figure 16).

Table 6. Characteristics of co- and homopolyamides from sebacic acid, 1,4-diaminobutane and diaminoisoidide. Reproduced with permission from reference (*87*). Copyright 2011, American Chemical Society

entry	***built-in composition*** *(DAB/DAII)*[a]	M_n [b] *[g·mol⁻¹]*	***PDI*** [b] *[-]*	T_m *[°C]*	$T_{5\%}$[d] *[°C]*
PA1	1.0/0	21,900	3.0	246	424
coPA2	0.89/0.11	21,300	2.7	242	388
coPA3	0.86/0.14	18,700	2.7	236	379
coPA4	0.80/0.20	20,400	2.9	232	377
coPA5	0.57/0.43	3,900	1.9	179,198	321
PA6[c]	0/1.0	4,200	2.3	152	300

[a] DAB = 1,4-diaminobutane, DAII = diaminoisoidide, molar ratio determined by NMR. [b] Determined for polyamides after Solid State Polymerization using SEC with PMMA standards in HFIP solvent. [c] PA obtained via interfacial polymerization. [d] $T_{5\%}$ = temperature of 5% mass loss.

An additional feature of the investigation was the evaluation of the DAII distribution over the crystalline and amorphous phase of the polyamides. The bands characteristic for the ethers asymmetric C-O-C stretching mode of diaminoisoidide units were found in the vicinity of 1080-1100 cm^{-1}. As the molar ratio of diaminoisoidide increases these bands together with the signals at 971 cm^{-1} assigned to CH_2 rocking vibrations show an increased intensity. FT-IR spectra of the materials containing DAII units show also the positive bands at 902-903 cm^{-1} assigned to amide stretching vibrations, which vanish close to the melting point of the copolymers. These changes can be easily explained as caused by the presence of diaminoisoidide in the crystalline phase of the copolyamides.

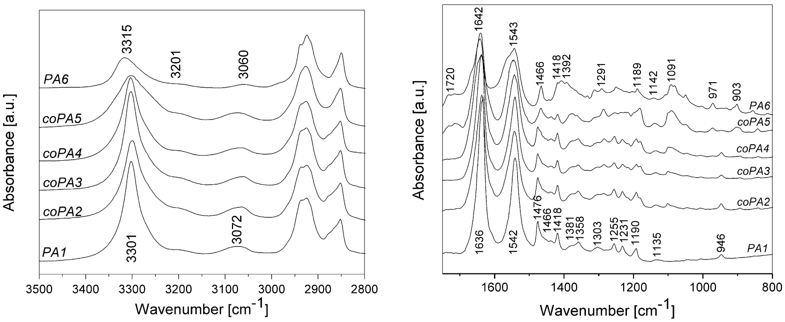

Figure 16. FT-IR spectra of the homopolyamides PA1, PA6 and copolyamides coPA2-coPA5, recorded at 30 °C. The spectra show frequency ranges of 2800-3500 cm^{-1} (left) and 800-1750 cm^{-1} (right). Reproduced with permission from reference (87). Copyright 2011, American Chemical Society.

X-ray diffraction techniques are commonly used for the analysis of polyamides chain organization and their crystal structure. To prove the cocrystallization of the DAII comonomers in the same crystal lattice of the PA 4.10 polyamide, Wide Angle X-ray Diffraction (WAXD) experiments were carried out. WAXD evaluations indicated that regardless of the chemical composition, all investigated materials are semi-crystalline. As presented in Figure 17 the X-ray diffraction patterns of PA1 and coPA2-coPA4 with DAII contents lower than 43 mol% show four reflections (001, 002, 100, and 010/110) in the vicinity of 3-7°, 10-12° and 18-25°. This suggests that the crystal structure of these materials consists of arranged side by side hydrogen-bonded sheets (*106*, *107*). Interestingly, upon increasing the DAII content in the polyamides their 010/110 reflection decreased in intensity and subsequently disappeared. As reported before, the absence of the individual 010/110 reflection, which corresponds to the intersheet distance, proved that coPA5 and PA6 structures changed into a hexagonal packing of polymer chains (*87*). This transition revealed equal interchain and intersheet distances in the crystal lattice of the polymers, which subsequently affects their properties. Furthermore, the analysis of the WAXD data shows that the position and intensities of the 001 reflection of the copolymers containing DAII units undergo visible changes. Their shift towards lower 2θ value reveals an increase of the c-axis dimension of the unit cell and cocrystallization of all comonomers in the same crystal lattice.

Downloaded by COLUMBIA UNIV on August 28, 2012 | http://pubs.acs.org
Publication Date (Web): August 16, 2012 | doi: 10.1021/bk-2012-1105.ch018

Downloaded by COLUMBIA UNIV on August 28, 2012 | http://pubs.acs.org
Publication Date (Web): August 16, 2012 | doi: 10.1021/bk-2012-1105.ch018

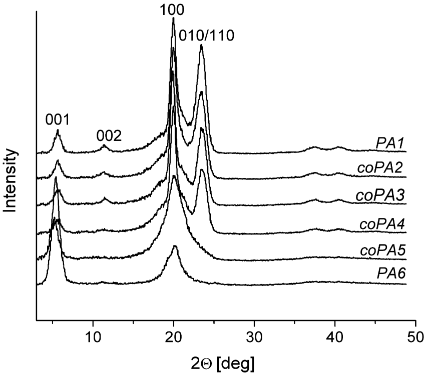

Figure 17. X-ray powder diffraction patterns of PA 4.10 (PA1) and diaminoisoidide-based co- and homopolyamides (coPA2-PA6). Reproduced with permission from reference (87). Copyright 2011, American Chemical Society.

Conclusions

Given the importance of biomass-based polymers we investigated polyamides from diaminoisoidide (the *exo-exo* diamine derivative of isomannide), 1,4-diaminobutane and sebacic acid. The polyamides were synthesized either by solvent-free bulk polycondensation followed by solid state polymerization or by interfacial polycondensation. By using mild reaction conditions white products with M_n values above 18,000 g·mol^{-1} and tunable melting temperatures were obtained. The influence of diaminoisoidide on the crystal structure and hydrogen bonding efficiency was probed by WAXD and FT-IR techniques. These methods allowed to prove the cocrystallization of DAII with DAB and SebA in the same crystal lattice and the reduced hydrogen bond density of the copolymers in comparison to PA 4.10.

Polyurethanes and Polyureas from Renewable Resources

Poly(ester urethane urea) and Poly(ether urea) Elastomers

Isocyanate-Route

Biomass-based and potentially biodegradable thermoplastic polyurethane or polyurea elastomers (TPUE) are of interest for engineering and biomedical applications. Several systems have been described in the open literature (*108*, *109*). Previously, low T_g polyesters were described, such as poly(1,2-dimethylethylene adipate) (PDMEA). These polydiols can be reacted with diisocyanates such as hexamethylenediisocyanate (HMDI) to form NCO-functional prepolymers, which can subsequently be chain-extended using low molecular weight diamines or diols (Scheme 5).

Downloaded by COLUMBIA UNIV on August 28, 2012 | http://pubs.acs.org
Publication Date (Web): August 16, 2012 | doi: 10.1021/bk-2012-1105.ch018

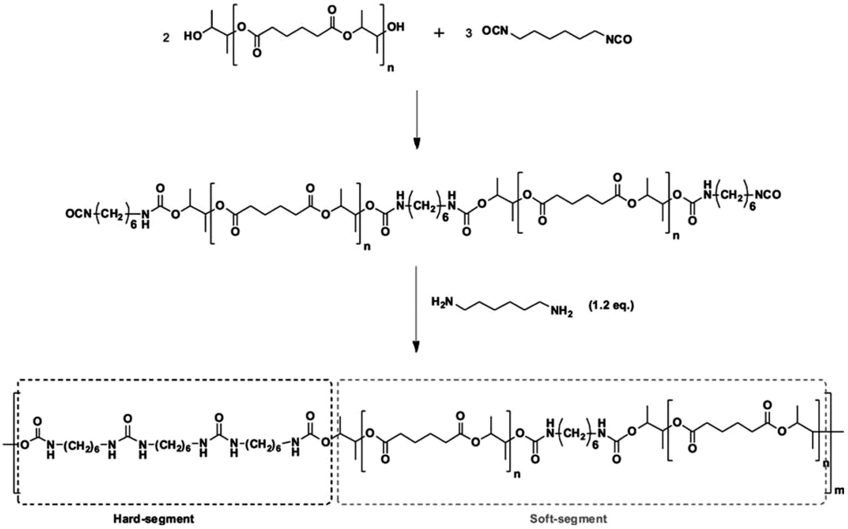

Scheme 5. Synthesis of poly(ester urethane urea)s based on PDMEA, HMDI and hexamethylenediamine (HMDA). Figure taken from reference (18). Copyright 2011, John Wiley & Sons. Reproduced with permission

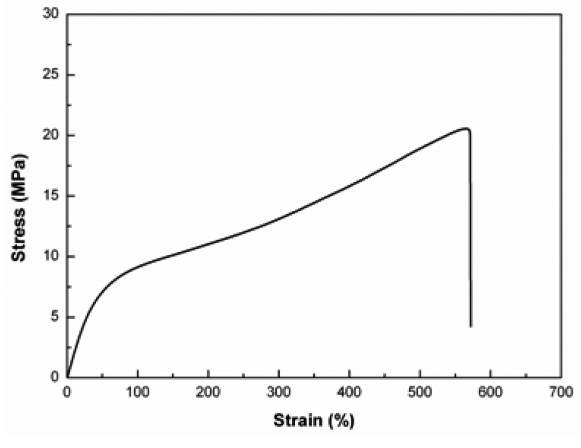

Figure 18. Stress-strain curve of a TPUE based on PDMEA, HMDI and HMDA. Figure taken from reference (18). Copyright 2011, John Wiley & Sons. Reproduced with permission.

The resulting poly(ester urethane urea)s have a phase-separated morphology, in which the hard segments can crystallize and act as physical cross-links dispersed in the amorphous, soft continuous phase. The presence of ester linkages along the polymer backbone as well as the amorphous nature of the continuous phase may improve the biodegradability of this type of polymers. Such TPUEs ideally have

Downloaded by COLUMBIA UNIV on August 28, 2012 | http://pubs.acs.org
Publication Date (Web): August 16, 2012 | doi: 10.1021/bk-2012-1105.ch018

a temperature-independent modulus above their T_g, determining their application window. The partly biobased polymer depicted in Scheme 5 is thermally stable up to approx. 260 °C, has a T_g of -3 °C and a flow temperature of 248 °C. From tensile testing (Figure 18), the E-modulus was found to be 20 MPa and the polymer has a strain at break of 560%. This combination of properties makes the polymer suitable for, e.g., biomedical applications (*18*).

Isocyanate-Free Route

One of the current developments in polyurethane chemistry is to investigate new synthetic routes which avoid the use of toxic diisocyanates (*110–114*). A particularly interesting option is to prepare dicarbamate hard segments, which can be reacted with amine- or hydroxy-functional prepolymers yielding polyureas or polyurethanes, respectively. This alternative synthetic strategy towards TPUEs offers great flexibility in terms of hard segment structure, a relatively high atom efficiency and a well-defined hard segment length. As the hard segment is prepared *ex-situ*, its length distribution is narrow, leading to enhanced crystallization and phase separation. The resulting TPUEs have T_g values close to the T_g of the soft segment, more temperature-independent shear moduli and sharper thermal transitions. Scheme 6 summarizes the isocyanate-free synthesis of polyureas and lists some of the dicarbamate hard segment structures studied in our laboratories. These dicarbamates can be prepared through efficient TBD-catalyzed reactions between 1,4-diaminobutane (DAB) and dimethylcarbonate (DMC).

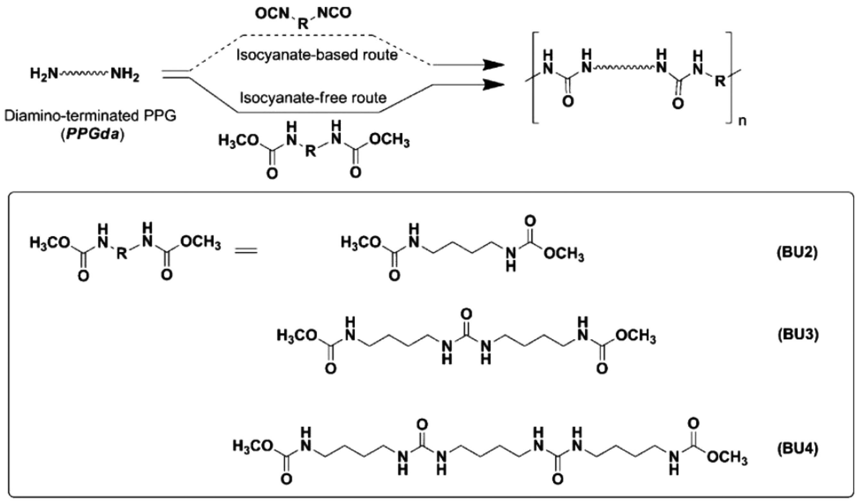

Scheme 6. Synthesis of biobased poly(ether urea)s through reactions of dicarbamate hard segments with the amino-functional poly(propylene glycol) (PPGda). Figure taken from reference (115). Copyright 2011, John Wiley & Sons. Reproduced with permission

Downloaded by COLUMBIA UNIV on August 28, 2012 | http://pubs.acs.org
Publication Date (Web): August 16, 2012 | doi: 10.1021/bk-2012-1105.ch018

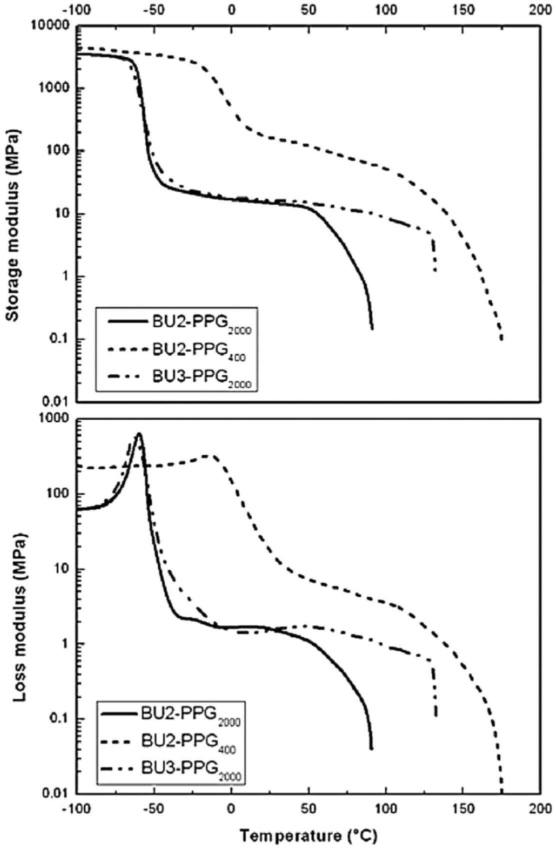

Figure 19. Storage and loss modulus curves for TPUEs prepared through an isocyanate-free route. Figure taken from reference (115). Copyright 2011, John Wiley & Sons. Reproduced with permission.

Dynamic Mechanical Thermal Analysis (DMTA) is the preferred characterization technique to study the storage (G') and loss (G'') moduli of elastomers as a function of temperature. Figure 19 shows the DMTA curves of several TPUEs synthesized according to the dicarbamate-route, using the hard segments shown in Scheme 6 in combination with amino-functional poly(propylene glycol)s (PPG) with molecular weights of 400 or 2000 g·mol^{-1}. The thermo-mechanical performance of the polyureas is determined by the hard segment length and content, as well as by the extent of phase separation and the length of the soft segment. By increasing the hard segment length, the flow temperature (T_{fl}, defined as the temperature at which G' drops below 0.1 MPa) of the material increases (compare BU2-PPG$_{2000}$ and BU3-PPG$_{2000}$), while the T_g stays constant. Shortening the soft segment from 2000 to 400 g·mol^{-1} (and thus, increasing the hard segment content from 9.3% to 31.7%) significantly increases the modulus of the rubbery plateau as well as the observed T_g (compare BU2-PPG$_{2000}$ and BU2-PPG$_{400}$). The latter effect is caused by an increased extent

Downloaded by COLUMBIA UNIV on August 28, 2012 | http://pubs.acs.org
Publication Date (Web): August 16, 2012 | doi: 10.1021/bk-2012-1105.ch018

of phase mixing, where the interaction between the soft and the hard segments leads to decreased mobility in the continous phase.

In general, it can be said that this isocyanate-free approach to thermoplastic elastomers leads to well-defined polymers, showing sufficient phase separation (especially at lower hard segment contents). As a results, these materials have rather sharp glass transitions and rubbery moduli which are fairly independent of temperature between T_g and T_{fl} (*115*).

DAH-Based Poly(ester/carbonate urethane) Cross-Linked Networks

Above, various hydroxy-functional polyesters and polycarbonates based on the 1,4:3,6-dianhydrohexitols (DAH) were described. The relatively rigid DAH skeletons present in the polymer backbones result in T_g values above room temperature. In addition, these polymers are amorphous materials, especially when isosorbide is used. These polydiols are therefore suitable starting materials for thermosetting coatings systems. In such systems, amorphous semi-aromatic polyesters are typically used, having either hydroxyl or carboxylic acid end-groups. The petrochemical aromatic constituents often lead to reduced UV-stability in outdoor applications, so a fully aliphatic, biomass-based alternative could be of significant interest. To assess the performance of the DAH-based polyester and polycarbonate resins as constituents of thermosetting coating systems, they can be cross-linked in a straightforward way using polyisocyanate curing agents. In this way, poly(ester urethane) (PEU) or poly(carbonate urethane) (PCU) networks are prepared, as shown in Figure 20 (*31*, *32*, *83*, *116*).

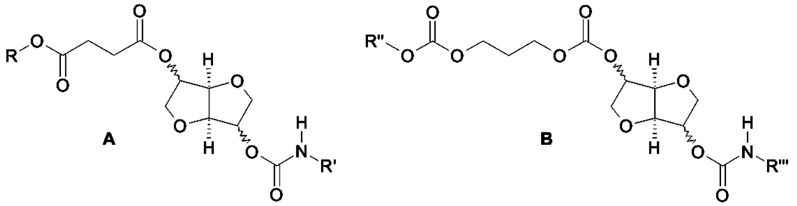

*Figure 20. DAH-based PEUs and PCUs, resulting from reactions between isocyanates and (**A**) an OH-functional poly(DAH succinate) or (**B**) an OH-functional poly(DAH-co-propylene carbonate).*

Examples of useful curing agents are depicted in Figure 21, where the HDI-based compound **I** is typically used in solvent-borne systems while the solid ε-caprolactam blocked, isophorone diisocyanate (IPDI)-based cross-linker **II** is often applied in powder coatings. Table 7 summarizes the performance of the different types of coatings in terms of solvent and impact resistance. In general, the obtained coatings are colourless to pale-yellow glossy, transparent films with a smooth surface, indicating sufficient flow of the polymer resins. In powder coating systems, flow plays a crucial role during film formation and coalescence of the resin particles. If the melt viscosity of the polymeric resin is too high, this

Downloaded by COLUMBIA UNIV on August 28, 2012 | http://pubs.acs.org
Publication Date (Web): August 16, 2012 | doi: 10.1021/bk-2012-1105.ch018

process does not occur properly and gelation of the formulation will occur before a smooth film is obtained. The melt viscosity of a polymer depends on the T_g, the molecular weight, the degree of branching and on intermolecular interactions such as hydrogen bonding. Obviously, the addition of additives such as pigments and flow agents also strongly affect the behavior of the formulated powder paint during film formation.

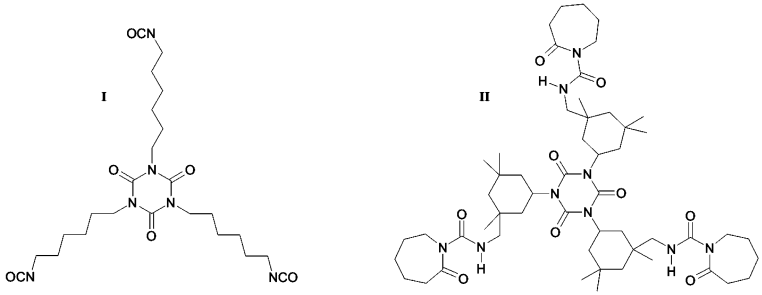

*Figure 21. Curing agents used to form poly(ester/carbonate urethane) networks from the corresponding DAH-based polyester or polycarbonate resins: (**I**) trimer of hexamethylene diisocyanate, (**II**) ε-caprolactam-blocked trimer of isophorone diisocyanate.*

Table 7. Performance of coatings from DAH-based polydiols

polymer topology	*curing agent*[a]	*acetone resistance*[b,c]	*impact res.*[b,d] *[100 kg.cm]*
polyesters			
linear	I	+	+
	II	+/-	-
branched	I	+	+
	II	+	+/-
polycarbonates			
linear / branched	I	+	+
	II	+	-

[a] see Figure 21. [b] + = passes test, +/- = minor damage, - = severe damage. [c] determined by rubbing the coating with an acetone-drenched cloth. [d] determined by reverse impact testing.

Polymer networks formed using curing agent **I** show better chemical and mechanical stability (determined by solvent resistance testing and falling dart reverse impact testing, respectively) than those cured with compound **II**. This is thought to be caused by the reduced combined reactivity of the IPDI moieties with the secondary, bulky DAH end-groups. In addition, dynamic mechanical analysis performed during the curing reaction demonstrated that a higher plateau modulus was reached when curing isoidide-based polyesters (90 kPa) compared to their isosorbide-based equivalents (55 kPa), indicating an enhanced cross-link density. These results suggest that the *exo*-oriented OH-groups of isoidide are more accessible for reaction with IPDI.

General Conclusion

In this chapter, several different groups of polymers were described, prepared through a range of polymerization techniques. The common denominator is the fact that all these materials are based on biomass, either fully or partially. Where possible, sustainable preparation methods were developed such as solvent-free, solid state or enzymatic polymerization. Efficient catalysts and modified monomers were used to reduce the required reaction temperatures and high atom efficiency was targeted. Our aim is not only to show the synthetic feasibility of these pathways, but also to demonstrate the merit of the resulting polymers in real-life applications. Clearly, unique polymer properties are obtained which can be adapted effectively once the chemistry and the structure-property relations are understood. Detailed molecular, thermal and mechanical characterization are essential in this respect. Linear high molecular weight polyesters, polyurethanes and polyamides were prepared, suitable for fiber, elastomer, biomedical or engineering plastic applications. In addition, well-defined polyester and polycarbonate resins with moderate molecular weight were successfully synthesized, having reactive end-groups. These prepolymers are very useful in thermosetting polymer networks for coating systems.

Downloaded by COLUMBIA UNIV on August 28, 2012 | http://pubs.acs.org
Publication Date (Web): August 16, 2012 | doi: 10.1021/bk-2012-1105.ch018

Glossary

1,3-PD	1,3-propanediol
1,4-BD	1,4-butanediol
^{13}C NMR	^{13}C Nuclear Magnetic Resonance spectroscopy
^{1}H NMR	^{1}H Nuclear Magnetic Resonance spectroscopy
2,3-BD	2,3-butanediol
2D	two-dimensional
4MeCL	4-methyl caprolactone
$\varepsilon_{\text{break}}$	strain at break
$\varepsilon_{\text{yield}}$	yield strain
σ_{break}	stress at break
σ_{yield}	yield stress
AA	Adipic acid
Am	ambrettolide
AV	acid value, determined by titration [mg KOH·g^{-1}]
BPA	bisphenol-A

Downloaded by COLUMBIA UNIV on August 28, 2012 | http://pubs.acs.org
Publication Date (Web): August 16, 2012 | doi: 10.1021/bk-2012-1105.ch018

CA	citric acid
CL	caprolactone
COSY	Correlation Spectroscopy
cROP	metal-catalyzed Ring-Opening Polymerization
DAB	1,4-diaminobutane
DAH	1,4:3,6-dianhydrohexitol
DAII	diaminoisoidide
DGT	diglycidyl terephthalate
DL	decalactone
DMC	dimethyl carbonate
DM(T)A	Dynamic Mechanical (Thermal) Analysis
DPC	diphenyl carbonate
DSC	Differential Scanning Calorimetry
DXO	1,5-dioxepan-2-one
E	tensile, elastic or Young's modulus [Pa]
eROP	enzymatic Ring-Opening Polymerization
F_n	functionality
FT-IR	Fourier Transform Infrared
G'	storage modulus [Pa]
G''	loss modulus [Pa]
Gl	globalide
GLY	glycerol
HDL	16-hexadecalactone
HEMA	hydroxyethyl methacrylate
HFIP	1,1,1,3,3,3-hexafluoro-2-propanol
HMBC	Heteronuclear Multiple-bond Correlation
HMDA	hexamethylenediamine
HMDI	hexamethylenediisocyanate
HT-SEC	high temperature Size Exclusion Chromatograpy
II	1,4:3,6-dianhydro-L-iditol (or: isoidide)
IM	1,4:3,6-dianhydro-D-mannitol (or: isomannide)
IPDI	isophorone diisocyanate
i-PP	isotactic polypropylene
IS	1,4:3,6-dianhydro-D-glucitol (or: isosorbide)
MA	maleic anhydride
MALDI-ToF-MS	Matrix-Assisted Laser Desorption/Ionization Time-of-Flight Mass Spectrometry
M_n	number average molecular weight $[\mathrm{g \cdot mol^{-1}}]$
M_w	weight average molecular weight $[\mathrm{g \cdot mol^{-1}}]$
n	number of repeating units in a polymer chain
NCO	isocyanate group
NMP	N-methyl-2-pyrrolidone
NMR	Nuclear Magnetic Resonance spectroscopy
NPG	neopentyl glycol
NVP	*N*-vinyl-2-pyrrolidinone
OHV	hydroxyl value, det. by titration $[\mathrm{mg\ KOH \cdot g^{-1}}]$
PA	polyamide

PAm	polyambrettolide
PBA	poly(1,4-butylene adipate)
PBS	phosphate buffered saline
PBT	poly(butylene terephthalate)
PCU	poly(carbonate urethane)
PDI	polydispersity index [-]
PDL	ω-pentadecalactone
PDMEA	poly(1,2-dimethylethylene adipate)
PDS	poly(1,12-dodecylene sebacate)
PEG	poly(ethylene glycol)
PEs	polyesters
PET	poly(ethylene terephthalate)
PEU	poly(ester urethane)
PGl	polyglobalide
PMMA	poly(methyl methacrylate)
PPA	poly(1,3-propylene adipate)
PPDL	polypentadecalactone
PPG	poly(propylene glycol)
PPGda	diamino-terminated poly(propylene glycol)
PS	polystyrene
ROP	Ring-Opening Polymerization
SA	succinic acid
SebA	Sebacic acid
SEC	Size Exclusion Chromatography
SSP	Solid State Polymerization
t	time [s]
T	temperature [°C]
$T_{5\%}$	temperature at which 5% mass loss is observed in TGA
T_c	crystallization temperature [°C]
T_fl	flow temperature [°C]
T_g	glass transition temperature [°C]
T_m	melting temperature [°C]
T_max	temperature of maximal rate of decomposition
TBD	1,5,7-triazabicyclo[4.4.0]dec-5-ene
TGA	ThermoGravimetric Analysis
TGT	triglycidyl trimellitate
TMP	trimethylolpropane
TPh	triphosgene
TPUE	thermoplastic polyurethane/polyurea elastomer
UL	undecalactone
UV	ultraviolet
VL	valerolactone
WAXD	Wide Angle X-ray Diffraction

Downloaded by COLUMBIA UNIV on August 28, 2012 | http://pubs.acs.org
Publication Date (Web): August 16, 2012 | doi: 10.1021/bk-2012-1105.ch018

Downloaded by COLUMBIA UNIV on August 28, 2012 | http://pubs.acs.org
Publication Date (Web): August 16, 2012 | doi: 10.1021/bk-2012-1105.ch018

References

1. Corma, A.; Iborra, S.; Velty, A. *Chem. Rev.* **2007**, *107*, 2411–2502.
2. Biebl, H.; Marten, S. *Appl. Microbiol. Biotechnol.* **1995**, *44* (1-2), 15–19.
3. Mu, Y.; Teng, H.; Zhang, D. J.; Wang, W.; Xiu, Z. L. *Biotechnol. Lett.* **2006**, *28* (21), 1755–1759.
4. Meynial-Salles, I.; Dorotyn, S.; Soucaille, P. *Biotechnol. Bioeng.* **2008**, *99* (1), 129–135.
5. Saha, B. C.; Bothast, R. J. *Appl. Microbiol. Biotechnol.* **1999**, *52* (3), 321–326.
6. Qin, J. Y.; Xiao, Z. J.; Ma, C. Q.; Xie, N. Z.; Liu, P. H.; Xu, P. *Chin. J. Chem. Eng.* **2006**, *14* (1), 132–136.
7. Hoydonckx, H. E.; De Vos, D. E.; Chavan, S. A.; Jacobs, P. A. *Top. Catal.* **2004**, *27*, 83–96.
8. Meher, L. C.; Vidya Sagar, D.; Naik, S. N. *Renewable Sustainable Energy Rev.* **2006**, *10*, 248–268.
9. Draths, K. M.; Frost, J. W. *J. Am. Chem. Soc.* **1994**, *116*, 399–400.
10. Lange, J. P.; Vestering, J. Z.; Haan, R. J. *Chem. Comm.* **2007** (33), 3488–3490.
11. Mutlu, H.; Meier, M. A. R. *Eur. J. Lipid Sci. Technol.* **2010**, *112* (1), 10–30.
12. Kiesewetter, M. K.; Shin, E. J.; Hedrick, J. L.; Waymouth, R. M. *Macromolecules* **2010**, *43* (5), 2093–2107.
13. Chuma, A.; Horn, H. W.; Swope, W. C.; Pratt, R. C.; Zhang, L.; Lohmeijer, B. G. G.; Wade, C. G.; Waymouth, R. M.; Hedrick, J. L.; Rice, J. E. *J. Am. Chem. Soc.* **2008**, *130* (21), 6749–6754.
14. Kiesewetter, M. K.; Scholten, M. D.; Kirn, N.; Weber, R. L.; Hedrick, J. L.; Waymouth, R. M. *J. Org. Chem.* **2009**, *74* (24), 9490–9496.
15. Fokou, P. A.; Meier, M. A. R. *Macromol. Rapid Commun.* **2008**, *29* (19), 1620–1625.
16. Turunc, O.; Meier, M. A. R. *Macromol. Rapid Commun.* **2010**, *31* (20), 1822–1826.
17. Liu, C.; Liu, F.; Cai, J. L.; Xie, W. C.; Long, T. E.; Turner, S. R.; Lyons, A.; Gross, R. A. *Biomacromolecules* **2011**, *12* (9), 3291–3298.
18. Tang, D.; Noordover, B. A. J.; Sablong, R. J.; Koning, C. E. *J. Polym. Sci., Part A: Polym. Chem.* **2011**, *49* (13), 2959–2968.
19. Stoss, P.; Hemmer, R. *Adv. Carbohydr. Chem. Biochem.* **1991**, *49*, 93–173.
20. Storbeck, R.; Ballauff, M. *J. Appl. Polym. Sci.* **1996**, *59*, 1199–1201.
21. Storbeck, R.; Rehahn, M.; Ballauff, M. *Makromol. Chem.* **1993**, *194*, 53–64.
22. Kricheldorf, H. R.; Behnken, G.; Sell, M. *J. Macromol. Sci., Part A: Pure Appl. Chem.* **2007**, *44* (7), 679–684.
23. Sablong, R.; Duchateau, R.; Koning, C. E.; De Wit, G.; Van Es, D.; Koelewijn, R.; Van Haveren, J. *Biomacromolecules* **2008**, *9*, 3090–3097.
24. Fenouillot, F.; Rousseau, A.; Colomines, G.; Saint-Loup, R.; Pascault, J.-P. *Prog. Polym. Sci.* **2010**, *35*, 578–622.
25. Okada, M.; Okada, Y.; Tao, A.; Aoi, K. *J. Appl. Polym. Sci.* **1996**, *62*, 2257–2265.

26. Okada, M.; Tsunoda, K.; Tachikawa, K.; Aoi, K. *J. Appl. Polym. Sci.* **2000**, *77*, 338–346.
27. Okada, M.; Okada, Y.; Aoi, K. *J. Polym. Sci., Part A: Polym. Chem.* **1995**, *33*, 2813–2820.
28. Braun, D.; Bergmann, M. *J. Prakt. Chem.* **1992**, *334*, 298–310.
29. Fleche, G.; Huchette, M. *Starch* **1986**, *38* (1), 26–30.
30. Chatti, S.; Bortolussi, M.; Loupy, A.; Blais, J. C.; Bogdal, D.; Roger, P. *J. Appl. Polym. Sci.* **2003**, *90*, 1255–1266.
31. Noordover, B. A. J.; Van Staalduinen, V. G.; Duchateau, R.; Koning, C. E.; Van Benthem, R. A. T. M.; Mak, M.; Heise, A.; Frissen, A. E.; Van Haveren, J. *Biomacromolecules* **2006**, *7* (12), 3406–3416.
32. Noordover, B. A. J.; Heise, A.; Malanowski, P.; Senatore, D.; Mak, M.; Molhoek, L.; Duchateau, R.; Koning, C. E.; Van Benthem, R. A. T. M. *Prog. Org. Coat.* **2009**, *65* (2), 187–196.
33. Noordover, B. A. J.; Duchateau, R.; Van Benthem, R. A. T. M.; Ming, W.; Koning, C. E. *Biomacromolecules* **2007**, *8*, 3860–3870.
34. Misev, T. A. *Powder coatings - chemistry and technology*, 1st ed.; John Wiley & Sons: New York, 1991.
35. Kricheldorf, H. R.; Chatti, S.; Schwarz, G.; Kruger, R. P. *J. Polym. Sci., Part A: Polym. Chem.* **2003**, *41*, 3414–3424.
36. Sapich, B.; Stumpe, J.; Krawinkel, T.; Kricheldorf, H. R. *Macromolecules* **1998**, *31*, 1016–1023.
37. Cognet-Georjon, E.; Mechin, F.; Pascault, J.-P. *Macromol. Chem. Phys.* **1996**, *197*, 3593–3612.
38. Beldi, M.; Medimagh, R.; Chatti, S.; Margue, S.; Prim, D.; Loupy, A.; Delolme, F. *Eur. Polym. J.* **2007**, *43* (8), 3415–3433.
39. Jasinska, L.; Koning, C. E. *J. Polym. Sci., Part A: Polym. Chem.* **2010**, *48* (13), 2885–2895.
40. Jasinska, L.; Koning, C. E. *J. Polym. Sci., Part A: Polym. Chem.* **2010**, *48* (24), 5907–5915.
41. Jo, S.; Shin, H.; Shung, A. K.; Fisher, J. P.; Mikos, A. G. *Macromolecules* **2001**, *34* (9), 2839–2844.
42. Zheng Shu, X.; Liu, Y.; Palumbo, F. S.; Luo, Y.; Prestwich, G. D. *Biomaterials* **2004**, *25* (7-8), 1339–1348.
43. Shin, H.; Temenoff, J. S.; Mikos, A. G. *Biomacromolecules* **2003**, *4* (3), 552–560.
44. Timmer, M. D.; Jo, S. B.; Wang, C. Y.; Ambrose, C. G.; Mikos, A. G. *Macromolecules* **2002**, *35* (11), 4373–4379.
45. Zhao, X. F.; Liu, L. X.; Dai, H. X.; Ma, C. X.; Tan, X. H.; Yu, R. H. *J. Appl. Polym. Sci.* **2009**, *113* (5), 3376–3381.
46. Mahmoudi, M.; Simchi, A.; Imani, M.; Hafeli, U. O. *J. Phys. Chem. C* **2009**, *113* (19), 8124–8131.
47. Chen, G. Q. *Chem. Soc. Rev.* **2009**, *38* (8), 2434–2446.
48. De Geus, M.; Van der Meulen, I.; Goderis, B.; Van Hecke, K.; Dorschu, M.; Van der Werff, H.; Koning, C. E.; Heise, A. *Polym. Chem.* **2010**, *1* (4), 525–533.

Downloaded by COLUMBIA UNIV on August 28, 2012 | http://pubs.acs.org
Publication Date (Web): August 16, 2012 | doi: 10.1021/bk-2012-1105.ch018

49. van der Meulen, I.; de Geus, M.; Antheunis, H.; Deumens, R.; Joosten, E. A. J.; Koning, C. E.; Heise, A. *Biomacromolecules* **2008**, *9* (12), 3404–3410.
50. Yang, Y. X.; Lu, W. H.; Zhang, X. Y.; Xie, W. C.; Cai, M. M.; Gross, R. A. *Biomacromolecules* **2010**, *11* (1), 259–268.
51. Quinzler, D.; Mecking, S. *Angew. Chem., Int. Ed.* **2010**, *49* (25), 4306–4308.
52. Jiang, Z. Z.; Azim, H.; Gross, R. A.; Focarete, M. L.; Scandola, M. *Biomacromolecules* **2007**, *8* (7), 2262–2269.
53. Hunsen, M.; Abul, A.; Xie, W. C.; Gross, R. *Biomacromolecules* **2008**, *9* (2), 518–522.
54. van der Meulen, I.; Li, Y.; Deumens, R.; Joosten, E. A. J.; Koning, C. E.; Heise, A. *Biomacromolecules* **2011**, *12* (3), 837–843.
55. Zhong, Z. Y.; Dijkstra, P. J.; Feijen, J. *Macromol. Chem. Phys.* **2000**, *201* (12), 1329–1333.
56. van der Meulen, I.; Gubbels, E.; Huijser, S.; Sablong, R.; Koning, C. E.; Heise, A.; Duchateau, R. *Macromolecules* **2011**, *44* (11), 4301–4305.
57. Andronova, N.; Finne, A.; Albertsson, A. C. *J. Polym. Sci., Part A: Polym. Chem.* **2003**, *41* (15), 2412–2423.
58. Tsujimoto, T.; Uyama, H.; Kobayashi, S. *Biomacromolecules* **2001**, *2* (1), 29–31.
59. van der Mee, L.; Helmich, F.; de Bruijn, R.; Vekemans, J.; Palmans, A. R. A.; Meijer, E. W. *Macromolecules* **2006**, *39* (15), 5021–5027.
60. Huisgen, R.; Ott, H. *Tetrahedron* **1959**, *6* (3), 253–267.
61. Uyama, H.; Takeya, K.; Hoshi, N.; Kobayashi, S. *Macromolecules* **1995**, *28* (21), 7046–7050.
62. Bisht, K. S.; Henderson, L. A.; Gross, R. A.; Kaplan, D. L.; Swift, G. *Macromolecules* **1997**, *30* (9), 2705–2711.
63. Duda, A.; Kowalski, A.; Penczek, S.; Uyama, H.; Kobayashi, S. *Macromolecules* **2002**, *35* (11), 4266–4270.
64. Takwa, M.; Simpson, N.; Malmstrom, E.; Hult, K.; Martinelle, M. *Macromol. Rapid Commun.* **2006**, *27* (22), 1932–1936.
65. Schecter, A.; Malik, N.; Haffner, D.; Smith, S.; Harris, T. R.; Paepke, O.; Birnbaum, L. *Environ. Sci. Technol.* **2010**, *44* (24), 9425–9430.
66. Inoue, S.; Koinuma, H.; Tsuruta, T. *Polym. Lett.* **1969**, *7*, 287–292.
67. Rokicki, G.; Kowalczyk, T. *Polymer* **2000**, *41*, 9013–9031.
68. Kuran, W.; Sobczak, M.; Listos, T.; Debek, C.; Florjanczyk, Z. *Polymer* **2000**, *41*, 8531–8541.
69. Wang, X. L.; Zhuo, R. X.; Liu, L. J.; He, F.; G., L. *J. Polym. Sci., Part A: Polym. Chem.* **2002**, *40*, 70–75.
70. Van Meerendonk, W. J.; Duchateau, R.; Koning, C. E.; Gruter, G.-J. M. *Macromol. Rapid Commun.* **2004**, *25*, 382–386.
71. Schutze, E.-C.; Hornung, K.-H.; Nehring, R. Patent US3547889, 1970.
72. Collins, J. R. Patent GB1079686, 1964.
73. Medem, H.; Schreckenberg, M.; Dhein, R.; Nouvertne, W.; Rudolph, H. Patent EP0025937, 1980.
74. Chatti, S.; Kricheldorf, H. R.; Schwarz, G. *J. Polym. Sci., Part A: Polym. Chem.* **2006**, *44*, 3616–3628.

Downloaded by COLUMBIA UNIV on August 28, 2012 | http://pubs.acs.org
Publication Date (Web): August 16, 2012 | doi: 10.1021/bk-2012-1105.ch018

75. Chatti, S.; Schwarz, G.; Kricheldorf, H. R. *Macromolecules* **2006**, *39*, 9064–9070.
76. Kricheldorf, H. R.; Sun, S.-J. *Macromol. Chem. Phys.* **1997**, *198*, 2197–2210.
77. Kricheldorf, H. R.; Sun, S. J.; Gerken, A.; Chang, T. C. *Macromolecules* **1996**, *29*, 8077–8082.
78. Yokoe, M.; Aoi, K.; Okada, M. *J. Polym. Sci., Part A: Polym. Chem.* **2003**, *41*, 2312–2321.
79. Yokoe, M.; Aoi, K.; Okada, M. *J. Appl. Polym. Sci.* **2005**, *98*, 1679–1687.
80. Ono, A.; Toyohara, K.; Minematsu, H.; Kageyama, Y. Patent EP1640400, 2006.
81. Schuhmacher, P.; Kricheldorf, H. R.; Sun, S.-J. Patent US6156866, 2000.
82. Dhara, D.; Shaiki, A. A. G.; Chatterjee, G.; Seetharaman, C. Patent WO2005066239, 2005.
83. Noordover, B. A. J.; Haveman, D.; Duchateau, R.; van Benthem, R. A. T. M.; Koning, C. E. *J. Appl. Polym. Sci.* **2011**, *121* (3), 1450–1463.
84. Szeja, W. *J. Chem. Soc., Chem. Commun.* **1981**, *5*, 215–216.
85. Buck, K. W.; Duxbury, J. M.; Foster, A. B.; Perry, A. R.; Webber, J. M. *Carbohydr. Res.* **1966**, *2*, 122–131.
86. Hsu, J.-P.; Wong, J.-J. *Ind. Eng. Chem. Res.* **2006**, *45*, 2672–2676.
87. Jasinska, L.; Villani, M.; Wu, J.; van Es, D.; Klop, E.; Rastogi, S.; Koning, C. E. *Macromolecules* **2011**, *44* (9), 3458–3466.
88. Thiem, J.; Bachmann, F. *Makromol. Chem.* **1991**, *192*, 2163.
89. Gomurashvili, Z.; Kricheldorf, H. R.; Katsarava, R. *J. Macromol. Sci. Pure.* **2000**, *37*, 215–227.
90. Philip, B.; Sreekumar, K. *Polym. Int.* **2001**, *50*, 1318–1323.
91. Okada, M.; Yamada, M.; Yokoe, M.; Aoi, K. *J. Appl. Polym. Sci.* **2001**, *81* (11), 2721–2734.
92. Wang, L. H.; Porter, R. S. *J. Polym. Sci., Part B: Polym. Phys.* **1995**, *33* (5), 785–790.
93. Johnson, C. G.; Mathias, L. J. *Polymer* **1993**, *34* (23), 4978–4981.
94. Prieto, A.; Iribarren, I.; Munoz-Guerra, S. *J. Mater. Sci.* **1993**, *28* (15), 4059–4062.
95. Wang, L. H.; Baltacalleja, F. J.; Kanamoto, T.; Porter, R. S. *Polymer* **1993**, *34* (22), 4688–4691.
96. Kricheldorf, H. R.; Bornhorst, K.; Schellenberg, J.; Schwarz, G. *J. Macromol. Sci. Pure.* **2007**, *44* (2), 119–124.
97. Ramesh, C. *Macromolecules* **1999**, *32* (11), 3721–3726.
98. Koning, C.; Teuwen, L.; de Jong, R.; Janssen, G.; Coussens, B. *High Perform. Polym.* **1999**, *11* (4), 387–394.
99. Jones, N. A.; Atkins, E. D. T.; Hill, M. J. *Macromolecules* **2000**, *33* (7), 2642–2650.
100. Jones, N. A.; Atkins, E. D. T.; Hill, M. J.; Cooper, S. J.; Franco, L. *Macromolecules* **1996**, *29* (18), 6011–6018.
101. Thiyagarajan, S.; Gootjes, L.; Vogelzang, W.; Wu, J.; van Haveren, J.; van Es, D. S. *Tetrahedron* **2011**, *67* (2), 383–389.

Downloaded by COLUMBIA UNIV on August 28, 2012 | http://pubs.acs.org
Publication Date (Web): August 16, 2012 | doi: 10.1021/bk-2012-1105.ch018

Downloaded by COLUMBIA UNIV on August 28, 2012 | http://pubs.acs.org
Publication Date (Web): August 16, 2012 | doi: 10.1021/bk-2012-1105.ch018

102. Cooper, S. J.; Coogan, M.; Everall, N.; Priestnall, I. *Polymer* **2001**, *42* (26), 10119–10132.
103. Nair, S. S.; Ramesh, C.; Tashiro, K. *Macromolecules* **2006**, *39* (8), 2841–2848.
104. Yoshioka, Y.; Tashiro, K.; Ramesh, C. *J. Polym. Sci., Part B: Polym. Phys.* **2003**, *41* (12), 1294–1307.
105. Yoshioka, Y.; Tashiro, K. *J. Phys. Chem. B* **2003**, *107* (43), 11835–11842.
106. Jones, N. A.; Atkins, E. D. T.; Hill, M. J.; Cooper, S. J.; Franco, L. *Polymer* **1997**, *38* (11), 2689–2699.
107. Bunn, C. W.; Garner, E. V. *Proc. R. Soc. London, Ser. A* **1947**, *189* (1016), 39–68.
108. Liu, Y.; Soderquist Lindblad, M.; Ranucci, E.; Albertsson, A.-C. *J. Polym. Sci., Part A: Polym. Chem.* **2001**, *39*, 630–639.
109. Sonnenschein, M. F.; Guillaudeu, S. J.; Landes, B. G.; Wendt, B. L. *Polymer* **2010**, *51* (16), 3685–3692.
110. Maier, S.; Loontjens, T.; Scholtens, B.; Mulhaupt, R. *Angew. Chem., Int. Ed. Engl.* **2003**, *42*, 5094–5097.
111. Versteegen, R. M.; Sijbesma, R. P.; Meijer, E. W. *Angew. Chem., Int. Ed.* **1999**, *38* (19), 2917–2919.
112. Figovsky, O. L.; Shapovalov, L. D. *Macromol. Symp.* **2002**, *187*, 325–332.
113. Deepa, P.; Jayakannan, M. *J. Polym. Sci., Part A: Polym. Chem.* **2007**, *45* (12), 2351–2366.
114. Deepa, P.; Jayakannan, M. *J. Polym. Sci., Part A: Polym. Chem.* **2008**, *46* (7), 2445–2458.
115. Tang, D.; Mulder, D.-J.; Noordover, B. A. J.; Koning, C. E. *Macromol. Rapid Commun.* **2011**, *32* (17), 1379–1385.
116. Van Haveren, J.; Oostveen, E. A.; Micciche, F.; Noordover, B. A. J.; Koning, C. E.; Van Benthem, R. A. T. M.; Frissen, A. E.; Weijnen, J. G. J. *J. Coat. Tech. Res.* **2007**, *4* (2), 177–186.

Downloaded by COLUMBIA UNIV on August 28, 2012 | http://pubs.acs.org
Publication Date (Web): August 16, 2012 | doi: 10.1021/bk-2012-1105.ch019

Chapter 19

Thermoplastic Starch Polymer Blends and Nanocomposites

C. M. Chaleat,[1] M. Nikolic,[2] R. W. Truss,[3] I. Tan,[3] S. A. McGlashan,[3] and P. J. Halley*,[1,3]

[1]AIBN, UQ QLD 4072, Australia
[2]Chemistry Discipline, QUT QLD 4000, Australia
[3]School of Chemical Engineering, UQ QLD 4072, Australia
***E-mail: p.halley@uq.edu.au**

This paper reviews the development of bio-based thermoplastic starch polymer blends and nanocomposites at the University of Queensland. Starch-based thermoplastics are relatively cheap and more importantly manufactured using a renewable biomaterial. However traditionally most thermoplastic starch polymers suffer from low water resistance and loss of mechanical properties when in contact with water. This paper will highlight the development of thermoplastic starch polymer blends and nanocomposite materials to overcome some of the challenges of thermoplastic starch. Specifically we will highlight understandings in the genetics-structure-property-biodegradation relationships for thermoplastic starch polymers, developments in blends, nanocomposite materials and reactive extrusion and highlights of scale-up of film blowing and injection molding grades.

Thermoplastic Starch Polymers

Starch Polymers

Starch-based biodegradable plastics were first developed in the 1980s (*1*, *2*) where thermoplastic starch (TPS) polymers were produced from starch and selected plasticisers and additives (eg. glycerol, water, urea, salts). Unlike traditional thermoplastics starch has a complex multiscale synthesis and subsequent structure as shown in Figure 1.

In Biobased Monomers, Polymers, and Materials; Smith, P., et al.;
ACS Symposium Series; American Chemical Society: Washington, DC, 2012.

Downloaded by COLUMBIA UNIV on August 28, 2012 | http://pubs.acs.org
Publication Date (Web): August 16, 2012 | doi: 10.1021/bk-2012-1105.ch019

Note also this structure itself undergoes changes (gelatinization (breakdown of granular structure), plasticization and recrystallisation during and after addition of plasticisers and polymer processing.

Thermoplastic starch polymers low cost base and hence cost-competitiveness compared to conventional plastics makes them an attractive choice platform material for biodegradable and renewable resource strategies. However due to poor properties and inherent water susceptibility, these materials have tended to focus on niche markets for low performance applications. Specifically some of these challenges include

- starch requires relatively high temperatures to be melt processed and at these temperatures starch may degrade by fragmentation (depolymerisation (*3*)) or lose volatile plasticisers
- even at these processing temperatures, gelatinisation (breakdown of starch granular structures), breakdown of residual crystallinity and melt mixing is difficult (*4*, *5*)
- starch has a relatively high processing viscosity (which increases the energy required for processing). It is rheologically equivalent to a power-law fluid (*6*) with physical entanglements and macromolecular interactions leading to a high dependence of viscosity on shear rate
- traditionally used plasticisers are hydroscopic and increase the water sensitivity of TPS properties (*7*)

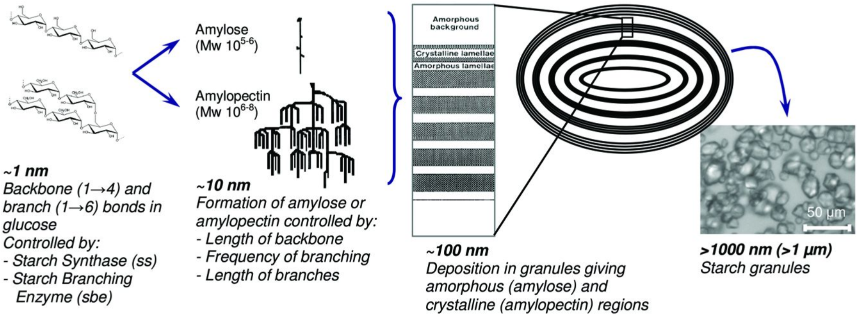
Amylose
(Mw 10^{5-6})
Amylopectin
(Mw 10^{6-8})
Amorphous background
Crystalline lamellae
Amorphous lamellae
50 µm
~1 nm
Backbone (1→4) and branch (1→6) bonds in glucose
Controlled by:
- Starch Synthase (ss)
- Starch Branching Enzyme (sbe)
~10 nm
Formation of amylose or amylopectin controlled by:
- Length of backbone
- Frequency of branching
- Length of branches
~100 nm
Deposition in granules giving amorphous (amylose) and crystalline (amylopectin) regions
>1000 nm (>1 µm)
Starch granules

Figure 1. Synthesis and structural hierarchy of starch polymers.

With this level of complexity and challenges, any research on developing new thermoplastic starch polymers requires a good grasp of the fundamental macromolecular science and engineering behavior.

Downloaded by COLUMBIA UNIV on August 28, 2012 | http://pubs.acs.org
Publication Date (Web): August 16, 2012 | doi: 10.1021/bk-2012-1105.ch019

Genetics-Structure-Property-Biodegradation Relationships

As seen from Figure 1, knowledge of the relationship between genetics-structure-processing-biodegradation for thermoplastic starch polymers is key to understanding their development.

In previous work (*8*) we examined the effects of manipulating the starch genetic pathway (as shown in Figure 2 below) on structure and properties of model thermoplastic starch polymers. Specifically we examined turning branching and debranching enzymes on or off, and the subsequent effects on macromolecular, granular and thermophysical properties.

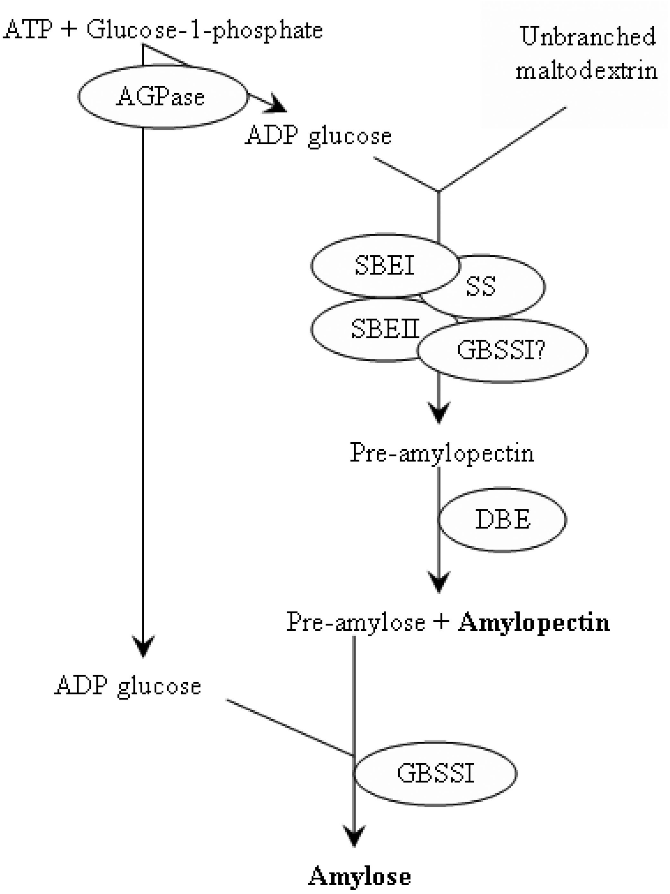
ATP + Glucose-1-phosphate
AGPase
ADP glucose
Unbranched maltodextrin
SBEI
SS
SBEII
GBSSI?
Pre-amylopectin
DBE
Pre-amylose + **Amylopectin**
ADP glucose
GBSSI
Amylose

Figure 2. Schematic representation of starch biosynthetic pathway in plants.

Downloaded by COLUMBIA UNIV on August 28, 2012 | http://pubs.acs.org
Publication Date (Web): August 16, 2012 | doi: 10.1021/bk-2012-1105.ch019

As an example for a range of Maize starch variants described in Table 1, the change in amylose content (Table 1) and a relative change in amylopectin molecular weight distribution (Figure 3; where the normalised distributions were analysed by subtracting the normal maize starch (W64A) distribution from those of others) can be seen.

Table 1. The novel starch varieties utilised as model materials

Plant origin	*Starch type*	*Description*	*Amylose content*
Maize	W64A	Normal (non-mutant) maize	13.6 ± 0.98
	Wx1M	Waxy maize - zero amylose	0.4 ± 0.03
	Du1R	dull1 mutant	25.4 ± 1.83
	Su1R	sugary1 mutant	49.9 ± 3.59
	High amylose	amylose extender mutant	75.3 ± 5.42

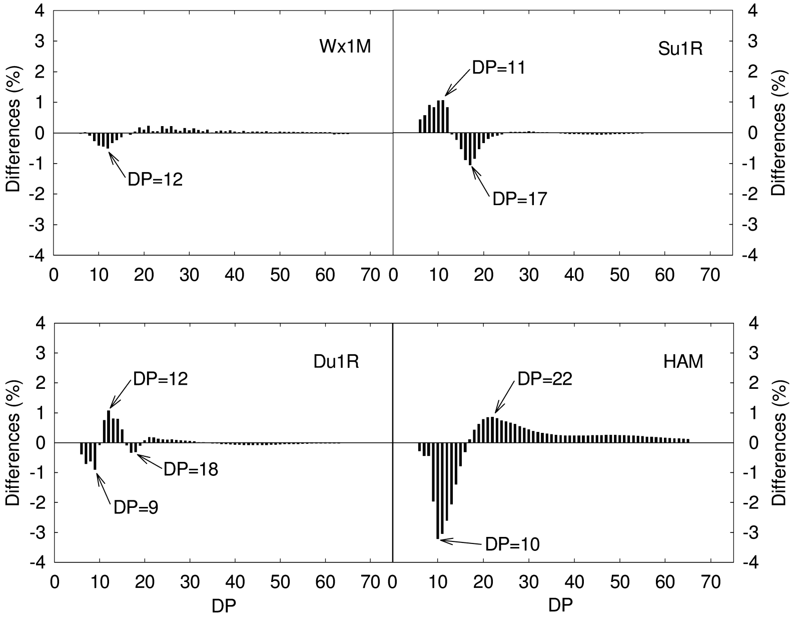

Figure 3. Comparison of the chain length distributions of isoamylase debranched amylopectin from various maize starches, relative to maize starch.

In Biobased Monomers, Polymers, and Materials; Smith, P., et al.;
ACS Symposium Series; American Chemical Society: Washington, DC, 2012.

Downloaded by COLUMBIA UNIV on August 28, 2012 | http://pubs.acs.org
Publication Date (Web): August 16, 2012 | doi: 10.1021/bk-2012-1105.ch019

Here amongst all maize starch varieties, the high amylose maize starch exhibits the most substantial differences in the amylopectin chain length profiles. The proportions of short chains with DP 6-16 are significantly reduced with the maximum reduction is detected at DP 10, while a considerable increase in the fractions of amylopectin chain lengths with DP > 16 is observed, which leads to the noticeable shift in the HAM amylopectin chain length profiles to longer chain lengths.

Further correlations of effects of genetics on crystallinity, granular structure and thermal properties have also been made in this work (*8–10*), and lead to a wealth of understanding for the effects of genetic varieties on macromolecular, granular, thermophysical and function starch polymer properties.

Thermoplastic Starch Polymer Blends

Further research in our laboratories (*7*, *11*, *12*) has extended the capabilities of low cost TPS by developing TPS-based polymer blends with improved performance. However once again a fundamental understanding of basic structure-function relationships needed to be developed,

For example we investigated the fundamental mechanical properties and fracture behaviour of plasticised thermoplastic starch/high molecular weight polyol blends (*11*). In this work the material was stored at various relative humidities to simulate a large range of storage conditions, and then the influence of the equilibrium moisture content on tensile and fracture properties was investigated. Results from effects of equilibrium content on thermal transitions (Figure 4), tensile properties (Figure 5) and fracture properties (Figure 6) are given here.

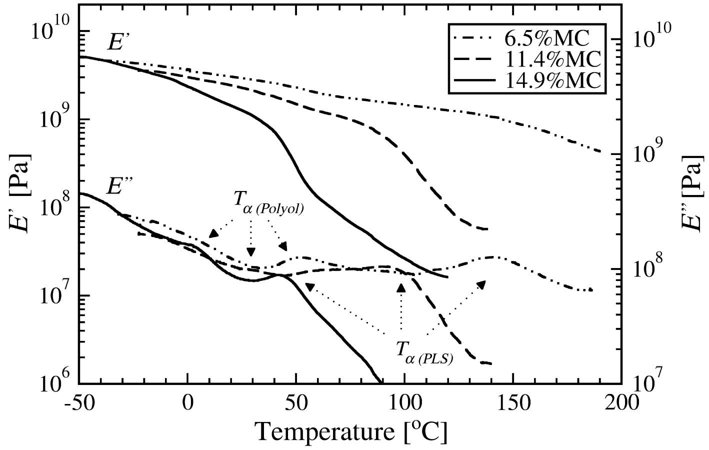

Figure 4. Thermal transitions of TPS blends as a function of moisture content.

Downloaded by COLUMBIA UNIV on August 28, 2012 | http://pubs.acs.org
Publication Date (Web): August 16, 2012 | doi: 10.1021/bk-2012-1105.ch019

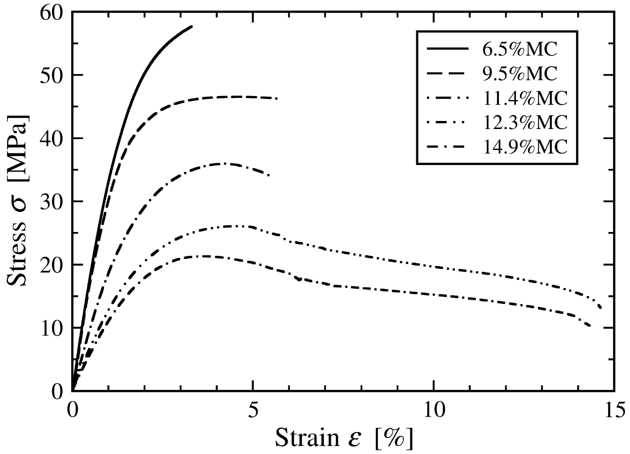

Figure 5. Stress-strain curves for the thermoplastic starch blend equilibrated at different moisture contents.

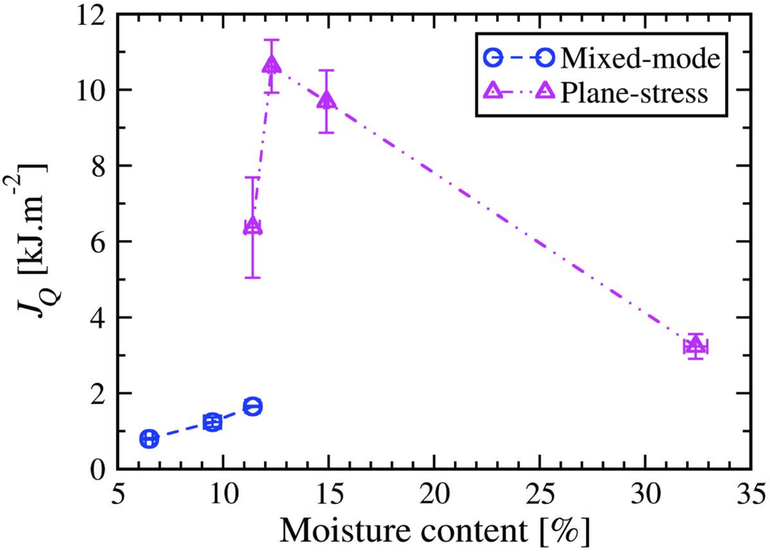

Figure 6. Variations of the strain energy release rate, J_Q for plane-stress and mixed-mode conditions with the equilibrium moisture content.

Downloaded by COLUMBIA UNIV on August 28, 2012 | http://pubs.acs.org
Publication Date (Web): August 16, 2012 | doi: 10.1021/bk-2012-1105.ch019

Clearly the moisture content was shown to strongly affect the tensile and ultimate properties of a plasticised starch/high molecular weight polyol blend due to changes in the glass transition temperature. As the moisture content increased, there was a reduction in the Young's modulus and yield stress. This was further supported by the effect of equilibrium content on fracture surfaces by SEM as shown below in Figure 7, where a more brittle surface is seen at low moisture.

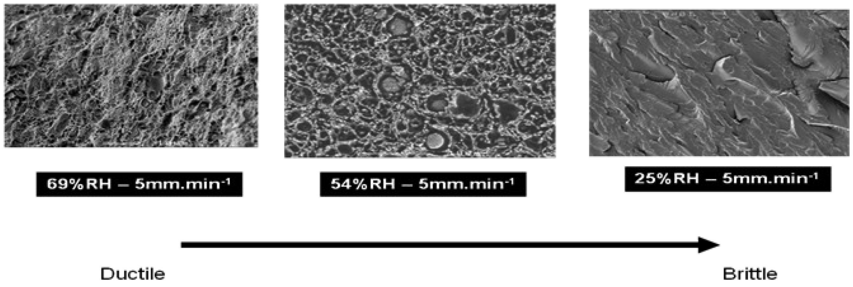

Figure 7. SEM fracture surfaces of thermoplastic starch blends as a function of moisture content.

Further work on dynamic mechanical thermal analysis (*13*) revealed the presence of two relaxations associated with the glass transition of each phase of the starch-high molecular weight polyol blend. The effect of moisture could be explained by a 'time-moisture' superposition demonstrating that the effect of the water content was analogous to the effect of temperature. The variation in the yield stress with strain rate and temperature was described accurately by a two-process Eyring's model. The process, which dominates the deformation behaviour at low strain rates and/or high temperatures correlated well with the relaxation of the plasticised starch-rich phase, while the second process involved at higher strain rates and/or lower temperatures could be associated with the relaxation of the polyol-rich phase

Very interesting results (*7*) on the effects of equilibrium moisture content on water diffusion in thermoplastic starch / high molecular weight polyol blends were observed by characterization of the water diffusion into these materials using MRI. Table 2 shows the values of diffusion (D_o), and Fickian model paramenters (A and n) for thermoplastic starch / high molecular weight polyol blends stored at various conditions, and tested with water at different temperatures.

In this work water diffusion was significantly affected by the temperature during the sorption study and by the relative humidity storage conditions of the material. Diffusion was faster into samples studied at higher water temperatures and those stored at higher relative humidity environments, due to an increase in free volume and plasticization within polymer.

Downloaded by COLUMBIA UNIV on August 28, 2012 | http://pubs.acs.org
Publication Date (Web): August 16, 2012 | doi: 10.1021/bk-2012-1105.ch019

Table 2. Summary of values of D_0, A and n determined from the analysis of the MRI images at (a) 25 °C, (b) 37 °C and (c) 45 °C

(a)

Condition	*$D_0 \times 10^{-7}$ (cm²/s)*	*A*	*n*
vac dried	0.6 ± 0.6	2.2 ± 0.1	0.50
23%	1.3 ± 0.7	2.3 ± 0.1	0.53
43%	1.6 ± 0.1	2.1 ± 0.3	0.51
54%	1.8 ± 0.6	2.3 ± 0.2	0.50
81%	2.4 ± 0.1	2.2 ± 0.2	0.47

(b)

Condition	*$D_0 \times 10^{-7}$ (cm²/s)*	*A*	*n*
vac dried	1.2 ± 0.4	2.3 ± 0.1	0.50
23%	1.8 ± 0.5	2.3 ± 0.1	0.57
43%	2.0 ± 0.2	2.2 ± 0.1	0.52
54%	2.7 ± 0.6	2.1 ± 0.5	0.51
81%	3.3 ± 0.4	2.2 ± 0.2	0.50

(c)

Condition	*$D_0 \times 10^{-7}$ (cm²/s)*	*A*	*n*
vac dried	2.3 ± 0.3	2.2 ± 0.2	0.53
23%	2.4 ± 0.5	2.3 ± 0.1	0.50
43%	2.5 ± 0.7	2.2 ± 0.2	0.50
54%	2.9 ± 0.1	1.6 ± 0.2	0.52
81%	3.8 ± 0.4	2.2 ± 0.1	0.50

Of course water diffusion is a vital first step in understanding biodegradation of biodegradable polymers and subsequent to these tests, the effects of equilibrium moisture and plasticisers were further examined on lab scale enzymatic degradation (*14*) and composting (*15*) behavior. Interesting observations were found with influence of high molecular weight polyol and low molecular weight plasticisers on lab enzyme degradation rates (*14*), and on substrate solubilisation on a COD basis in anaerobic digestion (*15*).

This extensive fundamental work has lead to understanding of performance of thermoplastic starch blends in various environments and subsequently has led to the development of sheet, thermoforming and injection molding grades (shown in Figure 8) that were developed by our CRC Food Packaging and Plantic Technologies Ltd.

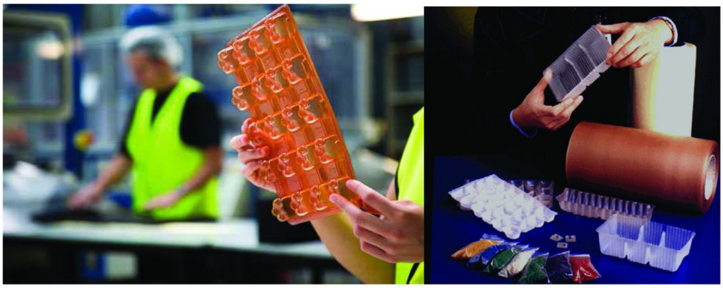

Figure 8. Examples of commercial uses of thermoplastic starch polymers.

Downloaded by COLUMBIA UNIV on August 28, 2012 | http://pubs.acs.org
Publication Date (Web): August 16, 2012 | doi: 10.1021/bk-2012-1105.ch019

Starch Polymer Nanocomposites

Work in our labs (*16*, *17*), developed starch polymer layered silicate nanocomposites systems that allowed processibility of TPS at higher temperatures enabling better melt mixing, increased clarity and antiblocking of blown films and improved tensile properties via an intercalated nanocomposite formation (*16*). For example Figure 9 shows the improvement in clarity in thermoplastic starch/Enpol™ polyester blend films with increasing level of cloisite 30B nanoclay (Southern Clay products).

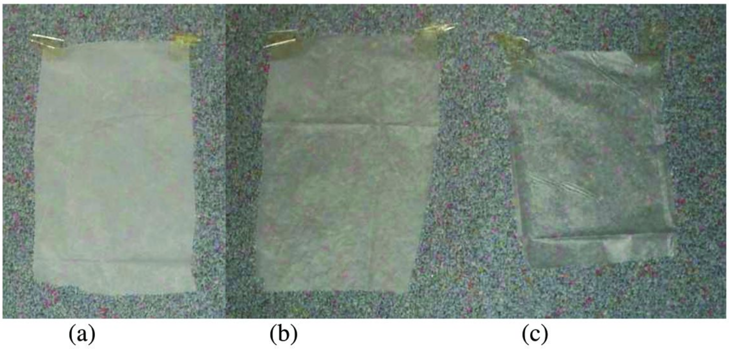

(a) (b) (c)

Figure 9. Thermoplastic starch/polyester blend films with (a) 0, (b) 2.5wt% and (c) 5wt% cloisite 30B nanoclay.

Further development of this nanocomposites work included the investigation of compatibilisation of the thermoplastic starch and Enpol™ polyester phases by using malaeic anhydride with dicumyl peroxide initiator (*18*). Figure 10 shows the improvement in compatibilisation of thermoplastic starch/ Enpol™ polyester / cloisite 30B nanocomposite materials, when extruded in a reactive extruder (*18*).

Downloaded by COLUMBIA UNIV on August 28, 2012 | http://pubs.acs.org
Publication Date (Web): August 16, 2012 | doi: 10.1021/bk-2012-1105.ch019

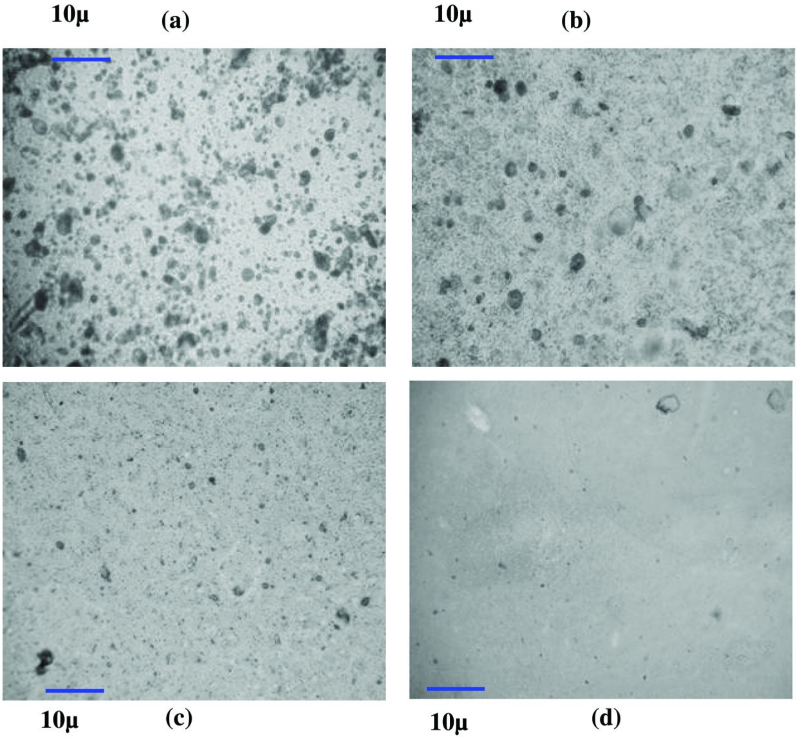

Figure 10. Thermoplastic starch/polyester (50:50 wt) blend with 2.5% Cloiste 30B nanocomposite with 1wt% malaeic anhydride compatibiliser and (a) 0.3, (b) 0.5, (c) 0.8 and (d) 1.2 wt% dicumyl peroxide initiator.

Averous (*19*) extended this work by incorporating a cationic starch nanomaterial masterbatch producing better exfoliation and dispersion of the nanoparticles in starch polymers resulting in superior properties. All these efforts highlight the importance of tailoring the nanomaterial-interface to produce superior processing and performance properties. However, these starch-nanocomposites have been formed via high temperature melt extrusion where, as reported by Dennis (*20*), some of the key parameters necessary for success are high shear rate (for exfoliation of the nanoparticles) and long residence times (for dispersion and distribution of the nanoparticles) in the extruder. Also as mentioned above, high temperature and high shear processing may also cause the starch to fragment or depolymerise, reducing the effectiveness of the nanocomposite enhancement. Thus clearly a major issue for processing of starch nanocomposites is to maximise exfoliation and dispersion to maximise interfacial surface area (and thus subsequent material and performance properties), whilst being able to reduce depolymerisation. Thus we believe there is an important role for rheology, polymer processing optimization and modeling in the further development of thermoplastic starch bionanocomposites. In this way starch nanocomposites may be able to achieve the remarkable property enhancements seen in conventional polymer systems (*21–23*)and be able to be used in more high performance and responsive polymer applications (such as for controlled drug release devices, smart packaging for release of antibacterial or anti microbial actives to foods or other controlled barrier property applications).

Conclusions

In this short review we have attempted to highlight the importance of conducting fundamental research work in parallel commercial development work for thermoplastic starch polymers. Specifically we have highlighted the importance of structure-processing-function relationships in developing thermoplastic starch polymers, blends and nanocomposites. There are abundant opportunities in the further development of thermoplastics starch polymers, especially in the areas of modified starch systems, novel plasticisers, novel processing (such as reactive extrusion, coextrusion and supercritical CO_2 processing) and new blends that will further expand the range of applications for thermoplastic starch polymers especially in the biomedical, pharmaceutical and higher value added agricultural and packaging applications.

Downloaded by COLUMBIA UNIV on August 28, 2012 | http://pubs.acs.org
Publication Date (Web): August 16, 2012 | doi: 10.1021/bk-2012-1105.ch019

References

1. Shogren, R. L.; Fanta, G. F.; Doane, W. M. *Starch/Starke* **1993**, *45* (8), 276–280.
2. Vansoest, J. J. G.; Vliegenthart, J. F. G. *Trends Biotechnol.* **1997**, *15* (6), 208–213.
3. Funke, U.; Bergthaller, W.; Lindhauer, M. G. *Polym. Degrad. Stab.* **1998**, *59*, 293–296.
4. Li, G.; Sarazin, P.; Favis, B. D. *Macromol. Chem. Phys.* **2008**, *209*, 991–1002.
5. Walenta, E.; Fink, H. P.; Weigel, P.; Ganster, J.; Schaaf, E. *Macromol. Mater. Eng.* **2001**, *286*, 462–471.
6. Willett, J. L.; Millardt, M. M.; Jasberg, B. K. *Polymer* **1997**, *38* (24), 5983–5989.
7. Russo, M.; Strounina, E.; Waret, M.; Nicholson, T.; Truss, R.; Halley, P. J. *Biomacromolecules* **2007**, *8* (1), 296–301.
8. Tan, I. *Characterisation of novel starch materials: structure-functionality relationship*. Ph.D. thesis, University of Queensland, 2005.
9. Tan, I.; Flanagan, B. M.; Halley, P. J.; Whittaker, A. K.; Gidley, M. J. *Biomacromolecules* **2007**, *8*, 885–891.
10. Tan, I.; Torley, P. J.; Halley, P. J. *Carbohydr. Polym.* **2008**, *72*, 272–286.
11. Chaléat, C. M.; Halley, P. J.; Truss, R. W. *Carbohydr. Polym.* **2008**, *71* (4), 535–543.

Downloaded by COLUMBIA UNIV on August 28, 2012 | http://pubs.acs.org
Publication Date (Web): August 16, 2012 | doi: 10.1021/bk-2012-1105.ch019

12. Halley, P. J.; Truss, R. W.; Markotsis, M. G.; Chaleat, C.; Russo, M.; Sargent, A. L.; Tan, I.; Sopade, P. A. A Review of Biodegradable Themoplastic Starch Polymers. In *Polymer Durability and Radiation Effects*; Celina, M. C., Assink, R. A., Eds.; ACS Symposium Series 978; American Chemical Society: Washington, DC, 2008.
13. Chaléat, C. M.; Michel-Amadry, G.; Halley, P. J.; Truss, R. W. *Carbohydr. Polym.* **2008**, *74*, 366–371.
14. Russo, M.; Truss, R. W.; Halley, P. J. *Carbohydr. Polym.* **2009**, *77*, 442–448.
15. Russo, M. A. L.; O'Sullivan, C.; Rounsefell, B.; Halley, P. J.; Truss, R.; Clarke, W. P. *Bioresour. Technol.* **2009**, *100*, 1705–1710.
16. McGlashan, S. A.; Halley, P. J. *Polym. Int.* **2003**, *52* (11), 1767–1773.
17. (a) Halley, P.; McGlashan, S.; Gralton, J. Patent WO200283784-A, 2002. (b) Halley, P.; McGlashan, S.; Gralton, J. Patents EP1392770-A4, 2002. (c) Halley, P.; McGlashan, S.; Gralton, J. Patent WO200283784-A1, 2002. (d) Halley, P.; McGlashan, S.; Gralton, J. Patent EP1392770-A1, 2002. (e) Halley, P.; McGlashan, S.; Gralton, J. Patent AU2002248988-A1, 2002. (f) Halley, P.; McGlashan, S.; Gralton, J. Patent US2004122135-A1, 2002. (g) Halley, P.; McGlashan, S.; Gralton, J. Patent AU2002248988-B2, 2002. (h) Halley, P.; McGlashan, S.; Gralton, J. Patent US7094817-B2, 2002.
18. Maliger, R. B.; McGlashan, S. A.; Halley, P. J.; Matthew, L. G. *Polym. Eng. Sci.* **2006**, *46*, 248–263.
19. Chivrac, F.; Pollet, E.; Schmutz, M.; Avérous, L. *Biomacromolecules* **2008**, *9*, 896–900.
20. Dennis, H. R.; Hunter, D. L.; Chang, D.; Kim, S.; White, J. L.; Cho, J. W.; Paul, D. R. *Polymer* **2001**, *42*, 9513–9522.
21. Kojima, Y.; Usuki, A.; Kawasumi, M.; Okada, A.; Fukushima, Y.; Karauchi, T.; Kamigaito, O. *J. Mater. Res* **1993**, *6*, 1185.
22. LeBaron, P. C.; Pinnavaia, T. J. *Chem Mater.* **2001**, *13*, 3760–3768.
23. Alexandre, M.; Dubois, P. *Mater. Sci. Eng.* **2000**, *28*, 1–10.

Downloaded by PENNSYLVANIA STATE UNIV on August 28, 2012 | http://pubs.acs.org
Publication Date (Web): August 16, 2012 | doi: 10.1021/bk-2012-1105.ch020

Chapter 20

Solution Blowing of Soy Protein Fibers

**S. Sinha-Ray,[1] Y. Zhang,[1] A. L. Yarin,*,[1,2] S. C. Davis,[3]
and B. Pourdeyhimi[3]**

**[1]Department of Mechanical and Industrial Engineering,
University of Illinois at Chicago,
842 W. Taylor St., Chicago, IL 60607-7022
[2]Center for Smart Interfaces, Technische Universität Darmstadt,
Petersen str. 32, 64287 Darmstadt, Germany
[3]3427 The Nonwovens Institute, Box 8301,
North Carolina State University,
Raleigh, NC 27695-8301
*E-mail: ayarin@uic.edu**

Solution blowing of soy protein (sp)/polymer blends was used to form monolithic nanofibers. The monolithic fibers were blown from blends of soy protein and nylon-6 in Formic Acid. The sp/nylon-6 ratio achieved in dry monolithic nanofibers formed using solution blowing of the blend was equal to 40/60. In addition, solution blowing of core−shell nanofibers was realized with soy protein being in the core and the supporting polymer in the shell. The shells were formed from either polyacrylonitrile (PAN), or nylon-6. The sp/nylon-6 ratio achieved in dry core−shell fibers was 32/68. For sp/PAN the ratio achieved in dry core−shell fibers was 29/71. The nanofibers developed in the present work contain significant amounts of soy protein and hold great potential in various applications of nonwovens.

Introduction

Modern technology is experiencing a significant shift towards biobased polymers caused by their biodegradablity, renewable sources, or just “green” agricultural biomolecular origin. The shift is driven by a necessity to reduce dependence on synthetic materials, namely on petroleum-derived polymers.

In Biobased Monomers, Polymers, and Materials; Smith, P., et al.;
ACS Symposium Series; American Chemical Society: Washington, DC, 2012.

As a result, significant efforts are directed toward production of biodegradable materials from cotton, corn, potato (*1–5*) and soy protein and development of biodegradable composites (*6–8*). In particular, there is a growing emphasis on making soy-based "green materials". The reason behind the drive towards soy-based materials can be attributed to the fact that soy protein is one of the cheapest and most widely grown vegetable products with a wide range of uses. Booming SoyDiesel production (*9*, *10*) facilitates increasing production of soy, while using only soy oil, and leaving behind abundant residual soy protein.

It is emphasized that soy nanofibers were unavailable at present until our recent work (*11*), as to our knowledge. In the present work we employ a novel method - solution blowing (*11*, *12*) - to produce monolithic and core−shell nanofibers containing soy protein. We denote as monolithic the fibers made of sp/polymer blends and distinguish them from core−shell fibers where sp is located in the core, and a polymer is predominantly in the shell. It is emphasized that in this work it was impossible to form pure sp fibers. Indeed, pure soy protein is very brittle and does not lend itself to fine fiber formation. In Ref. (*13*) electrospinning with pure sp was attempted and resulted in spraying only.

Downloaded by PENNSYLVANIA STATE UNIV on August 28, 2012 | http://pubs.acs.org
Publication Date (Web): August 16, 2012 | doi: 10.1021/bk-2012-1105.ch020

Experimental Section

Materials

Polyacrylonitrile (PAN) and nylon-6, two common industrial fiber-forming polymers were used. In particular, nylon-6 was chosen since it is soluble in formic acid which is also a solvent for soy protein isolate, enabling formation of homogeneous solution blends. On the other hand, PAN is soluble in N,N-Dimethyl Formamide (DMF), which is a non-solvent for soy protein isolate. The soy protein isolates PRO-FAM 955 (sp 955) and PRO-FAM 974 (sp 974) were generously donated by ADM Specialty Food Ingredients. PRO-FAM 955 and PRO-FAM 974 have the same composition but differ in the way they were processed, even though it might be expected that their denaturation in solution can make them practically indistinguishable. Both PRO-FAM 955 and PRO-FAM 974 were recommended by the United Soybean Board (USB) and furnished by ADM.

Solution Preparation

Solution preparation for blowing of sp/nylon-6 monolithic and core−shell fibers and their rheological characterization are described in detail in Ref. (*11*) and are not reproduced here. For the solution blowing of core−shell fibers with PAN in the shell of the fiber, a 10 wt% PAN solution dissolved in DMF (no soy protein added) was used. The core was formed from the following blend: 0.75 g of sp 955 was mixed in 10 g of DMF, and then 0.5 g of 8 wt% PAN solution in DMF was added to enhance core spinnability (viscoelasticity).

Setup and Experimental Procedure

A detailed description can be found in Refs. (*11*) and (*12*).

Downloaded by PENNSYLVANIA STATE UNIV on August 28, 2012 | http://pubs.acs.org
Publication Date (Web): August 16, 2012 | doi: 10.1021/bk-2012-1105.ch020

Results and Discussion

Blends of Soy Protein and Nylon-6: Monolithic Fibers

The fibers obtained from the blend of soy protein and nylon-6 are shown in Figure 1. They have no visible grains of protein, as it was completely dissolved in formic acid. Note that the fibers in the SEM images in Figure 1 a,b (PRO-FAM 955) look rather curly, and some knobs are also visible in Figure 1c where another type of soy protein (PRO-FAM 974) was used for comparison. A macroscale web image corresponding to Figure 1c is shown in Figure 1d.

In dry monolithic nanofibers formed using solution blowing of soy protein (PRO-FAM 955) blends with nylon-6 the protein/polymer ratio of sp/nylon=40/60 was achieved, as determined by the initial solution composition after the solvent had evaporated.

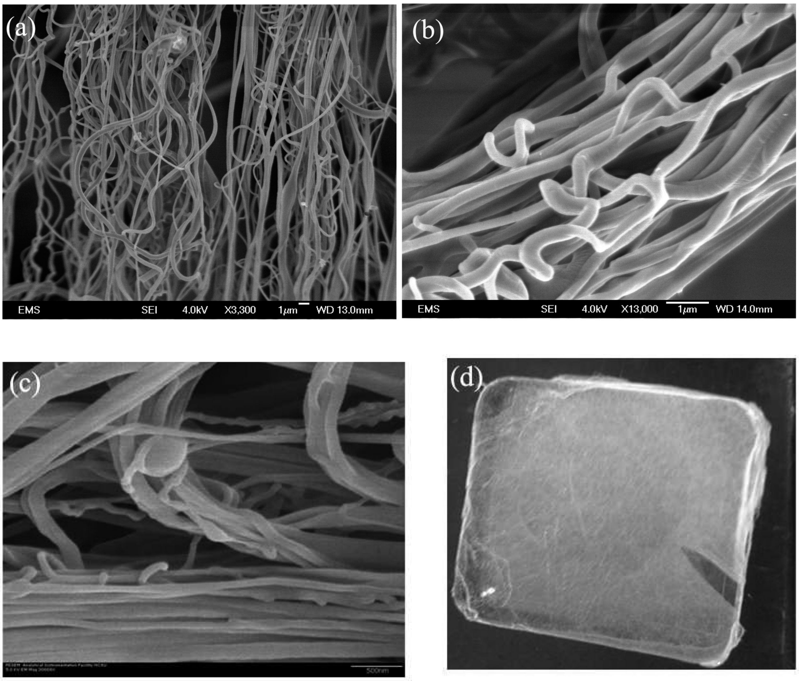
(a)
EMS SEI 4.0kV X3,300 1μm WD 13.0mm
(b)
EMS SEI 4.0kV X13,000 1μm WD 14.0mm
(c)
500nm
(d)

Figure 1. Panels (a) and (b) show SEM images of the monolithic fibers formed by blowing a blend of nylon-6 and soy protein PRO-FAM 955 in formic acid. The zoomed-in view of a section of (a) is shown in panel (b). The fibers are rather curly. Panel (c) shows for comparison fibers formed by blowing a blend of soy protein PRO-FAM 974 and nylon-6 in a 17/83 ratio in formic acid. The macroscale web shown in panel (d) corresponds to the nanofibers of panel (c). (Courtesy of the American Chemical Society).

PRO-FAM 974 product data shows nominal amino acid and other mineral contents, 0.62 wt% sulfur from cystine and methionine, and the elements Na (1.2-

Downloaded by PENNSYLVANIA STATE UNIV on August 28, 2012 | http://pubs.acs.org
Publication Date (Web): August 16, 2012 | doi: 10.1021/bk-2012-1105.ch020

1.6 wt%), K (0.024 - 0.3 wt%), Ca (0.05 – 0.15 wt%), P (0.7 – 1.0 wt%), Fe (0.008 – 0.013 wt%) and Mg (0.025 – 0.10 wt%). EDS spectra from SEM image collection was employed to detect the unique atomic markers from soy protein isolate to differentiate from nylon-6 in a monolithic blend of nanofibers such as shown in Figure 1c. Figure 2a shows the EDS spectra for a formic acid solution cast film of soy protein isolate PRO-FAM 974. The unique markers, P and S are clearly seen. An EDS spectra of 40/60 sp/nylon-6 monolithic blend nanofibers containing some beads is shown in Figure 2b. It is emphasized that the blend of sp/nylon-6 blown to form the fibers used in Figure 2 was absolutely clear, which is an indication that it was homogeneous and no undissolved protein grains were present. When such a blend is strongly stretched during the solution blowing process, solid nanofibers are formed. Sometimes some droplets are disconnected and emitted by high-speed gas stream, or beads are formed, which can be attributed to capillary instability. When the cast films of soy protein was examined using EDS unique markers, (P, S) can be clearly seen, which can also be seen clearly seen in the nanofiber. The quantities of S from the soy protein amino acids are comparable to theoretical (0.6 wt% in pure sp and 0.2% in the 40/60 sp/nylon-6 blend). It should be mentioned that Al was omitted in the analysis since it was due to the aluminum foil was used as nanofiber collection substrate. An EDS spectra was collected with SEM zoomed into a single bead as shown in Figure 2c. The P and S peaks are clearly visible indicating the presence of soy protein. Finally, the EDS spectra were collected with SEM zoomed to a nanofiber-only region as shown in the box labeled S3 of Figure 2d (image) and e (spectra). P and S are again clearly visible at levels consistent with a monolithic blend. These EDS spectral data suggest compositional uniformity of a monolithic sp/nylon-6 solution resulting in nanofibers and some beads with the same composition. The EDS analysis of the beads showed both S and P, which proves that soy protein precipitated in the beads. The EDS analysis of a visually fiber-only region (Figure 2e box labeled S3) clearly revealed P and S. In particular, such a region in box S3 in Figure 2d shows bundles of physically separated nanofibers with no matrix. This proves that the soy protein and nylon-6 co-precipitated to form monolithic fibers. In other words, the soy protein was mixed with nylon-6 in the nanofibers and not lying in between the fibers.

Core−Shell Nanofibers of Soy Protein and Polymer

Core−Shell Nanofibers of Soy Protein and PAN

The optical images of the core−shell PAN-based fibers formed at the core flow rate of 1.2 mL/h are shown in Figure 3 a,b, and at the core flow rate of 2.2 mL/h - in Figure 3 c,d. It can be seen that for the higher core flow rate the presence of the core is much more unambiguous compared to that at the lower core flow rate. However, it should be emphasized that an increase in the core flow rate makes the blowing process prone to interruptions and can result in dripping instead of core−shell fiber formation. It can be seen in Figure 3 d that in some cases the core was not present throughout the whole fiber (indicated by arrow), albeit such defects were relatively rare. Note also, that there are no visible soy protein grains.

Downloaded by PENNSYLVANIA STATE UNIV on August 28, 2012 | http://pubs.acs.org
Publication Date (Web): August 16, 2012 | doi: 10.1021/bk-2012-1105.ch020

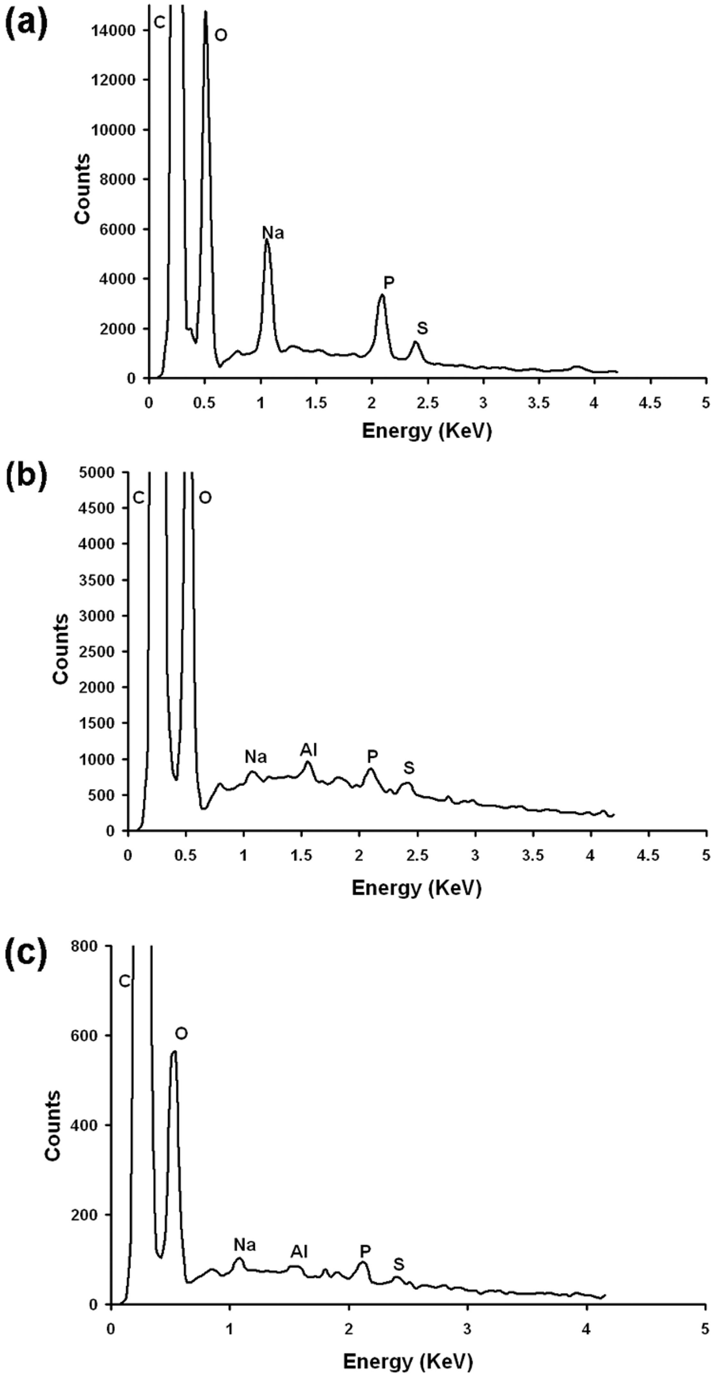

Downloaded by PENNSYLVANIA STATE UNIV on August 28, 2012 | http://pubs.acs.org
Publication Date (Web): August 16, 2012 | doi: 10.1021/bk-2012-1105.ch020

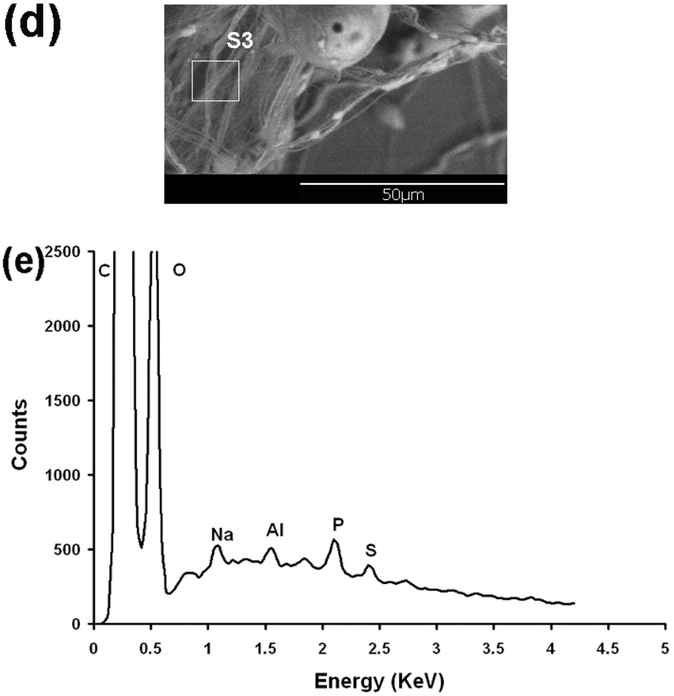

Figure 2. EDS spectra of (a) cast Pro-Fam 974 soy protein film; (b) 40/60 sp/nylon-6 nanofibers with beads; (c) single bead from 40/60 sp/nylon-6 blend; (d) SEM image of fiber only region (box S3) used for EDS collection in e; (e) nanofiber only region. (Courtesy of the American Chemical Society).

Several PAN-based core−shell samples were prepared for heat treatment followed by SEM observation. The resulting fibers were heated at 350 °C for 3 hours in air followed by heating at 750 °C for 1 hour in N_2 atmosphere. For control, soy protein isolate was also subjected to the same treatment and it was found that it was never fully destroyed and left residual quite comparable in volume to the original soy protein. Therefore, it was established that after such treatment the PAN-based core−shell samples will not be hollow, as in the case of PMMA-PAN samples in Ref. (*12*), even though the soy protein was subjected to such high temperatures when there must be some thermal degradation of it. Note that PAN shell definitely does not fully disappear under the same thermal treatment but rather carbonizes (*12*). In addition, it was expected that both materials (soy protein and PAN) shrink differently under such thermal treatment, and thus some cross-sectional differences will be visible in SEM images. It was expected that DMF in the core of the core−shell fiber should evaporate through the shell within about 10 sec (*14*). However, in contrast to Ref. (*14*), this process did not result in a hollow structure as in Ref. (*14*) where the core material was a relatively dilute polymer solution, which resulted in its precipitation onto the shell.

Downloaded by PENNSYLVANIA STATE UNIV on August 28, 2012 | http://pubs.acs.org
Publication Date (Web): August 16, 2012 | doi: 10.1021/bk-2012-1105.ch020

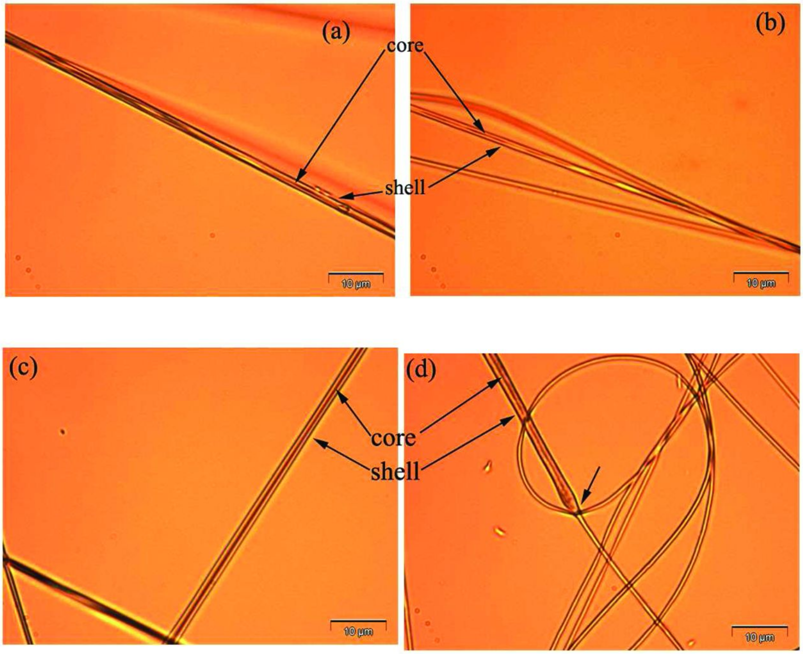

Figure 3. Optical images of the PAN-based core−shell fibers in the cases of the core flow rate of 1.2 mL/h in (a) and (b), and 2.2 mL/h in (c) and (d). The shell flow rate was kept constant at 4.5 mL/h in all the cases. Cores and shells are typically easily distinguishable. In (d) the core interruption at a certain location is marked by an arrow.

The SEM images in Figure 4 show the fracture pattern of the PAN-based core−shell nanofibers before heat treatment. The difference in the fracture between the core and the shell (a pit-like pattern of the core versus a straight cut of the shell) manifests different physical properties of soy protein coagulant in the core and PAN precipitant in the shell. The SEM images in Figure 5 show that the structure of the fibers after heat treatment is rough and possesses some nano-texture (indicated by arrows). The shell walls of the heat-treated PAN-based fibers possess porous structure resulting from DMF evaporation.

Two examples of macroscopic samples of core−shell soy protein-PAN nonwovens collected on a wire ring as a film or in a bucket as a bulky fluffy mass are given in Figure 6.

Core−Shell Nanofibers of Soy Protein and Nylon-6

The SEM images in Figure 7 show the cross-sectional view (Figure 7a) and side view (Figure 7b) of the nylon-6 based core−shell nanofibers. Denaturation of soy protein by formic acid results in complete solubilization of the former, while the evaporation of the latter after fibers were formed leaves a porous nylon-6 shell seen in Figure 7b. The mechanisms of pore formation in nanofibers were discussed before in the context of electrospinning in Refs. (*14*) and (*15*). They can be attributed to such factors as direct permeation of the shell by vapor escaping from the core, as well as to the breath figures, i.e. solvent evaporation cooling, which triggers water droplet condensation onto nanofibers from the surrounding humid air. The image in Figure 7a shows a significant grayness gradient between the core and the shell, which is attributed to a significant electron contrast of soy protein in the core and nylon-6 in the shell.

Downloaded by PENNSYLVANIA STATE UNIV on August 28, 2012 | http://pubs.acs.org
Publication Date (Web): August 16, 2012 | doi: 10.1021/bk-2012-1105.ch020

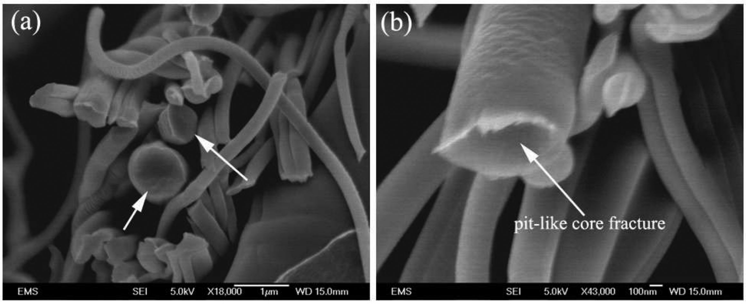
(a)
(b)
pit-like core fracture
EMS SEI 5.0kV X18,000 1μm WD 15.0mm
EMS SEI 5.0kV X43,000 100nm WD 15.0mm

Figure 4. Panels (a) and (b): SEM images of core−shell fibers (soy protein and a small amount of PAN in the core and 10 wt% of PAN in the shell) before heat treatment. In panels (a) and (b) the arrows point at the darker pit-like fracture of the core. This type of fracture is more prominent in panel (b). It looks like the core and shell have different stiffness, which results in different fracture patterns.

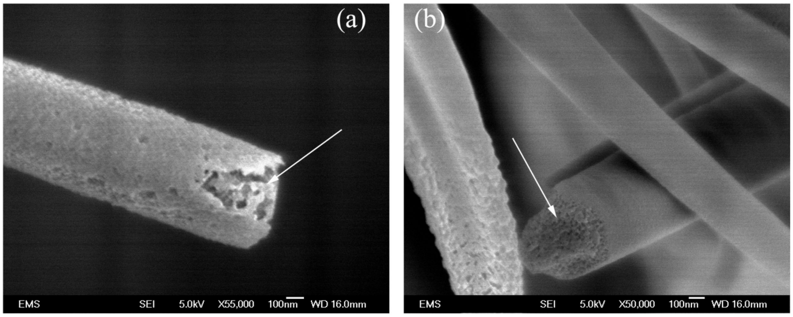
(a)
(b)
EMS SEI 5.0kV X55,000 100nm WD 16.0mm
EMS SEI 5.0kV X50,000 100nm WD 16.0mm

Figure 5. Panels (a) and (b): SEM images of the core−shell (soy protein/ PAN) fibers after heat treatment. The arrows indicate the presumably soy protein core surrounded by the porous carbon shell.

Downloaded by PENNSYLVANIA STATE UNIV on August 28, 2012 | http://pubs.acs.org
Publication Date (Web): August 16, 2012 | doi: 10.1021/bk-2012-1105.ch020

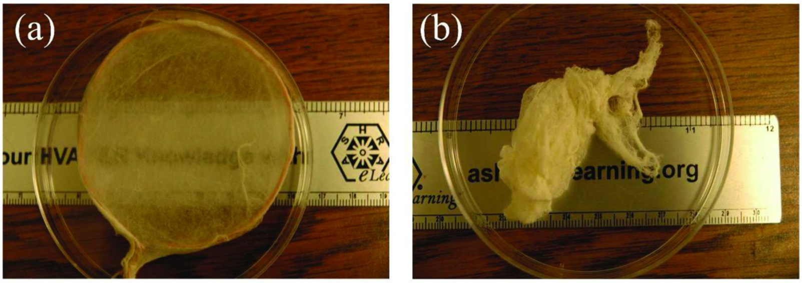

Figure 6. Macroscopic samples of core−shell soy protein-PAN nanofibers collected as a film on a wire ring (panel a), and as a bulky fluffy deposit in a bucket (panel b). Both samples were moved to Petri dishes also seen in the image.

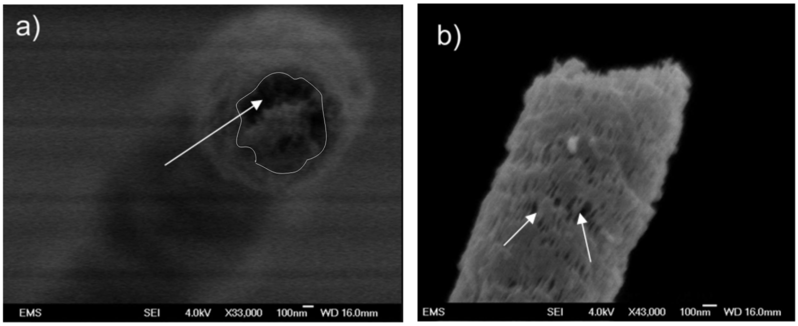
a)
EMS SEI 4.0kV X33,000 100nm WD 16.0mm
b)
EMS SEI 4.0kV X43,000 100nm WD 16.0mm

Figure 7. Panels (a) and (b) show SEM images of core−shell fibers made with fully denaturated soy protein and nylon-6. The core is clearly visible in the cross-sectional view in panel (a) because of a significant electron contrast between soy protein and nylon-6. The core boundary in panel (a) is also traced by a white contour to make it more visible in printed reproduction and marked by the arrow. The side view (b) shows that the nylon-6 shell of this core−shell fiber is porous. (Courtesy of the American Chemical Society).

In dry core−shell nanofibers the sp/nylon-6 ratio was 32/68, as determined by the initial solution compositions and the corresponding flow rates, after the solvent had evaporated.

Fluorescence Microscope Imaging

Fluorescence imaging was used to map soy protein inside fibers formed by solution blowing of blends of nylon-6 with sp in formic acid, and core−shell fibers with sp in the core and nylon-6 in the shell. The fiber mats were washed twice with phosphate-buffered saline (PBS) and then blocked with PBS containing 3%

BSA (500 µl per well) at room temperature for 30 min. Then the fiber mat was washed twice by PBS. After that, a rabbit anti-soy antibody at a dilution 1:2,000 in PBS was added overnight at 4 °C. Thereafter, the fiber mats were washed twice again with phosphate-buffered saline (PBS), and then a goat anti-rabbit IgG FITC antibody (Cat. No.10004302, Cayman, USA) was added at a dilution 1:100 in PBS for one hour at room temperature. Finally, the fiber mats were washed twice with phosphate-buffered saline (PBS). Fluorescent images were recorded using a Nikon microscope (Eclipse E800). Illuminating light was focused on the sample through a 20 ×/ 0.75 NA objective or a 10 ×/ 0.25 NA objective, and images were recorded using a CCD camera (CoolSnap fx, Roper Scientific, Tucson, AZ). Figure 8 demonstrates that soy protein is uniformly distributed in the fibers with the stained soy protein visible everywhere as green color. It is emphasized that soy protein can show some fluorescence under the illuminating light. However, typically staining is required for more reliable observation. On the other hand, nylon-6 does not possess any fluorescence of its own, and cannot be stained using the aforementioned procedure.

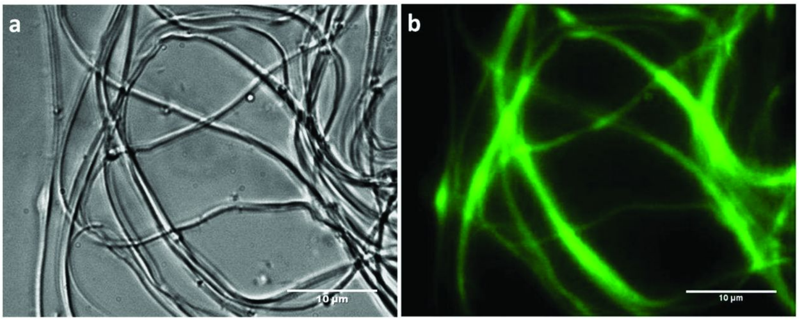

Figure 8. Optical image (panel a: black and white) versus fluorescent images (panel b: in color) of the fibers formed by solution blowing a blend of nylon-6 and soy protein in formic acid. Images (a) and (b) were taken exactly at the same place of a fiber mat. Both images were taken with a 100× microscope objective. The green color indicates the presence of soy protein. (Courtesy of the American Chemical Society).

The core−shell fibers are depicted in Figure 9. The images in Figure 9 reveal that the diameter of the green fluorescence fibers in panels (b) and (d) is smaller than the corresponding diameter of the same fibers in the black-and-white optical images in panels (a) and (c). In particular, in panel (a) the optical image of a fiber has a diameter of 1 µm, whereas the fluorescent image of the same fiber is only 0.4 µm in diameter. This proves that soy protein is, indeed, located in the core of the core−shell fibers as intended. It is emphasized that the fluorescent markers could easily reach the soy protein core via the nylon-6 shell through multiple pores clearly visible in Figure 7b and also reported previously for the other types of core−shell fibers (*14*, *15*).

Downloaded by PENNSYLVANIA STATE UNIV on August 28, 2012 | http://pubs.acs.org
Publication Date (Web): August 16, 2012 | doi: 10.1021/bk-2012-1105.ch020

Downloaded by PENNSYLVANIA STATE UNIV on August 28, 2012 | http://pubs.acs.org
Publication Date (Web): August 16, 2012 | doi: 10.1021/bk-2012-1105.ch020

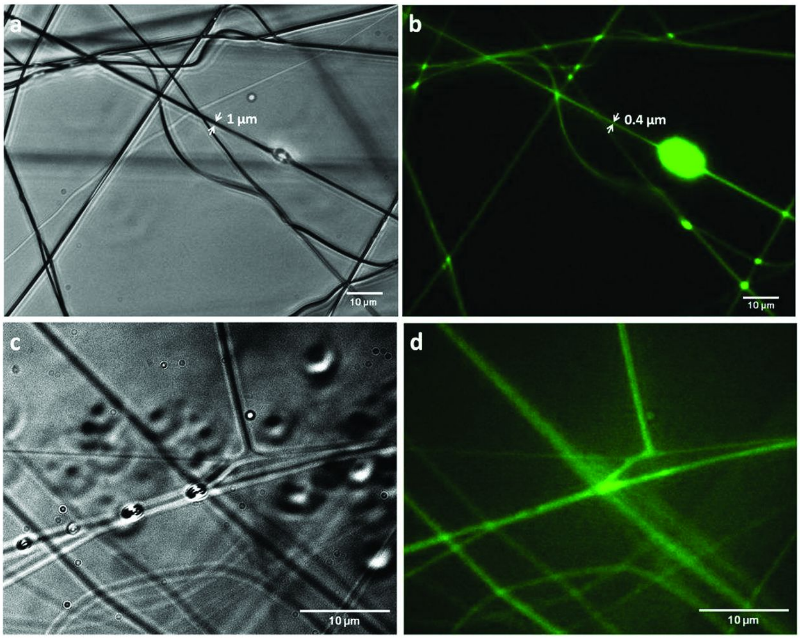

Figure 9. Optical images (panels a and c: black and white) and fluorescent images (panels b and d: in color) of core–shell fibers with soy protein and a small amount of nylon-6 in the core and 20 wt% solution of nylon-6 in formic acid used to form the shell. Panels (a) and (b) corresponding to exactly the same place in the fiber mat were taken with a 40× microscope objective. Panels (c) and (d) corresponding to exactly the same place in the fiber mat were taken with a 100× microscope objective. Green fluorescence indicates the presence of soy protein. (Courtesy of the American Chemical Society).

Statistical Image Analysis

Nonwovens produced by solution blowing are comprised of the entangled individual fibers. They practically never end until the process is stopped. In this sense, they are similar to electrospun nanofiber mats. Therefore, measurements of fiber lengths and aspect ratios are meaningless. On the other hand, cross-sectional diameter can vary even along the individual fibers due to the effect of the turbulent pulsations in gas and elastic wave propagation (*16*, *17*). Therefore, measurements of fiber diameter distribution can be important for the structural characterization of the solution-blown nonwovens and their further applications. Figure 10 depicts the diameter distributions measured from SEM images of sp/nylon-6 fibers blown from blends, while Figure 11 contains the corresponding data for sp/nylon-6 core–shell fibers. It is emphasized that the blend-blown (monolithic) fibers all belong to the submicron range, whereas the core–shell fibers can involve infrequent outliers as large as 2 µm. Still the core–shell fibers are submicron in average.

Downloaded by PENNSYLVANIA STATE UNIV on August 28, 2012 | http://pubs.acs.org
Publication Date (Web): August 16, 2012 | doi: 10.1021/bk-2012-1105.ch020

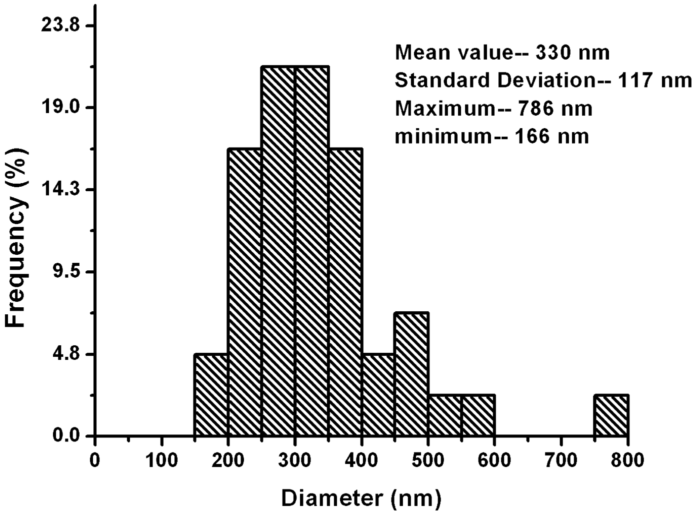

Figure 10. Diameter distribution in sp/nylon-6 blend solution blown nanofibers. (Courtesy of the American Chemical Society).

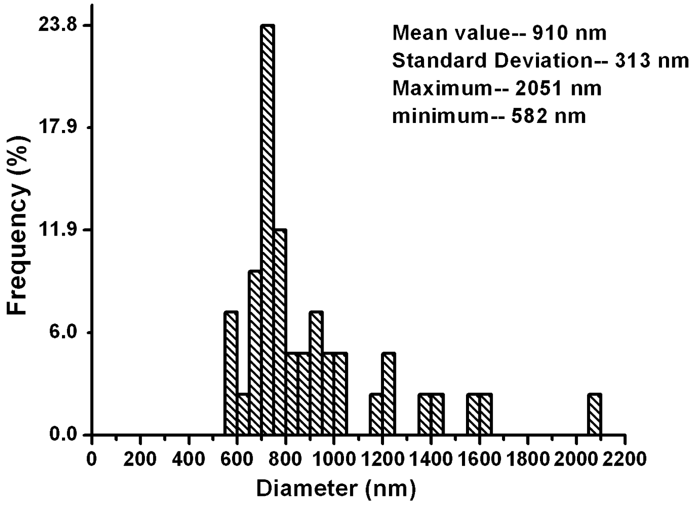

Figure 11. Diameter distribution in sp/nylon-6 core−shell solution blown fibers. (Courtesy of the American Chemical Society).

Downloaded by PENNSYLVANIA STATE UNIV on August 28, 2012 | http://pubs.acs.org
Publication Date (Web): August 16, 2012 | doi: 10.1021/bk-2012-1105.ch020

Conclusion

Solution blowing of monolithic and core−shell soy protein-polymer fibers was demonstrated. The blend fibers were produced from soy protein and nylon-6. They had a protein/polymer ratio of 40/60 in the dry sp/nylon-6 fibers. The core−shell fibers were produced from either protein/PAN, or protein/nylon-6 in the core and, respectively, PAN or nylon-6 in the shell. The protein/nylon-6 had a protein/polymer ratio of 32/68 in the dry core−shell fibers. The individual fibers and their nonwovens were analyzed using optical and scanning electron microscopy (with EDS). Soy protein and nylon-6 provided a significant electron contrast to make the protein core clearly distinguishable from the polymer shell. In the present work the monolithic nanofibers made from sp/nylon-6 blends were basically non-porous in the scale of 10-100 nm, since the images in this scale (e.g. Figure 1c) do not resolve any visible porosity, which still might be present on the smaller scale. The core−shell sp/nylon-6 fibers had pores in the shell in the scale of 10 nm (Figure 7b). Porous shells probably allow low molecular weight fluids to communicate with the core when core−shell fibers are submerged into them, which make them attractive for many applications. In addition, using staining with primary rabbit anti-soy antibody and secondary FITC antibody, soy protein has been successfully marked in the fibers. It was shown that in the blend-blown fibers, soy protein was distributed everywhere in the fibers. These results were in agreement with EDS data from SEM which indicated homogeneous sp/nylon-6 blends. In the core−shell sp/nylon 6 fibers, soy protein was located only in the fiber cores, as designed. The monolithic (blend-blown) fibers all belong to the submicron range, whereas the core−shell fibers can involve infrequent outliers as large as 2 μm. Nevertheless, the core−shell fibers are submicron in average.

The monolithic and core−shell nano- and micro-fibers containing significant amounts of soy protein developed in this work hold great potential as an effective method of utilizing of the one of the most abundant natural materials. In particular, it is foreseen as an effective method of utilization and valorisation of residual material left by Soy Diesel production, which can be useful in various applications of nonwovens. Moreover, Soy Protein Isolates (SPI) used in the present work contain 90% protein, while Soy Protein Concentrates (SPC) contain 50-70% protein (*18*). The highest protein content soy product commercially available was used for this study. Therefore, the use of SPC was not investigated.

In addition, note that solution blown the sp/nylon-6 nanofiber mats produced in the present work look stronger than many electrospun nanofiber mats reported so far (*19*) and are not brittle. A detailed study of their tensile properties is underway and will be reported in future.

Acknowledgments

This work was supported by a research contract with the United Soybean Board, Chesterfield, Missouri (research contract no. 0491). Dr M. Cho is acknowledged for his help with fluorescent microscopy, and A. Kolbasov for technical assistance.

Downloaded by PENNSYLVANIA STATE UNIV on August 28, 2012 | http://pubs.acs.org
Publication Date (Web): August 16, 2012 | doi: 10.1021/bk-2012-1105.ch020

References

1. Kanczler, J. M.; Ginty, P. J.; Bany, J. A.; Clarke, N. M. P.; Howdle, S. M.; Shakesheff, K. M.; Oreffo, R. O. C. *Biomaterials* **2009**, *29*, 1892–1900.
2. Yu, G.; Fan, Y. *J. Biomater. Sci. Polym. Ed.* **2008**, *19*, 87–98.
3. Greene, J. J. *Polym. Environ.* **2007**, *15*, 269–273.
4. Kim, C. W.; Frey, M. W.; Marquez, M.; Joo, Y. L. *Polymer* **2006**, *47*, 5097–5107.
5. Kim, C. W.; Frey, M. W.; Marquez, M.; Joo, Y. L. *J. Polym. Sci., Part B: Polym. Phys.* **2005**, *43*, 1673–1683.
6. Huang, X.; Netravali, A. A. N. *J. Macromol. Sci., Part A: Pure Appl. Chem.* **2008**, *45*, 899–906.
7. Huang, X.; Netravali, A. A. N. *J. Compos. Sci. Technol.* **2007**, *67*, 2005–2014.
8. Chabba, S.; Netravali, A. N. *J. Mater. Sci.* **2005**, *40*, 6275–6282.
9. Klass, D. L. *Biomass for Renewable Energy, Fuels, and Chemicals*; Academic Press: New York, 1998.
10. Ahmed, I.; Decker, J.; Morris, D. *How Much Does it Take to Make a Gallon of Soydiesel?* Report for the National SoyDiesel Development Board, Jefferson, Missouri, 1994.
11. Sinha Ray, S.; Zhang, Y.; Yarin, A. L.; Davis, S. C.; Pourdeyhimi, B. *Biomacromolecules* **2011**, *12*, 2357–2363.
12. Sinha-Ray, S; Yarin, A. L; Pourdeyhimi, B. *Carbon* **2010**, *48*, 3575–3578.
13. Phiriyawirut, M.; Rodchanacheewa, N.; Nensiri, N.; Supaphol, P. *Adv. Mat. Res.* **2008**, *55-57*, 733–736.
14. Dror, Y; Salalha, W; Avrahami, R; Zussman, E; Yarin, A. L; Dersch, R; Greiner, A; Wendorff, J. H. *Small* **2007**, *3*, 1064–1073.
15. Srikar, R.; Yarin, A. L.; Megaridis, C. M.; Bazilevsky, A. V.; Kelley, E. *Langmuir* **2008**, *24*, 965–974.
16. Sinha-Ray, S; Yarin, A. L; Pourdeyhimi, B. *J. Appl. Phys.* **2010**, *108*, 034912.
17. Yarin, A. L.; Sinha-Ray, S.; Pourdeyhimi, B. *J. Appl. Phys.* **2010**, *108*, 034913.
18. Liu, K. In *Soybeans-Chemistry, Technology and Utilization*; International Thomson Publishing: Florence, KY, 1997, pp. 25, 386.
19. Reneker, D. H.; Yarin, A. L.; Zussman, E.; Xu, H. *Adv. Appl. Mech.* **2007**, *41*, 43–195.

In Biobased Monomers, Polymers, and Materials; Smith, P., et al.;
ACS Symposium Series; American Chemical Society: Washington, DC, 2012.

Subject Index

A

α-Methylene-γ-butyrolactone (MBL)
  block copolymers, 202*s*
  butyrolactone ring, 206*s*
  chemical structure, 200*s*, 204*s*
  copypolymerization, 209*s*
  free-radical polymerization, 200*s*
  frustrated Lewis pair, 204*s*
  macromolecular architectures, 207*f*
  polymerization, 204*s*
  ring-opening polymerization, 208*f*
  ring-opening copolymerization, 205*s*
  temperature dependence, 207*f*
Amylose-grafted polysaccharide synthesis
  chemoenzymatic synthesis, 244, 244*f*, 245*f*, 247*f*, 248*f*, 249*f*
  enzymatic glycosylation, 239*f*
  enzymatic propagation, 243*f*
  enzymes, 240*f*
  film formation, 252*f*
  glycogen-based polysaccharide preparation, 251
  glycosylation, 239*f*
  overview, 237
  phosphorylase-catalyzed enzymatic polymerization, 241, 242*f*
  phosphorylase-catalyzed polymerization, 252*f*
  re-hydrogelation, 252*f*
  re-hydrogelation suppression, 252*f*
  xerogel dissolution, 252*f*
Avantium, 1

B

BD. *See* 1,4-butanediol (BD)
Biobased polymeric materials, cotton byproducts
  burr, 49*f*, 52*t*, 53*t*, 56*t*, 57*t*, 58*f*
  carboxymethylation, 57*t*
  cellulose esters, 50
  CMC, 58*f*
  CMX, 58*f*
  ester formation, 60
  ether formation, 60
  filler studies, 59
  hull, 49*f*, 52*t*, 53*t*, 55*t*, 57*t*, 58*f*
  iodine-catalyzed acetylation reaction, 55*t*, 56*t*
  LDPE, 49*f*, 53*t*
  overview, 47
  PLA, 49*f*, 52*t*
  polymer composites, 48
  polysaccharide carboxymethyl ethers, 51
Biobased polymers, plant-derived
  chemical structures, 199*c*
  classification, 198*t*
  copolymerization, 200
  free-radical homopolymerization, 200
  functional polymers, 204
  macromolecular architectures, 201
  MBL, 200, 203
  metal-catalyzed polymerization, 203
  overview, 197
  PMBL-b-PBA-b-PMBL, 202*f*
  precision polymerizations, 201
  specialty polymers, 204
  vinyl monomers, 198
Biobased pressure-sesitive adhesives
  DSO, 21*f*
  EMO polymer, 20*f*
  ESO, 21*f*, 22*f*, 23*f*, 24*f*
  H_3PO_4, 18*s*
  hydroxylated soybean oil, 18*s*
  overview, 15
  Polymer-1-2-P, 18*s*
  Polymer-5-6-P, 19*s*, 21*f*
  schematic representation, 17*f*
BiOH® polyols
  5000, 171*t*
  5300, 174
  5400, 174, 176*t*
  foam properties, 175*t*
  load bearing properties, 173*f*
  natural oils, 167
    incorporation level, 176
    polyurethanes, 169
  overview, 165
  properties, 171*t*
  soybean oil, 168*f*
  synthesis, 172*f*
Biological lactate-polymers
  characteristics
    enantiomeric purity, 226
    mechanical properties, 228, 230*t*
    molecular weights, 228
    sequential structures, 227
    thermal properties, 228, 230*t*
  enzyme, 216, 219
  high LA-containing polyesters, 225, 226*f*
  LA unit enrichment, 223

Downloaded by 217.66.152.26 on August 23, 2012 | http://pubs.acs.org
Publication Date (Web): August 16, 2012 | doi: 10.1021/bk-2012-1105.ix002

        - LA-based polyester biosynthesis, 216, 221
        - microbial cell factory, 221, 222*f*
        - overview, 213
        - PHA synthases, 217, 217*t*, 218*f*
        - polyester synthesis, 224
        - process conversion, 215*f*
        - in vitro polymerization assay system, 220*f*
- Biomass-based monomer synthesis
    - BD, 95*f*, 99*s*
    - biomass carbon ratio, 100, 101*t*, 102*t*, 103, 104*t*, 105*t*
        - measurement, 96
    - commercial plastics, 93*t*
    - DF, 100*s*
    - DS, 100*s*
    - FCA, 100*s*
    - furfural conversion, 98
    - overview, 91
    - PBS, 101
    - polycondensation
        - PBS, 97, 103*s*
        - PBT, 98, 106, 107*s*
    - ring-opening polymerization, 97, 106*s*
    - SA, 95*f*, 99*s*
    - THF, 100*s*
    - transesterification polycondensation, 97, 98
- Biomass-based plastics, 93*t*
- Biomass-based polydiols, 283*s*
- Biomass-based polymers
    - HEMA, 293*t*
    - isoidide, 284*f*
    - isomannide, 284*f*
    - isosorbide, 284*f*, 288*t*
    - macrolactones, ring-opening polymerization, 294
        - characterization, 297
        - enzymatic degradation, 300
        - hydrolytic degradation, 299*f*, 300
        - polymer synthesis, 294
    - overview, 281
    - polyamides, 305, 306*f*, 307*t*, 308*f*, 309*f*
        - diaminoisoidide, 306
    - polycarbonates, 300, 302*t*, 303*f*, 304*s*, 304*t*
    - polycondensation reaction, 285*s*
    - polydiols, 283*s*, 314*t*
    - polyureas, 309, 310*s*, 311*s*
        - elastomers, 309
    - polyurethanes, 309, 310*s*, 313*f*, 314*f*
        - elastomers, 309
    - saturated polyesters, 282
        - linear dihydroxyl-terminated polyesters, 282
        - polyester resins, 284
    - TBD-catalyzed synthesis, 283*s*
    - unsaturated polyesters, 289
- Biomass-based saturated polyesters, 282
    - linear dihydroxyl-terminated polyesters, 282
    - polyester resins, 284
- Biomass carbon ratio, 100, 101*t*, 102*t*, 103, 104*t*, 105*t*
    - measurement, 96
- Bottle application testing, FDCA, 5
- Branched polyester resins, 284
- 1,4-Butanediol (BD), 99*s*

C

- *C. tropicalis*, 78, 80
- Carbohydrate hydrogenolysis
    - C5 sugar, 188*t*
    - C6 sugar, 188*t*
    - overview, 183
    - pre-1970, 190
    - reaction mechanism, 185
    - 1970s, 190
    - 1980s, 190
    - 1990s, 191
    - 2000s, 191
    - sorbitol, 187*t*
    - sucrose, 185*f*
    - xylitol, 187*t*
        - hydrogenolysis, 186*f*
- Carboxymethylation, 57*t*
- Carboxymethyl cellulose (CMC), 58, 58*f*
- Carboxymethyl xylan (CMX), 58, 58*f*
- Cellulose esters, 50
- CMC. *See* carboxymethyl cellulose (CMC)
- CMX. *See* carboxymethyl xylan (CMX)
- Cotton burr, 49*f*, 52*t*, 53*t*, 56*t*, 57*t*, 58*f*
- Cotton hull, 49*f*, 52*t*, 53*t*, 55*t*, 57*t*, 58*f*

D

- DBTO-catalyzed condensation polymerization, 114, 118, 119*f*, 121*f*, 125*f*
- DF. *See* dimethyl fumarate (DF)
- Diglycidyl terephthalate (DGT), 288*f*
- Dimethyl fumarate (DF), 100*s*
- Dimethyl succinate (DS), 100*s*
- DS. *See* dimethyl succinate (DS)
- DSO, 21*f*

Downloaded by 217.66.152.26 on August 23, 2012 | http://pubs.acs.org
Publication Date (Web): August 16, 2012 | doi: 10.1021/bk-2012-1105.ix002

Downloaded by 217.66.152.26 on August 23, 2012 | http://pubs.acs.org
Publication Date (Web): August 16, 2012 | doi: 10.1021/bk-2012-1105.ix002

E

EBA-GMA. *See* ethylene/n-butyl acrylate/glycidyl methacrylate terpolymer elastomer (EBA-GMA)
EMO. *See* epoxidized methyl oleate (EMO) polymer
Energy balance, FDCA, 11
Enzymatic ring-opening polymerization, macrolactones, 295
Epoxidized methyl oleate (EMO) polymer, 19, 20*f*
Epoxidized soybean oil (ESO), 21*f*, 22*f*, 23*f*, 24*f*
ESO. *See* epoxidized soybean oil (ESO)
Ethylene/n-butyl acrylate/glycidyl methacrylate terpolymer elastomer (EBA-GMA), 38, 39*f*, 40*f*, 41*f*, 42*f*, 44*f*

F

Fatty acid oxidation, 79*f*, 84*f*
FCA. *See* furancarboxylic acid (FCA)
FDCA. *See* furandicarboxylic acid (FDCA)
FDCA-based polyesters, 3, 7*t*
Frustrated Lewis pair (FLP), 204*s*
Furan-based polyesters, 9
Furancarboxylic acid (FCA), 100*s*
Furandicarboxylic acid (FDCA)
  analytical techniques, 4
  bottle application testing, 5
  economical performance, 11
  energy balance, 11
  FDCA-based polyesters, 2, 7*t*
  furan-based polyesters, 9
  green house gas balance, 11
  overview, 1
  PBF production, 6*f*
  PEF, 6*t*, 8*f*, 9*t*, 10*f*, 11*f*
  PET, 9*t*, 10*t*, 11*f*
  polycondensation setup, 4
  polyester, 2
    production, 5
  polymer analyses, 5
  recycling, 10
  solid state polymerization, 8

G

Green house gas balance, FDCA, 11

H

HEMA. *See* 2-hydroxyethyl methacrylate (HEMA)
H_3PO_4, 18*s*
2-Hydroxyethyl methacrylate (HEMA), 293*t*
Hydroxylated soybean oil, 18*s*

I

Iodine-catalyzed acetylation reaction, 55*t*, 56*t*
Isoidide (II), 284*f*
Isomannide (IM), 284*f*
Isosorbide-derived unsaturated polyesters, 289
  properties, 292*t*
  structure, 290*f*, 301*f*

L

LDPE. *See* low density polyethylene (LDPE)
Linear dihydroxyl-terminated polyesters, 282
Linear polyester resins, 284
Long-chain polyesters
  alkoxycarbonylation, 155, 158*s*
  C_{19} polyester, 155
  C_{20} polyester, 154, 154*s*, 155*f*
  C_{23} polyester, 155
  catalytic hydrogenation, 161
  dimethyl-1,19-nonadecanedioate, 156*s*
  melting points, 157*f*
  methyl linoleate alkoxycarbonylation, 160, 161*f*, 162*f*
  monomers, 152*s*
  overview, 151
  polyamides, 152*s*
  WAXS diffraction, 158*f*
  α,ω-difunctional compounds, 153*s*, 154*s*, 157*s*
Low density polyethylene (LDPE), 49*f*, 53*t*

M

Macrolactones, 294
  characterization, 297
  enzymatic degradation, 300
  hydrolytic degradation, 300

Downloaded by 217.66.152.26 on August 23, 2012 | http://pubs.acs.org
Publication Date (Web): August 16, 2012 | doi: 10.1021/bk-2012-1105.ix002

  polymer synthesis, 294
MBL. *See* α-methylene-γ-butyrolactone (MBL)
McLafferty-type rearrangement, PU, 272*f*
MDO. *See* 2-methylene-1,3-dioxepane (MDO)
Melt polycondensation, polyesters, 282
Metal-catalyzed ring-opening polymerization, macrolactones, 295
Methyl methacrylate (MMA), chemical structures, 200*s*
2-Methylene-1,3-dioxepane (MDO), 208*f*
MMA. *See* methyl methacrylate (MMA)
Monomer biosynthesis, plastics
  C. tropicalis, 78, 80
  fatty acid oxidation, 79*f*, 84*f*
  fermentation, 81
  gene deletion, 78
  genotypes, 83*f*
  liquid chromatography-mass spectrometry, 81
  overview, 77
  purified alcohol dehydrogenase protein reactions, 80
  shake-flask oxidations, 80
  synthetic P450 expression, 79
  ω-hydroxyfatty acid production, 86*f*

N

Nanosized calcium carbonate (NPCC), 28, 33*f*, 34*f*, 34*t*, 37*f*
Natural oils, 167
  incorporation level, 176
  polyurethanes, 169
N435-catalyzed condensation polymerization, 114, 120, 123*f*, 126*f*
Nonreactive blending, PLA, 28
  biodegradable PBAT, toughening PLA, 28, 35
  inorganic rigid particles, toughening PLA, 32, 35
NPCC. *See* nanosized calcium carbonate (NPCC)
Nylon-6, 337

O

OL. *See* oleic acid (OL)
Oleic acid (OL), 269
OMMT. *See* organically modified montmorillonite (OMMT)
Organically modified montmorillonite (OMMT), 28, 33*f*, 34*f*, 34*t*, 37*f*

P

PAN. *See* polyacrylonitrile (PAN)
PBAT. *See* poly(butylene adipate-*co*-terephthalate) (PBAT)
PBS. *See* poly(butylene succinate) (PBS)
PBT. *See* poly(butylene terephthalate) (PBT)
PCL. *See* poly(epsilon-caprolactone) (PCL)
PEF. *See* polyethylene 2,5-furandicarboxylate (PEF)
PEOMA. *See* poly(ethylene oxide) methyl ether methacrylate (PEOMA)
PET. *See* polyethylene terephthalate (PET)
Polyacrylonitrile (PAN), 335, 341*f*, 342*f*, 343*f*
Polyamides, 305
  diaminoisoidide, 306
Poly(butylene adipate-*co*-terephthalate) (PBAT), 28, 30*f*, 31*f*, 31*t*, 36*f*, 37*f*
Poly(butylene succinate) (PBS), 96
Poly(butylene terephthalate) (PBT), 107*s*
Polycarbonates, 300
Polycondensation setup, FDCA, 4
Polydiols. *See* biomass-based polydiols
Poly(epsilon-caprolactone) (PCL), 257
Polyesters, 2
Polyethylene 2,5-furandicarboxylate (PEF), 6*t*, 8*f*, 9*t*, 10*f*, 10*t*, 11*f*
Poly(ethylene oxide) methyl ether methacrylate (PEOMA), 207*f*
Polyethylene terephthalate (PET), 9*t*, 10*t*, 11*f*
Poly(lactic acid) (PLA)
  EBA-GMA, 39*f*, 40*f*, 41*f*, 42*f*, 44*f*
  nonreactive blending, 28
    biodegradable PBAT, toughening PLA, 28, 35
    inorganic rigid particles, toughening PLA, 32, 35
  NPCC, 28, 33*f*, 34*f*, 34*t*, 37*f*
  OMMT, 28, 33*f*, 34*f*, 34*t*, 37*f*
  overview, 27
  PBAT, 30*f*, 31*f*, 31*t*, 36*f*, 37*f*
  reactive blending, 38
  synthetic route, 29*f*
Polymer analyses, FDCA, 5
Polymer-1-2-P, 18*s*
Polymer-5-6-P, 19*s*, 21*f*

Poly(oleic diacid-co-glycerol)
  characterization, 120*t*
  DBTO-catalyzed condensation polymerization, 114, 118, 119*f*, 121*f*, 125*f*
  DSC, 115
  N435-catalyzed condensation polymerization, 114, 120, 123*f*, 126*f*
  NMR, 115
  overview, 111
  size exclusion chromatography-multiangle laser light scattering, 115
  structure characterization, 116, 125*s*
  TGA, 115
  thermal properties, 126, 127*t*
Poly[(*R*)-3-hydroxybutyrate] (P(3HB))
  cold-drawing temperature effect, 68, 72*t*, 73*f*, 74*f*
  heat decomposition rate constant, 68*t*
  mechanical properties, 69, 70*f*
  melt-spinning time, 67*f*, 68*t*
  melt-spun fibers, 65
  molecular weight changes, melt spinning, 66
  molecular weight measurement, 65, 67*f*
  optimum conditions, melt spinning, 66
  overview, 63
  stress-strain test, 65, 69*f*, 70*f*
  X-ray diffraction, 71
  X-ray measurements, 66
Polysaccharide carboxymethyl ethers, 51
Polyureas, 309
  elastomers, 309
Polyurethanes, 309
  elastomers, 309
Poly(ω-hydroxyl tetradecanoic acid) (P(ω-OHC14)) synthesis
  DMTA, 136
  DSC, 136
  dynamic mechanical thermal analysis, 141
  FTIR, 135
  HDPE, 146
  molecular weight measurements, 135, 138*f*
  molecular weight progression, 139, 145*t*
  NMR, 135
  overview, 131
  preparation, 134
  reaction time, 139*f*
  SEC, 135
  temperature effect, 138
  tensile testing, 137, 142, 143*f*, 144*f*
  TGA, 136
  thermal properties, 140, 140*t*
  Ti(OiPr)4 concentration effect, 137
Purified alcohol dehydrogenase protein reactions, 80
P(ω-OHC14). *See* poly(ω-hydroxyl tetradecanoic acid) (P(ω-OHC14)) synthesis

R

Reactive blending, PLA, 38
Recycling, FDCA, 10

S

SA. *See* succinic acid (SA)
Saturated polyesters. *See* biomass-based saturated polyesters
Shake-flask oxidations, 80
Size exclusion chromatography-multiangle laser light scattering, 115
SNC. *See* starch nanocrystals (SNC)
Solid state polymerization, 8
Sorbitol, 187*t*
Soy protein fibers
  blends, 337, 337*f*
  core-shell nanofibers, 338, 343*f*
  films, 339*f*
  fluorescence microscope imaging, 343
  fluorescent image, 344*f*, 345*f*
  nylon-6, 337, 337*f*, 346*f*
  optical image, 344*f*, 345*f*
  overview, 335
  PAN, 341*f*, 342*f*, 343*f*
  statistical image analysis, 345
Starch nanocrystals (SNC)
  characterization, 260
  melt-blending preparation, 260, 260*t*, 263*f*, 264*f*, 264*t*, 265*f*, 266*t*
  nanohybrid synthesis, 261, 262*t*
  overview, 257
  PCL grafting, 262*f*
  PCL-based bio(nano)composites, 263
  preparation, 259
  ring-opening polymerization, 259, 261*f*
Succinic acid (SA), 99*s*
Sucrose, 185*f*
Synthetic P450 expression, 79
Synthetic route, PLA, 29*f*

Downloaded by 217.66.152.26 on August 23, 2012 | http://pubs.acs.org
Publication Date (Web): August 16, 2012 | doi: 10.1021/bk-2012-1105.ix002

Downloaded by 217.66.152.26 on August 23, 2012 | http://pubs.acs.org
Publication Date (Web): August 16, 2012 | doi: 10.1021/bk-2012-1105.ix002

T

Telechelic preparation, PU, 277*f*
Tetrahydrofuran (THF), 100*s*
Thermoplastic polyurethanes
  MALDI-TOF MS spectra, 278*f*
  McLafferty-type rearrangement, 272*f*
  MTT cytotoxicity, 277*f*
  OL-based, 273, 273*f*
  overview, 269
  polyaddition, 275*f*
  stress-strain curves, 276*f*
  telechelic preparation, 277*f*
  triglyceride molecule structure, 270*f*
  UD-based, 273, 273*f*
Thermoplastic starch polymer blends
  commercial uses, 331*f*
  films, 331*f*
  genetics-structure-property-biodegradation relationships, 325
  MRI, 330*t*
  nanocomposites, 331, 332*f*
  overview, 323
  schematic representation, 325*f*
  SEM fracture surfaces, 329*f*
  strain energy release rate, 328*f*
  stress-strain curves, 328*f*
  structural hierarchy, 324*f*
  synthesis, 324*f*
  thermal transitions, 327*f*
  varities, 326*t*
THF. *See* tetrahydrofuran (THF)
Transesterification polycondensation, 97, 98
Triglyceride molecule structure, 270*f*
Triglycidyl trimellitate (TGT), 288*f*
Tulipalin A monomer, 197

U

UD. *See* undecylenic acid (UD)
Undecylenic acid (UD), 269
Unsaturated polyesters. *See* isosorbide-derived unsaturated polyesters

W

ω-Hydroxyfatty acid production, 86*f*

X

Xylitol, 187*t*
Xylitol hydrogenolysis, 186*f*

Y

YXY building blocks, 1